AN IMPROVED METHOD FOR THE ESTIMATION OF THE ENERGY CONSUMPTION AND SAVINGS OF CODE-COMPLIANT OFFICE BUILDINGS IN DIFFERENT CLIMATES

A Dissertation

by

FARSHAD KHEIRI

Submitted to the Office of Graduate and Professional Studies of
Texas A&M University
in partial fulfillment of the requirements for the degree of

DOCTOR OF PHILOSOPHY

Chair of Committee,	Jeff S. Haberl
Co-Chair of Committee,	Juan-Carlos Baltazar
Committee Members,	Wei Yan
	David E. Claridge
Head of Department,	Gregory A. Luhan

December 2020

Major Subject: Architecture

ABSTRACT

Degree day methods are used in the estimation of building energy consumption and climate classification for buildings (e.g. in ASHRAE Standard 169-2013, which is adopted in ASHRAE Standard 90.1-2016). This study, first assessed the effectiveness of the conventional degree days in estimating building energy consumption in different moisture regimes. The analysis was done by comparing the energy performance of the DOE/PNNL medium office prototype building models in the 801 locations in the U.S. The results revealed large variations in the annual energy consumption of the models in the different moisture regimes within each climate zone. Furthermore, large differences in the estimated energy savings by utilization of daylight were shown in different locations. In addition, detailed pairwise analyses were performed to analyze the large variation in the cooling or heating energy consumption in sites with similar Cooling Degree Days (CDD) or Heating Degree Days (HDD), respectively. The analysis revealed that the influential weather parameters that affected the building energy consumption were not fully accounted for in a conventional degree day method. In other words, the level of aggregation of the data in the conventional degree day method masks some of the informative characteristics of the outdoor dry-bulb temperature.

To resolve these discrepancies, a split-degree day method was proposed to calculate the split-Cooling Degree Days (sCDD) and the split-Heating Degree Days (sHDD). The results show that in the regression models using the split degree days compared to the conventional degree days, the coefficient of determination of the estimations of the energy consumption increased for the total annual energy use (from 0.913 to 0.965), the heating energy use (from 0.891 to 0.981), the cooling energy use (from 0.979 to 0.982), and the fan energy use (from 0.383 to 0.722).

Similar results were shown for the models with higher thermal mass. The proposed method can be used for building energy consumption estimation, weather-normalized building energy savings calculation, and climate classification. Moreover, a new adjustment method was developed using the proposed split-degree day method that reduces the variations in the above code values in the performance compliance path in different locations from 14% to 2%.

DEDICATION

To my dear wife and beloved parents, sister, and brother

ACKNOWLEDGEMENTS

This dissertation was accomplished with the support and encouragement from multiple people. First, I would like to gratefully thank my chair, Professor Jeff S. Haberl, for his continuous support, essential guidance, and inspiration during my doctoral studies at Texas A&M University. I would also like to express my gratitude to my co-chair, Professor Juan-Carlos Baltazar, who devoted his time to effectively guide me through my studies, and for his continuous encouragements and support throughout my studies.

I would also like to thank my committee members, Professor Wei Yan for his valuable advices, inspirations, and comments; and Professor David E. Claridge for his valuable time and comments.

I would also like to extend my appreciation to the Energy Systems Laboratory where I have been supported during my doctoral studies with funding throughout the Texas Emissions Reduction Program (TERP). In addition, I would like to recognize the support by the Department of Architecture through teaching assistantship and several scholarships and Texas A&M University through different scholarships and grants. Furthermore, I would like to acknowledge the support from American Society of Heating, Refrigerating and Air-conditioning Engineers (ASHRAE) through the Houston student Chapter and Graduate Student Grant-In-Aid.

Finally, I am deeply grateful to my wife, parents, sister, and brother, with their positive and supportive attitude that has always encouraged me to accomplish my goals.

CONTRIBUTORS AND FUNDING SOURCES

This work was supervised by a dissertation committee consisting of Professors Jeff S. Haberl (chair), Juan-Carlos Baltazar (co-chair), and Wei Yan of the Department of Architecture and Professor David E. Claridge of the Department of Mechanical Engineering. All work for the dissertation was completed independently by the student.

Graduate study was partially supported by the ASHRAE Graduate Student Grant-In-Aid for the 2019-2020 academic year.

TABLE OF CONTENTS

Page

LIST OF FIGURES

Page

LIST OF TABLES

Page

CHAPTER I

INTRODUCTION

1.1. Background

Buildings are responsible for a considerable amount of global energy consumption and consume a large portion of the electricity generated all over the world. Currently, a considerable portion of this electricity is generated by the combustion of the non-renewable fuels, which lead to increasing amounts of emissions that have been shown to contribute to air pollution and climate change (EIA, 2018). Therefore, building energy efficiency is vital to help reduce future energy budgets and the related environmental issues.

Energy efficient buildings play an important role in national, statewide, and local energy policies. Building energy codes create an opportunity to reduce building energy use (Nelson, 2012). The minimum building energy codes (e.g. the American Society of Heating, Refrigerating and Air-Conditioning (ASHRAE) Standard 90.1 and International Code Council (ICC)) provide minimum efficiency provisions for various climate zones. Overall, the stringencies of the minimum standards and codes increase in each new revision to step forward toward the long-term energy-efficiency plans for various climates. ASHRAE Standard 90.1-2016 (ASHRAE, 2016) is the basis of most commercial codes in the U.S. (EPA, 2009). It provides the requirements for different climate zones mainly based on the analysis conducted using the prototype building energy simulation models (DOE, 2018). Besides the mandatory provisions, the requirements in Standard 90.1-2016 include either the prescriptive path provisions or the requisites for the performance path, which includes the Building Performance Factors (BPFs) that are updated in each version of the Standard 90.1 to assure a certain energy-efficiency level.

1.2. Motivation

The tabulated requirements in the prescriptive path are separated for different climate zones based on degree days. The BPFs in the performance path are also based on the prototype models, in which the envelope configurations are identical within each climate zone. However, each climate zone may have different moisture regimes, which can significantly influence building energy consumption.

A 2018 analysis conducted by the Pacific Northwest National Laboratory (PNNL) showed a 34.2% energy savings and energy cost savings for the buildings that meet the requirements of the ASHRAE Standard 90.1-2016 compared to ASHRAE Standard 90.1-2004 (Liu et al., 2018). The energy savings analysis for ASHRAE Standard 90.1-2016 compared to the previous version (ASHRAE Standard 90.1-2013) showed a 7.9% source energy savings with an approximate 5.2% source energy savings for medium office buildings (U.S. Department of Energy, 2017).

The analysis in the current study shows that the difference of the source energy consumption of the ASHRAE Standard 90.1-2016 medium office prototype models of different climate subtypes within one climate zone can vary up to 28%. The source energy savings of the ASHRAE Standard 90.1-2016 medium office prototype models versus the ASHRAE Standard 90.1-2004 medium office prototype models in different locations within one climate zone can vary up to 7.5%, which is considerable compared to the 7.9% average energy savings from 2013 to 2016 edition of the ASHRAE Standard 90.1.

Furthermore, there are certain requirements in ASHRAE 90.1-2016, such as the implementation of daylight responsive controls, which are mandated for certain types of the building (e.g., office buildings) regardless of the climate zone of the proposed building.

However, the associated energy savings with the implementation of daylight responsive controls can vary considerably in different climate conditions. Furthermore, previous studies have included discussions about daylighting design strategies that point to the need to refine daylighting design criteria because not all climates benefit uniformly from daylighting systems (Konis, 2013).

1.3. Objectives

The objective of this research is to develop a new improved procedure for a climate-based adjustment for code-compliant commercial buildings. The new procedure will be demonstrated using medium office prototype models that show that building energy loads in various moisture regimes (i.e., moist, dry, and marine) within each climate zone. The first task to resolve the current discrepancies in the predicted energy consumption of the different moisture regimes within each climate zone is to identify an improved climate indicator that captures the energy-related variations in different moisture regimes within each climate zone. Next, the adjustments for each location will then be demonstrated using the proposed new climate indicator applied to different locations within different climate zones and climate subtypes.

1.4. Significance and Limitations of the Study

This study is significant for the following reasons:

- It illustrates the variations in the simulated energy consumption of code-compliant, ASHRAE Standard 90.1-2016 medium office buildings in different moisture regimes.

- It reveals the energy savings related to daylighting in code-compliant, ASHRAE Standard 90.1-2016 medium office buildings in different climates and climate subtypes of the United States.
- It discusses the deficiencies in the conventional degree day methods.
- It develops a new, improved method, the split-degree day method, which overcomes some of the deficiencies in the conventional degree day methods[1] and allows better climate classifications.
- It proposes an adjustment procedure for the performance path of the ASHRAE Standard 90.1-2016 based on the new split-degree day method.

The current study has the following limitations:

- The analyses in this study were based on building energy simulation results using the EnergyPlus program, version 8.9.0.
- This study only focused on the eight climate zones in the United States.
- This study used the third version of Typical Meteorological Year (TMY3) weather files as the representative weather files. Hence, it assumes the TMY3 weather file limitations[2].

[1] Examples of the deficiencies in conventional degree day methods includes not fully accounting for various influential weather-related parameters on building energy performance (e.g., humidity, wind, and solar radiation) and the significant dependence of the accuracy of the energy consumption estimated using the conventional degree days on the base-temperature.

[2] Examples of the limitations in TMY3 weather files include that a TMY3 weather file is a typical representation rather than the actual representation of the weather in a location in TMY3 and the higher priorities on certain parameters, such as solar radiation, in creating the representative TMY3 weather files results in less accurate representation of the weather file for other parameters, such as wind

- The analyses in this study were only applied to the Department of Energy (DOE) medium office prototype models that were used by the PNNL and U.S.D.O.E. to analyze Standard 90.1.
- The improved method in this study is a modification of the degree day method, which ASHRAE uses to define the climate classifications in ASHRAE Standard 169-2013, which is used in ASHRAE Standard 90.1-2016.
- The analysis for daylighting in this study was restricted to the specifications of the DOE medium office prototype models and does not include other geometrical configurations, such as different shading, light-shelves, and/or dynamic glazing systems.

1.5. Document Overview

This dissertation is organized as follows:

In Chapter I, the study background is provided as well as the study motivation and objectives, followed by the study significance and the limitations.

In Chapter II, the literature review of the related materials is provided. This section includes the literature review of the building energy codes and standards, thermal and daylighting analysis and simulation tools, and different weather normalization methods.

In Chapter III, the new methodology is explained. The methodology includes an illustration of the DOE prototype model, the procedure for simulation and analysis, and the procedure for weather normalization. Discussions related to the new split-degree day method are also provided.

In Chapter IV the first part of the results are presented. This chapter includes the results of the medium office prototype models in different locations. Then, it illustrates the impact of different influential, weather-related parameters on building energy consumption. Finally, the results of the impact of the variations due to the weather-related parameters on energy savings and commercial code-compliant procedure are illustrated.

In Chapter V, the second part of the results are presented. This chapter includes the results of applying the improved method for building energy predictions as well as the results of applying the improved method in commercial, code-compliant office buildings.

In Chapter VI, a summary of this study is presented. Furthermore, potential future studies that can expand the analysis in this study are mentioned.

CHAPTER II

LITERATURE REVIEW

2.1. Overview

During the past decades, minimum building energy standards and codes (e.g. ASHRAE Standard 90.1 and IECC) have improved the energy-efficiency in the building sector by regulating the minimum efficiency requirements in buildings in the U.S. ASHRAE Standard 90.1-2016 (ASHRAE, 2016) is the basis of most commercial building energy codes in the U.S. (EPA, 2009). In ASHRAE Standard 90.1, mandatory provisions are included as well as tabulated provisions in the prescriptive path or performance path. Each newer version of the ASHRAE Standard 90.1 delivers a more stringent version of the code when compared to previous versions. The stringencies are compared to 2004 edition of the ASHRAE Standard 90.1, which is the baseline building energy code. In the building energy code the user must choose one of the prescriptive or performance paths. To address the varying building requirements in different climate zones, the prescriptive path provides tabulated values to be followed for different climate zones. On the other hand, performance path specifies certain calculation procedures to assure that the proposed building has an improved energy performance compared to a reference case. Therefore, the performance path is more flexible and has been widely used in commercial building code-compliance.

The building energy codes program of the U.S. Department of Energy (DOE) supports the Pacific Northwest National Laboratory (PNNL) to analyze the energy savings from code-compliant buildings using DOE commercial prototype building models, which are provided for different climate zones and climate zone subtypes (DOE, 2018). The envelope configurations in

these models are identical for the prototype models within each climate zone. While an average reduction in building energy consumption can be achieved by the different requirements for different climate zones, the weather-related parameters can vary the building energy consumption to a considerable extent within each climate zone. This is mainly due to the fact that the degree days, which is the basis for the classification by the ASHRAE Standard 169-2013 (ASHRAE, 2013a), does not fully account for the influence of the weather-related parameters on a building's energy and daylighting performance.

2.2. Daylighting

Daylighting is the utilization of natural light in a building while considering visual comfort issues. Effective daylighting can offset supplemental artificial lighting loads in a building without causing visual discomfort in a space. Since artificial, electric lighting has one of the highest end-use, energy uses in commercial buildings, daylighting can be utilized as a means of energy savings in buildings. In office buildings in particular, daylighting can reduce the annual energy consumption to a considerable extent. In addition, recently there have been studies showing the significance of the impact of daylighting on building occupant comfort, health, and performance (Boyce, et al. 2003; Edwards and Torcellini, 2002). These studies showed that the utilization of the daylighting can improve occupants' performance, health, and comfort, when compared to buildings without daylighting.

However, although daylighting has positive effects on occupants and can save energy, care should be taken to make sure that it does not cause visual discomfort, such as glare (Nazzal, 2000; Suk, et al. 2013; Wienold, 2009). Furthermore, energy savings in daylighting should be investigated carefully because it impacts the heating and cooling loads in a building as well as

lighting loads (Hee et al., 2015; Li and Lam, 2003). Daylight utilization can also reduce supplemental lighting loads, which can be a major internal heat source. Therefore, the use of daylighting can reduce the cooling load or increase the heating load depending on the orientation, fenestration layers, shading, climate zone, etc. Consequently, the use of daylighting requires careful assessment (Raji et al., 2015; Shen & Tzempelikos, 2013).

The assessment of daylighting covers direct, diffuse, and reflected light from the sun, sky, and surroundings. The origins of daylight assessments goes back to the measurement of outdoor illumination in 1895 (Walsh, 1951). Over time, different methods have been proposed to assess daylighting performance in a building. These methods include initial graphical methods derived from mathematical formulae, such as Waldram diagrams (as cited in Hopkinson et al., 1966), Pliejel's pepper-pot diagrams (as cited in Hopkinson et al., 1966), Building Research Establishment (BRE) daylight protractors (as cited in Hopkinson et al., 1966), the Graphic Daylight Design Method (GDDM) method (Moore, 1985), as well as empirical methods (Hopkinson et al., 1966), quick calculation tools (Altman, 2005; Moore, 1985), and sophisticated daylighting analysis tools, such as Radiance (Ward and Rubinstein, 1988), Daysim (Reinhart & Herkel, 2000).

2.2.1. Complex Fenestration Systems

Complex Fenestration Systems (CFS) seek to improve the distribution of indoor daylighting, typically by collecting and redirecting the daylight (Basurto et al., 2017). Due to the two main functions of CFS, lighting redirection and sun shading, an appropriate CFS can decrease the risk of glare and overheating normally associated with a daylighting system. Hence, it can contribute to improving visual and thermal comfort (Basurto et al., 2017).

There are different types of CFS currently used to enhance the building daylight performance, including laser-cut panels, daylight redirecting film, and micro-structured daylighting systems. A laser-cut panel is a type of CFS, which is based on the principles of light deflection and internal reflection. A laser-cut panel is made up of arrays of laser cut plastic or acrylic sheets that produces internal reflecting interfaces in the material (Edmonds, 1993; Ruck et al., 2000). Daylight redirecting film is another CFS that uses microstructure prisms to redirect the light towards the ceiling (Padiyath, 2013; Padiyath et al., 2013). Micro-structured daylighting systems are another type of CFS that redirect incident solar radiation for angles of incidence between 15° and 65° from the horizontal surface. Therefore, micro-structured daylighting systems can broaden the range of solar altitude angles that it efficiently redirects (Klammt et al., 2012).

The daylight propagation through CFS typically requires the measurement of the photometric properties of the CFS (e.g., visible transmittance and reflectance) to be assessed by a gonio-photometer, that is capable of measuring the intensity of light at varying angles. Once these measurements are made, a RADIANCE (Ward, 1989) simulation using a Bi-directional Scattering Distribution Function (BSDF) can be carried out to assess the CFS daylight performance.

2.2.2. Lighting Controls and the Daylighting Associated Energy Savings

Energy savings associated with lighting controls have been the focus of different studies for more than 30 years (Williams et al., 2011). Automatic daylighting control is a lighting control system that generally dims the indoor electric lighting to a lower level or switches it off in response to the available daylighting levels measured by a photosensor. In order to determine

what information is available and what actions the system can take, a control strategy should be selected before choosing a photosensor (Bierman, 2007).

One of the main distinctions between control strategies is whether the control is open-loop or close-loop. In the open-loop control system the electric lighting is controlled by the outside daylight level and the photocell is not influenced by the lighting, which means there is no feedback[3]. On the other hand, in the closed-loop, the sensor is influenced by the light that it is controlling. Therefore, the feedback can differ based on the daylight sensor placement and its optics (Bierman, 2007).

The current lighting control systems include on-off switched, bi-level, and continuous dimming systems, each of which can be chosen for the open- or closed-loop strategies. In the switched daylighting system, electric lights are turned-off when the daylight satisfies a minimum lighting level. In order to avoid frequent on-off behavior, the switched system uses hysteresis, which delays the system response (Lutron Co., 2014). The duration of the delay to turn the electric light off is controlled by the threshold of the minimum daylighting (e.g., 20% or more) (Bierman, 2007). A bi-level system is another daylighting control system similar to a switched system with the difference that in the bi-level system an intermediate state of 50% electric lighting can be used when the daylight availability exceeds 50% of the desired illuminance (Lutron Co., 2014). Finally, a continuous dimming system smoothly adjusts the electric lighting based on the available daylight level ensuring that the minimum desired illumination is met (Lutron Co., 2014). The effectiveness of a controller is defined as the “control effectiveness”,

[3] The term *feedback* is used when the output influences the input in a system (Bierman, 2007).

which is the division of the *actual savings* over *ideal achievable savings* (Hackel and Schuetter, 2013).

2.3. Building Energy Standards and Codes

Reducing the energy use in the building sector is one of the goals of minimum building energy standards as well as high-performance building energy standards. In general, building energy codes create an opportunity to reduce building energy use (Nelson, 2012). There are different minimum building energy codes and standards, such as ASHRAE Standard 90.1 and the International Energy Conservation Code. This section describes different compliance paths and discusses the related provisions to the daylighting in ASHRAE Standard 90.1-2016 (ASHRAE, 2016).

2.3.1. ASHRAE Standard 90.1

ASHRAE Standard 90.1 is the basis of most of the non-residential (i.e., commercial) codes in the United States. Currently, there are several different compliance paths to determine if a candidate building meets the standard (ASHRAE, 2016). ASHRAE Standard 90.1-2016 contains two paths for compliance, including: a prescriptive path; and performance path. There are two methods for performance path: the Energy Cost Budget (ECB) method, and the Performance Rating Method (PRM). Regardless of which path is chosen, the proposed designs must meet mandatory provisions, such as the provisions for Heating, Ventilation, and Air Conditioning (HVAC) system construction and insulation, equipment efficiencies, verification, and labeling requirements, etc. The three compliance paths in ASHRAE Standard 90.1-2016 are illustrated in Figure 1.

The prescriptive path specifies energy-related criteria for each building component that must be met. Therefore, compliance using the prescriptive path requires meeting all the specified provisions in the path. On the other hand, performance-based paths provide more flexibility to meet code compliance. The ECB method allows trade-offs of some of the prescriptive requirements not met through the use of more stringent requirements for other areas of the energy code. In order to comply with Standard 90.1-2016 in the ECB method, the total annual energy cost of the proposed design should not be greater than the total annual energy cost of the baseline design that meets the code. In addition to the ECB method, Appendix G of the Standard 90.1-2016 provides the PRM, which is the second performance-based path for code compliance. Compliance using the PRM requires calculating a Performance Cost Index (PCI) using a whole-building energy simulation that must be less than the target PCI that meets the ASHRAE Standard 90.1-2016 for the building type being considered (Rosenberg and Hart, 2016).

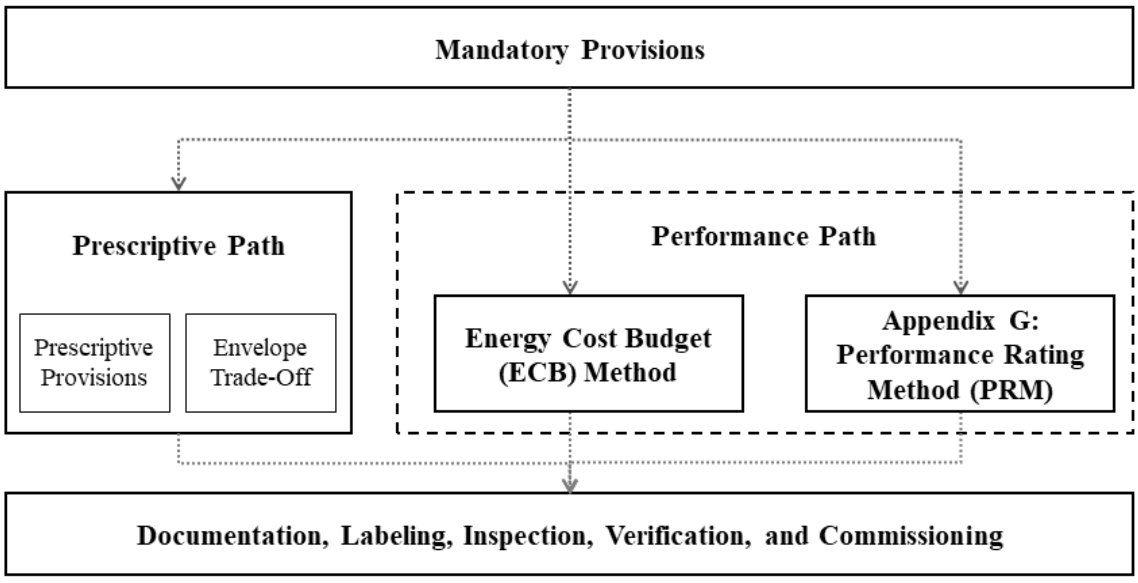

Figure 1: ASHRAE Standard 90.1 Compliance Paths for Building Envelope (ASHRAE, 2016)

Although the ECB method and PRM are both simulation-based methods, there are some differences between them. For example, in the ECB method, the specifications of the baseline design must match with the proposed building for all components meeting the prescriptive requirements. Whereas, in the PRM, there is one standard baseline design that meets the code, which is then compared against all the proposed designs (Rosenberg and Eley, 2013). While both the ECB method and PRM can demonstrate code compliance and both benefit from the simulated annual performance of selected components of the proposed design, the PRM has other advantages as well. One of the advantages of the PRM over the ECB method is that the baseline design remains the same for the minimum codes and the beyond code evaluations (i.e., ANSI/ASHRAE/ U.S. Green Building Council (USGBC)/ Illuminating Engineering Society (IES) Standard 189, the International Green Construction Code (IgCC), etc.). Also, in the PRM, the baseline design, which is based on ASHRAE Standard 90.1-2004, will remain the same and only the PCI will be updated (i.e., more stringent) in newer codes and above code rating systems (Rosenberg and Hart, 2016). Overall, performance paths provide more flexibility and have been widely-used in commercial building energy code compliance.

2.3.2. Daylighting in ASHRAE Standard 90.1

Besides the performance path, beginning with Standard 90.1-2010, the prescriptive path has mandatory requirements and credits for daylighting. These requirements are based on the analysis by the PNNL collaborated with Heschong Mahone Group (HMG) (Athalye et al., 2013). However, further investigations that account for all the different parameters are required to fully credit the daylighting saving potentials for different building configurations in different climates. As described in Section 4.2.1.1 of the ASHRAE Standard 90.1-2016 (ASHRAE, 2016), in order

to comply using the Prescriptive Method, provisions of the "Building Envelope", "Heating, Ventilating, and Air Conditioning", "Service Water Heating", "Power", "Lighting", and "Other Equipment" shall be met. Among these provisions, "Building Envelope" (Section 5 of the ASHRAE 90.1-2016) and "Lighting" includes provisions, such as fenestration configurations and daylight responsive controls, which are related to daylight utilization.

The fenestration provisions in ASHRAE Standard 90.1-2016 (Section 5.5.4) provides the requirements in the building envelope that highly impact thermal and daylighting performance of a building. The U-factor and SHGC indicate the thermal conductivity and the fraction of incident solar radiation admitted through a window, respectively, which identify the main thermal characteristics of the window. On the other hand, the Visible Transmittance (VT), which is an optical property of a window that shows the fraction of visible light transmitted through the window, can significantly impact the daylighting performance of a window. General provisions for fenestrations in ASHRAE 90.1-2016 include U-factor, SHGC, and VT/SHGC compliance requirements provided for different climate zones. Furthermore, there are provisions for the fenestration area, such as the maximum allowed Window-to-Wall Ratio (WWR) for vertical fenestration, maximum/minimum skylight area, and fenestration orientation. In general, fenestration area and orientation directly impact the heat transfer and the daylighting of a building.

There are two types of daylight zones defined in ASHRAE Standard 90.1, *primary sidelighted area* and *secondary sidelighted area*. Within each space, the total *primary sidelighted area* is the combination of each *primary sidelighted area*, which is directly adjacent to vertical fenestration below the ceiling. The total *secondary sidelighted area* is the combination of each *secondary sidelighted area*, which is directly adjacent to *primary sidelighted area*. Figure 2 and

Figure 3 illustrate how to compute *primary* and *secondary sidelighted area*, respectively (ASHRAE, 2016).

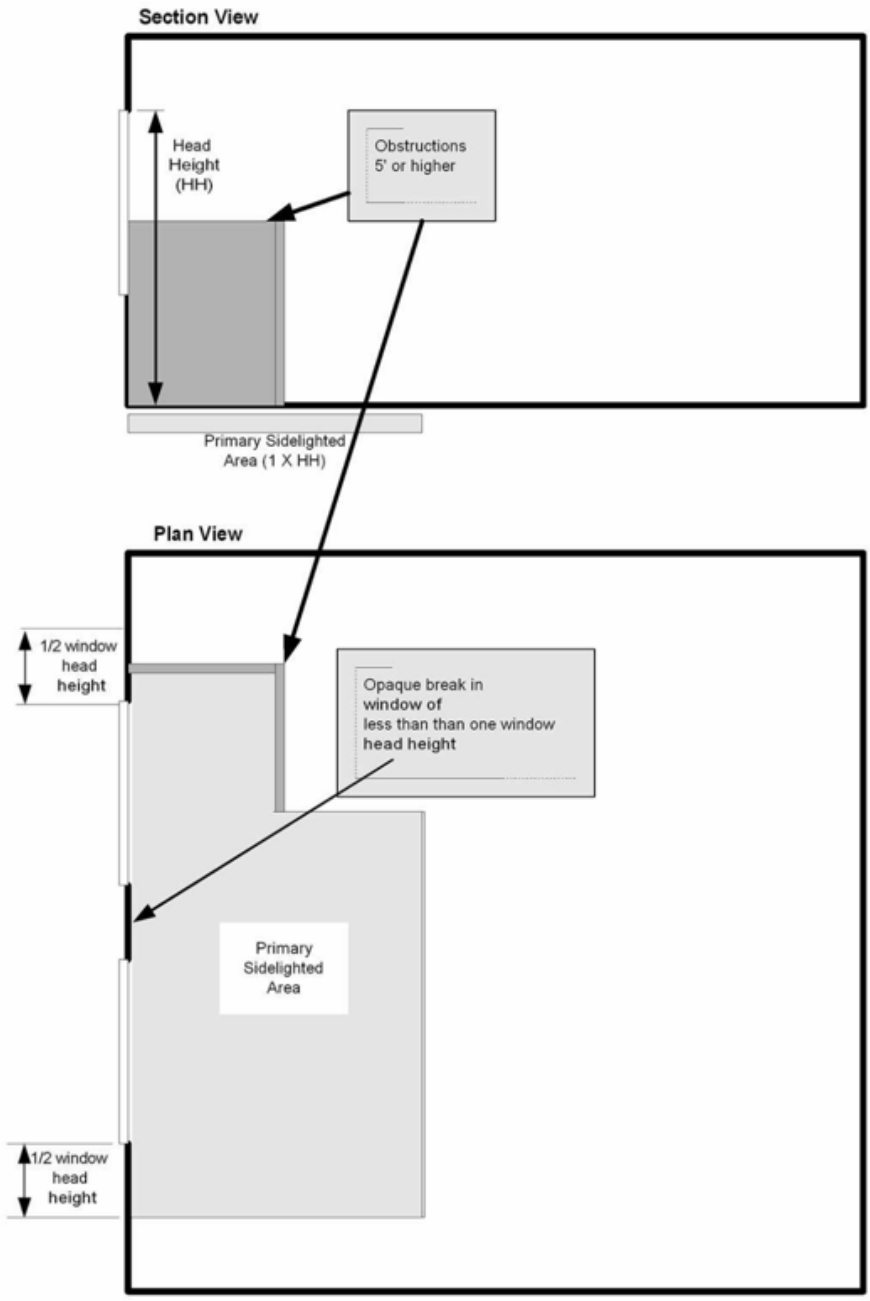

Figure 2: Computing the Primary Sidelighted Area. ©ASHRAE, www.ashrae.org. Original figure used with permission from 2016 ASHRAE Standard-90.1 (ASHRAE, 2016)

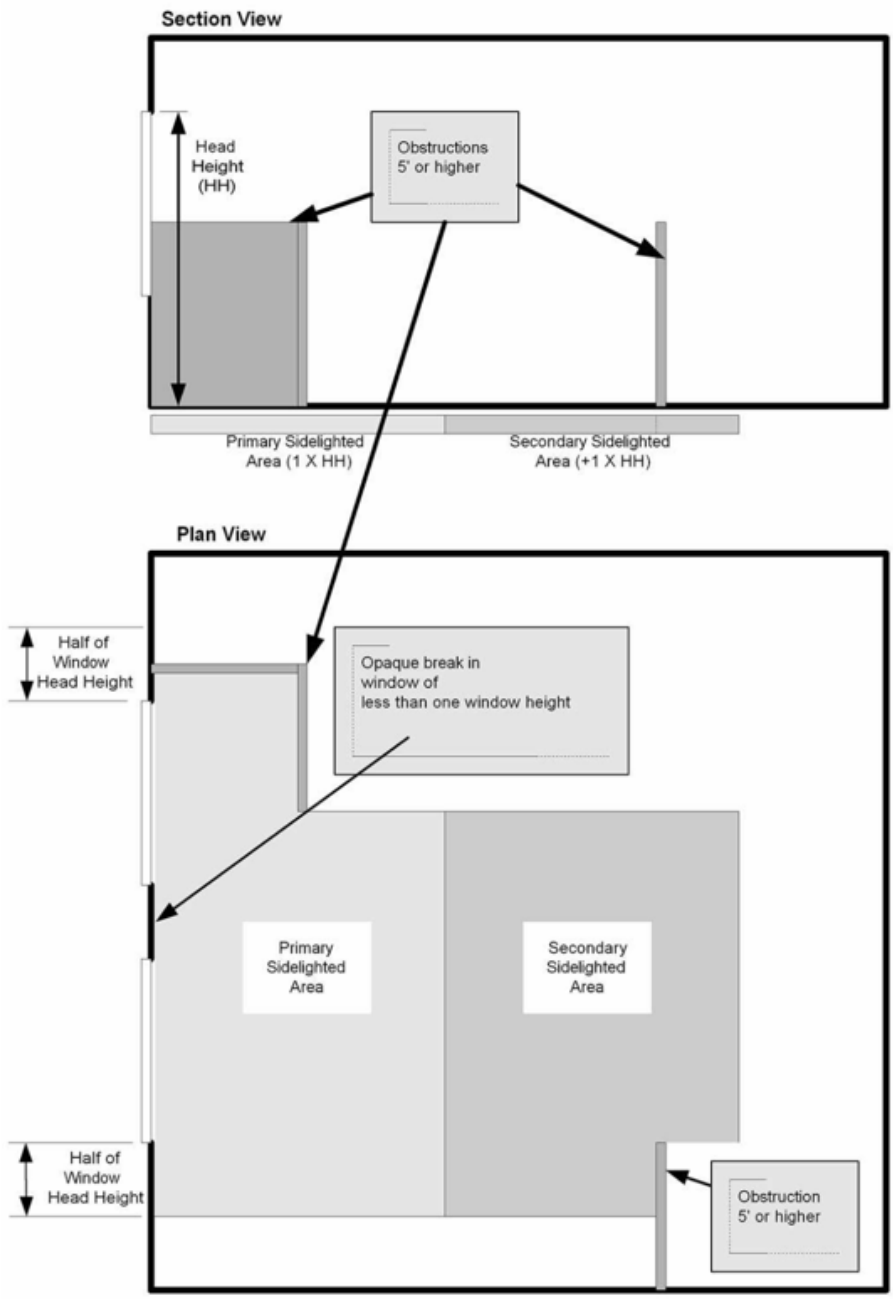

Figure 3: Computing the Secondary Sidelighted Area. ©ASHRAE, www.ashrae.org. Original figure used with permission from 2016 ASHRAE Standard-90.1 (ASHRAE, 2016)

Besides the fenestration provisions, ASHRAE Standard 90.1-2016 requires specific lighting controls for different types of the buildings. These provisions include specific

requirements for office buildings As indicated in Section 9.2.1 of the ASHRAE Standard 90.1-2016, the proposed lighting systems must comply with all “General”, “Mandatory Provisions”, “Submittals”, and prescriptive requirements in the Standard 90.1-2016. The prescriptive requirements must also comply with either Section 9.5, “Building Area Method Compliance Path”, or Section 9.6, “Alternative Compliance Path: Space-by-Space Method”. The “Building Area Method” is a simplified approach that determines the *interior lighting power allowance* while the “Space-by-Space Method” allows more flexibility.

The required controls in office buildings related to daylighting include “*automatic daylight responsive controls for sidelighting*” with equal or greater than 150 W combined input power of general lighting completely or partially in the primary sidelighted areas and 300 W combined input power of general lighting in the primary and secondary sidelighted areas as indicated in Section 9.4.1.1, Interior Lighting Controls of the ASHRAE Standard 90.1-2016 (ASHRAE, 2016). Similar requirements are established for the “*automatic daylight responsive controls for toplighting*” as indicated in Section 9.4.1.1, Interior Lighting Controls of the ASHRAE Standard 90.1-2016 (ASHRAE, 2016). Automatic control devices, which are capable of turning loads on and off without manual intervention, can reduce lighting load. Consequently, the reduction in the lighting load will impact the internal heat gain loads with possibly decreasing the cooling loads and increasing the heating loads. All of the lighting control functions listed in Table 9.6.1 of the ASHRAE Standard 90.1-2016 must be implemented for each affected space in the building (Figure 4).

Additional lighting power allowance can be calculated using a control factor, which is based on the installment of the identified non-mandatory controls, “*automatic continuous daylight dimming in secondary sidelighted area*”. As indicated in Section 9.6.3 of the ASHRAE

Standard 90.1-2016 (ASHRAE, 2016), the "Additional Interior Lighting Power Allowance" can be calculated by multiplying the "Lighting Power Under Control" and the "Control Factor". The "Lighting Power Under Control" is the total input Watts of all lamps being controlled using the controlled method, and the "Control Factor" is the value given in Table 9.6.3 of the ASHRAE Standard 90.1-2016 (see Figure 5) for the corresponding space type and control method.

Informative Note: This table is divided into two sections; this first section covers *space* types that can be commonly found in multiple *building* types. The second part of this table covers *space* types that are typically found in a single *building* type.			The *control* functions below shall be implemented in accordance with the descriptions found in the referenced paragraphs within Section 9.4.1.1. For each *space* type: (1) All REQs shall be implemented. (2) At least one ADD1 (when present) shall be implemented. (3) At least one ADD2 (when present) shall be implemented.								
			Local *Control* (See Section 9.4.1.1[a])	Restricted to *Manual* ON (See Section 9.4.1.1[b])	Restricted to Partial *Automatic* ON (See Section 9.4.1.1[c])	Bilevel Lighting *Control* (See Section 9.4.1.1[d])	*Automatic* Daylight Responsive *Controls* for Sidelighting (See Section 9.4.1.1[e][6])	*Automatic* Daylight Responsive *Controls* for *Toplighting* (See Section 9.4.1.1[f][6])	*Automatic* Partial OFF (See Section 9.4.1.1[g] [Full Off complies])	*Automatic* Full OFF (See Section 9.4.1.1[h])	Scheduled Shutoff (See Section 9.4.1.1[i])
Common *Space* Types[1]	*LPD*, W/ft^2	*RCR* Threshold	a	b	c	d	e	f	g	h	i
Office											
Enclosed and ≤250 ft^2	0.93	8	REQ	ADD1	ADD1	REQ	REQ	REQ		REQ	
Enclosed and >250 ft^2	0.93	8	REQ	ADD1	ADD1	REQ	REQ	REQ		ADD2	ADD2
Open plan	0.81	4	REQ	ADD1	ADD1	REQ	REQ	REQ		ADD2	ADD2
Parking Area, Interior	0.14	4	See Section 9.4.1.2.								
Pharmacy Area	1.34	6	REQ	ADD1	ADD1	REQ	REQ	REQ		ADD2	ADD2
Restroom											
Facility for the visually impaired (and not used primarily by the staff)[3]	0.96	8					REQ	REQ		REQ	
All other restrooms	0.85	8					REQ	REQ		REQ	
Sales Area[4]	1.22	6	REQ	ADD1	ADD1	REQ		REQ		ADD2	ADD2
Seating Area, General	0.42	4	REQ	ADD1	ADD1		REQ	REQ		ADD2	ADD2
Stairway	The *space* containing the stairway shall determine the *LPD* and *control* requirements for the stairway.										
Stairwell	0.58	10				REQ	REQ	REQ	REQ	ADD2	ADD2
Storage Room											
<50 ft^2	0.97	6	REQ							ADD2	ADD2
≥50 ft^2 and ≤1000 ft^2	0.46	6	REQ	ADD1	ADD1		REQ	REQ		REQ	
All other storage rooms	0.46	6	REQ	ADD1	ADD1		REQ	REQ	REQ	ADD2	ADD2
Vehicular Maintenance Area	0.56	4	REQ	ADD1	ADD1	REQ	REQ	REQ		ADD2	ADD2
Workshop	1.14	6	REQ	ADD1	ADD1	REQ	REQ	REQ		ADD2	ADD2

1. In cases where both a common *space* type and a *building* area specific *space* type are listed, the *building* area specific *space* type shall apply
2. In corridors, the extra *lighting power density* allowance is permitted when the width of the corridor is less than 8 ft and is not based on the *RCR*.
3. A "Facility for the Visually Impaired" is a facility that can be documented as being designed to comply with the light levels in ANSI/IES RP-28 and is licensed or will be licensed by local/state authorities for either senior long-term care, adult daycare, senior support and/or people with special visual needs.
4. For accent lighting, see Section 9.6.2(b).
5. Sometimes referred to as a "Picking Area."
6. *Automatic* daylight responsive *controls* are mandatory only if the requirements of the specified sections are present.
7. An additional 0.52 W/ft^2 shall be allowed, provided that the additional lighting is controlled separately from the base allowance of 0.43 W/ft^2. The additional 0.52 W/ft^2 allowance shall not be used for any other purpose.
8. Class of play as defined by IES RP-6.

Figure 4: Lighting Power Density Allowance Using the Space-by-Space Method and Minimum Control Requirements Using Either Building Area Method or Space-by-Space Method in ASHRAE Standard 90.1-2016. ©ASHRAE, www.ashrae.org. Original table used with permission from 2016 ASHRAE Standard-90.1 (ASHRAE, 2016)

Additional *Control* Method (In Addition to Mandatory Requirements)	*Space* Type				
	Open Office	Private Office	Conference Room, Meeting Room, Classroom (Lecture/ Training)	Retail Sales Area	Lobby, Atrium, Dining Area, Corridors/ Stairways, Gym/ *Pool*, Mall Concourse, Parking Garage
Manual, continuous dimming *control* or programmable multilevel dimming *control*	0.05	0.05	0.10	0.10	0
Programmable multilevel dimming *control* using programmable time scheduling	0.05	0.05	0.10	0.10	0.10
Occupancy sensors controlling the downlight component of workstation specific *luminaires* with continuous dimming to off capabilities	0.25[a]	0	0	0	0
Occupancy sensors controlling the downlight component of workstation specific *luminaires* with continuous dimming to off operation, in combination with personal continuous dimming *control* of downlight illumination by workstation occupant	0.30[a,b]	0	0	0	0
Automatic continuous daylight dimming in *secondary sidelighted areas*	0.10[c]	0.10[c]	0.10[c]	0.10[c]	0.10[c]

a. *Control* factor is limited to workstation-specific *luminaires* in partitioned single occupant work *spaces* contained within an open office environment (i.e. direct-indirect *luminaires* with separately controlled downlight and uplight components, with the downward component providing illumination to a single occupant in an open plan workstation). Within 30 minutes of the occupant leaving the *space*, the downward component shall continuously dim to off over a minimum of two minutes. Upon the occupant entering the *space*, the downward component shall turn on at the minimum level and continuously raise the illumination to a preset level over a minimum of 30 seconds. The uplight component of workstation specific *luminaire* shall comply with Section 9.4.1.1(h) (*automatic* full off).

b. In addition to the requirements described in footnote (a), the *control* shall allow the occupant to select their preferred light level via a personal computer, handheld device, or similarly accessible device located within the workstation.

c. *Control* factors may not be used if *controls* are used to satisfy exceptions to Section 5.5.4.2.3

Figure 5: Control Factors Used in Calculating Additional Interior Lighting Power Allowance in ASHRAE Standard 90.1-2016, Table 9.6.3. ©ASHRAE, www.ashrae.org. Original table used with permission from 2016 ASHRAE Standard-90.1 (ASHRAE, 2016)

2.4. Building Energy and Daylighting Assessment Tools

There are different methods and tools developed to assess building energy and daylighting performance. This section includes a discussions about the related materials regarding the assessment of daylighting in a building as well as an overview of building energy assessment tools.

2.4.1. Daylighting

This section discusses the related materials regarding the assessment of daylighting in a building. It includes the discussions on different sky models, daylighting performance indicators, daylighting calculation methods, and daylighting simulation tools.

2.4.1.1. Sky Models

Illumination from the sky can impact interior lighting levels if properly designed daylight systems are installed and maintained. The measurement of the sky brightness and daylight illumination began with Kimball and Hand in 1922 (Kimball and Hand, 1922). In 1921, an equation was proposed by Pokrowski to calculate the luminance distribution of a clear sky (Hopkinson et al., 1966). Later in 1942, an empirical formulae was proposed by Moon and Spencer to estimate the luminance distribution of an overcast sky, which was adopted by International Commission on Illumination (CIE) to calculate the overcast sky luminance distribution in 1955 (Hopkinson et al., 1966). In 1965, the CIE adopted the formulae proposed by Kettler for clear sky (Hopkinson et al., 1966). In the 1960s, a new formula to calculate the luminance distribution of fully overcast sky was proposed by McDermott and Gordon-Smith (Hopkinson et al., 1966). Finally, in 1993 Perez et al. (Perez et al., 1993) proposed new sky models for all clear, overcast and partly cloudy skies.

2.4.1.2. Daylighting Performance Indicators

Daylight performance indicators specify the daylighting performance of a building. In order to comprehensively analyze daylighting performance of a building the available daylight should be assessed while considering the visual comfort criteria of the space being lite. There have been different methods proposed to analyze the daylighting performance of a building. These methods include the quantification of the available daylight, including the Daylight Factor, Daylight Autonomy, Useful Daylight Illuminance, etc., as well as the analysis of the visual comfort in a building, including British Glare Index, Discomfort Glare Index, CIE Glare Index, etc.

2.4.1.2.1. Daylight Factor

In 1895, the Daylight Factor (DF) method was proposed by Trotter (Trotter, 1911) to evaluate the daylight availability of an interior space. The DF is defined as the ratio of daylight illuminance at an interior point in a space to the exterior illuminance under an unobstructed overcast sky. Hopkinson et al. (1966) mentions the advantages of the DF method as it can evaluate the daylighting performance of a room and also that it is in accordance with human perception, which is a relative perception rather than absolute. However, the DF method was proposed for an overcast sky. Therefore, sky conditions other than an overcast sky cannot be evaluated by DF method. Furthermore, because of the fact that in the overcast sky the luminance of the sky patches are radially the same with respect to the zenith, the DF is not sensitive to the orientation of the window. Furthermore, the DF is not an informative metric for glare.

Later, the Coefficient of Utilization method was developed for analyzing daylighting by providing illuminations on a work-plane with given sky conditions (Brackett, 1983). However, the Coefficient of Utilization covers only a limited number of cases (Love and Navvab, 1994). Currently, different software have the capability to calculate a DF fast and efficiently. Although, the limitations with DF method should still be considered while using these tools. Finally, neither the DF method nor Coefficient of Utilization method accounts for glare.

2.4.1.2.2. Daylight Autonomy

In 1985, the Association Suisse des Electriciens, proposed the Daylight Autonomy (DA) metric as the first dynamic daylight assessment. The DA is an annual daylight metric, defined as the percentage of annual daytime hours that the illumination level at a given point in a space is above a specified illumination level.

As stated by Galatioto and Beccali (Galatioto and Beccali, 2016), the DA accounts for different variables, such as the time frame, spatial consideration, target illuminance and the location and climate. However, the DA does not provide for lighting values below the specified lighting threshold nor for lighting values over the lighting threshold. Besides the incremental method of using the DA calculation, which adds one point for daylight illuminance exceeding the required illuminance for the given time, the continuous Daylight Autonomy (cDA) is another variation for calculating DA, which accounts for the fractional levels of daylight (Rogers, 2006).

2.4.1.2.3. Useful Daylight Illuminance

Nabil and Mardaljevic (Nabil and Mardaljevic, 2005) developed the Useful daylight illuminance (UDI), defined as the annual occurrence of illumination across the work plane where all the illuminances are within the specified range. Although both DA and UDI consider a fraction of the annual daytime hours and the illumination level at a given point in a space for the daylighting assessment, there are major differences between these two metrics. Unlike the DA, which is developed for an overcast sky, the UDI is based on an annual absolute illuminance values predicted under realistic skies generated from standard meteorological datasets. Furthermore, a high-threshold for the illumination level at a given point in a space is included in the UDI. Therefore, the UDI considers the visual discomfort created by excessive daylight.

2.4.1.2.4. Glare Indices

Glare is the visual discomfort caused by excessive natural or artificial light. Insuring visual comfort is an indispensable part of daylighting assessment. Glare not only depends on

absolute luminance value, but also depends on the contrast and relative luminance (Carlucci et al., 2015).

2.4.1.2.4.1. British Glare Index

Petherbridge and Hopkinson developed the British Glare Index (BGI) empirical equation at the Building Research Station (BRS) (Petherbridge and Hopkinson, 1950). The BGI was developed for small light sources (Chauvel et al., 1982). Therefore, the BGI is better suited for artificial light sources. However, it cannot accurately evaluate the glare associated with windows because of the large area that covers. BGI also does not account for the effect of adaptation (Carlucci et al., 2015).

2.4.1.2.4.2. Daylight Glare Probability

The Daylight Glare Probability (DGP) is derived from the experimental studies on office buildings with the involvement of subjects (Guth, 1963; Luckiesh and Guth, 1949). According to the equation proposed by Wienold and Christoffersen (Wienold and Christoffersen, 2006), the DGP provides a comprehensive annual analysis of glare and is calculated based on the vertical illuminance at the eye, luminance of the source, solid angle of the source, and Guth position index, which is a function of the glare source position in the observer's field of view and varies smoothly with the horizontal and vertical viewing angles (Ashdown, 2005). DGP considers occupants lighting perception during that time. However, different glare sources are not considered in DGP (Galatioto and Beccali, 2016).

2.4.1.2.4.3. Discomfort Glare Index

Daylight Glare Index (DGI) is a version of the BGI that was originally developed to determine the discomfort glare from large artificial light sources based on the *Cornell Formulae* (Bellia et al., 2008). DGI and DGP are two of the most widely used indices for assessing daylight glare (McNeil and Burrell, 2016). However, DGI works only when the direct sunlight does not enter the space (Jakubiec and Reinhart, 2012) and is based on a human subject study performed in a large open office space. Also, DGI is unable to accurately evaluate the discomfort glare experienced by the participants (Hirning et al., 2014; Hirning et al., 2013).

2.4.1.2.4.4. CIE Glare Index

The CIE Glare Index (CGI) is used to evaluate the perceived degree of glare intensity. Einhorn (Einhorn, 1979) proposed this new index, later called the CGI, to fix the mathematical inconsistency of the BGI for multiple glare sources. The CGI calculation requires the illuminances due to both direct and diffuse lighting evaluated on the horizontal plane passing through observer′s eyes (Carlucci et al., 2015). Navvab and Altland (1997) stated that the calculated CGI are correlated to human assessment of glare impression. However, the results have not been consistent in the related studies. For example, in an experimental study by Suk et al. (2017) it was concluded that the CGI tends to overestimate glare levels.

2.4.1.2.5. Summary of Daylight Performance Indicators

While most of the previous studies have focused on the assessment of daylight availability and glare, common daylighting performance indices generally do not consider the uniformity of the illuminance level of a room (Galatioto and Beccali, 2016). In addition, another

issue in daylighting assessment is the variations in available daylight. Finally, in addition to the previously discussed shortcomings, daylight assessment methods and daylight analysis tools can also impact the evaluation of daylighting performance.

2.4.1.3. Daylight Calculation Methods

In general, in order to analyze the daylighting performance of a building, three components should be considered: the Sky Component (SC), the External Reflected Component (ERC), and the Internal Reflected Component (IRC). To date, to model the sky component four different methods have been developed, including: a clear cloudless sky model, an intermediate or partly cloudy sky model, a fully overcast sky model (Hopkinson et al., 1966), and the all-weather sky model (Perez et al., 1993). Finally, there are also different daylighting calculation methods for the IRC. These methods include: the daylight factor method (Trotter, 1911; Walsh, 1951), the daylight coefficient method (Tregenza and Waters, 1983), and the Ray-Tracing method (Whitted, 1979).

2.4.1.3.1. Daylight Factor Method

The Daylight Factor (DF) is a ratio of the illuminance at a point on a plane (e.g., vertical or horizontal) to the simultaneous illuminance on a horizontal exterior plane. The illuminance at the point on the plane is the summation of the SC, ERC, and IRC. Each of these three components can be calculated using different methods, including: graphical methods, non-graphical methods or computational methods such as, the split-flux Method, the radiosity Method, etc.

2.4.1.3.2. Daylight Coefficient Methods

The Daylight Coefficient (DC) method was proposed by Tregenza and Waters (Tregenza and Waters, 1983) to overcome the deficiencies of the DF method (Kota and Haberl, 2009). The issues with the DF method include the fact that the DF method cannot predict the illumination levels at a point on a plane for time varying sun and sky luminance distribution. To resolve this issue in the DC method, the sky is divided into small segments (Tregenza and Waters, 1983). Also, the DCs are calculated based on the space dimensions and surface characteristics. Internal illumination is then calculated by multiplying the calculated DCs, sky luminance values and solid angle constants. In the DC method the illumination on the reference point on a plane accounts for the illumination of each segment. Therefore, unlike the DF method, the illumination level at the reference point can be predicted for different sky conditions using the DCs (Tregenza and Waters, 1983). In addition, in the DC method, the illumination on more than a single reference point can be predicted using Finite Element Methods (FEMs) (Kota and Haberl, 2009).

2.4.1.3.2.1. Graphical Methods

Graphical methods have been used to calculate the DF or a component of the DF. The Waldram diagram, proposed by Waldram in 1923, and the pepper-dot chart method, developed by Pleijel in 1954, are two graphical methods to calculate the SC of the DF (Hopkinson et al., 1966). In addition, the dot-chart method by Turner in 1969 (as cited in Moore, 1985) and the Graphic Daylight Design Method (GDDM) by Millet in 1978 (as cited in Moore, 1985) are other graphical mehods that can be used to calculate the overall DF (Moore, 1985).

2.4.1.3.2.2. Non-graphical Methods

There are several different non-graphical methods proposed to calculate the DF or a component of the DF. These methods include geometrical devices such as daylight protractor developed by Dufton in 1946 for an overcast sky and the daylight protractors developed by Bryan and Clasberg for clear sky in 1982, slide rulers, empirical formulae, such as the Lumen Method (Dresler, 1954), as well as the methods that use graphs, and tables (Hopkinson et al., 1966).

2.4.1.3.2.3. Split-Flux Method

The split-flux method, proposed by Hopkinson et al. in 1954, is an empirical formula for calculating the IRC based on the formula proposed by Arndt (Hopkinson et al.1954). The split-flux method splits the luminous flux coming into a space into two parts; with one coming from the sky and external obstructions passing downward through a horizontal plane that bisects a vertical window; and the flux coming up from the ground and external obstructions passing through a horizontal plane that bisects a vertical window. The summation of the flux passing up through the window plane is then multiplied by the reflectance of the surfaces above the horizontal line passing through the middle of the window. The summation of the flux passing down through the middle plane is multiplied by the average reflectance of the surfaces below the horizontal line passing through the middle of the window. In the next step, the unit sphere method is applied for the inter-reflection of light (Figure 6 and Figure 7).

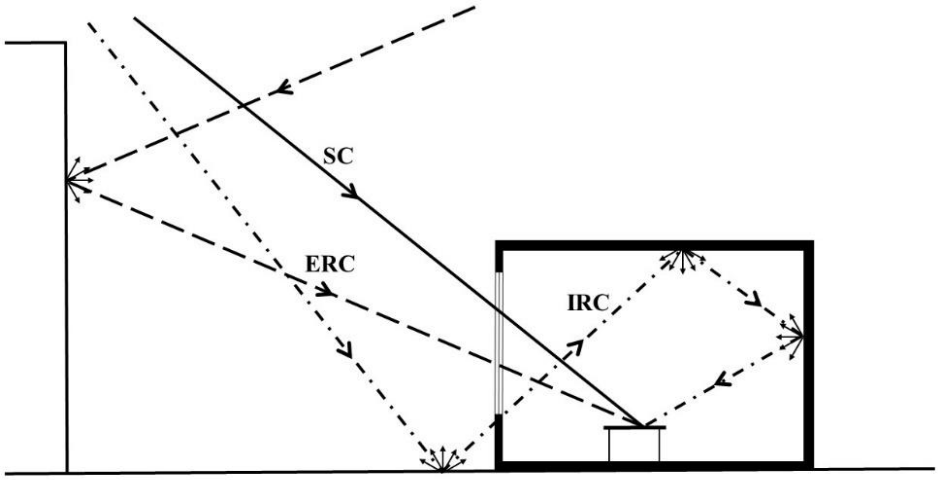

Figure 6: Components of the DF (Bryan and Clear, 1980)

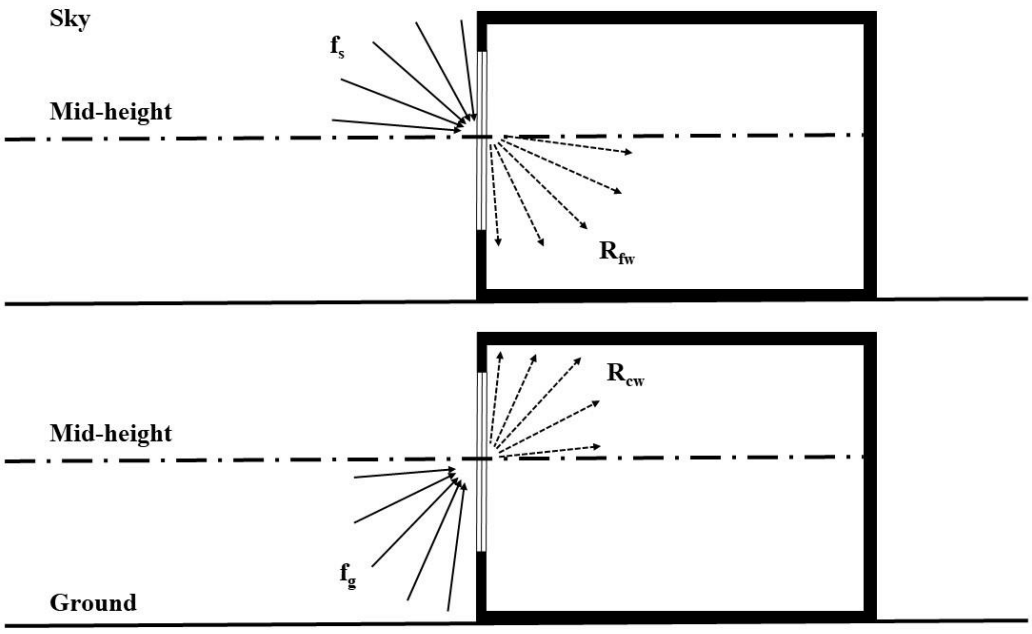

R_{fw} = Average reflectance of the floor and the parts of the walls below the plane of the mid-height of the window (excluding the window-wall)

R_{cw} = Average reflectance of the ceiling and the parts of the walls above the plane of the mid-height of the window (excluding the window-wall)

f_s = Window factor due to the light incident on the window from sky

f_g = Window factor due to the light incident on the window from ground

Figure 7: The Split-Flux Concept (Bryan and Clear, 1980)

One of the drawbacks of the split-flux method is that it was proposed for spherical spaces. Consequently, it works fine for cube-shaped spaces. However, the further the geometry of the space deviates from a cube shape, the more the accuracy will decrease (Hopkinson et al., 1966). In general, it is not recommended to use the split-flux method to calculate the DF of spaces with the depth/height ratio of more than three (Winkelmann and Selkowitz, 1985). The other limitation of the split-flux is that it cannot be used to analyze certain complex fenestration systems, such as light shelves (Baker, 1990).

2.4.1.3.2.4. Radiosity Method

In the radiosity method, the surfaces are divided into multiple patches, which are considered as Lambertian reflectors. In an iterative process, all the reflected fluxes between different patches are calculated using Lambert's cosine law (Tsangrassoulis and Bourdakis, 2003). A limitation of the radiosity method is that it assumes that all the surfaces are Lambertian. Therefore, it does not account for the specular reflectances in the IRC calculation.

2.4.1.3.3. Ray-tracing Methods

Ray-tracing is a computer graphic technique, first developed by Whitted in 1979 (Whitted, 1979), which can be used to analyze the interreflections between Lambertian and specular surfaces. There are two different types of ray-tracing, forward ray-tracing and backward ray-tracing. In forward ray-tracing the rays are distributed from the light source in all directions. Then, based on the *scene* being viewed geometry characteristics and surfaces specifications, the *light rays* are scattered and dispersed. Finally, in the forward ray-tracing method a portion of the lights reaches the viewpoint through an image plane (Kota and Haberl, 2009; Oh and Haberl,

2016). Therefore, although accurate, the forward ray-tracing is computationally time consuming process.

On the other hand, in 1986, the concept of the backward ray-tracing method was introduced by Arvo to generate images more efficiently (Arvo, 1986). Backward ray-tracing distributes the rays from the viewpoint toward the image plane and determines if they reach light sources after all interreflections and before the light has decayed. Therefore, backward ray-tracing is a more efficient ray-tracing technique for daylight analysis. However, as the backward ray-tracing distributes the light rays from a specific viewpoint, the ray-tracing process should be repeated whenever the viewpoint of interest changes.

2.4.1.3.4. Summary of Daylight Calculation Methods

In this section the daylight factor, daylight coefficient, and the ray-tracing methods have been reviewed. In general, there are different methods to estimate the daylight performance of a building. The DF method can be used to assess building daylighting performance. However, there are limitations and assumptions that should be considered while using DF method. For example, the DF method is designed for a spherical geometry. Therefore, the inaccuracy in DF method calculation will increase in rooms with higher depth to height ratios. Another deficiency in the DF method is that the sky is only considered as fully-overcast. Furthermore, the DF method can not account for certain advanced fenestration systems such as light shelves. On the other hand, the DC method resolves some of the issues in the DF by accounting for different sky types and sunlight. However, in order to analyze the impact of fenestration systems more accurately, ray-tracing method can be used. The ray-tracing method accounts for both diffuse

and specular surfaces and can be considered as one of the most reliable methods for daylighting analysis.

2.4.1.4. Daylighting Simulation Tools

Beginning in the 1960s a number of different daylighting simulation tools were developed. These daylighting simulation tools can be divided into different groups, including daylight factor tools and daylight coefficient tools.

2.4.1.4.1. Daylight Factor Tools

There are different tools that utilize the DF to assess the daylighting. This section provides the overview of the DF tools, including: DF Quick Tools, SUPERLITE, DOE-2, eQuest, EnergyPlus, and Ecotect.

2.4.1.4.1.1. Daylight Factor Quick Tools

Different tools has been developed that use the DF method for daylighting calculation, including quick tools such as Lumen_I, Lumen-II, Lumen-III, Lumen-Micro, Quicklite-I, and ENERGY. Lumen-I, the lighting simulation tool developed by DiLaura in 1968 is among the earliest computer packages that used the DF method. Lumen-II was later developed by DiLaura in 1970 (as cited in Altman, 2005) and in 1981, Lumen-III was developed by DiLaura and Kambich. Lumen-Micro version 1.0, the enhanced version of Lumen III, was released in 1983 for use on a PC. Lumen-Micro 2000, which uses the CIE clear, partly cloudy or overcast sky models, is the latest version of this tool, which uses the radiosity approach to calculate the IRC. Lumen-Micro accounts for diffuse glazing, overhangs, and selected controls such as venetian

blinds, external obstructions, and sky lit surfaces inside and outside the room (Moore, 1985). Other quick tools that use the DF method include: Quicklite-I, developed by Bryan in 1981, and ENERGY, developed by DiLaura and the Lighting Technologies company (Moore, 1985).

2.4.1.4.1.2. SUPERLITE

SUPERLITE, developed by Selkowitz et al. (1982), is a program that can be used to predict the spatial distribution of the illumination in a building. SUPERLITE uses uniformly overcast; CIE standard overcast and CIE clear sky (Hopkinson et al., 1966) with or without sun for daylighting (Ubbelohde and Humann, 1998). SUPERLITE uses a modified radiosity algorithm for computing the IRC (as cited in Hitchcock and Carroll, 2003).

2.4.1.4.1.3. DOE-2

DOE-2 is a detailed hourly whole-building energy simulation. A daylighting module was added to DOE-2 in version 2.1B for determining the impact of daylighting strategies on the energy consumption of the building, which uses the following three stages:

Stage I: In this stage a preprocessor calculates the DF, which will be used later in the hourly load calculation. DOE-2 integrates over the area of each window or skylight to obtain the contribution of direct light and reflected light from the walls, floors, and ceiling before reaching the one or two user-defined reference points. Parameters that are taken into account includes luminance distribution of the sky, geometrical properties (i.e., window size, slope, and orientation, sun control devices, such as drapes and overhangs, and external obstructions) and material properties (i.e., glass transmittance, and interior surface reflectances).

Stage II: In stage II for every hour that the sun is above the horizon, the illuminance of the window is calculated by multiplying the stored DF for the sun position and cloud cover of each specific hour, by exterior horizontal illuminance at that hour. If the glare control option is specified, the program automatically closes blinds or drapes, or uses window shading devices to reduce the glare below the specified comfort level.

Stage III: In this stage, the lighting control determines the required electric lighting to satisfy the design illuminance considering the daylighting level. After this stage, the lighting electricity requirements will be transferred for thermal analysis.

DOE-2 uses the split-flux Method (Bryan and Clear, 1980) to calculate the Internally Reflected Component (IRC). DOE-2 also calculates the daylight discomfort glare (Winkelmann, 1983; Winkelmann and Selkowitz, 1985). The discomfort glare is calculated using the Cornell-BRS "large-source" formulae (Hopkinson, 1970, 1972). In order to calculate the discomfort glare constant, in a similar fashion to the process of calculating the direct component of interior illuminance, the window surface is divided into rectangular subdivisions to calculate the average luminance of the window as seen from the reference point. The average illuminance from the window, and other parameters, including the solid angle subtended by the window with respect to the reference point, and solid angle subtended by the window, modified to take account for the direction of the occupant view. In addition, the luminance of the background area surrounding the window, is taken into account in the glare calculation process. The net daylight glare at a reference point, then, accounts for glare constant at the reference point due to each window.

2.4.1.4.1.4. eQuest

eQuest (eQUEST, 2017) uses the DOE-2.2 or DOE-2.3 simulation engines, which are derivatives of the DOE-2.1E program, as the simulation engine. The daylight calculation method in eQUEST is similar to DOE-2.1E, which uses the split-flux method. Therefore, the benefits and limitations of using eQuest (DOE-2.2 and DOE-2.3) for daylighting analysis is similar to DOE-2.

2.4.1.4.1.5. EnergyPlus

The daylighting calculations in EnergyPlus can be performed using either the split flux method, which is derived from the daylighting calculation in DOE-2.1E and is described in Winkelmann and Selkowitz (1985), or DElight, a simulation engine for daylight and electric lighting analysis in buildings (EnergyPlus, 2016). DElight version 1.0 was proposed based on the DOE-2.1E daylighting algorithms (Hitchcock and Carroll, 2003) and uses the split-flux method. As stated by Hitchcock and Caroll (2003), the IRC calculation method in DElight daylighting analysis incorporated the radiosity method in version 2. Furthermore, in DElight version 2, the new algorithms for analyzing Complex Fenestration Systems (CFS) were implemented. The daylighting simulation engine in DElight version 2.0 was further enhanced compared to version 1.0 through the implementation of the radiosity interreflection calculations, derived from SUPERLITE (Hitchcock and Carroll, 2003).

2.4.1.4.1.6. Ecotect

Ecotect can also be used to analyze the daylighting performance of a building. There are two approaches to analyze the daylighting performance of a building in Ecotect. One approach uses a built-in engine, which uses the split-flux method to compute the IRC and has three CIE

sky models—overcast, intermediate, and clear (Marsh, 2003). The built-in daylighting analysis module of Ecotect performs the analysis for a single day (Kota and Haberl, 2009). The other approach exports the geometry to a more sophisticated daylighting analysis tools, such as Radiance (Ward, 1989) and Daysim (Reinhart and Herkel, 2000). In this approach, Ecotect acts as an interface for Radiance and Daysim to model and visualize the results (Kota and Haberl, 2009).

2.4.1.4.2. Daylight Coefficient Tools

Different tools have been developed to assess the daylighting performance of a building using Daylight Coefficients (DCs). This section provides an overview of the daylight coefficient tools, including the Radiance, Daysim, and ESP-r.

2.4.1.4.2.1. Radiance

Radiance, developed by Lawrence Berkeley National Laboratories (LBNL), is a hybrid finite element analysis program that uses Monte-Carlo techniques to compute the interreflection between specular surfaces in complex geometries using ray-tracing methods (Ward and Rubinstein, 1988). There are two Radiance sky generators. The Gensky program offers sky model types based on CIE standard (CIE, 2002). Besides the standard CIE overcast model, gensky can also generate the sun descriptions and sky brightness distributions for the CIE clear or intermediate skies. Another Radiance sky generator program is Gendaylit, which generates sky conditions such as overcast, intermediate, clear, etc. based on the Perez All-Weather model (Mardaljevic, 2000).

2.4.1.4.2.2. Daysim

Daysim, (Reinhart and Herkel, 2000) is a Radiance-based program for estimating annual lighting and daylighting illuminance distribution. Daysim uses the Daylight Coefficient method and the Perez all-weather sky luminance model to calculate the illumination at a point in a space for the 8,760 hours of the year (Kota and Haberl, 2009). Daysim can be also used for simulating complex fenestration systems (CFS) and light-shelves.

2.4.1.4.2.3. ESP-r

ESP-r, initially developed in 1974, is a transient energy simulation system that can be used for different building performance analyses (Clarke et al., 1998). Energy and fluid flows within combined building and plant systems can be modeled considering control actions.

The central Program Manager (PM) in ESP-r performs the daylighting analysis using Radiance. After the daylight component is determined by Radiance, the ESP-r control algorithm adds the artificial lighting component (Janak, 1997).

2.4.1.4.3. Summary of Daylighting Simulation Tools

This section provided a review of daylighting simulation tools. The daylighting simulation tools reviewed in this section were classified into daylight factor tools and daylight coefficient tools. The pros and cons of different daylighting simulation tool were discussed in this section.

In a survey of one hundred and eighty five lighting simulation experts from 27 countries, it was determined that the complexity of tools and insufficient program documentation were the two main weaknesses of the current daylighting simulation programs currently in use for

daylighting simulations (Reinhart and Fitz, 2006). In the survey it was found that the usage of these tools were significantly higher in the later stages of design, such as in design development, compared to schematic design phase. Therefore, daylighting simulation tools are seldom used to *inform* design (Cutler et al., 2008).

Daylighting simulation is a complex process. In general, the time consuming process of modeling and simulation using Radiance was felt to be a hindrance by 50% of the survey respondents (Cutler et al., 2008; Reinhart and Fitz, 2006). On the other hand, easy-to-use software that performs both thermal and daylighting analysis have limitations in the daylighting analysis. For example, the DOE-2 and eQUEST uses the split-flux Method, which cannot model advanced fenestration systems, such as light shelves. On the other hand, the EnergyPlus program uses either the split flux or radiosity methods. Although the radiosity methid is an improvement over the split flux method, it also has limitations in diffuse interreflection calculation (Willmott and Heckbert, 1997).

2.4.2. Building Thermal Assessment Tools

Heat transfer in buildings involve non-linear heat flow through and among its components, including surfaces and volumes, which corresponds to a set of coupled differential equations with complex boundary and initial conditions (Birdsall et al., 1985). Detailed building energy simulation tools are used to solve the mathematical equations to simulate the dynamic behavior of the building (Birdsall et al., 1985). Over time, there have been different whole-building energy simulation programs introduced to assist engineers/architects in calculating the energy consumption of proposed buildings. Programs such as TRNSYS (Klein, 1976), DOE-2.1E (Winkelmann et al. 1993) and eQUEST/DOE-2.2 (Lawrence Berkeley National Laboratory

[LBNL] and James J. Hirsch & Associates [JJH] 1998), TRACE (Trance, 2010), and EnergyPlus (Crawley et al. 2001), are some of the most widely–used programs that have been applied in building energy analysis area.

Today, such whole-building energy simulation tools are used to assess annual building energy consumption. Currently, there are different methods used in the detailed building energy simulation tools. These methods include: the Transfer Function Method (TFM) or Weighting Factor Method (WFM) (Cumali et al. , 1979) and the Heat Balance Method (HBM) for calculating time-varying cooling loads for energy analysis (Pedersen et al., 1997). However, in all the above tools there are limitations in the daylighting performance analysis procedures currently being used in detailed building energy simulation tools. These limitations include the limitations of the analysis methods as well as other limitations such as the indices, number of sensors, etc. that are used in the analysis. Consequently, in order to have an accurate comprehensive analysis of building thermal and daylighting performance, there is a need to utilize the most accurate tools for each analysis.

2.4.2.1. TRNSYS

TRNSYS (TRaNsient SYstem Simulation) is a transient simulation program of HVAC and solar systems for multi-zone buildings that uses a modular structure (Klein, 2010). It has been available since 1975 and continues to be developed by an international collaboration of the United States, France, and Germany (Klein et al., 2018). TRNSYS is well suited to the detailed analyses of any system with the time-varying behavior (Klein et al., 2018). Furthermore, the source code of TRNSYS (the kernel and the component models) is publically available for all

users. This simplifies the extension of existing models to make them better fit a user's specific needs (Klein et al., 2018).

TRNSYS consists of two parts, an engine called the kernel and a library of components. The kernel reads and processes the input file, iteratively solves the system, determines the convergence, plots system variables, and provides utilities that determine the thermophysical properties, inverts matrices, perform linear regressions, and interpolate external data files. The TRNSYS library of components models the performance of each part of the system. TRNSYS models are constructed in such a way that users can modify existing components or write their own models, extending the capabilities of the environment (Klein et al., 2018). In addition, users can add custom components by creating new components, compiling them and linking them into an external Dynamic Link Library (DLL) (Solar Energy Laboratory-UWM et al., 2017).

In the TRNBuild sub-program, where the detailed information about every zone of the building is described, the user specifies the building properties such as, the thermal characteristics, structural components, schedules, infiltration etc. In addition, fenestration systems can be chosen from the available TRNSYS library. Currently, in TRNSYS 18 (Klein et al., 2018), a model for simulating Complex Fenestration Systems (CFSs) has been developed and has been integrated into the multi-zone building model (Type 56) that allows the user to represent the bidirectional scattering of radiation that occurs in slat systems or honeycomb structures. These features enable the users to simulate the optical model based on BSDF, including up to six layers with different gas mixtures, modeling infrared transparent systems, natural convection around shading layers, and mechanical ventilation (up to two gaps).

2.4.2.2. DOE-2

The DOE-2 building energy analysis computer program allows architects and engineers to simulate the whole-building energy use under varying weather conditions (Birdsall et al., 1985). The energy analysis in DOE-2 is performed in the four sequential steps: LOADS, SYSTEMS, PLANT, ECONOMICS. Birdsall et al. (1985) described these steps:

The LOADS program is defined as the energy rate (i.e., heating or cooling) that must be added or removed from a space (a user-defined subsection of a building) to maintain the pre-defined set-point temperature in the space. The calculation of the cooling and heating loads of a space has two steps in DOE-2, including the calculation of the space heat gains or heat losses and the total space loads, which are calculated from the sum of the space loads. DOE-2 uses either pre-calculated or custom weighting factors together with transfer functions to calculate the dynamic heat conduction into or out of a space, which involve one dimensional dynamic heat transfer equations. DOE-2 uses triangular temperature pulses as excitation functions in the time-series solution. The hourly simulation then uses these solutions, called “response factors”, to account for the heat gain or loss from the indoor and outdoor temperatures.

The SYSTEMS program simulates HVAC systems that provide the hourly heating or cooling defined by the LOADS program. The interaction between the equipment and the envelope are calculated by the simultaneous solution of the space air-temperature weighting factor equation with the equipment controller relation. The calculated sensible and latent coil loads are then either passed to the PLANT program, or the energy conversion is simulated directly in SYSTEMS in the case of direct-expansion systems or packaged cooling equipment.

The PLANT program simulates the primary hourly HVAC systems using empirically determined performance curves to determine the thermal performance of the equipment based on

the user-defined parameters, such as the part load, entering fluid temperatures, duct supply temperature, etc. The PLANT program also allows the users to define the time schedules and/or load ranges for every piece of equipment.

The ECONOMICS program calculates the costs of the hourly energy consumed by each piece of equipment. The program provides various tariff or cost schedules so the user can evaluate the different costs of operations of the building system and plant equipments. ECONOMICS can also simulate the purchase or sale of the electricity that is generated at the building. Furthermore, the user can simulate the life-cycle costs of the building over a multi-year period using the ECONOMICS program. In general, DOE-2 is a widely used, whole-building energy simulation program that has been verified against other software programs and against field measurements on existing buildings (LANL, 1981).

2.4.2.3. TRACE

TRACE 700 is a comprehensive analysis software for the energy and economic analysis of different architectural features, HVAC systems, HVAC equipment, building utilization or scheduling and financial options in a building. TRACE 700 was developed by the Trane company. In TRACE 700, zones divide the building to separate areas. Each zone contains one or more rooms. A room is the smallest space for calculating heating and cooling loads. The distribution of air to and from the conditioned spaces in the building is handled by the system. TRACE 700 includes more than 30 types of systems in five categories, including: variable volume, constant-volume mixing, constant volume non-mixing, heating only, and induction. The TRACE 700 Plant refers to the mechanical equipment that conditions the air in the conditioned spaces. Templates are also provided that can be used for applying a set of predetermined settings

for the different rooms. Also, Libraries include common design parameters for construction materials, equipment, base utilities, weather, and scheduling, which are mostly derived from the ASHRAE Handbook–Fundamentals or similar industry references (Trane, 2010).

2.4.2.4. EnergyPlus

EnergyPlus is a whole-building energy simulation program designed for modeling and simulating buildings and HVAC equipment based on fundamental heat balance principles. Many of the simulation characteristics of EnergyPlus have been inherited from the BLAST (Building Loads Analysis and System Thermodynamics) (Hittle, 1977) and DOE–2 energy and load simulation tools, which were developed and released in the late 1970s and early 1980s. There have been improvements implemented in EnergyPlus such as the structure and simulation management, modularity (which enables established links to other popular simulation environments/components), integration of loads, systems, and plants, feedback from the HVAC system to the zone conditions etc. (US Department of Energy, 2015).

One of the advancements of EnergyPlus over other programs is the integration of the simulation, which means, unlike sequential programs, such as BLAST and DOE-2, that all three parts of the building, systems, and plants, are solved simultaneously, which overcomes the unmatched loads in the sequential solution process. In the sequential solution, the process starts with a zone heat balance, which updates the zone conditions and determines the heating/cooling loads of the zone at all time steps. This information is then passed to the air-handling simulation where the system response is determined. However, if this system response does not resolve zone heating/cooling conditions, it is possible that the sequential process end up to unmatched loads. To decrease the unmatched loads issue in the sequential method, the system response should be a

well-defined function of the air temperature of the zone. However, in most situations, the air temperature of the zone is not the only influential parameter on system capacity and system capacity is dependent on outside conditions and/or other parameters of the zone (US Department of Energy, 2015).

EnergyPlus overcomes this issue by integrating functional elements connected by loops, divided into supply and demand sides, using the Integrated Solution Manage (ISM). The ISM uses a successive substitution iteration using the Gauss-Seidell philosophy to continuously update the supply and demand in the integrated process (US Department of Energy, 2015).

EnergyPlus Simulation Manager integrates different internal elements, including Surface Heat Balance Manager, Air Heat Balance Manager, Building Systems Simulation Manager, each of which is linked to different modules. Consequently, similar to other simulation programs, EnergyPlus consists of more than just an executable file. For example, the EP-Launch Program assists running the program in the Windows environment, which includes finding input files and storing or further processing the output files. There are also advanced techniques of executing the EnergyPlus program, including the advanced uses of the EP-Launch program, command line DOS commands, etc. (US Department of Energy, 2015).

2.4.2.5. Window Modeling Methods in Building Energy Simulation

The solar transmittance, reflectance, and absorptance properties of the individual layers in a window impact the direct solar gains by the interior surfaces of the building that then effect building thermal loads. Furthermore, the visible transmittance of the glazing affects the interior daylight illuminance, which impacts the building energy consumption of buildings with daylight responsive controls.

In general, there are two modeling approaches for windows in building energy simulation. These approaches include a simplified method or the Transmittance, Absorptance and Reflectance (TAR) method (Mitalas and Stephenson, 1962) and a more detailed layer-by-layer approach, the Multi-Layer Window (MLW) method (Mitchell et al., 2017).

The Energyplus simple window model[4] allows users to model window components using simple performance parameters of the entire glazing system, the U-Factor, and the SHGC. This model converts the inputs into an equivalent single layer window (EnergyPlus, 2016).

Building codes, standards, and voluntary code programs are developed that allow the use of a simplified model in the prescriptive path. The simplified window model in EnergyPlus only requires the U-Factor and SHGC indices. Energy codes and standards use these terms to provide a generic classification of the code-complied windows. However, as stated by Arasteh (2010), although there are beneficial points about using only the U-Factor and SHGC for window modeling, any method that uses only these two indices for modeling window components in building simulation software may provide less accurate results due to the following factors:

- The directly transmitted solar radiation and solar radiation that is absorbed by the glass that flows inward are combined in the SHGC. However, the directly transmitted and absorbed solar radiation have different implications for space heating and cooling. In addition, different windows with the same SHGC usually have different ratios of transmitted to absorbed solar radiation.

[4] This model can be accessed with "WindowMaterial:SimpleGlazingSystem" input object in EnergyPlus 8.9.0.

- The SHGC is determined at a normal incidence angle. However, since angular properties of glazing varies with the number of layers, tints, coatings, and angle of incident, products with the same SHGC can have different angular properties.
- U-factors vary with temperatures. However, the U-factors used in the simplified TAR window model is a fixed value.

The U-value/SHGC window modeling method uses a simple "Block Model" concept to map a given U-value, SHGC, VT to the properties of a fictitious "layer" in EnergyPlus. The effective conductivity of this single layer model represents the whole window component using a given U-Factor. In addition, the solar transmittances at normal incidence are defined based on the given SHGC while for the non-normal incidence angles properties the angular properties of multiple glazing layers are used.

In EnergyPlus the following steps are used to model the energy impacts of windows in whole buildings using the common window indices U-factor and SHGC (and optionally VT) (Arasteh, 2010):

Step 1: EnergyPlus determines the glass-to-glass resistance by calculating interior and exterior film coefficients for every time step.

Step 2: The thickness of the window will be determined by the U-factor. A 2 mm thick glass is used for U-factor of 7 W/m2-K and a 52 mm thick glass for U-factor of 1 W/m2-K. The fitted line interpolates glass thickness for the U-factors between 1-7 W/m2-k. For a U-factor greater than 7 W/m2-K, a thickness of 2 mm is selected for the glass.

Step 3: The effective thermal conductivity is determined by dividing the thickness of the window by the resistance of "Representative Layer" (m2-K/W) under winter conditions (also referred to as the glass-to-glass resistance).

Step 4: A reasonable solar transmittance will be determined for a given SHGC using the LBNL International Glazing Data-Base (IGDB) (Lawrence Berkeley National Laboratory, 2019) considering that the SHGC equals solar transmittance plus the multiplication of the inward flowing fraction for the Representative Layer and the absorptance of the Representative Layer. It also differentiates the relationship between solar transmittance and SHGC for single and double glazing.

Step 5: The front side, solar reflectance at a normal incidence angle is determined by knowing the sum of the solar transmittance, front side solar reflectance, at normal incidence, and the solar absorptance of the Representative Layer (*As*), which is equal to one. The SHGC is then divided by the inward flowing fraction for the Representative Layer (N), where N is calculated with the assumption that the absorbed solar radiation is absorbed in the center of the representative layer. The back side solar reflectance, at normal incidence is set equal to the front side solar reflectance at normal incidence.

Step 6: The visible transmittance of the window is equal to the VT, if given. If VT is not given, it will be assumed that the visible properties for the Representative Layer are the same as the solar properties.

Step 7: The angular properties of the glazing system are determined using the U-factor and SHGC that are used to determine the most probable window properties as well as the normalized transmission and reflectance.

Step 8: The hemispherical or diffuse transmittance is calculated by integrating the transmittance at angles of incidence from 0 to 90 in EnergyPlus.

2.4.2.6. Summary of Building Thermal Assessment Tools

The analysis of the building energy consumption can be carried out using building energy simulation tools, where the outputs are translated into suitable quantifications of performance indicators (Malkawi and Augenbroe, 2003). The advancements in hardware and software have increased the use of building energy simulation tools in the building design analysis process. Depending on the purpose of the analysis, different building energy simulation tools, such as TRNSYS, DOE-2/eQUEST, EnergyPlus, TRACE, etc. can be used to analyze a building's energy performance.

2.5. Weather-Normalized Building Energy Comparisons

Weather-related parameters influence building energy consumption. Therefore, different weather-normalization methods have been proposed over the years to account for the weather-related varying parameters when comparing building energy consumption or savings. These methods can be used to either remove the inconsistencies of the weather parameters before and after the retrofit periods in the same location or they can be used to account for weather parameters when comparing the energy consumption in various climates, such as in benchmarking. This section discusses different weather-normalization methods, including the degree day methods, the Modified Utilization Factor (MUF) method used in EN-ISO 13790, the Climate Severity Index (CSI) method, and the Climate Coefficients for the U.S. Building Energy Asset Score, that can be used to adjust the building energy use in different climates.

2.5.1. Degree-Days

The concept of degree days was initially proposed by Sir Richard Strachey (1878) in England to analyze a farmer's crop growth, where the base temperature was determined according to the temperature required for the plant growth. In addition to the early discussions of the temperature sums above a critical threshold in agriculture (Hann, 1903), since the 1940s, the history of the snowmelt runoff (Braithwaite, 2011) also included the discussions of the application of degree days in the calculation of the snow and ice runoff (Wilson, 1941). It was not until the 1920s (ASHVE, 1933) in the United States when the American Gas Association used degree days for the first time in buildings (CIBSE TM41, 2006). This section includes an introductory discussion of the degree days and its different variations, the calculation of the balance-point temperature, and the calculation of building heating and cooling loads using degree days.

Degree day methods are methods used in the energy analysis of the buildings that have constant internal energy use and HVAC equipment efficiency (ASHRAE, 2001). Consequently, Heating Degree-Days (HDD) and Cooling Degree-Days (CDD) measurements have been used to classify weather conditions with respect to the expected heating or cooling loads, respectively. In the degree day methods, the average daily temperature and a critical threshold is used to calculate the degree days (A more detailed discussion on the various degree day calculation methods is provided in Section 2.5.1.2). As stated by Day (CIBSE TM41, 2006), Strachey and the Meteorological Office in England initiated the use of daily minimum and maximum temperature measurements in the degree day calculation to facilitate the calculation process (The Meteorological Office, 1928). The use of minimum and maximum temperature was facilitated by

the invention and widespread use of the minimum–maximum thermometers, which simplified and standardized daily minimum–maximum temperature measurements.

Besides the use of daily minimum and maximum temperature measurements in the degree day calculation, another approach is the arithmetic average daily method to calculate the degree day. In the arithmetic average daily method the average temperatures from different hours of a day is used to calculate the degree day.

Various methods have also been proposed to calculate degree days based on the monthly temperatures. The monthly mean temperature is one of the simplest methods to estimate degree days. It is calculated by dividing the difference between the base temperature and monthly mean temperature by the number of the days in the month (Hitchin, 1981). However, it may not fully represent the data that is available in smaller time interval measurements. Also, the hourly data may not be available for long, continuous period of time for a given location. Several methods have been proposed for more accurate estimations of the degree days based on the monthly data. For example, Thom's method can be used to estimate the mean values of the heating degree days that are below the base temperatures (Thom, 1954a) and above base temperatures for cooling degree days (Thom, 1966) using the monthly averages air temperature, standard deviations, and empirical correction factors (Thom, 1954b). Thom's procedure assumes that the daily mean temperature is normally distributed within the month (Hitchin, 1983). The empirical term in Thom's method varies with the standard deviation of the normal distribution of the daily mean temperatures within the month.

Similarly, Steadman proposed a method to estimate the degree-days based on the average monthly temperature and the standard deviation of the temperature (Steadman, 1978). Compared to Thom's method, Steadman's method does not use empirical correction factors. Another

method is the Choffe's method, in which the degree day is estimated using the average and minimum temperature in the period of interest. Schoenau–Kehrig's monthly mean temperature method (Schoenau and Kehrig, 1990) is also a widely adopted method to calculate monthly degree days using the number of days in the month, the difference between base temperature and monthly mean temperature, and the standard deviation of the daily mean temperature. Other studies have analyzed the relationship of the degree days and the annual mean temperature and standard deviation of monthly mean temperature to calculate degree days for low resolution weather data. In addition, Mourshed (2012) proposed non-linear regression models to estimate HDD and CDD based on the annual mean temperatures. In this method, he found the accuracy of the estimation can be increased by including the standard deviation of monthly mean temperature and the latitude in the calculation.

2.5.1.1. Balance-Point Temperatures in Degree-Day Calculations

In the degree day calculation, the critical threshold is often called the balance-point temperature, T_b, which is defined as the outdoor temperature at which the total heat loss, q_{gain}, equals the heat gain from various sources, including solar gain and internal heat gains (ASHRAE, 2001). Therefore, typically, the base temperature is lower than the thermostat set-point since the internal heat gain is considered in the determination of the base temperature (CIBSE TM41, 2006), which lowers the ambient temperature that signifies the onset of heating. The q_{gain} can be calculated using equation 2.1.

$$q_{gain} = K_t(T_i - T_b) \tag{2.1}$$

where, K_t is the total heat loss coefficient of the building. By rearranging equation 2.1, the balance-point temperature can be calculated using equation 2.2.

$$T_b = T_i - \frac{q_{gain}}{K_t} \tag{2.2}$$

Determination of the base temperature depends on various parameters, including the building heat loss coefficient, the thermal capacity, infiltration, and the internal heat gains. However, for the most part, these influential parameters vary during a day. For example, the heat gains in a space are not always constant for most buildings. In addition, the indoor temperature can be controlled by thermostat setback controls, which result in varying indoor temperatures during the day. In the case of these varying parameters, the average values of these parameters can be used to determine the base temperature (CIBSE TM41, 2006). However, the intermittencies of various parameters (some parameters may have different daily periodicities) and the thermal storage effect in a building can make the degree day method less accurate in representing the dynamic heat transfer between a building and its surrounding. Consequently, the uncertainty in the estimation of the energy consumption increases when one decreases the time scale (Day and Karayiannis, 1999a). Therefore, different methods have been proposed to account for the variability of solar gains, the effect of building mass, and the different aspects of heating system control and performance. These methods try to account for the variabilities in internal and solar gains and variable part load ratios using utilization factors (Hitchin, 1990) as well as calculating the degree days with varying T_b is also used.

Various methods have been proposed to determine the base temperatures. These methods vary based on the calculation methods for T_b, T_i, and q_{gain}. For example, daily base methods use average daily values for T_i and q_{gain}. There are two variations for the daily base methods with different definitions for T_b, which can be either average daily or, in the case of varying set point temperatures during a day, the desired indoor temperature during occupied hours (Knight and Cornell, 1958). In a similar fashion to the daily base methods, there are monthly base methods, where the T_b and q_{gain} are average monthly values. In the monthly methods, the T_i can also be determined using either the average monthly value or the desired indoor temperature during occupied hours (Day and Karayiannis, 1999a).

The hourly-based methods are another approach that uses hourly values for T_b and q_{gain}. The T_i in the hourly methods, however, has three variations, including: the hourly value; the desired indoor temperature during occupied hours; or the average daily value. In general, in many cases in the hourly methods, the assumption of instantaneous response to the heat gains ignores the thermal storage effects in the building.

In cases where the desired indoor temperature during occupied hours is used for T_b, correction factors are needed to account for the unoccupied periods (Day and Karayiannis, 1999a). In the previous literature several studies have developed correction factors. However, the use of average indoor temperature to determine the base temperature is more reliable than applying correction factors that require additional measurements.

In practice, the mean indoor temperature, the magnitude of heat gains, and the heat loss coefficients are not known for a given building and have to be estimated, which may increase the uncertainties. The previous studies includes methods to estimate the base temperature for heating and cooling degree days in different locations using regression models (Bakirci et al. 2008;

Büyükalaca et al. 2001; Idchabani et al. 2015; Ihm et al. 2014; Indraganti and Boussaa, 2017; Lee et al. 2014; Papakostas and Kyriakis, 2005).

2.5.1.2. Degree-Day Calculation Methods

There are different methods that have been proposed to calculate degree days. This section describes the degree day calculation methods, including the Mean Daily Temperature, the Mean Degree Day method, the Meteorological Office (MO) equation, Variable Base Degree Day (VBDD) method, and the degree day estimation methods based on monthly temperatures.

2.5.1.2.1. Mean Daily Temperature

In the Mean Daily Temperature method, the average daily temperature is used to calculate the degree day. The HDD for each day is calculated by subtracting the mean daily temperature from the base temperature for the HDD, if it is a positive value. Similarly, the CDD for each day is calculated by subtracting the base temperature for CDD from the mean daily temperature, if it is a positive value. Figure 8 shows an example for the HDD calculation using Mean Daily Temperature method. The daily HDD in the Mean Daily Temperature method can be calculated using equation 2.3.

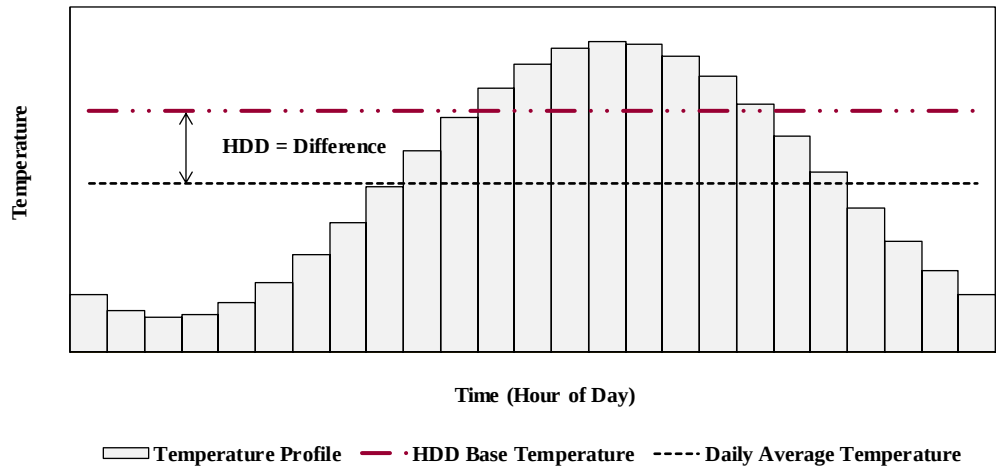

Figure 8: Degree Day Calculation Using Average Daily Temperature

$$HDD_{daily} = \left(T_{base,HDD} - \bar{T}_o\right)^+ \tag{2.3}$$

where, $T_{base,HDD}$ is the base temperature for HDD, which is typically assumed to be 18°C, $\bar{T}_o$ is the average daily outdoor air temperature. The positive sign denotes that only positive values should be summed.

Similarly, equation 2.4 shows how to calculate CDD in the Mean Daily Temperature method.

$$CDD_{daily} = \left(\bar{T}_o - T_{base,CDD}\right)^+ \tag{2.4}$$

where, $T_{base,CDD}$ is the base temperature for CDD, which is typically assumed to be 10°C.

As shown in equation 2.5, there are two different approaches to calculate $\bar{T}_o$. It can be either calculated using the daily maximum and minimum temperature or it can be the average daily temperature.

$$\bar{T}_o = \begin{cases} \frac{T_{max} + T_{min}}{2}, Daily\ Maximum - Minimum\ Approach \\ \frac{\sum_{n=1}^{24} T_{o,n}}{24}, Average\ Daily\ Approach \end{cases} \quad (2.5)$$

where, T_{max} is the maximum daily outdoor temperature, T_{min} is the minimum outdoor daily temperature, and $T_{o,n}$ is the outdoor temperature at hour *n* of a day.

The annual sum of the HDD and CDD can then be calculated using equations 2.6 and 2.7, respectively, for the daily minimum-maximum approach, and with equations 2.8 and 2.9, respectively, for the daily average approach.

$$HDD_{annual} = \sum_{i=1}^{365} \{T_{base,HDD} - [(T_{i,max} + T_{i,min})/2)]\}^{+} \quad (2.6)$$

where, $T_{base,HDD}$ is the base temperature for HDD, $T_{i,max}$ is the maximum outdoor temperature at day *i* of the year, and $T_{i,min}$ is the minimum outdoor temperature at day *i* of the year.

$$CDD_{annual} = \sum_{i=1}^{365} \{[(T_{i,max} + T_{i,min})/2)] - T_{base,CDD}\}^{+} \quad (2.7)$$

where, $T_{base,CDD}$ is the base temperature for CDD

$$HDD_{annual} = \sum_{i=1}^{365} \left(T_{base,HDD} - \frac{\sum_{n=1}^{24} T_{o,i,n}}{24} \right)^{+} \tag{2.8}$$

where, $T_{o,i,n}$ is the outdoor temperature at hour *n* of day *i* of the year.

$$CDD_{annual} = \sum_{i=1}^{365} \left(\frac{\sum_{n=1}^{24} T_{o,i,n}}{24} - T_{base,CDD} \right)^{+} \tag{2.9}$$

2.5.1.2.2. Mean Degree-Day

The calculation of degree day using the Mean Degree-Day method requires calculating the Heating Degree Hours (HDH) or Cooling Degree Hours (CDH) and then taking the average of these values for each day. Figure 9 shows an example of the calculation of the HDH. The average HDH is the HDD for that day in the Mean Degree-Day method.

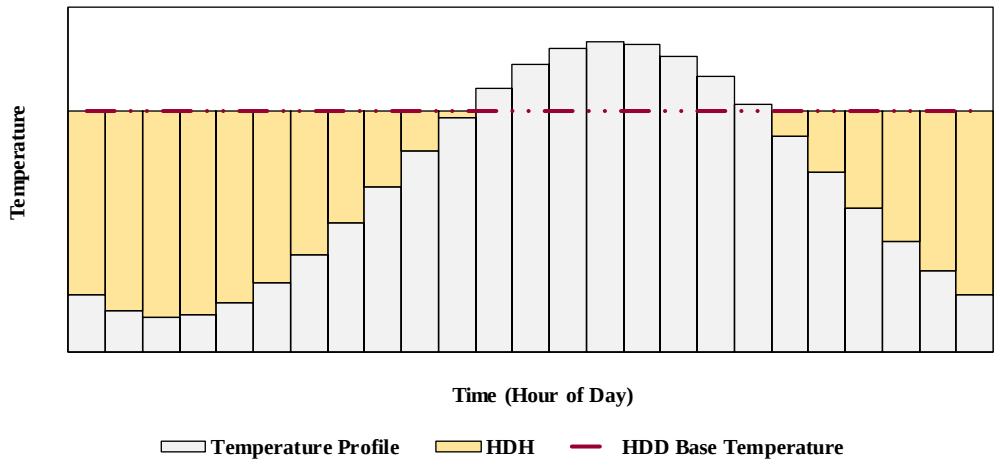

Figure 9: HDH Calculation

The HDD_{daily} in the mean degree day method can be calculated using equation 2.10:

$$HDD_{daily} = (1/24) \cdot \sum_{n=1}^{24} \left(T_{base,HDD} - T_{o,n}\right)^{+} \tag{2.10}$$

where, $T_{base,HDD}$ is the base temperature for HDD, which is typically assumed to be 18°C, $T_{o,n}$ is the outdoor air temperature in hour *n*. The positive sign denotes that only positive values should be summed.

Similarly, equation 2.11 shows how to calculate CDD in the mean degree day method.

$$CDD_{daily} = (1/24) \cdot \sum_{n=1}^{24} \left(T_{o,n} - T_{base,CDD}\right)^{+} \tag{2.11}$$

where, $T_{base,CDD}$ is the base temperature for CDD, which is typically assumed to be 10°C.

The annual HDD and CDD can then be calculated using equations 2.12 and 2.13, respectively.

$$HDD_{annual} = (1/24) \cdot \sum_{i=1}^{365} \sum_{n=1}^{24} \left(T_{base,HDD} - T_{o,i,n}\right)^{+} \tag{2.12}$$

$$CDD_{annual} = (1/24) \cdot \sum_{i=1}^{365} \sum_{n=1}^{24} \left(T_{o,i,n} - T_{base,CDD}\right)^{+} \tag{2.13}$$

2.5.1.2.3. The Meteorological Office Equations

The Meteorological Office (MO) equations, also called the UK Meteorological Office equations, 'McVicker', or the 'British Gas' formulae, is an approximation for the equations 2.14 and 2.15 using daily maximum and minimum temperature (The Meteorological Office, 1928).

$$HDD = \int \left(T_{base,HDD} - T_o\right) dt \tag{2.14}$$

$$CDD = \int \left(T_o - T_{base,CDD}\right) dt \tag{2.15}$$

The Meteorological Office equations for HDD and CDD are represented in Figure 10 and equations 2.16 and 2.17 respectively.

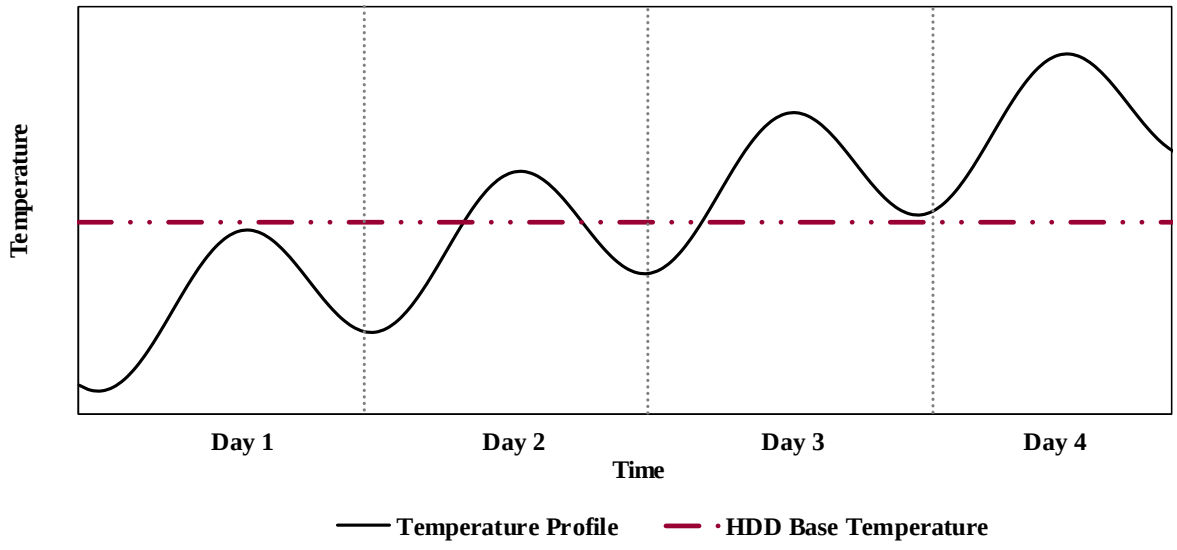

Figure 10: Representation for the Meteorological Office (MO) Equations

$$\begin{cases} if\ T_{max} \le T_{base,HDD} \rightarrow HDD_{daily} = T_{base,HDD} - 0.5(T_{max} + T_{min}) \\ if\ T_{min} < T_{base,HDD}; and\ \left(T_{max} - T_{base,HDD}\right) < \left(T_{base,HDD} - T_{min}\right) \rightarrow \\ \quad HDD_{daily} = 0.5\left(T_{base,HDD} - T_{min}\right) - 0.25(T_{max} - T_{base,HDD}) \\ if\ T_{max} > T_{base,HDD}; and\ \left(T_{max} - T_{base,HDD}\right) > (T_{base,HDD} - T_{min}) \rightarrow \\ \quad HDD_{daily} = 0.25(T_{base,HDD} - T_{min}) \\ if\ T_{max} \ge T_{base,HDD} \rightarrow HDD_{daily} = 0 \end{cases} \quad (2.16)$$

$$\begin{cases} if\ T_{min} \ge T_{base,CDD} \rightarrow CDD_{daily} = 0.5(T_{max} + T_{min}) - T_{base,CDD} \\ if\ T_{max} > T_{base,CDD}; and\ (T_{min} - T_{base,CDD}) > (T_{base,CDD} - T_{min}) \rightarrow \\ \quad CDD_{daily} = 0.5(T_{base,HDD} - T_{min}) - 0.25(T_{max} - T_{base,HDD}) \\ if\ T_{min} < T_{base,CDD}; and\ (T_{max} - T_{base,CDD}) < (T_{base,CDD} - T_{min}) \rightarrow \\ \quad CDD_{daily} = 0.25(T_{max} - T_{base,CDD}) \\ if\ T_{max} \le T_{base,CDD} \rightarrow CDD_{daily} = 0 \end{cases} \quad (2.17)$$

Similar to the previous methods, the annual HDD and CDD using the Meteorological Office equations can be calculated by summing the HDD and CDD for the 365 days of the year.

2.5.1.2.4. Variable Base Degree Day (VBDD)

The standard 10°C for cooling base temperature and 18°C for heating base temperature may not represent the actual temperatures, above or below which the building requires cooling or heating, respectively. Therefore, a Variable Base Degree Day method (VBDD) was developed. The VBDD method determines the heating and cooling loads by first determining the appropriate base temperature for each building. VBDD requires determining the base temperature that appropriately represents the cooling and heating requirements of a building.

The PRInceton Scorekeeping Method (PRISM) was one of the earliest VBDD methods. The application of different variations of PRISM to heating and cooling models of electrically heated houses was studied by Stram and Fels (Stram & Fels, 1986). Results showed reliable savings estimations using the PRISM model. The VBDD method has been widely used to determine appropriate base temperatures (Bakirci et al., 2008; Shanmuga Priya Selvanathan & Joanna Migdalska, 2015), calculate building energy loads (Degelman, 1985), and estimate the building energy savings (Wortman & Christensen, 1985). The VBDD method is also included in the ASHRAE Inverse Model Toolkit (IMT) although the algorithm used in the IMT differs from the algorithm used in PRISM (Haberl et al., 2003).

2.5.1.2.5. Degree-Day Estimation Methods Based on Monthly Temperatures

Different methods have been proposed to estimate the daily HDD or CDD based on the monthly temperatures. A number of widely used methods and variations of these methods are discussed in this section, including Thom's method, Hitchin's method, and Schoenau's and Kehrig's method.

Thom (1954b) proposed the following equation to estimate the mean monthly HDD, which is denoted as $\overline{HDD_{daily}}$:

$$\overline{HDD_{daily}} = N(T_{base,HDD} - \overline{T_o} + l\sqrt{N}\sigma_m) \tag{2.18}$$

where, N is the number of days in the month, $T_{base,HDD}$ is the base temperature, $\overline{T_o}$ is the mean monthly air temperature, l can be function of $(T_{base,HDD} - \overline{T_o})/\sigma$, σ is the standard deviation for the average day[5], and σ_m the standard deviation of the monthly average.

Hitchin (1983) proposed another equation to estimate the mean monthly HDD. Equation 2.19 shows Hitchin's equation, in which with large positive $(T_{base,HDD} - T_o)$, the HDD value approaches $N(T_{base,HDD} - T_o)$, and with large negative $(T_{base,HDD} - T_o)$, the HDD approaches zero.

$$\overline{HDD_{daily}} = \frac{N(T_{base,HDD} - \overline{T_o})}{1 - e^{-k(T_{base,HDD} - T_o)}} \tag{2.19}$$

where, N is the number of days in the month, $T_{base,HDD}$ is the base temperature, $\overline{T_o}$ is the mean monthly air temperature, k is a constant for the location. The importance of the value of k is more pronounced in small $(T_{base,HDD} - \overline{T_o})$ and when the weather is cold enough to result in large $(T_{base,HDD} - \overline{T_o})$, the variations in different days is less important hence the value of k is not critical (Hitchin, 1990).

Hitchin's method is simpler to Thom's method, in which k can be calculated using $2.5/\sigma$ when the standard deviation of daily mean temperature within a month, σ, is known. However, σ is often not known. Hitchin (Hitchin, 1983) argued that $\sqrt{N}\sigma_m$ results in poor estimate of σ and although the empirical term in Thom's method compensates a portion of the error, major errors

[5] The average day is a hypothetical day with a mean and standard deviation that results in the mean degree days for the month after the conversion is made to degree days and the result is multiplied by the number of days in the month (Thom, 1954b).

remain. An study by Erbs et al. (Erbs et al., 1981) shows that the actual values of σ are approximately half of the estimations using $\sqrt{N}\sigma_m$ with a dispersed scatter. This impacts the accuracy of Thom's procedure since the errors in estimation are larger than the errors when the base temperature is close to the external temperature (Hitchin, 1981). In the case of not knowing σ, when the standard deviation of the monthly mean temperature is available, $\sqrt{N}\sigma_m$, the values of *k* calculated using $5.26/\sqrt{N}\sigma_m$ are identical to the Thom's procedure (Hitchin, 1983). However, Hitchin has provided the best values of *k* for different sites (Hitchin, 1983).

Schoenau and Kehrig (1990) proposed a normal distribution method assuming an annual normal distribution of the daily mean temperatures around the monthly mean temperature to calculate degree days at any base temperature.

$$HDD_{monthly} = NS_d \int_{-\infty}^{Z_b} (Z_b - Z) f(Z) dZ \tag{2.20}$$

where, *N* is the number of days in the month, S_d is the standard deviation of the monthly mean temperature, *Z* is equal to $(T - T_m)S_d^{-1}$, where *T* is the daily mean temperature and T_m is the mean monthly temperature, and Z_b is equal to $(T_b - T_m)S_d^{-1}$, where T_b is the base temperature.

The function *f(Z)* is the Gaussian probability density function:

$$f(Z) = \frac{1}{\sqrt{2\pi}} e^{\left(\frac{-Z^2}{2}\right)} \tag{2.21}$$

By integrating equation 2.20, the estimation of the monthly HDD can be calculated using:

$$F(Z_b) = \int_{-\infty}^{Z_b} f(Z)dZ \tag{2.22}$$

The value of $F(Z_b)$ can be calculated or retrieved from normal probability tables as there is no explicit solution of the integral. Similarly, the monthly CDD can be calculated using:

$$CDD_{monthly} = NS_d \int_{Z_b}^{+\infty} (Z_b - Z) f(Z)dZ \tag{2.23}$$

Other equations, retrieved from regression models, have also provided by different researchers (e.g., as in (Mourshed, 2012)) that yield HDD and/or CDD based on the monthly temperatures.

2.5.1.3. Calculating the Building Energy Consumption Using the Degree-Days

There are different approaches to estimate building energy consumption, including forward methods (i.e., a law-driven method) and backward methods (i.e., data-driven methods or inverse methods) (ASHRAE, 2013b; Coakley et al. 2014). The previous literature includes estimations based on the forward methods, in which the physical properties of a building are taken into account to calculate building energy use or savings using a system of first principle equations. Backward methods are also widely used to estimate the energy consumption and savings of the buildings, such as the Inverse Model Toolkit (Haberl et al. 2003), in which the savings are estimated using the numerical algorithms. To account for the impact of the weather on building energy estimations, the weather parameters can be either used directly (e.g. using

outdoor temperature to estimate the heating or cooling loads) or processed to reveal specific points of interest for building energy load calculations (e.g., as in CDD, which only add up the temperature values larger than a designated base temperature).

Building energy consumption can be calculated using degree day method. The rate of heating energy consumption and the annual heating energy consumption of a building can be calculated using the equations 2.24 and 2.25, respectively.

$$q_h = \frac{K_t}{\eta_h}[T_b - T_o(t)]^+ \tag{2.24}$$

where, η_h is the Annual Fuel Use Efficiency (AFUE) of the heating system, *t* is time, and the plus sign indicates that only positive values should be added.

$$Q_h = \frac{K_t}{\eta_h}\int [T_b - T_o(t)]^+ dt \tag{2.25}$$

The discrete form of the equation yields:

$$Q_h = \frac{24.K_t.HDD_b}{\eta_h} \tag{2.26}$$

Similarly, the cooling energy consumption can be calculated using equation 2.27. To use this equation the assumptions for instantaneous steady-state sensible cooling rate extended to

longer time spans requires replacing the quantities by appropriate average values for that period (Claridge et al. 1987).

$$Q_c = \frac{24.K_t.CDD_b}{COP} \tag{2.27}$$

where, the *COP* is the coefficient of performance of the cooling system.

There are two approaches to account for the ground losses in this equation (Claridge et al., 1987). In one approach, the ground losses can be included in the calculation of the base temperature as a negative heat gain (equations 2.28 to 2.30).

$$Q_c = \frac{24.K_{t_1}.CDD_{T_{b_1}} + Q_L}{COP} \tag{2.28}$$

where, Q_L is the latent load (Btu) of the building in the period of the analysis.

$$T_{b_1} = T_i - \frac{Q_{IG} + Q_{SG} - Q_{Gr}}{K_{t_1}} \tag{2.29}$$

where, Q_{IG} is the average internal gain rate (Btu/h), Q_{SG} is the average solar gain rate (Btu/h), Q_{Gr} is the average rate of below grade heat loss (Btu/h) of the building in the period of the analysis. The parameter K_{t_1} can be calculated with:

$$K_{t_1} = \sum_i UA_i + \sum_i UA_{inf} \tag{2.30}$$

where, *i* is the number of above-grade components, UA_i is the product of the heat loss coefficient and the area for each of the above-grade components, and the UA_{inf} is the effective UA for infiltration.

In the other approach, the ground heat loss can be included the calculation of the building loss coefficient (equations 2.31 to 2.33).

$$Q_c = \frac{24.K_{t_2}.CDD_{T_{b_2}} + Q_L}{COP} \tag{2.31}$$

$$T_{b_2} = T_i - \frac{Q_{IG} + Q_{SG}}{K_{t_2}} \tag{2.32}$$

$$K_{t_2} = \sum_i UA_i + \sum_i UA_{inf} + \sum_i UA_{Gr} \tag{2.33}$$

where, UA_{Gr} can be calculated using equation 2.34.

$$UA_{Gr} = \frac{Q_{Gr}}{\bar{T}_i - \bar{T}_o} \tag{2.34}$$

where, $\bar{T}_i$ is the average indoor temperature and $\bar{T}_o$ is the average ambient temperature.

The concept and application of degree day methods and balance-point temperature are still considered as a valuable tool. In case of relatively constant indoor temperature and internal gains, degree day methods can be used to estimate building annual energy load. Since the degree day is the summation of temperature differences between a reference temperature and the outdoor air temperature over time, it represents both the extremity and duration of outdoor temperatures (CIBSE TM41, 2006). However, degree days do not fully account for several influential weather parameters that impact building energy consumption, including solar radiation, humidity, and wind speed. While the previous research have proposed different variations of the degree day to account for the time-varying parameters within one day, such as the varying internal gains or setpoints, the standard degree day remains a crude proxy of several weather-related parameters that impact building energy consumption. Furthermore, the degree day does not account for the daily fluctuations in outdoor temperature, which makes the building energy consumption differ with varying operation schedules.

Uncertainties in the degree day calculation have also been the focus of different research. Holmes et al. (2017) discussed higher uncertainties in the estimation of the building heating and cooling energy use when the temperature is close to the threshold temperature. Furthermore, the variations of the HDD and CDD due to various data sources used in the calculation of the degree day also adds to the uncertainties. Significant statistical variability has been reported by OrtizBeviá et al. (2012) in an investigation on the evolution of the HDD and CDD obtained from temperature records at 31 stations in Spain for the period of 1958–2005 as well as future atmosphere composition, which were estimated with simulations performed under scenario A1B of the IPCC scenario conditions for the period of 2001–2050.

Consequently, various researchers have proposed modifications to the degree day calculation to increase the accuracy of the predictions of the energy consumption when using regression models developed from degree days. The proposed modifications to increase the accuracy of the energy consumption predictions using the degree day calculation try to either improve the accounting of the weather parameters or include the geometrical features of buildings. The previous literature also includes studies that have compared the accuracy of the prediction of the energy use and savings using various methods (Eto, 1988).

Huang et al. (1987) recommended including enthalpy and solar insolation along with degree day equation to better correlate building loads with weather parameters. Results of this study showed that the total heating loads can be better estimated with moderate accuracy using the variable-based daily HDD. However, this study also showed that adding the heating insolation-hours, defined as the total insolation incident on a one-square-foot vertical surface during the hours when temperature is below a certain value, will improve the correlation and allows using the standard HDD base temperature of 65 ^{o}F. A reliable estimation of the total cooling loads, however, requires at least two weather-related parameters. These parameters are the latent enthalpy hours, defined as the amount of energy that must be removed from the air at each hour that without changing the drybulb temperature lowers the enthalpy so that the indoor conditions are in the ASHRAE comfort zone, and either variable-base hourly cooling degree-days with the 75 ^{o}F base temperature modified to omit vented hours, or the cooling insolation-hours with the 70 ^{o}F base temperature.

The enthalpy-latent load has also been used in other research to estimate the cooling loads using regression models (Krese et al., 2011; Sailor, 2001; Sailor and Muñoz, 1997). In order to account for the latent loads into the cooling degree days concept, a performance surface

was proposed, which is represented as the 3-D plot of electric energy consumption as a function of cooling degree days and latent enthalpy days (Krese et al., 2011). In addition, Shin and Do (Shin and Do, 2016) proposed an enthalpy-based CDD method to account for latent and sensible heat. Comparisons of the measured data and the linear regression models derived from the temperature-based and enthalpy-based CDDs showed a 2% increase in the accuracy of predicting the cooling energy consumption using the enthalpy-based CDD versus the temperature-based CDD.

Similar to the concept to enthalpy latent days, Ihara et al. (2008) included specific air humidity to account for both air temperature and humidity in the estimation of building electricity use. Another approach to account for the humidity in load estimations was carried out by Krese et al. (2012), where a wet bulb CDD was proposed to better account for the latent loads as well as sensible loads. The comparisons of the correlations of the actual electric energy consumption and the wet bulb CDD showed a 5% higher explained variance compared to the conventional CDD. The wet-bulb based temperature is also shown to have less dependence on the chosen determination method, such as energy signature and performance line method. However, it should be mentioned that while the percentage differences between actual and predicted monthly electric energy consumption in the comparison conducted in this study shows better estimations by the wet bulb CDD compared to the conventional CDD in the period of July through October, the conventional CDD better estimated the monthly electric energy consumption in other months.

Non-climatic features of a building have also been proposed as independent variables in regressions to estimate building heating and cooling loads. Ciulla et al. (2016) analyzed including several building-related specifications along with the degree day and other weather-

related parameters. The parameters included in this analysis were the wind speed, shape factor (surface-to-volume ratio), the window-to-opaque surface ratio, the window transmittance, the global average of opaque transmittance surfaces, the global average of transmittance, the solar gains, and the yearly total hours of heating operation.

An analysis conducted by D'Amico et al. (2019) is another study that included building geometrical features to better estimate the energy consumption of a building using degree day. In this analysis, the relation between HDD and heating energy consumption of non-residential buildings was investigated using three climate data-sets in Italy. The analysis continued with correlations of the HDD and surface-to-volume ratio versus building heating energy consumption. This study emphasized that the validity of the assessment of building energy consumption using degree day method depends on the determination of the climate index as a function of the same weather data, as the results showed higher correlation coefficients when the climate index was calculated using the same weather file in the simulations.

2.5.1.4. Degree-Day Summary

Overall, the degree day calculation has been widely used to estimate building heating and cooling energy consumption. Various researchers have proposed different methods to increase the accuracy of the estimations of building heating and/or cooling loads using the conventional degree day calculation. The proposed methods are mainly modifications to the original degree day calculation, calculations that include weather-related parameters other than dry bulb temperature, or calculations that account for building geometrical features in the estimations.

2.5.2. Modified Utilization Factor-EN-ISO 13790

Having its root in the European standard of International Organization for Standardization (prEN-ISO 13790) (EN ISO, 2008), the Modified Utilization Factor (MUF) method was proposed to normalize the space heating energy use while taking into account the solar gains and the intermittent set-point temperature by applying a quasi, steady-state approximation (Roulet, 2002; Santamouris, 2004). In the prEN-ISO 13790 method, the dynamic effect of passive solar and internal heat gains were taken into account using a utilization factor. The utilization factor for the internal and passive solar heat gains treated part of the internal and passive solar heat gains as an offset in the heating load and allows for extra heat gains that can lead to cooling needs (Roulet, 2002). The following equations described the procedure of calculating the heating and cooling loads in prEN-ISO 13790 method (EN ISO, 2008).

In the prEN-ISO 13790 method the total heating energy requirement for a space can be calculated using:

$$Q_{h,n} = \left[Q_{h,i} - \eta_{h,g} Q_{h,g}\right]^{+} \tag{2.35}$$

where $Q_{h,i}$ is the total heat transfer for the heating mode in MJ, $Q_{h,g}$ is the total heat gains for the heating mode in MJ, $\eta_{h,g}$ is the gain utilization factor for heating and can be calculated using the equation 2.36. The plus sign indicates only the positive values should be considered.

$$\eta_{h,g} = \begin{cases} \dfrac{1-\gamma_h^{a_h}}{1-\gamma_h^{a_h+1}} & if\ \gamma_h > 0\ and\ \gamma_h \neq 1 \\ \dfrac{\gamma_h}{\gamma_h+1} & if \gamma_h = 1 \\ \dfrac{1}{\gamma_h} & if \gamma_h < 0 \end{cases} \quad (2.36)$$

In the method γ_h is the heat balance ratio for the heating mode that can be calculated using equation 2.37, and a_h is a parameter that includes a time constant, τ_h, that can be calculated using equation 2.38.

$$\gamma_h = \frac{Q_{h,g}}{Q_{h,i}} \quad (2.37)$$

$$a_h = a_{h,r} + \frac{\tau_h}{\tau_{h,r}} \quad (2.38)$$

In equation 2.38 $a_{h,r}$ is a dimensionless reference numerical parameter that can be found from tabulated data for continuously heated buildings and building heated during day-time only (Roulet, 2002), τ_h is the time constant of the building or building zone, and $\tau_{h,r}$ is a reference time constant that can be found in tabulated data for continuously heated buildings and building heated during day-time only (Roulet, 2002).

The $Q_{h,g}$, is the sum of the solar heat gains and the internal heat gains for the calculation period, which consists of the heat flow rate from occupants, appliances, lighting, hot and mains water and swege, HVAC system, and processes and goods. For the monthly and seasonal periods

as well as the hourly periods in simple hourly method, the sum of solar or internal heat gains during the considered month or season, $Q_{\propto}$ (MJ), can be calculated using the equation 2.39.

$$Q_{\propto} = t \cdot \sum_{k} \phi_{\propto,mn,k} + t \cdot \sum_{l} (1 - b_l)\phi_{\propto,mn,l} \tag{2.39}$$

where $\phi_{\propto,mn,k}$ (W) is the time-average heat flow rate from internal heat source *k* or solar heat gains, $\phi_{\propto,mn,l}$ (W) is the time-average heat flow rate from internal heat source *l* or solar heat gains in the adjacent unconditioned space, $\propto$ can be either internal heat gains or solar heat gains, b_l is the reduction factor for the adjacent unconditioned space with internal heat source *l*, defined in ISO/DIS 13789:2005 (ISO 13789, 2006).

The total cooling energy requirement for a space can be calculated using:

$$Q_{c,n} = \left[Q_{c,i} - \eta_{c,g} Q_{c,g}\right]^{+} \tag{2.40}$$

where $Q_{c,i}$, in MJ, is the total heat transfer for the cooling mode, $Q_{c,g}$, in MJ, is the total heat gains for the cooling mode, $\eta_{c,g}$ is the utilization factor for heat losses and can be calculated using the equation 2.41, and the plus sign indicates only the positive values should be considered.

$$\eta_{c,g} = \begin{cases} \dfrac{1-\gamma_c^{a_c}}{1-\gamma_c^{a_c+1}} & if\ \gamma_c > 0\ and\ \gamma_c \neq 1 \\ \dfrac{\gamma_c}{\gamma_c+1} & if \gamma_c = 1 \\ \dfrac{1}{\gamma_c} & if \gamma_c < 0 \end{cases} \quad (2.41)$$

where γ_c is the heat balance ratio for the cooling mode and can be calculated using the equation 2.42, and a_c is a parameter depending on the time constant, τ_c, and can be calculated using equation 2.43.

$$\gamma_c = \frac{Q_{c,g}}{Q_{c,i}} \quad (2.42)$$

$$a_c = a_{c,r} + \frac{\tau_c}{\tau_{c,r}} \quad (2.43)$$

where $a_{c,r}$ is a dimensionless reference numerical parameter that can be retrieved from a tabulated data, τ_c is the time constant of the building or building zone, and $\tau_{c,r}$ is a reference time constant that can be retrieved from a tabulated data.

While the prEN-ISO 13790 takes into account the solar gains and the intermittent set-point temperature, the limitations of the MUF method are more pronounced when applying to commercial buildings and the calculations become complicated by including the space cooling (Wang et al., 2017). A study by Jokisalo and Kurnitski (2007) on the numerical parameters of the EN ISO 13790, showed that although there is a reasonable application for the parameters in

residential buildings, they are not applicable for office buildings. Measuring the indoor and outdoor temperature profiles throughout the year, estimating the solar gains delivered to the space according to the energy auditor's judgment and site experience are other complications that can increase the uncertainties (Santamouris, 2004; Wang et al., 2017).

2.5.3. Climate Severity Index (CSI)

The Climate Severity Index (CSI) can be used as a weather normalization method that accounts for the ambient air temperature, useful solar radiation, and wind (Markus, 1982). The development of CSI can be either developed using multiple regression models (equation 2.44), actual measurements, or detailed building energy simulations. One of the early formulation of the CSI was proposed by Markus (1982) and is shown in equation 2.44.

$$CSI = K(aT - bR + cW) \tag{2.44}$$

Where, T is a selected value of outdoor temperature, R is a selected value of total solar radiation (W/m^2), W is a selected value of wind velocity (m/s), and a, b, and c are appropriate coefficients for each type of the buildings. The term $(aT - bR + cW)$ is the annual heat loss Q (kWh/m^3).

The coefficient a corresponds to defining the mass/insulation, the coefficient b corresponds to defining the solar admittance, and the coefficient c corresponds to defining the wind permeability characteristics of houses. Assuming that a single linear index can define the relationship between the mass/insulation and temperature (e.g., using Muncey's Response Factor technique (Muncey, 1979)), a can be interpreted as the slope for specific construction with a

certain mass/insulation. Similarly, assuming a linear relationship between the radiation admittance and the solar radiation, *b* represents the slope of the relation between *Q* and solar radiation. The wind permeability coefficient, *c*, was defined as the combined effect of wind speed and stack ventilation caused by the temperature difference of the indoor and outdoor. The combined effect of wind speed and stack effect was expressed as a relation between heat loss and wind permeability with a speed at which the building has zero loss.

Later, Markus et al. (1984) formulated the CSIs using regression models from simulation results. The multiple linear regression model estimates the monthly energy consumption (kWh), *E*, using:

$$E = at + bR_d + cR_f + dV + e \tag{2.45}$$

where, t is the average monthly temperature (°C), R_d is the average monthly direct normal solar radiation (W/m^2), R_f is the average monthly diffuse horizontal radiation, V is the average monthly wind speed (m/s), and the *a*, *b*, *c*, *d*, and *e* are the coefficients in regression model.

The following procedure was used to generate the CSI (Markus et al., 1984):

- The difference between the maximum and minimum energy loads for each climatic variable and house type are determined using the maximum and minimum of that climate variable and the appropriate regression model.
- The relative contribution of each parameter to the energy loads for each building type is calculated by dividing the difference, described in previous step, by the total difference.

- The contribution of each individual climatic parameter to the CSI is then determined by normalization based on the values of the lowest and highest energy loads.
- A group of curves can then be determined for the CSI for the energy consumption of each type of the houses.

While the CSI accounts for various weather-related parameters, it still does not account for the diurnal temperature variations in the ambient temperature. Also, it requires separate calculations for different weather-related parameters. Similar to the concept of the base temperature in degree days, each of these parameters has an intercept where the energy load is zero. Therefore, all the limitations in degree days base temperature applies to the determination of the value of each of these parameters, at which the building load will be zero. Consequently, the accuracy of the CSI index depends on the accurate determination of the base values.

Finally, the utilization of the CSI method depends highly on the availability of the climate data for the location of interest (Wang et al., 2017). While there is only a limited number of pre-calculated CSIs that were developed, the accuracy of using this method, specifically for the locations that do not have a CSI remains to be seen (Wang et al., 2017).

2.5.4. Climate Coefficients for U.S. Building Energy Asset Score

Wang et al. (2017) developed simulation-based climate coefficients for each weather station in the U.S. to separately adjust building heating, cooling, and fan energy consumption. The simulations of multiple building types with 1,020 TMY3 weather station files in the U.S. revealed that representative cities were not adequate for summarizing building performance in all cities in each climate zone (Makhmalbaf et al., 2013). In this study, the location-specific

normalized EUI for each site, denoted as the site EUI-ratio for an arbiturary site *m*, was calculated separately for weather-sensitive loads, such as space heating, space cooling, fan, and pumps using:

$$EUI - ratio_{j,m}^{\alpha} = \frac{EUI_m^{\alpha}}{\frac{1}{n}\sum_{i=1}^{n} EUI_i^{\alpha}} \tag{2.46}$$

where, α is the end-use (space heating, space cooling, fan, or pumps), *j* is the building prototype, *n* is the number of weather sites, and *i* is the site number.

Based on values calculated from equation 2.46, specific climate adjustment coefficients were developed for a prototype building *j*, weather site *m*, and end-use α, using:

$$C_{j,m}^{\alpha} = \frac{1}{EUI_{j,m}^{\alpha}} \tag{2.47}$$

For the energy asset score, three sets of coefficients for heating, cooling, and fan were developed for each of the 1,020 available weather stations in the U.S. The EUI for each end-use of each site was then normalized using:

$$NormalizedEUI_m^{\alpha} = C_m^{\alpha} \cdot EUI_m^{\alpha} \tag{2.48}$$

where, α is the end-use (space heating, space cooling, or fan) and *i* is the site number.

This method resulted in the reduction of the variations of the energy consumption in each climate zone and allowed for a fair comparison of the building energy performance that was normalized for the weather-related parameters in different locations.

The utilization of this methods required the available climate coefficients for the location or coefficients that are extrapolated from nearby locations. This method was developed based on TMY3 weather files, therefore the proposed climate coefficients may not necessarily agree with the coefficients from an actual weather file. While this method captures the variations due to the weather-related parameters, there is the limitation that this method requires the data in different locations to calculate the adjustments for each location. Also, development of new coefficients requires a large number of simulations to achieve the normalization for each site.

2.5.5. Summary of the Weather-Normalization Methods for Building Energy Consumption

Use of the previously-developed weather-normalization methods allows one to account for the weather-related influences on the energy consumption of buildings in different locations. The degree day method is a widely used method that is currently the main basis for the climate classification in ASHRAE Standard 169-2013 (ASHRAE, 2013a), which is used in ASHRAE Standard 90.1-2016 (ASHRAE, 2016) and ASHRAE 189.1-2018 (ASHRAE, 2018). However, there are several limitations in the degree day method:

- First, the degree day method does not fully account for all influential weather parameters (e.g., solar radiation, humidity, and wind).
- Second, defining the optimal base temperature requires detailed information about the building thermal configurations, which is not always known for a given building at certain location.

- Third, the degree day method does not account for the varying performance of a building's heating and cooling equipment during each day.
- Fourth, while there has been previous research addressing varying internal gains, a diurnal variation of the heat loss coefficient that includes sol-air and wind speed variables cannot be accounted for in the degree day method.

Different studies have proposed various methods to increase the accuracy of the estimation of building heating and/or cooling energy consumption using the conventional degree days. These methods include the modifications in the degree day calculation by including more weather-related parameters (e.g., solar radiation, humidity, wind speed, etc.) and/or geometrical features of buildings. While overall the correlations of the proposed methods show improved results compared to the results of the conventional degree day, in these studies the results were for certain cases with designated base temperatures, which can be different for other building types. Therefore, it limited their application in climate classification where the method should account for various building types without having the geometrical information of the buildings.

Another shortcoming is where new methods show better results in specific periods of time while in other periods, the conventional degree day method shows better estimations. In addition, various studies have proposed site-specific correction factors. However, the development of new correction factors for the weather data that does not have a correction factors require simulating buildings for all other weather files. Also, not all the previous methods were tested for the impact of various end-uses. Therefore, while they have a slight improvement in one end-use, there may be no guarantee to have improved predictions in other end-uses. Finally, adding more variables, which is the case in a considerable number in the proposed new methods, can introduce more complexities and can add to uncertainties if the data is not available

with the preferred resolution. Therefore, there is a need for an improved degree day method that accounts for influential weather parameters on building energy consumption, maintains the improved accuracy for different base temperatures, and can be easily applied for each location.

CHAPTER III

METHODOLOGY

This chapter illustrates the new methodology used in this dissertation. The description includes the general specifications of the DOE medium office prototype models for ASHRAE Standard 90.1-2016. In addition, it includes the procedures used for the simulation and analysis. Finally, the procedure used for applying the new weather normalization is provided.

3.1.General Specifications of the ASHRAE Standard 90.1-2016 Medium Office Prototype Models

In the U.S., the Building Energy Codes Program of the U.S. Department of Energy supports the development, adoption, and implementation of building energy standards and codes. To support the U.S. Department of Energy Building Energy Codes Program PNNL developed a suite of prototype buildings covering 80% of the commercial building floor area in the United States for new construction, including medium office buildings, across all U.S. climate zones. The Standard 90.1 medium office prototype building models, retrieved from the Building Energy Codes Program of the U.S. Department of Energy (DOE, 2018), were used to carry out this analysis. In this analysis seventeen prototype office models were analyzed for each climate zone and subtype across the U.S. Figure 11 shows the 3D view of the DOE medium office prototype building model (left) and a plan view of the thermal zoning (right).

3.1.1. Geometry and Envelope Configurations

The DOE medium office building prototypes are three-story models with the length of 163.8 ft, width of 109.2 ft, and the total conditioned floor area of 53,600 ft^2. The floor-to-floor height is 13 ft and the floor-to-ceiling height is 9 ft. The Window-to-Wall Ratio (WWR) is 33% for each exterior wall. The model includes six exterior doors, two doors on the south side, two doors on the north side, one door on the east side, and one door on the west side. Table 1 and Table 2 show the gross area and general specifications of the ASHRAE Standard 90.1-2016 medium office prototypes. Figure 13 through Figure 18 show the schedules of lighting, equipment, elevator, fan, heating set-point, and cooling set-point of the ASHRAE Standard 90.1-2016 medium office, respectively.

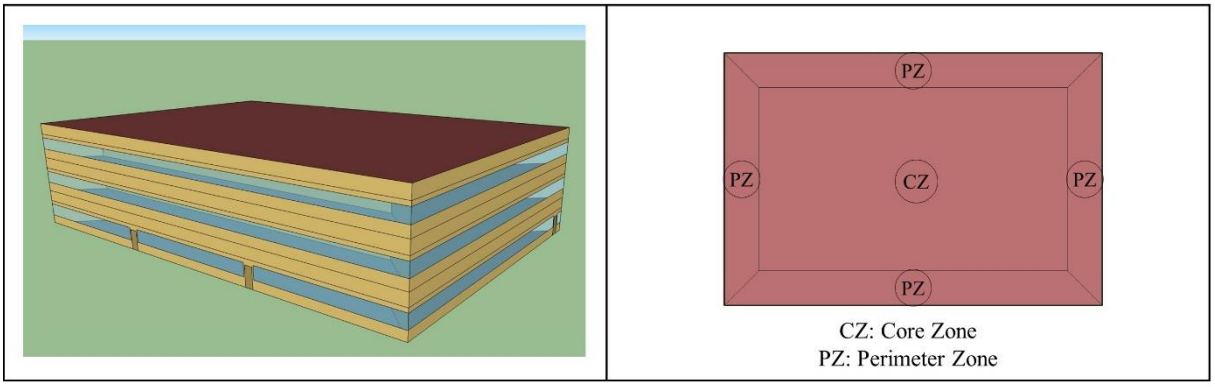

Figure 11: DOE Medium Office Prototype Model; Left: 3D View of the Building Model; Right: Plan View of the Thermal Zoning (DOE Medium Office Prototype Models (DOE, 2018))

Table 1: Gross Areas of the ASHRAE Standard 90.1-2016 Medium Office Prototypes (Data Retrieved from DOE Medium Office Prototype Models (DOE, 2018))

Location	Gross Wall Area	Gross Roof Area	Window Opening Area	Window-Wall Ratio
	[ft^2]	[ft^2]	[ft^2]	[%]
North and South	6386		2107	33
East and West	4257		1405	33
Total	21287	17876	7025	33

Table 2: General specifications of the ASHRAE Standard 90.1-2016 Medium Office Prototypes (Data retrieved from DOE Medium Office Prototype Models (DOE, 2018))

Zone Location			Area	Part of Total Floor Area	Volume	Gross Wall Area	Window Glass Area	Lighting	People	Plug and Process
			[ft^2]	(Y/N)	[ft^3]	[ft^2]	[ft^2]	[W/m2]	[m^2/person]	[W/m2]
Core Zones	First Floor		10587	Yes	95280	0	0	0.79	18.58	3.79
	Second Floor		10587	Yes	95280	0	0	0.79	18.58	0.75
	Third Floor		10587	Yes	95280	0	0	0.79	18.58	0.75
Perimeter Zones	First Floor	South Zone	2232	Yes	20086	1474	702	0.79	18.58	0.75
		East Zone	1413	Yes	12716	983	468	0.79	18.58	0.75
		West	2232	Yes	20086	1474	702	0.79	18.58	0.75
		North	1413	Yes	12715	983	468	0.79	18.58	0.75
	Second Floor	South Zone	2232	Yes	20086	1474	702	0.79	18.58	0.75
		East Zone	1413	Yes	12716	983	468	0.79	18.58	0.75
		West	2232	Yes	20086	1474	702	0.79	18.58	0.75
		North	1413	Yes	12715	983	468	0.79	18.58	0.75
	Third Floor	South Zone	2232	Yes	20086	1474	702	0.79	18.58	0.75
		East Zone	1413	Yes	12716	983	468	0.79	18.58	0.75
		West	2232	Yes	20086	1474	702	0.79	18.58	0.75
		North	1413	Yes	12715	983	468	0.79	18.58	0.75
Plenums	First Floor		17876	No	71504	2183	0	0.00	0.00	0.00
	Second Floor		17876	No	71504	2183	0	0.00	0.00	0.00
	Third Floor		17876	No	71504	2183	0	0.00	0.00	0.00
Total			53628		482650	14738	7025	0.79	18.58	1.35

3.1.2. Schedules

This section represents the schedules used in the DOE medium office prototype models. The schedules include occupancy (Figure 12), lighting (Figure 13), equipment (Figure 14), elevator (Figure 15), fan (Figure 16), heating setpoint (Figure 17), and cooling setpoint (Figure 18). Each of these figures represent the corresponding schedules for weekdays and weekends (which were also used for the holidays and all other days not defined in other categories), as well as the schedules for summer and winter design days, which are used for sizing the HVAC system.

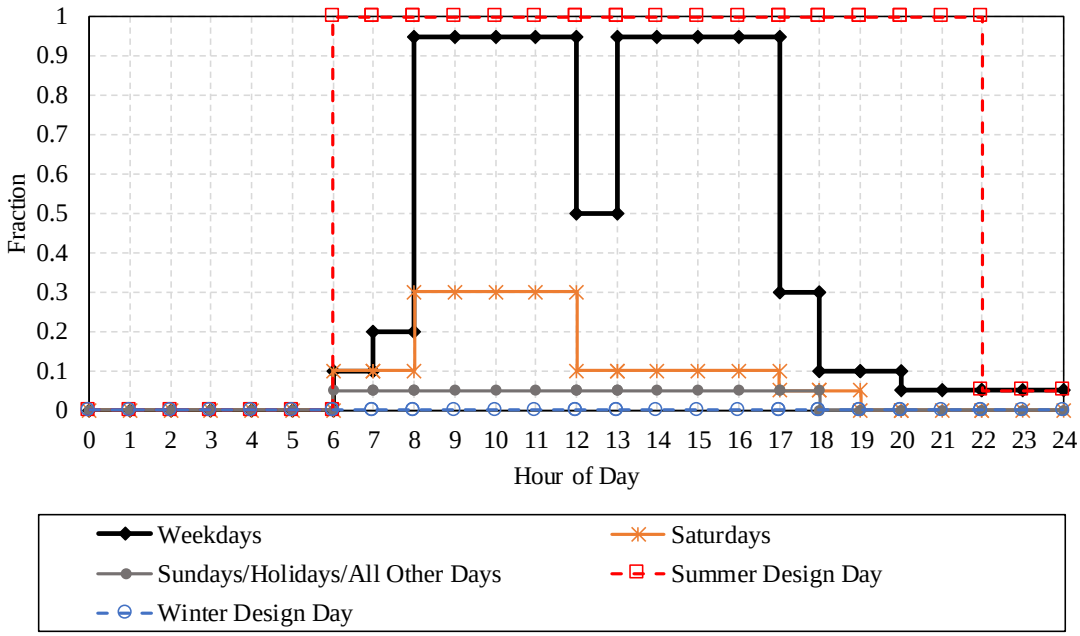

Figure 12: Occupancy Schedule of the ASHRAE Standard 90.1-2016 Medium Office Prototype Models (Data Retrieved from the DOE Medium Office Prototype Models (DOE, 2018))

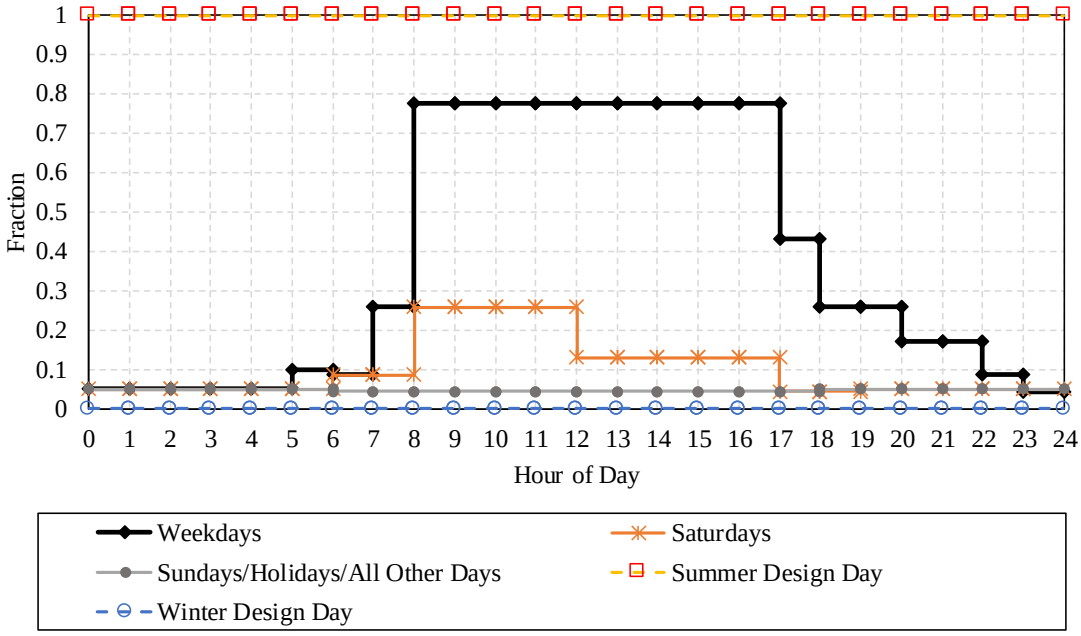

Figure 13: Lighting Schedule of the ASHRAE Standard 90.1-2016 Medium Office Prototype Models (Data Retrieved from the DOE Medium Office Prototype Models (DOE, 2018))

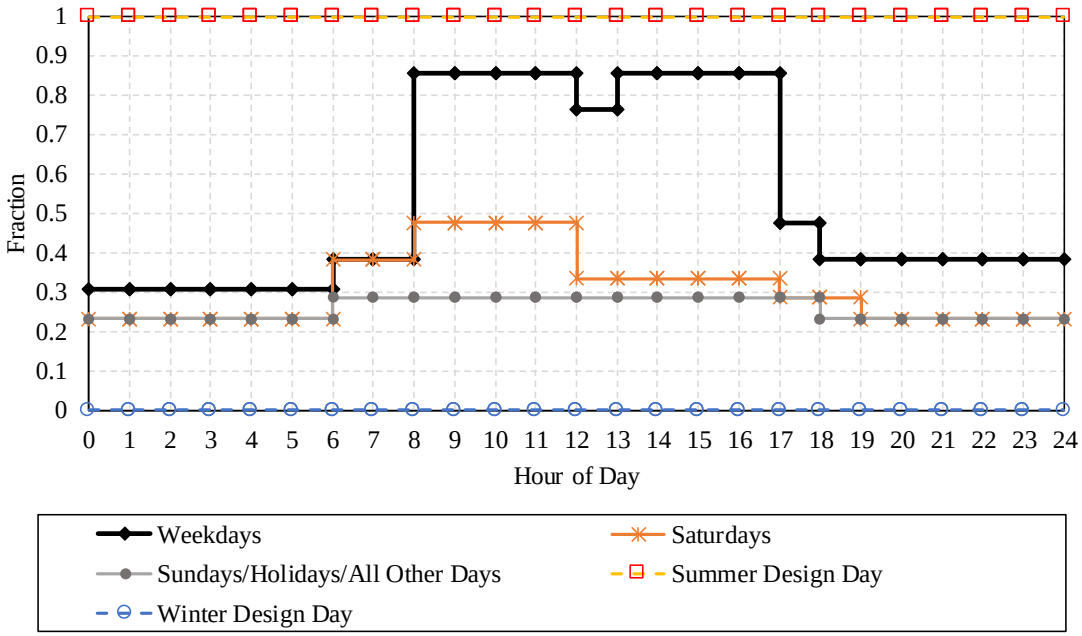

Figure 14: Equipment Schedules of the ASHRAE Standard 90.1-2016 Medium Office Prototype Models (Data Retrieved from the DOE Medium Office Prototype Models (DOE, 2018))

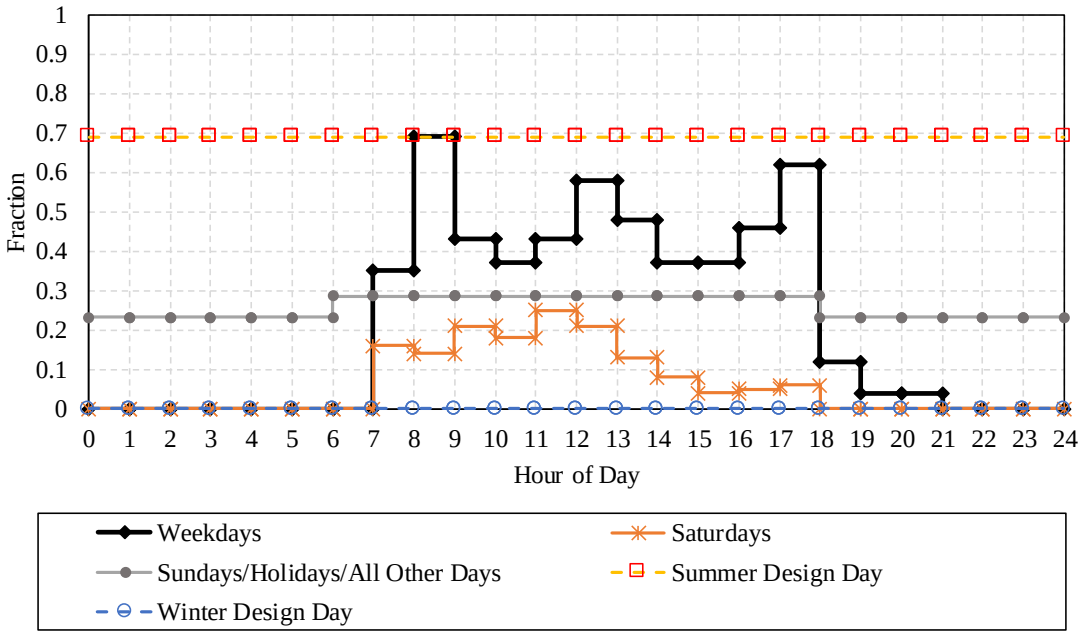

Figure 15: Elevator Schedules of the ASHRAE Standard 90.1-2016 Medium Office Prototype Models (Data Retrieved from the DOE Medium Office Prototype Models (DOE, 2018))

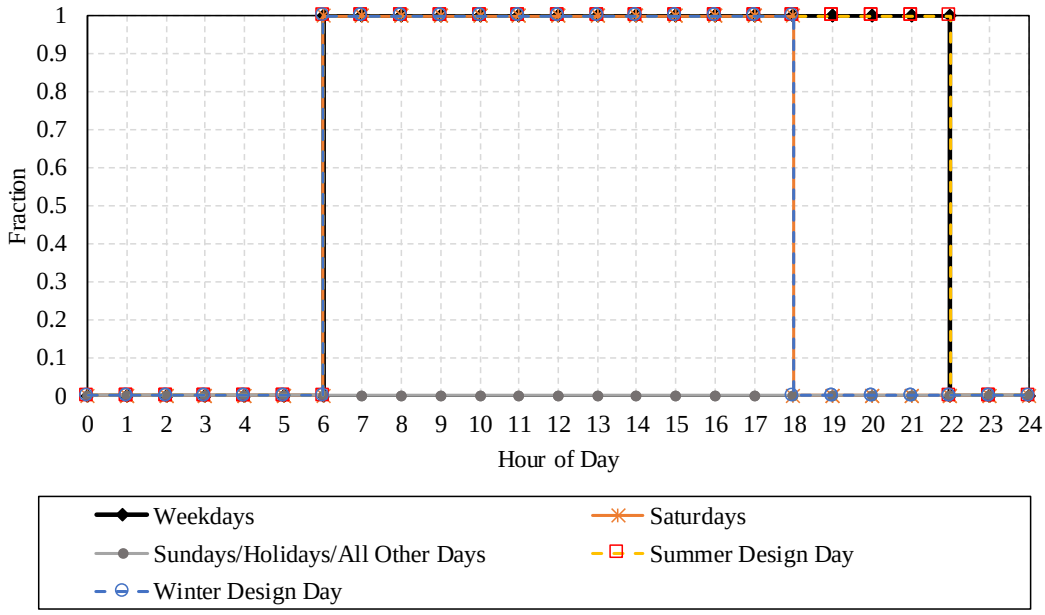

Figure 16: Fan Schedules of the ASHRAE Standard 90.1-2016 Medium Office Prototype Models (Data Retrieved from the DOE Medium Office Prototype Models (DOE, 2018))

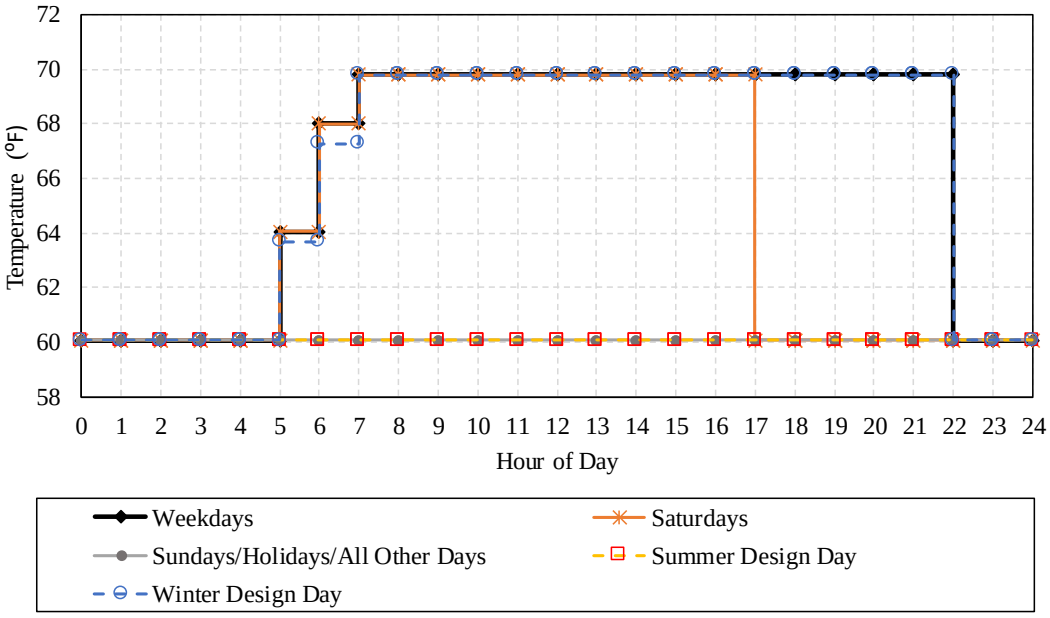

Figure 17: Heating Setpoint Schedule of the ASHRAE Standard 90.1-2016 Medium Office Prototype Models (Data Retrieved from the DOE Medium Office Prototype Models (DOE, 2018))

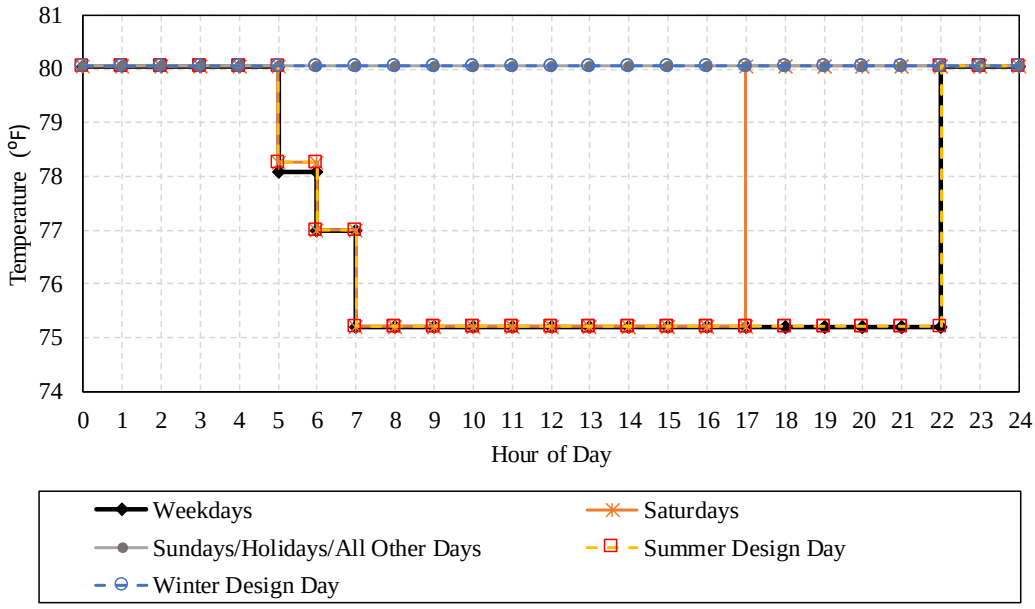

Figure 18: Cooling Setpoint Schedule of the ASHRAE Standard 90.1-2016 Medium Office Prototype Models (Data Retrieved from the DOE Medium Office Prototype Models (DOE, 2018))

3.1.3. HVAC Systems Configurations

The HVAC system consists of a packaged air-conditioning unit as the cooling system type and a gas furnace as the heating system type. The distribution and terminal units include Variable Air Volume (VAV) terminal box with dampers and an electric reheating coil. The service water temperature setpoint is 140 ^{0}F, and has a 100 gallon storage tank. Equation 3.1 shows the total capacity of the direct expansion coil as a function of cooling coil inlet air temperature.

$$Total\ Cooling\ Capacity = 1.39072 - 0.05291 \cdot T_{wb,i} + 0.001842 \cdot T_{wb,i}^2 + 0.000583 \cdot T_{c,i} - 0.00019 \cdot T_{c,i}^2 + 0.000265 \cdot T_{wb,i} \cdot T_{c,i} \quad (3.1)$$

where, $T_{wb,i}$ is the cooling coil inlet air wet-bulb temperature (ºC) and $T_{c,i}$ is the outdoor condenser inlet air dry-bulb temperature (ºC).

3.1.4. Energy Efficiency Measures and Daylight Responsive Controls

The energy efficiency measures include daylight responsive controls that were implemented in the perimeter zones of the medium office prototype model. In these measures stepped lighting controls with 3-steps were implemented in the perimeter zones. Each perimeter zone included two daylight reference points; one for primary sidelighted area and the second one for secondary sidelighted area. The fraction of the zone controlled by the daylight reference points for primary sidelighted area and primary sidelighted area are 38.35% and 13.95% of the area of the zone, respectively. The illumination setpoint for all the daylight reference point was set to 375 lux (35 fc).

3.2. Split-Degree Days

In the degree day method, the overall heat transfer coefficient, the area, and the degree days are used in the calculation of the energy consumption (equation 3.2). However, in this method the heat transfer coefficient and the temperature difference vary in each time step. Figure 19 provides an example of the steady-state resistances in a multilayer wall and equation 3.3 shows the equation of the overall heat transfer coefficient. Since the surface convective heat transfer varies in each time-step, the overall heat transfer coefficient also varies. The temperature difference also varies based on the fluctuations in outdoor temperature for a fixed indoor temperature. These variations cause inaccuracies in the estimated energy consumption using the

conventional degree day method. Therefore, there is a need to define a more accurate accounting procedure that accounts for these variations.

One such procedure would be a split-Heating Degree Day (sHDD) and split-Cooling Degree Day (sCDD). The sHDD and sCDD are defined as shown in Figure 20 and Figure 21, respectively, in which the calculation of the sHDD and sCDD are shown for three days. In Figure 20 and Figure 21, typical sinusoidal daily temperature profile that constantly increases over three consecutive days is presented as an example to show different scenarios (i.e., Day 1, Day 2, Day3). In Figure 20 and Figure 21 each day is divided into two sections. The first section represents the beginning of the day up until hour *n* and the period of the day from hour *m* until the end of the day, where hour *n* and hour *m* represent the beginning and end of a symmetrical period around the peak daily temperature. The second section of the day represents the period from hour *n* to hour *m*. In Day 1, the average of both the split sections (i.e., section 1 and 2) are lower than the base temperature. In Day 2, the average of split section 1 is lower than the base temperature while the average of section 2 is higher than the base temperature. In Day 3, the average of both split sections (i.e., section 1 and 2) are higher than the base temperature.

Equations 3.4 and 3.5 denote the calculation of the sHDD and sCDD, respectively, where the same approach in the calculation of the degree day is applied to two intervals within one day, one interval between hour *n* and *m* ($1 \leq n, m \leq 24$), denoted as $\{n,m\}$, and the other interval for the complement hours of the day, represented as $\{n,m\}^{'}$.

$$Q_d = 24 \cdot U \cdot A \cdot DD \tag{3.2}$$

Where, *U* is the overall heat transfer coefficient, *A* is the area, and *DD* is the degree day.

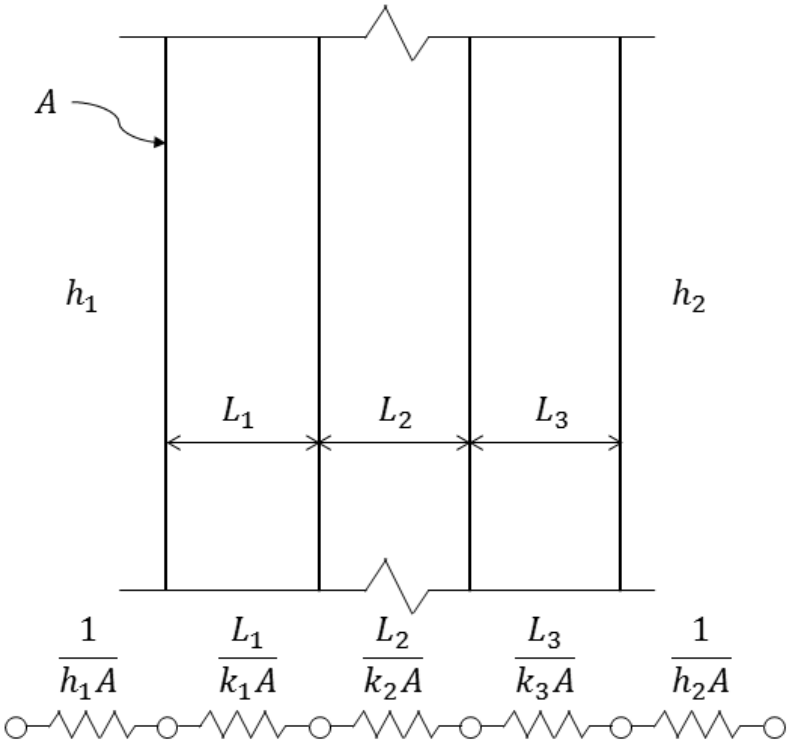

Figure 19: Representation of Steady-State Thermal Resistances in a Multilayer Wall (Adopted from Incropera et al. (2007))

$$U = \frac{1}{\frac{1}{h_1} + \sum_i \frac{L_i}{k_i} + \frac{1}{h_2}} \tag{3.3}$$

where, h_1 and h_2 are the convective/radiative heat transfer coefficients of the two sides of the wall, L is the thickness and k is the thermal conductivity of the material layer i.

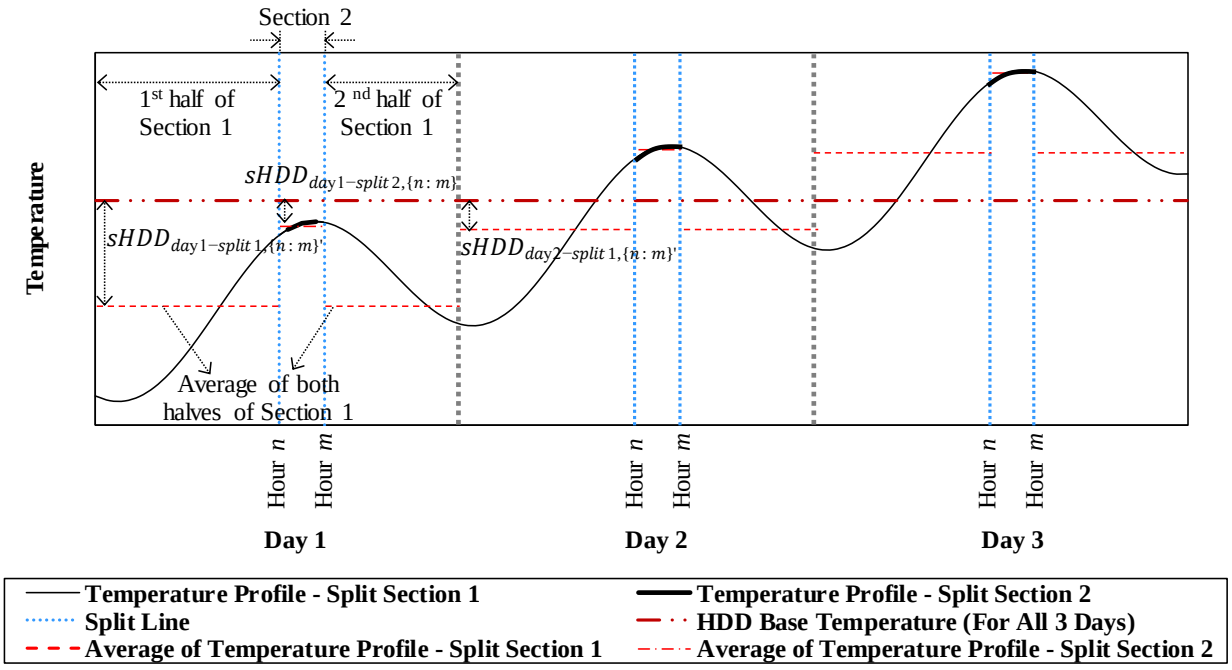

Figure 20: Representation of the sHDD

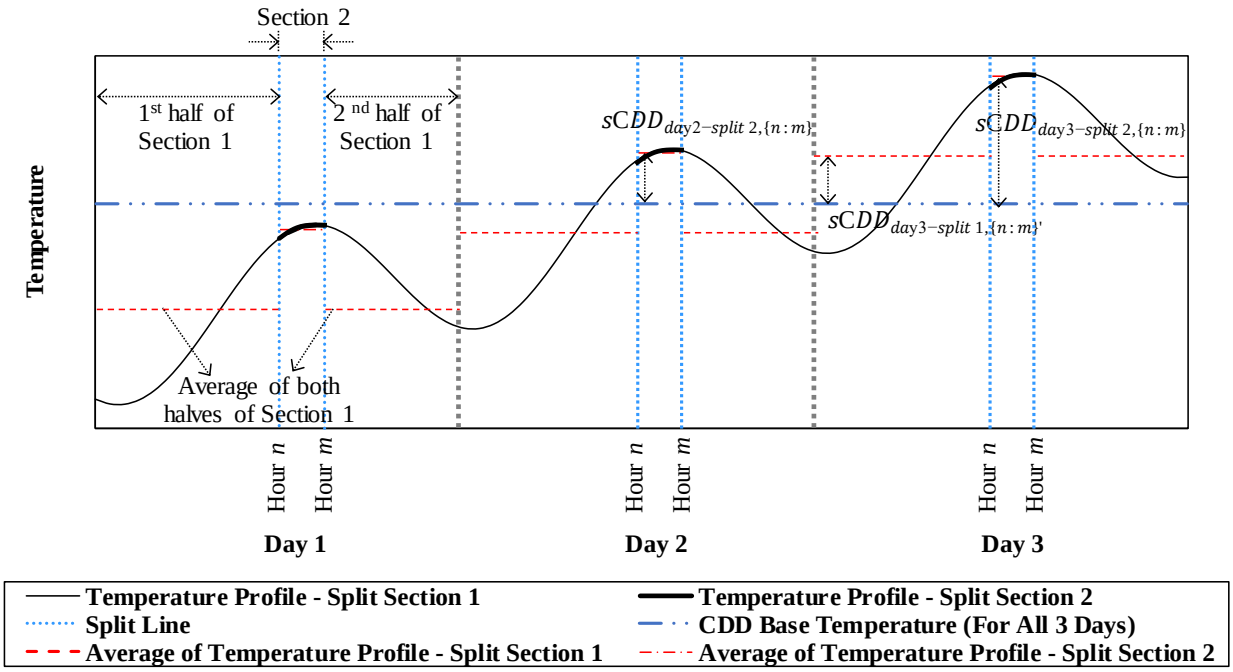

Figure 21: Representation of the sCDD

$$sHDD_{daily-split\ 1,\{n:\ m\}} = \left(T_{base,HDD} - \frac{T_{\{n\ :m\},max} + T_{\{n\ :m\},min}}{2}\right)^{+}$$

$$sHDD_{daily-split\ 2,\{n:\ m\}'} = \left(T_{base,HDD} - \frac{T_{\{n\ :m\}',max} + T_{\{n\ :m\}',min}}{2}\right)^{+} \quad (3.4)$$

where, $T_{base,HDD}$ is the base temperature for HDD, which is assumed to be 18°C.

$$sCDD_{daily-split\ 1,\{n:\ m\}} = \left(\frac{T_{\{n\ :m\},max} + T_{\{n\ :m\},min}}{2} - T_{base,CDD}\right)^{+}$$

$$sCDD_{daily-split\ 2,\{n:\ m\}'} = \left(\frac{T_{\{n\ :m\}',max} + T_{\{n\ :m\}',min}}{2} - T_{base,CDD}\right)^{+} \quad (3.5)$$

where, $T_{base,CDD}$ is the base temperature for CDD, which is assumed to be 10°C

The annual sHDD and sCDD can then be calculated using equations 3.6 and 3.7.

$$sHDD_{annual-split\ 1,\{n:\ m\}} = \sum_{i=1}^{365}\left(T_{base,HDD} - \frac{T_{n_{\{n\ :m\}},max} + T_{n_{\{n\ :m\}},min}}{2}\right)^{+}$$

$$sHDD_{annual-split\ 2,\{n:\ m\}'} = \sum_{i=1}^{365}\left(T_{base,HDD} - \frac{T_{i_{\{n\ :m\}'},max} + T_{i_{\{n\ :m\}'},min}}{2}\right)^{+} \quad (3.6)$$

$$sCDD_{annual-split\ 1,\{n:m\}} = \sum_{i=1}^{365}\left(\frac{T_{i_{\{n:m\}},max} + T_{i_{\{n:m\}},min}}{2} - T_{base,CDD}\right)^{+}$$

$$sCDD_{annual-split\ 2,\{n:m\}'} = \sum_{i=1}^{365}\left(\frac{T_{i_{\{n:m\}'},max} + T_{i_{\{n:m\}'},min}}{2} - T_{base,CDD}\right)^{+} \quad (3.7)$$

In the split-degree days methods similar procedure for the degree days calculation is applied for two time spans during the day. Therefore, the split-degree days include more information about the diurnal temperature range compared to the degree days. Also, separate heat loss coefficients can be calculated for the two time spans. Similar to the calculation of the daily energy consumption using the degree days method (equation 3.2), the daily energy consumption can be calculated using the split-degree days as shown in equation 3.8.

$$Q_d = n_{split1} \cdot U_{split1} \cdot A \cdot DD_{split1} + n_{split2} \cdot U_{split2} \cdot A \cdot DD_{split2} \quad (3.8)$$

where, n_{split1} and n_{split2} are the number of hours in each of the time spans, U_{split1} and U_{split2} are the overall heat transfer coefficients in the two daily time spans, A is the area, DD_{split1} and DD_{split1} are the HDD or CDD of the two daily time spans.

Due to the thermal storage effect in buildings, the energy consumption in a building in each of the two time spans during a day may require accounting for the energy use in previous intervals. This effect may be more pronounced for smaller time intervals within each time span. Such dependence between the two variables can be included using the interaction term in a regression model. Equation 3.9 shows the calculation of the daily energy consumption including an interaction term.

$$Q_d = n_{split1} \cdot U_{split1} \cdot A \cdot DD_{split1} + n_{split2} \cdot U_{split2} \cdot A \cdot DD_{split2} + c \cdot DD_{split1} \cdot DD_{split2} \quad (3.9)$$

where, *c* is a factor to control the impact of the interaction term.

The annual energy consumption can be calculated using equation 3.10 by summing the daily energy consumptions over the period of a year.

$$Q_a = \sum_{i=1}^{365} (n_{split1} \cdot U_{split1} \cdot A \cdot DD_{split1}(i) + n_{split2} \cdot U_{split2} \cdot A \cdot DD_{split2}(i)) \quad (3.10)$$

The daily heating and cooling energy consumption can be calculated using equations 3.11 and 3.12, respectively.

$$Q_{h,d} = \frac{n_{split1}.K_{t1}.sHDD_{split1} + n_{split2}.K_{t2}.sHDD_{split2}}{\eta_h} \quad (3.11)$$

where, K_{t1} and K_{t2} are the total heat loss coefficients of the building in the two time-spans and η_h is the Annual Fuel Use Efficiency (AFUE) of the heating system.

$$Q_{c,d} = \frac{n_{split1}.K_{t1}.sCDD_{split1} + n_{split2}.K_{t2}.sCDD_{split2}}{COP} \quad (3.12)$$

where, *COP* is the coefficient of performance of the cooling system.

3.3. Prediction of the Annual Energy Consumption by Regression Models Using Degree Day Methods

The energy consumption of a building can be estimated using ambient temperature (Figure 22). Similarly, degree days can be used to estimate the energy consumption of a building. Equations 3.14 and 3.15 show the estimation of building heating and cooling energy consumption, respectively, where the coefficients are derived from a regression model based on measured or simulated data. In a similar fashion to the estimation of heating and cooling energy use, the total energy consumption can be estimated using the HDD and CDD (equation 3.15). APPENDIX A provides the discussions for developing simple and multiple linear regression models as well as calculating the coefficients of determination.

$$Q_{h,p} = \beta_{h,0} + \beta_{h,1} \cdot HDD_p \tag{3.13}$$

where, p is the period of time, $\beta_{h,0}$ is the constant and $\beta_{h,1}$ is the slope of the model derived from the regression analysis.

$$Q_{c,p} = \beta_{c,0} + \beta_{c,1} \cdot CDD_p \tag{3.14}$$

where, $\beta_{c,0}$ and $\beta_{c,1}$ are the constant and slope of the model derived from the regression analysis.

$$Q_{t,p} = \beta_{t,0} + \beta_{t,1} \cdot HDD_p + \beta_{t,2} \cdot CDD_p \tag{3.15}$$

where, $\beta_{t,0}$, is the constant and $\beta_{t,1}$ and $\beta_{t,2}$ are the slopes of the model derived from the regression analysis.

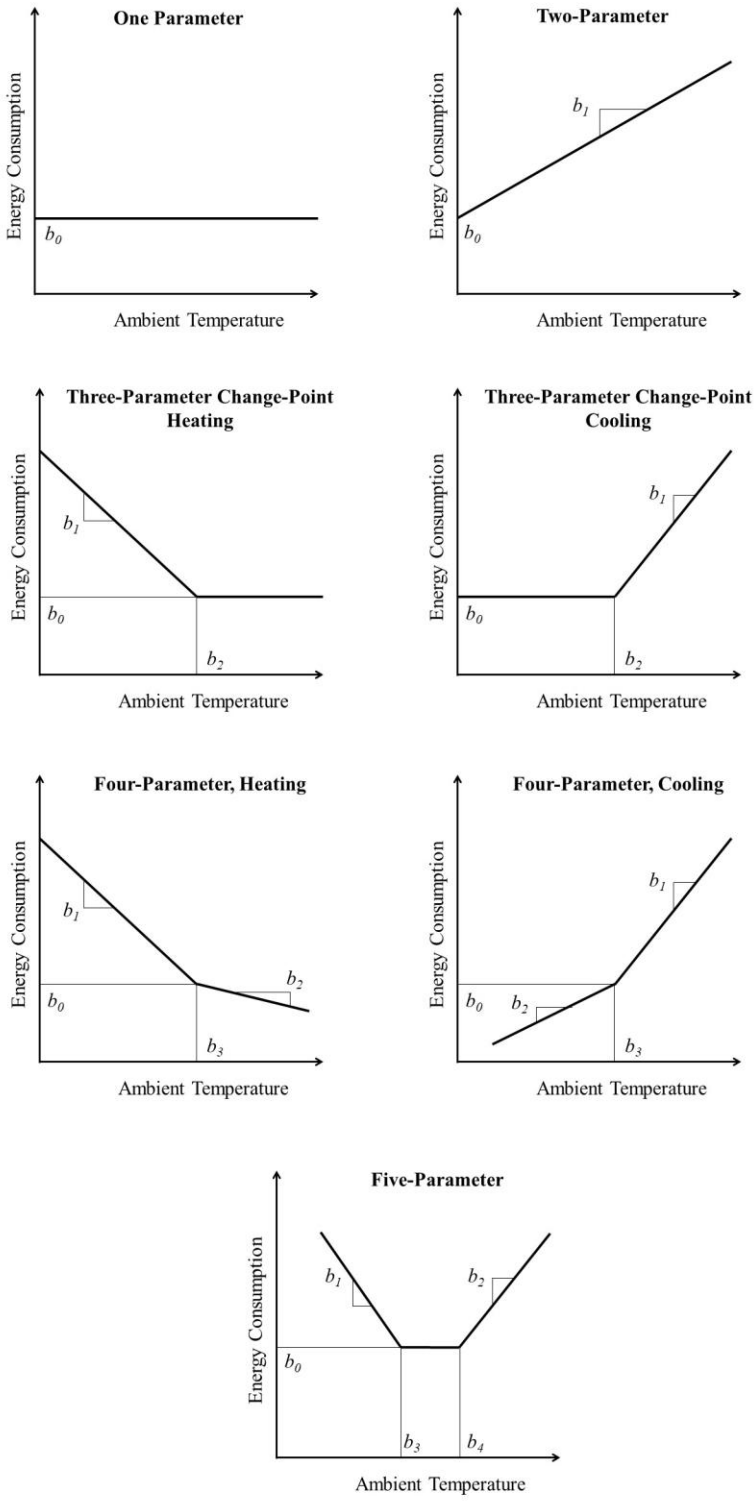

Figure 22: Estimation of Building Energy Consumption Using linear and Change-Point Linear Models with Ambient Temperature (ASHRAE, 2002)

3.4. Simulations and Analysis Procedure

This section describes the procedure for the simulations and analyses carried out in this study. It also describes the format for the representation of the results.

3.4.1. Simulation Procedure

This section describes the different steps for the building energy simulations that used the ASHRAE Standard 90.1-2016 medium office prototype models with and without daylight-responsive controls, and the ASHRAE Standard 90.1-2004 medium office prototype models (without daylighting) as the baseline buildings for this study where 2004 was defined as the baseline in the ASHRAE Standard 90.1-2016.

The procedure for the preparation of the building energy simulation models, and the post-processing analysis of the results can be divided into three main parts. As shown in Figure 23, these three parts are: data collection, pre-processing of building energy simulation models, and the simulation and post-processing. The preparation, simulation, and extraction of the results are carried out using a custom Python 3.7.0 script.

3.4.1.1. Data Collection

There are several tasks in data collection section, including: retrieving the medium office prototype models; weather files and the design day files; calculation of the CDD and HDD for each weather file; retrieving the subtype from ASHRAE Standard 169-2013; and generating a master list that lists the weather file name, design day file name, and climate zone and subtype for each location.

In order to quantify the variations of the energy consumption and energy savings in different climates, 801 simulations were carried out using the available EnergyPlus Weather Files (EPW) that have corresponding Design Day Files (DDY) for the cities in the U.S. Seventeen ASHRAE Standard 90.1-2016 medium office prototypes and seventeen ASHRAE Standard 90.1-2004 medium office prototypes were retrieved from the DOE Website (DOE, 2018). Also, 1,030 available TMY3-EPW were retrieved from the EnergyPlus weather data online source (DOE-NREL, 2018), of the 1,030 available TMY3-EPW files 801 EPW files that had available Design Day files (DDY) were selected across the continental U.S. to carry out the analysis. Figure 24 shows the number of the weather files selected in each climate zone.

The moisture classification was retrieved from the ASHRAE Standard 169-2013 (ASHRAE, 2013a), which classifies locations in climate zones 1 to 6 into different moisture regimes. Moist, dry, and marine moisture classification are defined as subtype A (moist), B (dry), and C (marine), respectively. Finally, a master list was generated that includes the EPW and DDY file names with the corresponding climate zone for each location (APPENDIX B).

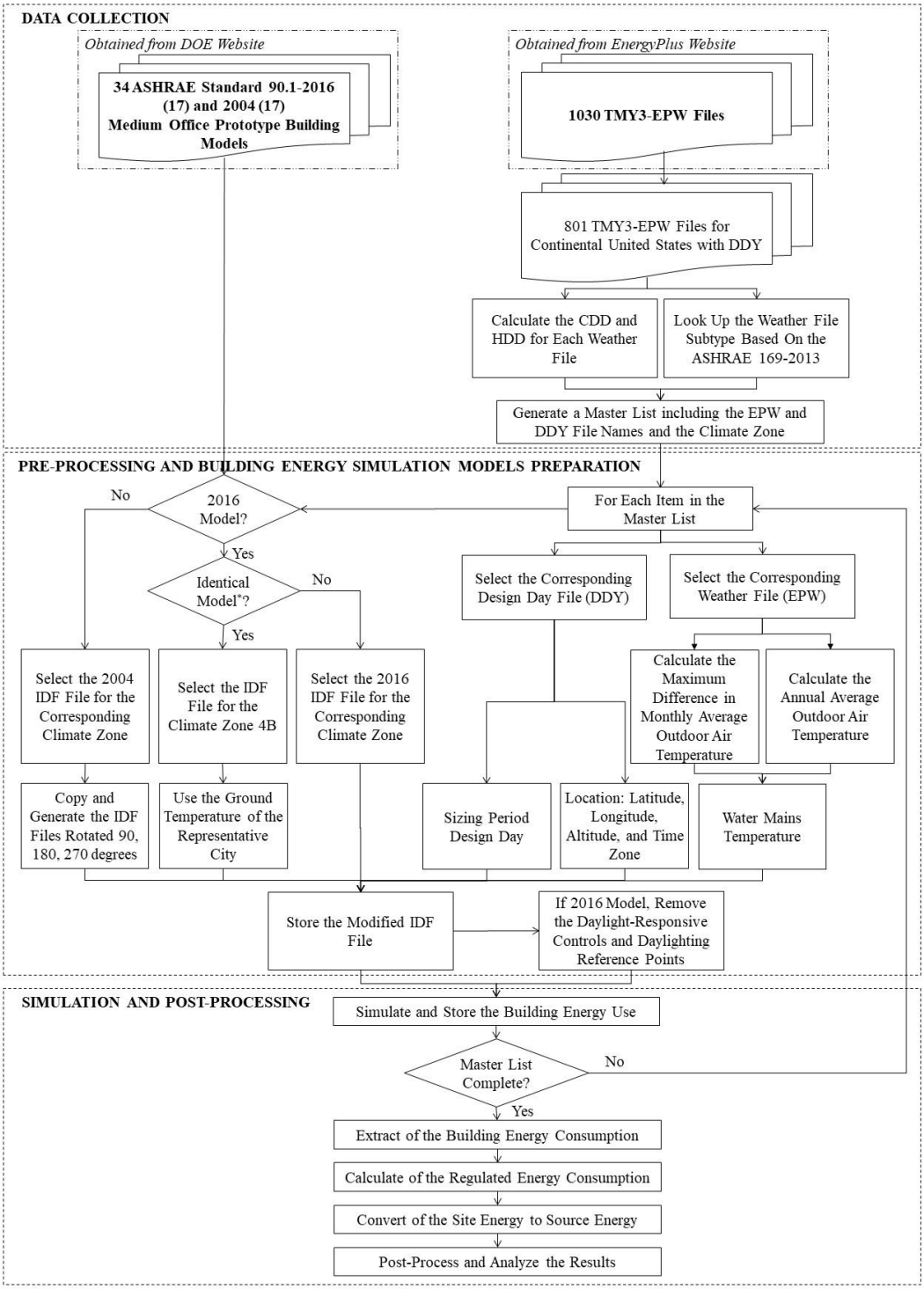

* The identical model refers to both of the following models:
1) The DOE medium office prototype model for ASHRAE Standard 90.1-2016 for climate zone 4B
2) The modified DOE medium office prototype model for ASHRAE Standard 90.1-2016 for climate zone 4B with high thermal mass

Figure 23: Flowchart of the Analysis of the Energy Consumption of ASHRAE Standard 90.1-2016 with and without Daylight Responsive Controls and -2004 Prototype Models

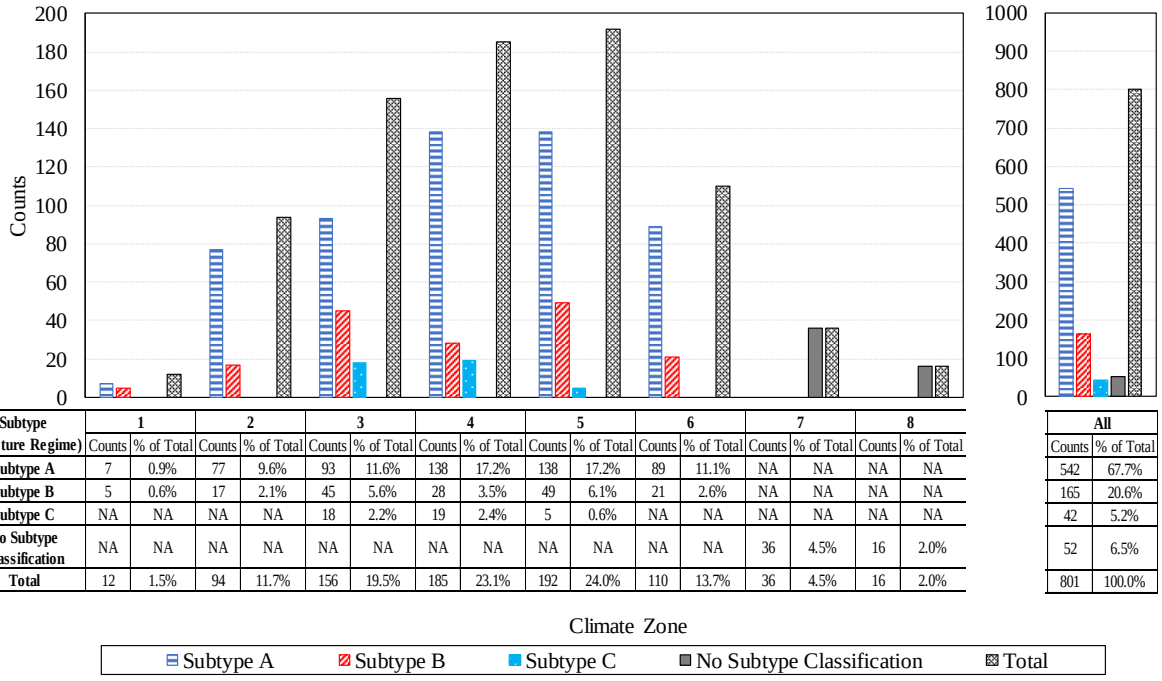

Subtype (Moisture Regime)	1		2		3		4		5		6		7		8		All	
	Counts	% of Total	Counts	% of Total	Counts	% of Total	Counts	% of Total	Counts	% of Total	Counts	% of Total	Counts	% of Total	Counts	% of Total	Counts	% of Total
Subtype A	7	0.9%	77	9.6%	93	11.6%	138	17.2%	138	17.2%	89	11.1%	NA	NA	NA	NA	542	67.7%
Subtype B	5	0.6%	17	2.1%	45	5.6%	28	3.5%	49	6.1%	21	2.6%	NA	NA	NA	NA	165	20.6%
Subtype C	NA	NA	NA	NA	18	2.2%	19	2.4%	5	0.6%	NA	NA	NA	NA	NA	NA	42	5.2%
No Subtype Classification	NA	NA	NA	NA	NA	NA	NA	NA	NA	NA	NA	NA	36	4.5%	16	2.0%	52	6.5%
Total	12	1.5%	94	11.7%	156	19.5%	185	23.1%	192	24.0%	110	13.7%	36	4.5%	16	2.0%	801	100.0%

Figure 24: Number of the Weather Files Selected in Each Climate Zone

For each weather file, the HDD and CDD were calculated using equations 3.16 and 3.17, respectively (ASHRAE, 2013a).

$$HDD = \sum_{n=1}^{365} \left(T_{base,HDD} - \frac{T_{n,max} + T_{n,min}}{2} \right)^{+} \tag{3.16}$$

Where $T_{base,HDD}$ is the base temperature, which is assumed to be 18 ºC (64.4 ºF), and $T_{n,max}$ and $T_{n,min}$ are the maximum and minimum outdoor air dry-bulb temperatures for the nth day of the year.

$$CDD = \sum_{n=1}^{365} \left(\frac{T_{n,max} + T_{n,min}}{2} - T_{base,CDD} \right)^{+} \quad (3.17)$$

Where $T_{base,CDD}$ is the base temperature, which is assumed to be 10°C (50°F), and $T_{n,max}$ and $T_{n,min}$ are the maximum and minimum outdoor air dry-bulb temperatures for the nth day of the year.

3.4.1.2. Pre-Processing of the Building Energy Simulation Models

The simulation for each file required selecting the appropriate medium office prototype model paramers for the corresponding climate zone (e.g., U-value, SHGC, etc.). Also, the simulation model required input for each locations (e.g., location, water mains temperature, design day, etc.) and modifying the model using the weather variables. This process was repeated for the 801 locations in the U.S. The parameters modified included the location, sizing, and water mains temperature.

There are different classes in an EnergyPlus model that include the location, sizing, and water mains temperature parameters. These classes include “Site:Location”, “SizingPeriod:DesignDay”, “Site:WaterMainsTemperature”, and “Site:GroundTemperature:BuildingSurface”.

The “Site:Location” class in EneryPlus, under the “Location and Climate” group, includes the name, latitude, longitude, time zone, and elevation, which were retrieved from the DDY file. These had to be modified for each of the 801 locations.

The “SizingPeriod:DesignDay” class of EnergyPlus is a common method used to provide the required information for performing the sizing simulation. The “SizingPeriod:DesignDay”

included one or more extreme weather conditions for each heating and cooling, typically representing 99.6% or 99% weather conditions, and allows for generating a daily weather profile used for sizing. The design days information for one heating day and one cooling day were retrieved from the corresponding DDY file and inserted in the EnergyPlus file for each location.

The "Site:WaterMainsTemperature" is another class that had to be modified for each weather station. The "Site:WaterMainsTemperature" includes annual average outdoor air temperature and maximum difference in monthly average outdoor air temperature. These values were calculated for each weather file using the hourly outdoor dry-bulb temperatures provided in the weather file. These values should be modified for all 801 locations as the water mains temperature impacts the energy consumption in a building.

It should also be mentioned that the "Site:GroundTemperature:BuildingSurface" class, which is specially used for the surfaces that are in contact with the ground, depends on the local weather information and can differ significantly in different locations. Although weather files include the "undisturbed" ground temperature, which represents the ground temperature for each month, these values are significantly different from the ground temperature under the conditioned building zones. Therefore, in this study the monthly ground temperature for each representative city in the seventeen climate zones and subtypes (i.e., 1A, 1B, etc.) were used for the simulation of all the models in that climate zone and subtype.

In order to analyze the impact of weather variables on the building total regulated energy consumption of the buildings in different climates, a set of simulations was carried out using an identical prototype model, the ASHRAE Standard 90.1-2016 Medium Office Prototype Model for climate zone 4B, for all climate zones to remove the impact of varying parameters in the prototype models. The preparation of the models for the simulation was the same as the process

described for the ASHRAE Standard 90.1-2016 Medium Office Prototype Models, in which the models complied with the requirements for each climate zone. The "Site:GroundTemperature:BuildingSurface" provided in the prototype model for the corresponding climate zone was used for the simulation.

Therefore, the parameters related to the location and weather (e.g. location, water mains temperature, sizing, and ground temperature) were modified for each location.

After the building model was modified for each weather location, a set of 801 EnergyPlus files was generated by removing the daylighting controls and reference points from the models to perform the simulations without daylight-responsive controls, leaving all other variables the same.

The ASHRAE Standard 90.1-2004 medium office prototypes were used in the analysis related to the performance path. It should be mentioned that since the ASHRAE Standard 90.1-2004 does not require the implementation of the daylight-responsive controls, the 2004 version of the medium office prototype models does not have daylight-responsive controls.

3.4.1.3. Simulation and Post-Processing

In this step, first the models with and without daylight-responsive controls were simulated using EnergyPlus and the corresponding EPW file for the 801 locations. Then, the annual electricity and natural gas consumption for the different end-uses was extracted from the output from each simulation. The regulated energy consumption was calculated by summing the total electricity and natural gas energy consumptions except for interior equipment. The site energy was converted to source energy using the 3.167 and 1.084 multipliers for the electricity

and natural gas, respectively (ICC, 2018). Overall, the following simulations were carried out in this study:

- 801 simulations using code-compliant 2016 DOE medium office prototype models, complied with the requirements for each location
- 801 simulations using 2016 DOE medium office prototype models without daylight responsive controls
- 801 simulations using an identical 2016 DOE medium office prototype model
- 801 simulations using an identical 2016 DOE medium office prototype model with high-thermal mass
- 801 simulations using an identical 2016 DOE medium office prototype model with 24 hour operating schedule
- 3204 (4 × 801) simulations using code-compliant 2004 DOE medium office prototype models, rotated 0, 90, 180, and 270 degrees, complied with the requirements for each location.

3.4.2. Analysis of the efficiency of the algorithm

In order to compare the efficiency of the algorithms, a function can be used to map the size of the input to the number of execution steps (time complexity) or the amount of memory required for the algorithm (space complexity) (Knuth, 1998).

The big O notation is an asymptotic analysis that is used to quantify the time complexity of an algorithm by estimating the upper-bound of an algorithm's runtime and to show how the processing time of an algorithm changes as the problem size becomes sufficiently large (Dasgupta et al., 2006). Given the functions $f : \mathbb{R} \to \mathbb{R}$, and $g : \mathbb{R} \to \mathbb{R}$, $f(x) = O(g(x))$, if and

only if there exists a positive constant M and a constant x_0, such that the $|f(x)| \leq M \cdot |g(x))|$ for $x \geq x_0$.

3.4.3. Analysis of the Impact of Schedules

The ASHRAE Standard 90.1-2016 and 90.1-2004 medium office prototype models used the typical office schedules. In order to analyze the impact of the operating schedule on the results, the schedules of the ASHRAE Standard 90.1-2016 medium office prototype models are modified to represent a 24-hours operation schedule for the 801 simulations.

In order to modify the model to represent 24-hour operating schedule, temperature set-points and different schedules were modified to have a flat value for all 24 hours of the day, during the whole year. The maximum values used in the typical office operating hours were used in the 24-hours models. The heating and cooling set-points were set to 21 °C and 24 °C, respectively. The schedules that were changed include: the HVAC operation schedule was set to 1, the lighting schedule was set to 0.776, the equipment schedule was set to 0.858, the occupancy schedule was set to 0.950, the elevator schedule was set to 0.690, the minimum outdoor air motorized damper schedule was set to 1, and all the infiltration schedules were set to 1.

3.4.4. Analysis of the Impact of Thermal Mass

To analyze the accuracy of the estimations of the conventional degree days and the split-degree days, a set of 801 simulations were carried out using an identical simulation model that has higher thermal mass compared to the DOE medium office prototype models. The modified model has the same specifications compared to the DOE medium office prototype model compliant with the requirements for the ASHRAE Standard 90.1-2016 for climate zone 4B,

except the changes mentioned in Table 3. Layers shown in bold and italic in Table 3 indicate the modified or added materials. The properties for the materials mentioned in Table 3 are provided in Table 4.

Table 3: Comparison of the Modified Building Components

	Layers	Building Component/Configurations	
		Prototype Model	Model with High Thermal Mass
Interior Slab: Floor	Layer 1*	100 mm Normal-Weight Concrete	***200 mm Normal-Weight Concrete***
	Layer 2	Carpet	Carpet
Exterior Wall	Layer 1*	25 mm stucco	25 mm stucco
	Layer 2	16 mm Gypsum Board	16 mm Gypsum Board
	Layer 3	Exterior Wall Insulation	Exterior Wall Insulation
	Layer 4	16 mm Gypsum Board	***100 mm Normal-Weight Concrete***
	Layer 5		G01 16mm gypsum board
Interior Wall	Layer 1*	13 mm Gypsum Board	13 mm Gypsum Board
	Layer 2	13 mm Gypsum Board	***100 mm Normal-Weight Concrete***
	Layer 3		13 mm Gypsum Board
Roof	Layer 1*	Built-up Roofing	Built-up Roofing
	Layer 2	Roof Insulation	Roof Insulation
	Layer 3	Metal Surface	Metal Surface
	Layer 4		***200 mm Normal-Weight Concrete***

* Outside Layer

Table 4: Description of the Materials Properties in Modified Building Model

Name	Unit	13 mm Gypsum Board	16 mm Gypsum Board	25 mm stucco	100 mm Normal-Weight Concrete	200 mm Normal-Weight Concrete	Built-up Roofing	Carpet	Exterior Wall Insulation	Metal Surface	Roof Insulation
Roughness	-	Smooth	Medium Smooth	Smooth	Medium Rough	Medium Rough	Rough	Very Rough	Medium Smooth	Smooth	Medium Smooth
Thickness	m	0.0127	0.0159	0.0254	0.1016	0.2032	0.0095	-	-	0.0008	-
Conductivity	W/m·°K	0.16	0.16	0.72	2.31	2.31	0.16	-	-	45.28	-
Density	Kg/m^3	800	800	1856	2322	2322	1120	-	-	7824	-
Specific Heat	J/kg·°K	1090	1090	840	832	832	1460	-	-	500	-
Thermal Resistance	m^2·°K/W	-	-	-	-	-	-	0.216	2.368	-	5.307
Thermal Absorptance	-	0.9	-	0.9	-	-	0.9	0.9	0.9	-	0.9
Solar Absorptance	-	0.7	-	0.7	-	-	0.7	0.7	0.7	-	0.7
Visible Absorptance	-	0.5	-	0.7	-	-	-	0.8	0.7	-	0.7

3.4.5. Analysis of the Influential Parameters of the Weather Files

The weather files used in this study were the EPW files based on TMY3 weather files. The data in each file contains various weather information, including: psychrometric parameters, solar radiation, illumination, and wind.

In a comparative analysis of the two locations, in order to analyze the impact of each of the influential parameters on the building energy consumption, a fictitious weather file was generated by replacing specific parts of one weather file with another. In the pairwise comparisons, one site was determined as the base case and the parameters in the other file were modified one-at-a-time. For example, to analyze the impact of the dry-bulb temperature on the energy consumption in a pairwise comparison, the dry-bulb temperature of the base-case weather file was used in the modified weather file of the other location while keeping other values as they were in the original weather file. Similarly, to analyze the impact of humidity, the dew-point temperature, relative humidity, and liquid precipitation depth were replaced, and to analyze the impact of wind, the wind speed and wind direction are replaced. For the analysis of the impact of solar radiation, the solar radiation and illuminance data are replaced. The reason that the illuminance data are changed along with the solar radiation data is that the illuminance data are calculated using luminous efficacy models developed by Perez et al. (1990) in TMY3 files (Wilcox and Marion, 2008). These parameters include extraterrestrial horizontal radiation, extraterrestrial direct normal radiation, horizontal infrared radiation intensity, global horizontal radiation, direct normal radiation, diffuse horizontal radiation, global horizontal illuminance, direct normal illuminance, diffuse horizontal illuminance, and zenith luminance.

The temperature diurnal profile is also a characteristic of a weather that can affect building energy consumption. However, using the data from another weather file might not

reveal the impact of temperature diurnal profile on building energy consumption. Therefore, for each comparative analysis, two sets of dry-bulb temperature data that yielded the same HDD or CDD were generated while all other parameters except atmospheric station pressure[6] were set to zero. These two sets include one with a constant value repeated throughout the weather file (i.e., one temperature for the year) and one with a sinusoidal profile with the same daily average temperature as the constant temperature cases (i.e., one cycle in 24-hours). The average dry-bulb temperature is calculated using the two weather files in the analyses so that the generated file has the same HDD or CDD. The temperature swing in the sinusoidal case was derived from the average diurnal swing of the two weather files in the analyses.

3.4.6. Analysis of the Energy Savings Associated with the Implementation of the Daylight Responsive Controls

The energy savings associated with the implementation of daylight responsive controls in ASHRAE Standard 90.1 medium office prototype models were calculated using equations 3.18 and 3.19, respectively.

$$Energy\ Savings = Energy_{v,\ e,\ woDL} - Energy_{v,\ e,\ wDL} \tag{3.18}$$

$$Energy\ Savings\ Percentage = \frac{100 \times (Energy_{v,\ e,\ woDL} - Energy_{v,\ e,\ wDL})}{Energy_{v,\ e,\ woDL}} \tag{3.19}$$

[6] The atmospheric station pressure was set to 101,325 Pascal (1 Atmosphere) throughout the weather file.

where, *v* is the version of the ASHRAE 90.1 medium office prototype models, *e* is the end-use or the total regulated energy consumption, and *woDL* and *wDL* mean without and with daylight responsive control, respectively.

3.4.7. Analysis of the Code-Compliance Using Performance Path-Appendix G

The Appendix G of the ASHRAE 90.1-2016 (ASHRAE, 2016) requires each building to have the Performance Cost Index (*PCI*) lower than the defined target Performance Cost Index (PCI_t), which is the maximum *PCI* for a proposed design to comply with a particular edition of Standard 90.1. The PCI_t is provided for each climate zone and subtype. The *PCI* and PCI_t can be calculated using equations 3.20 and 3.21, respectively. The Building Performance Factor (BPF) in equation 3.21 is calculated using the equation 3.22.

$$\mathrm{PCI} = \frac{BP_{Proposed}}{BP_{baseline}} \tag{3.20}$$

Where, the $BP_{proposed}$ is the proposed building performance, which is the annual energy cost for a proposed design calculated according to Standard 90.1-2016, Appendix G. The $BP_{baseline}$ is the baseline building performance is the annual energy cost for a baseline design calculated according to Standard 90.1-2016, Appendix G.

$$\mathrm{PCI}_t = \frac{(\mathrm{BBUEC} + (\mathrm{BPF} \times \mathrm{BBREC}))}{\mathrm{BBP}} \tag{3.21}$$

Where, the Baseline Building Unregulated Energy Cost (*BBUEC*) is the portion of the annual energy cost of a baseline building design that is due to unregulated energy use. The Baseline Building Regulated Energy Cost (*BBREC*) is the portion of the annual energy cost of a baseline building design that is due to regulated energy use. The Building Performance Factor (*BPF*) is calculated using equation 3.22, which can be retrieved from Tables 2.2, 2.3, and 2.4 of the ASHRAE Standard 90.1-2016 (ASHRAE, 2016). The Baseline Building Performance (*BBP*) is the annual energy cost of the baseline building design including both regulated and unregulated energy use.

$$\mathrm{BPF}_{year\ x} = \frac{(\sum \frac{\mathrm{PBREC}_{year\ x}}{\mathrm{PBREC}_{2004}})}{N_P} \qquad 3.22$$

Where, the Prototype Building Regulated Energy $\mathrm{Cost}_{\mathrm{year\ x}}$ ($BPREC_{year\ x}$) is the portion of annual energy cost due to regulated energy use from the DOE prototype buildings for a given building prototype, climate zone and edition of Standard 90.1. The Prototype Building Regulated Energy Cost_{2004} ($BPREC_{2004}$) is the portion of annual energy cost due to regulated energy use from the DOE prototype buildings for a given building prototype, climate zone and the 2004 edition of Standard 90.1, and the N_p is the number of prototype building models of a particular building type from Table 2.1 of the ASHRAE 90.1-2016 (ASHRAE, 2016).

The Baseline Building Performance is calculated by averaging the annual energy cost of a baseline building design that is due to regulated energy use of the baseline models with rotation angles of 0, 90, 180, 270 degrees.

The building energy costs were calculated using the 2018 U.S. average commercial building energy prices reported by Energy Information Administration (EIA) in Table 2 of the March 2017 Short Term Energy Outlook (EIA, 2019), which provides 7.82 $/thousands cubic feet for the U.S. natural gas retail prices for the commercial sector and 10.66 ¢/kWh for U.S. electricity retail prices for the commercial sector. After conversions, 7.19 $/GJ for natural gas and 29.61 $/GJ for electricity were used in this study.

3.4.8. Analysis of the Predictability of the Energy Consumption and Weather-Related Parameters by Various Degree Day Calculation Methods

In order to assess the predictability of the energy consumption and weather-related parameters by various degree day calculation methods, the HDD and CDD were calculated using the different degree day methods for each of the 801 TMY3 weather files. These methods are previously described in Section 2.5.1.2. Then, the annual sum of the HDD and CDD were calculated for each site. Next, different regression models were developed using the annual energy consumption of the end-use(s) of interest and either the HDD, or CDD, or both HDD and CDD values for each site. In these models, the annual energy consumption of the end-use(s) of interest for each case was the dependent variable, and the HDD, or CDD, or both HDD and CDD were the independent variable(s). Using these models, the appropriateness of the degree day predictions were assessed using the R^2, Adjusted R^2, and RMSE of the predicted values using the predicted values by the regression models and the actual simulated values. Similar procedures are applied for the calculation of the split Cooling Degree Days (sCDD) and split Heating Degree Days (sHDD) resulting in two sCDD and two sHDD for each site.

To analyze the impact of the base temperature on the accuracy of the prediction of the annual heating and cooling energy consumption, the HDD, CDD, sHDD, and sCDD were calculated for the different weather files using different temperatures as the base temperature with increments of 1°C. Then, for the heating, for each base temperature, a regression model was developed using the sum of the HDD or sHDD for the whole year for each location as the independent variable and the annual heating energy consumption for each location as the dependent variable. Similarly, for each base temperature, a regression model is developed for the cooling using the sum of the CDD or sCDD for the whole year for each location as the independent variable and the annual cooling energy consumption in each location as the dependent variable. The R^2 of the 801 different location predicted values using the regression model compared against the simulated annual energy consumption was used as a metric to assess the appropriateness of the base temperature.

3.5.Weather-Normalization for Building Energy Comparisons

First, using the procedure for the performance path defined in Appendix G of the ASHRAE Standard 90.1-2016 (ASHRAE, 2016), previously discussed in section 0 of this document, the *PCI* and PCI_t for each of the 801 locations were calculated. Next, the difference of the *PCI* and the PCI_t were calculated for the different locations. This difference shows that the compliant building configuration can differ by using the prescriptive path or performance path. In other words, a single *BPF* for each climate zone and subtype can result in variations in energy consumption and energy costs due to the different weather conditions within each climate zone and subtype lead. This variation leads to the variation in the differences between *PCI* and PCI_t in different locations within each climate zone and subtype.

The weather normalization for performance path was carried out with similar goal in the prescriptive path, which used the prototype building models provided for each climate zone and subtype as the benchmark for all locations within that climate zone and subtype. To achieve this goal in the performance path, ideally the *PCI* should equal PCI_t in different locations.

Different approaches could be used to eliminate the differences of the *PCI* and PCI_t at different locations in one climate zone and subtype. One approach could provide a separate *BPF* for each location. However, this would require numerous tabulated values for different building types and could not be applied for the locations that are not included in the list. The other approach, which was used in this study, was to generate a regression model using split degree days in each weather file to adjust the *BPF* for each location (equation 3.23). Using this equation, one can estimate the variation for any location within each climate zone and subtype by calculating the sHDD and sCDD for that weather file and then adjust the *BPF*.

To estimate the adjustment factor for the *BPF*:

$$minimize: PCI_t - PCI = \frac{E_{2004,i}^{Unregulated} + BPF \cdot E_{2004,i}^{Regulated}}{E_{2004,i}^{Total}} - \frac{E_{2016,i}^{Total}}{E_{2004,i}^{Total}}, \quad subject\ to\ PCI_t \geq PCI \tag{3.23}$$

Where, $E_{2004,i}^{Unregulated}$ is the unregulated energy consumption of the ASHRAE Standard 90.1-2004 model for site *i*, $E_{2004,i}^{Regulated}$ is the regulated energy consumption of the 2004 model for site *i*, $E_{2004,i}^{Total}$ is the total energy consumption of the 2004 model for site *i*, and $E_{2016,i}^{Total}$ is the total energy consumption of the ASHRAE Standard 90.1-2016 model for site *i*.

Equation 3.24 can be retrieved using the equation 3.**23** and defining an ideal *BPF* for location i, $BPF_{ideal,i}$.

$$\frac{E_{2004,i}^{Unregulated} + BPF_{ideal} \cdot E_{2004,i}^{Regulated}}{E_{2004,i}^{Total}} = \frac{E_{2016,i}^{Total}}{E_{2004,i}^{Total}} \tag{3.24}$$

Rearranging equation 3.24 to solve for $BPF_{ideal,i}$ yields equation 3.25. The weather-related parameters in equation 3.25 ($E_{2016,i}^{Total}$ and $E_{2004,i}^{Regulated}$) can be estimated by sDD (Section 5.1).

$$BPF_{ideal.\ i} = \frac{E_{2016,i}^{Total} - E_{2004,i}^{Unregulated}}{E_{2004,i}^{Regulated}} \tag{3.25}$$

The $BPF_{ideal.i}$ can be calculated using the multiplication of a coefficient for site i, defined as $BPF\_F_{ideal.i}$, and the BPF for the corresponding climate zone and subtype x, called BPF_x. Therefore, the $BPF\_F_{ideal.i}$ can be calculated by dividing the $BPF_{ideal,i}$ over the *BPF* of the corresponding climate zone, BPF_x (equation 3.26).

$$BPF\_F_{ideal.i} = \frac{BPF_{ideal.i}}{BPF_x} \tag{3.26}$$

The $BPF\_F_{ideal.i}$ is the estimated using the sDD.

$$\widehat{BPF\_F}_{ideal.i} = \beta_0 + \beta_1 \cdot sCDD_1 + \beta_2 \cdot sCDD_2 + \beta_3 \cdot sCDD_1 \cdot sCDD_2 + \beta_4 \cdot sHDD_1 + \beta_5 \cdot sHDD_2 + \beta_6 \cdot sHDD_1 \cdot sHDD_2 \quad (3.27)$$

where, $\widehat{BPF\_F}_{ideal.i}$ is the estimated ideal BPF for location *i*.

CHAPTER IV

RESULTS – PART I

4.1.Overview

This chapter includes the results of simulations of the DOE medium office prototype models used for ASHRAE Standard 90.1-2016. The simulation results include the results of the simulations of the models that complied with the requirements for each climate zone as well as the results of the simulations of one model that complied with the requirements of climate zone 4B that was used for all locations. In addition, an analysis of the influential weather-related parameters is provided for two cities with similar CDD values and two cities with similar HDD values with varying energy consumption as calculated by the DOE model. Finally, the results of the impact of varying energy consumption values for the code compliant models are illustrated.

4.2. Results of the Office Building Prototype Models

This section presents the energy consumption of the ASHRAE Standard 90.1-2016 medium office prototype models in different locations. The results are illustrated in two subsections for the models that complied with the requirements in each zone and the results of the simulations using one model for all climate zones.

4.2.1. Energy Consumption of the ASHRAE Standard 90.1-2016 Medium Office Prototype Models in Different Locations

Figure 25 to Figure 28 illustrate the regulated energy consumption of the ASHRAE Standard 90.1-2016 medium office prototype models. The results are presented using plots that

consist of a scatter plot that shows the energy consumption versus the CDD or HDD values for the different weather locations (Figure 25 and Figure 26). These plots include histograms illustrating the distribution of the HDD or CDD values, represented on the horizontal axis of the scatter plot, and the distribution of the energy consumption or energy savings, represented on the vertical axis of the scatter plot. In addition, different climate zones and subtypes are illustrated using data labeling and color notation in the scatter plots. In each plot, the average energy consumption or savings for each climate subtype is listed on the right hand side of the plot. In these plots, the average of energy consumption or savings for the locations in climate zones 7 and 8 (i.e. 3160 and 4137 for the energy consumption, etc.) are provided for each of these climate zones and are not divided into subtypes (see ASHRAE 169, 2013).

In Figure 25 and Figure 26 the regulated energy consumption is shown with respect to the CDD10°C (Figure 25) and HDD18°C (Figure 26) for the 801 locations in the U.S. The histograms at the top and right side of each figure shows the frequency of the individual points versus CDD10°C or HDD18°C (upper plot) and versus the regulated energy consumption (right plot).

Figure 27 and Figure 28 show the regulated energy consumption and the Energy Use Intensity (EUI) from the simulated energy use for the 801 locations. These energy intensity plots are used to show the energy consumption or savings of each simulation as scatter plots on the HDD versus CDD axis. In these plots, the climate zones and subtypes are illustrated using the overlaid boxes and different data labels for each climate subtype. Circles, triangles, and diamonds are used to represent climate subtypes A, B, and C, respectively, and the asterisk and plus signs represent climate zones 7 and 8, respectively.

In Figure 27, the regulated energy consumption from the simulations varies for the different climate zones, which is shown with varying colors. In the plots the average regulated energy use in different climate zones varied from 2819 GJ (in climate zone 4) to 4142 GJ (climate zone 8). In Figure 27, as one progresses from climate zone 1 to climate zone 2, climate zone 3, and climate zone 4, the average regulated energy consumption in the climate zone begins at 3681 GJ in climate zone 1, then drops across climate zones 2, 3, and 4, as the CDD10°C drops, then begins to rise again in climate zones 6, 7, and 8 as the HDD18°C rises. Within each climate zone, on average, subtype C has the lowest energy consumption and subtype A has the highest energy consumption.

The results of a study on the feasibility of zero net energy buildings in different climates by Eley (2017) has shown similar variations for the minimum Collector-to-Floor Area (CFA) ratio needed for net-zero energy office buildings. According to this study, the minimum CFA for net-zero energy office buildings that complied with ASHRAE Standard 90.1-2013 ranged from 0.3 in the Pacific coast to 1.04 in the Arctic. Similarly, the minimum CFA for a net-zero energy office buildings with a maximum technical potential range from 0.11 in the Pacific coast to 0.3 in the Arctic.

From the results of the analysis in this analysis, it can be seen that there is a systematic difference between the regulated energy consumption of the medium office prototype models in different locations. Figure 29 shows an analysis of the variance (ANOVA) of the different moisture regimes with a 0.05 level of significance for climate zone subtype A (moist), B (dry), and C (marine). The difference is significant with the F-ratio of 311.62 and the p-value of less than 0.0001, which means there is a systematic difference in the average regulated energy consumption of the medium office prototype models in different subtypes.

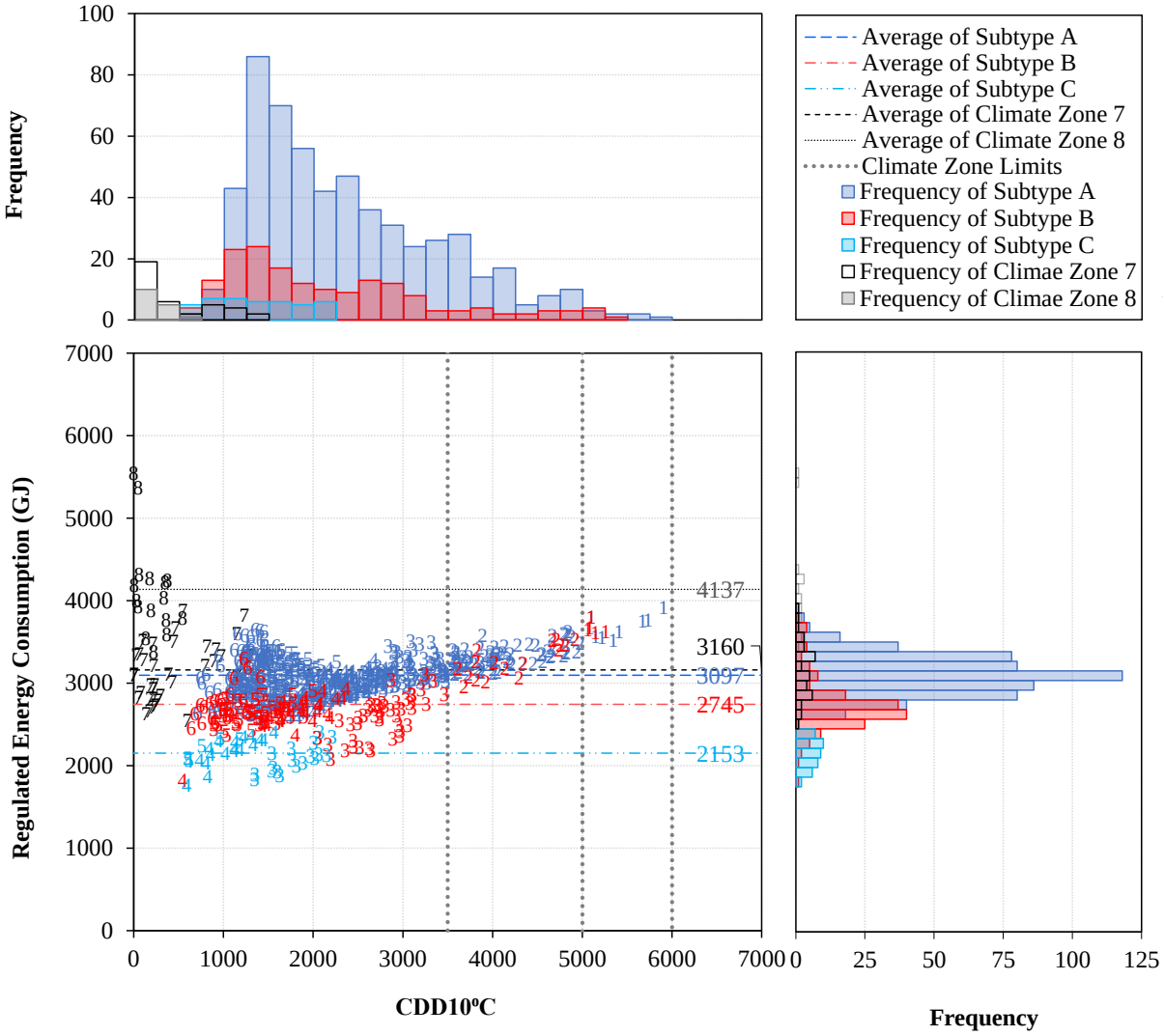

Figure 25: Regulated Energy Consumption of the ASHRAE Standard 90.1-2016 Medium Office Prototype Models with Respect to the CDD10°C of Different Weather Files

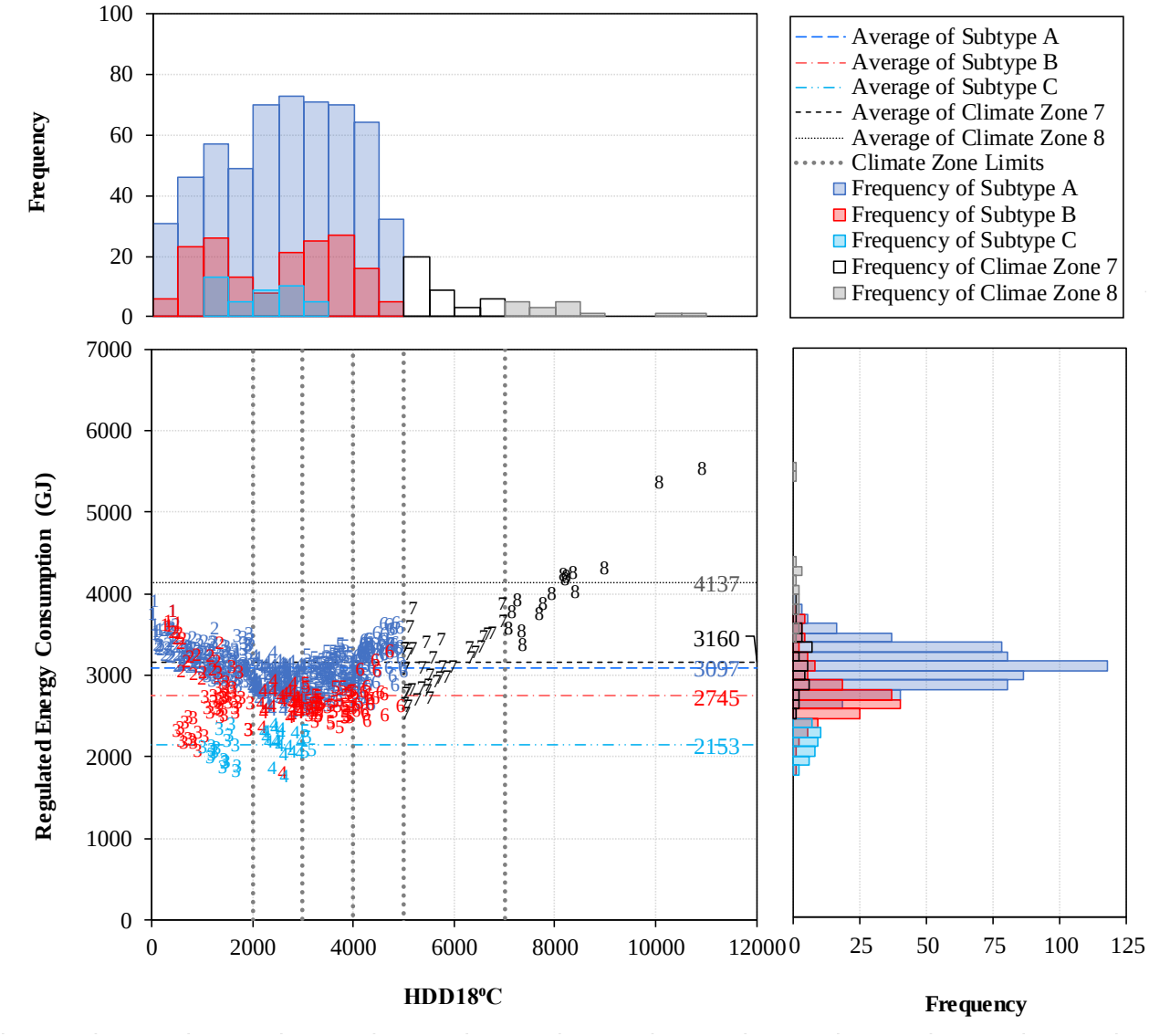

Figure 26: Regulated Energy Consumption of the ASHRAE Standard 90.1-2016 Medium Office Prototype Models with Respect to the HDD18°C of Different Weather Files

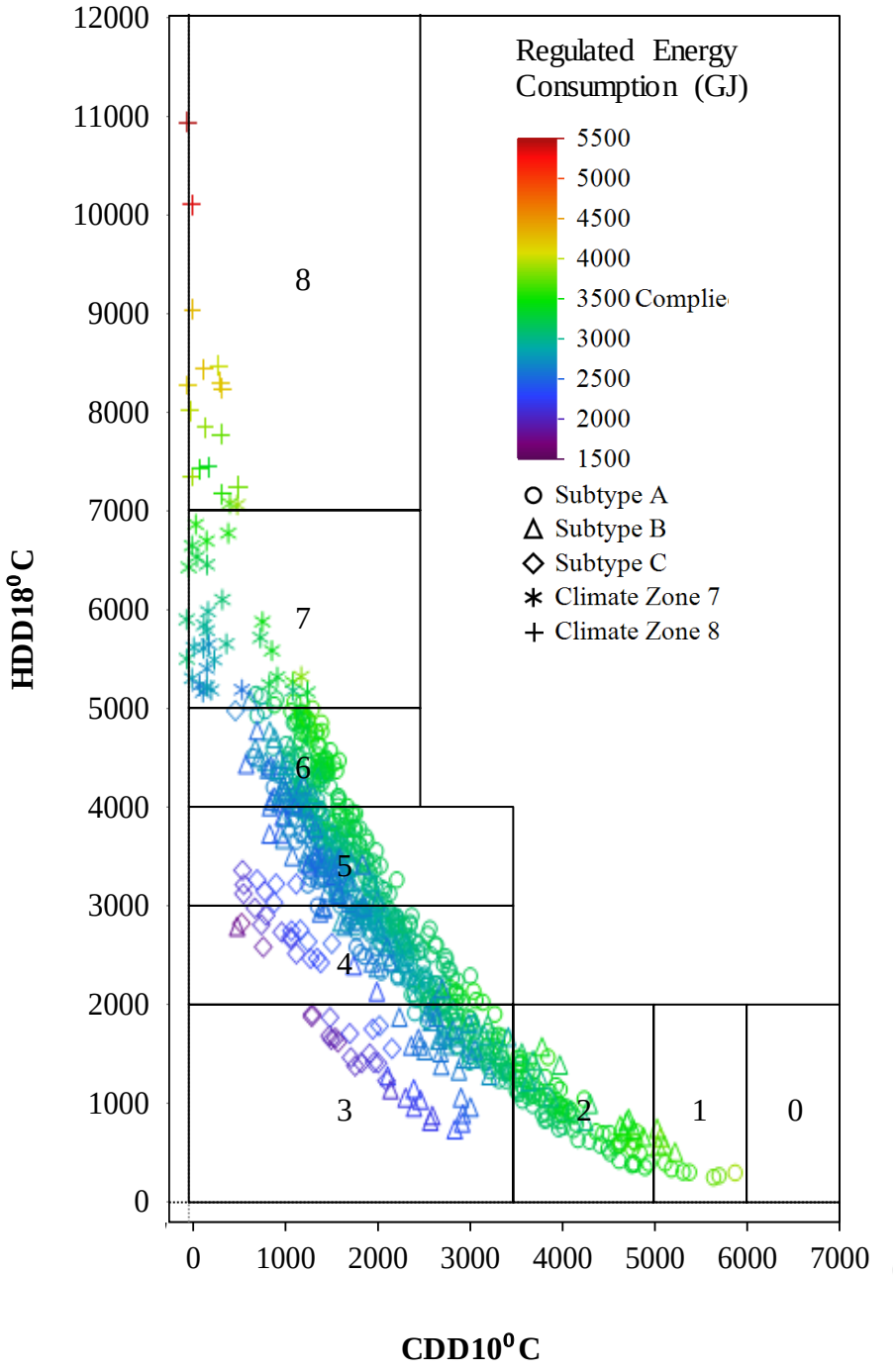

Figure 27: Regulated Energy Consumption of the ASHRAE Standard 90.1-2016 Medium Office Prototype Models in Different Climate Zones

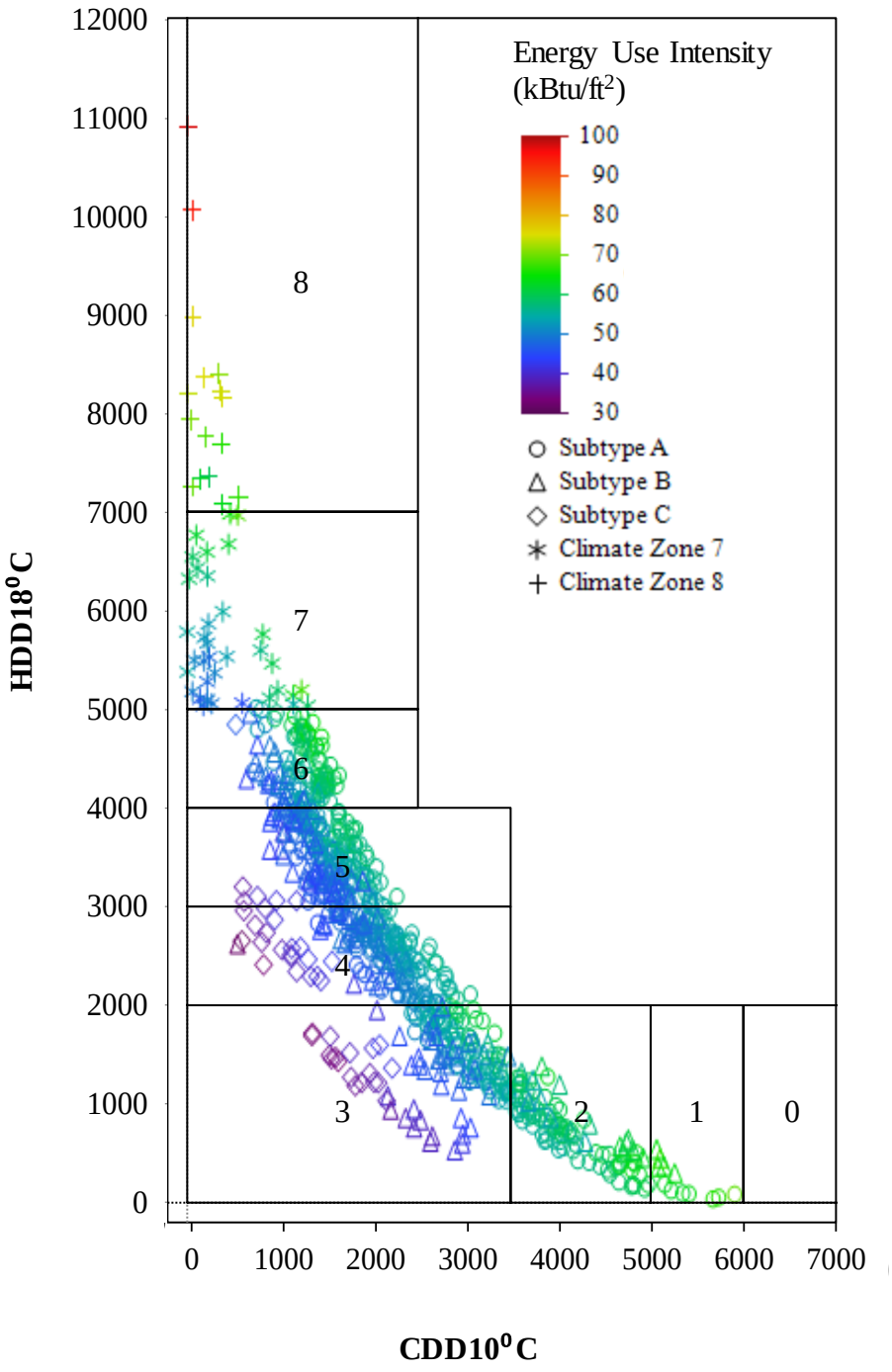

Figure 28: Energy Use Intensity of the ASHRAE Standard 90.1-2016 Medium Office Prototype Models in Different Climate Zones

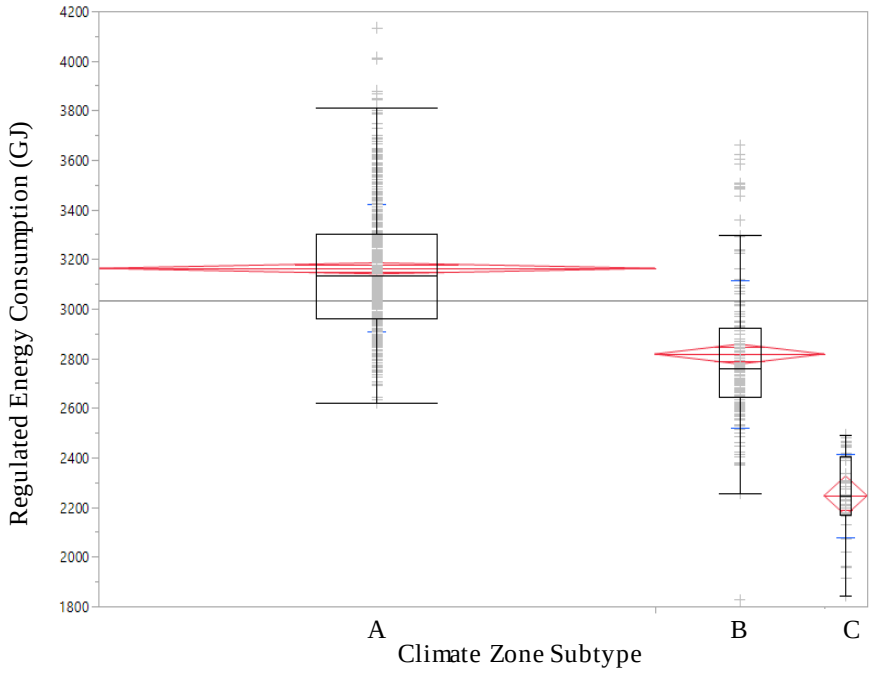

Figure 29: Analysis of Variance of the Regulated Energy Consumption in Different Subtypes

4.2.2. Energy Consumption of an Identical ASHRAE Standard 90.1-2016 Medium Office Prototype Model in Different Locations

Figure 30 to Figure 32, show the regulated energy consumption of the ASHRAE Standard 90.1-2016 medium office prototype model for climate zone 4B in different locations. The regulated energy consumption in Figure 30 and Figure 31 are shown with respect to the CDD10°C and HDD18°C of the different weather files. The histograms in the top and right side of each figure shows the frequency of the CDD10°C or HDD18°C and the regulated energy consumptions, respectively. Figure 32 shows the regulated energy consumption of the model in different climate zones.

Results of the simulated energy consumption of the identical model showed similar variations as in the simulated models that complied with the requirements in each climate zone.

However, the simulation results of the identical model showed higher energy consumption in very hot or very cold climates. This is mainly due to the fact that the identical model for climate zone 4B was chosen and the less stringent requirements for reducing heating loads in climate zone 4 compared to colder climates lead to significantly higher energy consumption of the model in regions with much higher heating loads (i.e. climate zone 8).

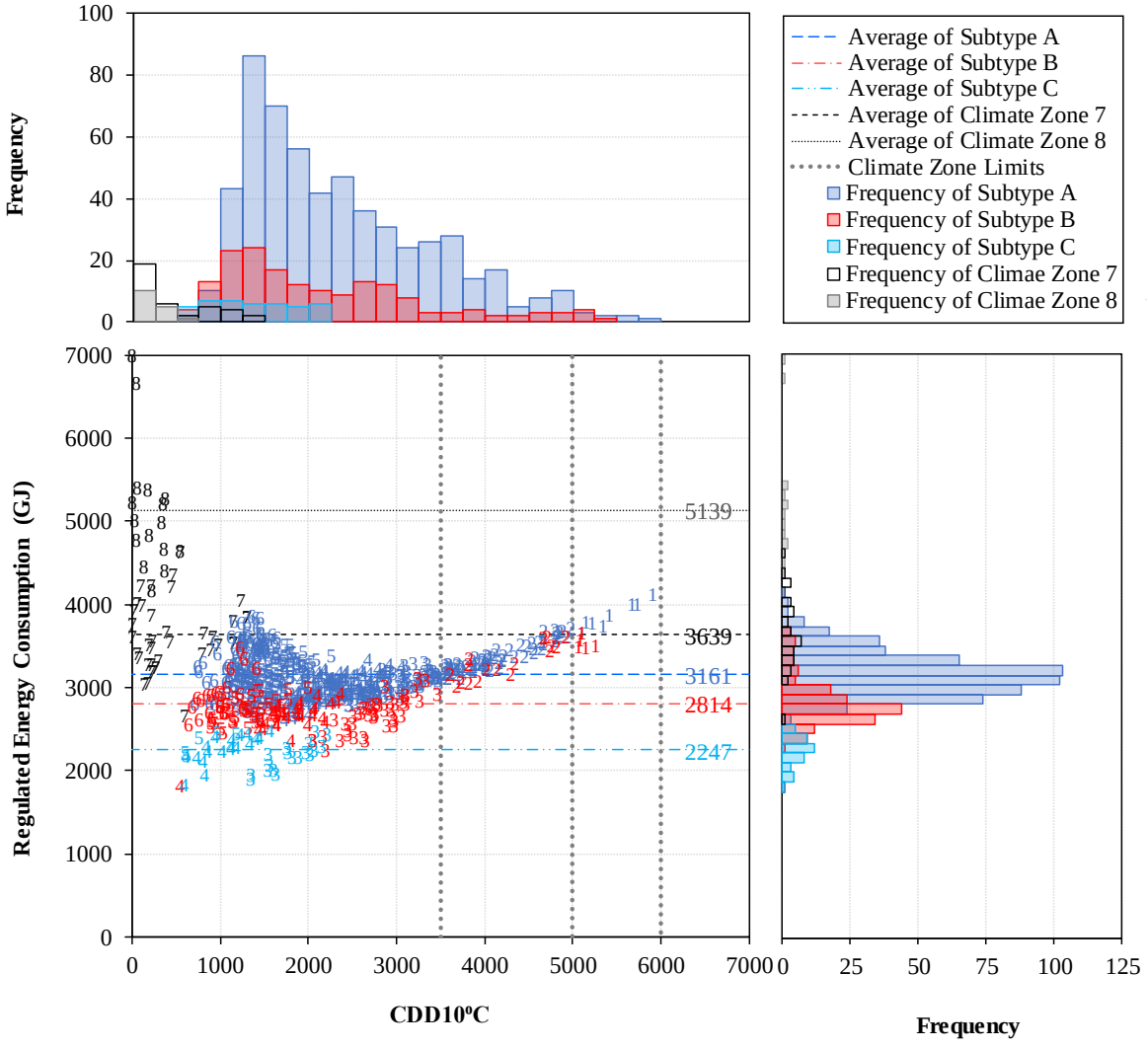

Figure 30: Regulated Energy Consumption of the ASHRAE Standard 90.1-2016 Medium Office Prototype Model for Climate Zone 4B with Respect to the CDD10°C of Different Weather Files

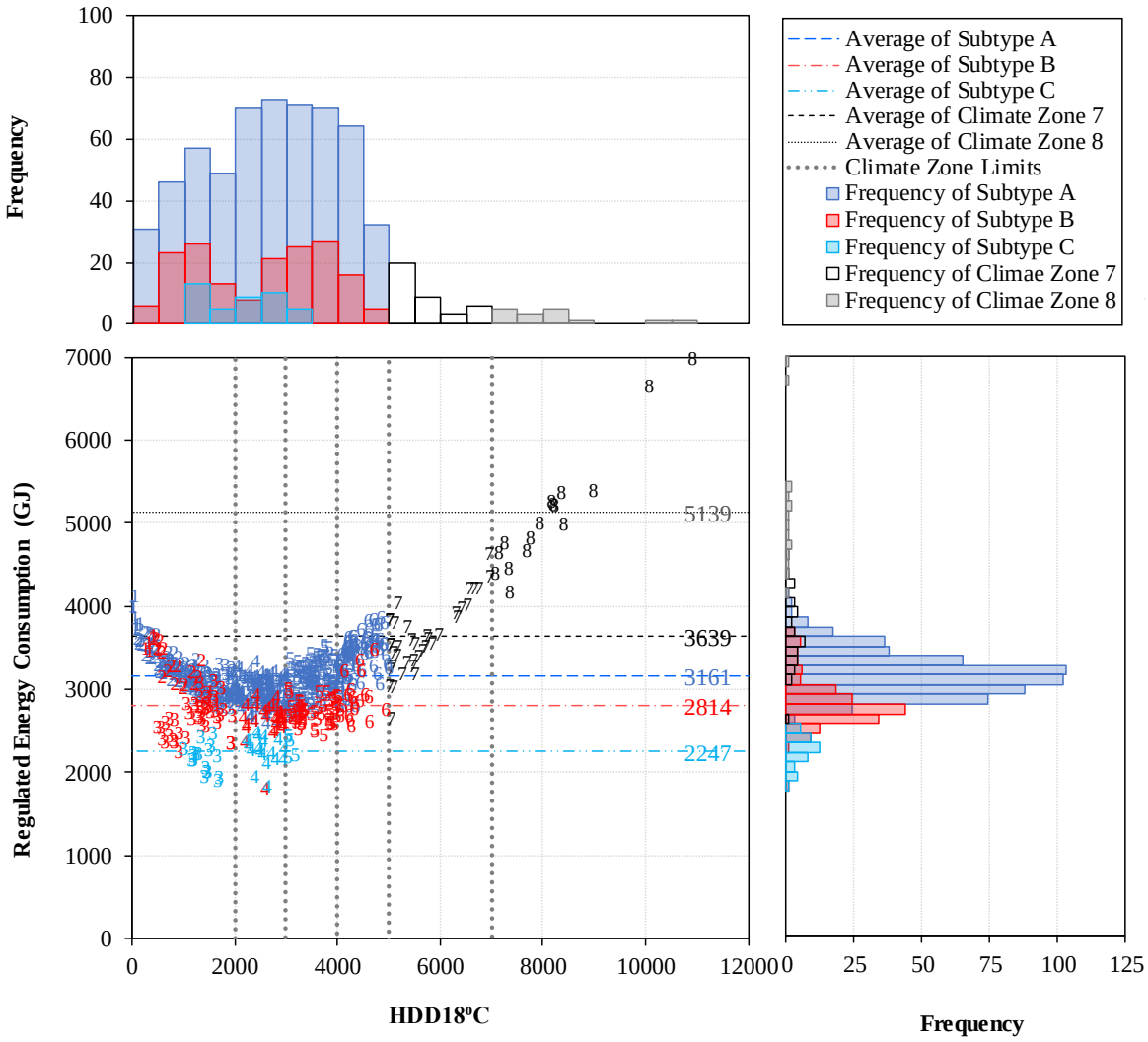

Figure 31: Regulated Energy Consumption of the ASHRAE Standard 90.1-2016 Medium Office Prototype Model for Climate Zone 4B with Respect to the HDD18°C of Different Weather Files

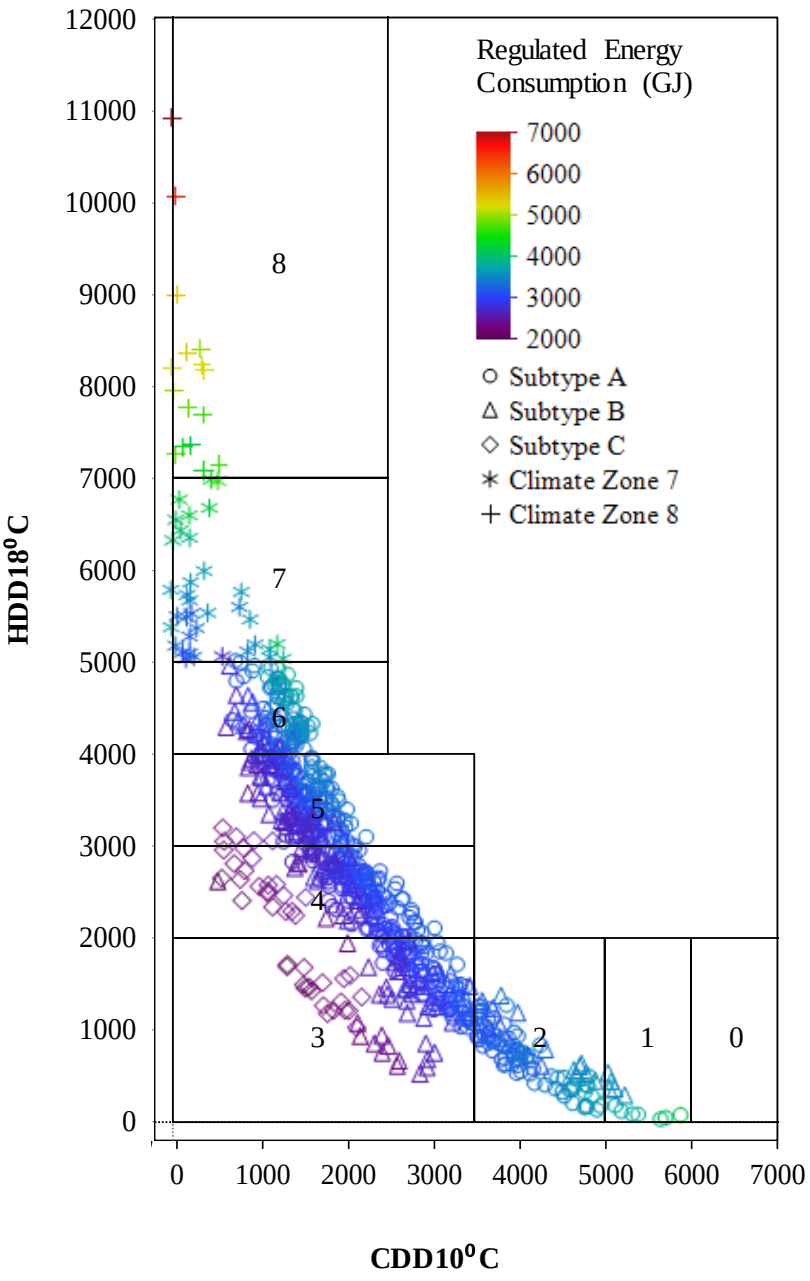

Figure 32: Regulated Energy Consumption of the ASHRAE Standard 90.1-2016 Medium Office Prototype Model for Climate Zone 4B in Different Climate Zones

4.3.Analysis of the Influential Weather Parameters Varying the Energy Consumption within Each Climate Zone

As illustrated in Section 4.2, the energy consumption of the DOE office building models vary for the different climate zones and within each climate zone. The variations can be distinguished between different subtypes. Typically, it can be seen that the simulations in subtype A on average show the largest energy consumption and subtype C show the lowest energy consumption compared to other subtypes. Section 4.3.1 includes the discussions for the variations in the energy consumption of the models in subtype C compared to subtypes A and B.

Besides the difference between subtype C and the other subtypes, there is a distinct difference in the energy consumption of the buildings in subtype A and B in the same climate zones. Sections 4.3.2 and 4.3.3 discuss the variation of the energy consumption of the identical medium office prototype model in different locations. To analyze the variation of the heating and cooling energy consumption within each climate zone, two locations with similar HDD (for the variations in heating energy use) and CDD (for the variations in cooling energy use) were selected. Then, an identical model is used to remove the impact of code-compliant building-related parameters in the results. The analysis was mainly focused on a single day with similar HDD or CDD. The purpose of the comparative analysis was to reveal the influential weather variables that define the variations in energy consumption using time-series representations.

4.3.1. Variations in the Energy Consumption of the Models in Marine Compared to Moist and Dry Moisture Regimes

As mentioned previously, the energy consumption of the models in subtype C is on average lower than the average consumption of the models in subtypes A and B. Figure 33 to

Figure 37 show the daily profile of the hourly average outdoor dry-bulb temperature for annual, spring, summer, fall, and winter, respectively. First, the average outdoor dry-bulb temperature for each site represents the average value for each hour of the day in 365 days. Next, the average value is calculated for all sites for each hour of the day. As illustrated in Figure 33, while the daily profile of climate zone 7 and 8 have lower temperatures compared to other climate zones, subtypes A, B, and C have very similar daily profiles for the annual hourly average outdoor dry-bulb temperature.

Since Figure 33 does not reveal the seasonal differences in the different subtypes, a similar calculation procedure to analyze the annual hourly average temperature was carried out for seasonal hourly average temperatures. Figure 34 to Figure 37 show the daily profiles of the hourly average outdoor dry-bulb temperature in the different seasons. It can be seen that among the different subtypes, by comparing the temperature at each hour in the different seasons, subtype C has the lowest difference in different seasons. In other words, while the three subtypes have approximately the same profile in spring and fall, there is a higher temperature for subtypes A and B in the summer and a lower temperature of subtypes A and B in the winter compared to subtype C. Figure 38 shows the daily profile of the maximum seasonal average hourly difference of outdoor dry-bulb temperature. This profile shows the difference in subtype C is lower when compared to other subtypes. HDD and CDD reflects this difference to some extent when one considers the weather files of sites with similar HDD in different subtypes. For example, the weather files in subtype C typically have a lower CDD compared to other subtypes. Similarly, by comparing the weather files with similar CDD we observe that the subtype C weather files typically have lower HDD compared to other subtypes. Therefore, in general, the least building energy consumption in each climate zone occur in subtype C.

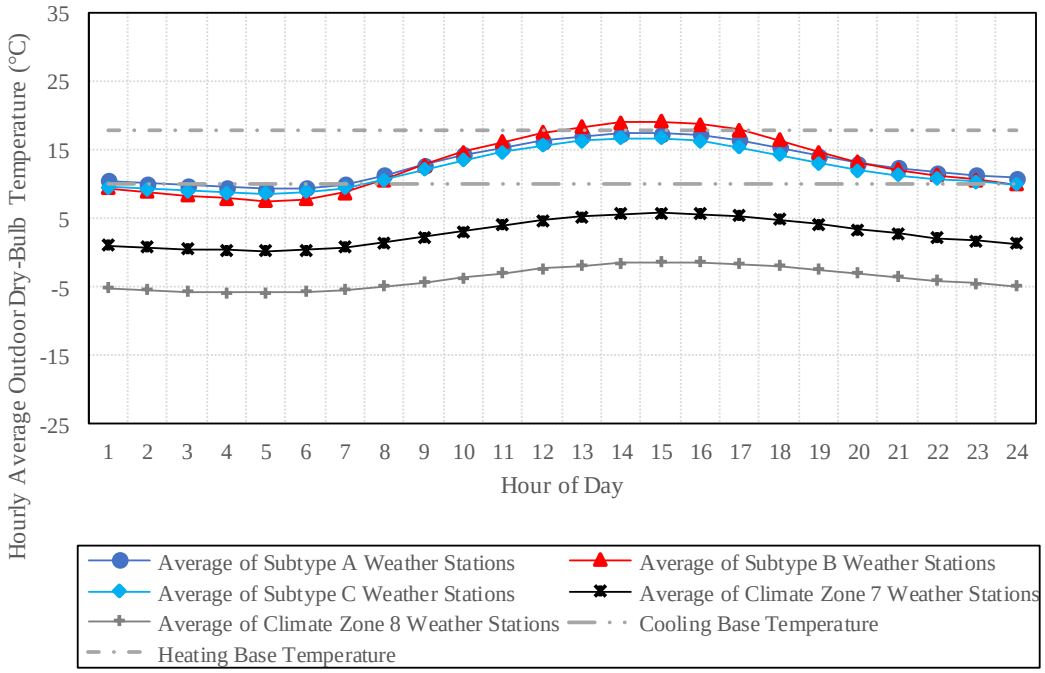

Figure 33: Daily Profile of the Annual Hourly Average Outdoor Dry-Bulb Temperature

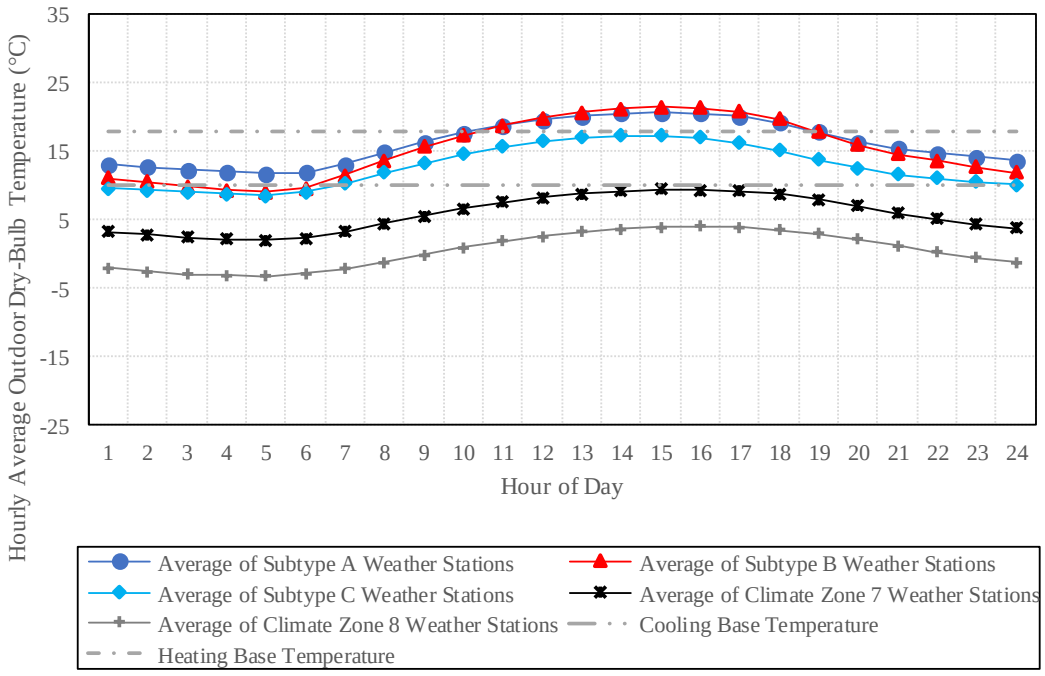

Figure 34: Daily Profile of the Spring Hourly Average Outdoor Dry-Bulb Temperature

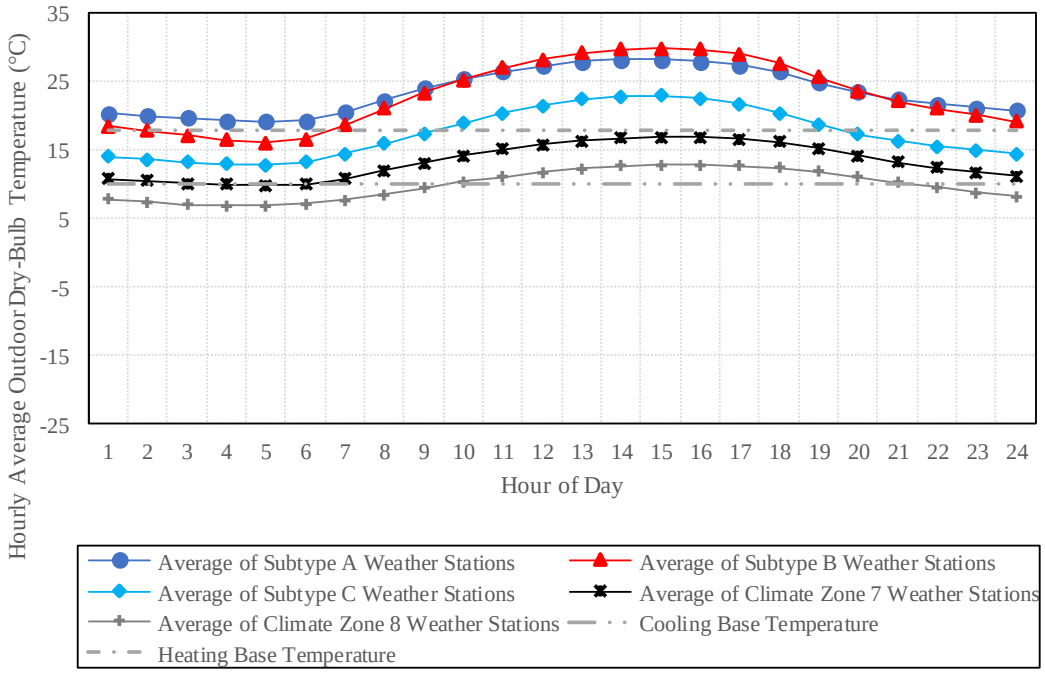

Figure 35: Daily Profile of the Summer Hourly Average Outdoor Dry-Bulb Temperature

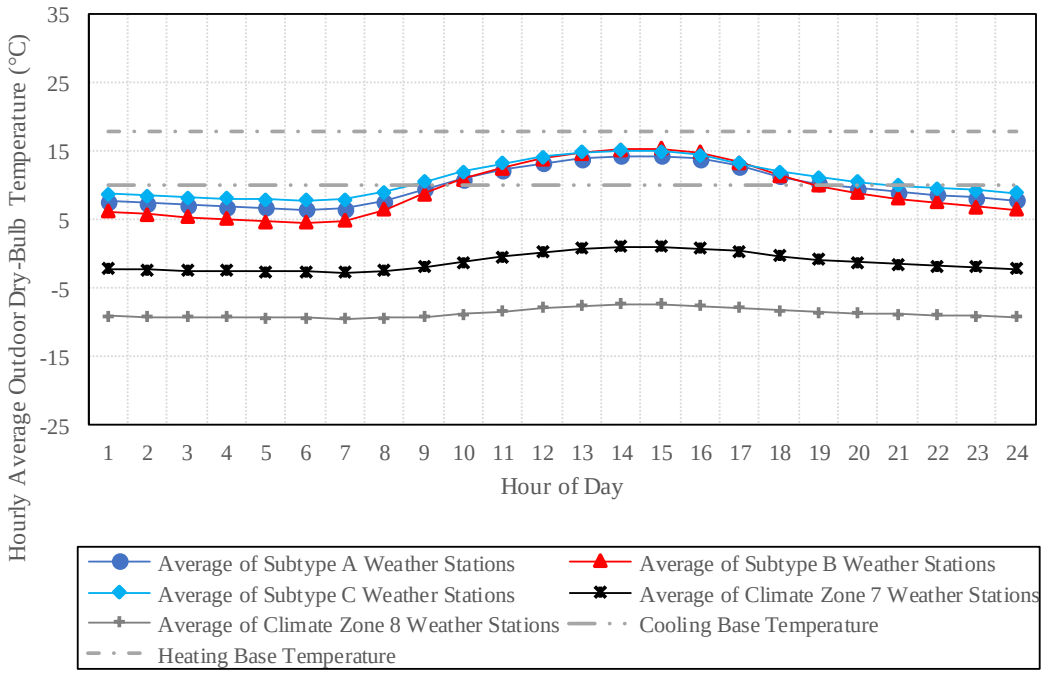

Figure 36: Daily Profile of the Fall Hourly Average Outdoor Dry-Bulb Temperature

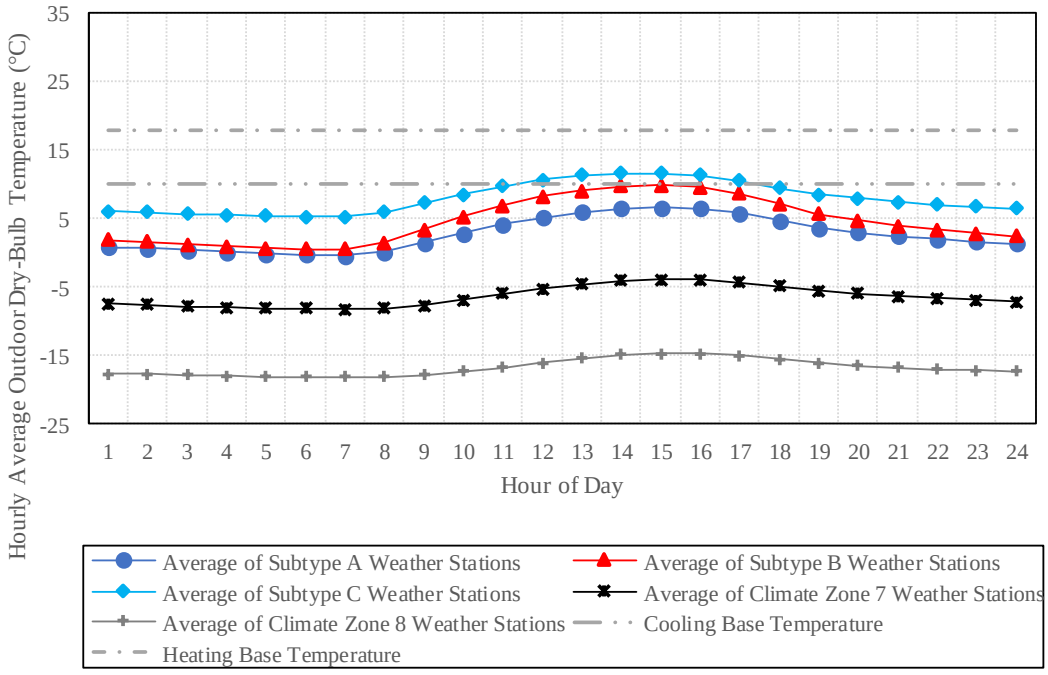

Figure 37: Daily Profile of the Winter Hourly Average Outdoor Dry-Bulb Temperature

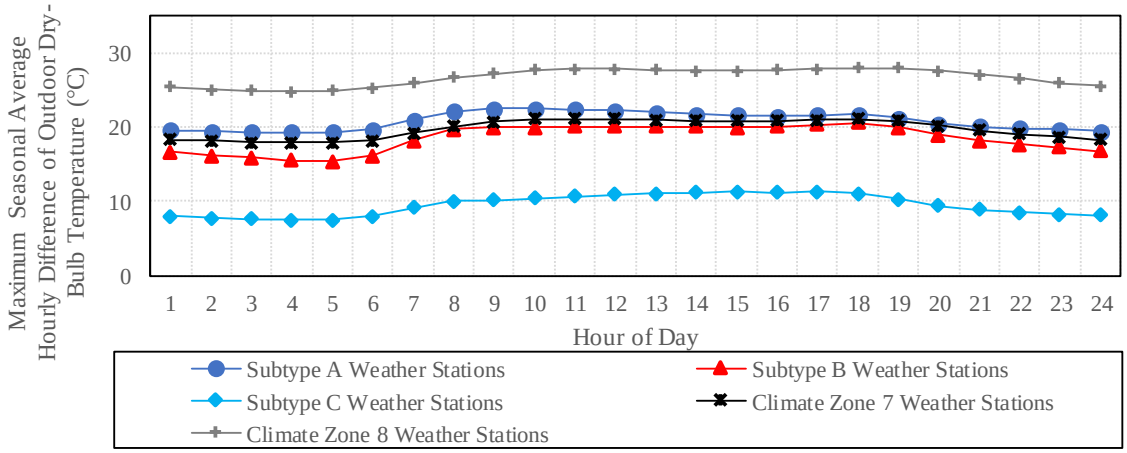

Figure 38: Daily Profile of the Maximum Seasonal Average Hourly Difference of Outdoor Dry-Bulb Temperature

4.3.2. Comparative Analysis of the Variations in Heating Energy Consumption in Locations with Similar HDD in Moist and Dry Moisture Regimes

The HDD in buildings is utilized as a method to classify the weather conditions with respect to the expected heating load in buildings. However, results of the current study show that the heating energy consumption can vary within similar ranges of HDD. For example, Figure 39 shows the heating energy consumption of the ASHRAE Standard 90.1-2016 medium office prototype models in different locations with respect to the calculated HDD of the corresponding weather files. This figure illustrates the variations within similar ranges of HDD. In order to remove the effect of various building configurations in the analysis, the results of the heating energy consumption of an identical ASHRAE Standard 90.1-2016 medium office prototype model that complied with climate zone 4B, with respect to the calculated HDD of the corresponding weather files are illustrated in Figure 40. Similar to the results of the models that complied with the requirements for each climate zone, the results of the simulations of the identical model show significant variations in heating energy consumption of the models within a similar HDD group.

In order to analyze the difference in heating energy consumption of the cases with similar HDDs, as shown in Figure 39 and Figure 40, two locations from Climate Zone 5 were selected: the Omaha-Eppley Airfield weather station (ID: 725500), located in Climate Zone 5, subtype A, and the Gallup-Sen Clarke Field weather station (ID: 723627), located in Climate Zone 5, subtype B (Figure 41). In the analysis, the same simulation model (ASHRAE Standard 90.1 prototype building model for climate zone 4B) was used to enable studying only the weather impacts (Figure 40). The HDDs of the selected city in climate zone 5A and 5B are 3,232 and 3241, respectively. The simulated annual heating energy consumption of the models in the

selected city in climate zone 5A and 5B were 816 GJ and 356 GJ for the models complied with each climate zone and 901 GJ and 388 GJ for the identical model. In Figure 39 it can be seen that although the HDD of the selected city in climate zone 5B is even slightly higher than the HDD of the selected city in climate zone 5A, the heating energy use was significantly higher in Omaha, Nebraska versus Gallup, New Mexico.

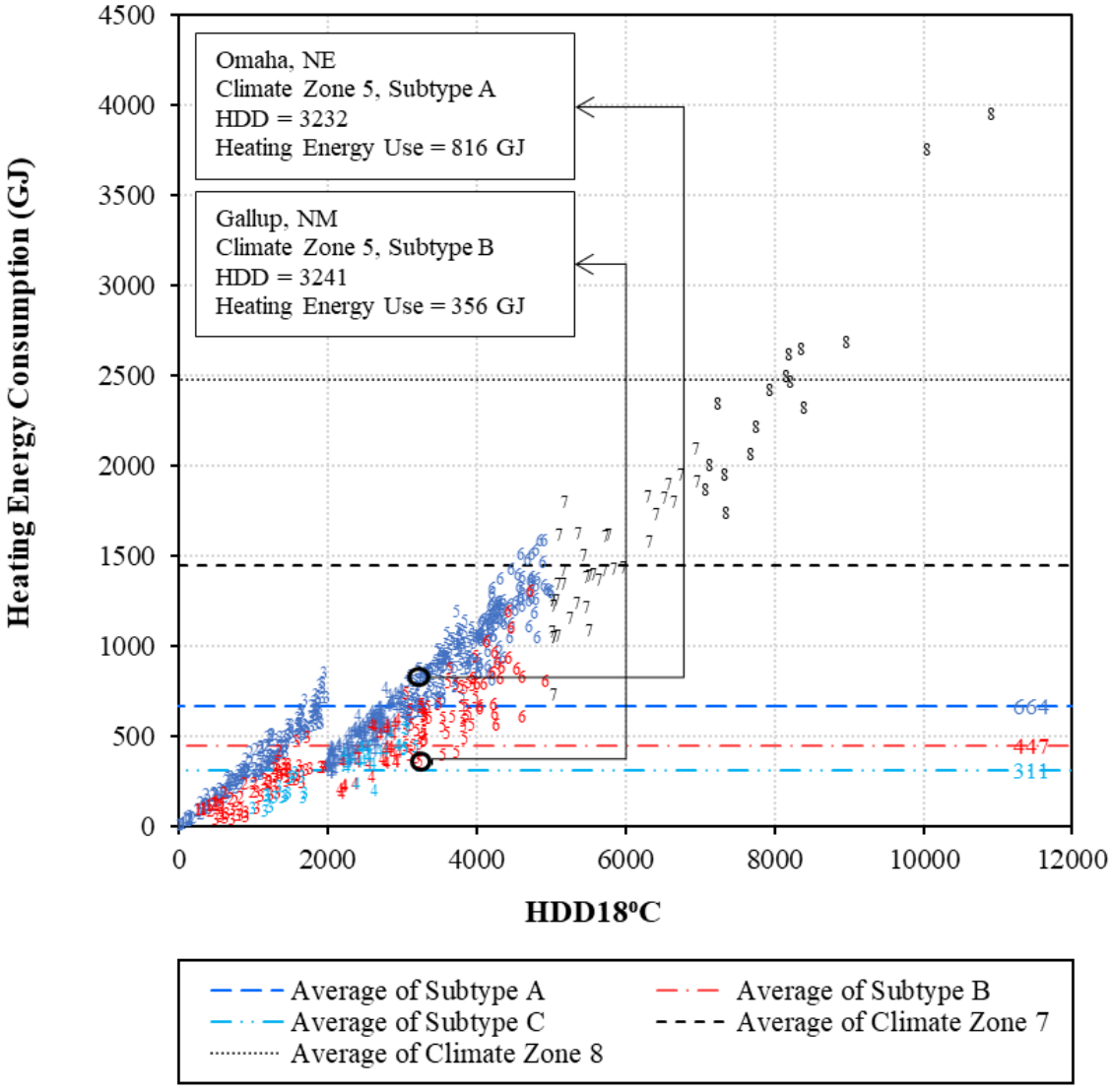

Figure 39: Variation of the Heating Energy Consumption of the Prototype Models Complied with Each Climate Zone and the Representation of the Two Selected Cases with Similar HDD and Different Heating Energy Consumption

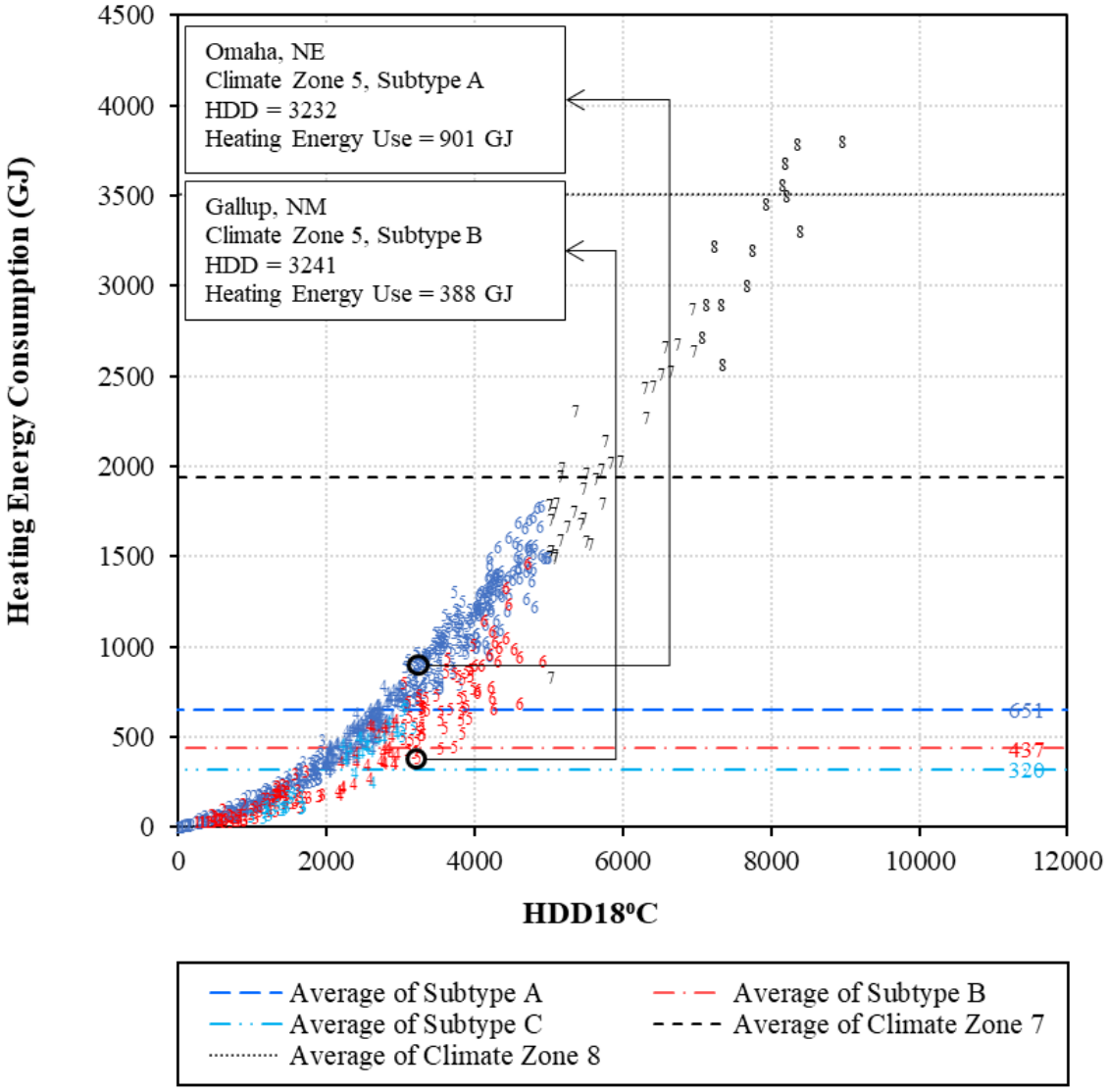

Figure 40: Variation of the Heating Energy Consumption of an Identical Model and the Representation of the Two Selected Cases with Similar HDD and Different Heating Energy Consumption

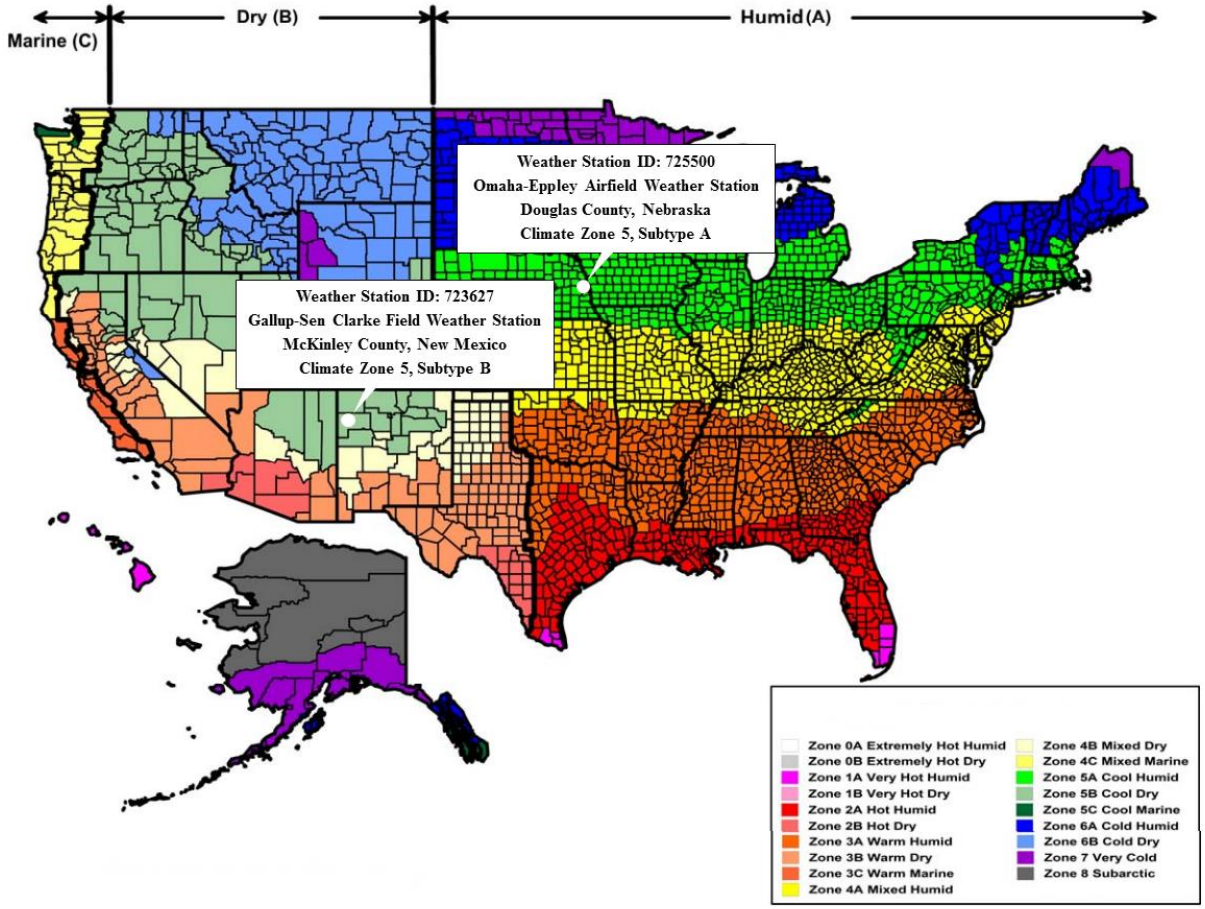

Figure 41: Selected Weather Stations in Climate Zone 5, subtypes A and B in the Climate Zones for United States Counties Map. ©ASHRAE, www.ashrae.org. Original map used with permission from 2013 ASHRAE Standard-169 (Map: (ASHRAE, 2013a))

4.3.2.1. Analysis of the Impact of Solar Radiation, Dry-Bulb Temperature, Humidity, and Wind on the Variations in Heating Energy Consumption in Locations with Similar HDD

This section seeks to analyze the impact of different weather parameters on the variations in the heating energy consumption using the DOE medium office prototype models. The analysis starts with simulating the two selected building models using the corresponding weather files. Then, four simulations were carried out to reveal the impact of solar radiation, dry-bulb

temperature, wind, and humidity on the building heating energy consumption. Then, to reveal the impact of the operating schedule, a 24-hour operating model was simulated using the two weather files.

In the analysis, it was observed that there were several additional influential weather variables that were not considered in the HDD groupings that impact the heating energy consumption, which can result in different daily energy use values. For example, weather data with different daily profiles can have similar HDD. Figure 42 shows the daily profile of the outdoor dry-bulb temperature, global horizontal solar radiation, relative humidity, wind speed, and the heating energy consumption for the two selected sites in January 11th. Although the two sites have almost the same HDD (approximately 16 °C), there is a large difference in the heating energy consumption in that day (7.8 GJ and 2.1 GJ for climate zones 5A and 5B, respectively). It can be seen that although the HDD is slightly lower in the site located in climate zone 5A (Omaha, Nebraska) compared to the site in climate zone 5B (Gallup, New Mexico), the daily heating energy consumption in Omaha is more than three times larger compared to Gallup.

For the two days shown in Figure 42 that both registered 16°C HDD, it can be clearly seen that the outdoor air temperature had completely different profiles. Although both days had approximately 16°C HDD, in the case of Omaha, there was overcast sky and very little solar radiation, resulting in the daily outdoor temperature remained relatively constant at approximately 0°C, with high humidity levels. In contrast in Gallup, New Mexico, there were clear sky, cold temperature during the evenings (approximately -5°C), and warmer, drier daytime temperature (approximately 10°C), which also yielded 16°C HDD. However, it should be mentioned that the

comparisons in the selected day do not mean that similar variations will necessarily apply for all days in different moisture regimes (in this case subtypes A and B).

Table 5 shows the impact of the weather parameters on both the annual heating energy consumption and for one selected day, January 11th. For the analysis, the Gallup, NM, weather station (ID: 723627), located in Climate Zone 5B, was selected as the basecase. Figure 43 shows the impact of the solar radiation on indoor temperatures for January 11th. Figure 44 to Figure 46 show the parameters and the results for January 11th, and Figure 48 illustrates the results of the simulations of the models with 24-hours operating schedules in January 11th.

One of the major influential weather variables that impact the heating energy consumption of a building is the solar radiation, which is not considered in the HDD calculation. The comparison of the solar radiation of the selected cities for January 11th is shown in Figure 42. To reveal the impact of solar radiation on heating demand, a model without HVAC systems and infiltration was simulated with all other parameters in the weather file set to zero (except the atmospheric station pressure, which was set to 101.3 kPa). Figure 43 shows the total transmitted solar radiation energy from the windows in middle floor zones and the mean air temperature of the zones. Figure 43 illustrates a temperature rise of approximately 10 °C in the south zone of the model in the selected city in climate zone 5B, which has higher solar radiation compared to the selected city in climate zone 5A while there was no significant increase in the zones temperatures of the selected city in climate zone 5A, where the model received lower amount of solar radiation.

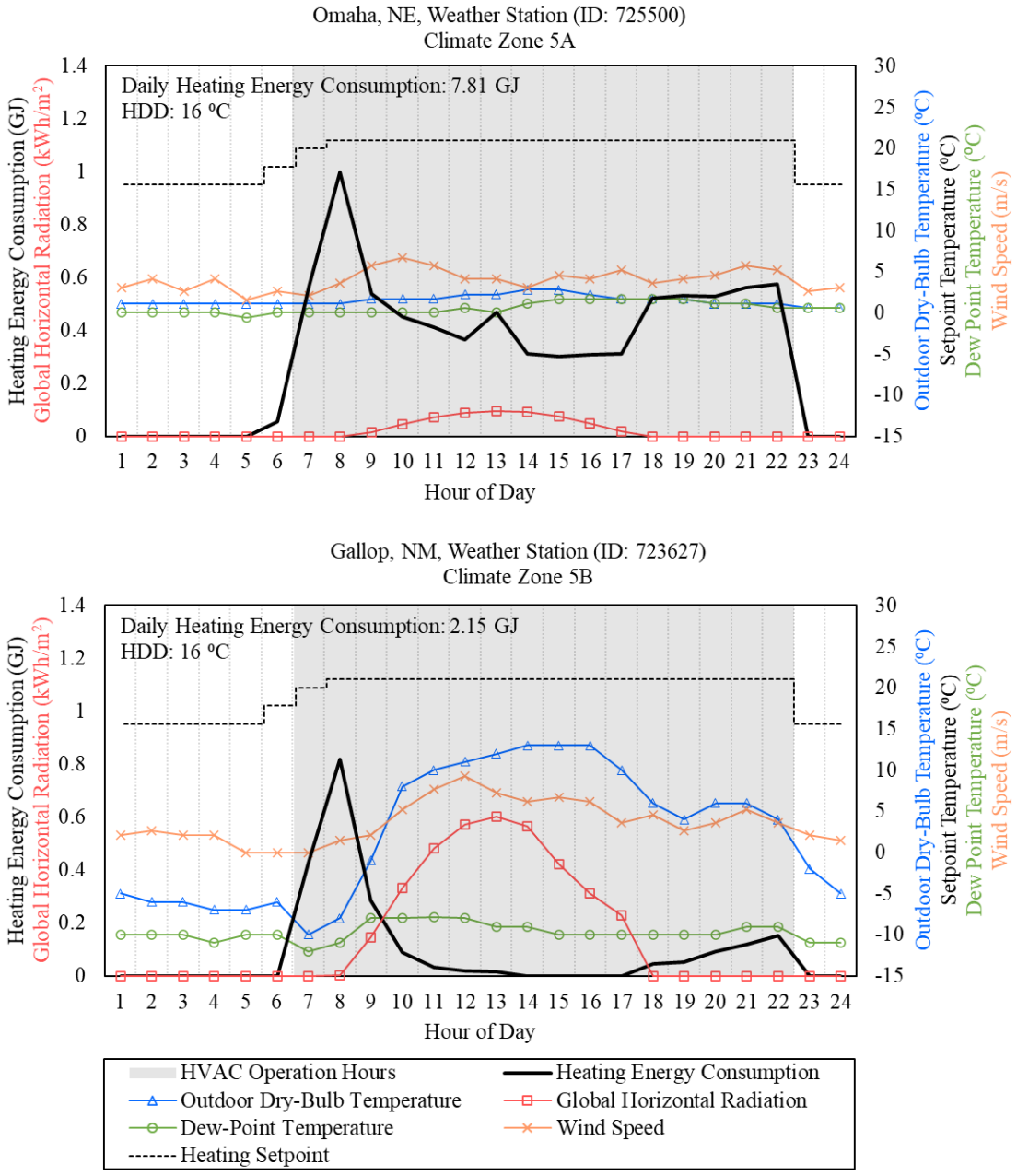

Figure 42: Comparison of the Heating Energy Consumption and the Influential Weather Parameters of Two Locations with Similar HDD for January 11th

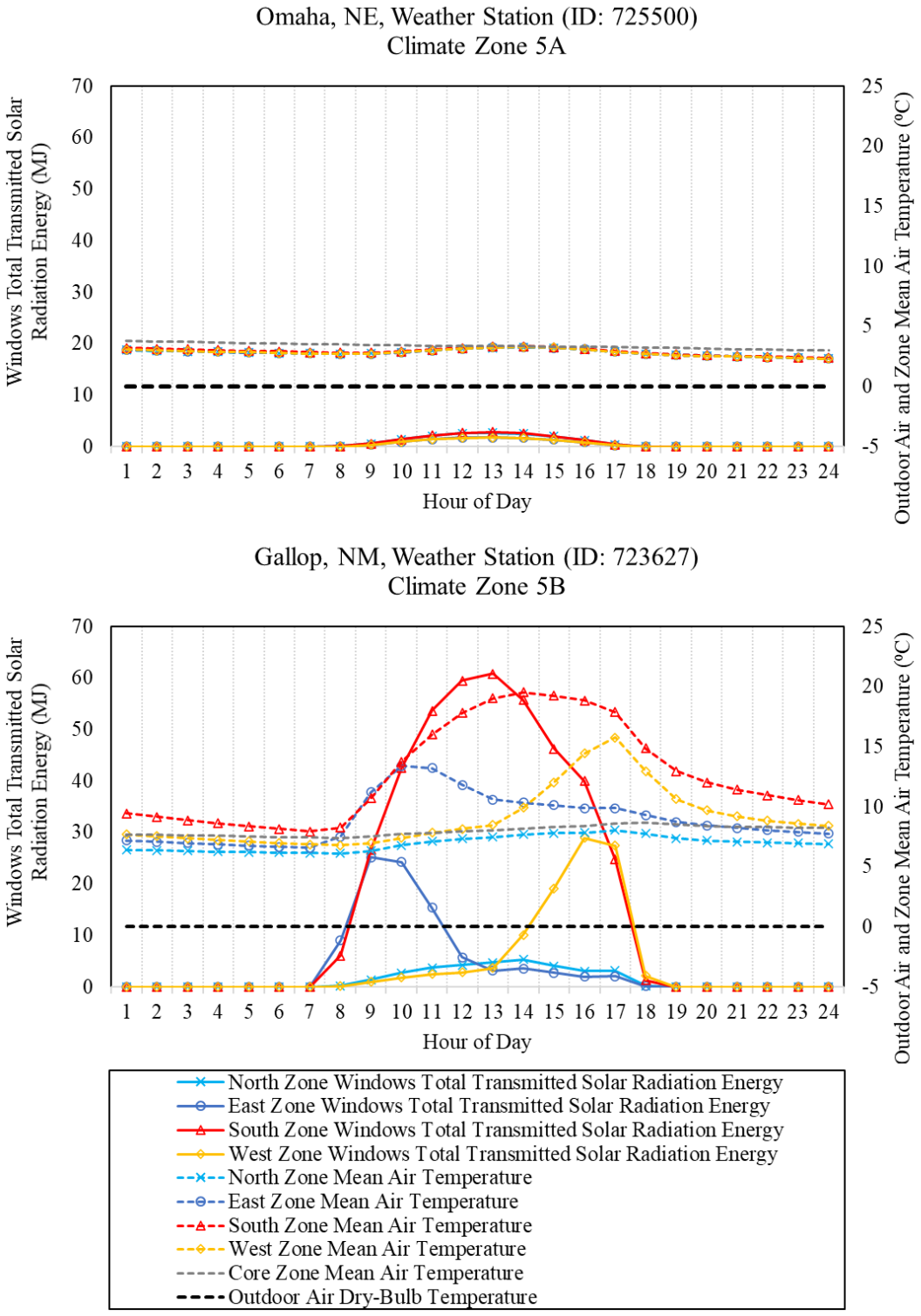

Figure 43: Total Transmitted Solar Radiation through the Windows and the Mean Air Temperature of the Middle Floor Zones for January 11th

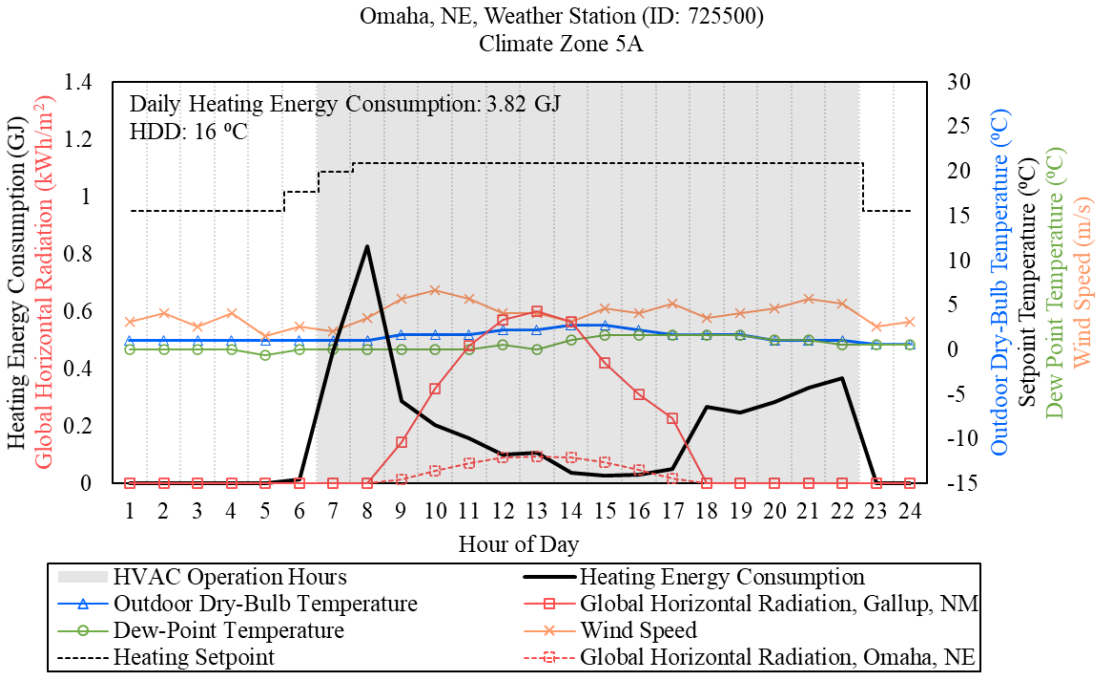

Figure 44: Heating Energy Consumption for January 11th Using the Solar Radiation Data from Gallup, NM

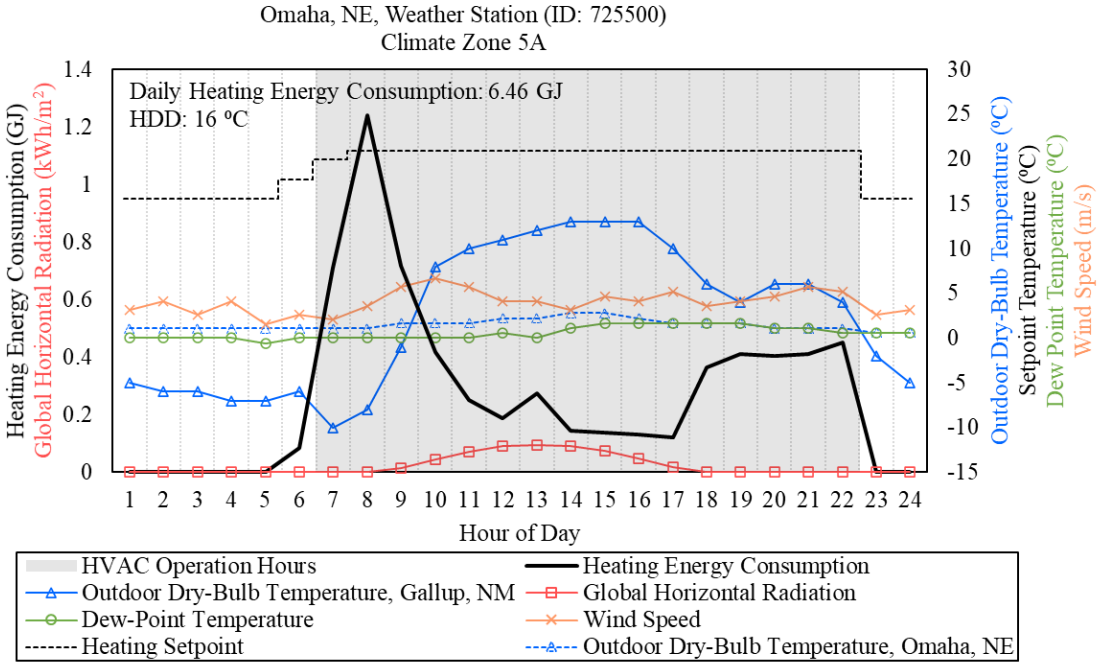

Figure 45: Heating Energy Consumption for January 11th Using the Dry-Bulb Temperature Data from Gallop, NM

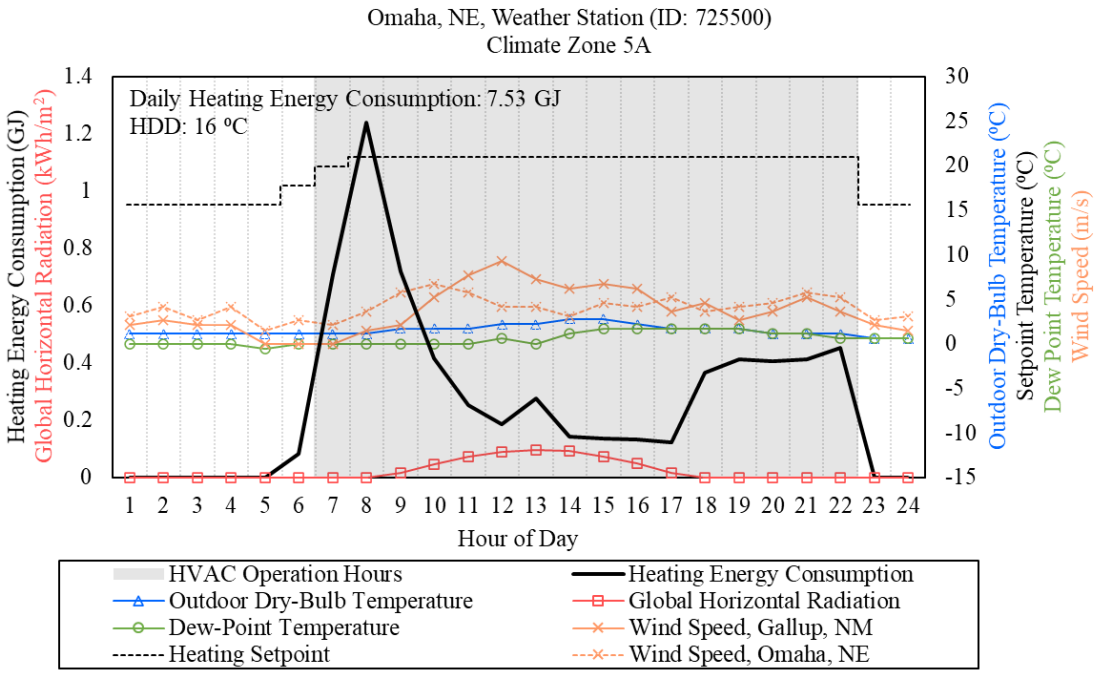

Figure 46: Heating Energy Consumption for January 11th Using the Wind Data from Gallop, NM

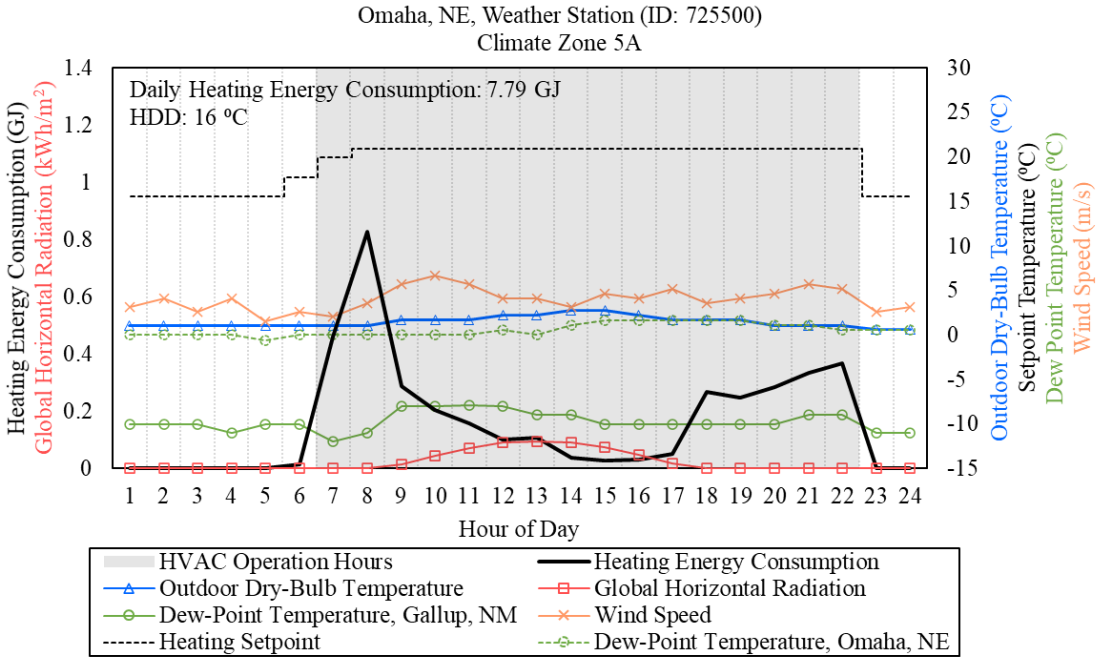

Figure 47: Heating Energy Consumption for January 11th Using the Humidity Data from Gallop, NM

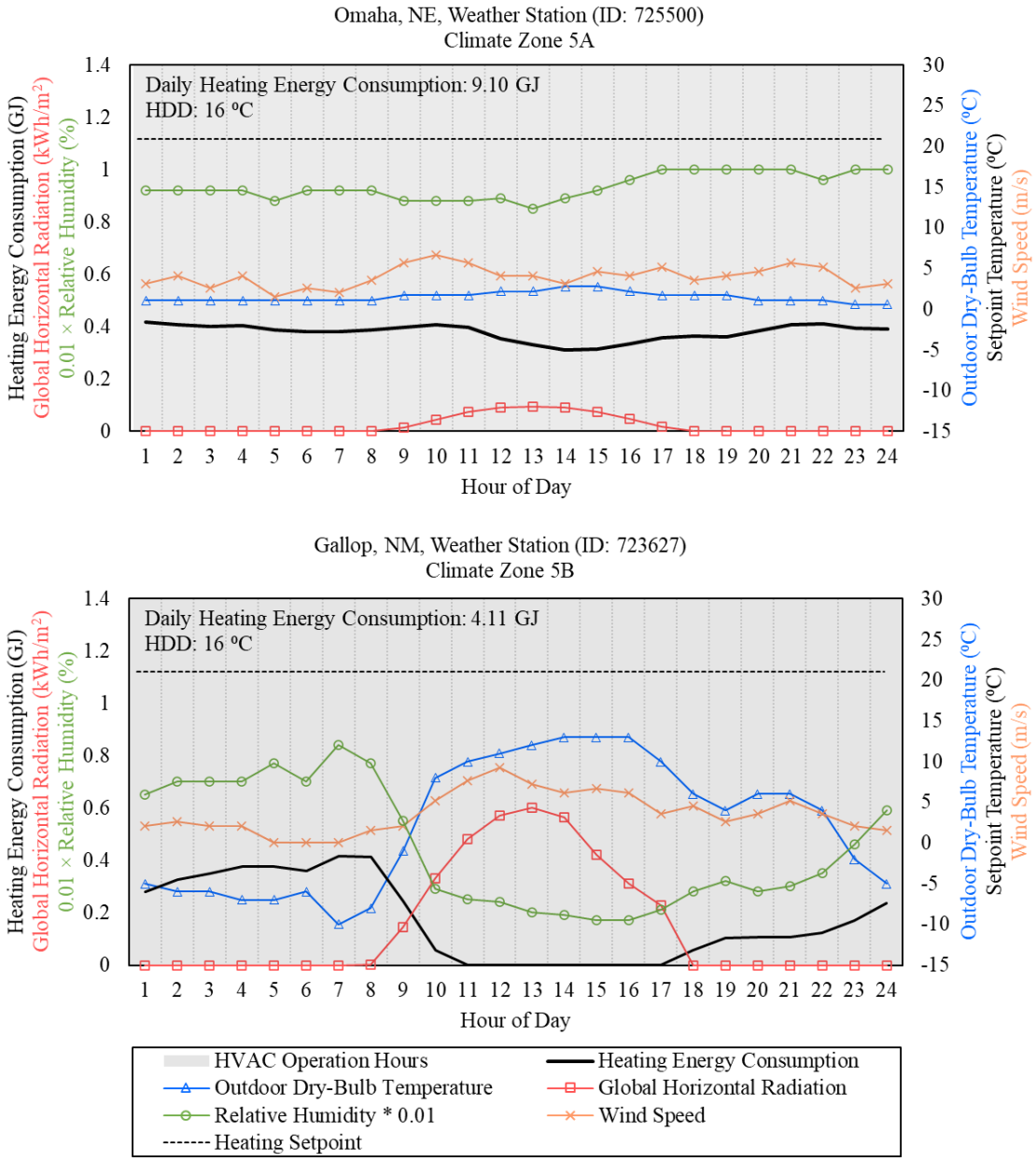

Figure 48: Comparison of the Heating Energy Consumption and the Influential Weather Parameters of the Two Locations with Similar HDD for January 11th in Models with 24-Hours Operating Schedule

To further analyze the impact of the solar radiation on the heating energy consumption, the model in climate zone 5A was simulated using a modified weather file, where the solar radiation data from the weather file for climate zone 5B was used in the modified weather file for climate zone 5A. The results, shown in Figure 44, reveal that similar solar radiation makes the heating energy consumption of the two locations much closer to each other. Specifically, the heating energy consumption in climate zone 5A was reduced from 7.8 GJ to 3.8 GJ, which is closer to the 2.1 GJ, which was the heating energy consumption in climate zone 5B. In other words, the heating energy consumption was 3.6 times larger in climate zone 5A compared to climate zone 5B using the actual weather files and only 1.8 times larger while using the identical solar radiation data, which means a large portion of the variation is attributable to the solar radiation parameter.

Besides the solar radiation data, replacing the dry-bulb temperature will also significantly reduce the difference (Figure 45). Furthermore, replacing the wind data also reduces the difference (Figure 46). However, compared to the impact of replacing the dry-bulb temperature, replacing the wind data had a lower impact in reducing the differences in the energy consumption between the two sites.

Replacing the humidity data only slightly reduces the difference due to the moisture content in the air (Figure 47). However, the impact of the humidity is less pronounced compared to other parameters. The contribution from the water vapor in the calculation of the heating load is relatively small since, as depicted in Figure 49 and illustrated in equation 4.1, the small value of the humidity ratio makes the impact of the moisture in the air less pronounced in the calculation of the total enthalpy change.

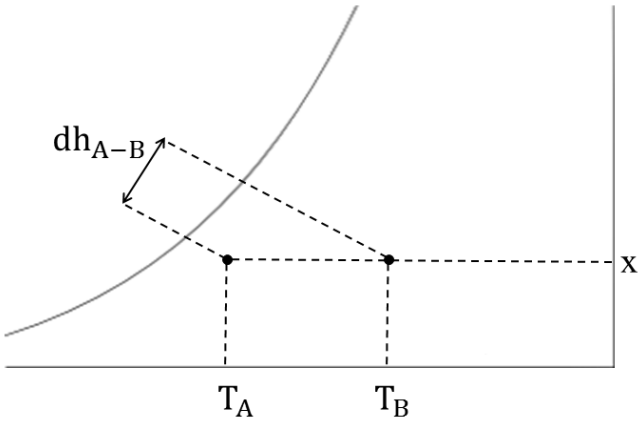

Figure 49: Schematic Representation of the Heating Process

$$dh_{A-B} = C_{p-air}(T_B - T_A) + xC_{p-water}(T_B - T_A) \quad (4.1)$$

Where dh_{A-B} represents the enthalpy difference of the moist air between A and B, C_{p-air} specific heat capacity of air, $C_{p-water}$ is the specific heat capacity of water, T_A and T_B are the dry-bulb temperature of points A and B, respectively, and x is the humidity ratio.

Figure 48 shows the heating energy consumption of the model in the 24-hour operating configurations at the two selected locations. In Figure 48, the peak demand in the first hours of operation using the office schedule (Figure 42) was no longer seen in the results of the heating energy use of the 24-hour schedule model due to the continuous operation of the heating equipment and internal loads. The lower temperature during the night-time and early morning in the case located in climate zone 5B resulted in a higher heating demand during the night and early morning, which lead to a closer daily heating use between the two locations. The results show the ratio of the heating energy consumption reduces from 3.6 times larger in climate zone 5A compared to climate zone 5B to 2.2 times larger in climate zone 5A compared to climate zone 5B. However,

although the difference in heating energy consumption was reduced, there was still a significant difference between two locations. The significant difference in heating energy use of the 24-hour operating model in the two locations shows that the difference in heating energy consumption is not only caused by the operation schedules and verifies the impact of other influential parameters on the variation in the heating energy consumption of each location.

As illustrated in Figure 48, it can be seen that while there was a lower temperature at night in case of climate zone 5B, the heating energy use during those hours was not significantly higher than the case of climate zone 5A. In fact, the thermal mass effect of the building impacts the heating demand in the hours proceeding the night. During the day, the direct solar gains result in lower energy consumption for the case of climate zone 5B. In fact, the internal gains and the solar radiation are shown to be sufficient to eliminate the heating demand for several hours (from 11 am to 5 pm) during the day.

Table 5: The Impact of Weather Parameters on the Heating Energy Consumption

Case No.	Weather File	Annual			Daily (January 11th)		
		Heating Energy Use	Difference with Base Case	Difference / Heating Energy Use	Heating Energy Use	Difference with Base Case	Difference / Heating Energy Use
		[GJ]	[GJ]	[%]	[GJ]	[GJ]	[%]
1	Gallup, NM[1] (Base Case)	387.86	0.00	0.00%	2.15	0.00	0.00%
2	Omaha, NE[2]	901.14	513.28	56.96%	7.81	5.66	72.47%
3	Omaha, NE, Except Solar Radiation Data from Gallup, NM	699.33	311.47	44.54%	3.82	1.67	43.75%
4	Omaha, NE, Except Dry-Bulb Temperature Data from Gallup, NM	763.43	375.57	49.19%	6.46	4.32	66.76%
5	Omaha, NE, Except Wind Data from Gallup, NM	828.61	440.75	53.19%	7.53	5.38	71.47%
6	Omaha, NE, Except Humidity Data from Gallup, NM	899.91	512.04	56.90%	7.79	5.64	72.41%

1. Gallup, NM, weather station (ID: 723627) is classified in climate zone 5B
2. Omaha, NE, weather station (ID: 725500) is classified in climate zone 5A

In summary, the analysis in this section showed that the solar radiation is a measure that is not fully accounted in HDD and has high impact on the differences in heating energy consumption of the two near-identical HDD locations in climate zone 5A and climate zone 5B.

4.3.2.2. Analysis of the Impact of Diurnal Temperature Profiles on the Variations in Heating Energy Consumption in Locations with Similar HDD

On average, the diurnal temperature range has different patterns in different moisture regimes. Figure 50 shows the annual average outdoor dry-bulb temperature of the two selected locations. In the figure it can be seen that location in subtype A has a narrower diurnal temperature difference range compared to the one in subtype B. Overall, the diurnal temperature in dry subtype has higher probability to have higher temperature swing during a day.

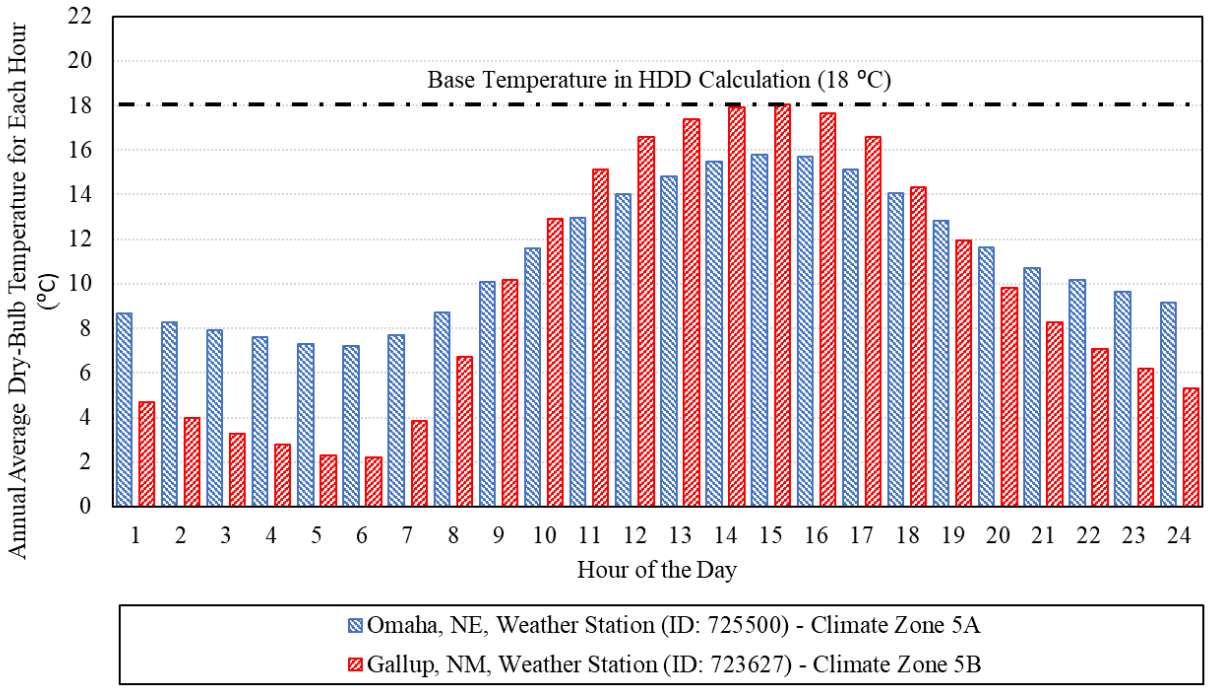

Figure 50: Comparison of the Annual Average Outdoor Dry-Bulb Temperature of Selected Weather Stations in Climate Zone 5, Subtypes A and B

This section presents the analysis of the impact of diurnal temperature profile on the variations in heating energy use. In the analysis, seven simulations were performed to show the impact of the diurnal temperature profile on building heating energy use. In the analysis, an identical model was used in all seven simulations to analyze the impact of different diurnal temperature profiles. Therefore, the only parameter changed in this analysis was the dry-bulb temperature of the weather files used in the simulations. The analysis included two types of daily temperature profiles, including a flat and a sinusoidal temperature profiles with one cycle in 24 hours. In the analysis, six variations of the sinusoidal temperature profile were studied with only a difference in the peak hour, ranging from 12:00 PM to 5:00 PM with increments of one hour. Figure 51 shows the flat temperature profile and different sinusoidal diurnal temperature profiles.

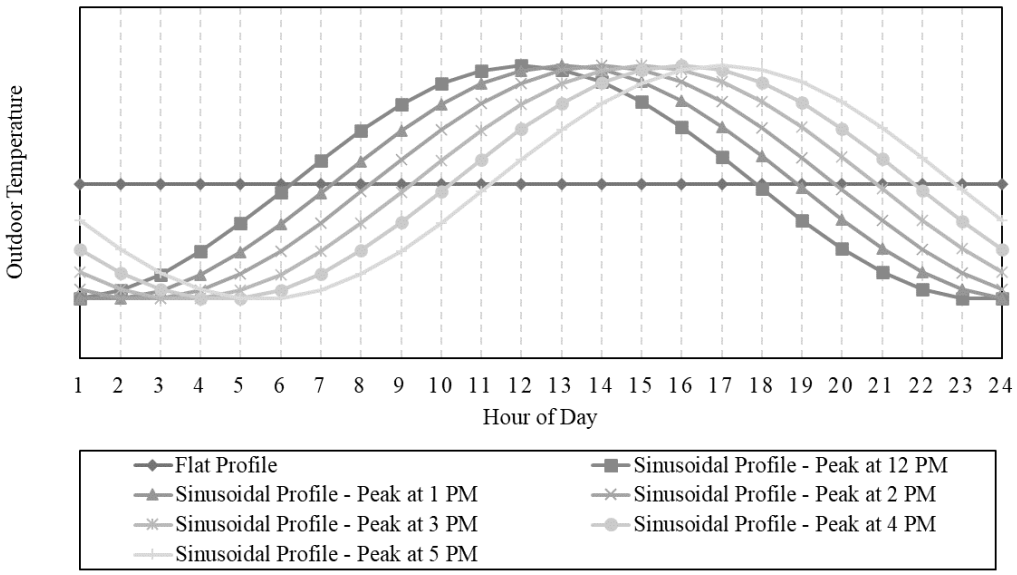

Figure 51: Representation of the Flat Temperature Profile and Different Sinusoidal Diurnal Temperature Profiles

A summary of the analysis of the impact of the diurnal temperature profile on the variations in heating energy consumption is shown in Table 6. In all six simulations, the heating

energy consumption using the sinusoidal temperature profile was higher than the heating energy consumption with flat average temperature. Figure 52 shows the cumulative heating energy use for the different simulations using the sinusoidal temperature profiles versus the cumulative heating energy using a flat average temperature profile. In a cumulative heating energy consumption the heating energy use of the previous hours are added in each hour and allows comparing the total heating energy consumption up to each hour of the day. While the flat and the sinusoidal temperature profile yield the same HDD, the impact of the higher heating demand in the early operating hours in sinusoidal temperature profile is more pronounced than the slightly lower heating consumption during the day. An example of comparative analysis of the flat and sinusoidal temperature profile is shown in Figure 53. Overall, the results for the heating energy consumption using sinusoidal temperature profile is slightly higher than the flat temperature profile using the identical ASHRAE Standard 90.1-2016 medium office prototype model. However, the difference is negligible compared to the variations in the heating energy consumption of the two selected cities using the corresponding actual weather file for each city.

Overall, the diurnal temperature profile has a very small impact on the heating energy consumption. Typically, locations in subtype A have a narrower diurnal temperature range compared to the one in subtype B. Although the impact of the diurnal temperature range shows that flat average temperature profile has slightly less heating energy compared to the sinusoidal profiles, the results of heating energy consumption show higher energy consumption in subtype A. This is mainly due to the fact that the impact of the other influential parameters are more pronounced compared to the diurnal temperature profile shape. Furthermore, the actual weather files in subtype A are still sinusoidal, which makes the small difference between the flat and sinusoidal temperature profiles even less.

Table 6: The Impact of Diurnal Temperature Profile on the Heating Energy Consumption

Case No.	Weather File[1]	Annual			Daily		
		Heating Energy Use	Difference with Base Case	Difference / Heating Energy Use	Heating Energy Use	Difference with Base Case	Difference / Heating Energy Use
		[GJ]	[GJ]	[%]	[GJ]	[GJ]	[%]
1	Flat Dry-Bulb Temperature Profile (Base Case)	1114.20	0.00	0.00%	3.55	0.00	0.00%
2	Sinusoidal Dry-Bulb Temperature Profile with Maximum at 12:00 PM	1191.06	76.86	6.45%	3.86	0.31	8.15%
3	Sinusoidal Dry-Bulb Temperature Profile with Maximum at 1:00 PM	1177.13	62.93	5.35%	3.75	0.20	5.42%
4	Sinusoidal Dry-Bulb Temperature Profile with Maximum at 2:00 PM	1180.89	66.69	5.65%	3.70	0.15	4.13%
5	Sinusoidal Dry-Bulb Temperature Profile with Maximum at 3:00 PM	1202.60	88.40	7.35%	3.72	0.18	4.78%
6	Sinusoidal Dry-Bulb Temperature Profile with Maximum at 4:00 PM	1240.55	126.35	10.19%	3.82	0.27	7.17%
7	Sinusoidal Dry-Bulb Temperature Profile with Maximum at 5:00 PM	1286.11	171.91	13.37%	3.98	0.43	10.86%

1. Parameters other than the dry-bulb temperature were set to zero throughout the weather file except the atmospheric station pressure, which is set to 101.3 kPa

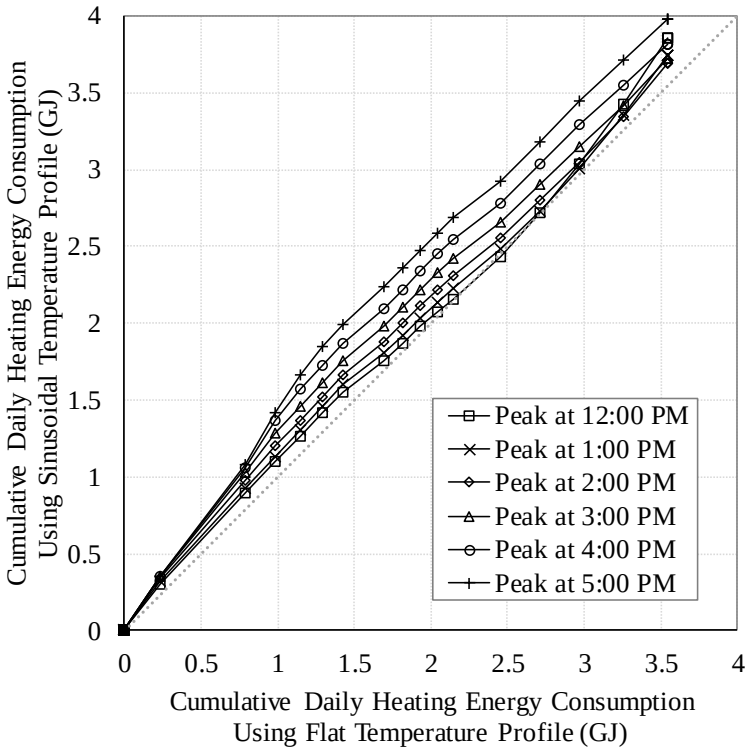

Figure 52: Comparison of the Cumulative Heating Energy Consumption of the Simulations Using a Sinusoidal Temperature Profile Versus a Flat Average Temperature Profile

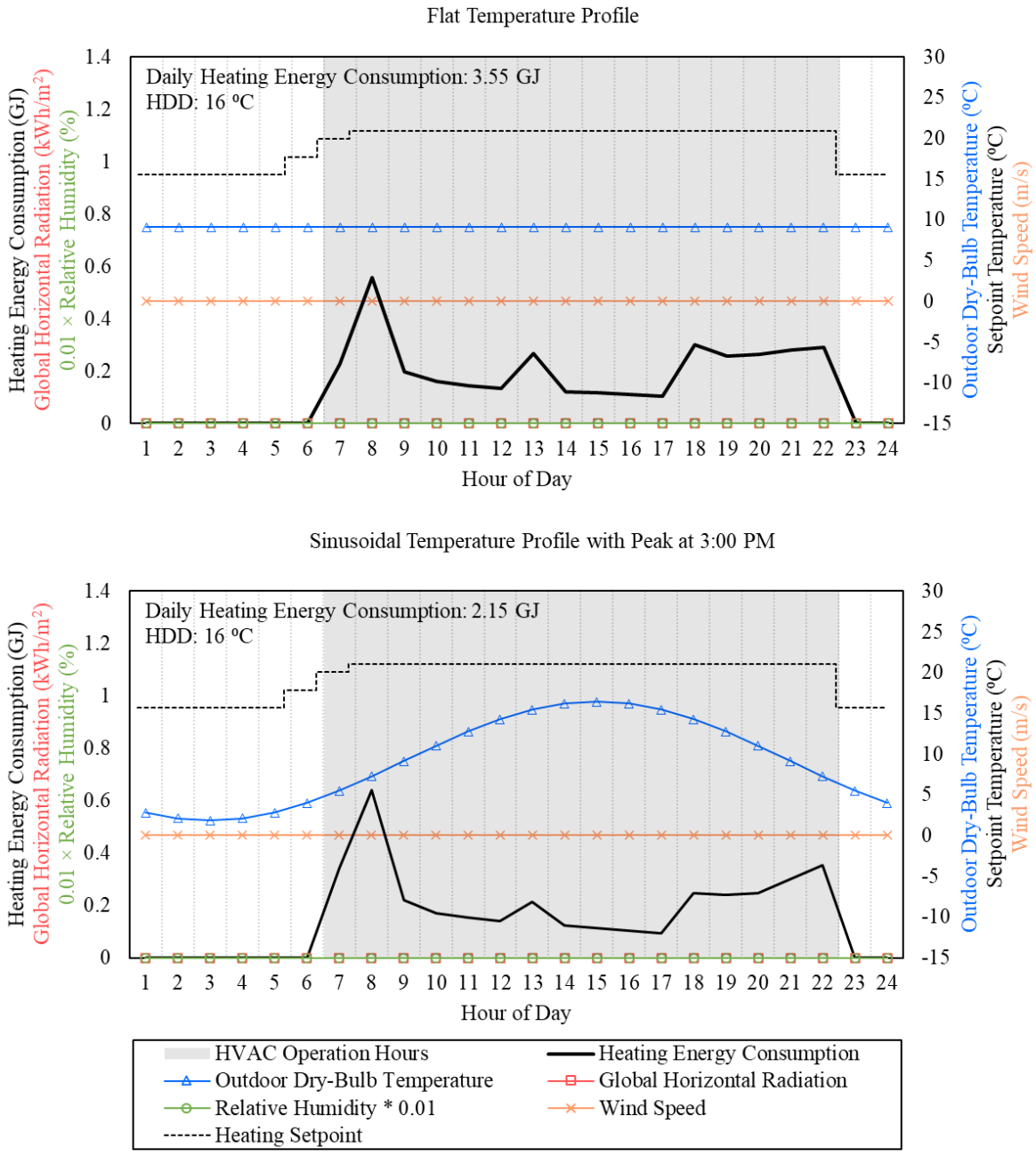

Figure 53: The Impact of the Diurnal Temperature Profile on the Heating Energy Consumption-The Case with Sinusoidal Peak Temperature at 3:00 PM

In addition to the direct impact of the diurnal temperature profile, it was observed that it roughly correlates with other influential parameters (e.g. solar radiation). Figure 54 shows the annual average hourly global horizontal radiation versus the annual average diurnal temperature

range of 801 different locations. In the figure it can be seen that there is a distinct difference between the annual average hourly global horizontal solar radiation between the dry and the moist and marine moisture regimes when looking at either the annual average diurnal temperature range or the annual average hourly global horizontal radiation. As shown in Figure 54, there is also a modest agreement between the increase of the annual average diurnal temperature range and the increase in annual average hourly global horizontal radiation in different subtypes. This correlation is more pronounced when using the exact hourly data instead of annual average values. Consequently, more important than the direct impact of the diurnal temperature, diurnal temperature can be used to crudely capture the differences in other influential weather parameters in different subtypes.

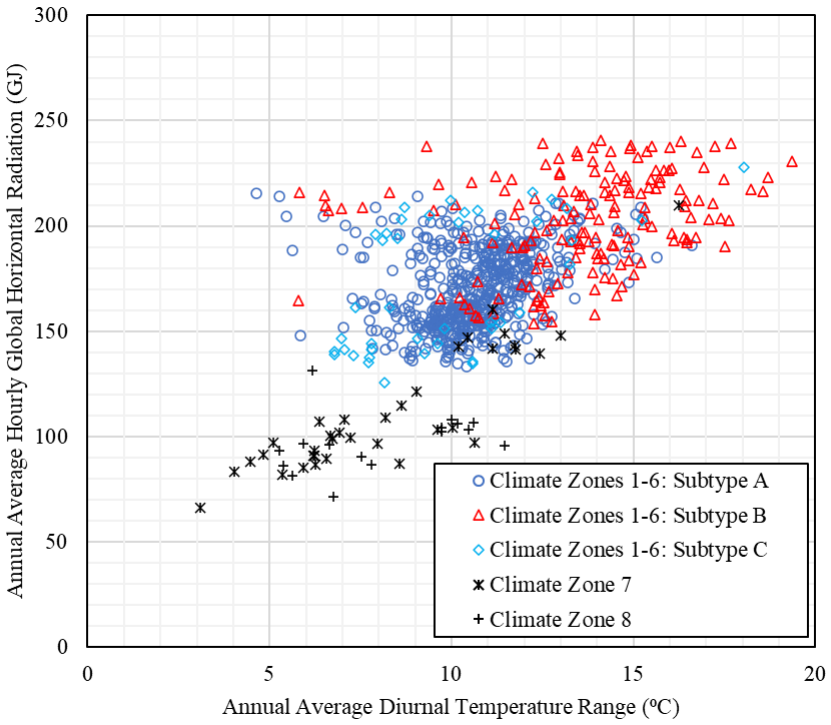

Figure 54: The Distinction of the Annual Average Solar Radiation in Dry versus Moist and Marine Moisture Regimes and Its General Increasing Trend with the Annual Average Diurnal Temperature Range

4.3.2.3. Summary of the Analysis of the Variations in Heating Energy Consumption in Locations with Similar HDD

In general, there are different weather parameters that influence building heating energy consumption, which are not accounted in the HDD measurements. Among these influential parameters, the highest impact is from the solar radiation. Other influential parameters are the wind dry-bulb temperature profile, wind, and humidity. Furthermore, the diurnal temperature range impacts building energy consumption. Although dry-bulb temperature is included in the calculations of the HDD, the replacement of the dry-bulb temperature still impacts the heating energy consumption. Besides the direct impact of the diurnal temperature range on building energy consumption, the diurnal temperature range roughly correlates with other influential weather parameters on heating energy use (e.g., global horizontal radiation).

4.3.3. Comparative analysis of the Variations in Cooling Energy Consumption in Locations with Similar CDD in Moist and Dry Moisture Regimes

While the CDD is a measurement used to classify the weather condition with respect to the anticipated cooling load in buildings, the results show that the cooling energy consumption can vary within the same ranges of CDD. Figure 55 shows the cooling energy consumption of the ASHRAE Standard 90.1-2016 medium office prototype models, complied with the requirements of each climate zone, in different locations with respect to the calculated CDD of the corresponding weather files and illustrates the variations within similar ranges of the CDD. Besides the overall trend of increasing the cooling energy consumption with increased CDD, it can be seen that, on average, the cooling energy consumption of the locations with similar CDD tends to be higher in moist areas compared to dry areas.

Therefore, to study this further, two locations with similar CDDs that have different cooling energy consumption were chosen in moist (Subtype A) and dry (Subtype B) areas for further analysis. As shown in Figure 55, these locations are: the Chattanooga-Lovell Field Airport (weather station ID: 723240), located in Hamilton county, Tennessee, classified in climate zone 3A, and the Truth or Consequences Municipal Airport (weather station ID: 722710), located in Sierra county, New Mexico, classified in climate zone 3B. It can be seen that while the CDD in the Truth or Consequences Municipal Airport was slightly higher than the CDD in the Chattanooga-Lovell Field Airport (2687 versus 2678), the cooling energy consumption in Chattanooga-Lovell Field Airport was significantly higher than in Truth or Consequences Municipal Airport (1025 GJ versus 869 GJ).

In order to remove the impact of various building configurations in the analysis, the results of the cooling energy consumption of an identical ASHRAE Standard 90.1-2016 medium office prototype model that complied with climate zone 4B with respect to the calculated CDD of the corresponding weather files are illustrated in Figure 56. Similar to the results of the models complied with the requirements for each climate zone, the results of the simulations of the identical model show variations in cooling energy consumption of the models within similar CDD. In the analysis it was observed that the moisture regimes seemed to have distinct separate patterns in cooling energy consumption. By comparing the cooling energy consumption in locations with similar CDD, on average, the dry locations seems to have lower cooling energy consumption compared to the moist locations.

The two selected locations with similar CDD and different cooling energy consumption in the two moisture regimes, shown in Figure 55, are also illustrated in Figure 56. Figure 57 locates the selected cities on the county-wide U.S. climate classification map. In this analysis, the

same simulation model (ASHRAE Standard 90.1 prototype building model for climate zone 4B) was used to enable studying only the weather impacts (Figure 40). The CDD of the selected city in climate zone 3A and 3B were 2678 and 2687, respectively. The annual cooling energy consumption of the models in the selected city in climate zone 3A and 3B were 1025 GJ and 869 GJ for the models complied with each climate zone and 1160 GJ and 996 GJ for the identical model. It can be seen that although the CDD of the selected city in climate zone 3B was slightly higher than the CDD of the selected city in climate zone 3A, the cooling energy was significantly higher in the selected city in climate zone 3A compared to the selected city in 3B.

Similar to HDD, there are different influential weather variables that are not considered in the CDD measurement that impact the heating energy consumption. For example, weather data with different daily profiles can have similar CDD. These different daily profiles can lead to varying cooling energy consumption in locations with similar CDD.

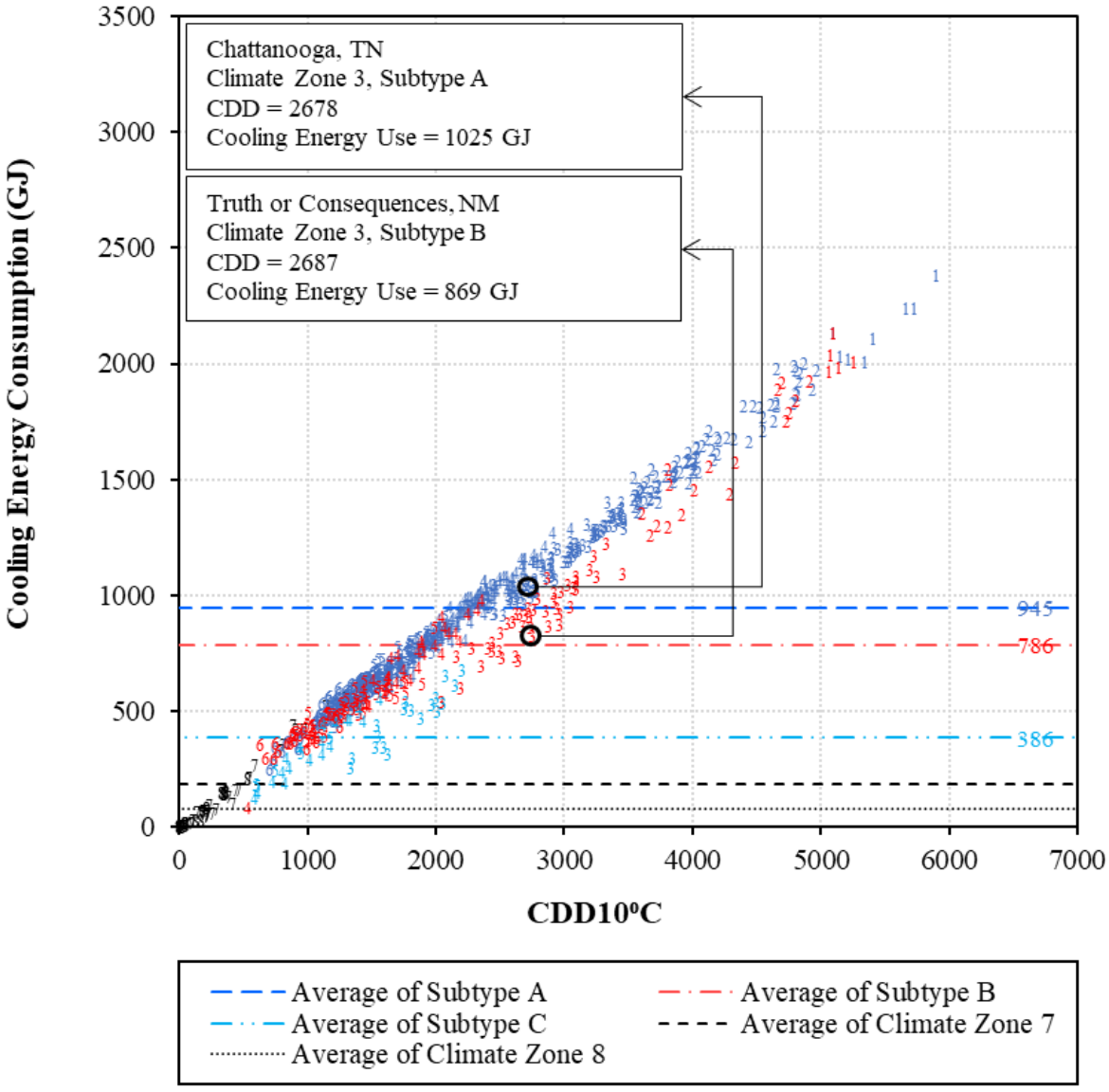

Figure 55: Variation of the Cooling Energy Consumption Using the Prototype Models Complied with Each Zone and the Representation of the Two Selected Cases with Similar CDD and Different Cooling Energy Consumption

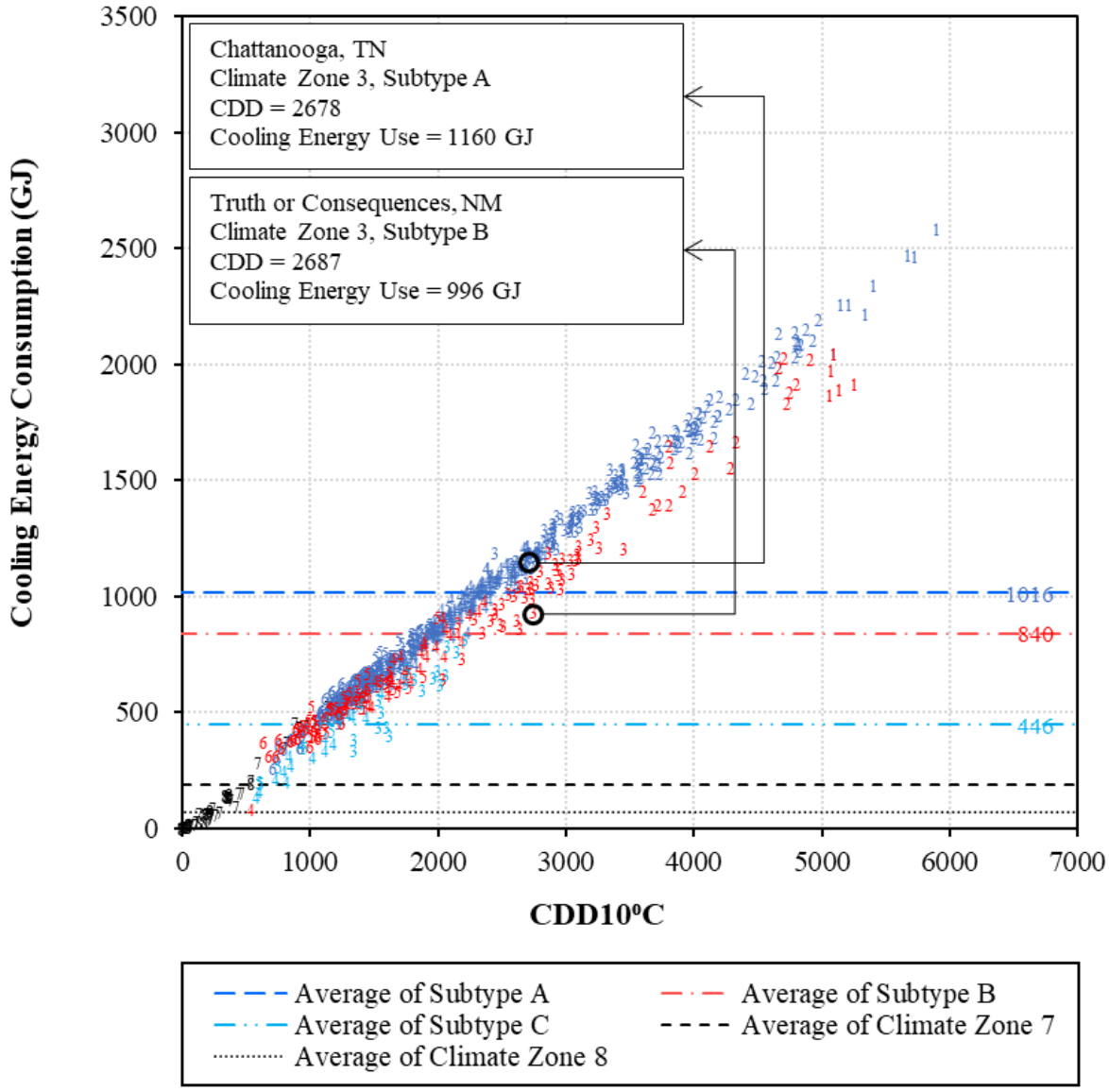

Figure 56: Variation of the Cooling Energy Consumption Using an Identical Model and the Representation of the Two Selected Cases with Similar CDD and Different Cooling Energy Consumption

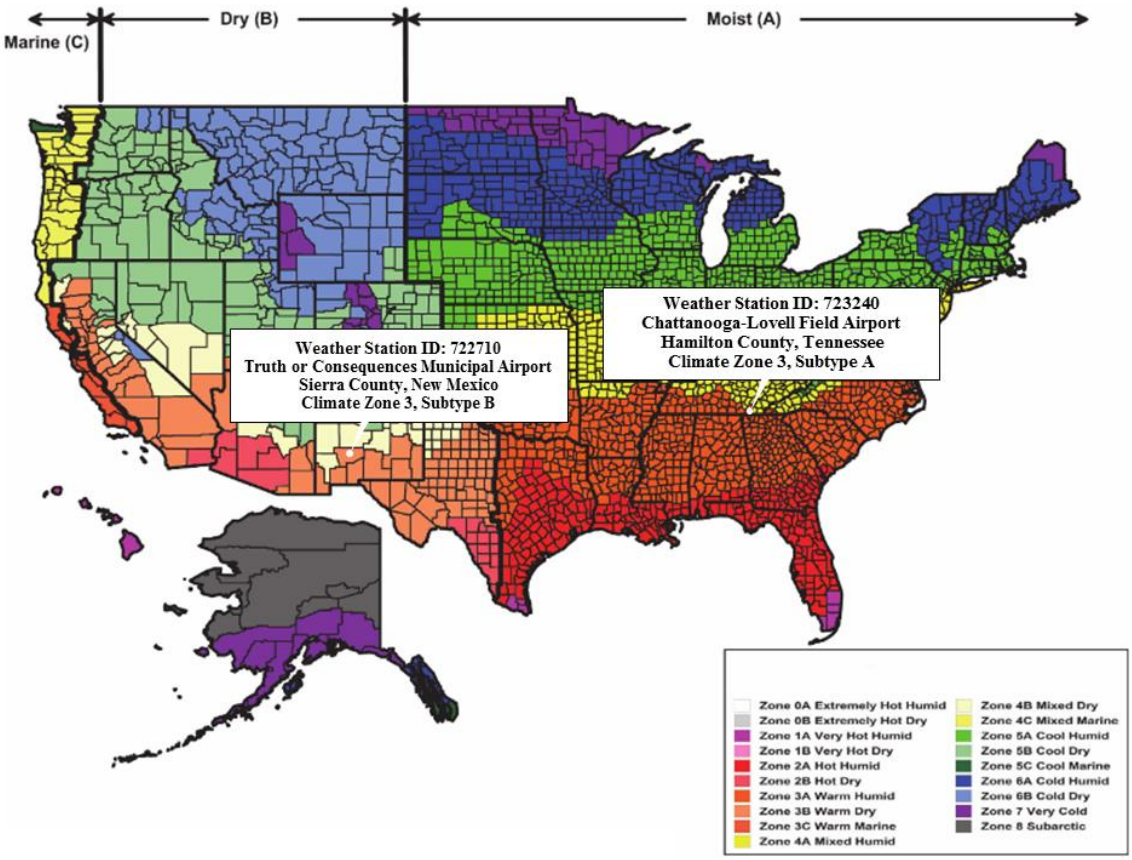

Figure 57: Selected Weather Stations in Climate Zone 3, Subtypes A and B. ©ASHRAE, www.ashrae.org. Original map used with permission from 2013 ASHRAE Standard-169 (Map: (ASHRAE, 2013a))

4.3.3.1. Analysis of the Impact of Solar Radiation, Dry-Bulb Temperature, Humidity, and Wind on the Variations in Cooling Energy Consumption in Locations with Similar CDD

This section seeks to analyze the variations in cooling energy consumption for locations with similar CDDs. The analysis starts by simulating a similar selected building model using the corresponding weather files. Then, four simulations are carried out to reveal the impact of solar radiation, dry-bulb temperature, wind, and humidity on the building cooling energy consumption.

Finally, to reveal the impact of the operating schedule, a 24-hour operating model was simulated using these two weather files.

Figure 58 shows the daily profile of the outdoor dry-bulb temperature, global horizontal solar radiation, relative humidity, wind speed, and the heating energy consumption at the two selected sites on June 22nd. Although the two sites have almost the same CDD (approximately 15 ºC), there was a difference in the cooling energy consumption on that day (8.74 GJ and 6.22 GJ for climate zones 3A and 3B, respectively). In the analysis it could be seen that although the CDD was slightly lower at the site located in climate zone 3A compared to the site in climate zone 3B, the daily cooling energy consumption in the site located in climate zone 3A was more than the the site located in climate zone 3B. It is worthwhile to mention that the comparisons in the selected day do not mean that similar variations will necessarily apply for all days in different moisture regimes (in this case subtypes A and B).

Table 7 shows the impact of the weather parameters on both the annual cooling energy consumption and for the selected day, June 22nd. Truth or Consequences Municipal Airport weather station (ID: 722710), located in Climate Zone 3B, is selected as the basecase. Figure 59 to Figure 62 show the parameters and the results for June 22nd and Figure 63 illustrates the results of the simulations of the models with 24-hours operating schedules in June 22nd.

Similar to the analysis of the variations in hearing energy consumption, the cooling energy consumption is also affected by the weather parameters that are not included in CDD. However, the weather parameters affect the cooling energy consumption differently compared to the analysis on heating energy consumption in section 4.3.2.1.

First, the main difference with the results of the analysis conducted for the variations in heating energy consumption is the more pronounced impact of humidity on cooling energy

consumption. In fact, replacing the humidity data variable of the Chattanooga-Lovell Field Airport weather station (ID: 723240), located in Climate Zone 3A with the corresponding data the Truth or Consequences Municipal Airport weather station (ID: 722710), located in Climate Zone 3B creates a large enough difference to make the cooling energy consumption in 3A lower than 3B (Figure 62). The contribution from the water vapor in the calculation of the cooling load is much higher than in the calculation of heating loads since besides the sensible cooling load, the cooling procedure may include dehumidification, which impacts the total enthalpy change.

Furthermore, unlike the analysis on heating energy consumption in Section 4.3.2.1, replacing the solar radiation variable (Figure 59) and dry-bulb temperature variable (Figure 60) of the location in 3A with the corresponding data from 3B increased the difference. This increase is mainly due to the higher solar radiation in 3B and higher dry-bulb temperature during the operation hours. Replacing the wind data trivially reduces the difference (Figure 61).

Table 7: The Impact of Weather Parameters on the Cooling Energy Consumption

Case No.	Weather File	Annual			Daily (June 22nd)		
		Cooling Energy Use	Difference with Base Case	Difference / Cooling Energy Use	Cooling Energy Use	Difference with Base Case	Difference / Cooling Energy Use
		[GJ]	[GJ]	[%]	[GJ]	[GJ]	[%]
1	Truth or Consequences, NM[1] (Base Case)	996.0	0.00	0.00%	6.22	0.00	0.00%
2	Chattanooga, TN[2]	1160.0	164.06	14.14%	8.74	2.52	28.83%
3	Chattanooga, TN, Except Solar Radiation Data from Truth or Consequences, NM	1242.8	246.78	19.86%	8.78	2.56	29.16%
4	Chattanooga, TN, Except Dry-Bulb Temperature Data from Truth or Consequences, NM	1260.4	264.42	20.98%	9.08	2.86	31.52%
5	Chattanooga, TN, Except Wind Data from Truth or Consequences, NM	1154.3	158.31	13.71%	8.67	2.44	28.21%
6	Chattanooga, TN, Except Humidity Data from Truth or Consequences, NM	857.2	-138.75	-16.19%	5.55	-0.67	-12.09%

1. Truth or Consequences, NM, weather station (ID: 722710) is classified in climate zone 3B
2. Chattanooga, TN, weather station (ID: 723240) is classified in climate zone 3A

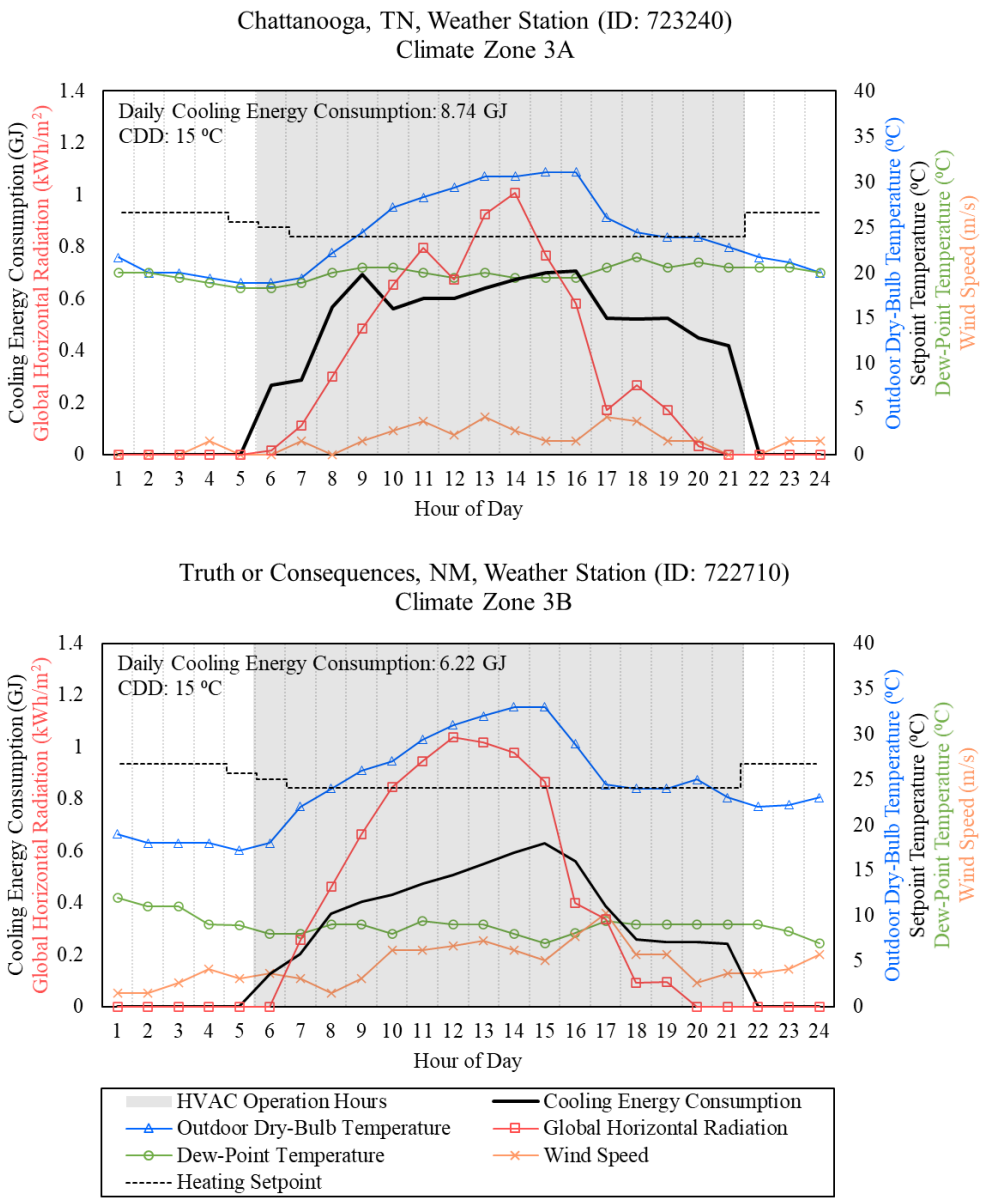

Figure 58: Comparison of the Cooling Energy Consumption and the Influential Weather Parameters of Two Locations with Similar CDD on June 22nd

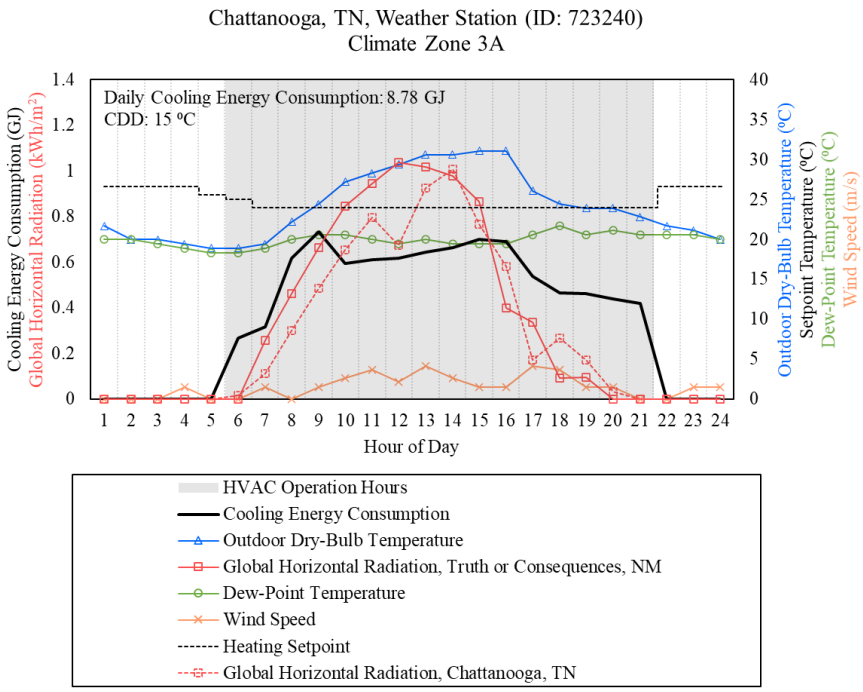

Figure 59: Cooling Energy Consumption Using the Solar Radiation Data from Truth or Consequences, NM

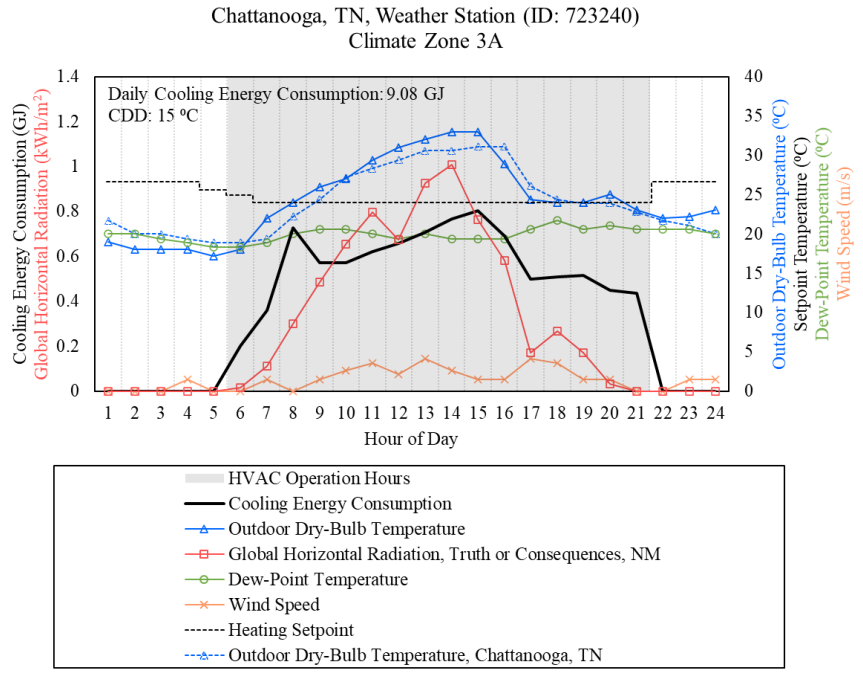

Figure 60: Cooling Energy Consumption Using the Dry-Bulb Temperature Data from Truth or Consequences, NM

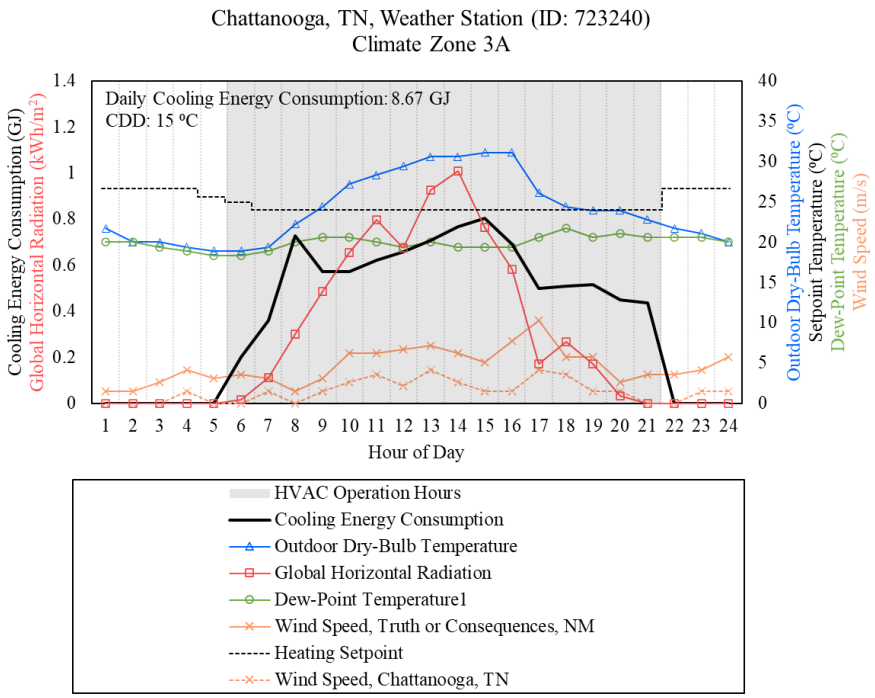

Figure 61: Cooling Energy Consumption Using the Wind Data from Truth or Consequences, NM

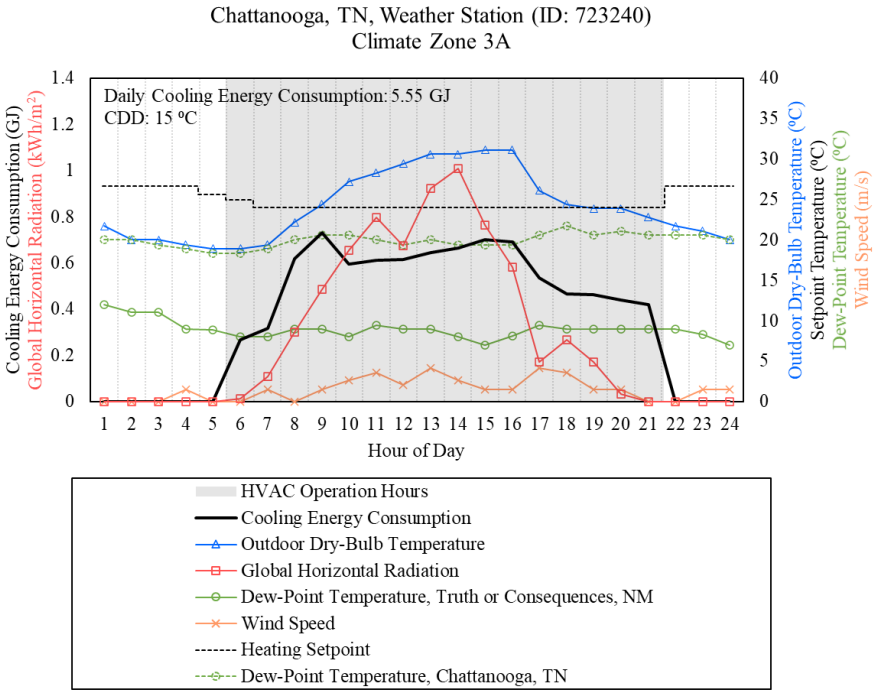

Figure 62: Cooling Energy Consumption Using the Humidity Data from Truth or Consequences, NM

Figure 63 shows the cooling energy consumption of the model in the 24-hour operating configuration in the two selected locations. In the figure it can be seen that the peak demand in the first hours of operation in the case with regular office schedule (Figure 58) is no longer seen in the results of the cooling energy use of the 24-hour schedule due to the continuous operation of the cooling equipment and internal loads. Unlike the cases discussed in Section 4.3.2.1, the solar radiation and dry-bulb temperature in the analysis of the cooling energy consumption in the two locations have similar patterns since the chosen date was June 22nd and both sites have almost clear sky conditions during the day. While the lower temperature during the night requires less cooling, the higher humidity during the night in 3A requires more cooling than 3B. However, it can be seen that the ratio of the cooling energy consumption reduces from 2.2 times larger in 3A compared to 3B to 1.6 times larger in 3A compared to 3B in the 24-hours operating schedule. Therefore, although the difference in cooling energy consumption is reduced, there still is a significant difference between the two locations. This invalidates justifying the difference in cooling energy consumption only by the operation schedules and verifies the impact of other influential parameters on the cooling energy consumption of each location.

Overall, the analysis in this section shows that the difference in the humidity data in the different moisture regimes is an important parameter that varies the cooling energy consumption in the locations with similar CDDs. Figure 64 shows the annual average of the daily average hourly dew-point temperature versus annual average diurnal temperature range in 801 different locations. In the figure there is a distinct separation between dry and moist/marine regimes using the annual average diurnal temperature range. It can also be seen that the dry locations have an average lower humidity compared to the moist and marine locations. Therefore, besides the direct impact of the

diurnal temperature range, diurnal temperature can be used to crudely capture the differences in other influential weather parameters in different subtypes.

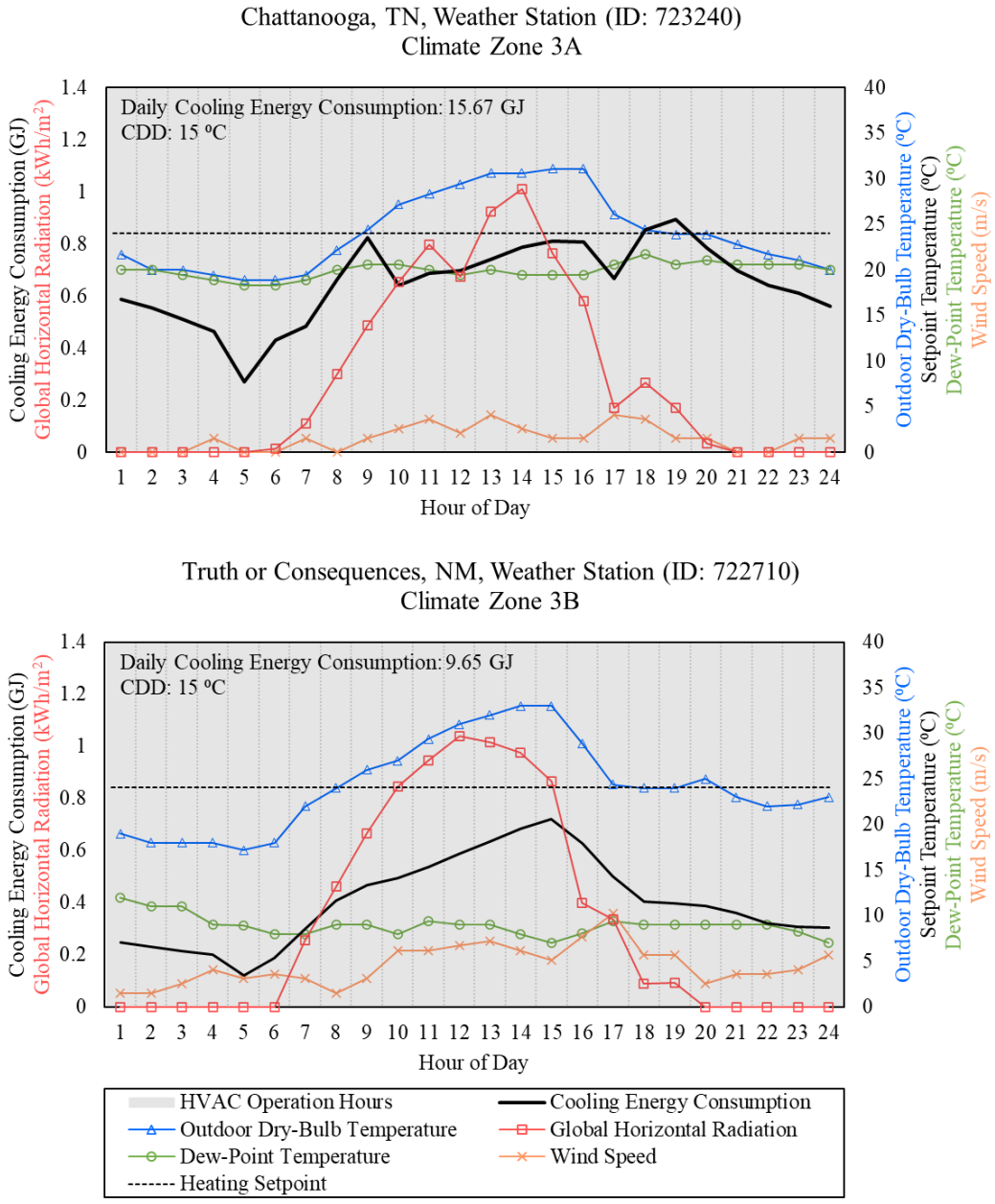

Figure 63: Comparison of the Cooling Energy Consumption and the Influential Weather Parameters of the Two Locations with Similar CDD on June 22nd in Models with 24-Hour Operating Schedule

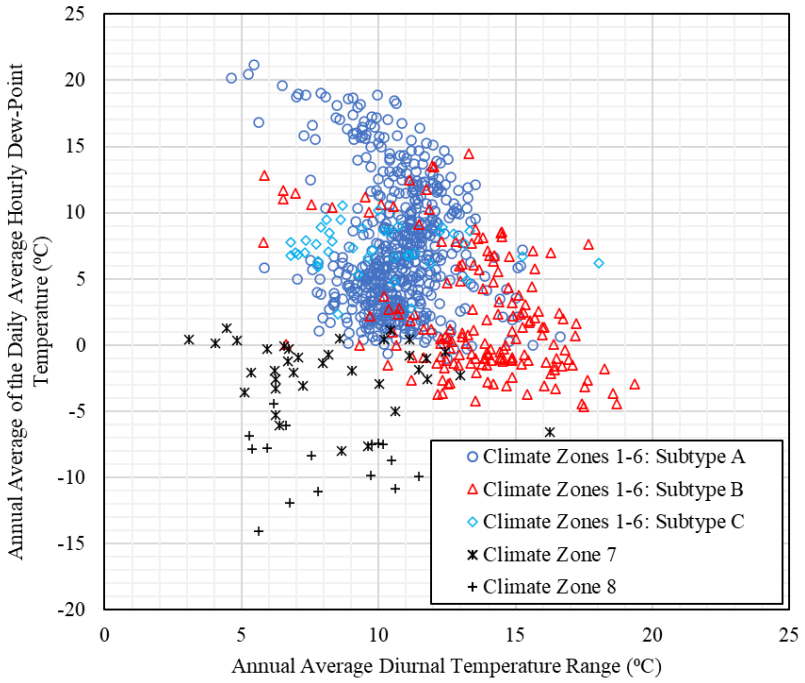

Figure 64: The Distinction of the Annual Average of the Daily Average Hourly Dew-Point Temperature in Dry (Subtype B) versus Moist (Subtype A) and Marine (Subtype C) Moisture Regimes

4.3.3.2. Analysis of the Impact of Diurnal Temperature Profiles on the Variations in Cooling Energy Consumption in Locations with Similar CDD

This section presents the analysis of the impact of the diurnal temperature profile on the variations in cooling energy consumption. In the analysis seven simulations were carried out to show the impact of the diurnal temperature profile on the building heating energy use. In the analysis an identical model was used for all seven simulations to review the impact of different diurnal temperature profiles. Therefore, the only parameter changing in this analysis is the dry-bulb temperature of the weather files used in the simulations. This analysis includes two types of daily temperature profiles, a flat and a sinusoidal temperature profile with a 24-hour cycle. Six

variations of the sinusoidal temperature profile were studied where the only difference was the peak hour, ranging from 12:00 PM to 5:00 PM with increments of one hour.

The summary of the results of the analysis of the impact of diurnal temperature profile on the variations in cooling energy consumption is shown in Table 8, which shows the cooling energy consumption in all six simulations using the sinusoidal temperature profile was higher than the one with a flat average temperature. Figure 65 shows the cumulative cooling energy use for the different simulations using the sinusoidal temperature profiles versus the cumulative cooling energy using a flat average temperature profile. While the flat and the sinusoidal temperature profiles yielded the same CDD, unlike in the heating energy consumption, the impact of the lower cooling demand in the early operating hours in the sinusoidal temperature profile was less pronounced than the largely higher cooling consumption during the day. An example comparative analysis of the flat and sinusoidal temperature profile is shown in Figure 66, which juxtaposes the case with flat profile and the case with sinusoidal profile with the peak temperature at 2:00 PM. Consequently, the results for the cooling energy consumption using sinusoidal temperature profile is higher than the flat temperature profile using the identical ASHRAE Standard 90.1 medium office prototype.

Table 8: The Impact of Diurnal Temperature Profile on the Cooling Energy Consumption

Case No.	Weather File[1]	Annual			Daily (June 22nd)		
		Cooling Energy Use	Difference with Base Case	Difference / Cooling Energy Use	Cooling Energy Use	Difference with Base Case	Difference / Cooling Energy Use
		[GJ]	[GJ]	[%]	[GJ]	[GJ]	[%]
1	Flat Dry-Bulb Temperature Profile (Base Case)	376.68	0.00	0.00%	1.34	0.00	0.00%
2	Sinusoidal Dry-Bulb Temperature Profile with Maximum at 12:00 PM	597.17	220.49	36.92%	2.10	0.76	36.19%
3	Sinusoidal Dry-Bulb Temperature Profile with Maximum at 1:00 PM	604.02	227.34	37.64%	2.13	0.79	37.06%
4	Sinusoidal Dry-Bulb Temperature Profile with Maximum at 2:00 PM	596.78	220.10	36.88%	2.11	0.77	36.50%
5	Sinusoidal Dry-Bulb Temperature Profile with Maximum at 3:00 PM	577.33	200.65	34.75%	2.05	0.71	34.58%
6	Sinusoidal Dry-Bulb Temperature Profile with Maximum at 4:00 PM	547.25	170.58	31.17%	1.94	0.60	31.08%
7	Sinusoidal Dry-Bulb Temperature Profile with Maximum at 5:00 PM	507.74	131.06	25.81%	1.80	0.46	25.76%

1. Parameters other than the dry-bulb temperature are set to zero throughout the weather file except the atmospheric station pressure, which is set to 101325 Pa

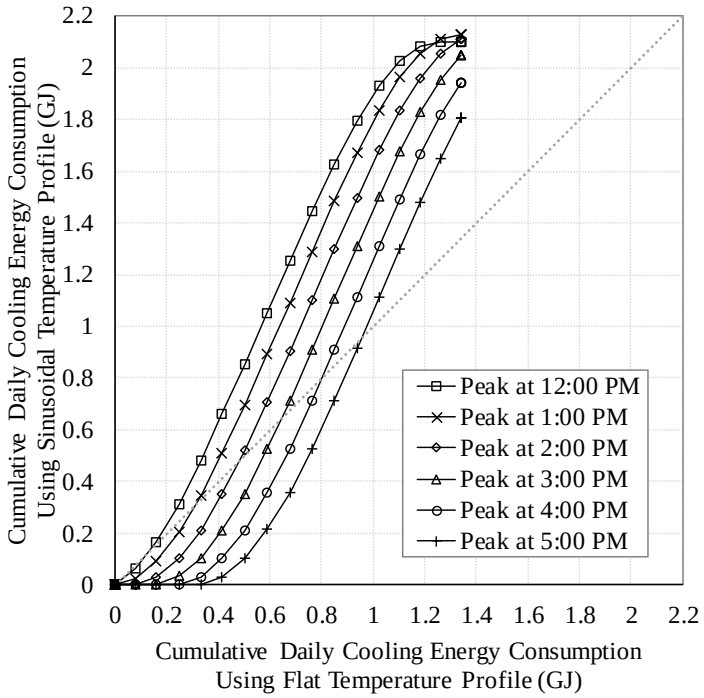

Figure 65: Comparison of the Cumulative Cooling Energy Consumption of the Simulations Using a Sinusoidal Temperature Profile versus a Flat Average Temperature Profile

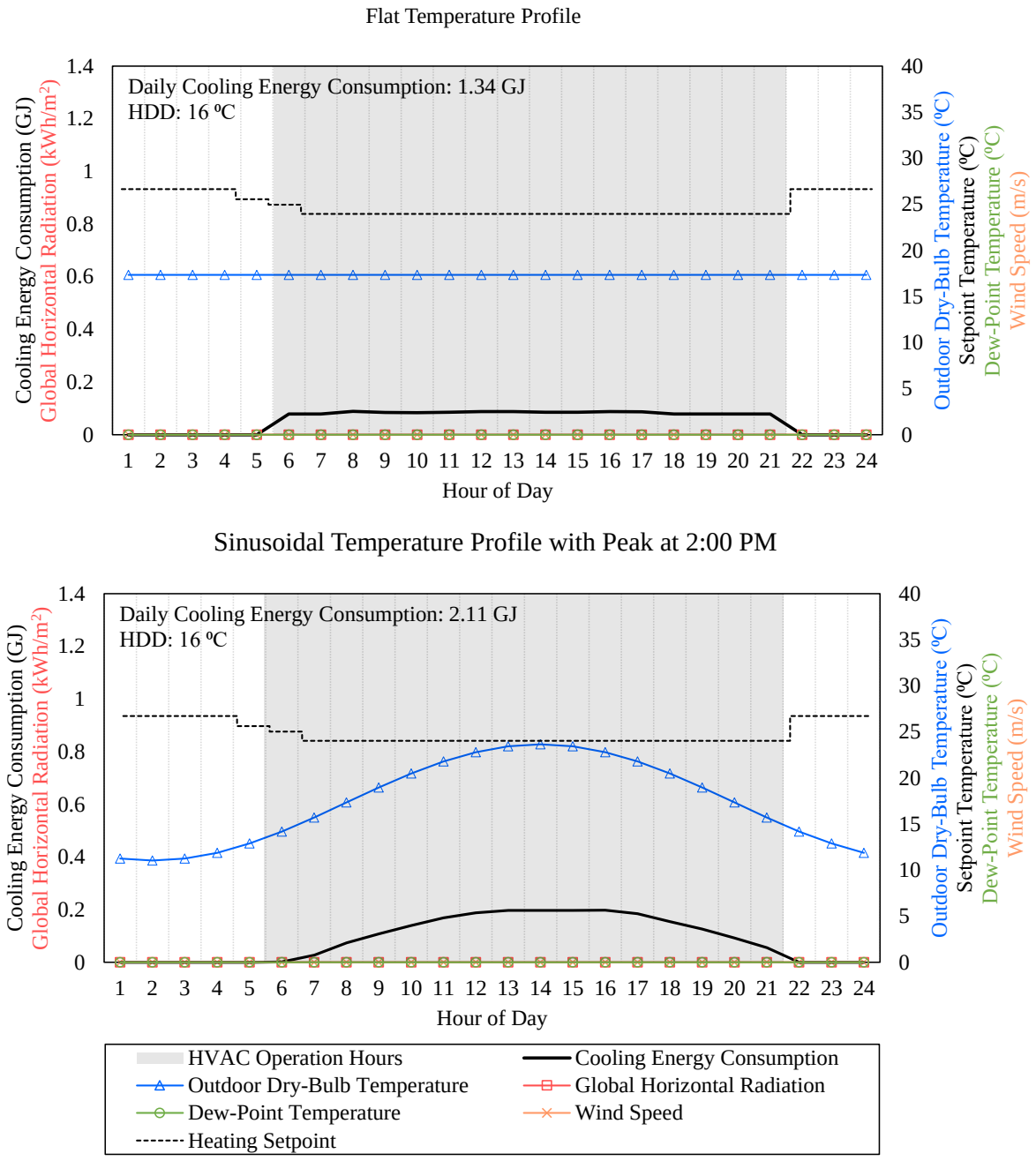

Figure 66: The Impact of the Diurnal Temperature Profile on the Cooling Energy Consumption-The Case with Sinusoidal Peak Temperature at 2:00 PM

4.3.3.3. Summary of the Analysis of the Variations in Cooling Energy Consumption in Locations with Similar CDD

In summary, this section has shown that there are different weather parameters that influence building cooling energy consumption, which are not accounted in CDD measurements. By comparing the two locations with similar CDD in different moisture regimes, the highest impact of these influential parameters was led by the various humidity in the two locations. Other influential parameters were the solar radiation, the dry-bulb temperature, and the wind. Although dry-bulb temperature is included in the calculations of the CDD, the replacement of the dry-bulb temperature still impacts the cooling energy consumption. Furthermore, the diurnal temperature range impacts building energy consumption. Besides the direct impact of the diurnal temperature range on building energy consumption, the diurnal temperature range roughly correlates with other influential weather parameters on heating energy use (e.g., humidity).

4.4. The Impact of Varying Energy Consumption on Code-Compliant Office Buildings

This section discusses the impact of the varying energy consumption from the medium office prototype models (DOE, 2018). In this Section there are two Sub-Sections: Section 4.4.1 discusses the variation in energy savings associated with the implementation of the daylight responsive controls, in which the variations in energy savings in different locations are discussed, indicating how the variations in the baseline energy consumption impact the total savings percentages; and section 4.4.2 discusses how the variations in the energy consumption impact the compliance using performance path.

4.4.1. Variation of the Energy Savings: A Case Study of the Associated Energy Savings with the Implementation of the Daylight Responsive Controls

This section includes the results of the simulations performed using the ASHRAE Standard 90.1-2016 medium office prototype models, which were complied with the code requirements for each climate zone, in different locations. The results include the regulated energy consumption of the models with and without daylight responsive controls followed by the total energy savings and the total energy savings percentage for each case.

APPENDIX C presents the results for the ASHRAE Standard 90.1-2016 medium office prototype models in each climate zone. It also includes the results for the analysis that used the identical model and the model for 24-hour operation schedule. The results of the regulated energy consumption, total energy savings, and total energy savings percentages in each climate zone are provided in Appendix C.1. The results of the simulations carried out using the identical ASHRAE Standard 90.1-2016 medium office prototype model in different climate zones is provided in Appendix C.2. The results of the models with 24-hour operating schedule is shown in Appendix C.3.

The results of the regulated energy consumption of the ASHRAE Standard 90.1-2016 medium office prototype models, which has the daylight responsive controls as required by the code, are presented in Section 4.2.1. Figure 67 through Figure 69 illustrate the regulated energy consumption of the models without daylight responsive controls. Similar trends and variations can be seen in the simulation of the models without daylight responsive controls.

Figure 67 consists of different plots. The main plot in Figure 67 shows the regulated energy consumption of an identical model with respect to the CDD10 °C. The frequencies of the CDD10 °C of the different subtypes is juxtaposed in the top plot. The frequencies of the

locations in Subtypes A and B sharply increases with increasing the CDD10 °C and meets their maximum in the 1250 to 1500 CDD10 °C. Then they gently decrease with increasing the CDD10 °C. Subtype C, climate zone 7, and climate zone 8 are less spread across the CDD10 °C frequencies and are spread across lower ranges of CDD10 °C. Similar to the representation of the frequencies of the CDD10 °C in the top frequency plot, the frequencies of the total regulated energy consumption is shown on the frequency plot on the right side of the main plot. The frequency plots show that the largest number of locations are in Subtype A. Subtype B has the second largest number of locations.

One important feature that the frequency plots for CDD10 °C and total regulated energy consumption show is that the frequencies of CDD10 °C for Subtype A and Subtype B are mixed in the frequency plot for CDD10 °C. However, there is a distinct separation between the frequencies of Subtype A and Subtype B in the frequency plot for the total regulated energy consumption, which shows that the CDD10 °C has not discriminated these two Subtypes effectively in terms of their energy consumption. Similar feature can be seen in Figure 68. While the frequency plot for the HDD18 °C, represented in the top frequency plot in Figure 68 shows a mixed pattern for Subtype A and Subtype B, the total regulated frequency plot on the right side of the main plot in Figure 68 (which is the same as in Figure 67) shows a distinct separation between the frequencies for the total regulated energy consumption of these two Subtypes.

Similar results are shown in Figure 69, which represents the results shown in Figure 67 and Figure 68 by including both CDD10 °C and HDD18 °C. Figure 69 also shows that the total regulated energy consumption can vary more than two times within one climate zone. For example, by looking at the results in climate zone 3, it can be seen that there are different

locations in Subtype A with total regulated energy consumption as more than twice higher than the sites in Subtype C. The difference between the regulated energy consumption in different Subtypes can be seen in other climate zones as well.

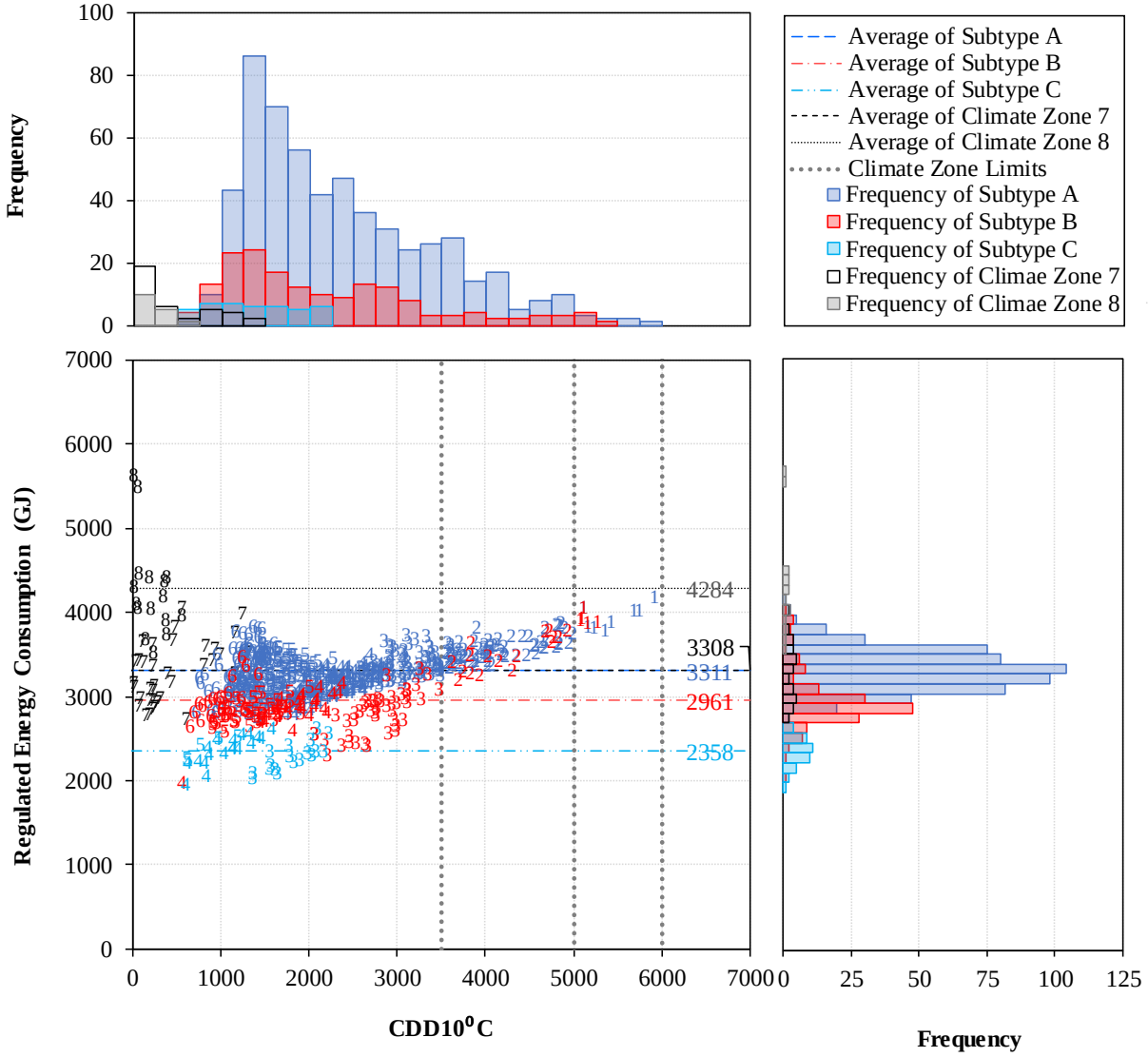

Figure 67: Regulated Energy Consumption of the ASHRAE Standard 90.1-2016 Medium Office Prototype Models without Daylight Responsive Controls with Respect to the CDD10°C of Different Weather Files

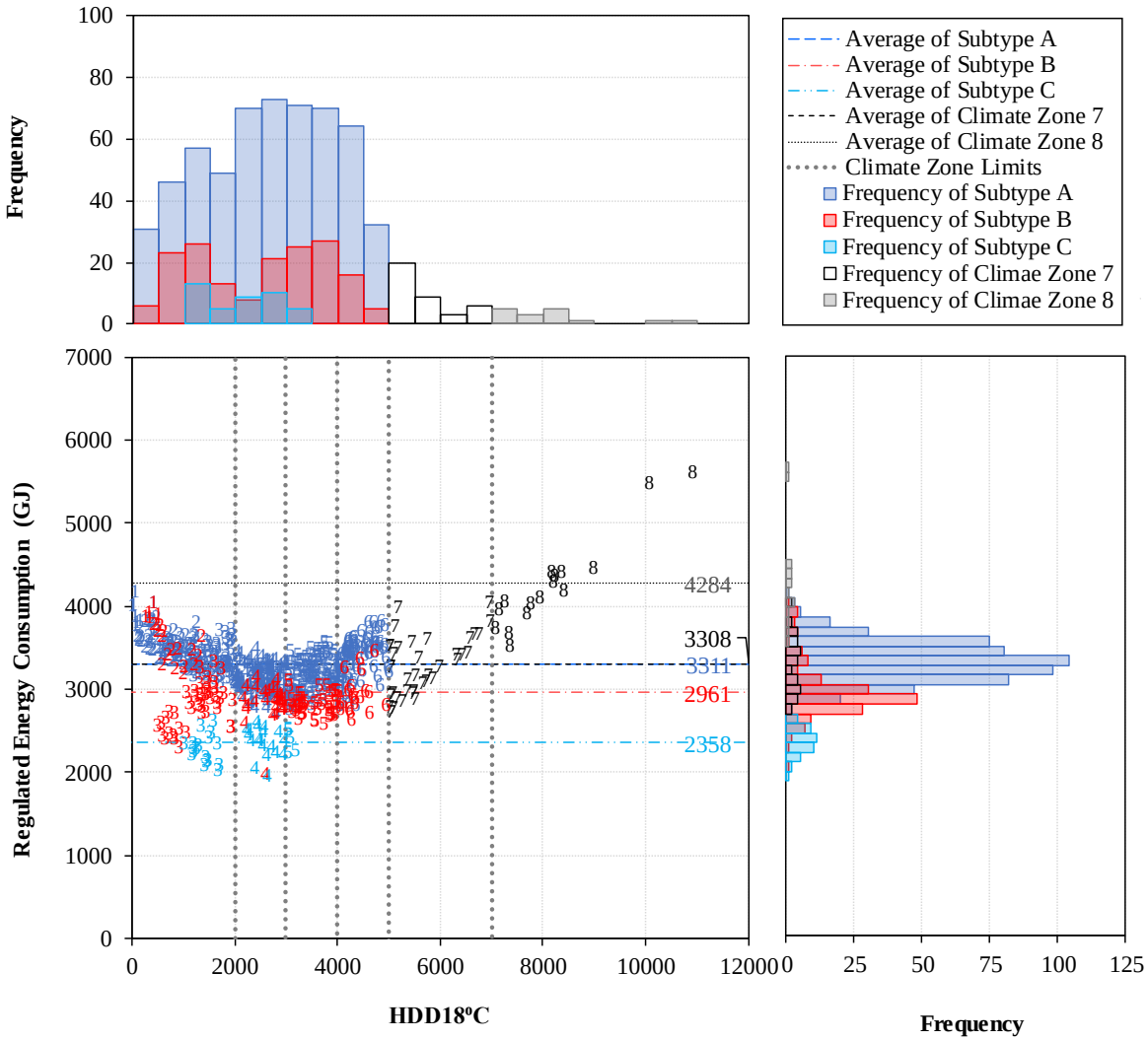

Figure 68: Regulated Energy Consumption of the ASHRAE Standard 90.1-2016 Medium Office Prototype Models without Daylight Responsive Controls with Respect to the HDD18°C of Different Weather Files

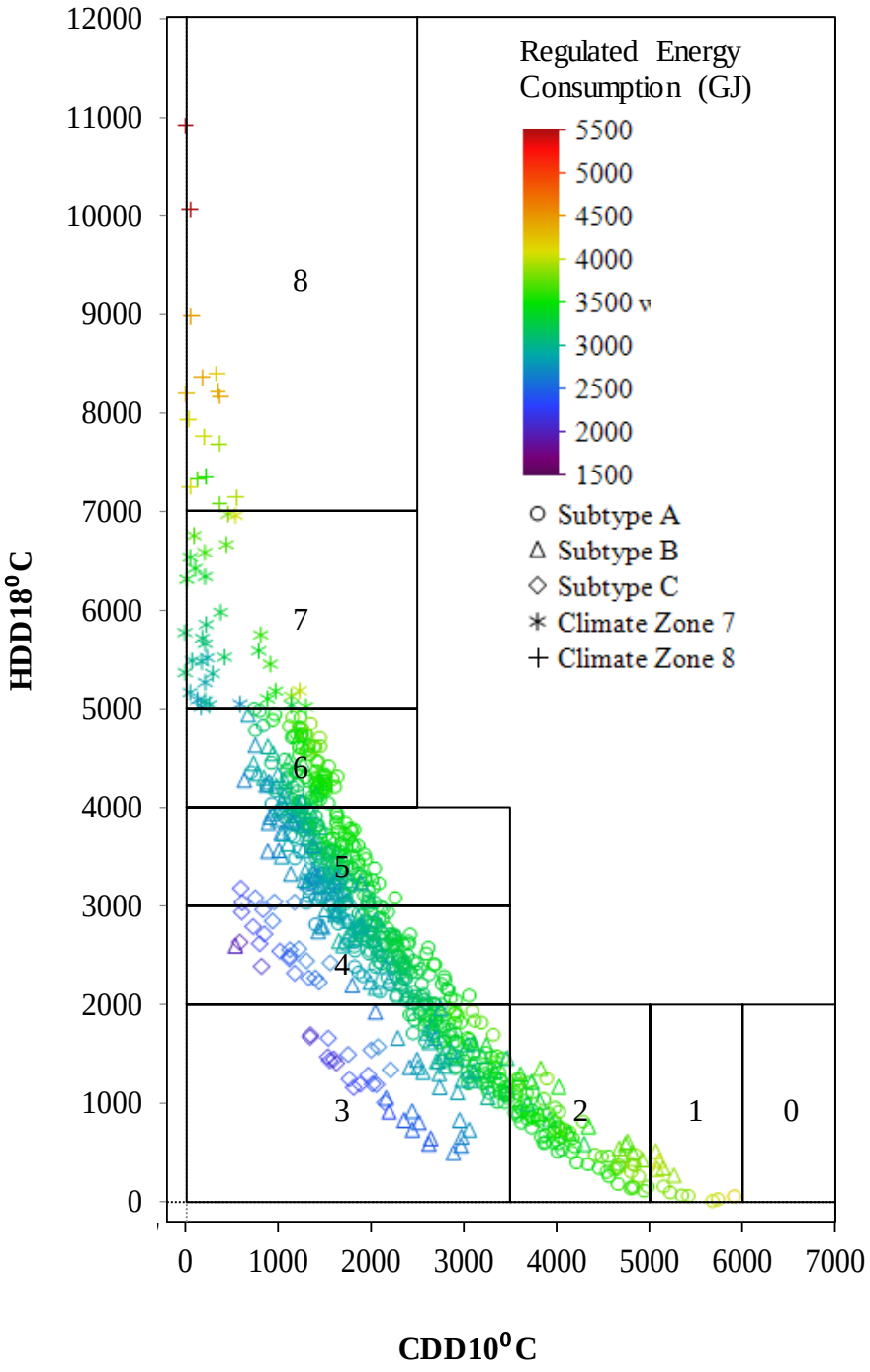

Figure 69: Regulated Energy Consumption of the ASHRAE Standard 90.1-2016 Medium Office Prototype Models without Daylight Responsive Controls in Different Climate Zones

The results of the analysis show a difference in the energy consumption of the models with and without daylight controls that show different patterns in lighting, heating, and cooling use. Figure 70 shows that the implementation of the daylight responsive controls results in approximately similar lighting energy savings in different locations in climate zones 1 to 6. In addition, it can be observed that there was no considerable difference between the lighting energy savings in different subtypes. However, climate zones 7 and 8 tended to have lower lighting energy savings.

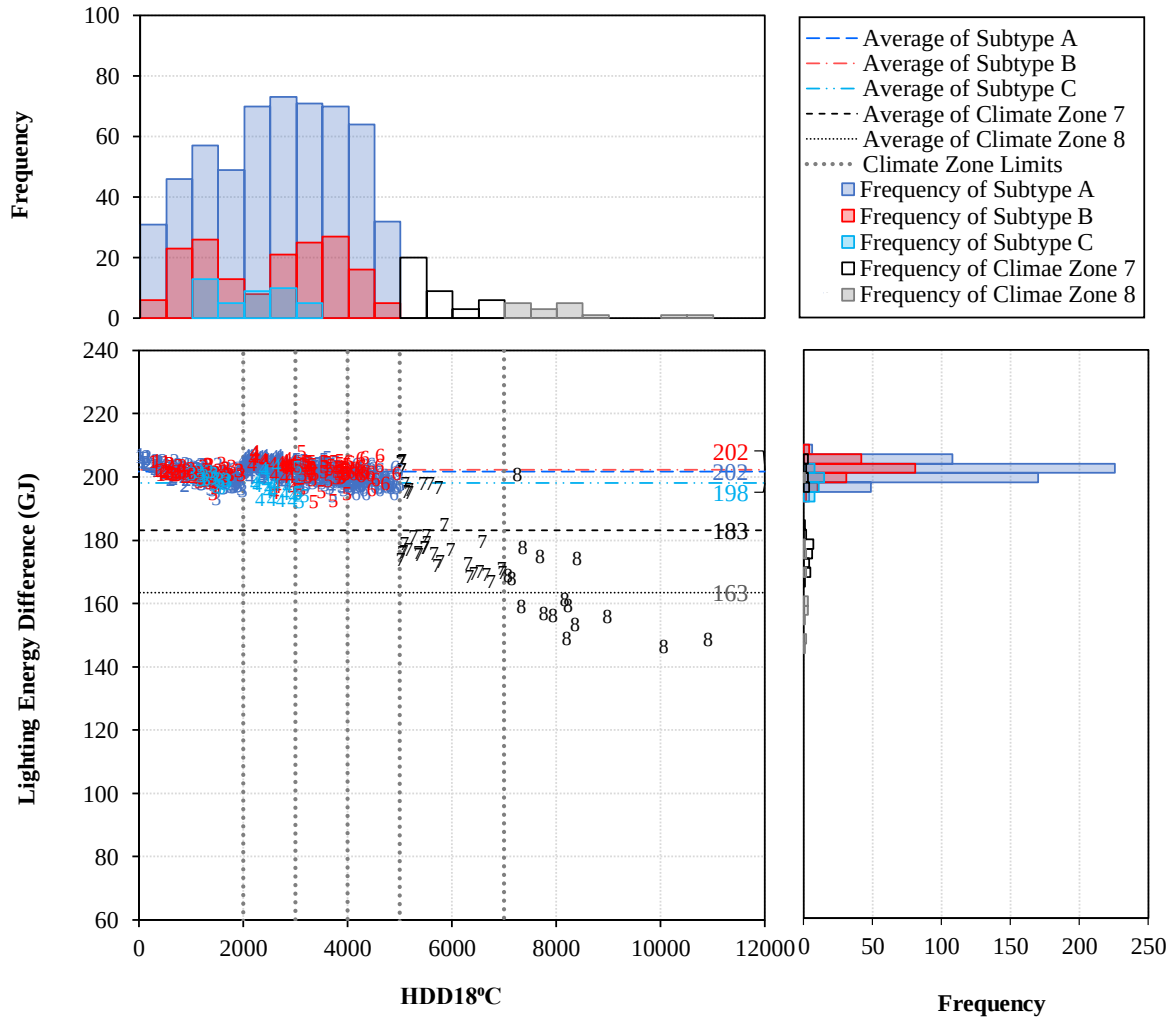

Figure 70: Lighting Energy Difference of the ASHRAE Standard 90.1-2016 Medium Office Prototype Models Associated with the Implementation of Daylight Responsive Controls

As shown in Figure 71, apart from a few exceptions, the heating energy increases with the implementation of the daylight responsive controls at the different sites. This is mainly due to the reduction in the lighting internal heat gains. Similar results that have the opposite impact can be seen in the cooling energy consumption in Figure 72, where the cooling energy consumption of different locations decreased with reduction in the lighting internal loads.

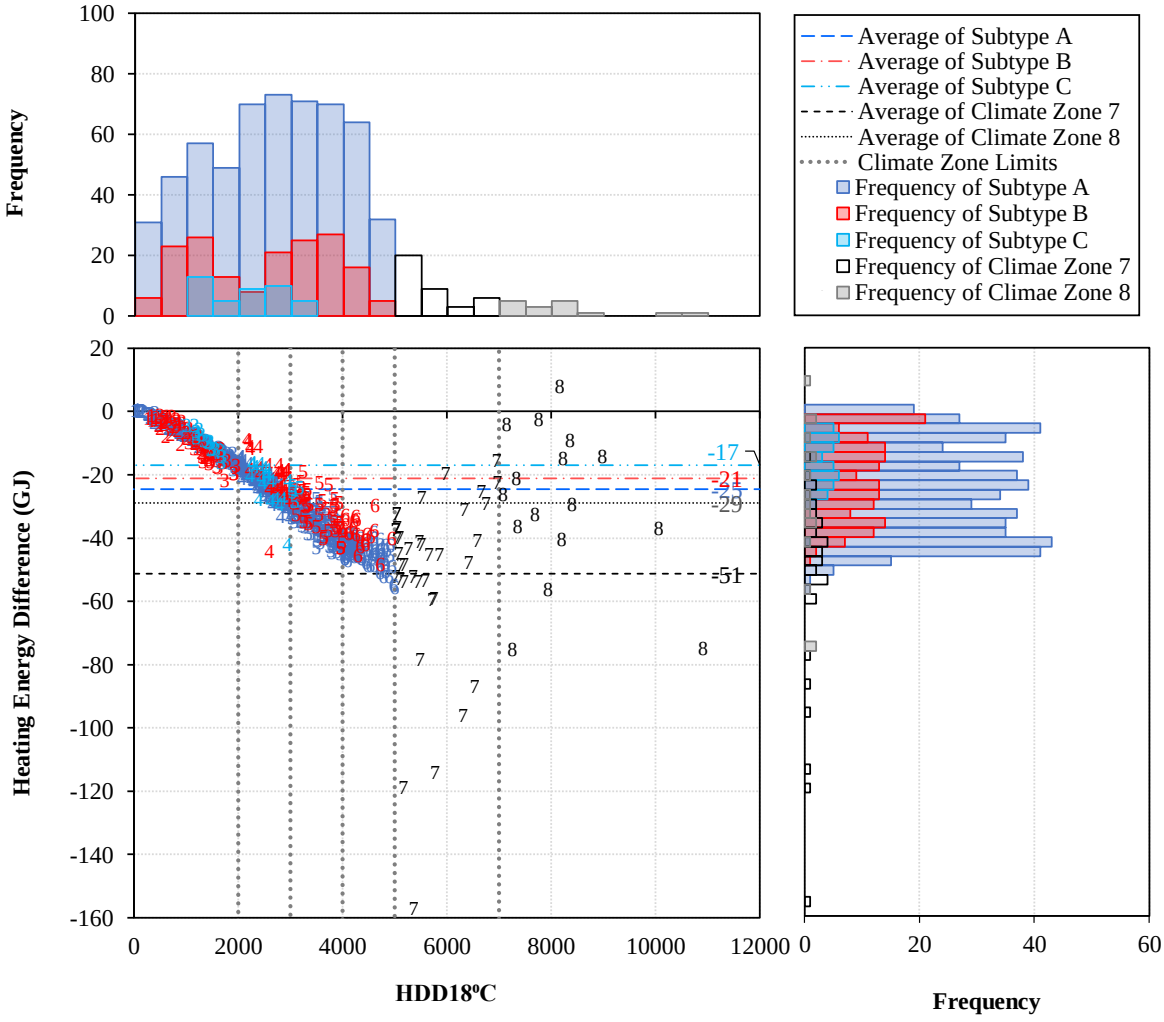

Figure 71: Heating Energy Difference of the ASHRAE Standard 90.1-2016 Medium Office Prototype Models Associated with the Implementation of Daylight Responsive Controls

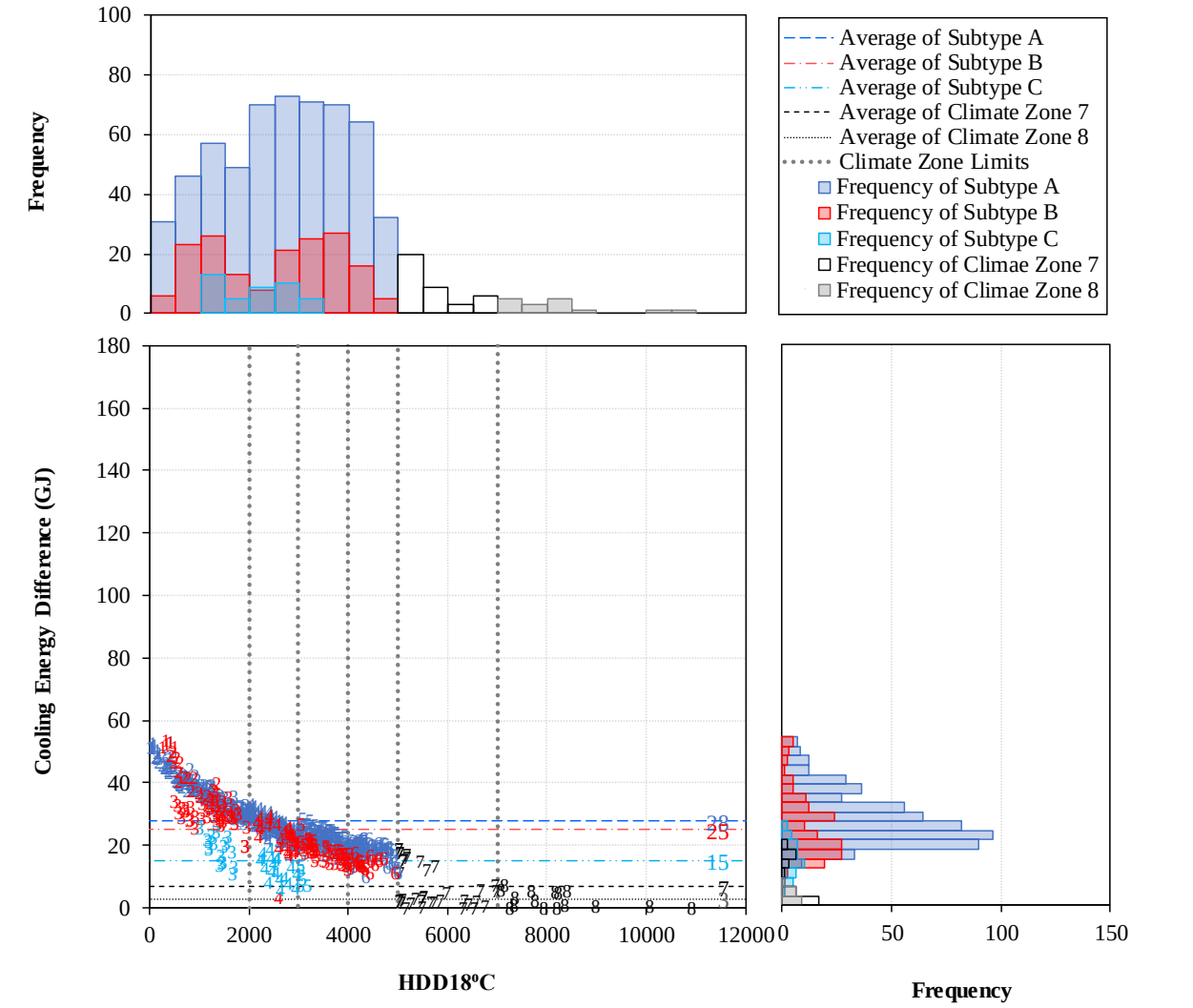

Figure 72: Cooling Energy Difference of the ASHRAE Standard 90.1-2016 Medium Office Prototype Models Associated with the Implementation of Daylight Responsive Controls

The results of the analysis of the total energy savings associated with the implementation of daylight responsive controls in ASHRAE Standard 90.1-2016 using the medium office prototype models is shown in Figure 73 to Figure 75. The results show that although the implementation of the daylight responsive controls has resulted in total energy savings in all the locations, the total energy savings of the daylight harvesting is higher in climate zones with higher cooling demands. While the lighting energy savings is close in different climate zones

(mainly climate zones 1 to 6) (Figure 70), the impact of the electrical lighting on the internal heat gains varies the total energy savings differently based on the heating/cooling demand (Figure 71 and Figure 72). For example, in the climate zones with higher cooling demand the reduction in electrical lighting will have a more advantageous effect on reducing the cooling load than the adverse effect on increasing the heating load. However, in the climates with higher heating demand, the effect of the increase in the heating demand is more pronounced than the reduction of the cooling demand, resulting in lower total energy savings. Therefore, it can be concluded that the daylight harvesting strategies in medium office prototype models are more beneficial for hot climates, whereas they can result in trivial energy savings in very cold climates.

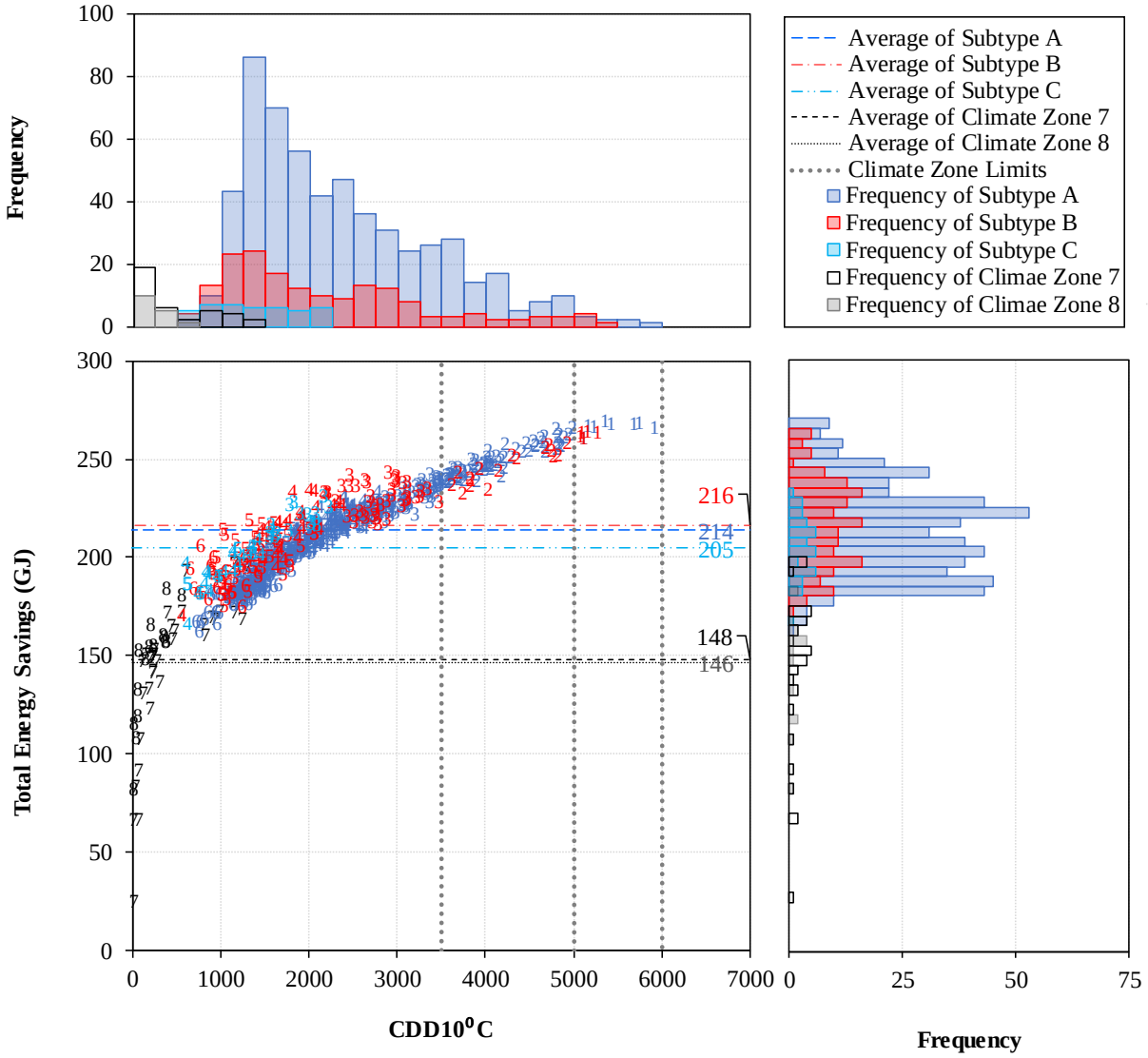

Figure 73: Total Energy Savings of the ASHRAE Standard 90.1-2016 Medium Office Prototype Models Associated with the Implementation of Daylight Responsive Controls with Respect to the CDD10°C of Different Weather Files

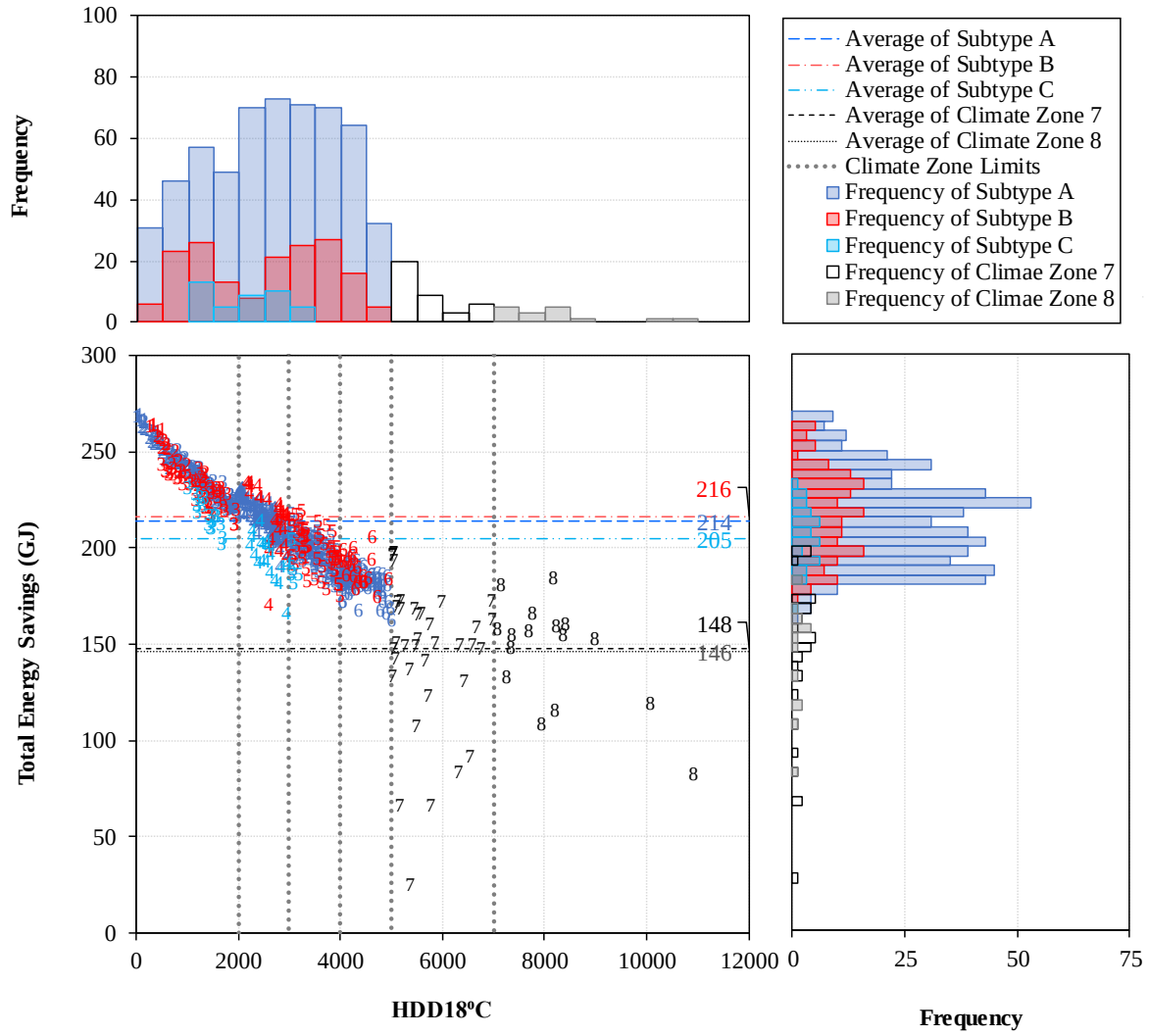

Figure 74: Total Energy Savings of the ASHRAE Standard 90.1-2016 Medium Office Prototype Models Associated with the Implementation of Daylight Responsive Controls with Respect to the HDD18°C of Different Weather Files

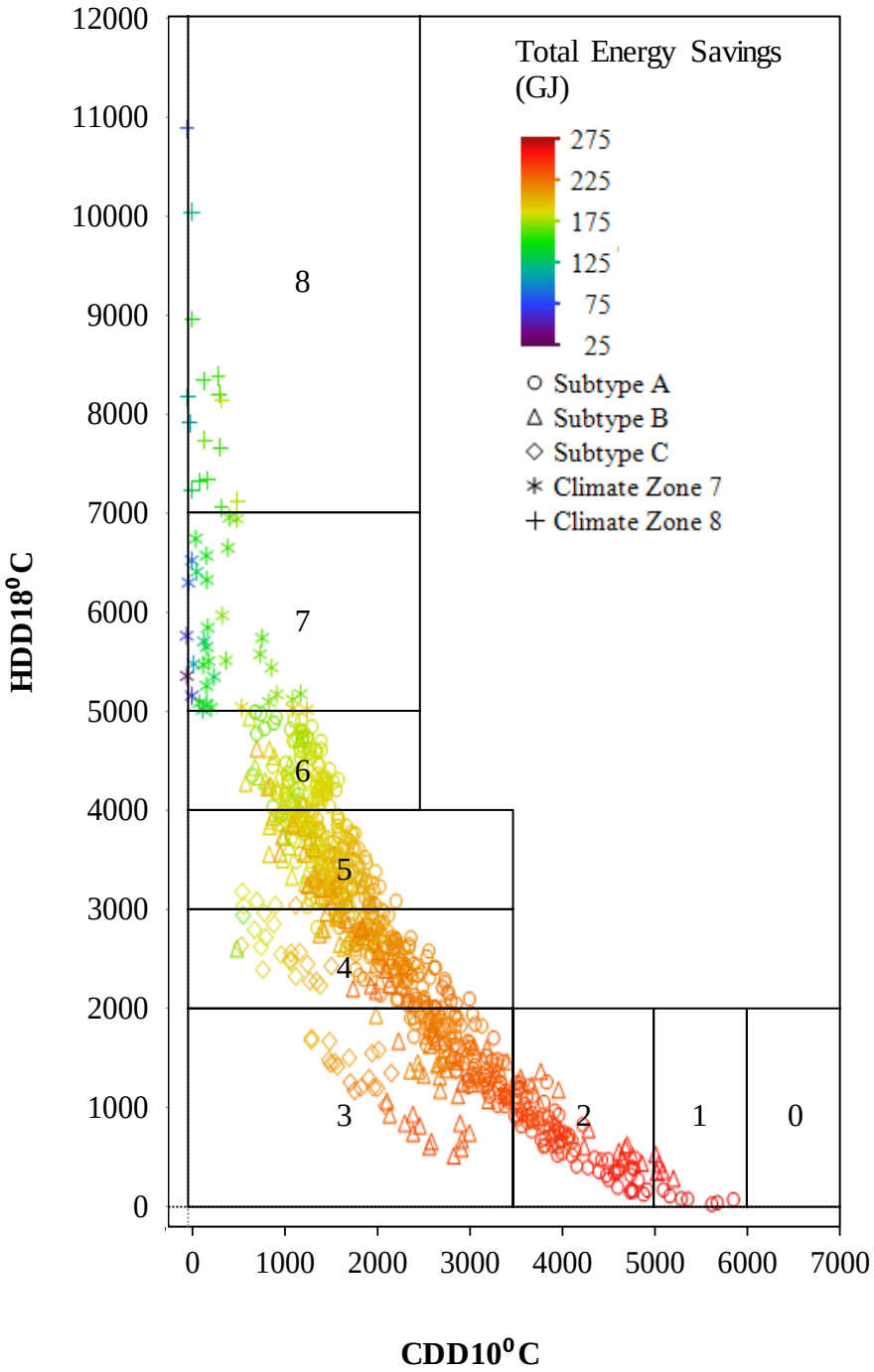

Figure 75: Total Energy Savings of the ASHRAE Standard 90.1-2016 Medium Office Prototype Models associated with the implementation of Daylight Responsive Controls in Different Climate Zones

In order to have a comparative point of view on the energy savings associated with the implementation of daylight responsive controls with respect to the total energy consumption, the total energy savings percentages are shown in Figure 76 to Figure 78. Figure 76 and Figure 77 show the energy savings for the daylighting in different sites with respect to CDD10 °C and HDD18 °C, respectively. Figure 78 shows these results with respect to CDD10 °C and HDD18 °C, allowing to represent the variations in energy savings percentages within each climate zone.

It can be seen that the total energy savings percentage starts with average values of the whole range of savings in hot climates zones (climate zones 1 and 2), then the total savings percentages peak at climate zone 3, subtype C (represented with light blue color), and in general, the savings start to decrease by moving toward colder climates until it reaches the minimum savings at the very cold climates. Also, in general it can be seen that subtype C has the highest energy savings percentages within each climate zone and the energy savings percentages in subtype B is higher than A. The most influential parameter in this variation is the trend of the energy consumption in the denominator. Also, the variation in the energy savings impacts the percentages. Altogether, the total savings percentages show that while the implementation of the daylight responsive controls can play an important role as an energy reduction strategy in certain climates, it may only have a small impact in other climates.

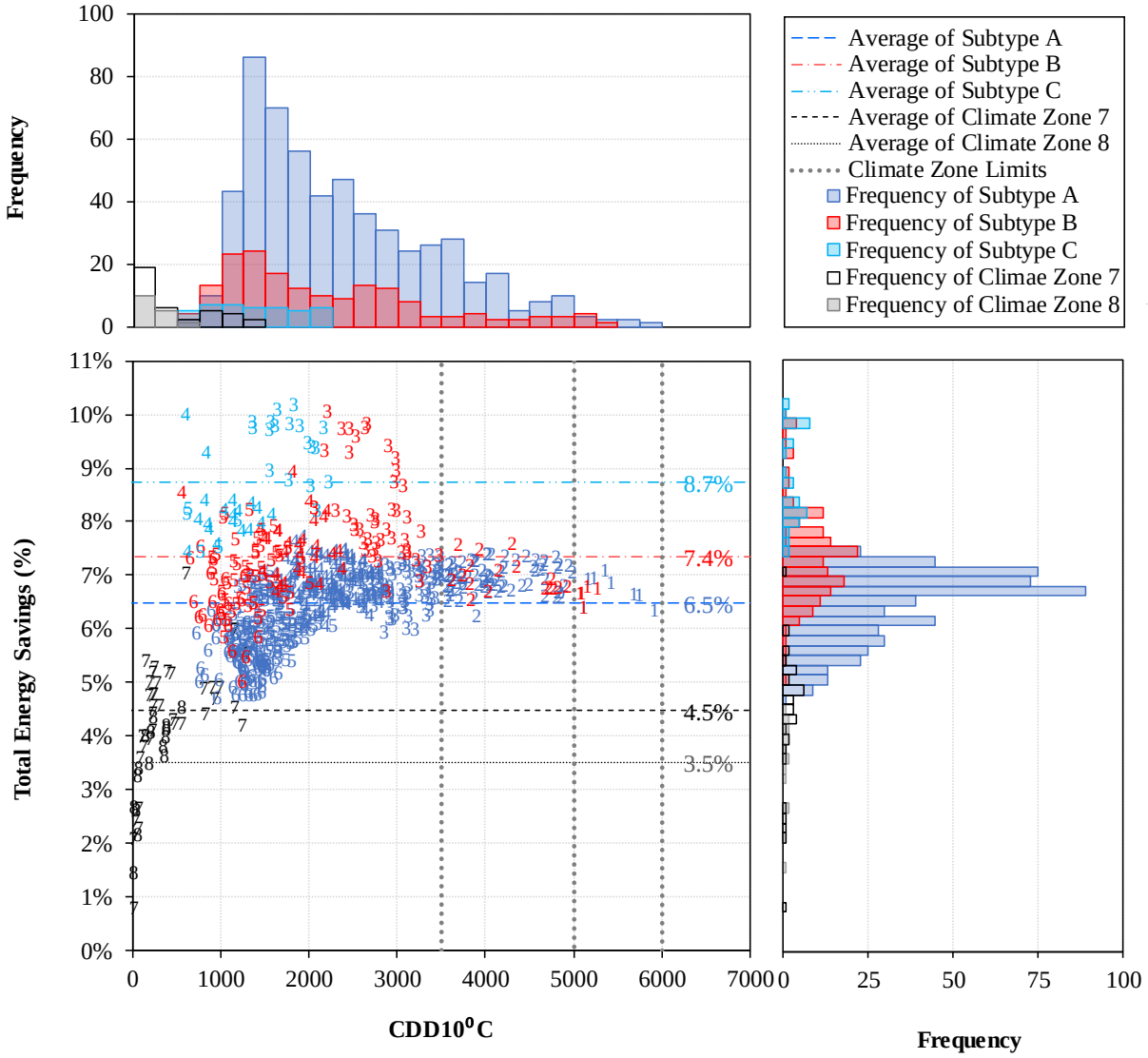

Figure 76: Total Energy Savings (%) of the ASHRAE Standard 90.1-2016 Medium Office Prototype Models Associated with the Implementation of Daylight Responsive Controls with Respect to the CDD10°C of Different Weather Files

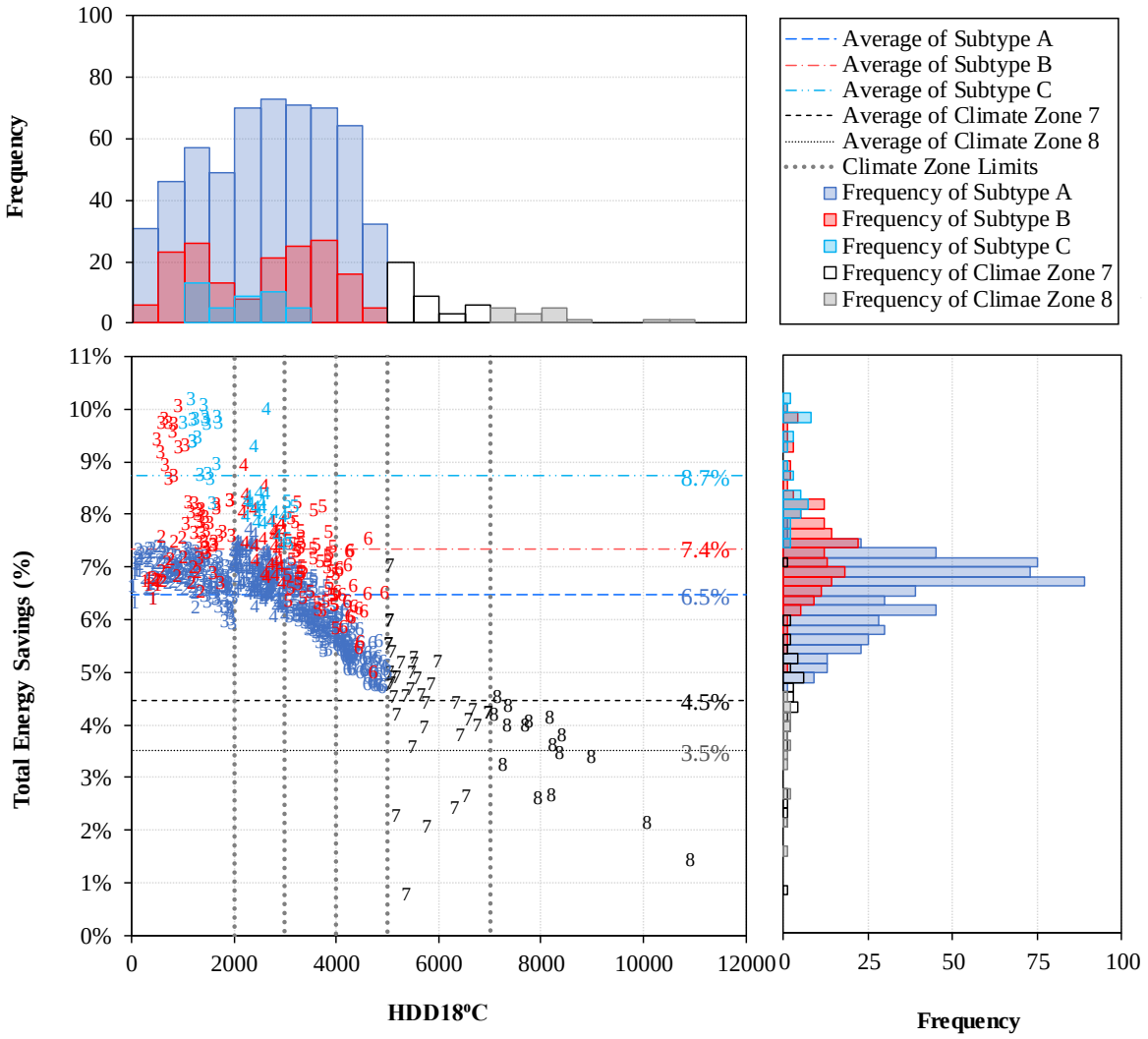

Figure 77: Total Energy Savings (%) of the ASHRAE Standard 90.1-2016 Medium Office Prototype Models Associated with the Implementation of Daylight Responsive Controls with Respect to the HDD18°C of Different Weather Files

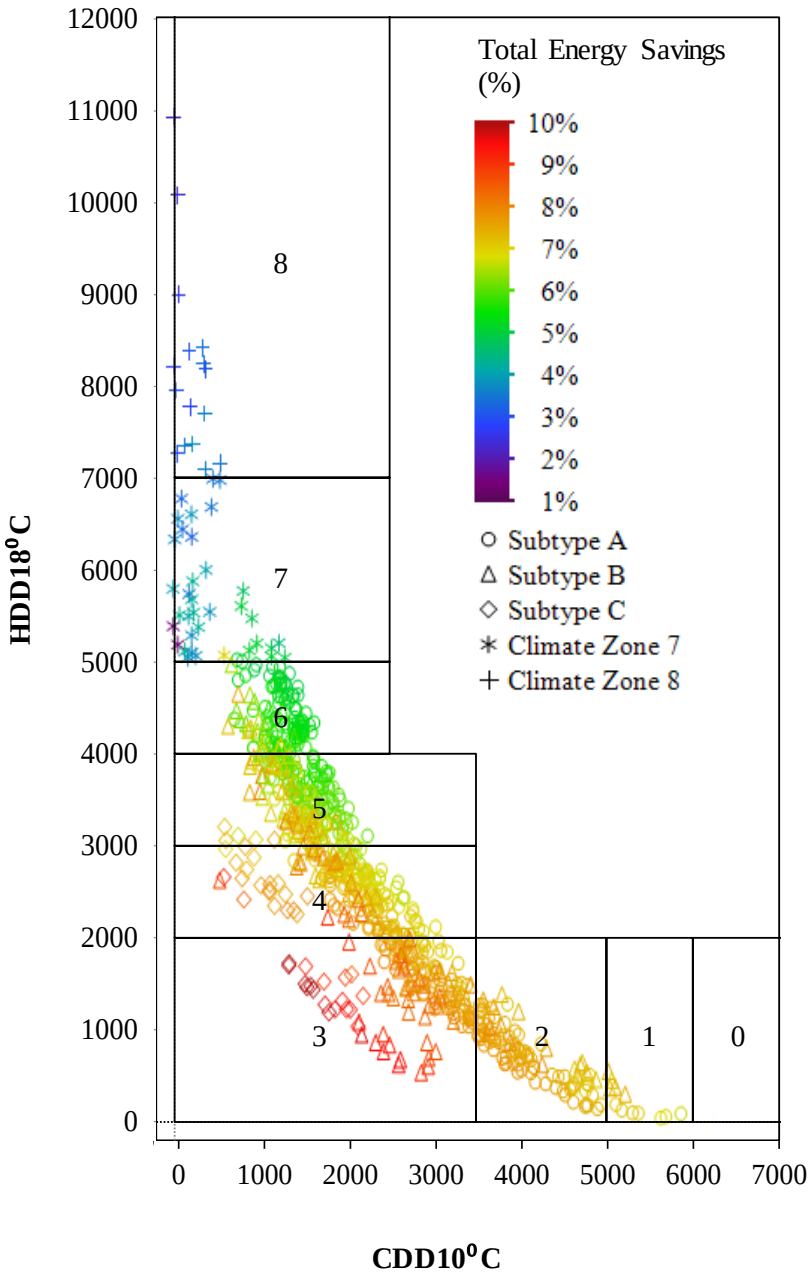

Figure 78: Total Energy Savings (%) of the ASHRAE Standard 90.1-2016 Medium Office Prototype Models Associated with the Implementation of Daylight Responsive Controls in Different Climates

4.4.2. Variation in Code-Compliance Using Performance Path

Compliance of a building using Appendix G performance path requires demonstrating a lower Performance Cost Index (PCI) compared to a target PCI, which is called PCI_t. The PCI of 1 represents that the building has the same stringency as required by ASHRAE Standard 90.1-2004 and PCI of 0 represents a net zero building. ASHRAE Standard 90.1-2016 requires at least a certain reduction in building annual source energy cost compared to ASHRAE Standard 90.1-2004. To acomplish this goal, a specific Building Performance Factor (BPF) is proposed for each building type in each climate zone and subtype to ensure the preferred reduction in the annual regulated energy consumption in each case. Table 9 shows the BPF for the office building type in different ASHRAE Standard 90.1 editions and shows the decreasing trend of the BPF for office buildings in each climate zone as the versions of ASHRAE Standard 90.1 progresses. In the table it can be seen that, on average, the BPF has decreased The required BPF will then impact the calculated PCI_t as shown in equation 3.21 in Section 0 of this document.

Table 9: Building Performance Factors (BPF) for Compliance of Office Buildings with Standard 90.1 (Rosenberg and Hart, 2016)

ASHRAE Standard 90.1 Edition	Climate Zone																	Average
	1A	1B	2A	2B	3A	3B	3C	4A	4B	4C	5A	5B	5C	6A	6B	7	8	
2010	0.74	0.77	0.73	0.76	0.72	0.76	0.66	0.70	0.73	0.70	0.72	0.73	0.70	0.71	0.72	0.70	0.75	0.72
2013	0.63	0.67	0.62	0.67	0.65	0.69	0.59	0.63	0.65	0.63	0.65	0.66	0.63	0.66	0.66	0.62	0.66	0.65
2016	0.58	0.62	0.57	0.62	0.60	0.64	0.54	0.58	0.60	0.58	0.60	0.61	0.58	0.61	0.61	0.57	0.61	0.60
2019	0.52	0.57	0.50	0.56	0.53	0.56	0.48	0.51	0.52	0.49	0.51	0.51	0.49	0.52	0.51	0.49	0.51	0.51

The calculated PCI_t and PCI for the ASHRAE Standard 90.1-2016 medium office prototype models in different locations are illustrated in Figure 79 and Figure 80, respectively. In these figures, subtype A is represented in dark blue, subtype B sis represented in red, subtype C

is represented in light blue, and climate zones 7 and 8 are represented in grey and black, respectively. It can be seen in the figure that the average PCI_t and PCI is 0.72 and 0.63, respectively.[7] The PCI_t of 0.72 is 0.28 lower than the 2004 baseline.

Commercial buildings meeting the requirements of ASHRAE Standard 90.1-2016 show 8.2% in energy cost savings, 7.9% in source energy savings, and 6.7% in site energy savings compared to the ASHRAE Standard 90.1-2013 (US DOE, 2017). The difference of PCI_t and PCI, shown in Figure 81, is within the range of 0.06 to 0.12 with the average 0.09 difference. It can be seen that the average difference of 0.09 and the range of 0.06 are significant compared to 0.28 difference with 2004 baseline and 0.08 energy cost savings compared to ASHRAE Stanbdard 90.1-2013.

Figure 82 shows the difference of PCI_t and PCI in different climate zones and subtypes, respectively, which are the box plot representaion of the same data shown in Figure 81. Figure 83 show similar data by grouping the data for each subtype in different climate zones. In Figure 82 and Figure 83 it can be seen that the difference varies with climate zone and subtype. Subtype A is shown to have a lower difference of PCI_t and PCI compared to subtype B and subtype C. For example in climate zone 3, all the locations in subtype A have lower difference of PCI_t and PCI compared to subtype B and C. Similar pattern can be seen by comparing the average values in diffirent subtypes within each climate zone (Figure 82). Furthermore, by grouping the data for each subtype in different climate zone, subtype A shows to have lower difference of PCI_t and PCI compared to subtype B and subtype C (Figure 83).

[7] Note that the PCI_t in this study is calculated only for the ASHRAE Standard 90.1-2016 DOE medium office prototype models while DOE small, medium, and large office prototype models are used for the calculation of the BPF of the office buildings in ASHRAE Standard 90.1-2016.

The difference of PCI and PCI_t in Figure 82, which shows how much above code is the building in each location, shows that the medium office prototype passes the code using the performance path. However, while the BPFs are provided for each climate zone and subtype, the variation within each climate zone and subtype can be substantially different compared to others. This means certain climates take benefit of the weather-related parameters that are not considered in the code, which will allow some locations to escape from the stringencies in the building energy Standard 90.1-2016. Therefore, the conventional degree-day for climate classification can not group different locations for their estimated energy consumption and results in giving extra credits for subtypes B and C compared to subtype A.

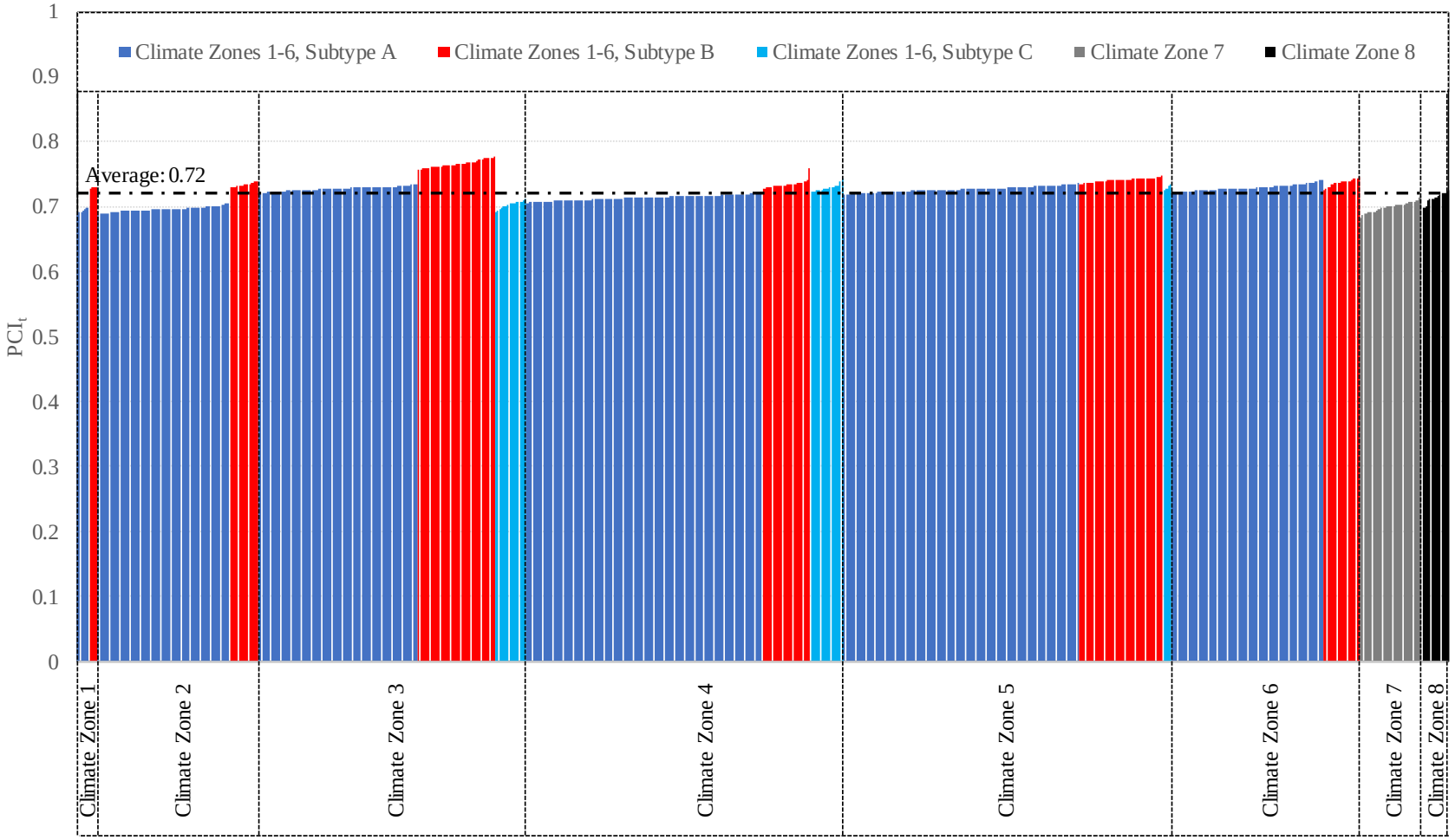

Figure 79: PCI_t of the ASHRAE Standard 90.1-2016 Medium Office Prototype Models in Different Locations

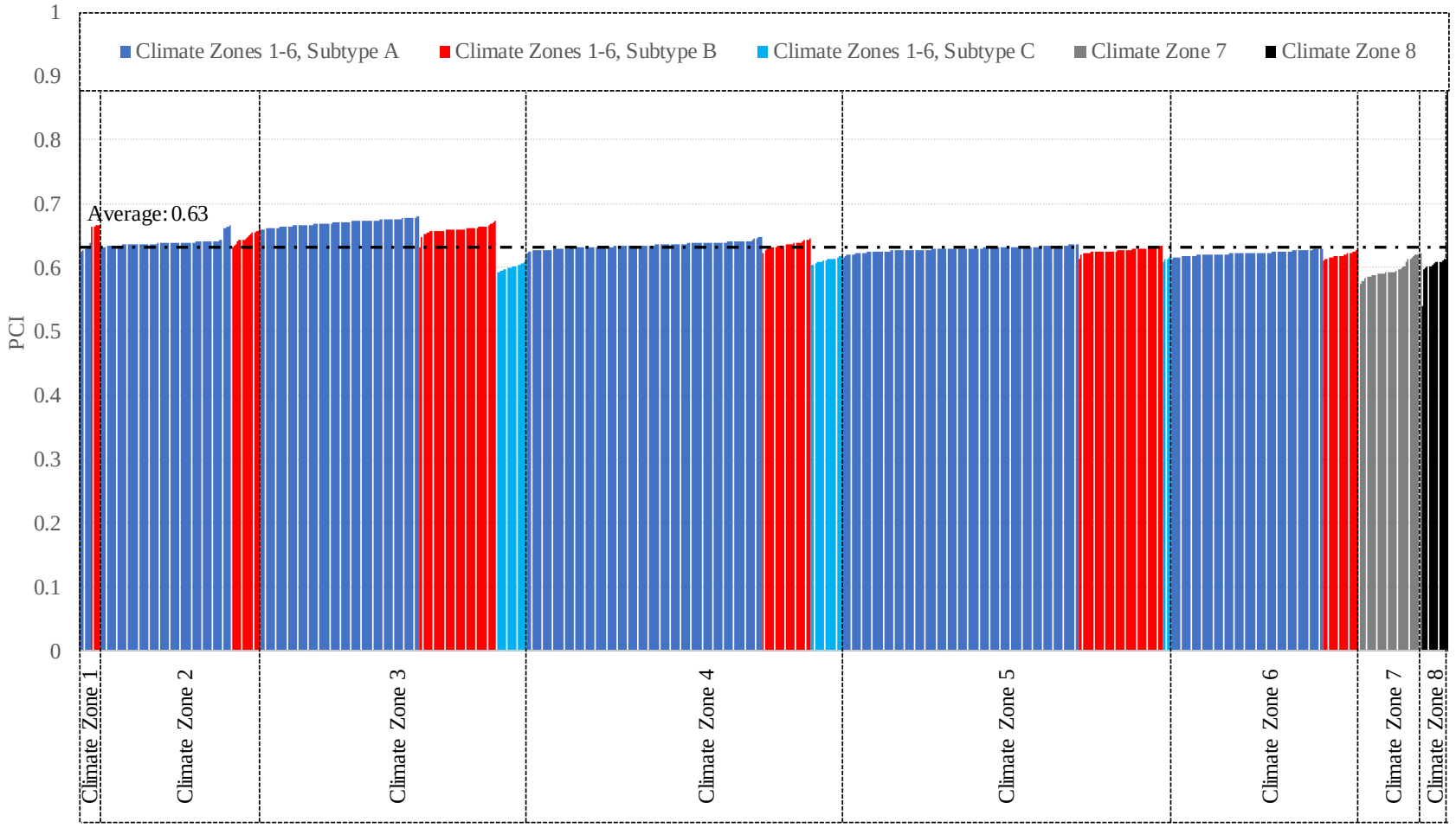

Figure 80: PCI of the ASHRAE Standard 90.1-2016 Medium Office Prototype Models in Different Locations

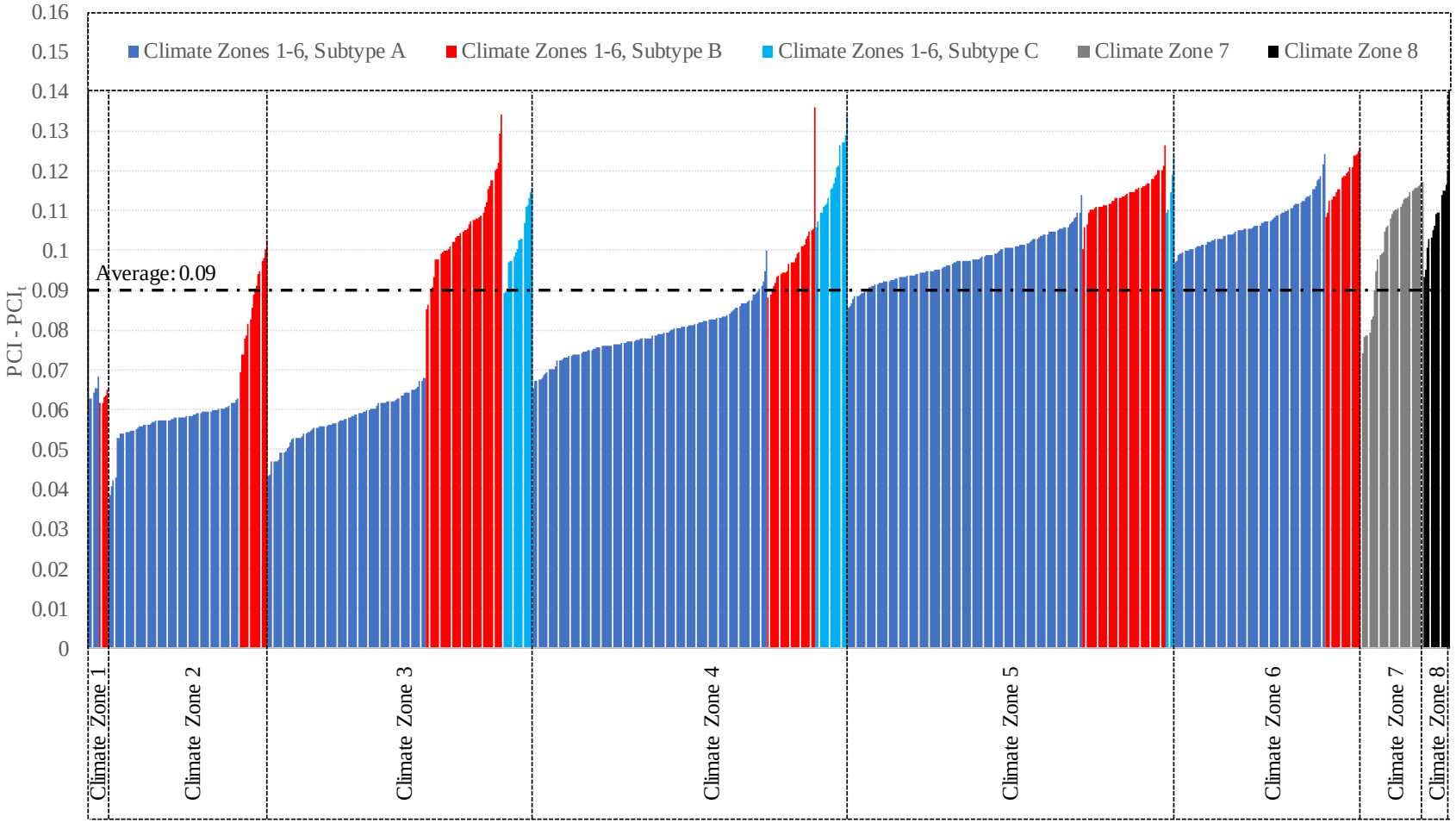

Figure 81: Difference of the PCI and PCI_t of the ASHRAE Standard 90.1-2016 Medium Office Prototype Models in Different Locations

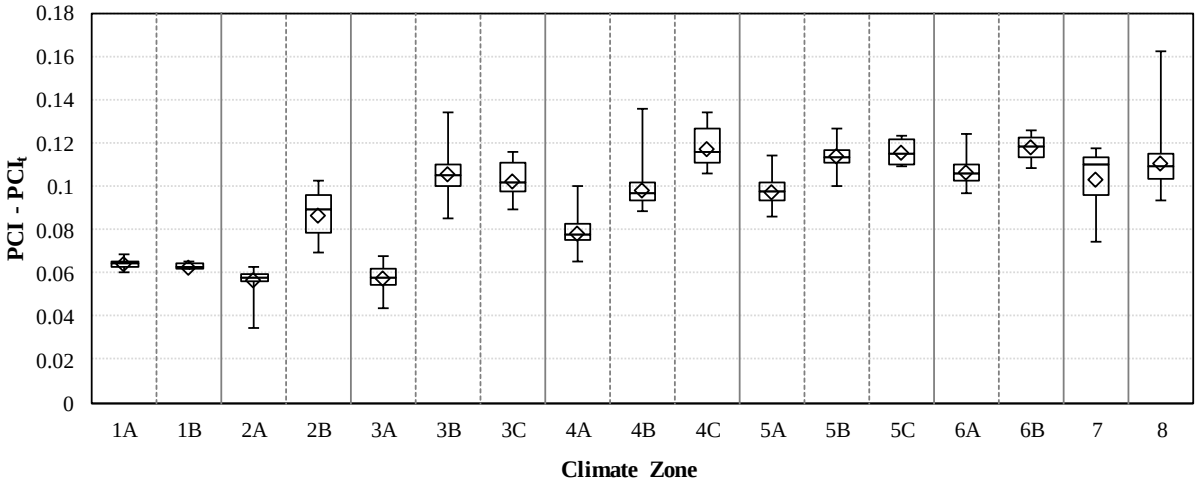

Figure 82: Difference of the PCI and PCI_t of the ASHRAE Standard 90.1-2016 Medium Office Prototype Models in Different Climate Zones

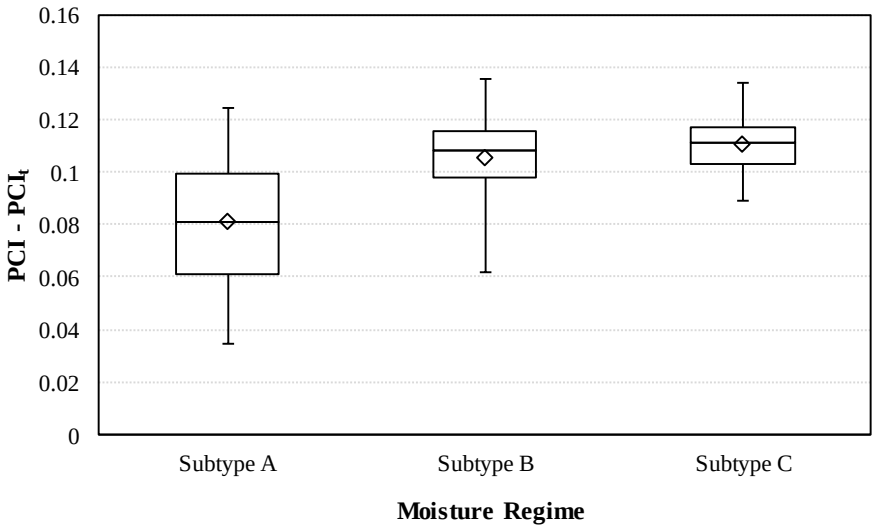

Figure 83: Difference of the PCI and PCI_t of the ASHRAE Standard 90.1-2016 Medium Office Prototype Models in Different Climate Subtypes

4.5. Summary of the Impact of Varying Energy Consumption on Building Code-Compliance

As discussed in previous sections, the energy consumption of the ASHRAE 90.1 medium office prototype buildings vary along different climate zones as well as different moisture

regimes within each climate zone. The variation leads to varying energy saving in different locations associated with the daylight responsive controls.

On average, in many cases the inconsistency of the energy consumption in different moisture regimes is even more substantial compared to the inconsistency of the energy consumption in different climate zones. One main reason is that there are differences in the climate conditions of the different subtypes that are not accounted in the degree day method. Based on the analysis in this section, the influential weather-related parameters that are not fully accounted in the degree day method are the solar radiation, humidity, and wind speed. Furthermore, the diurnal temperature range is a weather-related characteristic that is an indicator for the energy consumption that is not accounted in the degree day method. Consequently, the degree day method as a classification index fails to discriminate the potential varying energy consumption in different moisture regimes.

CHAPTER V

RESULTS – PART II

This chapter, discusses the potential improvements in the degree day method to better discriminate the difference in energy consumption of the ASHRAE Standard 90.1-2016 medium office prototype building models used at different locations. As discussed in the previous chapter, there are varying influential parameters in different moisture regimes that impact buildings energy consumption, however, they are not fully accounted for in the degree day method. The discussions in this chapter will introduce the shortcomings in the degree day method and describe a new approach to overcome these issues. This is then followed by the comparison of the accuracy of the estimation of the influential weather parameters using the conventional degree day method and the new approach. In these estimations, the simulation results from an identical model, compliant with the requirements for climate zone 4, were used to eliminate parameters other than climate variables. Therefore, the estimations are based on the results of specific models with specific thermal properties and the utilization of the same models with the same coefficients may not be the best representative model for other building configurations. However, this analysis allows for the comparison of the accuracy of the estimation of the building energy consumption using the conventional degree day versus the proposed method and allows to quantify the differences in the accuracies. Then, a comparison of the estimation of the building energy consumption using the conventional degree day method and the new approach is provided. Finally, the application of the proposed method in the prescriptive and performance compliance paths of ASHRAE Standard 90.1-2016 is discussed.

5.1. Improved Method to Predict the Building Energy Consumption

The high-level of aggregation of the data in the traditional degree day method can invalidate the representation of the heating and cooling requirements of a building in each location. Figure 84 illustrates two daily temperature profiles with different diurnal temperature ranges. In Figure 84 it can be seen that while the two temperature profiles fluctuate differently during the day, the daily average temperature of the two profiles is the same, which leads to the same CDD or HDD. Therefore, conventional degree day method does not account for the diurnal temperature range.

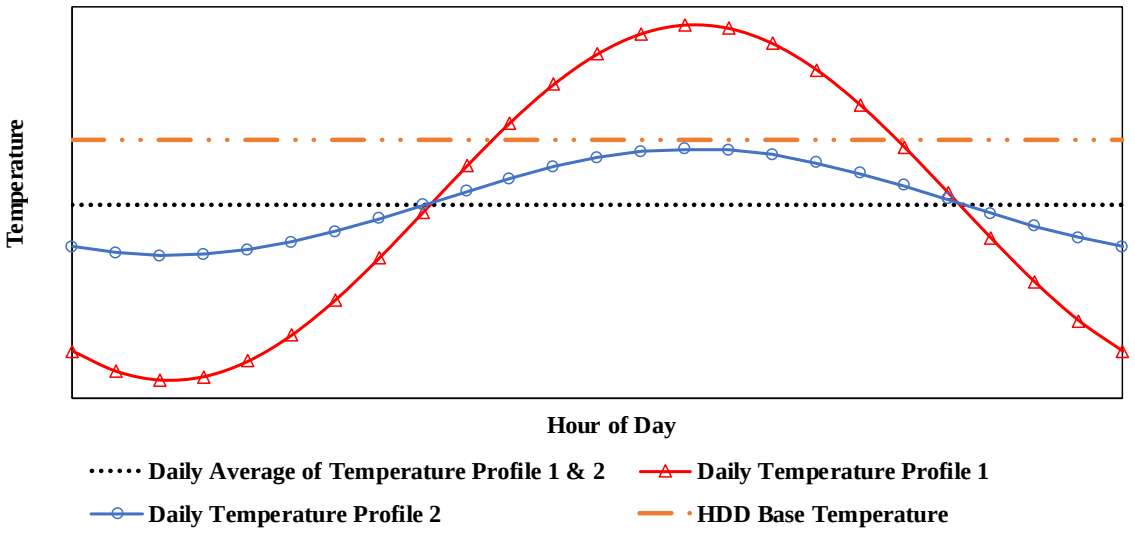

Figure 84: Representation of Two Daily Temperature Profiles in the Conventional Degree day Method

Consequently, conventional degree day or degree hour methods do not discriminate between different moisture regimes[8]. Figure 85 shows the normalized frequencies of the annual

[8] The lower consumption in marine (subtype C) locations compared to the moist (sybtype A) and dry (subtype B) locations is discussed in Section 4.3.1 of this dissertation.

sum of the minimum, maximum, and average outdoor dry-bulb temperature, as well as the CDD, HDD, CDH, and HDH for different locations in moist and dry areas. The distributions are normalized by dividing the counts in each bin by the total number of sites in that subtype. In the top part of the Figure 85, it can be seen that the distributions for the minimum and maximum in the two subtypes are mixed, which results in a mixed distribution for the average values and then eventually results in mixed distributions for degree days and degree hours in different locations in moist and dry regions.

However, the daily fluctuation of the outdoor temperature is an essential weather-related characteristic that is normally associated with other influential weather-related parameters that are not included in the conventional degree day method. While the diurnal temperature range can directly impact the energy consumption of a building (as discussed in Sections 4.3.2.2 and 4.3.3.2 of this dissertation), the significance of accounting for the diurnal temperature range is the discriminatory attribute of this quantity that discriminates the locations with different moisture regimes.

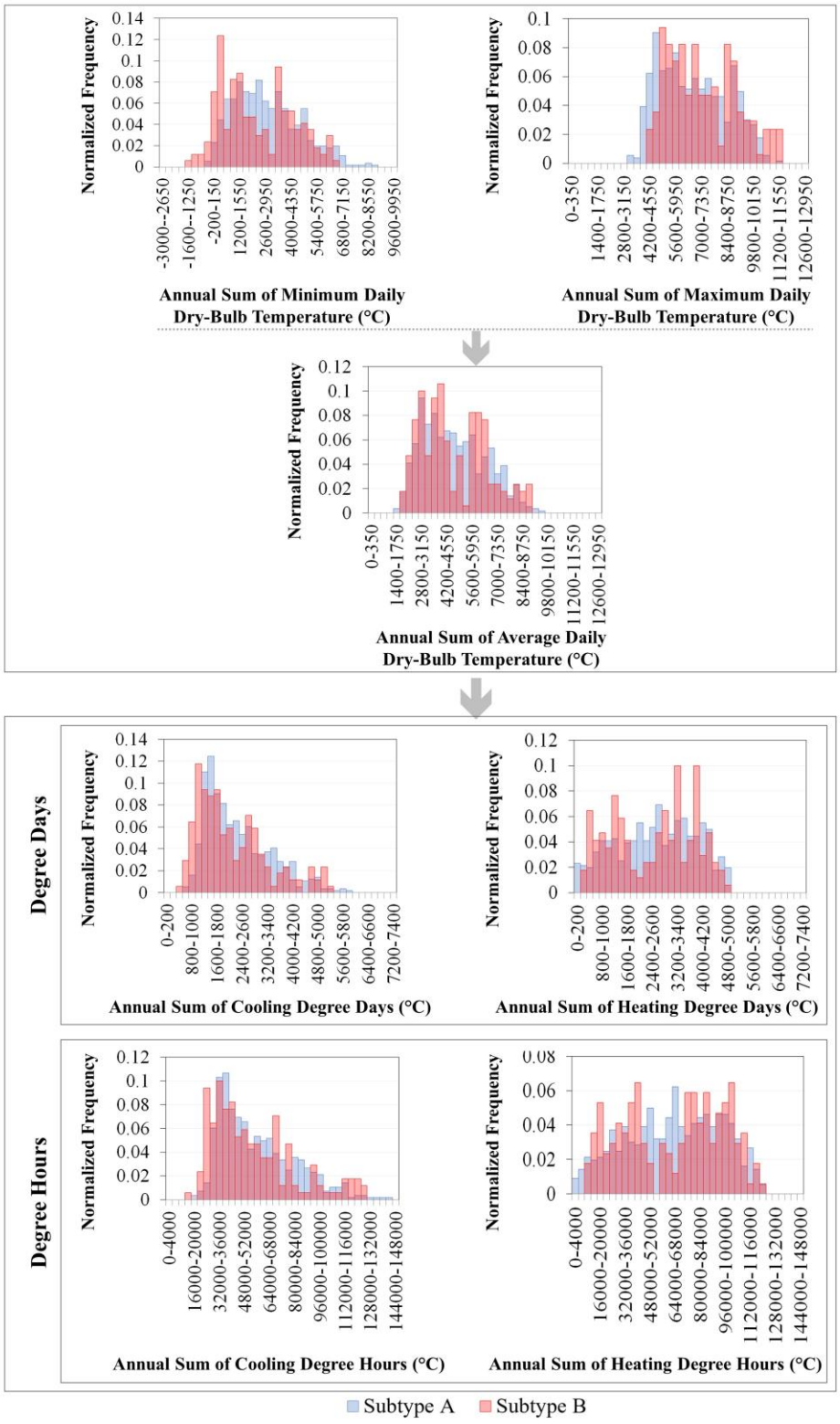

Figure 85: Nondiscriminatory attribute of the conventional degree days and degree hours approaches for moist (subtype A) and dry (subtype B) locations

As shown in Figure 86 the annual sum of the diurnal temperature range varies considerably in different locations. Among all 801 weather files used in this study, the annual sum varies from 2,439 to 5,168. In Figure 86, in general, subtype A, which is shown in dark blue color, has a relatively close annual sum of the diurnal temperature range to subtype C, which is shown in light blue color. Subtype B, however, has a higher annual sum of the diurnal temperature range compared to A and C. This trend can also be seen in Figure 87 where the total annual regulated energy consumption is shown versus the annual sum of the diurnal temperature range. In the figure it can be seen that how the subtype B points, shown in red, are separated from other subtypes by comparing their distributions along the horizontal axis. In fact, the higher annual sum of the diurnal temperature range in subtype B separates the majority of the subtype B points from the other locations. A comparison of the distribution of the normalized frequencies of the annual sum of the diurnal temperature range in locations in subtype A versus subtype B is provided in Figure 88. In Figure 88, it can be seen that in contrary to the minimum, maximum, and consequently the average values (shown in Figure 85), the diurnal temperature better discriminates the two moist and dry subtypes, which allows for better energy use estimations. However, while the diurnal temperature range can be included in the models, in this study the diurnal temperature range is captured through the split-degree day approach rather than directly including the diurnal temperature range in the models. While the selected split-degree day and the model with the conventional degree days along with the diurnal temperature range showed to have comparable R-square values, the split-degree day is selected as the coefficients in this regression model have more meaningful insights and associates the split-degree day values with varying U-values.

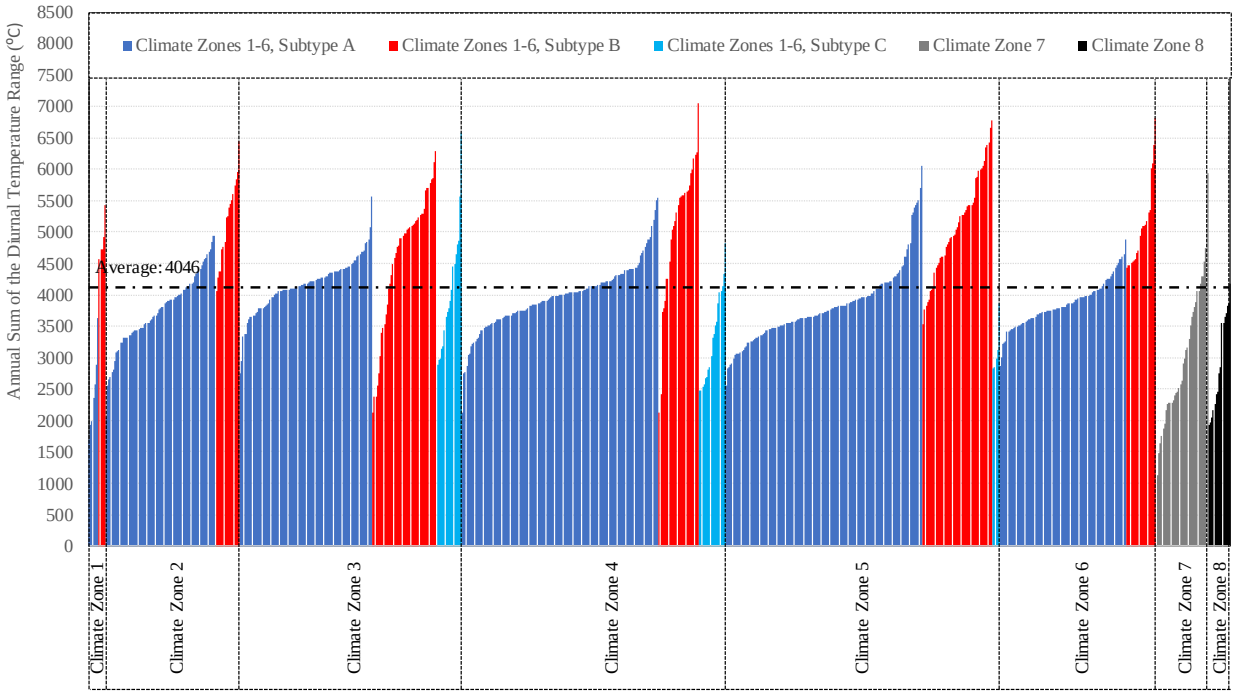

Figure 86: Annual Sum of the Diurnal Temperature Range in Different Locations

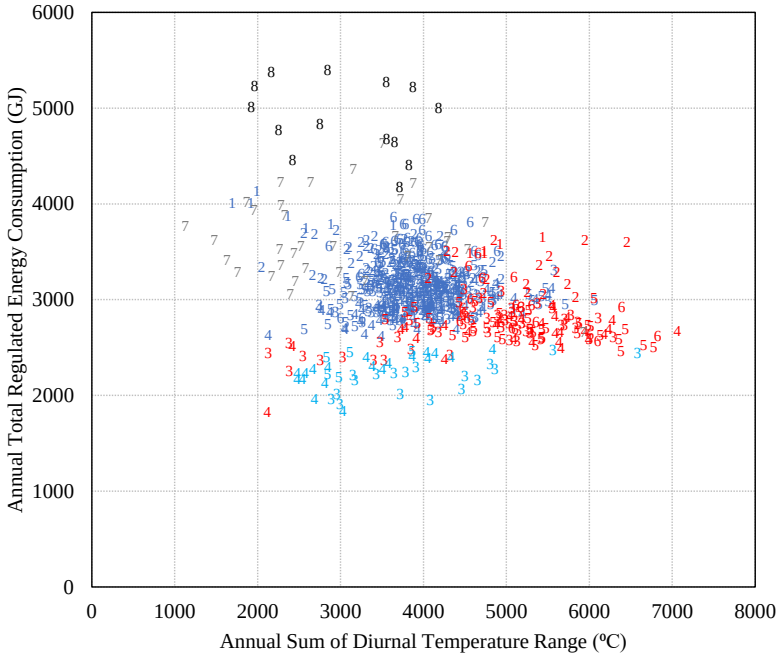

Figure 87: Plot of the Annual Total Regulated Energy Use versus the Annual Sum of the Diurnal Temperature Range

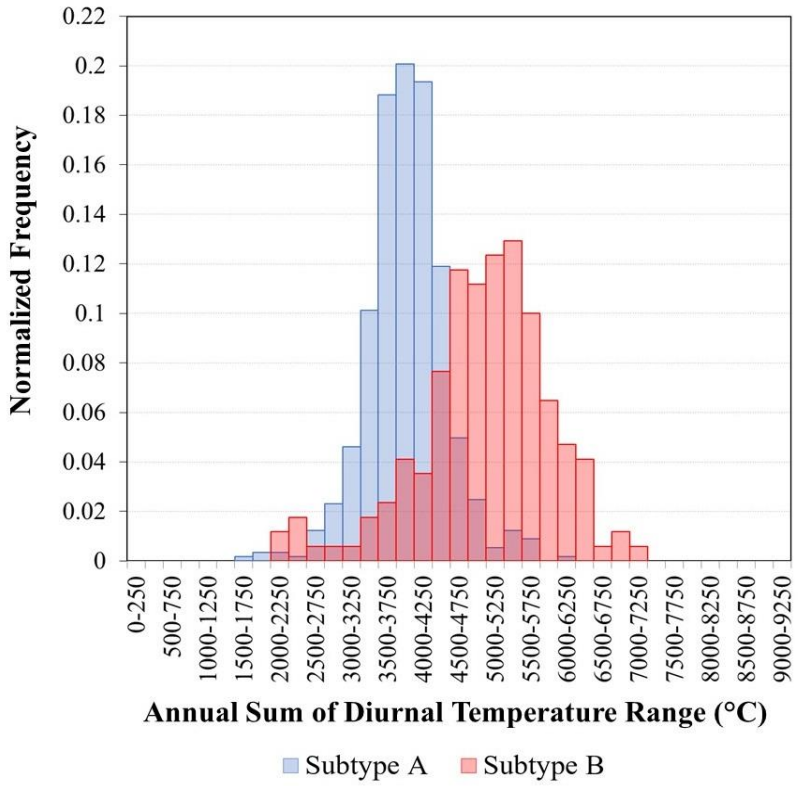

Figure 88: Discriminatory attribute of the diurnal temperature range for moist (subtype A) and dry (subtype B) locations

One approach to overcome the issue that the degree day method does not account for the diurnal temperature range is to divide the average 24-hour temperature span used in the calculation of degree days into two sections. Figure 89 shows an example of splitting the daily temperature profile into two sections and then determining how it impacts the averages in each section. Without splitting the temperature profile, the two profiles yield the same average temperature for the degree days calculation. Splitting the temperature profile into two sections, however, yields two averages for each temperature profile, one for each interval. In this example, the section of the intervals in the morning and night is called section 1 and the section of the interval in the middle of the day is called section 2. The average for each section is calculated using the average of the maximum and minimum hourly temperatures in that section. In Figure

89 an imaginary HDD base temperature, which is assumed to be in between the maximum and minimum temperatures in the day, is represented as well. The same principle applies in the calculation of the CDD as well.

As shown in Figure 89, the difference in the average temperatures in the two sections is larger in the temperature profile with larger diurnal temperature range. This implies that splitting a daily temperature profile and taking the average for each section includes the information for the diurnal temperature range. Specifically, the averages in section 1 of the temperature profile 1 is lower than the corresponding value for temperature profile 2 while the averages in section 2 of the temperature profile 1 is higher than the corresponding value for temperature profile 2. This could lead to a better estimation of the heating and cooling loads. For example, in this example, the section 1 of the temperature profile 1 yields a significantly larger heating degree days (HDD) for that portion of the day compared to the section 1 of the temperature profile 2. However, section 2 of the temperature profile 2 shows zero HDD for that portion of the day compared to a small nonzero value for the section 2 of the temperature profile 2. Overall, using the weighted average method for the calculated split degree day, the heating degrees in temperature profile 1 were 88% higher than the temperature profile 2 while the conventional HDD yield the same value for both temperature profile.

5.1.1. Determination of the Split Points in the Split-Degree Days

This section describes the coefficient of determination of the estimation of the energy consumption of the medium office prototype building models using split-degree days with different split hours, which is the start hour for splitting the day, as well as span hours, which is the number of hours from the start hour to split the 24 hours in a day. For example, a split-degree

day with a start time of 14 and span of 3 hours splits a day into two spans, one from the 14th hour of the day up to 16th hour of the day, which includes the start time as well, and the other span includes the rest of the day. Various split and span hours make up the 288 variations (24 multiplied by 12, considering the symmetry). In this study, the start time is selected to vary 24 hours and the time span to vary 12 hours.

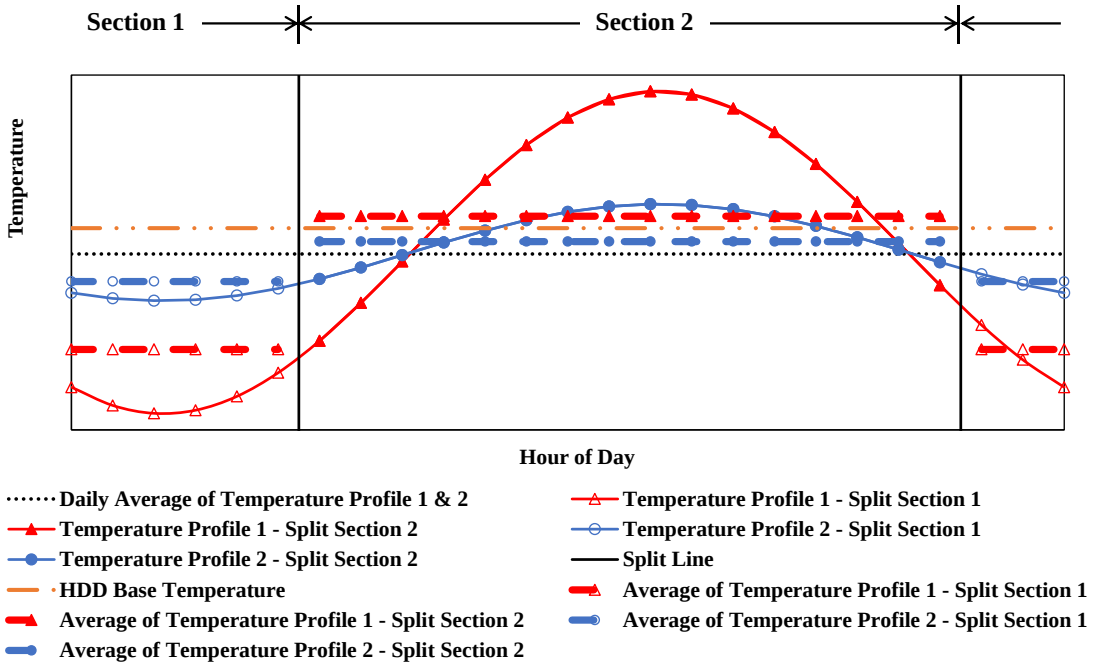

Figure 89: Example of a Split the Daily Temperature Profile for the Degree Day Calculation Using Two Sections

The results include the estimations of energy consumption for the total regulated (Figure 90), heating (Figure 91), cooling (Figure 92), and fan (Figure 93) energy use. Each point in the top figures of Figure 90 to Figure 93, and similarly each bar in the bottom figures in Figure 90 to Figure 93, represent the R-square for the estimation of the energy consumption for one variation of the split-degree days. To calculate the R-square for each point or each bar in Figure 90 to Figure 93, the R-square of the estimation of the 801 simulated results of the end-uses of interest

in each case (total regulated, heating, cooling, or fan energy use) using the corresponding split-degree days configuration is calculated.

Figure 90 shows that the R-square for estimating the total regulated energy consumption can vary approximately 3% using different split-degree days with the best configurations of start point at 14 and time span of two or three hours. Figure 91 shows that the R-square for estimating the heating energy consumption can vary approximately 2% using different split-degree days. The R-square for estimating the cooling energy consumption, shown in Figure 92 vary less compared to the variations in R-square for the total regulated and heating energy consumption. On the other hand, as shown in Figure 93, the R-square for estimating the fan energy consumption varies significantly (approximately 35%) using different split-degree days[9].

There are also similarities in the trends of the changes in the R-squares in the estimation of each of the total regulated, heating, cooling, and fan energy consumption with different split-degree day configurations. Moving along the split hour axis, the R-square has two points where it drops. As an example, in Figure 90, the R-square in three hours split spans, denoted with black lines with solid rectangles, remains approximately constant by varying the split start hour from 1 to 5. Then it drops to the minimum value when using 9 as the start time. This is mainly due to the fact that in general most of the weather files used in this study have the minimum daily temperature at night and before sunrise. Therefore, split-degree days with start time of 1 to 5 and three hours of time span represent a value close to the minimum daily temperature.

Considering the values for split-degree days for each split interval, the estimations have higher R-square due to the higher discrimination of the diurnal temperature range in these cases.

[9] Please note that the vertical axis in Figure 93 is different from the axis used in Figure 90 to Figure 92.

However, at the start time of around 9 am, and for the three hour split span the two values of the split-degree days for heating and the two values for cooling are very close to each other as in general, it is highly expected to experience the average daily temperature at around this time span. Therefore, splitting the day will not improve the R-square significantly compared to the conventional degree days. By moving along the start hour span, the R-square increases to its maximum when it incorporates the hours in which the highest daily temperature of the weather files are. The two values in the split-degree days, in this case, represents more information about the temperature profile and is more discriminative as it discriminates different diurnal temperature range for the temperature profile with similar conventional degree days. It should be noted that since the diurnal temperature range is better described, it is a better accounting of other weather-related parameters, such as solar radiation and humidity, since these parameters associate with diurnal temperature range. Finally, similar to the case of start time at 9 am, by moving along the horizontal axis, the R-square drops first and then slightly increases.

Overall, the split-degree days with start time of 2 pm and span period of three hours is selected as the final configuration. This configuration is selected considering various considerations. Considering the accuracy of the estimation of different end-uses using different split-degree days variation, overall, the split-degree days with start time of 2 pm and span period of three hours shows the highest accuracy. While there are other configurations in the case of cooling with higher R-square, the difference is trivial and the selected split-degree days is very close to the maximum value. Also, in the case of the fan, there are other split-degree days with a higher R-square. However, since the portion of the fan energy in the total energy is small and the selected split-degree days has high enough accuracy, the split-degree days with start time of 2 pm and span period of three hours is selected.

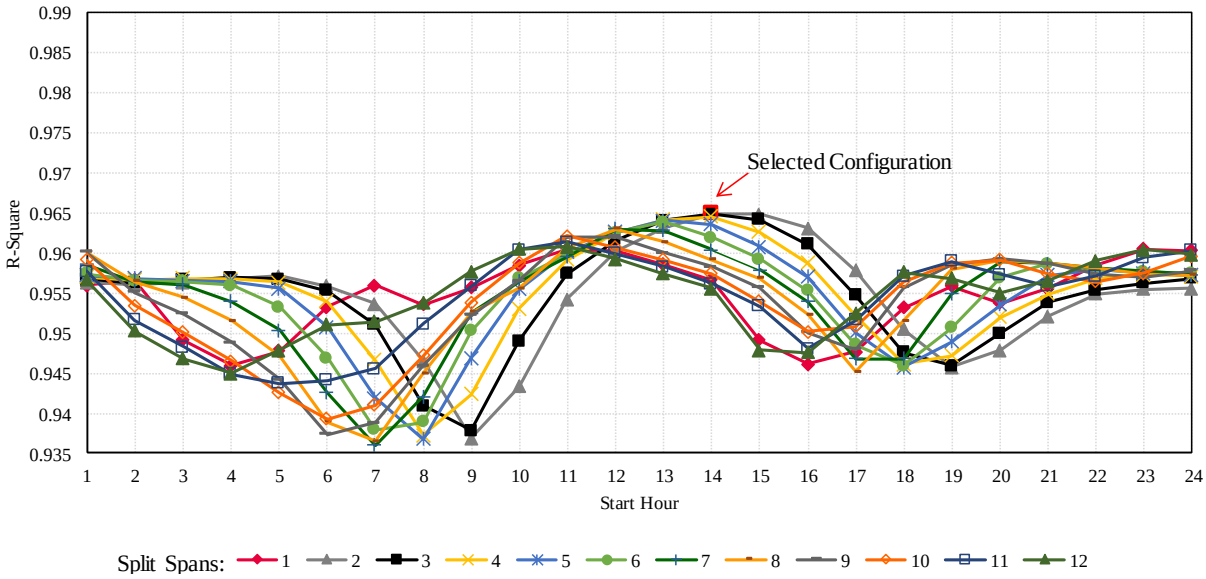

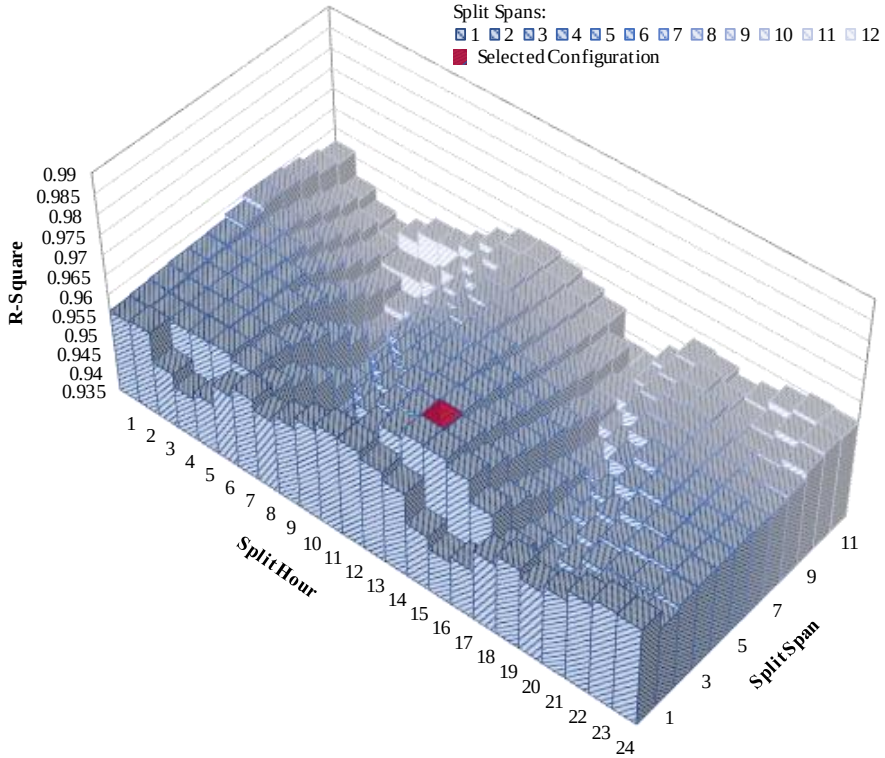

Figure 90: The Accuracy of the Estimated Total Regulated Energy Consumption Using Split-Degree Days with Different Split and Span Hours

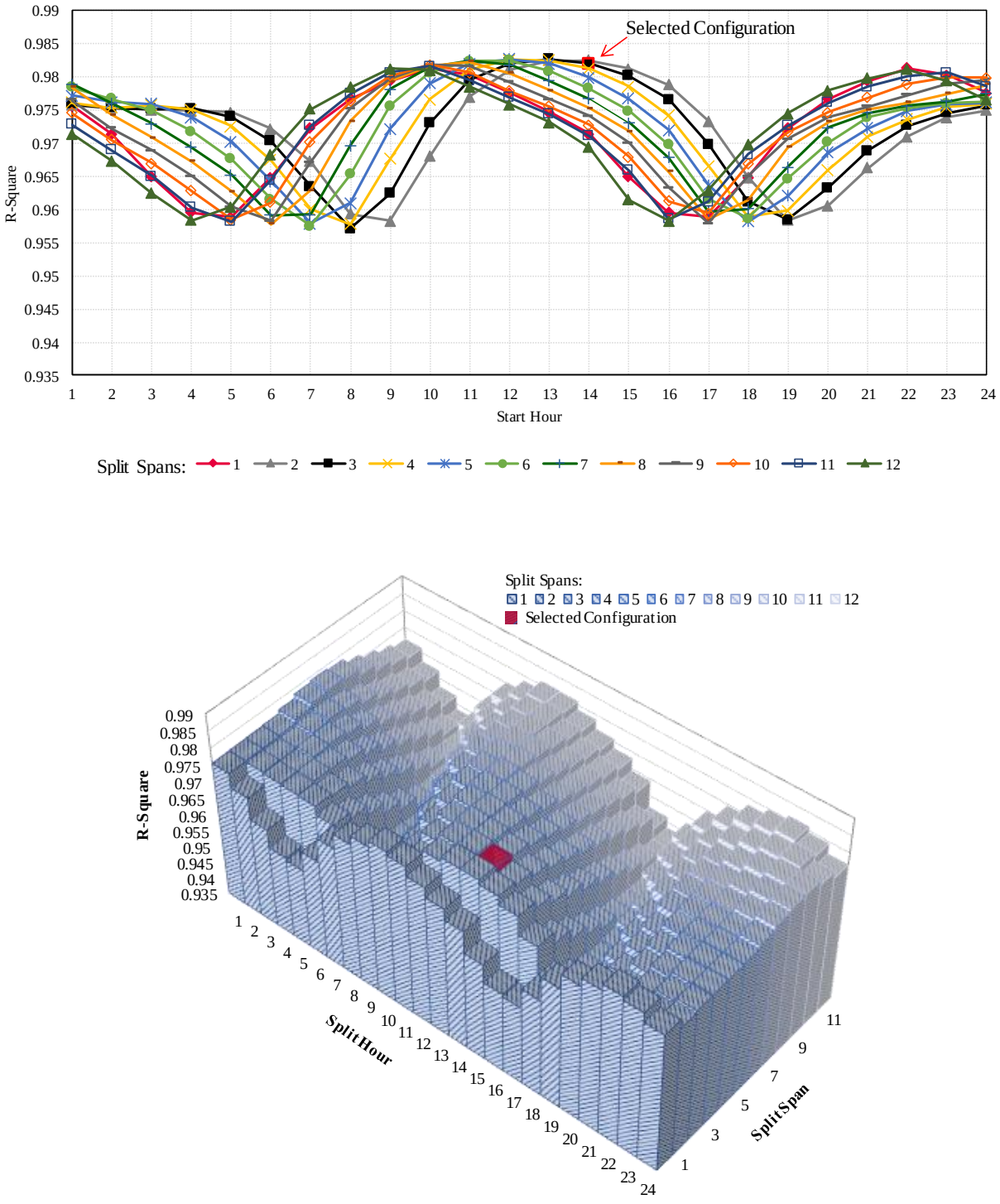

Figure 91: The Accuracy of the Estimated Heating Energy Consumption Using Split-Degree Days with Different Split and Span Hours

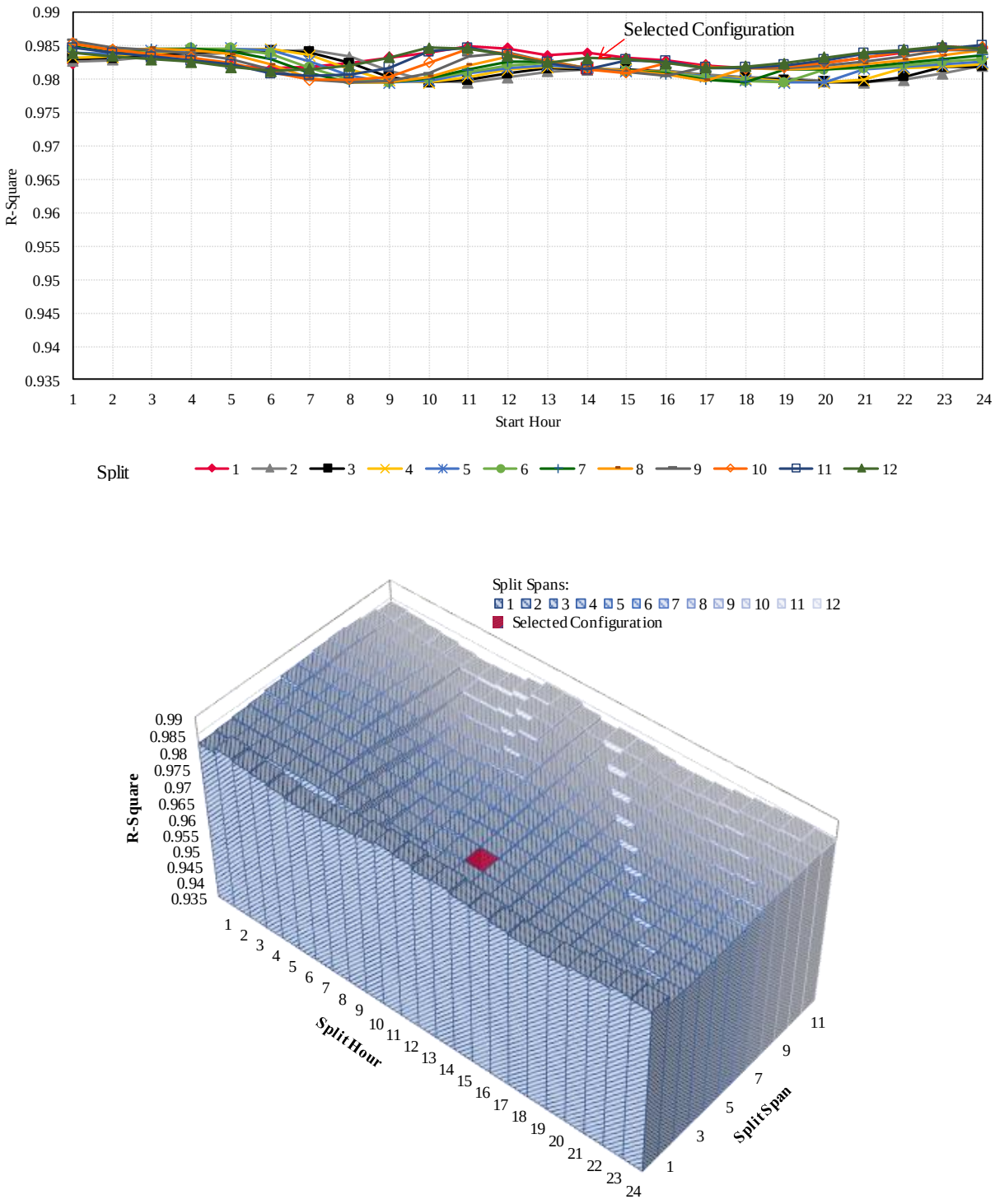

Figure 92: The Accuracy of the Estimated Cooling Energy Consumption Using Split-Degree Days with Different Split and Span Hours

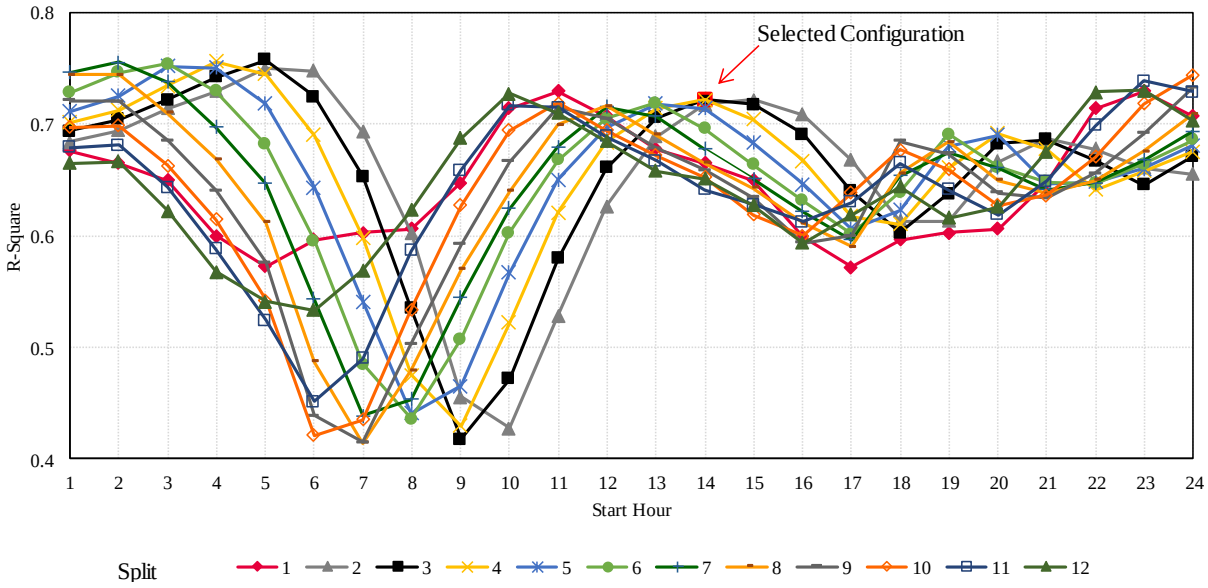

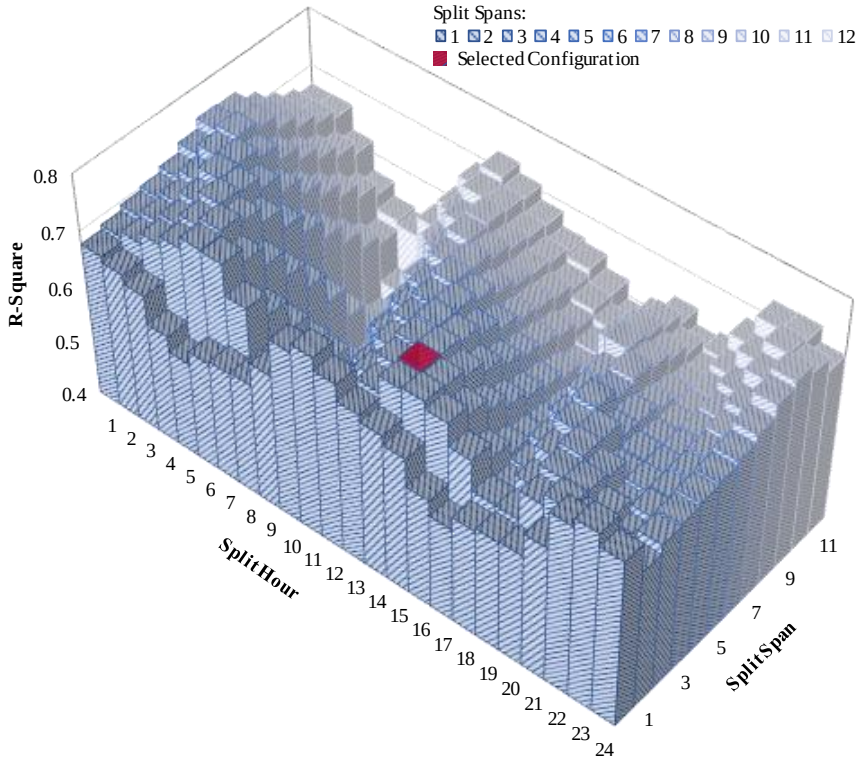

Figure 93: The Accuracy of the Estimated Fan Energy Consumption Using Split-Degree Days with Different Split and Span Hours

In order to find the best points to split the temperature range, various configurations are studied. The analysis included regressing the total regulated energy consumption, heating, cooling, and fan energy consumption at various possible split-CDD and split–HDD, hereafter called sCDD and sHDD, respectively. Based on the results, the sHDD and sCDD, or in general the split-DD, called sDD selected in this study is defined using the following equations:

$$sHDD_{P1} = \sum_{n=1}^{365} \left(T_{base,HDD} - \frac{T_{P1,max} + T_{P1,min}}{2} \right)^{+} \quad 5.1$$

$$sHDD_{P2} = \sum_{n=1}^{365} \left(T_{base,HDD} - \frac{T_{P2,max} + T_{P2,min}}{2} \right)^{+} \quad 5.2$$

where, $T_{base,HDD}$ is the base temperature for the HDD, which is assumed to be 18 ºC (65 ºF), $T_{P1,max}$ and $T_{P1,min}$ are the maximum and minimum outdoor air dry-bulb temperatures, respectively, during the time periods from 12:00 am to 1:00 pm and 5:00 pm to 11:00 pm, and $T_{P2,max}$ and $T_{P2,min}$ are the maximum and minimum outdoor air dry-bulb temperatures, respectively, during the hours 2:00 pm, 3:00 pm, and 4:00 pm.

$$sCDD_{P1} = \sum_{n=1}^{365} \left(\frac{T_{P1,max} + T_{P1,min}}{2} - T_{base,CDD} \right)^{+} \quad 5.3$$

$$sCDD_{P2} = \sum_{n=1}^{365} \left(\frac{T_{P2,max} + T_{P2,min}}{2} - T_{base,CDD} \right)^{+} \quad 5.4$$

where, $T_{base,CDD}$ is the base temperature for CDD, which is assumed to be 10°C (50 °F).

The representation of the sDD applied for the two temperature profile examples is shown in Figure 94. Figure 95 shows the frequency of each hour of the day. The distribution of the daily maximum temperature at the 801 different locations (Figure 95) shows that the maximum daily temperature most likely occurs in the 14:00 to 16:00 time intervals. The selected split interval allows the sDD to account for the diurnal temperature range by including the average in the interval within which mostly the daily peak values occur. The dual values for sCDD and sHDD allows for a more accurate estimation of the building cooling and heating energy consumption, respectively, by discriminating between the coefficients for the two time-spans.

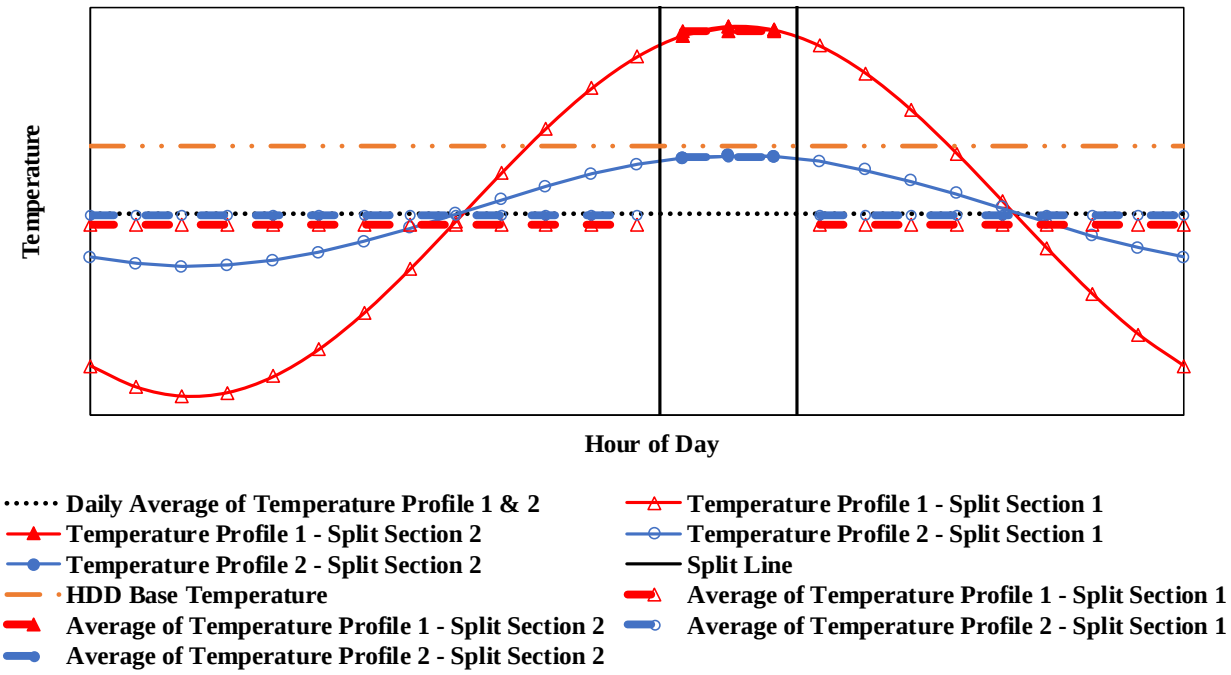

Figure 94: Representation of the Selected Split-DD Applied on Two Temperature Profiles

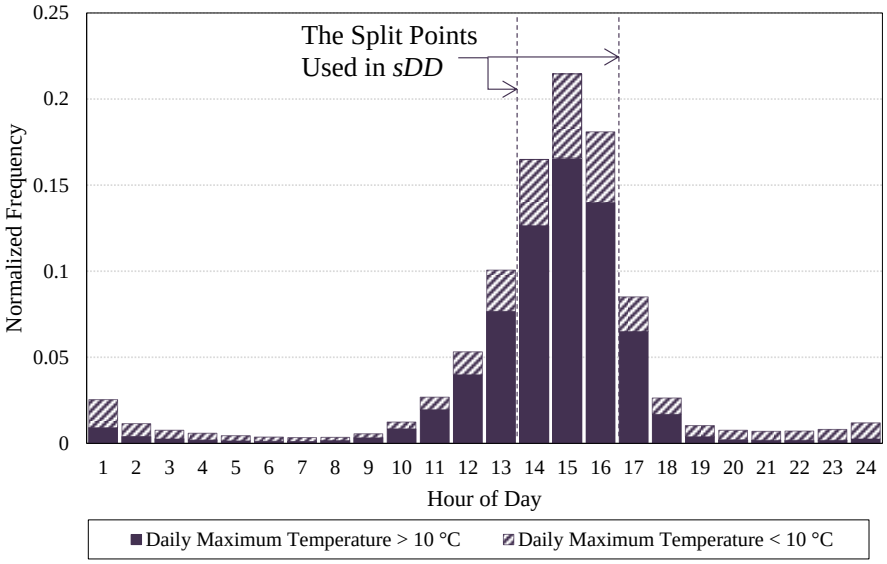

Figure 95: The Distribution of the Daily Maximum Temperature in 801 Different Locations

While considering the improvement of the accuracy of the estimations of the energy consumption, the complexity of the models should also be considered. As described in Appendix A.2, to develop multiple regression models, the desired vector of coefficients, $\widehat{\boldsymbol{\beta}}$, can be calculated using $(\mathbf{X}^{\mathrm{T}}\mathbf{X})^{-1}\mathbf{X}^{\mathrm{T}}\mathbf{Y}$, where $\mathbf{X}$ is an $n \times (k + 1)$ matrix of k independent variables and $\mathbf{Y}$ is an $n \times 1$ vector of outputs. Assuming m equals $k + 1$, transposing the $n \times m$ matrix of $\mathbf{X}$, demoted as $\mathbf{X}^{\mathrm{T}}$, has time complexity of the form $O(n \cdot m)$. The multiplication of the $n \times m$ matrix $\mathbf{X}$ and the $m \times n$ matrix $\mathbf{X}^{\mathrm{T}}$ has n calculation for each element of output, $n \times m$ calculations for each row in the output matrix, and total $O(n \cdot m^2)$ time complexity to calculate the $m \times m$ matrix of $\mathbf{X}^{\mathrm{T}}\mathbf{X}$. The time complexity for the matrix inversion, $(\mathbf{X}^{\mathrm{T}}\mathbf{X})^{-1}$, is $O(m^3)$. The $\mathbf{X}^{\mathrm{T}}\mathbf{Y}$ has $O(n \cdot m)$ time complexity and the multiplication of the $m \times m$ matrix of $(\mathbf{X}^{\mathrm{T}}\mathbf{X})^{-1}$ and the $m \times 1$ matrix of $\mathbf{X}^{\mathrm{T}}\mathbf{Y}$ has $O(m^2)$ time complexity. By including the terms with higher degrees (m^3 instead of m^2 and $n \cdot m^2$ instead of $n \cdot m$, the overall regression procedure results in the time complexity of the

form $O(m^2 \cdot (n+m))$. This means that, as the inputs get larger, the execution time for developing the regression models exponentially increases relative to the inputs.

After developing the regression models, the execution time to calculate the energy consumption using the regression models that were developed from the conventional degree day method and the split-degree day method without the interaction term has time complexity of the form O(n). However, including the interaction term(s) in the split-degree day method increases the time to $O(n^2)$. It should be mentioned, though, that practically, the computation time is higher in the estimations using the split-degree day method (either with or without interaction terms) compared to the conventional degree day method. In other words, while the O(n) time complexity represents the asymptotic behavior of both the conventional degree day method and the split-degree day method without the interaction term, the calculations in the estimations using the split-degree day method without the interaction term require two more multiplications and then their additions for the calculations. Similarly, the numbers in the case with interaction is higher for the four more extra multiplications, which is finally summed. Similarly, as the number of parameters increase in the models, the space complexity increases. However, for the time complexity, to better compare the growth of the models and their scalabilities, the Big-O notation is used here.

A split-degree days can be defined using different number of segmentations in a day (23-split configurations, from 2-split to 24-split, assuming an hourly resolution for the data). To analyze the performance of the split configurations other than the 2-split, two cases were studied. One is the 3-split configuration, assuming that the period of hours 2 pm to 4 pm is fixed. The total number of possible ways to split the 24-hour in a day into 3 segments is 2048. To analyze a number of cases with 3-split configuration, 20 possible cases by fixing one segment of 2 pm to 4

pm were used to see the performance of these 3-plit configurations while the fixed period of time allows for capturing the diurnal temperature range by separating the hours at which maximum ambient temperature in a day is most likely to happen (as discussed in the 2-split configurations). Another study was done on the 24-split configuration. This R-square is calculated for the 20 cases of the 3-split configuration, both with and without interaction terms. However, based on the $O(m^2 \cdot (n+m))$, developing the model for 24 segmentation configuration with interaction terms is considerably more complex in terms of runtime. Also, the calculations using the developed model for the 24 segmentation without the interaction term has O(n) time complexity while the model with all the interaction terms has $O(n^{24})$. In this case, the R-square is only calculated for the model without interaction terms for comparisons.

Figure 96 shows the comparison of the calculated R-squares for the models with the conventional degree days as well as the 2-split configurations, with and without interaction terms. The results for both the identical DOE medium office prototype model for ASHRAE Standard 90.1, climate zone 4B (top) and the model with higher thermal mass (bottom) are provided. In Figure 96, it can be seen that the split-degree days have higher R-square values compared to the conventional degree days. Comparing different split configurations, the 24-split and the 3-split segmentation with interaction terms have the highest R-square. However, the 3-split models without interaction terms have significantly lower accuracy. On the other hand, the 2-split models with and without interaction have comparatively high accuracy. Overall, as a balance between the accuracy, complexity, and considering potentially lower resolution of ambient temperature data in practice, the 2-split configuration is selected for this study, while there is a room to further study the optimal configurations of other split configurations for the future studies.

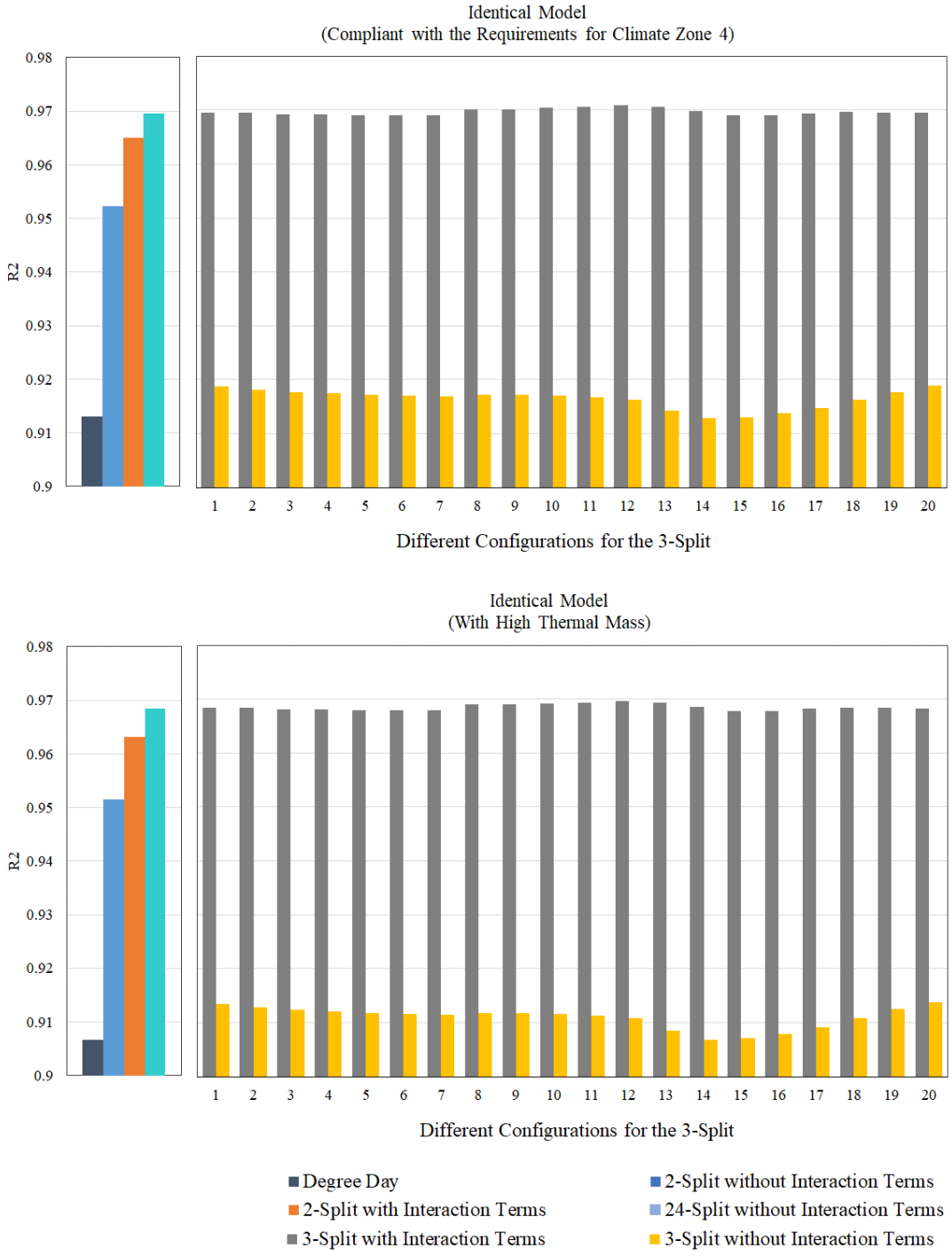

Figure 96: Comparisons of the Accuracy of the Estimations of the Selected Cases with Different Split Configurations and the Conventional Degree Day Method; Top: Results for the Identical DOE Medium Office Prototype Model for Climate Zone 4B for ASHRAE Standard 90.1-2016; Bottom: Modified Identical DOE Medium Office Prototype Model with Higher Thermal Mass.

5.1.2. Association of the Influential Climatic Parameters and the Degree Days and Split-Degree Days Methods

This section represents the results of the comparative analysis of the predictions of the influential climatic parameters using degree days and split-degree days as the dependent variables. The results utilize the linear regressions derived from either conventional degree days (HDD and CDD) or split-Degree Days (sHDD and sCDD). The plots for the analysis of the predictions include the scatter plots of the predicted values using the regression model versus the actual simulated values as well as the residuals. The mathematical regression models, R-square, adjusted R-square, and the RMSE are included in each result. Except for the diurnal temperature range, which yields a single value for each day, daily average hourly values are calculated for other parameters. The annual sum of these parameters are then used in the regressions. The bar in the regression models indicate the average, the "AnnSum" superscript indicates the annual sum, and the "d, h" subscript indicates the daily average hourly.

5.1.2.1. The Association of Diurnal Temperature Range and the Degree Days and Split-Degree Days

As shown in Figure 87, the points for the 801 locations are widely distributed along the horizontal axis, which shows that the diurnal temperature range vary significantly in different locations. On average, subtype B has higher diurnal temperature range compared to other locations. This can be seen in the grouping of the subtype B (red) toward the highest ranges. However, this difference and grouping can not be seen when using the average or maximum daily values (Figure 97). In other words, the three clusters of the three different moisture regimes

in Figure 97 are not horizontally separated by the values on the horizontal axes. Therefore, the average values (or maximum or minimum values) do not represent the diurnal temperature range, which can be used as a discriminating parameter between different moisture regimes.

Figure 87 also shows that there is no significant relationship between the climate zone numbers and the diurnal temperature range, although the diurnal temperature range in climate zones 7 and 8 have slightly lower diurnal temperature range compared to others.

In order to assess the predictability of the diurnal temperature range using either the conventional degree days or split-degree days, the annual sum of the diurnal temperature range ($\overline{\mathrm{DTR}}_{\mathrm{d,h}}^{\mathrm{Ann.Sum}}$) was regressed against the conventional HDD and CDD and then against the sHDD and sCDD. Figure 98 shows the prediction of the $\overline{\mathrm{DTR}}_{\mathrm{d,h}}^{\mathrm{Ann.Sum}}$ by conventional HDD and CDD. The regression model is shown in equation 5.5. The R^2 of the model is 0.032, the adjusted R^2 is 0.029, and the Root Mean Square Error (RMSE) is 859.594. The very low R^2 of the linear regression shows that there is approximately no indication of the $\overline{\mathrm{DTR}}_{\mathrm{d,h}}^{\mathrm{Ann.Sum}}$ in conventional degree days.

On the other hand, the linear regressions using sHDD and sCDD, either without including the interaction term (Figure 99), or with the interaction term of the two sHDDs and two sCDDs (Figure 100), shows a significant improvement in the prediction of the $\overline{\mathrm{DTR}}_{\mathrm{d,h}}^{\mathrm{Ann.Sum}}$ with the sHDD and sCDD. The regression model using sHDD and sCDD without including the interaction term (Figure 99) is shown in equation 5.6. The R^2 and the adjusted R^2 of the model are 0.964, and the RMSE is 165.671. The regression model using sHDD and sCDD with the interaction term included (Figure 100) is shown in equation 5.7. The R^2 and the adjusted R^2 of the model are 0.968, and the RMSE is 156.192.

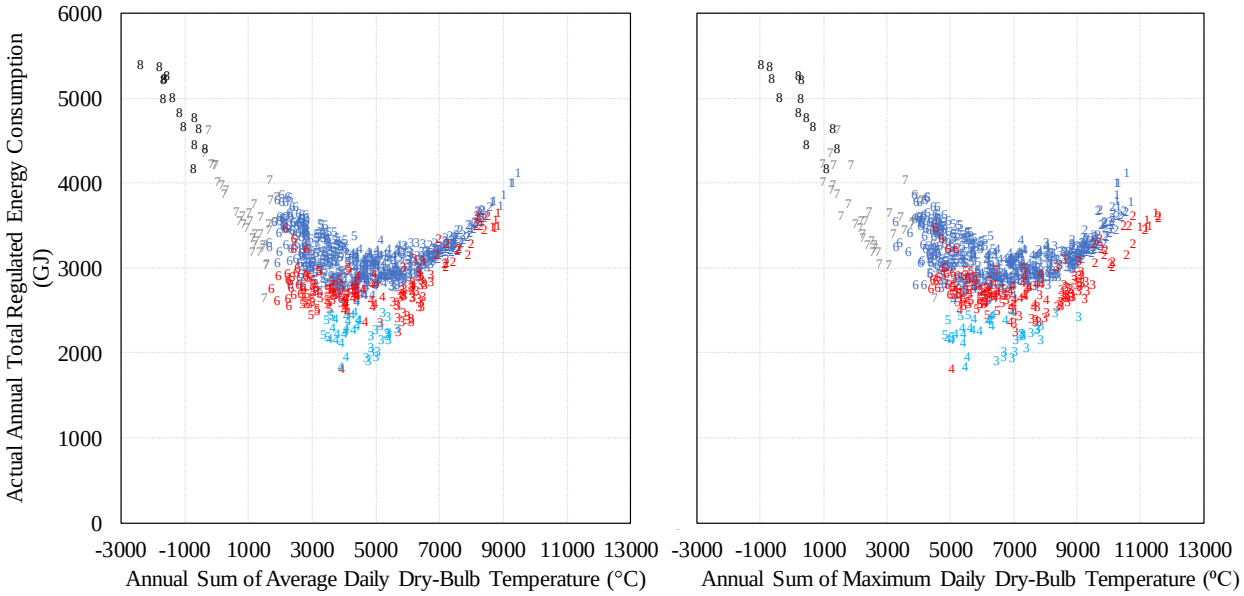

Figure 97: Distribution of the Annual Sum of Average Daily Dry-Bulb Temperature (Left) and Maximum Daily Dry-Bulb Temperature (Right)

$$\overline{\mathrm{DTR}}_{\mathrm{d,h}}^{\mathrm{Ann.Sum}}(CDD,\ HDD) = 4572.4826 - 0.066822 \cdot CDD - 0.136582 \cdot HDD \quad (5.5)$$

$$\overline{\mathrm{DTR}}_{\mathrm{d,h}}^{\mathrm{Ann.Sum}}(sCDD_{P1},\ sCDD_{P2}, sHDD_{P1},\ sHDD_{P2}) = -241.5932 - 1.090981 \cdot sCDD_{P1} + 1.3794276 \cdot sCDD_{P2} + 1.8052363 \cdot sHDD_{P1} - 1.617339 \cdot sHDD_{P2} \quad (5.6)$$

where, $sCDD_{P1}$ and $sCDD_{P2}$ are the split cooling degree days in section 1 and 2 of a daily temperature profile (Figure 89), respectively, and $sHDD_{P1}$ and $sHDD_{P2}$ are the split heating degree days in section 1 and 2 of a daily temperature profile (Figure 89), respectively.

$$\overline{\mathrm{DTR}}_{\mathrm{d,h}}^{\mathrm{Ann.Sum}}(sCDD_{P1},\ sCDD_{P2}, sHDD_{P1},\ sHDD_{P2}) \tag{5.7}$$

$$= -659.0309 - 1.016862 \cdot sCDD_{P1} + 1.4656489 \cdot sCDD_{P2}$$

$$- 0.000018 \cdot sCDD_{P1} \cdot sCDD_{P2} + 1.7436697 \cdot sHDD_{P1}$$

$$- 1.418671 \cdot sHDD_{P2} - 0.00001219 \cdot sHDD_{P1} \cdot sHDD_{P2}$$

The main reason that the $\overline{\mathrm{DTR}}_{\mathrm{d,h}}^{\mathrm{Ann.Sum}}$ can be well predicted using split-degree days is that the two values in the split-degree days correlates well with the diurnal temperature range and provides improved information. In contrast to the split-degree days, the average values taken in degree days loses all the information related to the diurnal temperature range.

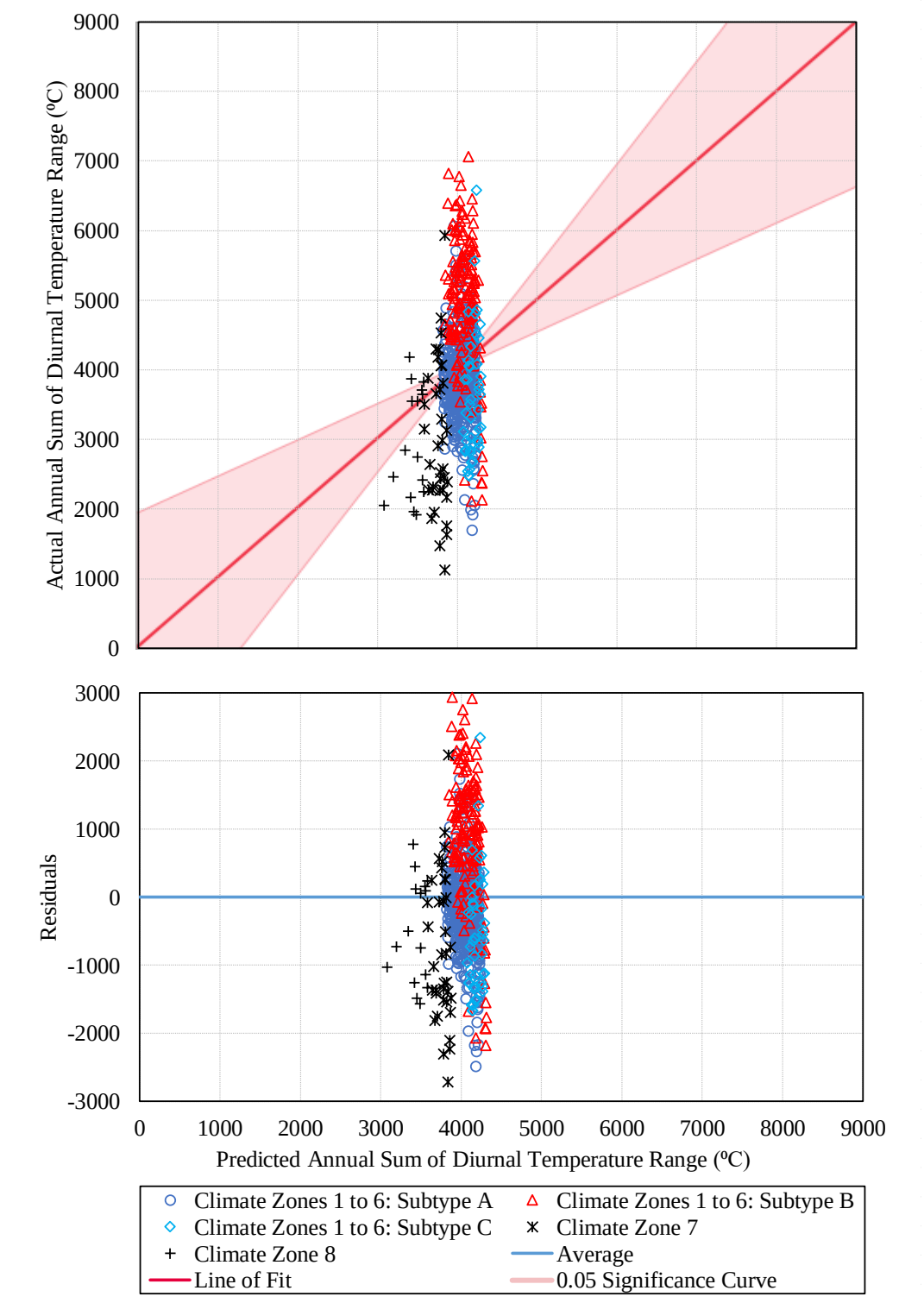

Figure 98: Prediction of the Annual Sum of Diurnal Temperature Range Using Conventional Degree Day

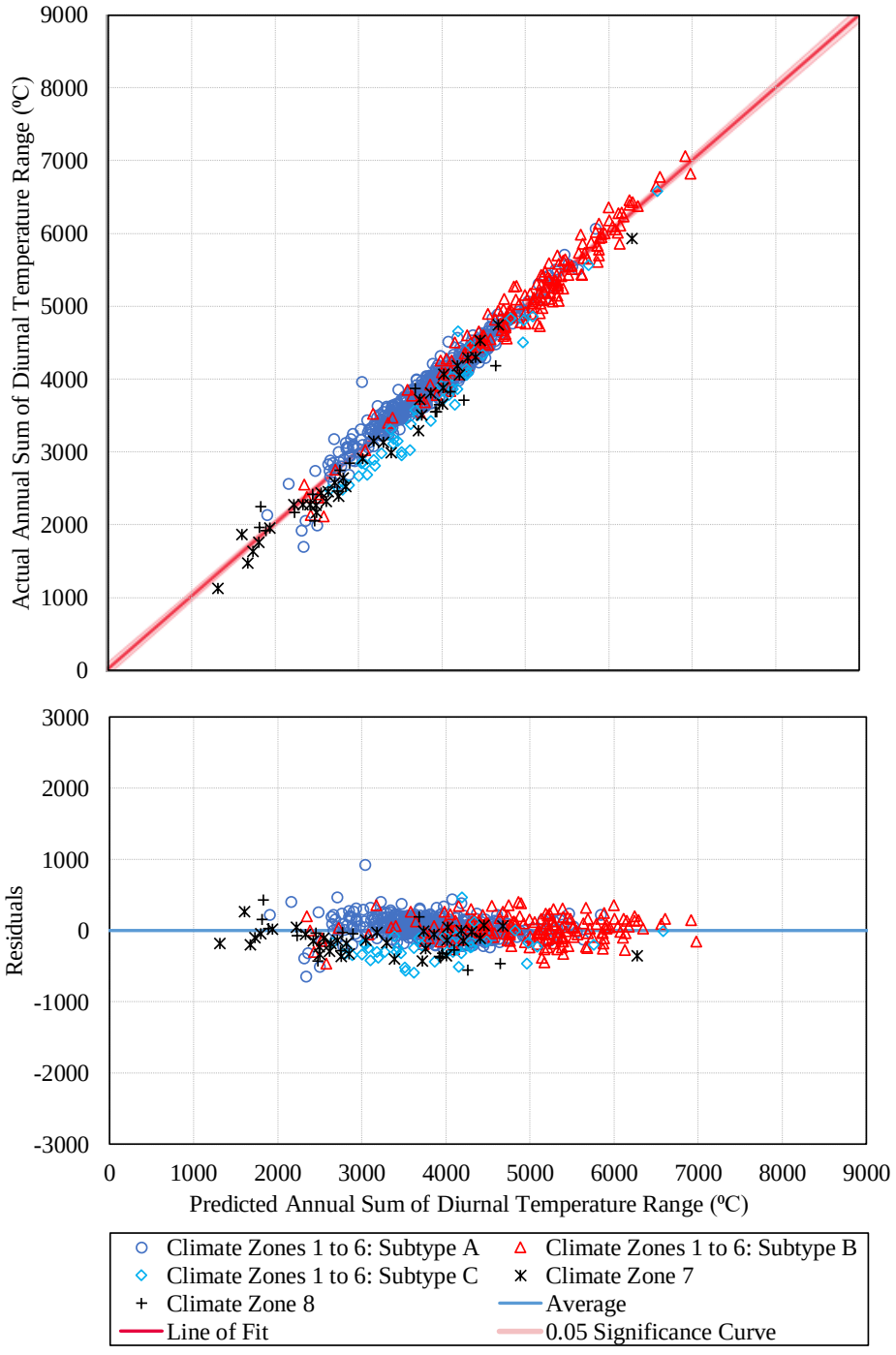

Figure 99: Prediction of the Annual Sum of Diurnal Temperature Range Using Split-Degree Day without Interaction Terms

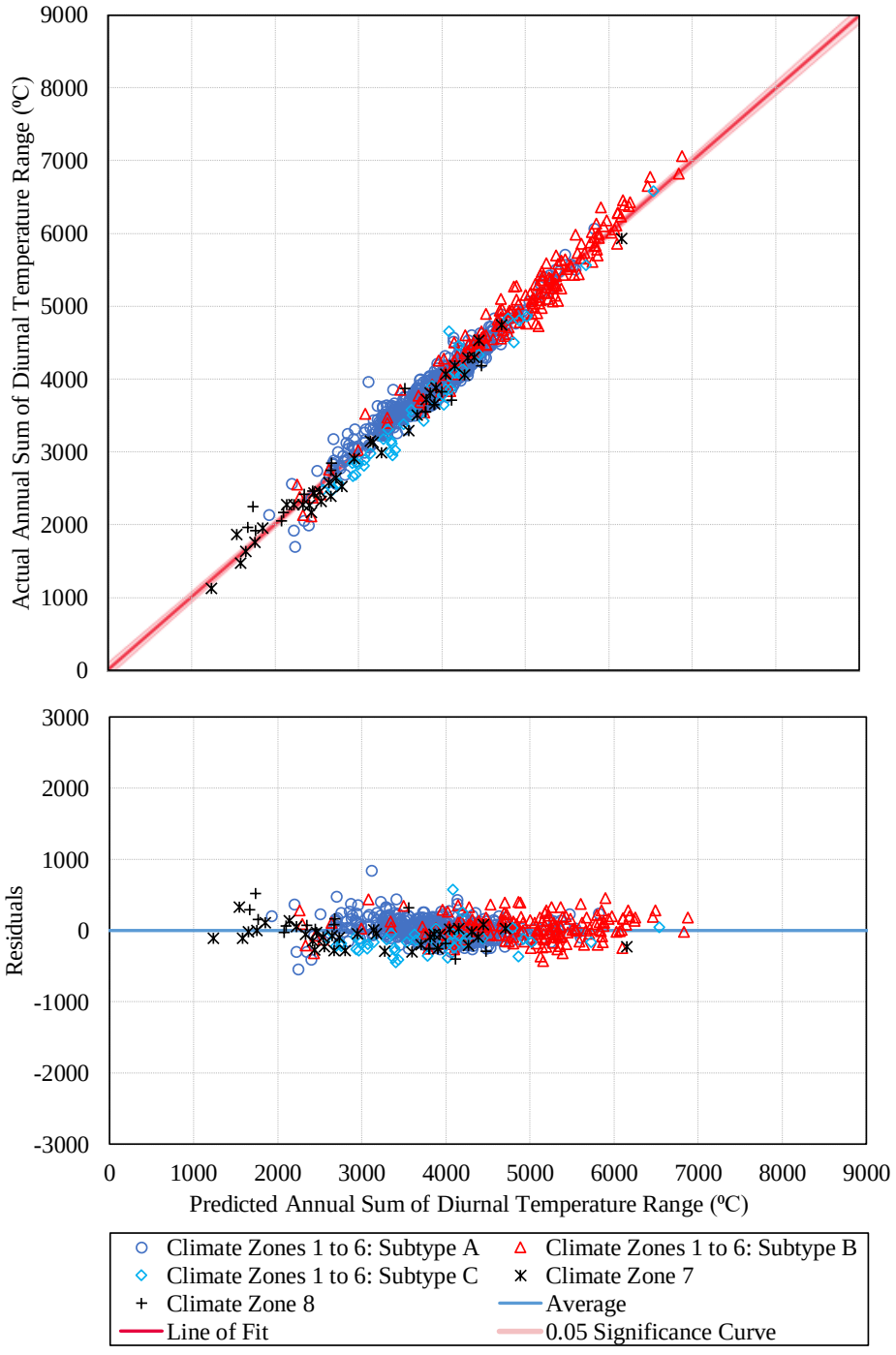

Figure 100: Prediction of the Annual Sum of Diurnal Temperature Range Using Split-Degree Day with Interaction Terms

5.1.2.2. The Association of Solar Radiation and the Degree Days and Split-Degree Days

The global horizontal solar radiation is used to represent the solar radiation characteristics of each location. The daily average hourly global horizontal solar radiation ($\overline{GHR}_{d,h}^{Ann.Sum}$) is calculated for each location and then the annual sum provides a single value for each location. As shown in Figure 101, similar to the diurnal temperature range, the $\overline{GHR}_{d,h}^{Ann.Sum}$ in dry moisture regimes is higher than other subtypes. In other words, the clusters of subtype A and B are horizontally separated showing that there is a distinct difference between the $\overline{GHR}_{d,h}^{Ann.Sum}$ in subtype A and B. Also, Figure 101 also shows that the $\overline{GHR}_{d,h}^{Ann.Sum}$ decreases with increasing the climate zone number. The highest $\overline{GHR}_{d,h}^{Ann.Sum}$ can be seen at climate zones with lower numbers and the lowest $\overline{GHR}_{d,h}^{Ann.Sum}$ can be seen at 7 and 8.

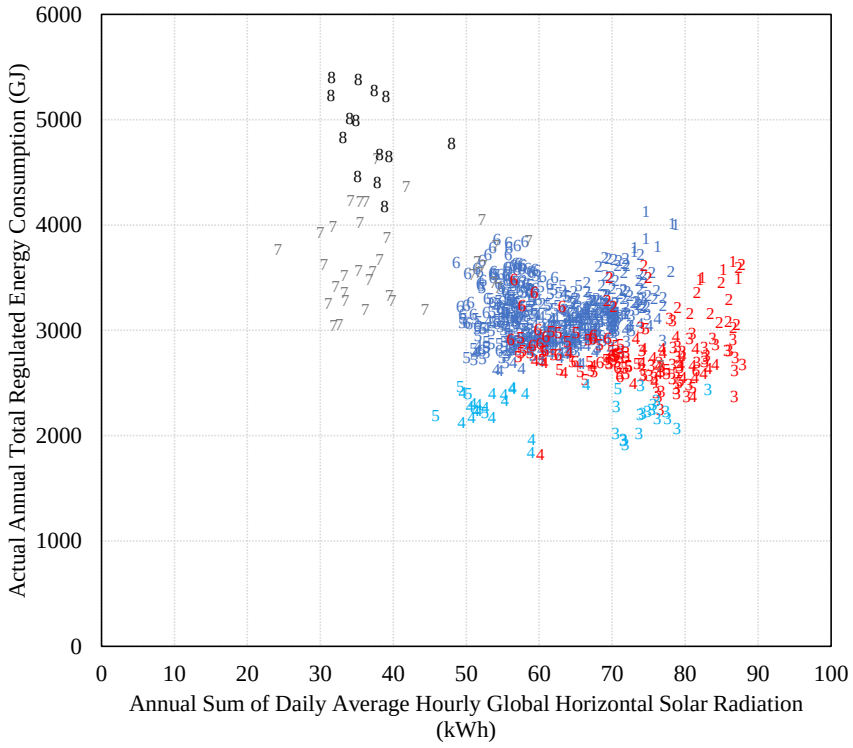

Figure 101: Various Global Horizontal Solar Radiation in Different Subtypes for Similar Regulated Energy Consumptions

Since $\overline{\mathrm{GHR}}_{\mathrm{d,h}}^{\mathrm{Ann.Sum}}$ classifies different moisture regimes into approximately distinct clusters, it can be potentially considered as a covariate for the estimation of the building energy consumption. To evaluate this, linear regressions were conducted for $\overline{\mathrm{GHR}}_{\mathrm{d,h}}^{\mathrm{Ann.Sum}}$ as the dependent variable and either the conventional degree days or the split-degree days as the independent variables. Results show that the estimations using the split-degree days were considerably better than the estimations using the conventional degree days.

Figure 102 shows that the estimation of the $\overline{\mathrm{GHR}}_{\mathrm{d,h}}^{\mathrm{Ann.Sum}}$ using the conventional degree days. The regression model is shown in equation 5.8. The R^2 of the model is 0.578, the adjusted R^2 is 0.577, and the RMSE is 7.106. Figure 102 shows that the estimation of the $\overline{\mathrm{GHR}}_{\mathrm{d,h}}^{\mathrm{Ann.Sum}}$ using the conventional degree days can vary to a large extent within different ranges of $\overline{\mathrm{GHR}}_{\mathrm{d,h}}^{\mathrm{Ann.Sum}}$. The more numbers of point in subtype A play a significant role in the regression model. The figure shows that the model underestimates the actual values of $\overline{\mathrm{GHR}}_{\mathrm{d,h}}^{\mathrm{Ann.Sum}}$ for the majority of points in subtype B. Also, the prediction for the dry moisture regime is underestimated in the majority of the cases while $\overline{\mathrm{GHR}}_{\mathrm{d,h}}^{\mathrm{Ann.Sum}}$ is mainly overestimated in climate zone 7.

$$\overline{\mathrm{GHR}}_{\mathrm{d,h}}^{\mathrm{Ann.Sum}}(CDD,\ HDD) = 75.784278 + 0.0005362 \cdot CDD - 0.004884 \cdot HDD \quad (5.8)$$

On the other hand, the analysis showed the prediction of the $\overline{\mathrm{GHR}}_{\mathrm{d,h}}^{\mathrm{Ann.Sum}}$ using split-degree days, either without including the interaction terms (Figure 103) or with the interaction

terms (Figure 104) show considerably higher R-square values. The regression model without the interaction terms (Figure 103) is shown in equation 5.9. The R^2 of the model is 0.807, the adjusted R^2 is 0.806, and the RMSE is 4.814.

$$\overline{\mathrm{GHR}}_{\mathrm{d,\ h}}^{\mathrm{Ann.\ Sum}}(sCDD_{P1},\ sCDD_{P2}, sHDD_{P1},\ sHDD_{P2}) \tag{5.9}$$
$$= 45.335365 - 0.004573 \cdot sCDD_{P1} + 0.0076949 \cdot sCDD_{P2}$$
$$+ 0.0087627 \cdot sHDD_{P1} - 0.011727 \cdot sHDD_{P2}$$

The regression model with the interaction terms (Figure 104) is shown in equation 5.10. The R^2 of the model is 0.811, the adjusted R^2 is 0.810, and the RMSE is 4.770.

$$\overline{\mathrm{GHR}}_{\mathrm{d,\ h}}^{\mathrm{Ann.\ Sum}}(sCDD_{P1},\ sCDD_{P2}, sHDD_{P1},\ sHDD_{P2}) \tag{5.10}$$
$$= 46.327788 - 0.003005 \cdot sCDD_{P1} + 0.0075216 \cdot sCDD_{P2}$$
$$- 0.0000002633 \cdot sCDD_{P1} \cdot sCDD_{P2} + 0.009132 \cdot sHDD_{P1}$$
$$- 0.013858 \cdot sHDD_{P2} + 0.00000022568 \cdot sHDD_{P1} \cdot sHDD_{P2}$$

The issue with the underestimation for dry regions and overestimation for very cold climates was resolved to a considerable extent in regression models using split-degree days, since the dual values provided for sHDD and sCDD associated with different moisture regimes *indirectly* included the information of different subtypes.

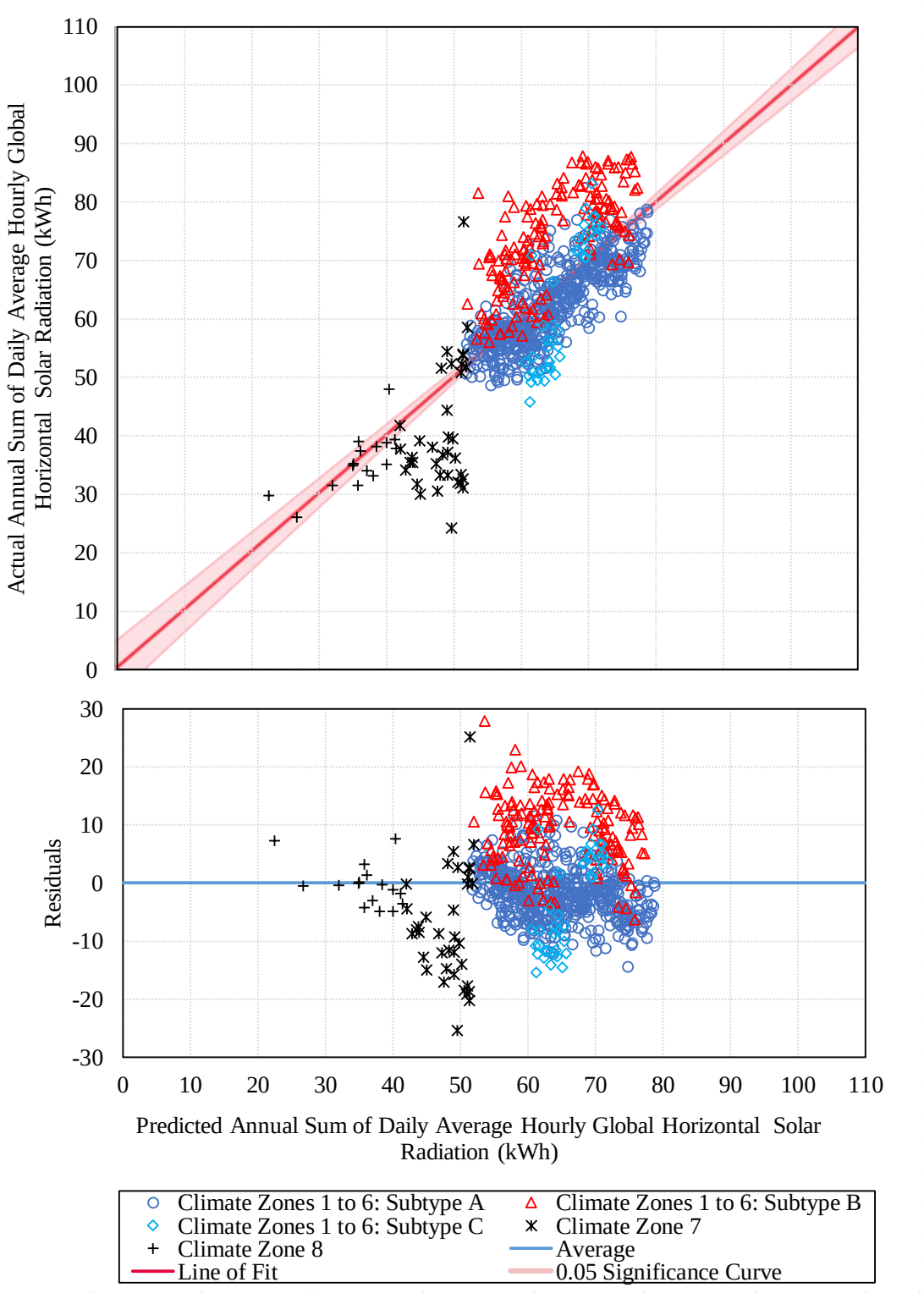

Figure 102: Prediction of the Annual Sum of the Daily Average Hourly Global Horizontal Solar Radiation Using Conventional Degree Days

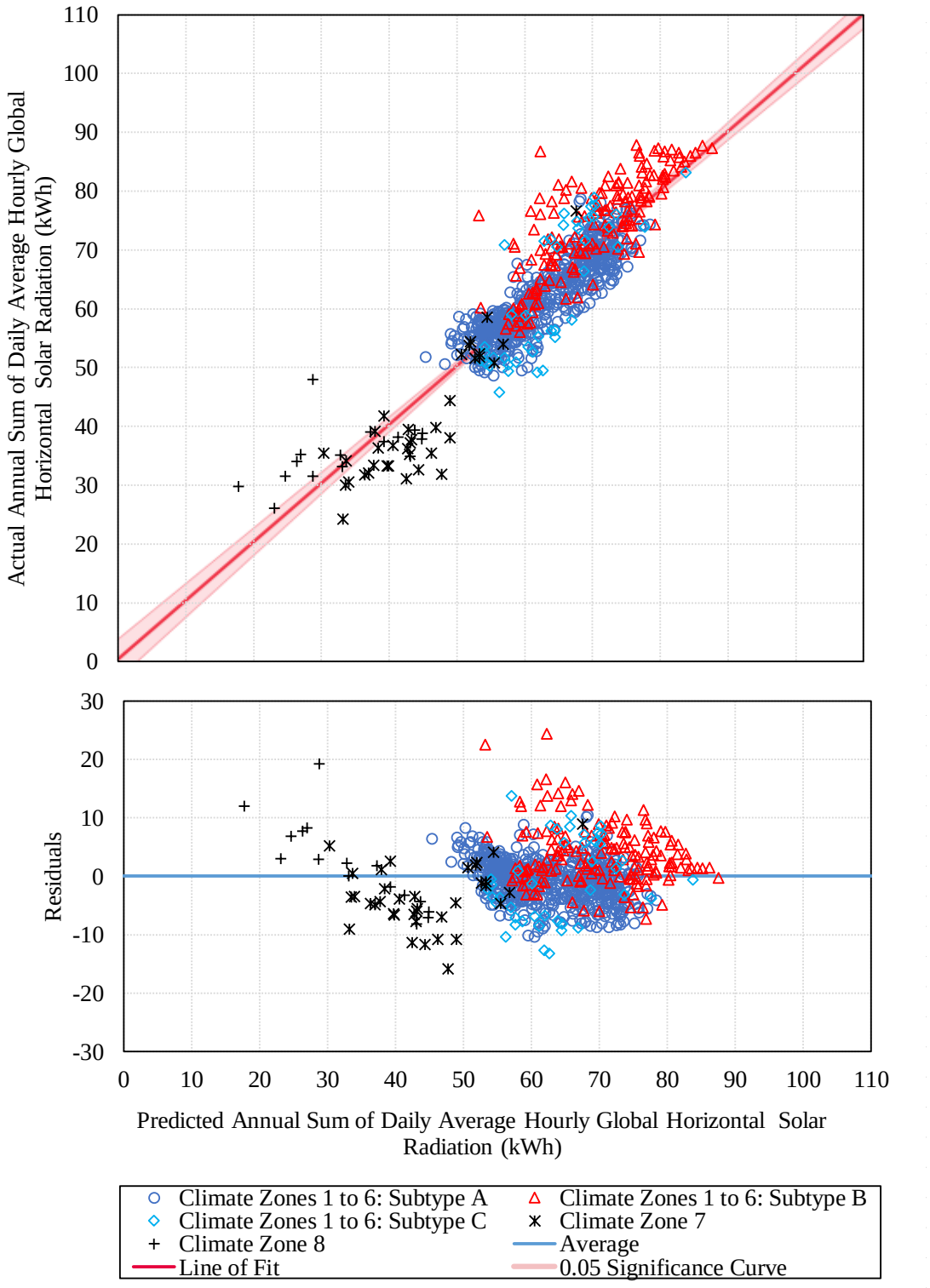

Figure 103: Prediction of the Annual Sum of the Daily Average Hourly Global Horizontal Solar Radiation Using Split-Degree Days without Interaction Terms

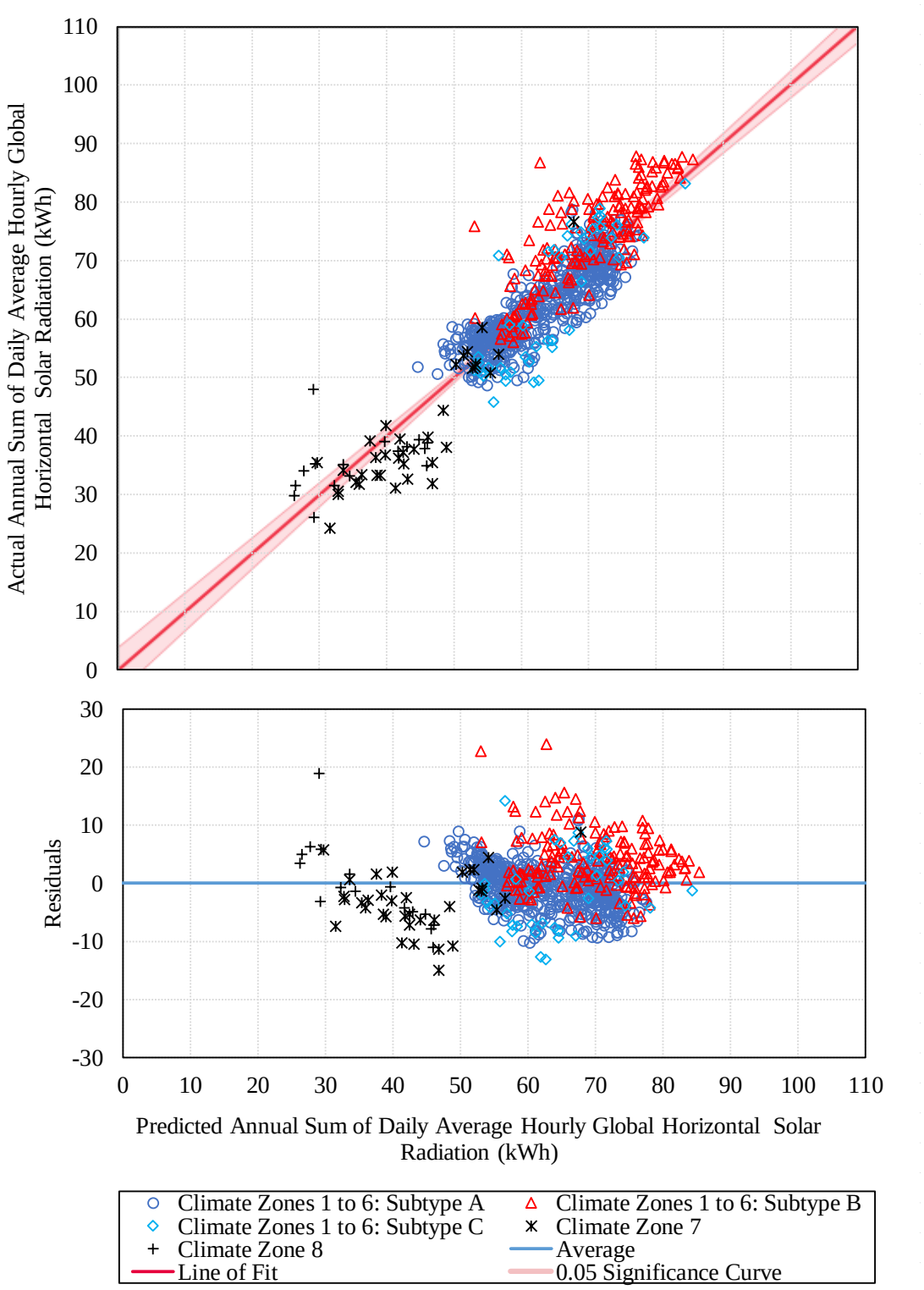

Figure 104: Prediction of the Annual Sum of the Daily Average Hourly Global Horizontal Solar Radiation Using Split-Degree Days with Interaction Terms

5.1.2.3. The Association of Humidity with the Degree Days and Split-Degree Days

Humidity is a weather-related parameter that impacts building energy consumption in buildings where cooling and dehumidification occur. In this section, the dew-point temperature is selected as the representative parameter for the humidity of each weather file. More specifically, the annual sum of the daily average hourly dew-point temperature ($\overline{\mathrm{DP}}_{\mathrm{d,h}}^{\mathrm{AnnSum}}$) was used in the analysis of this section. Figure 105 shows that within each climate zone number, the $\overline{\mathrm{DP}}_{\mathrm{d,h}}^{\mathrm{AnnSum}}$ is slightly lower in dry locations compared to moist and marine locations. The separation of the different moisture regimes in Figure 105 shows that $\overline{\mathrm{DP}}_{\mathrm{d,h}}^{\mathrm{AnnSum}}$ could be considered as a covariate in the estimation of the total regulated energy consumption by including the information to discriminate various moisture regimes.

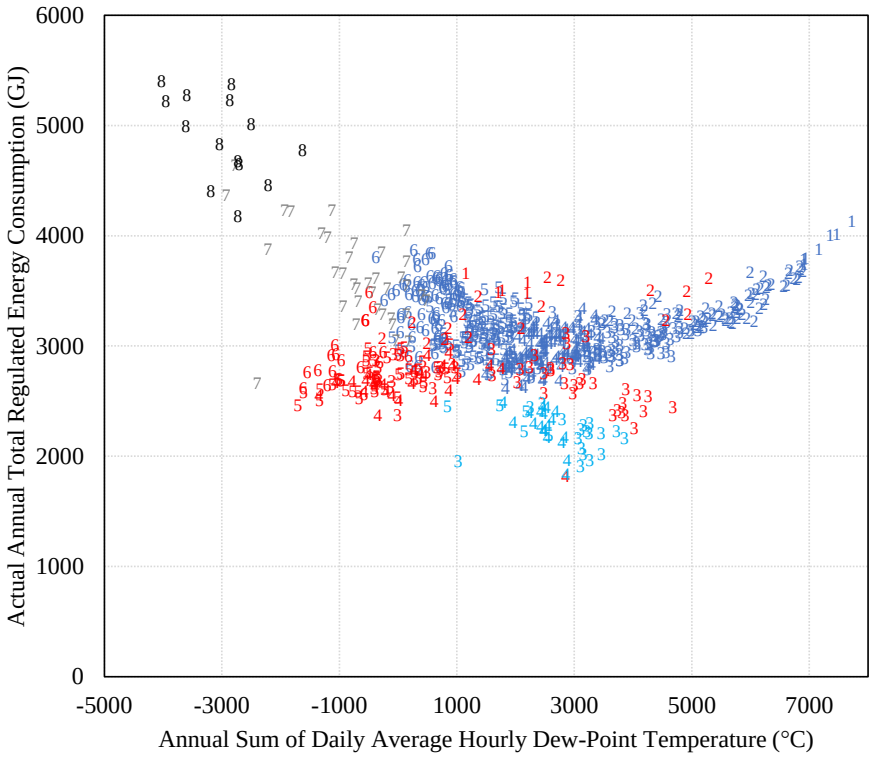

Figure 105: Various Dew-Point Temperature in Different Subtypes for Similar Regulated Energy Consumptions

The $\overline{\mathrm{DP}}_{\mathrm{d,h}}^{\mathrm{AnnSum}}$ was used as the dependent variable for either the conventional degree days or split-degree days as the independent variables to develop linear regression models. Figure 106 shows the estimation of the $\overline{\mathrm{DP}}_{\mathrm{d,h}}^{\mathrm{AnnSum}}$ using the conventional degree days. The regression model is shown in equation 5.11. The R^2 and the adjusted R^2 of the model are 0.756, and the RMSE is 1009.388.

$$\overline{\mathrm{DP}}_{\mathrm{d,h}}^{\mathrm{AnnSum}}\,(CDD,\ HDD) = 3061.7175 + 0.5251119 \cdot CDD - 0.775979 \cdot HDD \qquad 5.11$$

In the Figure 106 it can be seen that, in general, the $\overline{\mathrm{DP}}_{\mathrm{d,h}}^{\mathrm{AnnSum}}$ for subtype A is underestimated while it is overestimated for subtype B. Also, there is a large variation in the estimations of the $\overline{\mathrm{DP}}_{\mathrm{d,h}}^{\mathrm{AnnSum}}$ for the locations subtype B within similar ranges of the HDD and CDD. There is also a slight underestimation in the prediction of $\overline{\mathrm{DP}}_{\mathrm{d,h}}^{\mathrm{AnnSum}}$ for the locations in climate zone 7.

On the other hand, the estimation of the $\overline{\mathrm{DP}}_{\mathrm{d,h}}^{\mathrm{AnnSum}}$ using sDD, either without interaction terms (Figure 107) or with interaction terms (Figure 108) shows less discrepancies in the prediction of the $\overline{\mathrm{DP}}_{\mathrm{d,h}}^{\mathrm{AnnSum}}$ for different moisture regimes. Furthermore, the issue of the overestimation in climate zone 7 is resolved by using sDD as the independent variables.

The regression model without the interaction terms (Figure 107) is shown in equation 5.12. The R^2 of the model is 0.877, the adjusted R^2 is 0.876, and the RMSE is 718.352.

$$\overline{\mathrm{DP}}_{\mathrm{d,h}}^{\mathrm{AnnSum}}\left(sCDD_{P1},\ sCDD_{P2}, sHDD_{P1},\ sHDD_{P2}\right) \qquad 5.12$$

$$= 6618.7851 + 2.2461651 \cdot sCDD_{P1} - 1.757061 \cdot sCDD_{P2}$$

$$- 1.324498 \cdot sHDD_{P1} + 0.2103839 \cdot sHDD_{P2}$$

The regression model with the interaction terms (Figure 108) is shown in equation 5.13. The R^2 of the model is 0.882, the adjusted R^2 is 0.881, and the RMSE is 703.040.

$$\overline{\mathrm{DP}}_{\mathrm{d,h}}^{\mathrm{AnnSum}}\left(sCDD_{P1},\ sCDD_{P2}, sHDD_{P1},\ sHDD_{P2}\right) \qquad 5.13$$

$$= 5752.6857 + 2.761751 \cdot sCDD_{P1} - 1.571594 \cdot sCDD_{P2}$$

$$- 0.000101 \cdot sCDD_{P1} \cdot sCDD_{P2} - 1.405983 \cdot sHDD_{P1}$$

$$+ 0.2784268 \cdot sHDD_{P2} + 0.000015527 \cdot sHDD_{P1} \cdot sHDD_{P2}$$

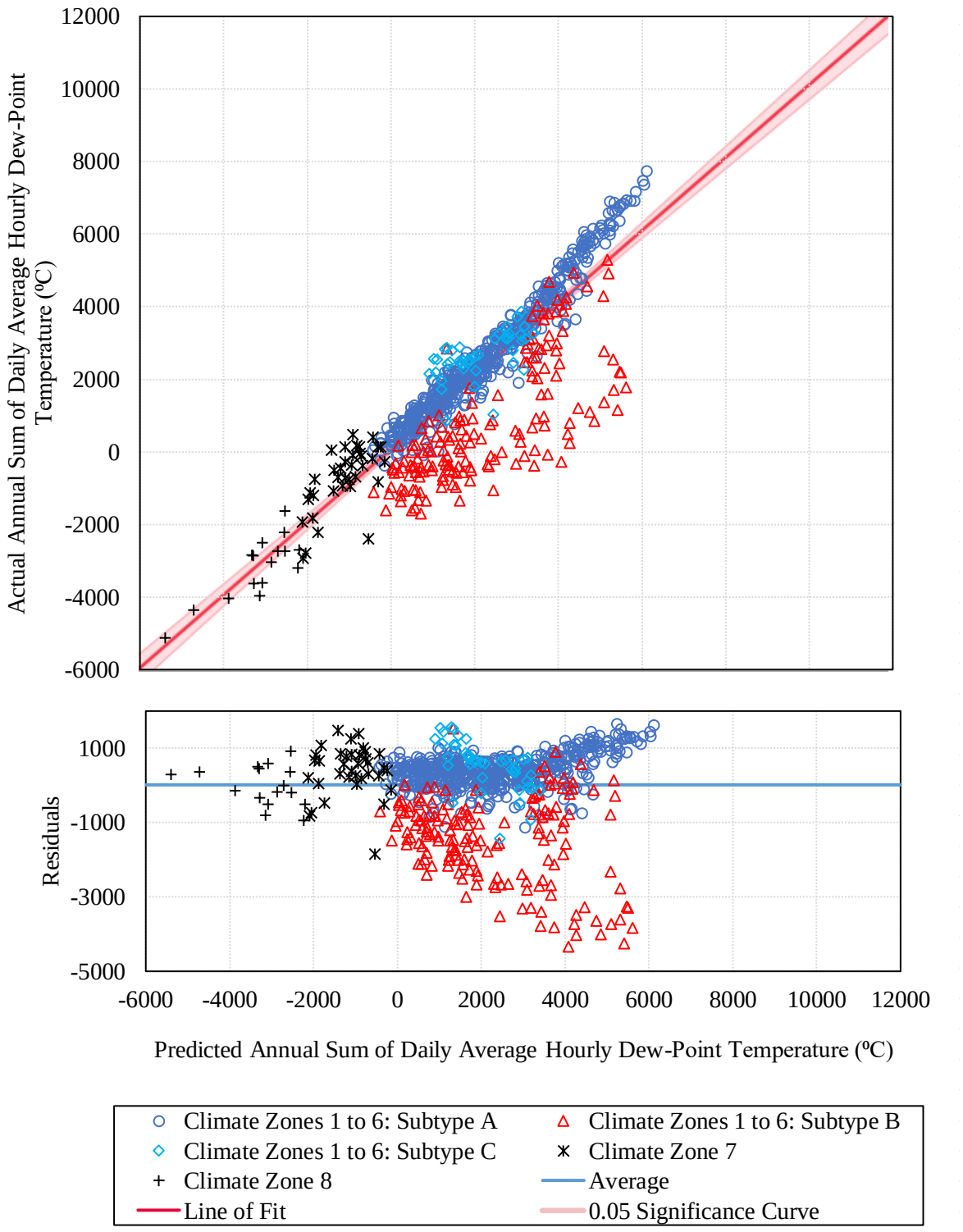

Figure 106: Prediction of the Annual Sum of the Daily Average Hourly Dew-Point Temperature Using Conventional Degree Days

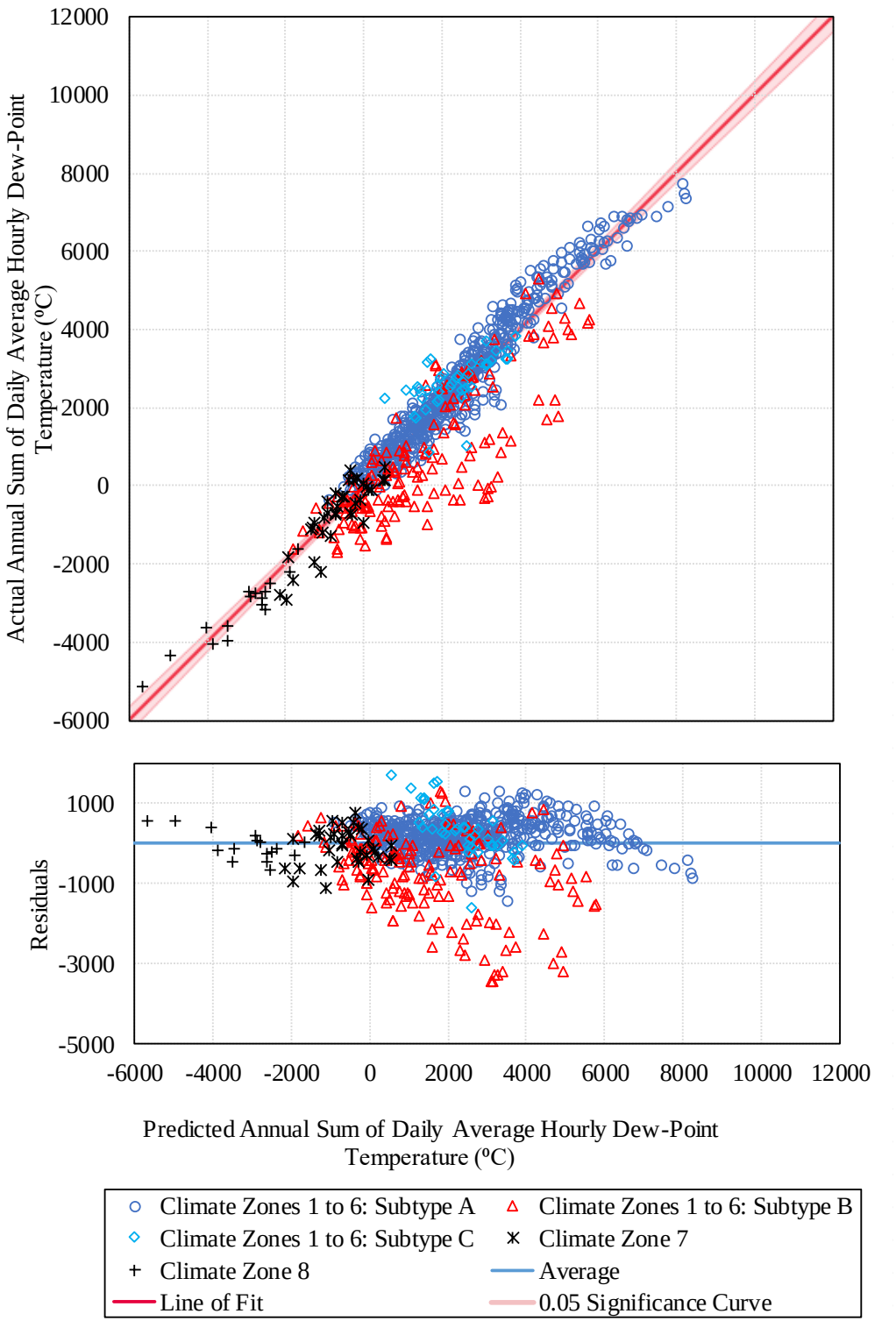

Figure 107: Prediction of the Annual Sum of the Daily Average Hourly Dew-Point Temperature Using Split-Degree Days without Interaction Terms

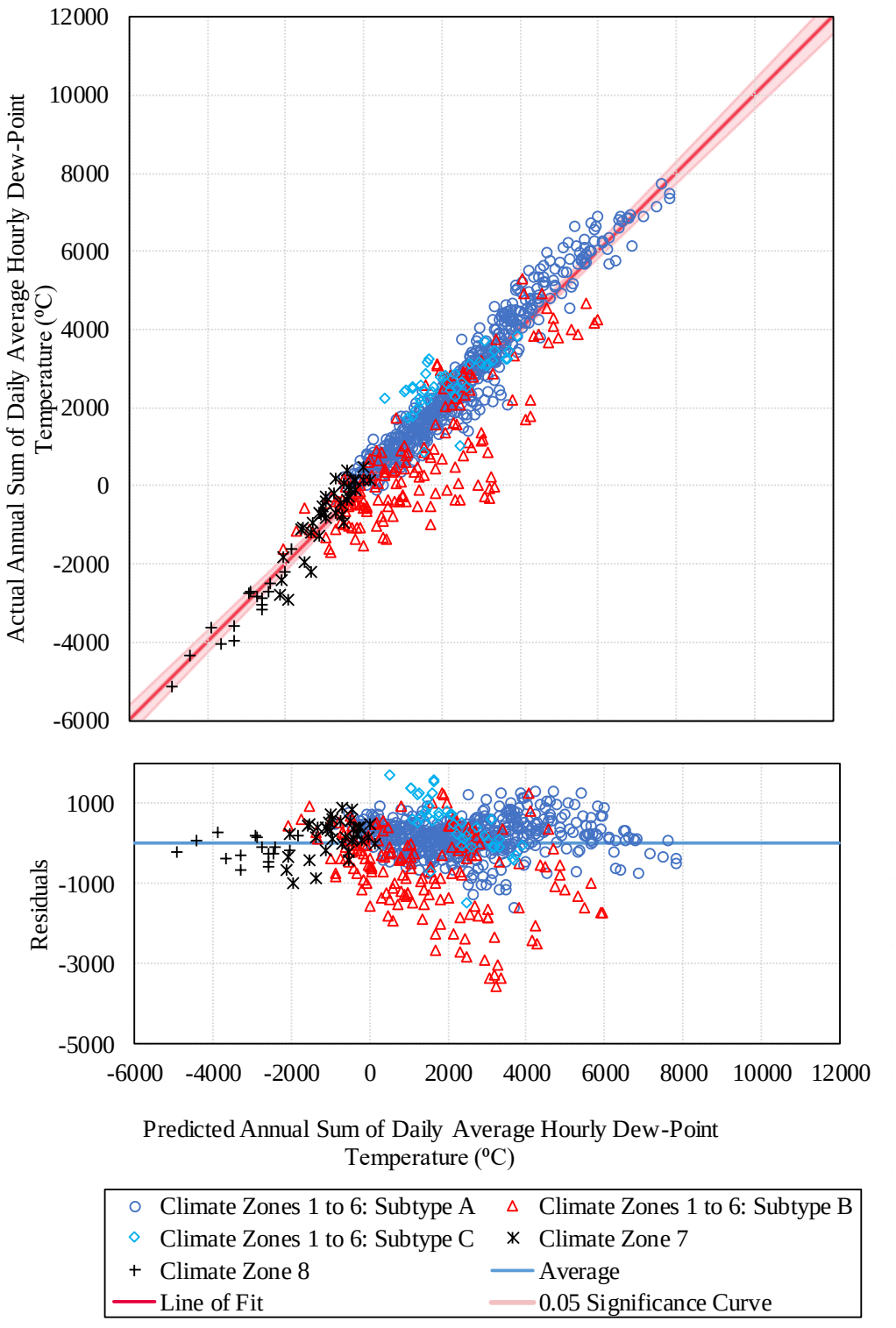

Figure 108: Prediction of the Annual Sum of the Daily Average Hourly Dew-Point Temperature Using Split-Degree Days with Interaction Terms

5.1.2.4. The Association of the Wind and the Degree Days and Split-Degree Days

Wind speed is also a weather-related parameter that can influence building energy consumption. The annual sum of the daily average hourly wind speed ($\overline{WS}_{d,h}^{Ann.Sum}$) was used to represent the wind speed characteristics in each location. However, compared to other influential weather-related parameters, there was not a significant difference in $\overline{WS}_{d,h}^{Ann.Sum}$ of different subtypes and the $\overline{WS}_{d,h}^{Ann.Sum}$ was not expected to be an appropriate covariate. Consequently, this section does not discuss the regression models for predicting $\overline{WS}_{d,h}^{Ann.Sum}$.

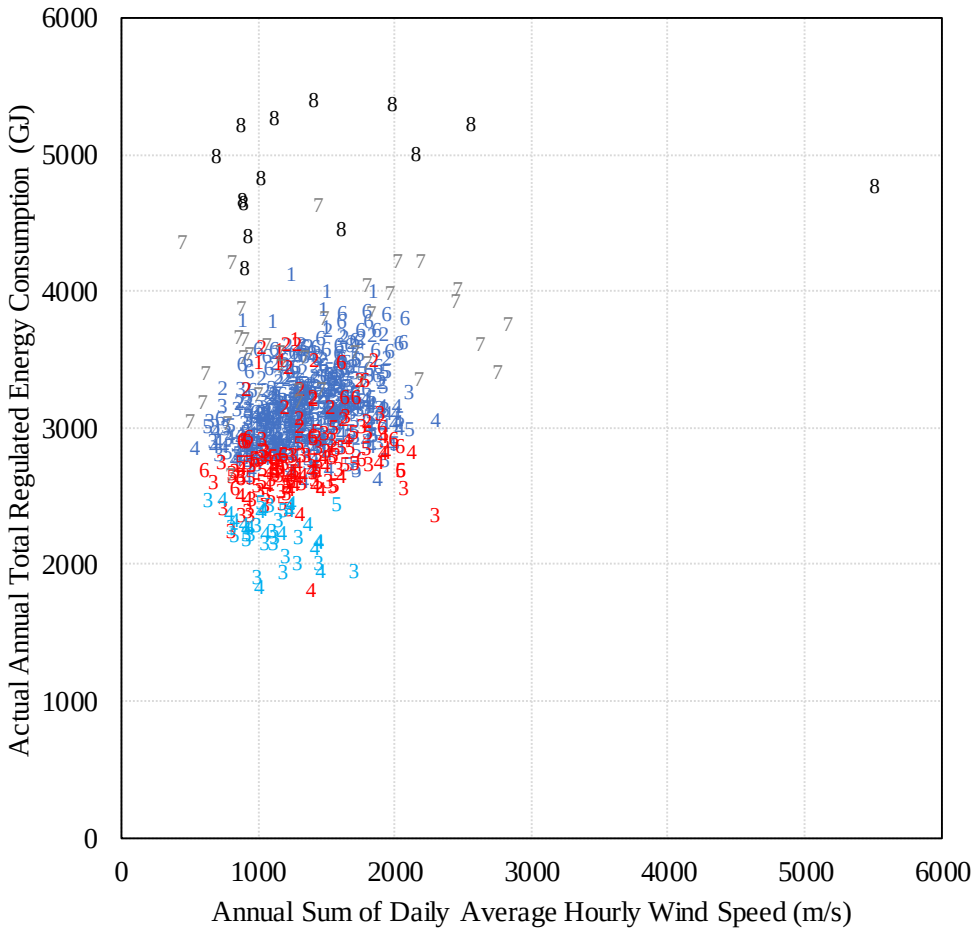

Figure 109: Various Dew-Point Temperature in Different Subtypes for Similar Regulated Energy Consumptions

5.1.3. Predicting the Regulated Energy Consumption

This section provides the results of the regression models for predicting the total annual regulated energy consumption ($E_{Regulated}^{Annual}$) of the medium office prototype in different locations using the conventional degree days, the conventional degree days plus the influential weather-related parameters, and the split-degree days. In the case of the conventional degree days, the predictors were CDD and HDD. In the case of the conventional degree days plus the influential weather-related parameters, the regressions used the conventional degree days and other influential parameters, CDD, HDD, $\overline{GHR}_{d,h}^{Ann.Sum}$, $\overline{DP}_{d,h}^{AnnSum}$, $\overline{WS}_{d,h}^{Ann.Sum}$, $\overline{DTR}_{d,h}^{Ann.Sum}$, and $\overline{DBT}_{d,max}^{Ann.Sum}$. The split-degree days results included the regression models using sHDD and sCDD without and with the interaction terms, where the interaction terms are the interaction terms of the $sHDD_{P1}$ and $sHDD_{P2}$, and the interaction terms of the $sCDD_{P1}$ and $sCDD_{P2}$.

Figure 110 illustrates the results of the predicted versus actual $E_{Regulated}^{Annual}$ using the conventional degree days. Figure 111 shows the results for the predictions using the conventional degree days and other influential parameters. Figure 112 and Figure 113 show the results using split-degree days without the interaction terms and with the interaction terms, respectively. The results show that the predictions by split-degree days are less dispersed and have the highest R^2 and adjusted R^2 and the lowest RMSE. There is an overestimation in the prediction of the energy consumption of the subtype B by the model with the conventional degree days variables (Figure 110). Also, there is an underestimation for the energy use of the climate zone 8. The regression model is shown in equation 5.14. The R^2 and the adjusted R^2 of the model are 0.913, and the RMSE is 143.248.

$$\mathrm{E}_{\mathrm{Regulated}}^{\mathrm{Annual}}\,(CDD,\,HDD) \qquad 5.14$$

$$= -\,144.4533\;+\;0.7397604\cdot CDD + 0.5955554\cdot HDD$$

The regression model with the conventional degree days and other influential weather parameters is shown in equation 5.15. The R^2 of the model is 0.958, the adjusted R^2 is 0.951, and the RMSE is 99.709. Although the overestimation of the energy use in subtype B is resolved in the model with the conventional degree days and other influential weather parameters, the underestimation of the energy use of climate zone 8 still exists (Figure 111). Also, the model has a large number of parameters that require further preparation compared to the degree days and split-degree days.

$$\mathrm{E}_{\mathrm{Regulated}}^{\mathrm{Annual}}\,(CDD,\,HDD,\,GHR,\,DP,\,WS,\,DTR,\,DBT_{max}) \qquad 5.15$$

$$= 3162.0099\;+\;1.0387216\cdot CDD\;+\;0.1220186\cdot HDD$$

$$-\;8.563456\cdot GHR\;+\;0.0232175\cdot DP\;+\;0.1039635\cdot WS$$

$$+\;0.2322308\cdot DTR\;-\;0.491139\cdot DBT_{max}$$

The regression model with the split-degree days parameters without interaction terms (Figure 112) is shown in equation 5.16. The R^2 and the adjusted R^2 of the model are 0.952, and the RMSE is 106.295. The model has slightly lower, but a comparable result in terms of accuracy to the model with the conventional degree days and other influential weather parameters.

$$\mathrm{E}_{\mathrm{Regulated}}^{\mathrm{Annual}}\left(sCDD_{P1},\ sCDD_{P2}, sHDD_{P1},\ sHDD_{P2}\right) \quad 5.16$$

$$= 451.16497 + 0.5114318 \cdot sCDD_{P1} + 0.1100748 \cdot sCDD_{P2}$$

$$+ 0.0431021 \cdot sHDD_{P1} + 0.5438452 \cdot sHDD_{P2}$$

The regression model with the split-degree days parameters with interaction terms (Figure 113) is shown in equation 5.17. The R^2 of the model is 0.965, the adjusted R^2 is 0.964, and the RMSE is 91.773. The model results in the highest accuracy. The issue of the overestimation of climate zone 8, which was seen in other models, is resolved in this model.

$$\mathrm{E}_{\mathrm{Regulated}}^{\mathrm{Annual}}\left(sCDD_{P1},\ sCDD_{P2}, sHDD_{P1},\ sHDD_{P2}\right) \quad 5.17$$

$$= 514.33402 + 0.6379942 \cdot sCDD_{P1} + 0.0995313 \cdot sCDD_{P2}$$

$$- 0.00002146 \cdot sCDD_{P1} \cdot sCDD_{P2} + 0.0700323 \cdot sHDD_{P1}$$

$$+ 0.382724 \cdot sHDD_{P2} + 0.000017385 \cdot sHDD_{P1} \cdot sHDD_{P2}$$

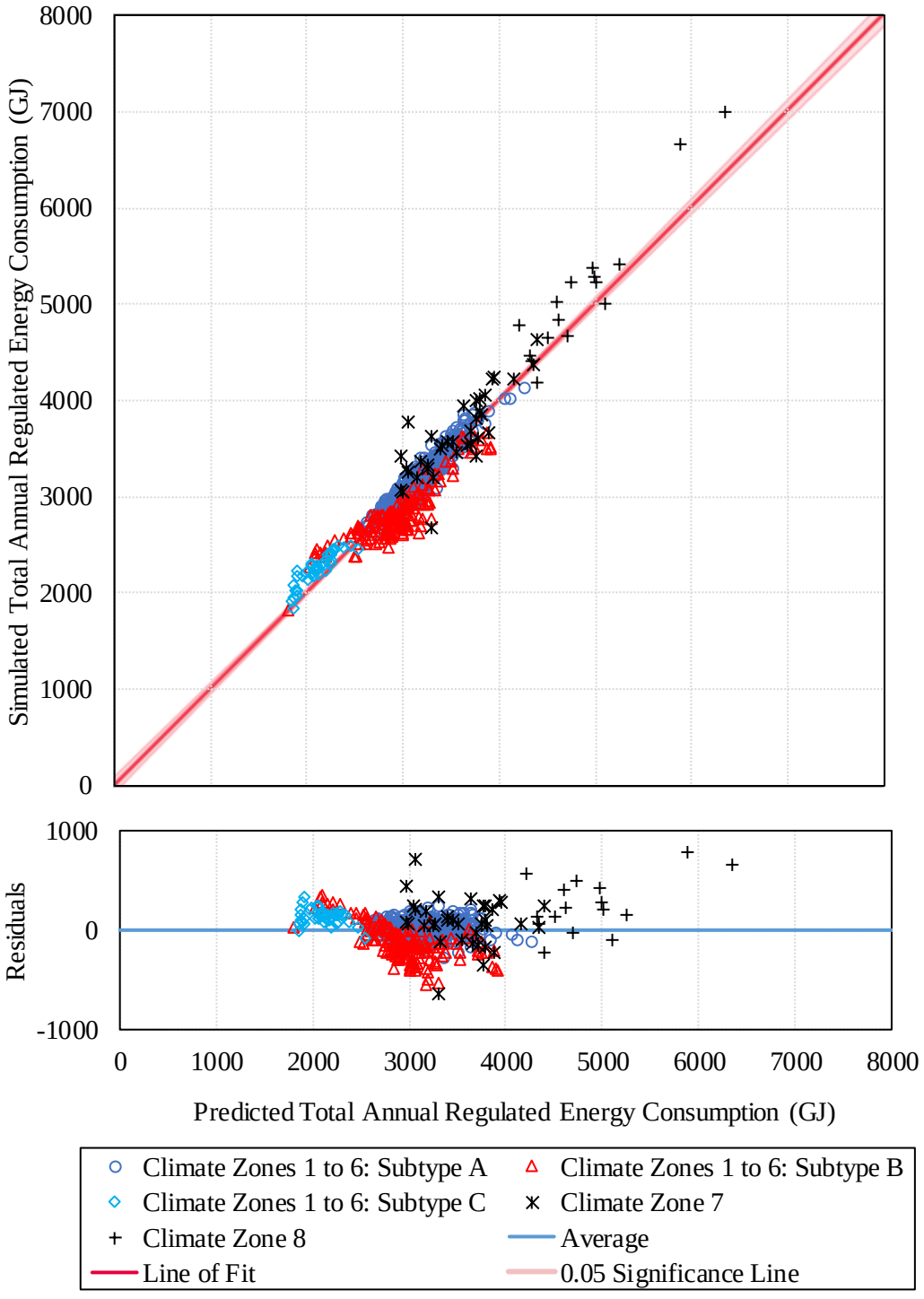

Figure 110: Predicting the Total Regulated Energy Consumption Using the Conventional Degree Days

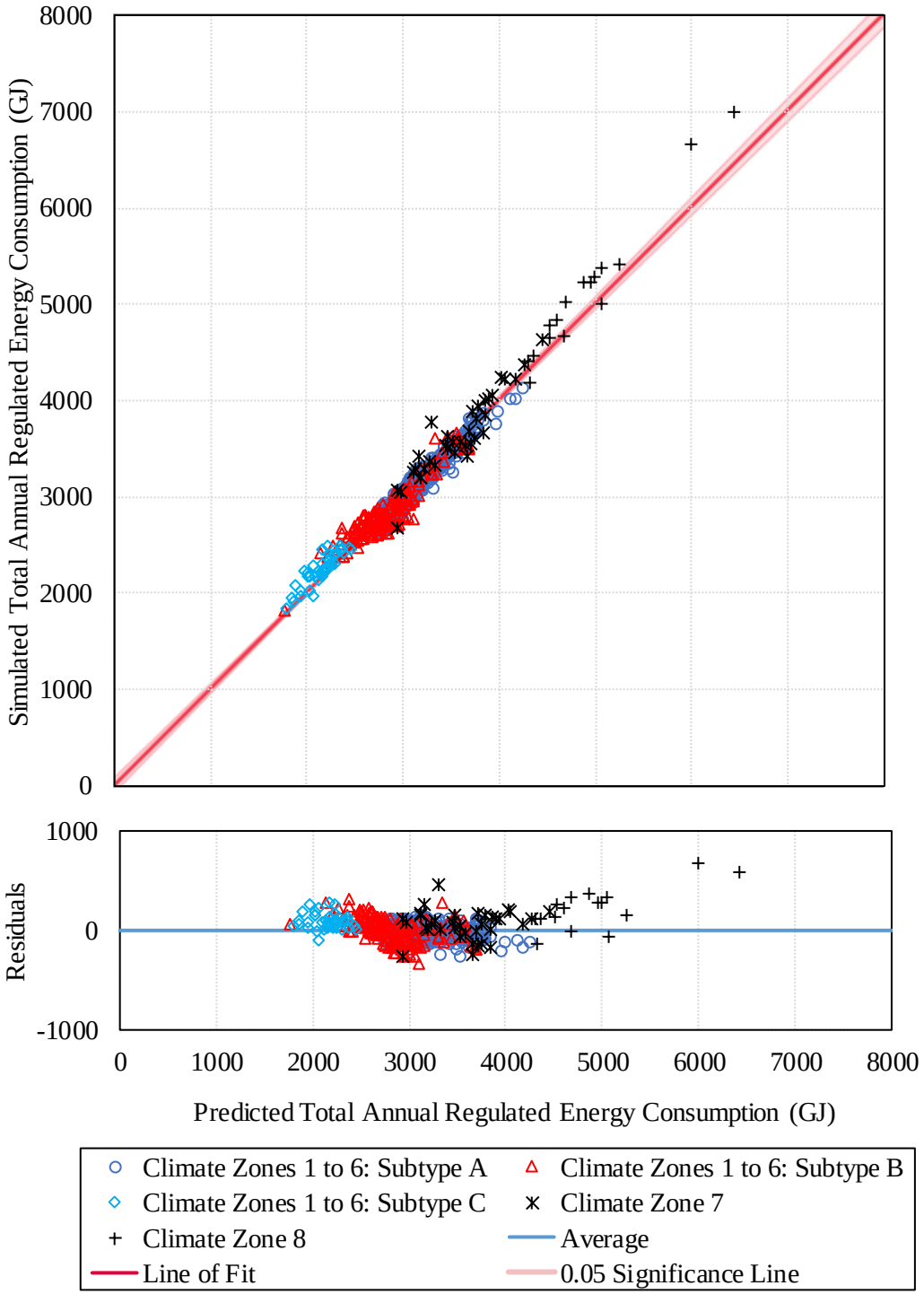

Figure 111: Predicting the Total Regulated Energy Consumption Using the Conventional Degree Days, GHR, DP, WS, DTR, and DBT_{max}

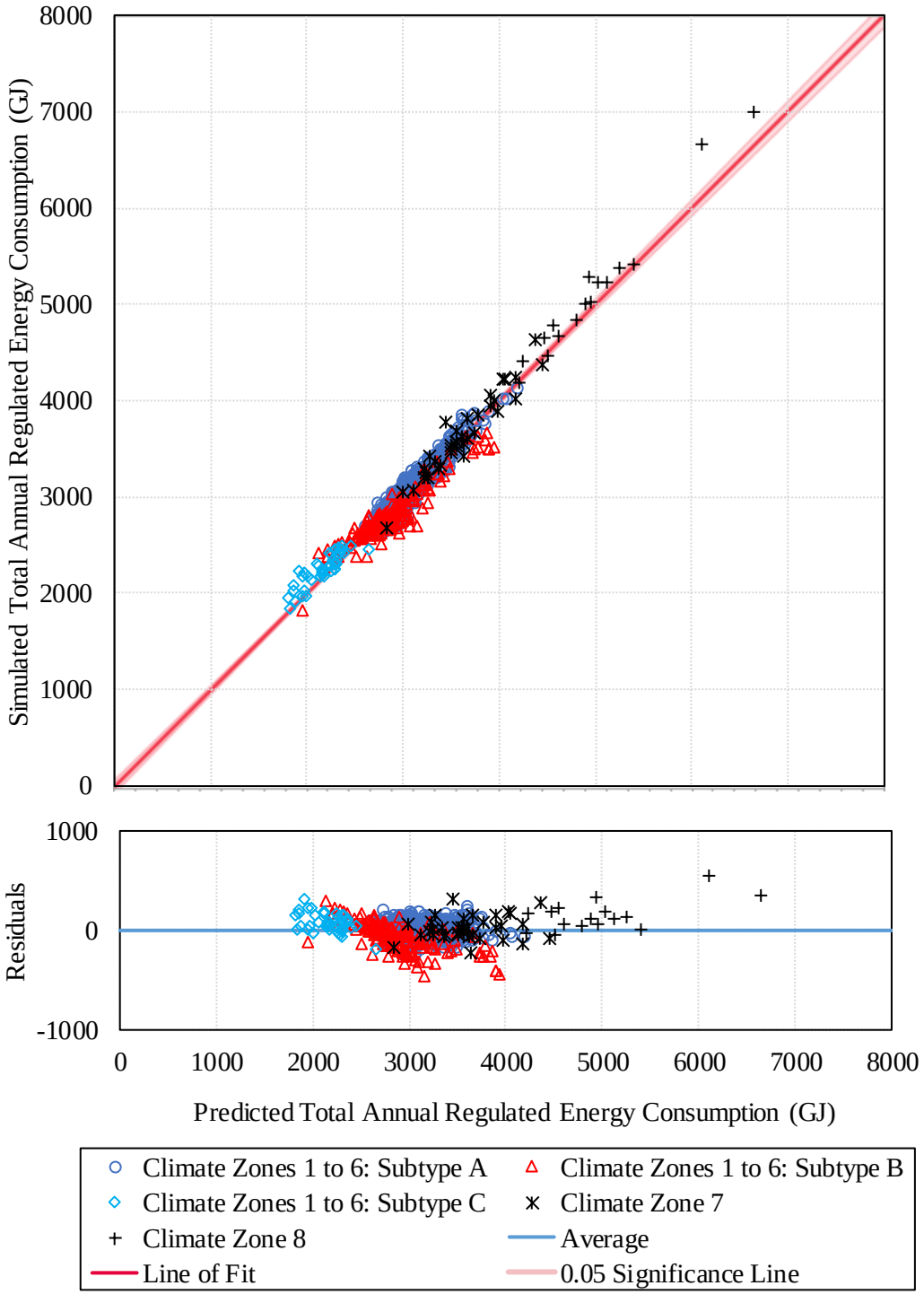

Figure 112: Predicting the Total Regulated Energy Consumption Using the Split-Degree Days without the Interaction Terms

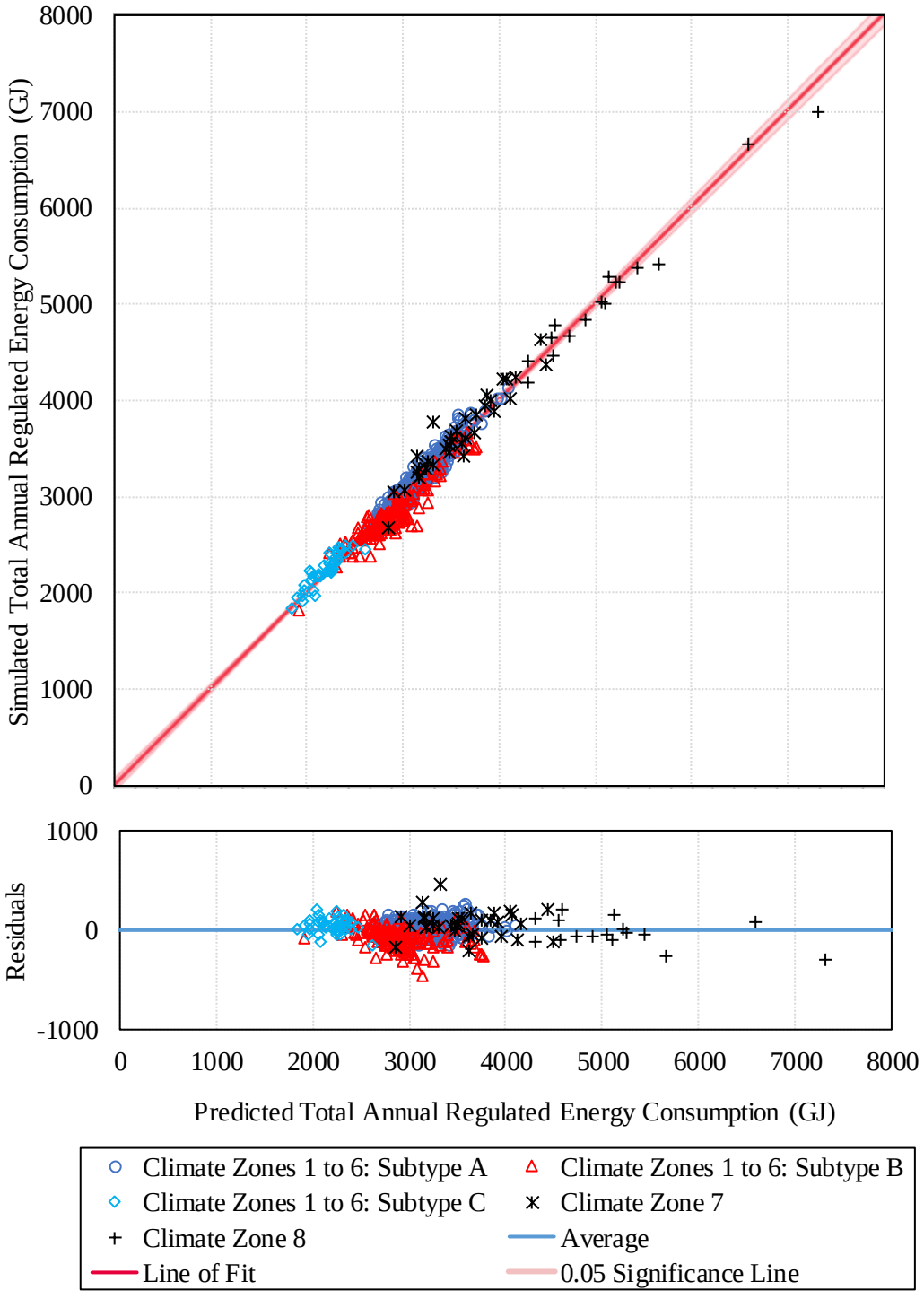

Figure 113: Predicting the Total Regulated Energy Consumption Using the Split-Degree Days with the Interaction Terms

5.1.4. Predicting the Heating Energy Consumption

This section includes the estimation of the annual heating energy consumption, $E_{Heating}^{Annual}$, using the Heating Degree Days (HDD) and split-Heating Degree Days (sHDD). Figure 114 shows the predicted heating energy consumption using the regression model derived from the HDD. The regression model is shown in equation 5.18. The R^2 and the adjusted R^2 of the model are 0.898 and the RMSE is 210.614.

$$E_{Heating}^{Annual}(HDD) = -396.3349 + 0.3922467 \cdot HDD \quad 5.18$$

The residual pattern in Figure 114 indicates a potential better correlation of the $E_{Heating}^{Annual}$ with higher degrees of HDD. Therefore, a polynomial regression model with the degree of two with the HDD as the indicator was also developed to allow for the comparison of the models with higher accuracy using the HDD when compared to the models using sHDD. Figure 115 shows the results of the predicted values $E_{Heating}^{Annual}$ by the degree two polynomial model. The regression model is shown in equation 5.19. The R^2 and the adjusted R^2 of the model are 0.957 and the RMSE is 135.901.

$$E_{Heating}^{Annual}(HDD) = -64.74019 + 0.1390695 \cdot HDD + 0.000036447 \cdot HDD^2 \quad 5.19$$

It can be seen that the relation of the heating energy consumption to the outdoor temperature is not linear when using the HDD as the independent variable. Previous research has shown U-shape relation between the energy consumption, mostly electricity, and the temperature

(e.g. Henley and Peirson, 1997; Moral-Carcedo and Vicéns-Otero, 2005; Bessec and Fouquau, 2008; and Lee and Chiu, 2011). There are several factors that make the energy consumption grow faster once the temperature deviates more from the comfort temperature. These parameters include: varying heat transfer coefficients (radiation and/or convection) that can result in more pronounced heat transfer through the building envelope, which can also result in radiant asymmetry and requiring further conditioning in order to reach comfort level; and for different systems, the varying efficiencies in different temperatures. However, the U-shape versus the V-shape energy consumption pattern is typically discussed for the electricity consumption. In this case, there seems to be a deficiency in HDD to accurately capture the extreme conditions. Hence, in this study, the residual pattern in the plot of the model with degree one of HDD was tried to be resolved only using statistical approach without considering the physical interpretation to allow for the comparison of the HDD model with higher accuracy versus the models using sHDDs. Therefore, a polynomial model was developed to statistically address the residual pattern in the model with degree one HDD. Results show that the polynomial model better fits the actual $E_{Heating}^{Annual}$ as the R^2 is increased from 0.898 to 0.957. However, in both cases, the $E_{Heating}^{Annual}$ in dry locations are overestimated by the model. However, actual $E_{Heating}^{Annual}$, is affected by various parameters, namely the solar radiation, which reduces the $E_{Heating}^{Annual}$ more in dry locations compared to the moist and marine areas. The low predictability of the solar radiation by the conventional HDD mainly leads to the discrepancy in the estimation of the $E_{Heating}^{Annual}$ in various moisture regimes.

The estimated $E_{Heating}^{Annual}$ using the sHDD for the model without including the interaction term is presented in Figure 116. The regression model is shown in equation 5.20. The R^2 and the adjusted R^2 of the model are 0.964 and the RMSE is 125.264.

$$E_{Heating}^{Annual}(sHDD_{P1},\ sHDD_{P2}) = -40.55628 - 0.197441 \cdot sHDD_{P1} + 0.6506595 \cdot sHDD_{P2} \quad (5.20)$$

The estimated $E_{Heating}^{Annual}$ using the sHDD for the model with the interaction term is presented in Figure 117. The regression model is shown in equation 5.21. The R^2 and the adjusted R^2 of the model are 0.981 and the RMSE is 90.345.

$$E_{Heating}^{Annual}(sHDD_{P1},\ sHDD_{P2}) = 19.615939 - 0.093186 \cdot sHDD_{P1} + 0.3782819 \cdot sHDD_{P2} + 0.0000236 \cdot sHDD_{P1} \cdot sHDD_{P2} \quad (5.21)$$

The R^2 in both models using sHDD, either with or without the interaction terms, are higher than the ones using the conventional HDD.

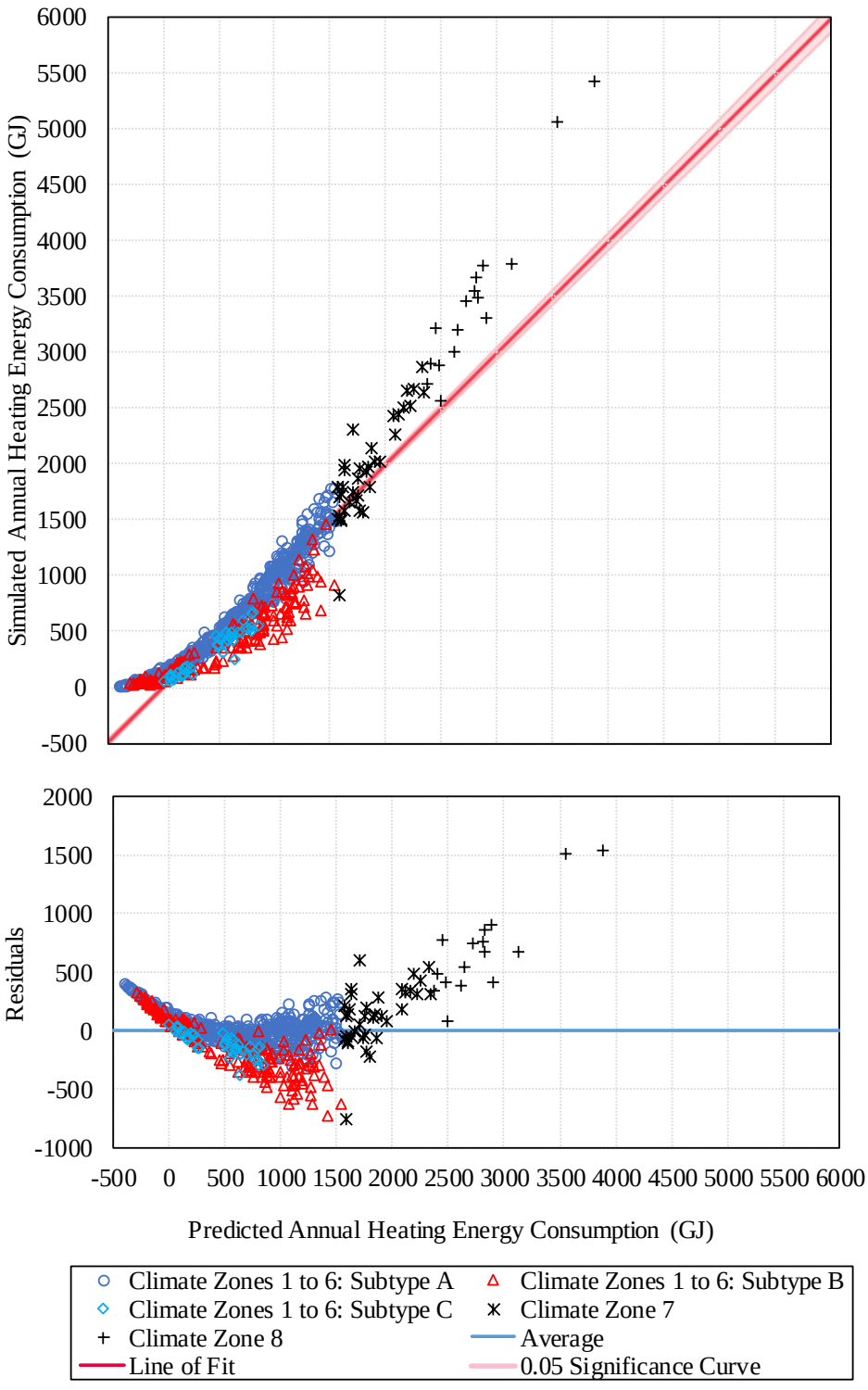

Figure 114: Predicting the Heating Energy Consumption Using the Conventional HDD

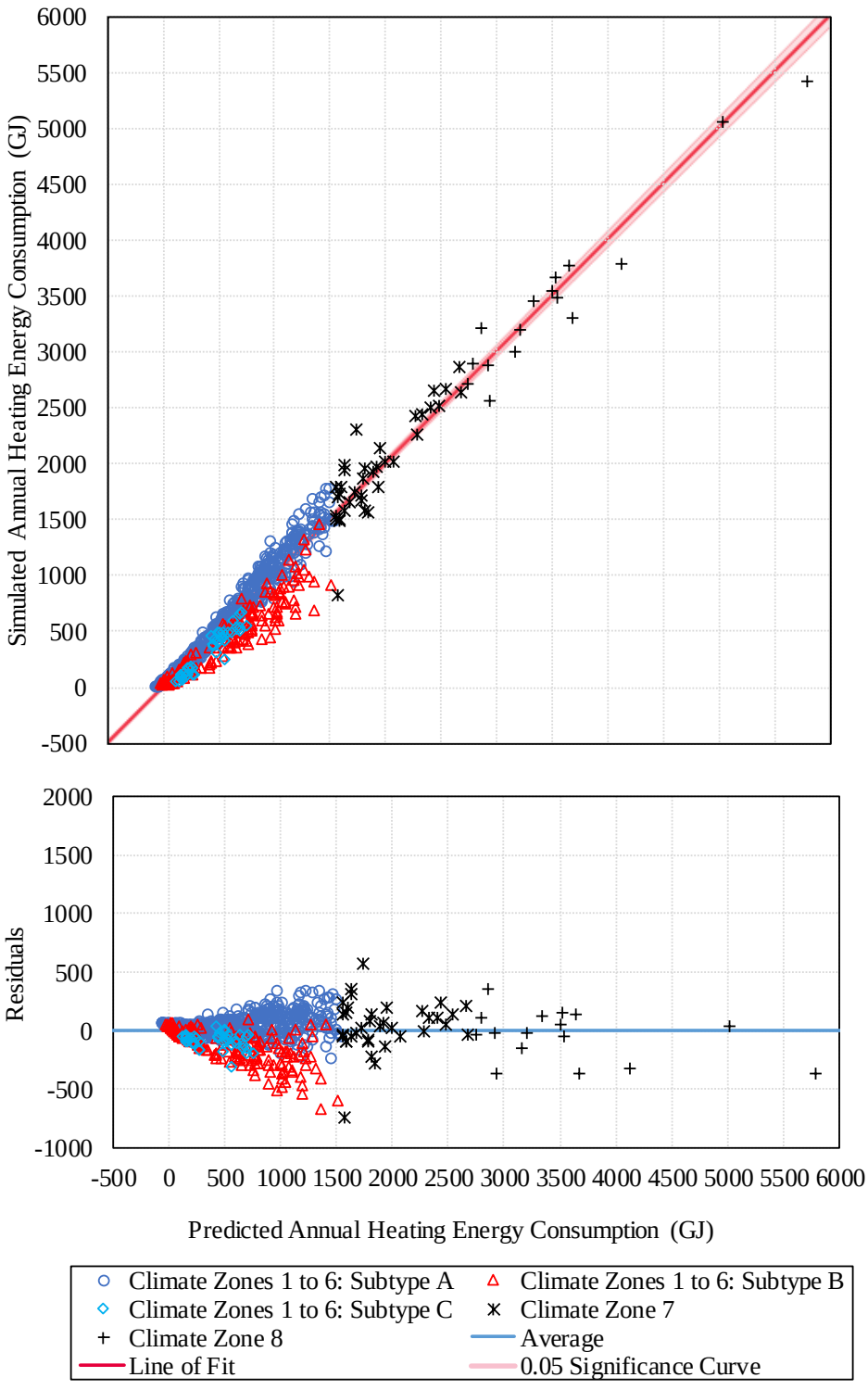

Figure 115: Predicting the Heating Energy Consumption Using the Conventional HDD with Degree Two Polynomial

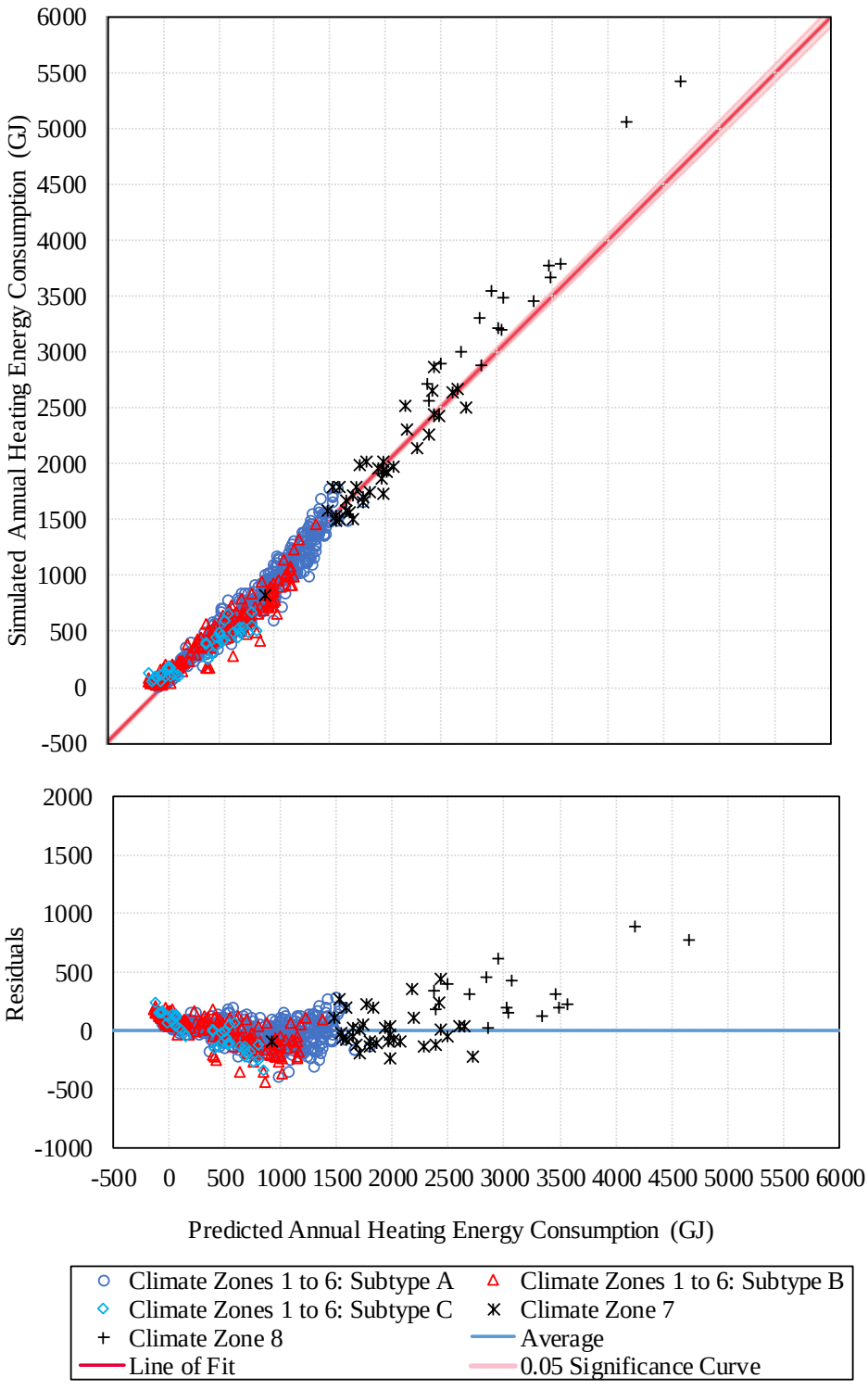

Figure 116: Predicting the Heating Energy Consumption Using the Split-HDD without the Interaction Terms

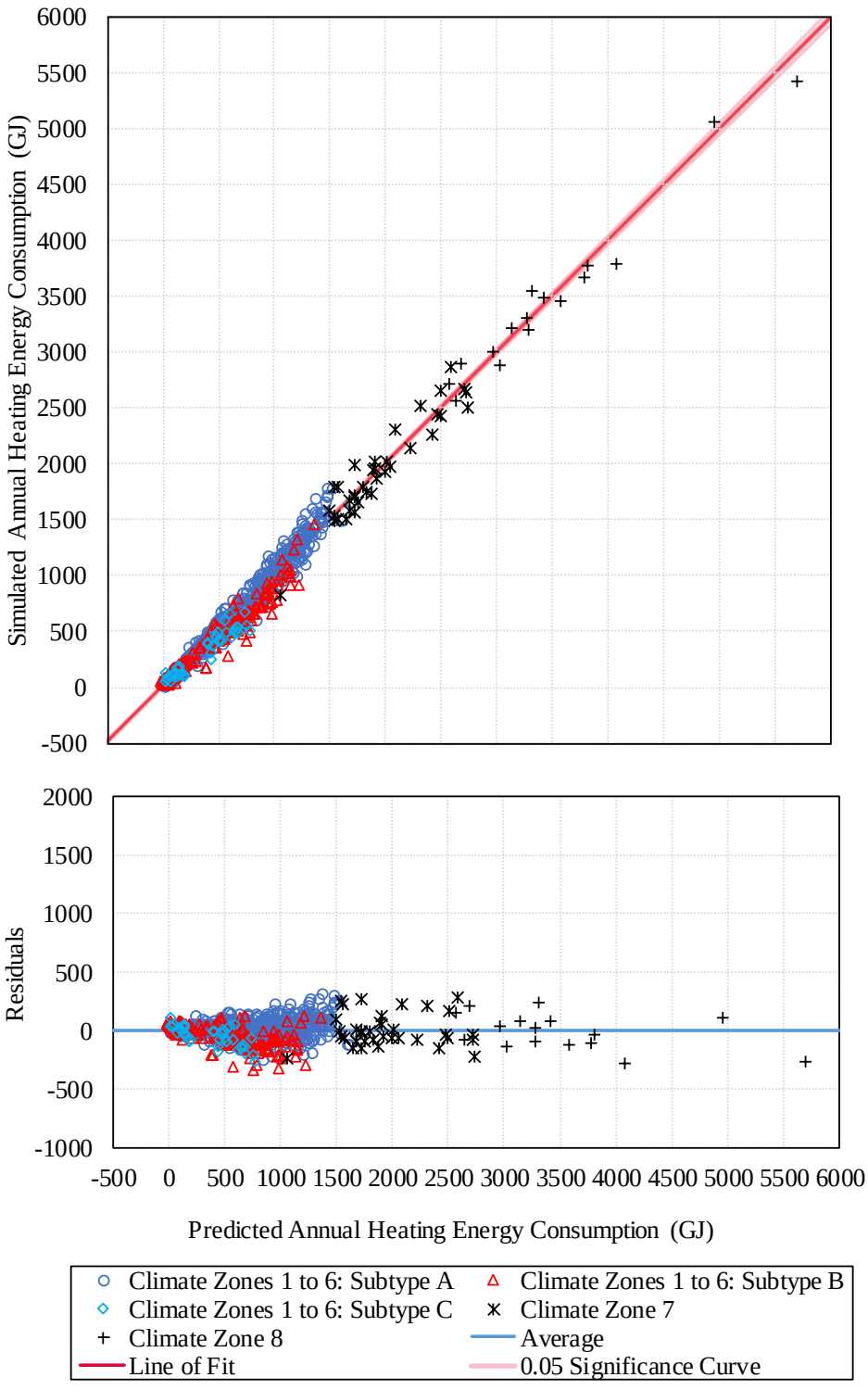

Figure 117: Predicting the Heating Energy Consumption Using the Split-HDD with the Interaction Terms

5.1.5. Predicting the Cooling Energy Consumption

This section presents the accuracy of the predictability of the annual cooling energy consumption ($E_{Coolting}^{Annual}$) using the conventional Cooling Degree Days (CDD) and split-Cooling Degree Days (sCDD). It includes the predicted $E_{Coolting}^{Annual}$ using the conventional CDD and sCDD with and without interaction terms.

The predicted $E_{Coolting}^{Annual}$ using the conventional CDD is shown in Figure 118. The regression model is shown in equation 5.22. The R^2 and the adjusted R^2 of the model are 0.979 and the RMSE is 70.052.

$$E_{Cooling}^{Annual}(CDD) = -12.10281 + 0.4257311 \cdot CDD \quad (5.22)$$

The predicted cooling energy consumption using the sCDD are shown in Figure 119 for the model without the interaction term, and in Figure 120 for the model with the interaction term. The regression model without the interaction term is shown in equation 5.23. The R^2 and the adjusted R^2 of the model are 0.981 and the RMSE is 67.807.

$$E_{Cooling}^{Annual}(sCDD_{P1}, sCDD_{P2}) = 18.074123 + 0.4640176 \cdot sCDD_{P1} - 0.026039 \cdot sCDD_{P2} \quad (5.23)$$

The regression model using the sCDD with the interaction term is shown in equation 5.24. The R^2 and the adjusted R^2 of the model are 0.982 and the RMSE is 66.058.

$$\mathrm{E}_{\mathrm{Cooling}}^{\mathrm{Annual}}(sCDD_{P1}, sCDD_{P2}) \quad 5.24$$

$$= 18.074123 + 0.4640176 \cdot sCDD_{P1} - 0.026039 \cdot sCDD_{P2}$$

Although the predicted $\mathrm{E}_{\mathrm{Coolting}}^{\mathrm{Annual}}$ using sCDD shows slightly better predictions, the improvement is not as pronounced as the accuracy of the prediction is high even in the models developed by the conventional CDD. Humidity is shown to have the highest impact in the analysis conducted in section 4.3.3. Therefore, better estimation of the $\overline{\mathrm{DP}}_{\mathrm{d,h}}^{\mathrm{AnnSum}}$ using the sDD compared to the conventional CDD, which was discussed in section 5.1.2.3, plays an important role in improving the accuracy of the estimations of $\mathrm{E}_{\mathrm{Coolting}}^{\mathrm{Annual}}$.

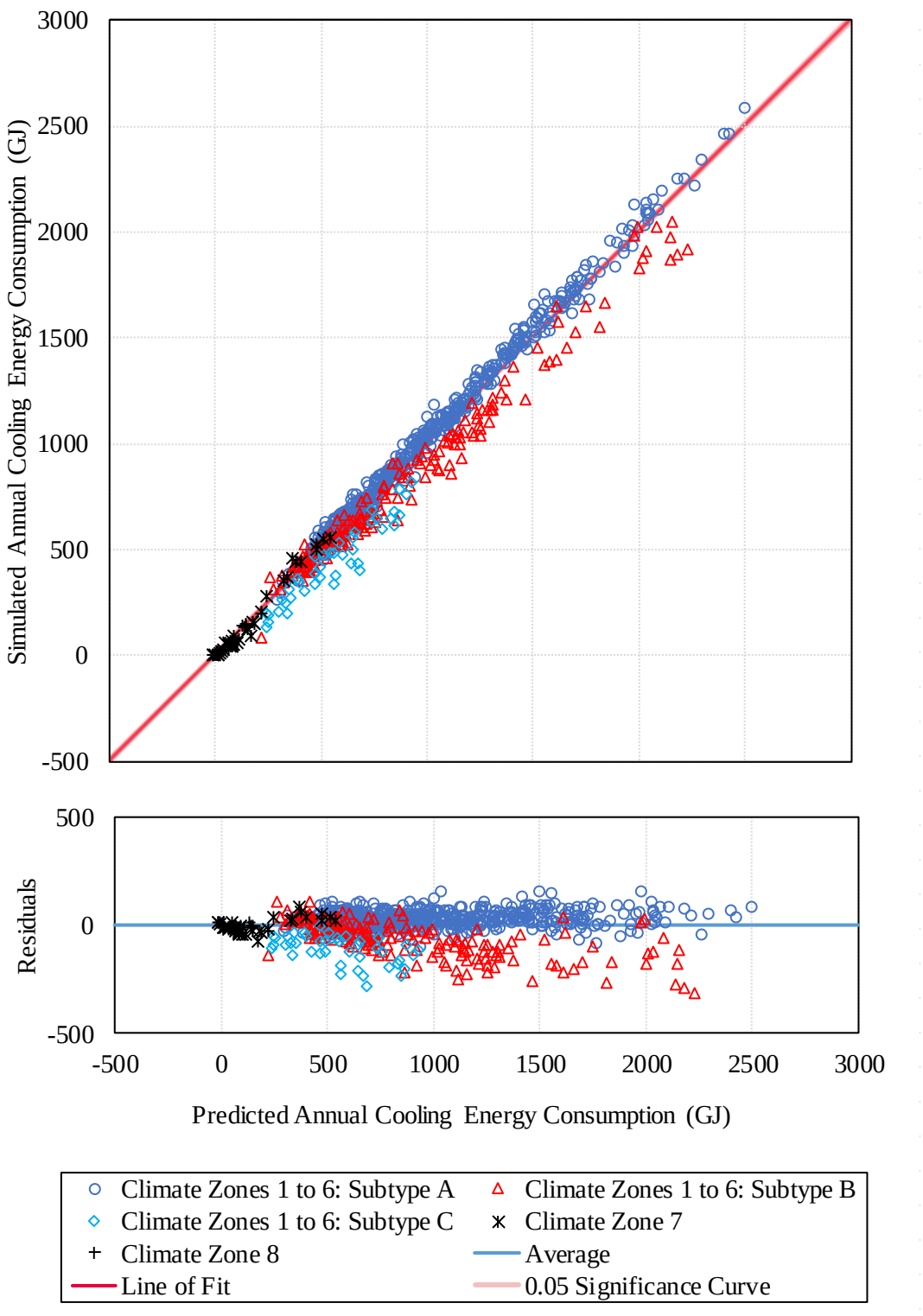

Figure 118: Predicting the Cooling Energy Consumption Using the Conventional CDD

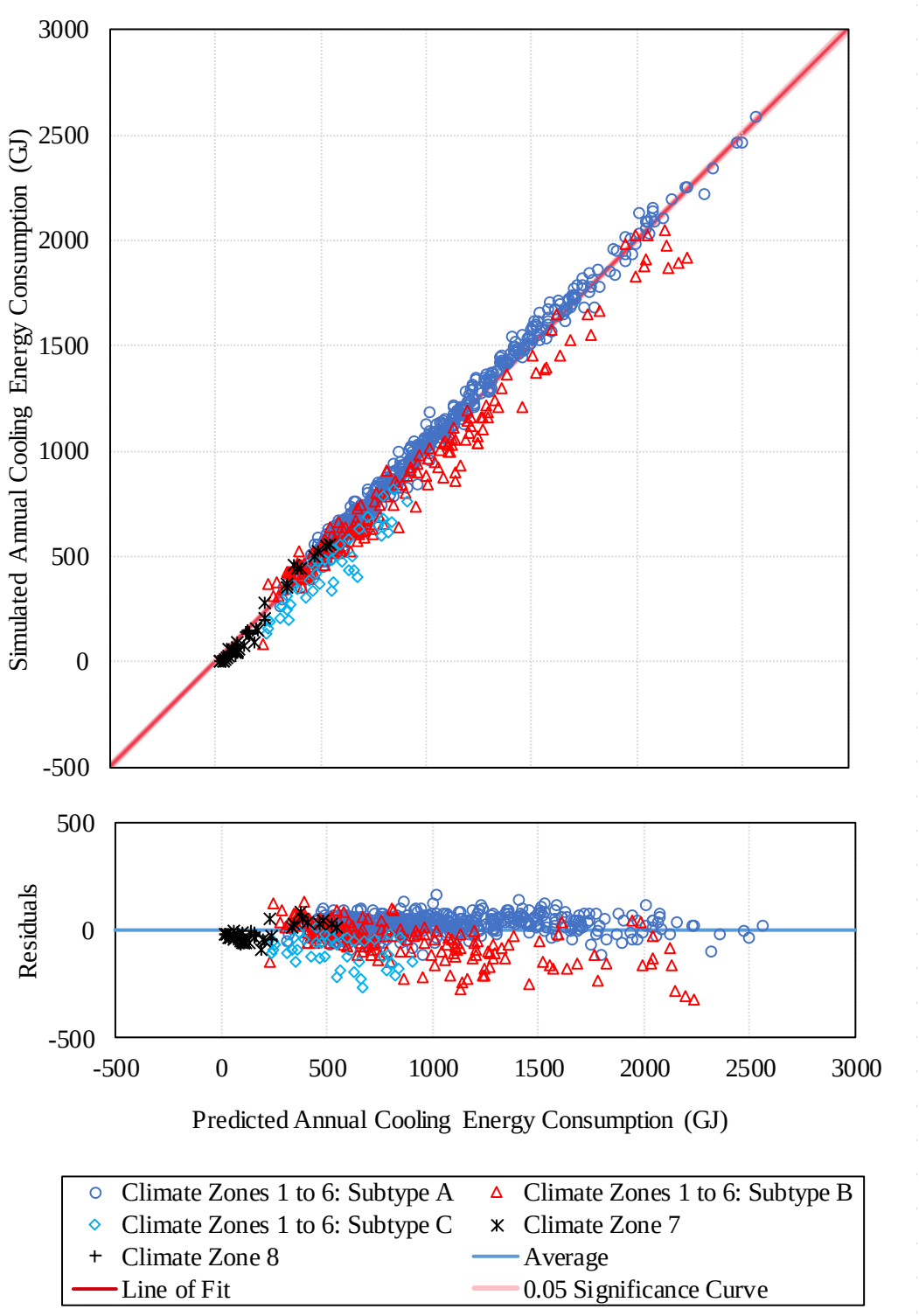

Figure 119: Predicting the Cooling Energy Consumption Using the Split-CDD without the Interaction Terms

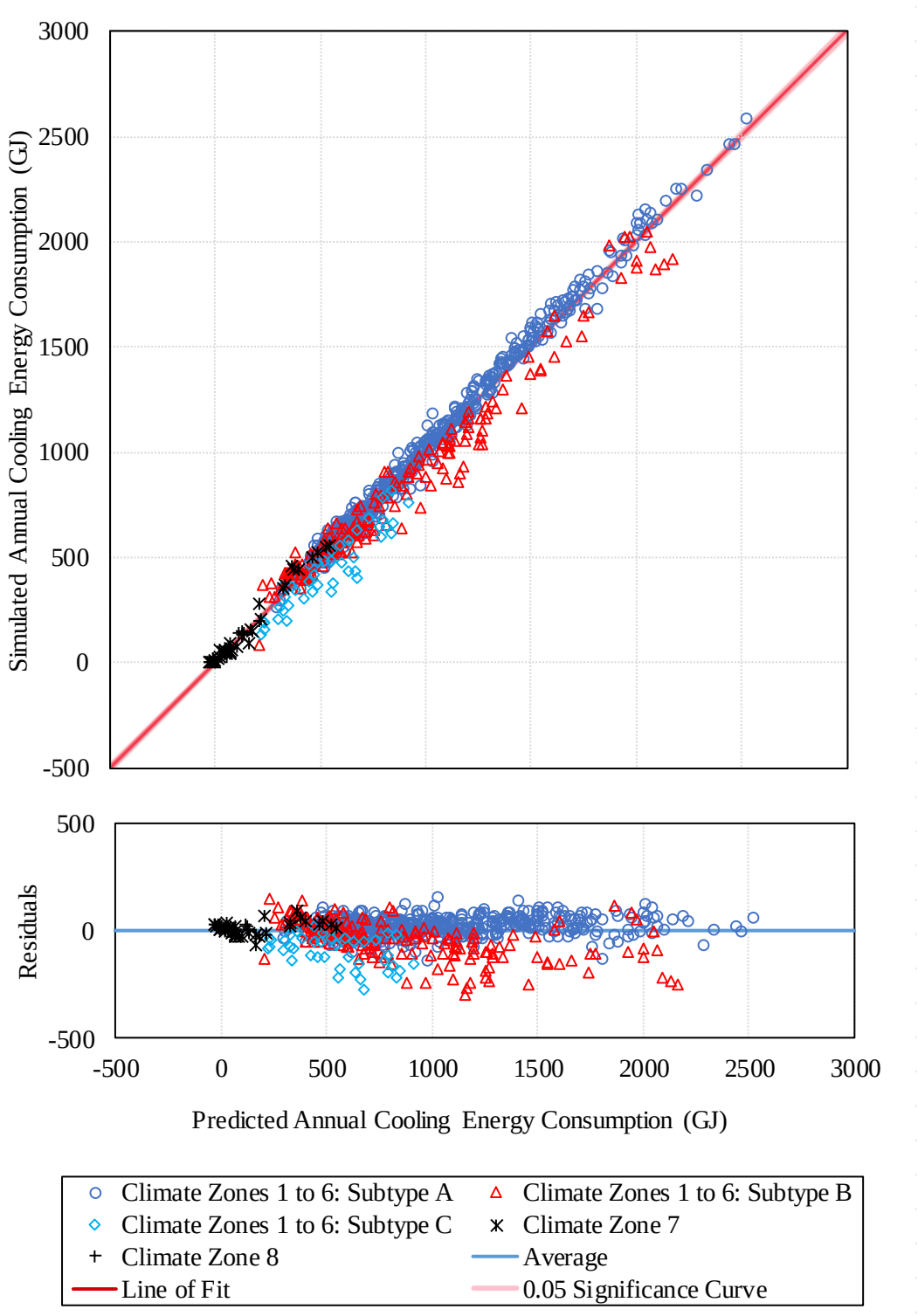

Figure 120: Predicting the Cooling Energy Consumption Using the Split-CDD with the Interaction Terms

5.1.6. Predicting the Fan Energy Consumption

This section includes the results for the prediction of the annual fan energy consumption (E_{Fan}^{Annual}) using the regression models developed by the conventional degree days and split-degree days. The regression model using the conventional degree days is shown in Figure 121 and equation 5.25. The R^2 of the model is 0.383, the adjusted R^2 is 0.381 and the RMSE is 24.812.

$$E_{Fan}^{Annual}(CDD, HDD) = 212.93043 + 0.0206718 \cdot CDD + 0.0028814 \cdot HDD \quad 5.25$$

The predicted fan energy consumption using the sCDD are shown in Figure 122 for the model without the interaction term, and in Figure 123 for the model with the interaction term. The regression model without the interaction term is shown in equation 5.26. The R^2 of the model is 0.708 and the adjusted R^2 of the model is 0.707 and the RMSE is 17.089.

$$E_{Heating}^{Annual}(sCDD_{P1}, sCDD_{P2}, sHDD_{P1}, sHDD_{P2}) \quad 5.26$$
$$= 110.72467 - 0.002521 \cdot sCDD_{P1} + 0.0306831 \cdot sCDD_{P2}$$
$$+ 0.0427832 \cdot sHDD_{P1} - 0.032883 \cdot sHDD_{P2}$$

The regression model without the interaction term is shown in equation 5.27. The R^2 of the model is 0.722 and the adjusted R^2 of the model is 0.720 and the RMSE is 16.693.

$$\mathrm{E}_{\mathrm{Heating}}^{\mathrm{Annual}}(sCDD_{P1}, sCDD_{P2}, sHDD_{P1}, sHDD_{P2}) \tag{5.27}$$

$$= 138.93311 - 0.012781 \cdot sCDD_{P1} + 0.0247612 \cdot sCDD_{P2}$$

$$+ 0.0000021314 \cdot sCDD_{P1} \cdot sCDD_{P2} + 0.0462724 \cdot sHDD_{P1}$$

$$- 0.041314 \cdot sHDD_{P2} + 0.00000023126 \cdot sHDD_{P1} \cdot sHDD_{P2}$$

Results show significant improvements in the prediction of the $\mathrm{E}_{\mathrm{Heating}}^{\mathrm{Annual}}$ using split-degree days compared to degree days. The comparison of the actual $\mathrm{E}_{\mathrm{Heating}}^{\mathrm{Annual}}$ versus the predicted $\mathrm{E}_{\mathrm{Heating}}^{\mathrm{Annual}}$ yields lower R^2 (0.383) compared to the predictions models using the split-degree days, either without the interaction term (0.708) or with the interaction terms (0.722). This is mainly due to the underestimation of $\mathrm{E}_{\mathrm{Heating}}^{\mathrm{Annual}}$ in dry locations and the overestimation of $\mathrm{E}_{\mathrm{Heating}}^{\mathrm{Annual}}$ in very cold climates by the models from the conventional degree days, which is resolved to a considerable extent in the models using split-degree days.

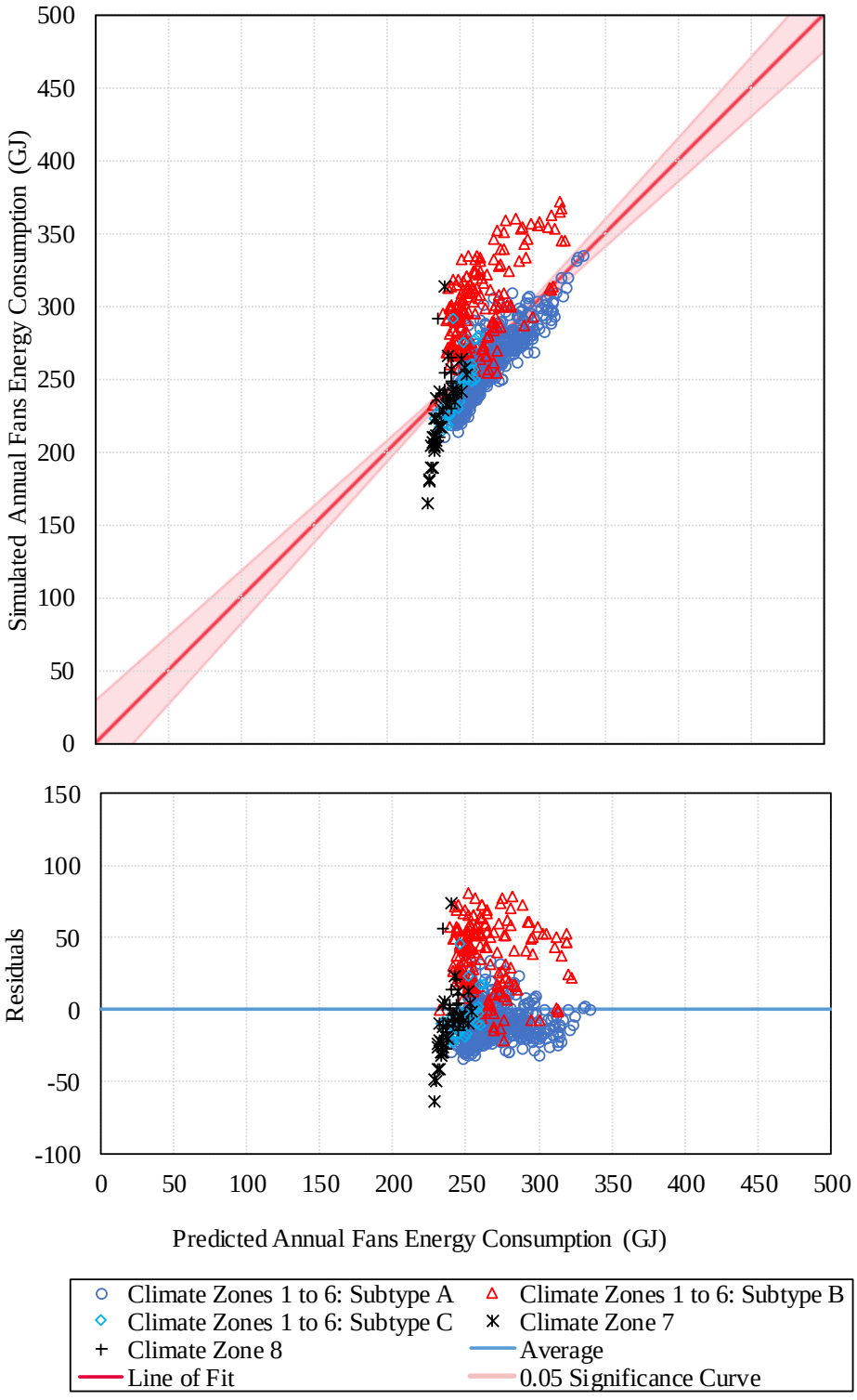

Figure 121: Predicting the Fan Energy Consumption Using the Conventional Degree Days

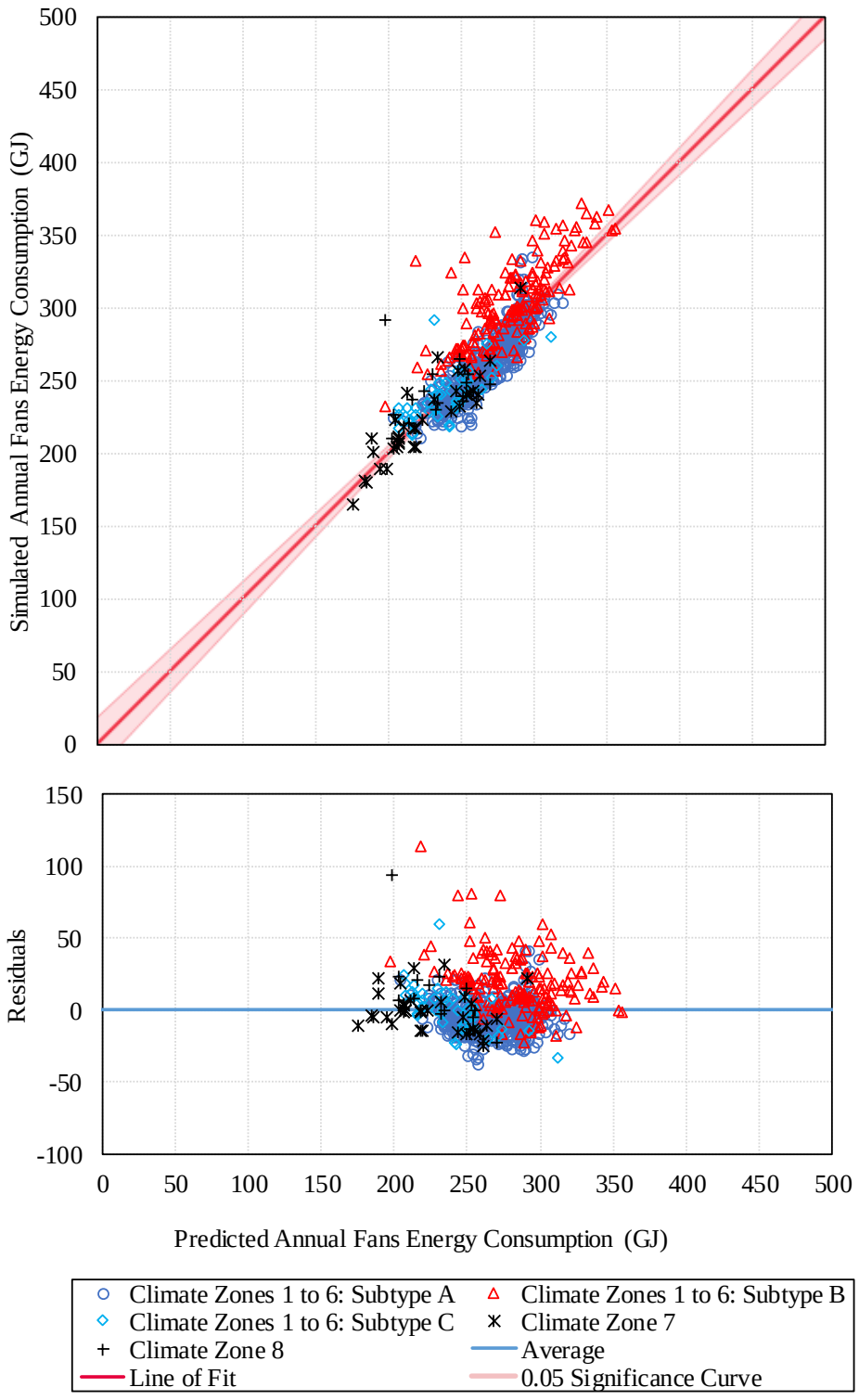

Figure 122: Predicting the Fan Energy Consumption Using the Split-Degree Days without the Interaction Terms

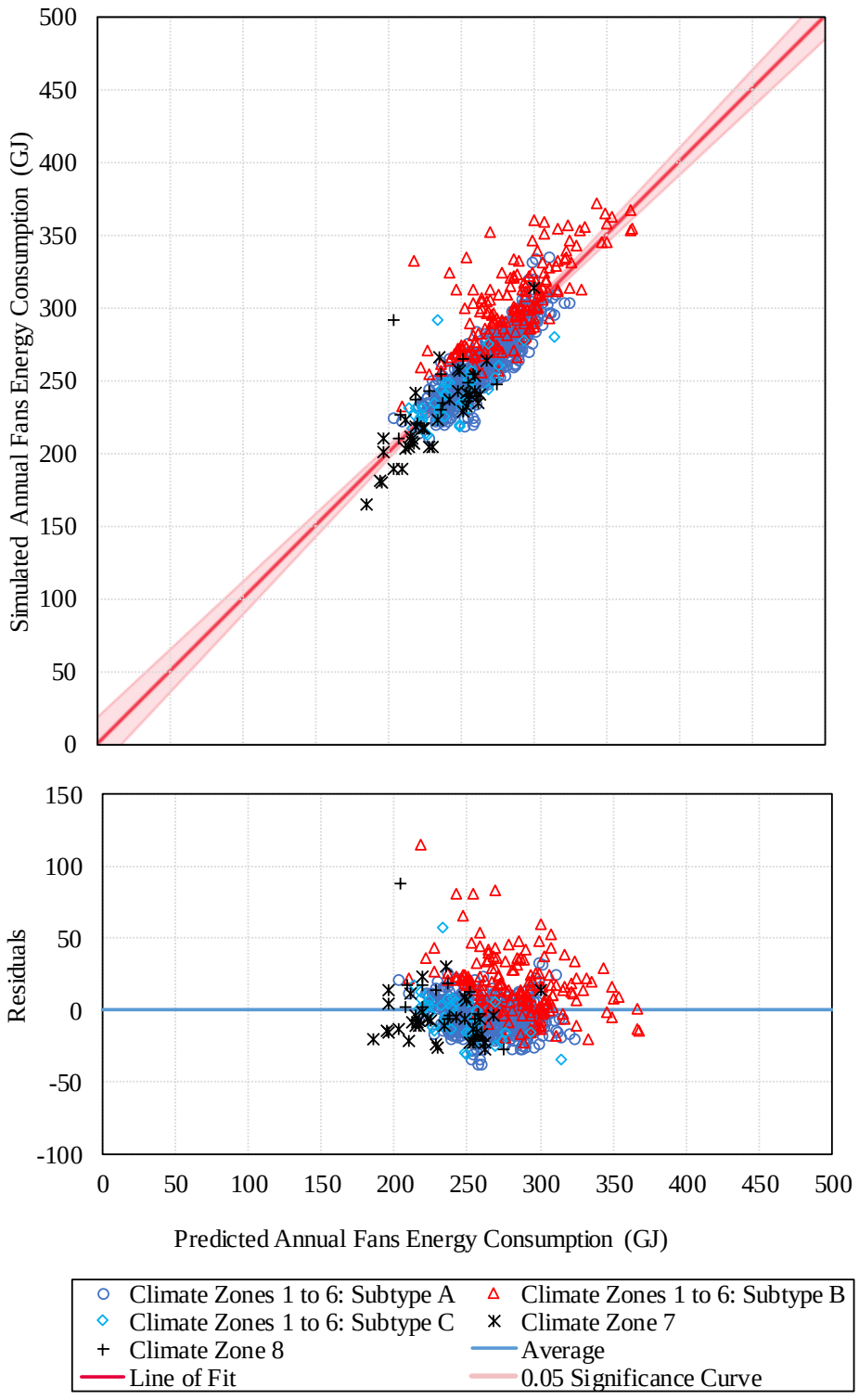

Figure 123: Predicting the Fan Energy Consumption Using the Split-Degree Days with the Interaction Terms

5.1.7. Estimation of the Annual Heating and Cooling Using the Variable-Degree Day and Split-Degree Day methods

In this section the results of predictions of the annual heating and cooling energy consumption in different locations are compared using various base temperatures used in HDD and CDD as well as sHDD and sCDD. Figure 124 illustrates the accuracy of the estimation of the annual heating and cooling energy consumption in different locations using the degree days and split-degree days with different base temperatures (left) and includes a closer representation of the predictions near to the optimal base temperatures (right). The results of the accuracy of the prediction of the annual heating and cooling energy consumption of different locations in Figure 124 are presented with red triangles (heating) and blue circles (cooling), respectively. Each point represents the R^2 of the predicted values using the regression model versus the actual heating or cooling of 801 locations for each base temperature. Hollow markers indicate the predictions using either HDD or CDD and the filled marker shows the predictions using either sHDD or sCDD.

As shown in Figure 124, the accuracy of the prediction of the annual heating and cooling energy consumption vary significantly with changes to the base temperature. In the case of heating, the R^2 increases significantly until it reaches an optimal base temperature. Calculating the HDD and sHDD using the represented lowest base temperatures yields zero for almost all of the 801 locations since there are very few sites with at least one day in which the average daily temperature is lower than those very low base temperatures. Therefore, the independent variables in the model are mostly the same value (zeros). Therefore, the model does not discriminate various heating loads in various locations. The more pronounced difference between the changes in the R^2 for total regulated energy consumption in the two methods is shown in Figure 125.

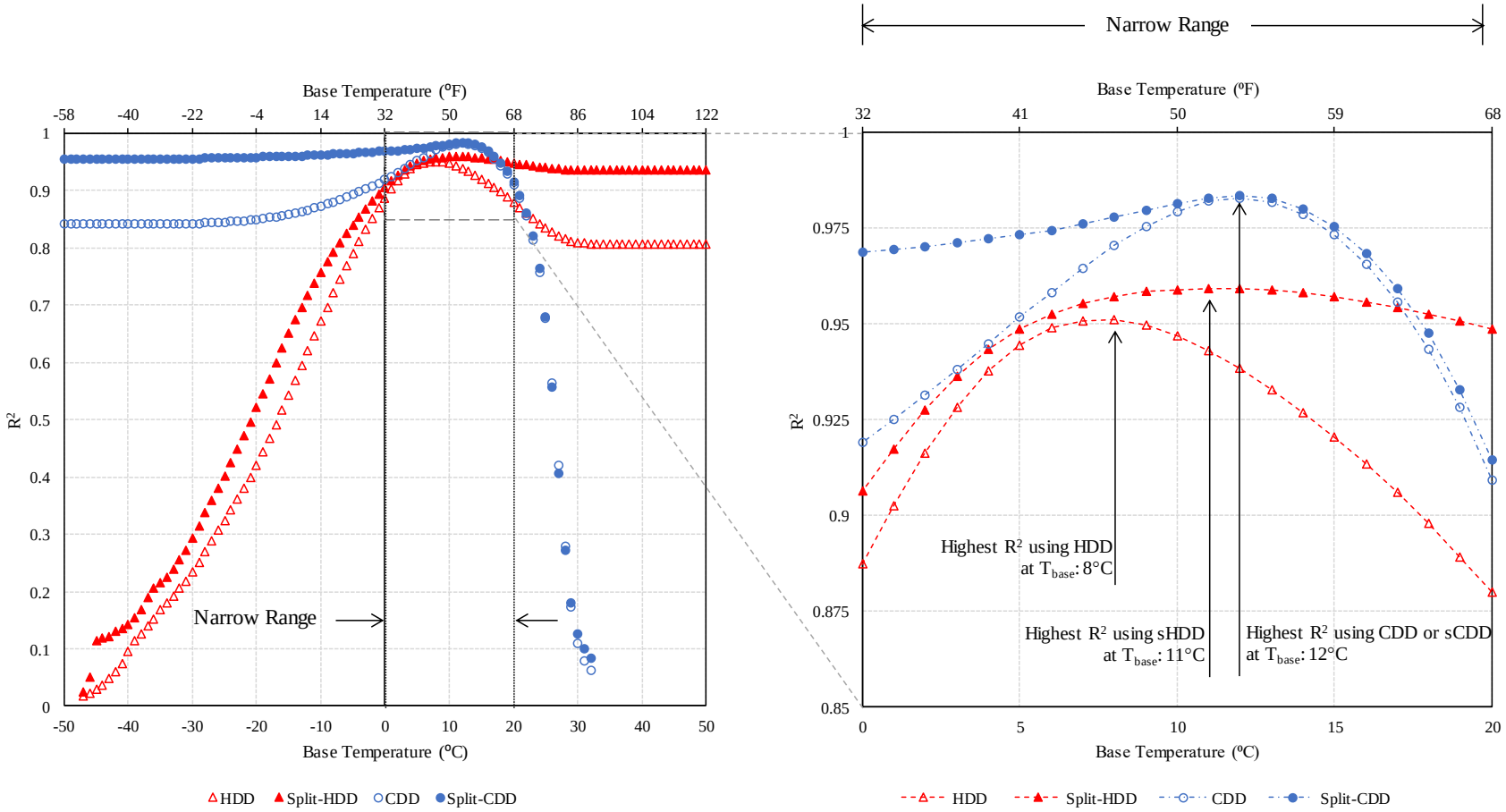

Figure 124: The Predictability of the Annual Heating and Cooling Energy Consumption Using the Conventional Degree Days and Split-Degree Days with Different Base Temperatures; Left: Representation for a Large Span of Base Temperature; Right: Representation for the Temperature Range Close to the Optimal Base Temperature.

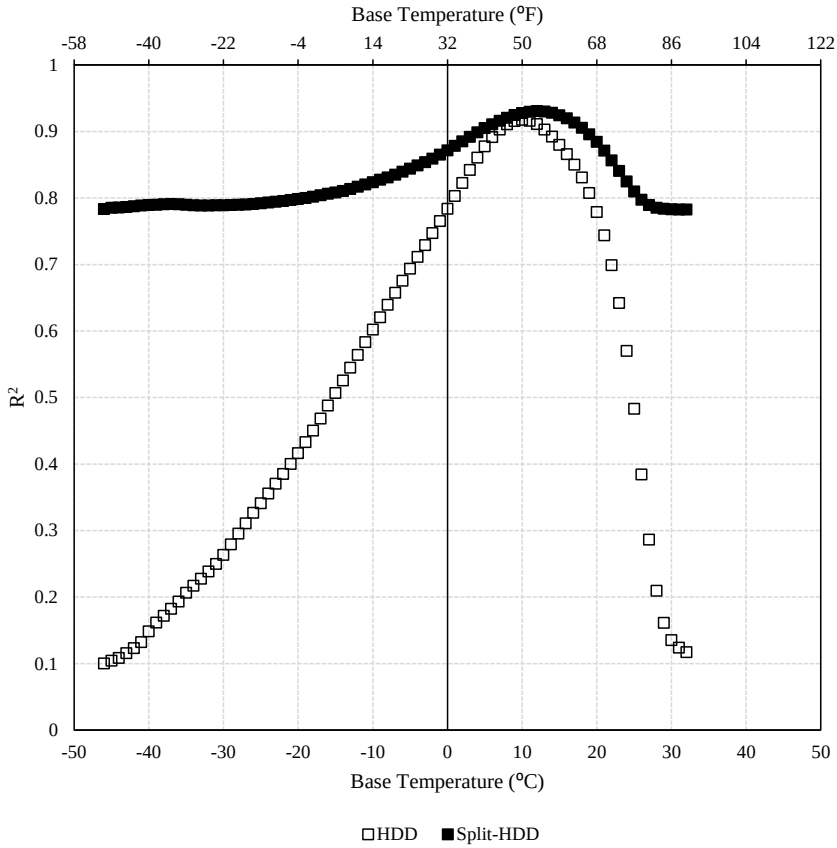

Figure 125: The Predictability of the Total Annual Regulated Energy Consumption Using the Conventional Degree Days and Split-Degree Days with Different Base Temperatures

The accuracy in the discrimination of the heating loads among different sites increases with increasing the base temperature until the base temperature reaches a certain point (8°C for HDD and 11°C for sHDD)[10]. From this point, increasing the base temperature reduces the R^2 since the higher base temperatures does not accurately represent the temperature above which heating loads are needed. Eventually, there is a base temperature that the average daily

[10] It should be noted that this optimal base temperature is specifically derived from the regressions from the energy simulations of the DOE medium office protoype building models and the 801 TMY3 weather files and may not apply for other building types, building configurations, and different pool of weather files.

temperature in the case of the HDD, and the average temperature in each interval in the case of the sHDD, in all days in different locations is lower than the base temperature. Consequently, the HDD and sHDD will simply be the base temperature minus the average temperature. Increasing the base temperature from this point will only add a constant value to all different sites, which does not change the R^2. This temperature varies in HDD and sHDD. It should be noted that, unlike the cases with very low base temperatures, by increasing the base temperature the R^2 does not decrease to very low numbers. This is mainly because of the fact that with even with very large base temperatures, the HDD or sHDD in various sites to some extents discriminates the heating loads in different locations while there is little or no discrimination in heating demands of different locations when using very low base temperatures, in which the HDD or sHDD is zero for most of the sites.

Similar but reverse scenario in the heating applies for the cooling. The R^2 remains approximately constant within the range of very low base temperatures since the base temperature is lower than the average daily temperature (or the average of each split interval in the case of the sCDD) in almost all days of all 801 weather files; hence, the values of all independent variables in very low base temperatures differ by a constant value, which is the temperature difference of the base temperatures and does not change the R^2. While these independet values to some extent discriminates the cooling demands in each location, but they do not accurately represent the base temperature, above which the building requires cooling. Therefore, the R^2 increases until it reaches the optimal base temperature (12℃ for both CDD and

sCDD with this building configurations and the 801 used weather files)[11]. The R^2 then significantly decreases as most of the days in most of the weather files result in zero CDD or sCDD, which will make no discrimination for the cooling loads.

One of the major advantages of the split-degree days compared to the conventional degree days is the roubust estimation of the energy consumption by the split-degree days, which plays a crucial rule in weather classification when there is limited or no information about the building configurations. As shown in Figure 124, the R^2 in both sHDD and sCDD throughout the whole range of the base temperatures was higher than the HDD and CDD of the corresponding base temperatures. Although the R^2 of the two methods are very close around the optimal base temperatures, the R^2 drops significantly in heating base temperatures above the optimal base temperature for heating and cooling temperatures below the optimal base temperature for cooling. However, the R^2 of the sHDD for the base temperatures above the optimal heating base temperature and the R^2 of the sCDD for the base temperatures below the optimal cooling base temperature remains very close to the optimal R^2. The prototype building models are representative models based on the surveys and current configurations of the built building. However, each building can have a different base temperature based on its unique heat loss and heat gains patterns and schedules. Furthermore, different building types can have different base temperatures. However, in weather classification, the classification should be inclusive for various buildings in different regions. Therefore, in weather classification, where there is limited or no information for the buildings, the roubustness of the classification plays an essential role as

[11] Similar to the case of heating, this optimal base temperature is specifically derived from the regressions of the energy simulations of the medium office protoype building models and the 801 TMY3 weather files and may not apply for other building types, building configurations, and different pool of weather files.

it should account for various building configurations that have different heat loss coefficients, internal gains, schedules, and consquently different base temperatures.

5.1.8. Comparative Analysis on the Estimation of the Energy Consumption using the Split-Degree Day and the Conventional Degree Day Methods

This section provides a comprehensive comparison of the accuracy of the estimation of energy consumption by various degree day methods. Besides the comparisons between the conventional degree days and the split-degree days, which were provided in the previous subsections, other methods are compared in this section as well.

To begin, the HDD and CDD based on different degree day calculation methods as well as the Heating Degree Hours (HDH) and Cooling Degree Hours (CDH) were calculated for the 801 weather data. Then, regression models were developed using the different parameter as the independent variable and total regulated, heating, cooling, and fan annual energy consumption as the dependent variable. Results are shown in Figure 126 and Table 10. Figure 126 and Table 10 include the R^2, the adjusted R^2, and the RMSE of the developed regression models in 801 locations for total regulated, heating, cooling, and fan energy consumption. The regression models are developed using the conventional degree days with maximum/minimum temperature approach, the conventional degree days with average temperature approach, the degree hours, the mean degree hours, the meteorological office equations, and the split-degree days. From the figure and table it can be seen that the proportion of the variance in the total regulated energy consumption that is predictable using the split-degree days is more than 5% higher than the one from the degree days. In addition, significant improvement in predictability can be seen for the

heating and fan energy use. The high predictability in various methods for cooling, however, yields a smaller improvement in the estimation of cooling energy consumption using sCDD.

Comparisons of different methods with the optimal base temperature for degree day method (discussed in Section 5.1.7) are provided in Figure 127 and Table 11. The optimal base temperature refers to the optimal values for the conventional CDD and HDD, as illustrated in Figure 124. The optimal values differ in different methods. Therefore, the accuracies are lower in some cases when compared to the standard base temperature. In this figure and table it can be seen that similar to the comparisons conducted using the standard base temperatures, the results of split-degree days outperforms other methods in the estimation of different energy sectors.

While split-degree days outperforms other methods in predicting different energy end uses, there are different ways that the *split* method can be applied. For example, including or not including the interaction terms, utilization of the maximum–minimum or average approach, and the number of splits per day are some of the main variations in split-degree days. While Appendix C illustrates the determination of the best split time span in a 2-split approach, this sections provides the comparison of several other variations. The comparisons include the 2-split split-degree days including the interactions terms for the two $sHDD_{P1}$ and $sHDD_{P2}$, and also $sCDD_{P1}$ and $sCDD_{P2}$, each with maximum–minimum approach and the average approach. Furthermore, a 24-split approach, which is basically using 24 HDH and 24 CDH values, is also analyzed. Results are illustrated for the standard base temperatures (Table 12) and the optimal base temperatures (Table 13).

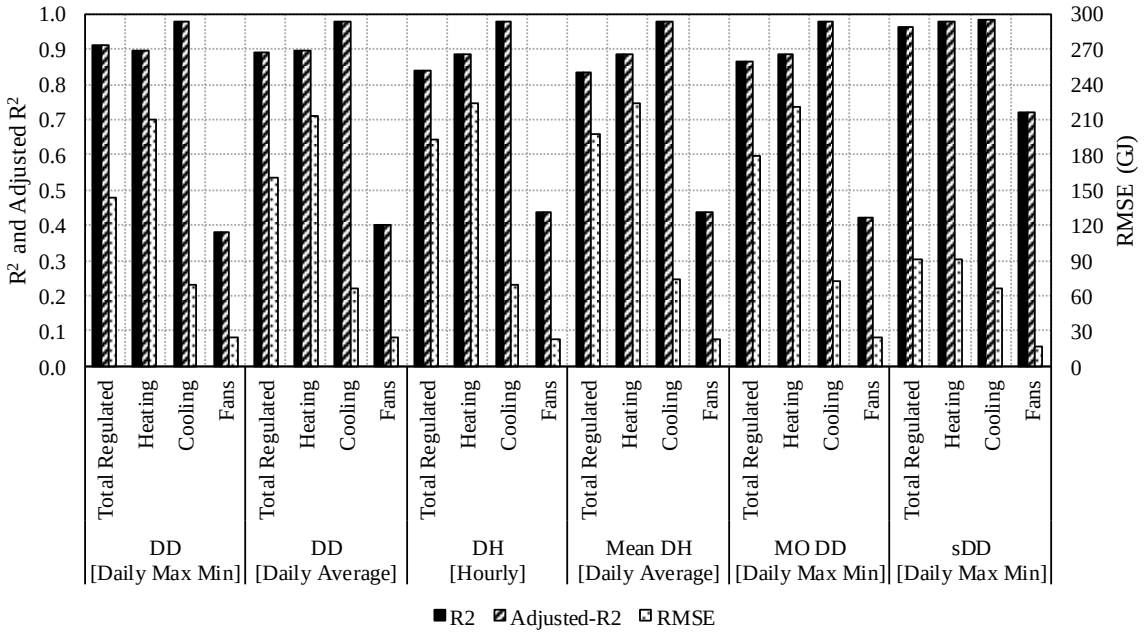

Figure 126: Representation of the Predictability of the Energy Consumption by Various Degree Day/Hour Methods Using the Standard Base Temperatures

Table 10: Predictability of the Energy Consumption by Various Degree Day/Hour Methods Using the Standard Base Temperatures

		Temperature	R^2				Adjusted-R^2				RMSE (GJ)			
			Total Regulated	Heating	Cooling	Fans	Total Regulated	Heating	Cooling	Fans	Total Regulated	Heating	Cooling	Fans
Base Temperature for Cooling: 10 ºC; Base Temperature for Heating: 18 ºC	**CDD**	Daily Max Min	0.913		0.979	0.383	0.913		0.979	0.381	143.248		70.052	24.812
	HDD	Daily Max Min		0.898				0.898				210.614		
	CDD	Daily Average	0.891		0.981	0.400	0.891		0.981	0.399	160.342		66.900	24.461
	HDD	Daily Average		0.895				0.895				213.423		
	CDH	Hourly	0.841		0.979	0.439	0.841		0.979	0.438	193.825		69.910	23.658
	HDH	Hourly		0.884				0.884				224.195		
	Mean CDH	Daily Average	0.834		0.977	0.439	0.834		0.977	0.438	198.012		73.567	23.658
	Mean HDH	Daily Average		0.884				0.884				224.195		
	MO[1] CDD	Daily Max Min	0.865		0.978	0.422	0.865		0.978	0.421	178.424		72.884	24.008
	MO[1] HDD	Daily Max Min		0.887				0.887				221.193		
	sCDD* (2-Split)	Daily Max Min	0.965		0.982	0.722	0.964		0.982	0.720	91.773		66.058	16.693
	sHDD* (2-Split)	Daily Max Min		0.981				0.981				90.345		

1. MO referes to the Metheorological Office equations

The asterisk symbol (*) indicates that the regression model includes the interaction terms

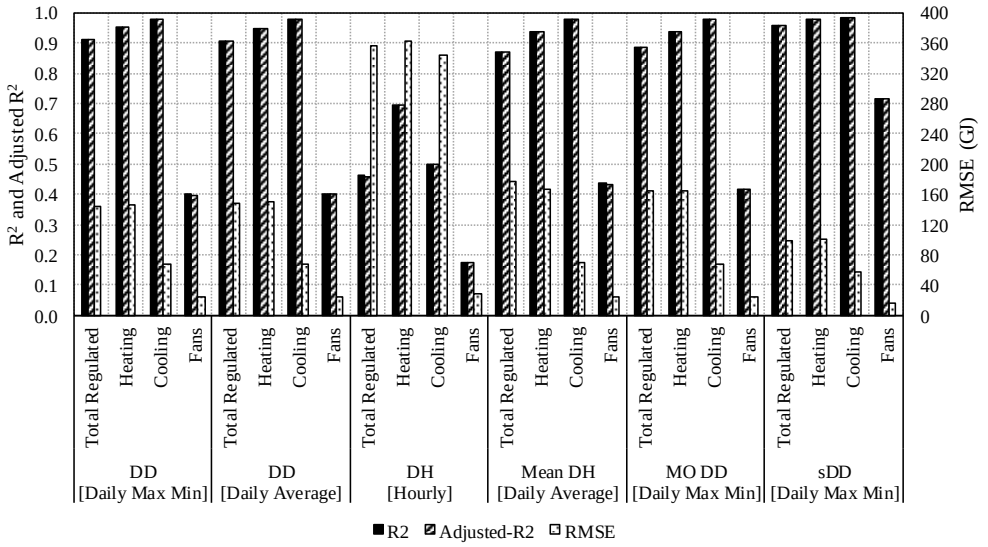

Figure 127: Representation of the Predictability of the Energy Consumption by Various Degree Day/Hour Methods Using the Optimal Base Temperatures[12]

Table 11: Predictability of the Energy Consumption by Various Degree Day/Hour Methods Using the Optimal Base Temperatures[12]

		Temperature	R^2				Adjusted-R^2				RMSE			
			Total Regu	Heating	Cooling	Fans	Total Regu	Heating	Cooling	Fans	Total Regulated	Heating	Cooling	Fans
Base Temperature for Cooling: 12 °C; Base Temperature for Heating: 8 °C	**CDD**	Daily Max Min	0.912		0.981	0.400	0.912		0.981	0.398	144.357		66.871	24.470
	HDD	Daily Max Min		0.951				0.951				145.761		
	CDD	Daily Average	0.907		0.981	0.401	0.907		0.981	0.400	148.155		66.871	24.443
	HDD	Daily Average		0.948				0.948				150.347		
	CDH	Hourly	0.462		0.500	0.176	0.461		0.499	0.174	356.672		344.411	28.681
	HDH	Hourly		0.695				0.695				363.521		
	Mean CDH	Daily Average	0.869		0.980	0.435	0.868		0.980	0.434	176.315		69.484	23.735
	Mean HDH	Daily Average		0.936				0.935				167.211		
	MO[1] CDD	Daily Max Min	0.886		0.981	0.419	0.885		0.981	0.418	164.499		67.664	24.075
	MO[1] HDD	Daily Max Min		0.938				0.937				164.634		
	sCDD* (2-Split	Daily Max Min	0.959		0.986	0.717	0.959		0.986	0.715	98.500		57.196	16.848
	sHDD* (2-Split	Daily Max Min		0.977				0.977				99.825		

1. MO referes to the Metheorological Office equations

The asterisk symbol (*) indicates that the regression model includes the interaction terms

[12] The optimal base temperatures refers to the temperatures at which the conventional CDD and HDD result in the highest accuracy of the estimations for the cooling loads and heating loads, respectively, as illustrated in Figure 124. This temperature differ from the optimal values for other methods. Therefore, besides the R^2 for the cooling and heating loads for CDD and HDD, other R^2 may be lower than the standard base temperature.

In Table 12, it can be seen that the split-degree days used in this study, which includes the interaction terms with the daily maximum–minimum approach has comparatively better results compared to other 2-split split-degree days results in the standard base temperatures in the predictions of the total regulated, heating, and with high accuracy in the estimation of cooling and fan. The average approach has higher R^2 in the predictions of the cooling and fan energy consumption. However, compared to conventional degree day methods, the accuracy of the prediction of all split-degree day methods for the fan energy consumption are much higher that the trivial difference between split-degree day methods can be considered negligible. Also, the accuracy of the estimation is high in all the cases and the trivial difference can be considered negligible. The predictions of the 24-split approach is slightly better than the 2-split approach. However, in some cases such as heating, the 2-split split-degree days outperforms the 24-split split-degree days. Results for the optimal base temperatures, shown in Table 13, have closer accuracy for different methods. Overall, due to the complexity and resolution of the data, and considering the relatively smaller improvement in 24-split split-degree days and 2-split split-degree days versus each split-degree days and conventional degree days, the 2-split split-degree days with interactions were selected in this study.

Table 12: Predictability of the Energy Consumption by Various Split-Degree Day Methods Using the Standard Base Temperatures

		Temperature	R^2				Adjusted-R^2				RMSE			
			Total Regulated	Heating	Cooling	Fans	Total Regulated	Heating	Cooling	Fans	Total Regulated	Heating	Cooling	Fans
Base Temperature for Cooling: 10 °C; Base Temperature for Heating: 18 °C	**sCDD (2-Split)**	Daily Max Min	0.952		0.981	0.708	0.952		0.981	0.707	106.295		67.807	17.089
	sHDD (2-Split)	Daily Max Min		0.964				0.964				125.264		
	sCDD* (2-Split)	Daily Max Min	0.965		0.982	0.722	0.964		0.982	0.720	91.773		66.058	16.693
	sHDD* (2-Split)	Daily Max Min		0.981				0.981				90.345		
	sCDD (2-Split)	Daily Average	0.946		0.983	0.728	0.945		0.983	0.727	113.509		63.588	16.493
	sHDD (2-Split)	Daily Average		0.963				0.962				127.496		
	sCDD* (2-Split)	Daily Average	0.961		0.984	0.741	0.961		0.984	0.739	96.114		61.605	16.112
	sHDD* (2-Split)	Daily Average		0.981				0.981				90.520		
	sCDD (24-Split)	Daily Average	0.970		0.991	0.814	0.968		0.991	0.802	87.354		46.255	14.031
	sHDD (24-Split)	Daily Average		0.970				0.970				114.871		

1. MO referes to the Metheorological Office equations

The asterisk symbol (*) indicates that the regression model includes the interaction terms

Table 13: Predictability of the Energy Consumption by Various Split-Degree Day Methods Using the Optimal Base Temperatures[13]

		Temperature	R^2				Adjusted-R^2				RMSE			
			Total Regulated	Heating	Cooling	Fans	Total Regulated	Heating	Cooling	Fans	Total Regulated	Heating	Cooling	Fans
Base Temperature for Cooling: 12 °C; Base Temperature for Heating: 8 °C	**sCDD (2-Split)**	Daily Max Min	0.959		0.983	0.690	0.959		0.983	0.689	98.506		63.126	17.604
	sHDD (2-Split)	Daily Max Min		0.976				0.976				101.681		
	sCDD* (2-Split)	Daily Max Min	0.959		0.986	0.717	0.959		0.986	0.715	98.500		57.196	16.848
	sHDD* (2-Split)	Daily Max Min		0.977				0.977				99.825		
	sCDD (2-Split)	Daily Average	0.960		0.982	0.699	0.960		0.982	0.697	97.416		65.348	17.352
	sHDD (2-Split)	Daily Average		0.977				0.977				100.686		
	sCDD* (2-Split)	Daily Average	0.960		0.985	0.729	0.960		0.985	0.727	97.443		59.901	16.499
	sHDD* (2-Split)	Daily Average		0.978				0.977				98.748		
	sCDD (24-Split)	Daily Average	0.972		0.992	0.789	0.970		0.991	0.776	84.338		45.072	14.936
	sHDD (24-Split)	Daily Average		0.979				0.979				96.286		

1. MO referes to the Metheorological Office equations

The asterisk symbol (*) indicates that the regression model includes the interaction terms

[13] The optimal base temperature refers to the temperatures at which the conventional CDD and HDD result in the highest accuracy of the estimations for the cooling loads and heating loads, respectively, as illustrated in Figure 124.

The results of the analysis of the accuracy of the estimation of the energy consumption using the split-degree days and the conventional degree days for the model with higher thermal mass (described in Section 3.4.4), shown in Table 14, showed that the R^2 using the split-degree days was higher than the R^2 using the conventional degree days. Also, the R^2 of the estimations for the identical model with high thermal mass using split-degree day was only trivially lower than the R^2 of the estimations of the selected identical DOE prototype model. However, the lower accuracy in the estimations of the energy use of the identical model with high thermal mass versus the selected identical DOE prototype model using the conventional degree day was more significant. For example, the R^2 of the estimation of the total regulated energy consumption of the cases with higher thermal mass showed to be 0.007 (0.913 to 0.907) lower than the corresponding R^2 of the selected identical DOE prototype model. However, the corresponding comparison for the estimations using the split-degree days shows a 0.001 decrease only, which shows that, similar to the analysis of the DOE medium office prototype, the split-degree day resulted in more accurate estimations for the energy use of the model with higher thermal mass compared to the conventional degree days.

5.2. Application of the Split-Degree Days Method

This section discusses the potential application of the split-degree days in the ASHRAE Standard 90.1. The potential application includes the utilization of the split-degree days in climate classification as well as the use of split-degree days as a correction factor in the performance path.

Table 14: Predictability of the Energy Consumption of the Selected DOE Identical Prototype Model and the Identical Model with High Thermal Mass Using the Conventional Degree Day and the Split-Degree Day Methods

	R^2								Difference in the R^2			
	Identical Prototype Model[1]				Identical Model[1] with High Thermal Mass				R^2 of the Identical Prototype Model - R^2 of the Identical Model with High Thermal Mass			
	Total Regulated	Heating	Coooling	Fan	Total Regulated	Heating	Coooling	Fan	Total Regulated	Heating	Coooling	Fan
CDD	0.913	0.898		0.383	0.907	0.893		0.477	0.007	0.005		-0.094
HDD			0.979				0.978				0.001	
sCDD*	0.965	0.981		0.722	0.963	0.981		0.773	0.001	0.001		-0.050
sHDD*			0.982				0.981				0.001	

1. Compliant with the requirements for Climate Zone 4 of the ASHRAE Standard 90.1-2016 Using the DOE Medium Office Prototype Model for Climate Zone 4B

The asterisk symbol (*) indicates that the regression model includes the interaction terms

5.2.1. Utilization of the Split-Degree Days method in Climate Classification

Currently, climate zones classification in ASHRAE Standard 169-2013 and other Standards that use the same classification (e.g. ASHRAE Standard 90.1-2016), are mainly based on the HDD and CDD. Then some of the climate zones are divided into subtypes based on their different moisture regimes. However, in previous sections of this document, it has been shown that the impact of moisture regime is significant within each climate zone. The prescriptive path provides tabulated values for each climate zone. Therefore, the significant variation within each climate zone is not normalized using the prescriptive path.

To more accurately classify the weather in different locations, it is more appropriate to use an index that similar to degree days that accounts for the climate severity, but better accounts for the moisture regimes. The split-degree days determines the severity of the weather similar to

degree days and is shown to have higher predictability of different moisture regime. Therefore, different weather conditions can be more accurately classified using the split-degree days.

5.2.2. Utilization of the Split-Degree Days Method for the PCI Adjustment

In section 4.4.2, it has been shown that currently, there is a considerable variation in the extent at which each location is above-code using the performance path. Therefore, there is a need to adjust the BPFs for each weather. This section provides the results of the complied buildings using the adjusted BPFs.

First of all, the extent to which each location is above code is calculated using the $PCI - PCI_t$. Then, as described in section 3.5 of this document, the $BPF\_F_{ideal.i}$, which is ratio of the BPF_{ideal} for location i over the *BPF* of the corresponding climate zone is calculated. Multiplying the $BPF\_F_{ideal.i}$ with the *BPF* of the corresponding weather file results in zero $PCI - PCI_t$ for each location. Then, a linear regression model is developed using the sHDD and sCDD as the independent variables and the BPF_F_{ideal} for different locations as the dependent variable. Then the adjustments are applied using the sHDD and sCDD of each site and the linear equation derived for each climate zone. The adjustments are applied using the sHDD and sCDD of each site, plugged into a linear equation derived for each climate zone. The calculated adjustment factor is multiplied with the provided *BPF* for each location.

It should be noted that the above code value is ideally calculated using the developed linear regression model. However, although split-degree days is shown to better estimate the energy performance of a building compared to the conventional degree days, split-degree days does not perfectly define all the variations in different locations. Therefore, there is an error term that makes the estimated above code value slightly smaller or larger than the actual calculated

above code value, which can result in below code rating in some cases. In order to assure that all the estimated above code values are equal or larger than zero, a constant value is added to the constant term of the linear regression that, among all cases, yields the minimum value of zero for the above code. Figure 128 shows the difference of the PCI and PCIt of the ASHRAE Standard 90.1-2016 medium office prototype models in different climate zones using the adjustment factors. Figure 129 shows the difference in the variations in the above code index of the ASHRAE Standard 90.1-2016 medium office prototype models in different locations with and without applying the adjustment factors, which is in fact the variations shown in the vertical axis of Figure 82 and Figure 128.

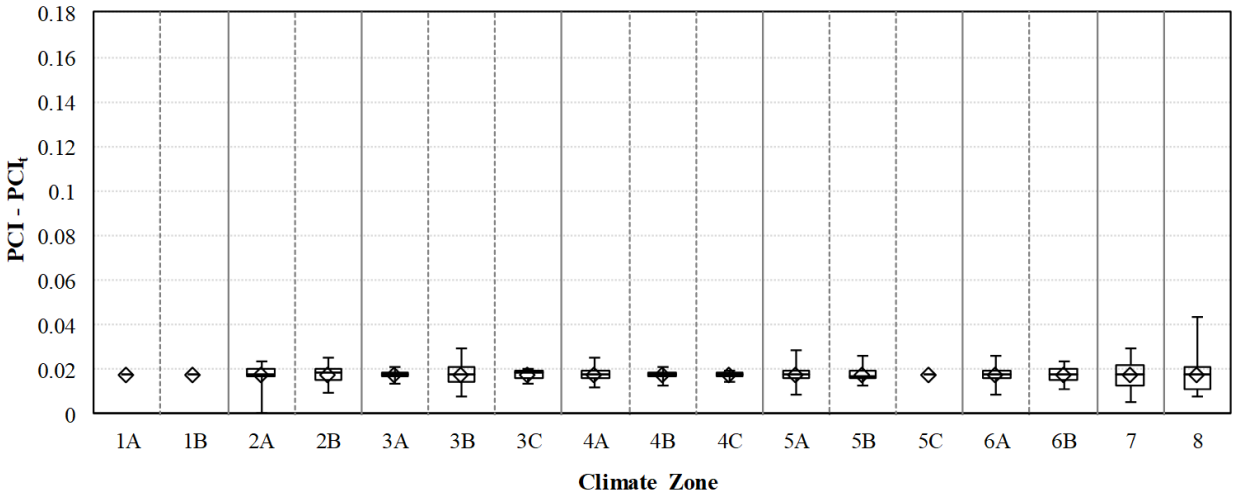

Figure 128: Difference of the PCI and PCI_t of the ASHRAE Standard 90.1-2016 Medium Office Prototype Models in Different Climate Zones Using the Adjustment Factors

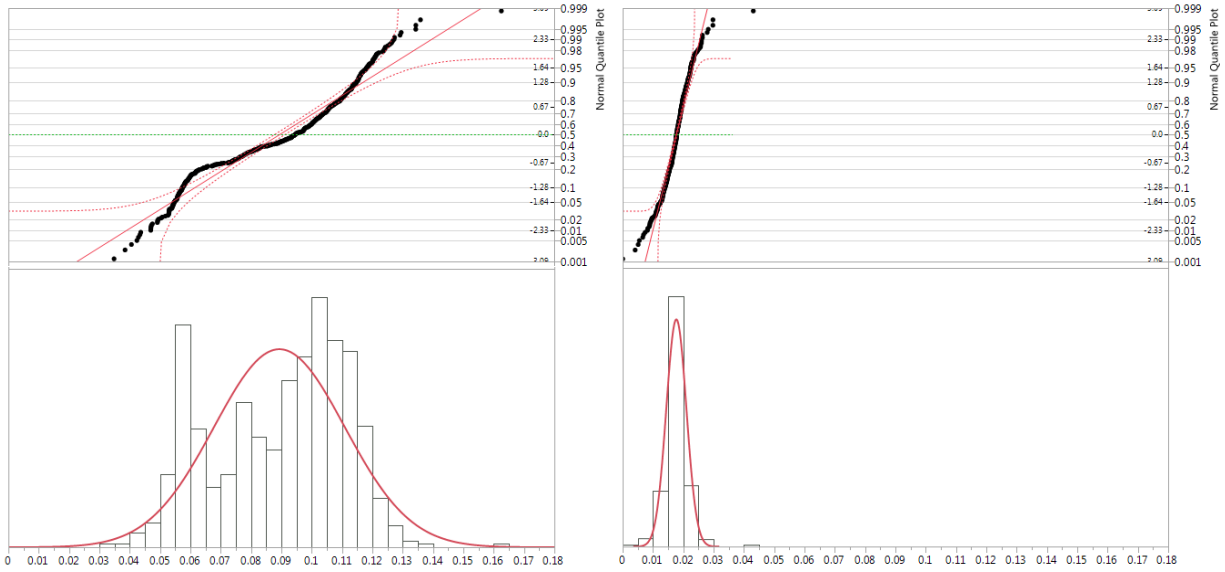

Figure 129: The Variations in the Above Code Index of the ASHRAE Standard 90.1-2016 Medium Office Prototype Models in Different Locations without (Left) and with (Right) Applying the Adjustment Factors

5.3. Summary of the Accuracy and Application of the Improved Method

This chapter illustrated the results of the comparisons between the proposed improved split-degree days and the conventional degree days and the application of the split-degree days method in commercial code compliance procedure. The results include the comparisons of the accuracy of the prediction of the influential weather parameters on building energy consumption (diurnal temperature range, solar radiation, and humidity) split-degree days and degree days. Then, the accuracy of the prediction of medium office building total regulated, heating, cooling, and fan energy consumption are compared using split-degree days versus degree days as the independent variable. Results of the comparative analysis shows that using the split-degree days as independent variable to estimate the weather parameters or the energy consumption of the models results in more accurate estimations compared to using the conventional degree days.

Then, the application of the new split-degree days is shown for a commercial building code compliance procedure. First, the use of the new split-degree day method is demonstrated for climate classification instead of the traditional degree day method. The new procedure more accurately classifies the climate of each location according to its weather characteristics by better estimating the building energy consumption in that location. Finally, an adjustment procedure is defined to help eliminate the variations in the above code values for each climate zone. The adjustment factors for each location can be calculated using the new split-degree days for each location, which are used with the new multi-linear regression model for the corresponding climate zone.

CHAPTER VI

SUMMARY AND FUTURE WORK

This Chapter includes a summary of the results and a discussion about future work. This study highlighted the variations in the energy consumption and the energy savings associated with the implementation of daylight responsive controls in different climate locations of the United States using the DOE medium office prototype models for ASHRAE Standard 90.1-2016 and 90.1-2004. The analysis of the prototype models that met the requirements in the prescriptive path showed a systematic difference in code-compliant buildings in different moisture regimes. Similar systematic differences were observed when using the performance path for the compliance (Performance Rating Method). Based on the analysis of the variations in different locations, a new index for climate classification was developed and demonstrated. The proposed index, called the split-degree day, can be used in the estimation of building energy consumption and weather-normalized energy savings calculation. Specifically related to building energy standards and codes, the proposed index can be used for an improved weather classification that better claassifies the provisions provided for each location. Furthermore, using the proposed index, an adjustment procedure was also developed for the performance path of ASHRAE Standard 90.1. Figure 130 is the flowchart that summarizes this study. The current status, analysis, the proposed method, and the application of the proposed method are shown in the figure. Current utilization of the conventional degree day method related to ASHRAE Standard 90.1 is traced using red arrows. The application of the proposed split-degree day is shown using the dashed red lines.

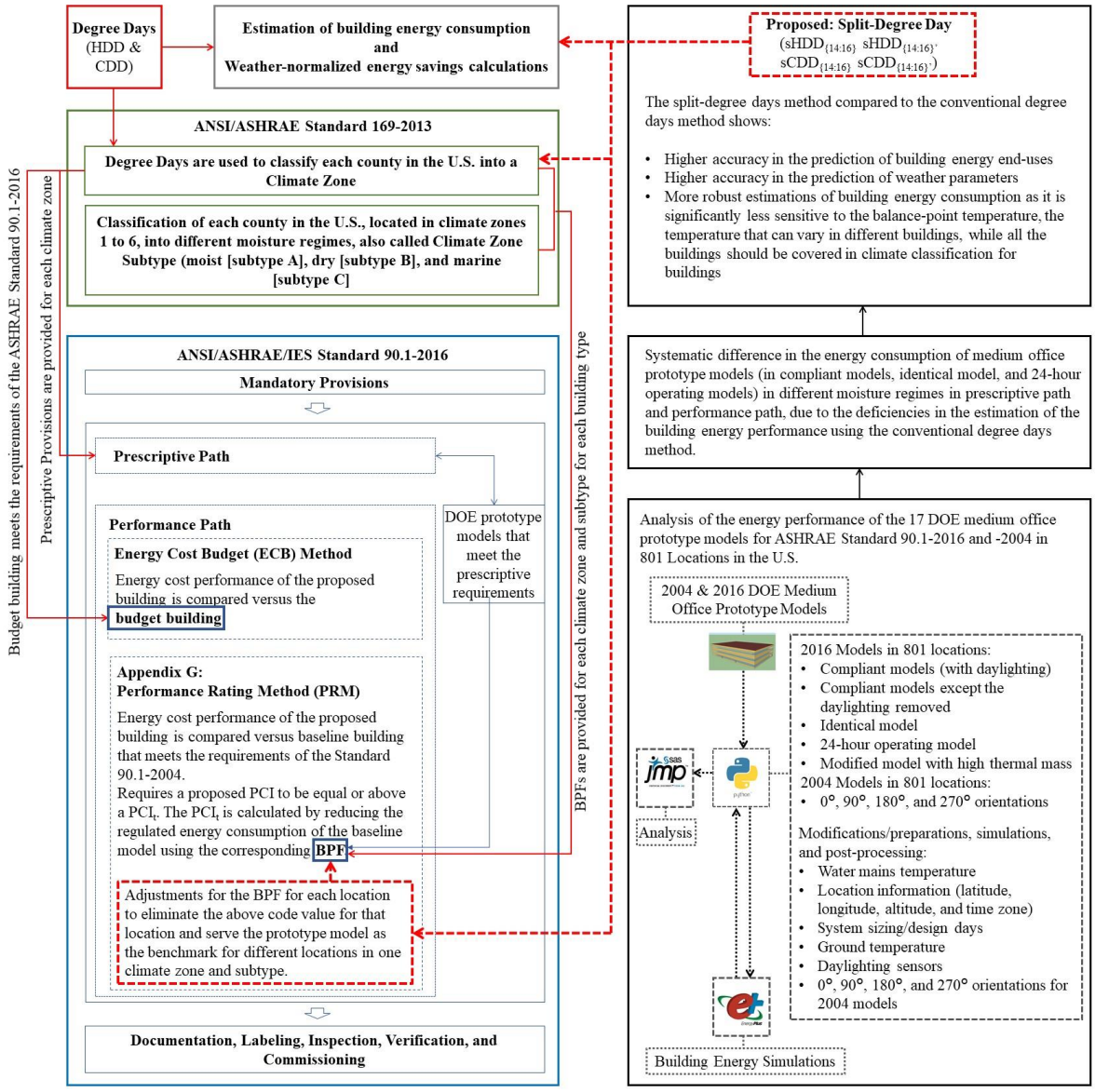

Abbreviations: BPF: Building Performance Factor; CDD: Cooling Degree Day; HDD: Heating Degree Day; PCI: Performance Cost Index; PCI_t = Target Performance Cost Index; sCDD: split-Cooling Degree Day; sHDD: split-Heating Degree Day

Figure 130: Overall Procedure: Current Status, Analysis Procedure, and the Application of the Proposed sDD Method

6.1.Summary of the Results of the Simulated Medium Office Models

The variation in the energy consumption of the DOE medium office models in different climatic locations are discussed in the first part of the results. Similarly, the variation in the

energy savings of the models with the implementation of the daylight responsive controls are discussed in this section. Furthermore, the variations in the amount of above code value at each location is also illustrated.

The analysis in this section shows that there is a systematic difference in the energy consumption of the models in different moisture regimes. While the solar radiation, dry-bulb temperature, humidity, and wind, impact building energy consumption, the most influential parameters in different moisture regimes that lead to different heating and cooling energy consumption were shown to be the solar radiation and humidity, respectively. Also, it is shown that while different diurnal temperature profiles directly impact building energy consumption, diurnal temperature range can be used to estimate other influential weather conditions.

Finally, the results show that there is a significant difference in energy savings associated with the implementation of daylight responsive controls in the different climate zones. The results show higher energy savings for buildings with daylighting features in hotter climates compared to colder climates.

6.2. Summary of the Proposed Split-Degree-Days Based Climate Classification Method

The analysis shows that the traditional degree days do not fully discriminate the influential parameters. A new modified degree days index for climate classification, split-degree days, is defined so that it includes the diurnal temperature range information. These new split-degree days can be calculated in a similar fashion as degree days, except that the new split-degree days should be calculated separately for two sections of each day. The analyses on the DOE medium office models in this study showed that the best split interval were the hours from 14:00 to 16:00 in one split and the remainder of the day in the other split. Considering that the

diurnal temperature range associates well with influential weather parameters on building thermal performance and the fact that the conventional degree days were not sensitive to the diurnal temperature range, the new split-degree days had a higher accuracy for predicting the building energy consumption compared to the conventional degree days.

Different regression models were developed to predict the total regulated, heating, cooling, and fan energy consumption in the DOE models in different locations as the dependent variable and either the degree days or the split-degree days of the corresponding locations as the independent variables. The comparisons of the accuracy of the estimations showed that the estimated energy consumption using split-degree days is significantly higher than the estimates using degree days. Furthermore, it is shown that by using split-degree days, there is less discrepancy in the estimated total regulated, heating, cooling, and fan energy consumption in the different moisture regimes.

6.3. Summary of the Results of the Application of the Proposed New Method

Based on the analysis on the energy consumption in different locations, a new index for climate classification is proposed. The accuracy of the estimation of the heating and cooling energy consumption using the proposed new method is shown to be less sensitive to the base temperature above a certain temperature for heating and below a certain temperature for cooling. Climate classification covers various building types and configurations, each of which can have a different base temperature. Therefore, the utilization of the split-degree days compared to the conventional degree days is more appropriate for the climate classification.

Finally, using the proposed new split-degree days, adjustment factors are proposed for use in the ASHRAE Standard 90.1 performance path to reduce the variation of the above code

rating at different locations. The adjustment factors are calculated using the new sHDD and sCDD values of the weather file in the new derived equations.

6.4. Recommendations for Future Research

This study showed the variations in building energy consumption in the DOE medium office prototype models in different locations of the United States. A new modified degree day method was developed to better estimate the energy consumption of the DOE models in different locations. Based on the limitations of this study, the following categories are recommended as the potential future work:

- Analysis of the accuracy of the estimation of the building energy consumption using the split-degree day method for different building types (i.e., different commercial buildings).
- Analysis of the accuracy of the estimation of the building energy consumption using the split-degree day method in weather conditions outside the United States.
- Comparisons and analysis of the potentially improved methods other than degree day methods.
- Analysis of the impact of various building energy systems on the variation of the building models energy consumption in different locations.
- Analysis of the impact of different configurations of building envelopes (e.g. different configurations of shadings, WWR, glazing types, interior space layout and materials, etc.) on the daylighting performance of the building models remain to be done.
- Analysis carried out using other thermal and daylighting simulation tools.

REFERENCES

Altman, E. (2005). Computers and Lighting, Century Series: Pioneers. *LD+A, December*, 57–62.

Arasteh, D., Kohler, C., Griffith, B. (2009). *Modeling windows in Energy Plus with simple performance indices*. Lawrence Berkeley National Laboratory Report, LBNL-2804E.

Arvo, J. (1986). Backward ray tracing. *SIGGRAPH '86 Developments in Ray Tracing Course Notes*, volume 12. Available at: www.cs.washington.edu/education/courses/cse457/06au/projects/trace/extra/Backward.pdf. Retrieved on August 16, 2017.

Ashdown, I. (2005). Sensitivity analysis of glare rating metrics. *LEUKOS – The Journal of Illuminating Engineering Society of North America*, *2*(2), 115–122. https://doi.org/10.1582/LEUKOS.2005.02.02.003.

ASHRAE. (2001). *Energy estimating and modelling methods, Ch. 31 in ASHRAE handbook: fundamentals*. Atlanta: ASHRAE.

ASHRAE. (2002). *ASHRAE Guideline 14-2002, Measurement of Energy and Demand Savings*. Atlanta: ASHRAE.

ASHRAE. (2013a). *ANSI/ASHRAE Standard 169-2013, Weather Data for Building Design Standards*. Atlanta: ASHRAE.

ASHRAE. (2013b). *ASHRAE Handbook-Fundamentals*. Atlanta: ASHRAE.

ASHRAE. (2016). *ANSI/ASHRAE/IES Standard 90.1-2016, Energy Standard for Buildings Except Low-Rise Residential Buildings*. Atlanta: ASHRAE.

ASHRAE. (2018). *ANSI/ASHRAE/ICC/USGBC/IES Standard 189.1-2017, Standards for the Design of High-Performance Green Buildings*. Atlanta: ASHRAE

ASHVE. (1933). *American Society of Heating and Ventilating Engineers Guide*. New York, NY: American Society of Heating and Ventilating Engineers.

Athalye, R., Xie, Y., Liu, B., and Rosenberg, M. (2013). Analysis of Daylighting Requirements within ASHRAE Standard 90.1. PNNL-22698.

Baker, S. M. (1990). Modeling Complex Daylighting with DOE-2.1C. *The DOE-2 User New*, *11*(1).

Bakirci, K., Ozyurt, O., Karagoz, S., and Erdogan, S. (2008). Variable-base degree-day analysis for provinces of the Eastern Anatolia in Turkey. *Energy Exploration and Exploitation*. *26*(2), 111–132. https://doi.org/10.1260/014459808785260490

Basurto, C., Kämpf, J. H., and Scartezzini, J.-L. (2017a). Multi-criteria analysis for the integrated performance assessment of complex fenestration systems. *Building Research and Information*, *45*(8), 926–942. https://doi.org/10.1080/09613218.2016.1235911

Bellia, L., Cesarano, A., Iuliano, G.F., and Spada, G. (2008). Daylight glare: A review of discomfort indexes. In: Visual quality and energy efficiency in indoor lighting: Today for tomorrow, International Workshop, 31 March 2008, Rome, Italy. Ente per le Nuove Tecnologie, L'Energia e L'Ambiente, ENEA. Retrieved from www.fedoa.unina.it/1312/1/Bellia_paper.pdf (accessed November 2019).

Bessec, M., and Fouquau, J. (2008). The non-linear link between electricity consumption and temperature in Europe: A threshold panel approach. Energy Economics, 30(5), 2705-2721.

Bierman, A. (2007). Photosensors, dimming and switching systems for daylight harvesting. National Lighting Product Information Program (NLPIP) Specifier Reports. 11(1).

Birdsall, B. E., Buhl, W. F., Curtis, R. B., Erdem, A. E., Eto, J. H., Hirsh, J. J., Oslon, K. H., and Winkelmann, F. C. (1985). The DOE-2 computer program for thermal simulation of buildings. In: David Hafmeister editor. *Energy Sources: Conservation and Renewables, American Institute of Physics*. 135, 642.

Boyce, P., Hunter, C., and Howlett, O. (2003). The Benefits of Daylight through Windows. Lighting Reasearch Center, 1(1), 1–88. https://doi.org/12180-3352

Brackett, W. E., and Applied Software Analysis Boulder CO. (1983). *Daylighting Coefficient of Utilization Tables*. Defense Technical Information Center.

Braithwaite, R. J. (2011). Degree-days. In: Singh V.P., Singh P., Haritashya U.K. (eds) Encyclopedia of Snow, Ice and Glaciers. Encyclopedia of Earth Sciences Series. Springer, Dordrecht, 196–199. https://doi.org/10.1007/978-90-481-2642-2_104

Bryan, H. J., and Clear, R. D. (1980). *A procedure for calculating interior daylight illumination with a programmable hand calculator*. Berkeley, CA. LBL-11687.

Büyükalaca, O., Bulut, H., and Yılmaz, T. (2001). Analysis of variable-base heating and cooling degree-days for turkey. *Applied Energy*, *69*(4), 269–283. https://doi.org/10.1016/S0306-2619(01)00017-4

Carlucci, S., Causone, F., De Rosa, F., and Pagliano, L. (2015). A review of indices for assessing visual comfort with a view to their use in optimization processes to support building integrated design. *Renewable and Sustainable Energy Reviews*, *47*, 1016–1033. https://doi.org/10.1016/j.rser.2015.03.062

Chauvel, P., Collins, J. B., Dogniaux, R., and Longmore, J. (1982). Glare from windows: current views of the problem. *Light Res Technol*, *14*(1), 31–46.

CIBSE TM41. (2006). *Degree-days: theory and application*. London, UK: Chartered Institution of Building Services Engineers.

CIE—Commission Internationale de l'Eclairage. *Spatial distribution of daylight—CIE standard general sky*. 2002, CIE: Wien, 7.

Ciulla, G., Lo Brano, V., and D'Amico, A. (2016). Modelling relationship among energy demand, climate and office building features: A cluster analysis at European level. *Applied Energy*, *183*, 1021–1034. https://doi.org/10.1016/j.apenergy.2016.09.046.

Claridge, D., Krarti, M., and Bida, M. (1987). A validation study of variable-base degree-day cooling calculations. ASHRAE. RP-384.

Clarke, J. H., Hensen, J. L. M., and Janak, M. (1998). Integrated Building Simulation: State-of-the-Art. *Proc. Indoor Climate of Buildings '98, Slovak Society for Environmental Technology (SSTP), Bratislava, ASHRAE Transactions, Vol. 104*, Part 1.

Coakley, D., Raftery, P., and Keane, M. (2014). A review of methods to match building energy simulation models to measured data. *Renewable and Sustainable Energy Reviews*, *37*, 123–141. https://doi.org/10.1016/j.rser.2014.05.007.

Crawley, D.B., L.K. Lawrie, F.C. Winkelmann, and C.O. Pedersen. (2001). EnergyPlus: New capabilities in a whole-building energy simulation program. *Proceedings of Building Simulation 2001*, Rio de Janeiro, Brazil, August 13–15, 2001, pp. 51–58.

Cumali, Z. O., Sezgen, A. O., and Sullivan, R. (1979). Passive solar calculation methods: Final Report, DSE–5221-T1. 15 Oct. 1978 - 15 Jun. 1979 CCB/Cumali Associates, Oakland, CA.

Cutler, B., Sheng, Y., Martin, S., Glaser, D., and Andersen, M. (2008). Interactive selection of optimal fenestration materials for schematic architectural daylighting design. *Automation in Construction*, *17*(7), 809–823. https://doi.org/10.1016/j.autcon.2008.01.002.

D'Amico, A., Ciulla, G., Panno, D., and Ferrari, S. (2019). Building energy demand assessment through heating degree days: The importance of a climatic dataset. *Applied Energy*, *242*, 1285–1306. https://doi.org/10.1016/j.apenergy.2019.03.167.

Dasgupta, S., Papadimitriou, C. and Vazirani, U. (2006). Algorithms: McGraw-Hill.

Day, A. R., and Karayiannis, T. G. (1999a). Identification of the uncertainties in degree-day-based energy estimates. *Building Services Engineering Research and Technology*, *20*(4), 165–172. https://doi.org/10.1177/014362449902000401.

Day, A. R., and Karayiannis, T. G. (1999b). New degree-day model for estimating energy demand in buildings. *Building Services Engineering Research and Technology*, *20*(4), 173–178. https://doi.org/10.1177/014362449902000402.

Degelman, L. O. (1985). Bin weather data for simplified energy calculations and variable base degree-day information. *ASHRAE Transactions*, *91*, pt 1A, 3–14.

Diamond, S.C., Hunn, B.D., and Cappiello, CC. (1981). DOE-2 Verification Project. Phase I Interim Report. Los Alamos, NM: Los Alamos Scientific Laboratory, Report No. LA-8295-MS.

DOE. (2018, October 24). U.S. DOE. Building Energy Codes Program. Retrieved from https://www.energycodes.gov/development/commercial/prototype_models. Retrieved on December 21, 2018.

DOE-NREL (2018). Weather Data. Available at: https://energyplus.net/weather. Retrieved on October 15, 2018.

Dresler, A. (1954). The "reflected component" in daylighting design. *Transactions of the Illuminating Engineering Society*, *19*(7), 50–60.

Edmonds, I. R. (1993). Performance of laser cut light deflecting panels in daylighting applications. *Solar Energy Materials and Solar Cells*, *29*(1), 1–26. https://doi.org/10.1016/0927-0248(93)90088-K.

Edwards, L., and Torcellini, P. (2002). *A Literature Review of the Effects of Natural Light on Building Occupants*. Colorado: National Renewable Energy Laboratory – U.S. Department of Energy, (July), NREL/TP-550-30769. https://doi.org/10.2172/15000841.

Energy Information Administration (EIA). (2018a). Annual Energy Outlook 2018. Washington, DC: Energy Information Administration, U.S. Department of Energy.

Energy Information Administration (EIA). (2018b). U.S. Energy Information Administration: Sales (consumption), revenue, prices & customers. Washington, DC: Energy Information Administration, U.S. Department of Energy.

Energy Information Administration (EIA). (2019). Short-Term Energy Outlook. Washington, DC: Energy Information Administration, U.S. Department of Energy. Retrieved from https://www.eia.gov/outlooks/steo/.

Einhorn, H. D. (1979). Discomfort glare: A formula to bridge differences. *Lighting Research & Technology*, *11*(2), 90–94. https://doi.org/10.1177/14771535790110020401.

Eley, C. (2017). Feasibility of ZNE by building type and climate. *ASHRAE Journal*, *59*(7), 32–37.

EN ISO. 13790: Energy performance of buildings–Calculation of energy use for space heating and cooling (EN ISO 13790: 2008). , European Committee for Standardization (CEN), Brussels § (2008).

Erbs, D. G., Beckman, W. A., and Klein, S. A. (1981). Degree-days for variable base temperatures. *Proc. 6th National Passive Solar Conference*, Portland, OR, 1981, American Solar Energy Society, 387 - 391.

Eto, J. H. (1988). On using degree-days to account for the effects of weather on annual energy use in office buildings. *Energy and Buildings*, *12*(2), 113–127.

Galatioto, A., and Beccali, M. (2016). Aspects and issues of daylighting assessment: A review study. *Renewable and Sustainable Energy Reviews*, 66, 852–860. https://doi.org/10.1016/j.rser.2016.08.018.

Guth, S. K. (1963). A method for the evaluation of discomfort glare. *Illum. Eng.*, *57*(5), 351–364.

Haberl, J. S., Claridge, D. E., and Kissock, J. K. (2003). Inverse model toolkit: Application and testing. *ASHRAE Transactions*, *109* Part 2, 435–448.

Hackel, S., and Schuetter, S. (2013). Automatic daylighting controls. *ASHRAE Journal*, *55*(9), 46–56.

Hann, J. (1903). *Handbook of climatology: Part 1. General Climatology*. New York: The MacMillan Company.

Hee, W. J., Alghoul, M. A., Bakhtyar, B., Elayeb, O., Shameri, M. A., Alrubaih, M. S., and Sopian, K. (2015). The role of window glazing on daylighting and energy saving in buildings. *Renewable and Sustainable Energy Reviews*, *42*, 323–343. https://doi.org/10.1016/j.rser.2014.09.020.

Henley, A., and Peirson, J. (1997). Non-linearities in electricity demand and temperature: parametric versus non-parametric methods. Oxford bulletin of economics and statistics, 59(1), 149-162.

Hirning, M. B., Isoardi, G. L., and Cowling, I. (2014). Discomfort glare in open plan green buildings. *Energy and Buildings*, *70*, 427–440. https://doi.org/10.1016/j.enbuild.2013.11.053.

Hirning, M. B., Isoardi, G. L., Coyne, S., Garcia Hansen, V. R., and Cowling, I. (2013). Post occupancy evaluations relating to discomfort glare: A study of green buildings in Brisbane. *Building and Environment*, *59*, 349–357. https://doi.org/10.1016/j.buildenv.2012.08.032.

Hirsch, J. J and Associates. (2011). eQUEST: the QUick Energy Simulation Tool. Available at: http://www.doe2.com/. Last Retrieved on July 26, 2017.

Hitchcock, R. J., and Carroll, W. L. (2003). DElight: A daylighting and electric lighting simulation engine. *Eighth International IBPSA Conference*. Eindhoven, Netherlands.

Hitchin, E. R. (1981). Degree-days in Britain. *Building Services Engineering Research and Technology*, *2*(2), 73–82. https://doi.org/10.1177/014362448100200202.

Hitchin, E. R. (1983). Estimating monthly degree-days. *Building Services Engineering Research and Technology*, *4*(4), 159–162. https://doi.org/10.1177/014362448300400404.

Hitchin, E. R. (1990). Developments in degree-day methods of estimating energy use. *Building and Environment*, *25*(1), 1–6. https://doi.org/10.1016/0360-1323(90)90034-O.

Hittle, D. C. (1977). Use of the Building Loads Analysis and System Thermodynamics Program to Perform Total Energy System Analysis (No. CERL-IR-E-108). *Construction Engineering Research Lab (Army) Technical Report CERL-IR-E-108*. Champaign, IL.

Holmes, C., Tett, S., and Butler, A. (2017). What is the uncertainty in degree-day projections due to different calibration methodologies? *Journal of Climate*, *30*(22), 9059–9075. https://doi.org/10.1175/JCLI-D-16-0826.1.

Hopkinson, R.G. (1970). Glare from Windows. *Construction Research and Development Journal*, *2*(3) 98-105; *2*(4) 169-175.

Hopkinson, R.G. (1972). Glare from Daylighting in Buildings. *Applied Ergonomics*, *3*(4), 206–215.

Hopkinson, R.G., Petherbridge, P., and Longmore, J. (1954). An Empirical Formula for the Computation of Indirect Component of Daylight Factor. *Transactions of the Illuminating Engineering Society*, *19*(7), 201–219.

Hopkinson, R. G., Petherbridge, P., and Longmore, J. (1966). *Daylighting*. London : Heinemann.

Huang, J., Ritschard, R. L., Bull, J. C., and Chang, L. (1987). Climatic indicators for estimating residential heating and cooling loads. *ASHRAE Transactions*, *93*(pt 1), 72–111.

Idchabani, R., Garoum, M., and Khaldoun, A. (2015). Analysis and mapping of the heating and cooling degree-days for Morocco at variable base temperatures. *International Journal of Ambient Energy*, *36*(4), 190–198. https://doi.org/10.1080/01430750.2013.842497.

Ihara, T., Genchi, Y., Sato, T., Yamaguchi, K., and Endo, Y. (2008). City-block-scale sensitivity of electricity consumption to air temperature and air humidity in business districts of Tokyo, Japan. *Energy*, *33*(11), 1634–1645. https://doi.org/10.1016/j.energy.2008.06.005.

Ihm, P., Jung, S.-S., and Seo, D. (2014). Estimating Cooling and Heating Degree Days for Variable Base Temperature. *Korean Journal of Air-Conditioning and Refrigeration Engineering*, *26*(2), 79–85. https://doi.org/10.6110/kjacr.2014.26.2.079.

Incropera, F.P., DeWitt, D.P., Bergman, T.L., Lavine, A.S. (2007). Fundamentals of Heat and Mass Transfer 6th Edition. doi:10.1016/j.applthermaleng.2011.03.022.

Lutron Electronics Co. Inc., (2014). Daylight sensor: design and application guide. Retrieved from http://www.lutron.com/en-US/pages/default.aspx.

Indraganti, M., and Boussaa, D. (2017). A method to estimate the heating and cooling degree-days for different climatic zones of Saudi Arabia. *Building Services Engineering Research and Technology*, *38*(3), 327–350. https://doi.org/10.1177/0143624416681383.

International Code Council (ICC). (2018). *International Green Construction Code (IgCC)*.

ISO 13789. (2006). *Thermal performance of buildings – Transmission and ventilation heat transfer coefficients – Calculation method*.

Jakubiec, J. A., and Reinhart, C. F. (2012). The 'adaptive zone'-A concept for assessing discomfort glare throughout daylit spaces. *Lighting Research and Technology*, *44*(2), 149–170. https://doi.org/10.1177/1477153511420097.

Janak, M. (1997). Coupling Building Energy and Lighting Simulation. *In: 5th International IBPSA Conference*. 8–10 September 1997, Prague, vol. II, pp. 313–319.

Jokisalo, J., and Kurnitski, J. (2007). Performance of EN ISO 13790 utilisation factor heat demand calculation method in a cold climate. *Energy and Buildings*, *39*(2), 236–247. https://doi.org/10.1016/j.enbuild.2006.06.007.

Kim, J. J., Papamichael, K. M., Selkowitz, S., and Spitzglas, M. (1986). Determining Daylight Illuminance in Rooms Having Complex Fenestration Systems. *Proceedings of the International Daylighting Conference*. November 5-7, Long Beach, CA.

Kimball, H. H., and Hand, I. F. (1922). Daylight Illumination on Horizontal, Vertical, and Sloping. *Monthly Weather Review*, *50*(12), 615–628.

Klammt, S., Neyer, A., and Müller, H. F. O. (2012). Redirection of sunlight by microstructured components - Simulation, fabrication and experimental results. *Solar Energy*, *86*(5), 1660–1666. https://doi.org/10.1016/j.solener.2012.02.034.

Klein, S.A. (1976). A design procedure for solar heating systems. Doctoral Dissertation, University of Wisconsin–Madison, Madison, WI.

Klein, S.A., Beckman, W.A., Mitchell, J.W., Duffie, J.A., Duffie, N.A., Freeman, T.L., et al. (2018). *TRNSYS 18: A Transient System Simulation Program. Updates in Version 2017*. Solar Energy Laboratory, University of Wisconsin-Madison.

Klein, S.A., Beckman, W.A., Mitchell, J.W., Duffie, J.A., Duffie, N.A., Freeman, T.L., et al. (2017). *TRNSYS 17 a transient system simulation program*. Solar Energy Laboratory, University of Wisconsin-Madison.

Knight, J. C., and Cornell, A. A. (1958). Degree-days and fuel consumption for office buildings. *J. Inst. Heating Ventilating Engineers*, 26, 309–328.

Knuth, D. E. (1998). The art of computer programming: sorting and searching. Pearson Education, vol. 3.

Konis, K. (2013). Evaluating daylighting effectiveness and occupant visual comfort in a side-lit open-plan office building in San Francisco, California. *Building and Environment*, *59*, 662–677. https://doi.org/10.1016/j.buildenv.2012.09.017.

Kota, S., and Haberl, J. S. (2009). Historical Survey of Daylighting Calculations Methods and Their Use in Energy Performance Simulations. *Proceedings of the 9th international conference for enhanced building operation.* 2009: Austin, Texas (USA). p. 1–9.

Krese, G., Prek, M., and Butala, V. (2011). Incorporation of latent loads into the cooling degree days concept. *Energy and Buildings*, *43*(7), 1757–1764. https://doi.org/10.1016/j.enbuild.2011.03.042.

Krese, G., Prek, M., and Butala, V. (2012). Analysis of building electric energy consumption data using an improved cooling degree day method. Strojniski Vestnik – Journal of Mechanical Engineering, 58(2), 107–114. https://doi.org/10.5545/sv-jme.2011.160.

Lawrence Berkeley National Laboratory (LBNL) and James J. Hirsch & Associates (JJH). 1998. Overview of DOE-2.2. www.doe2.com/download/Docs/22 Oview.pdf.

Lawrence Berkeley National Laboratory (LBNL). (2019). Windows & Daylighting. Building Technology & Urban Systems Division, Energy Technologies Area, Lawrence Berkeley National Laboratory, University of California. Available at: windows.lbl.gov/software. Retrieved on July 29, 2020.

Lee, C. C., and Chiu, Y. B. (2011). Electricity demand elasticities and temperature: Evidence from panel smooth transition regression with instrumental variable approach. Energy Economics, 33(5), 896-902.

Lee, K., Baek, H. J., and Cho, C. H. (2014). The estimation of base temperature for heating and cooling degree-days for South Korea. *Journal of Applied Meteorology and Climatology*, *53*(2), 300–309. https://doi.org/10.1175/JAMC-D-13-0220.1.

Li, D. H. W., and Lam, J. C. (2003). An investigation of daylighting performance and energy saving in a daylit corridor. *Energy and Buildings*, *35*(4), 365–373. https://doi.org/10.1016/S0378-7788(02)00107-X.

Liu, B., Rosenberg, M., and Athalye, R. (2018). National Impact of ANSI/ASHRAE/IES Standard 90.1-2016. *2018 Building Performance Analysis Conference and SimBuild Co-Organized by ASHRAE and IBPSA-USA*. Chicago, IL. September 26-28, 2018.

Love, J. A., and Navvab, M. (1994). The Vertical-to-Horizontal Illuminance Ratio: A New Indicator of Daylighting Performance. *J Illum Eng Soc*, *23*, 50–61.

Luckiesh, M., and Guth, S. (1949). Brightness invisual field at borderline between comfort and discomfort (BCD). *J Illum Eng Soc*, *44*, 650–667.

Lyman Ott, R., and Longnecker, M. (2001). *An Introduction to Statistical Methods and Data Analysis*. Cengage Learning, Belmont, CA.

Makhmalbaf, A., Srivastava, V., and Wang, N. (2013). Simulation-based weather normalization approach to study the impact of weather on energy use of buildings in the U.S. *Proceedings of BS 2013: 13th Conference of the International Building Performance Simulation Association*, Le Bourget Du Lac, France, 1436–1444.

Malkawi, A., and Augenbroe, G. (2003). *Advanced Building Simulation*. Spon Press, New York.

Mardaljevic, J. (2000). *Daylight simulation: validation, sky models and daylight coefficients*. Ph.D. Thesis, De Montfort University, Leicester, UK.

Markus, T. A., Clarke, J. A., Morris, E. N., and Collins, T. G. (1984). The influence of climate on housing: A simple technique for the assessment of dynamic energy behaviour. *Energy and Buildings*, *7*(3), 243–259. https://doi.org/10.1016/0378-7788(84)90029-X.

Markus, Thomas A. (1982). Development of a cold climate severity index. *Energy and Buildings*, *4*(4), 277–283. https://doi.org/10.1016/0378-7788(82)90057-3.

Marsh, A. (2003). ECOTECT and EnergyPlus. *Building Energy Simulation User News*, *24*(6), 2–3.

McNeil, A., and Burrell, G. (2016). Applicability of DGP and DGI for evaluating glare in a brightly daylit space. *ASHRAE and IBPSA-USA SimBuild*. Salt Lake City, UT.

Mitalas, G., Stephenson, D. (1962). *Absorption and transmission of thermal radiation by single and double glazed windows*. Research paper no. 173, National Research Council of Canada, Ottawa.

Mitchell, R., Kohler, C., Curcija, D., Zhu, L., Vidanovic, S., Czarnecki, S., Arasteh, D., Carmody. J., and Huizenga, C. (2017). *THERM 7 / WINDOW 7 NFRC Simulation Manual*. National Fenestration Rating Council, Inc.

Modest, M. F. (1982). A general model for the calculation of daylighting in interior spaces. *Energy and Buildings*, *5*(1), 69–79. https://doi.org/10.1016/0378-7788(82)90030-5.

Moore, F. (1985). *Concepts and Practice of Architectural Daylighting*. New York: Van Nostrans Reinhold.

Moral-Carcedo, J., and Vicéns-Otero, J. (2005). Modelling the non-linear response of Spanish electricity demand to temperature variations. Energy economics, 27(3), 477-494.

Mourshed, M. (2012). Relationship between annual mean temperature and degree-days. *Energy and Buildings*, *54*, 418–425. https://doi.org/10.1016/j.enbuild.2012.07.024.

Muncey, R. W. R. (1979). *Heat transfer calculations for buildings*. Applied Science, London.

Nabil, A., and Mardaljevic, J. (2005). Useful daylight illuminance: a new paradigm for assessing daylight in buildings. *Lighting Research and Technology*, *37*(1), 41–59. https://doi.org/10.1191/1365782805li128oa.

Navvab, M., and Altland, G. (1997). Application of CIE glare index for daylighting evaluation. *Journal of the Illuminating Engineering Society*, *26*(2), 115–128. https://doi.org/10.1080/00994480.1997.10748196.

Nazzal, A. A. (2000). A New Daylight Glare Evaluation Method. *Journal of Light & Visual Environment*, *24*(2), 19–27. https://doi.org/10.2150/jlve.24.2_19.

Nelson, H. T. (2012). Lost opportunities: Modeling commercial building energy code adoption in the United States. *Energy Policy*, *49*, 182–191. https://doi.org/10.1016/j.enpol.2012.05.033.

Oh, S., and Haberl, J. S. (2016). Origins of analysis methods used to design high-performance commercial buildings: Solar energy analysis. *Science and Technology for the Built Environment*, *22*(1), 87–106. https://doi.org/10.1080/23744731.2015.1090277.

OrtizBeviá, M. J., Sánchez-López, G., Alvarez-Garcìa, F. J., and RuizdeElvira, A. (2012). Evolution of heating and cooling degree-days in Spain: Trends and interannual variability. *Global and Planetary Change*, *92–93*, 236–247. https://doi.org/10.1016/j.gloplacha.2012.05.023.

Padiyath, R. (2013). *Daylight redirecting window films*. (No. LOT-2829). 3M Company St. Pauk, MN.

Padiyath, R., Marttila, C. S., and Al., E. (2013). *Light redirecting constructions*. St. Pauk, MN, US.

Papakostas, K., and Kyriakis, N. (2005). Heating and cooling degree-hours for Athens and Thessaloniki, Greece. *Renewable Energy*, *30*(12), 1873–1880. https://doi.org/10.1016/j.renene.2004.12.002.

Pedersen, C. O., Fisher, D. E., and Liesen, R. J. (1997). Development of a heat balance procedure for calculating cooling loads. *ASHRAE Transactions*, *103*(pt 2), 459–468.

Perez, R., Ineichen, P., Seals, R., Michalsky, J., Stewart, R. (1990). Modeling Daylight Availability and Irradiance Components from Direct and Global Irradiance. *Solar Energy*, *44*(5), pp. 271-289.

Perez, R., Seals, R., and Michalsky, J. (1993). All-weather model for sky luminance distribution-Preliminary configuration and validation. *Solar Energy*, *50*(3), 235–245. https://doi.org/10.1016/0038-092X(93)90017-I.

Petherbridge, P., and Hopkinson, R. G. (1950). Discomfort glare and the lighting of buildings. *Trans Illum Eng Soc*, *15*, 29–79.

Raji, B., Tenpierik, M. J., and van den Dobbelsteen, A. (2015). An assessment of energy-saving solutions for the envelope design of high-rise buildings in temperate climates: A case study in the Netherlands. *Energy and Buildings*, 124, 210–221 https://doi.org/10.1016/j.enbuild.2015.10.049.

Reinhart, C. F., and Herkel, S. (2000a). The Simulation of annual daylight illuminance distributions-a state-of-the-art comparison of six RADIANCE-based methods. *Energy and Buildings*, *32*(2), 167–187. https://doi.org/10.1016/S0378-7788(00)00042-6.

Reinhart, C., and Fitz, A. (2006). Findings from a survey on the current use of daylight simulations in building design. *Energy and Buildings*, *38*(7), 824–835. https://doi.org/10.1016/j.enbuild.2006.03.012.

Rogers, Z. (2006). *Daylighting metric development using daylight autonomy calculations in the sensor placement optimization tool*. Architectural Energy Corporation, Boulder, CO.

Rosenberg, M., and Hart, R. (2016). *Developing Performance Cost Index Targets for ASHRAE Standard 90.1 Appendix G – Performance Rating Method*. PNNL-25202.

Rosenberg, M. I., and Eley, C. (2013). A Stable Whole Building Performance Method for Standard 90.1. *ASHRAE Journal*, *55*(5), 33–45.

Roulet, C. A. (2002). prEN-ISO 13790 - A simplified method to assess the annual heating energy use in buildings. *ASHRAE Transactions*, *108*, Part 2, 911–918.

Ruck, N., Aydinli, S., and Al., E. (2000). *Daylight in buildings: a source book on daylighting systems and components*. Lawrence Berkeley National Laboratory, Berkeley, USA. LBNL-47493.

Sailor, D. J. (2001). Relating residential and commercial sector electricity loads to climate - Evaluating state level sensitivities and vulnerabilities. *Energy*, *26*(7), 645–657. https://doi.org/10.1016/S0360-5442(01)00023-8.

Sailor, D. J., and Muñoz, J. R. (1997). Sensitivity of electricity and natural gas consumption to climate in the U.S.A. - Methodology and results for eight states. *Energy*, *22*(10), 987–998. https://doi.org/10.1016/S0360-5442(97)00034-0.

Santamouris, M. (2004). Energy performance of residential buildings: A practical guide for energy rating and efficiency. In Energy Performance of Residential Buildings: A Practical

Guide for Energy Rating and Efficiency. Earthscan, UK. https://doi.org/10.4324/9781849776059.

Schoenau, G. J., and Kehrig, R. A. (1990). Method for calculating degree-days to any base temperature. *Energy and Buildings*, *14*(4), 299–302. https://doi.org/10.1016/0378-7788(90)90092-W.

Selkowitz, S., Kim, J. J., Navvab, M., and Winkelmann, F. (1982). The DOE-2 and SUPERLITE daylighting programs. *Proceeding of the 7th National Passive Solar Conference*. Knoxville, TX.

Shanmuga Priya Selvanathan, and Joanna Migdalska. (2015). Cooling Degree Day Analysis as a Climate Impact. *International Journal of Advances in Science Engineering and Technology*, (4), 43–51.

Shen, H., and Tzempelikos, A. (2013). Sensitivity analysis on daylighting and energy performance of perimeter offices with automated shading. *Building and Environment*, *59*, 303–314. https://doi.org/10.1016/j.buildenv.2012.08.028.

Shin, M., and Do, S. L. (2016). Prediction of cooling energy use in buildings using an enthalpy-based cooling degree days method in a hot and humid climate. *Energy and Buildings*, *110*, 57–70. https://doi.org/10.1016/j.enbuild.2015.10.035.

Steadman, R. G. (1978). The determination and metrication of degree days. *ASHRAE Journal*, *20*(12), 38.

Strachey, R. (1878). Paper on the computation and quantity of heat in excess of a fixed base temperature received at any place during the course of the year to supply a standard comparison with the progress of vegetation. *Quarterly Weather Report Appendix II*.

Stram, D. O., and Fels, M. F. (1986). The applicability of PRISM to electric heating and cooling. *Energy and Buildings*, *9*(1–2), 101–110. https://doi.org/10.1016/0378-7788(86)90011-3.

Suk, J. Y., Schiler, M., and Kensek, K. (2013). Development of new daylight glare analysis methodology using absolute glare factor and relative glare factor. *Energy and Buildings*, *64*, 113–122. https://doi.org/10.1016/j.enbuild.2013.04.020.

Suk, J. Y., Schiler, M., and Kensek, K. (2017). Investigation of existing discomfort glare indices using human subject study data. *Building and Environment*, *113*, 121–130. https://doi.org/10.1016/j.buildenv.2016.09.018.

The Meteorological Office. (1928). *The Weekly Weather Report 26th Feb*, 1928 (London: History Majesty's Stationery Office).

Thom, H. C. S. (1954a). Normal degree days below any base. *Monthly Weather Review*, *82*(5), 111–115. https://doi.org/10.1175/1520-0493(1954)082<0111:nddbab>2.0.co;2.

Thom, H. C. S. (1954b). The rational relationship between heating degree days and temperature. *Monthly Weather Review*, *82*(1), 1–6. https://doi.org/10.1175/1520-0493(1954)082<0001:trrbhd>2.0.co;2.

Thom, H. C. S. (1966). Normal degree days above any base by the universal truncation coefficient. *Monthly Weather Review*, *94*(7), 461–465. https://doi.org/10.1175/1520-0493(1966)094<0461:nddaab>2.3.co;2.

Trane. (2010). *TRACE 700 Building Energy and Economic Analysis User's Manual. Version 6.2*.

Tregenza, P. R., and Waters, I. M. (1983). Daylight coefficients. *Lighting Research and Technology*, *15*(2), 65–71. https://doi.org/10.1177/096032718301500201.

Trotter, A. P. (1911). *Illumination, Its Distribution and Measurements*. London: Macmillan.

Tsangrassoulis, A., and Bourdakis, V. (2003). Comparison of radiosity and ray-tracing techniques with a practical design procedure for the prediction of daylight levels in atria. *Renewable Energy*, *28*(13), 2157–2162. https://doi.org/10.1016/S0960-1481(03)00078-8.

Athalye, R., Halverson, M., Rosenberg, M., Liu, B., Zhang, J., Hart, R., Mendon, V., Goel, S., Chen, Y., Xie, Y., Zhao, M. (2017). Energy Savings Analysis: ANSI/ASHRAE/IES Standard 90.1-2016. *U.S. Department of Energy, Office of Energy Efficiency and Renewable Energy, Building Technologies Office*.

Ubbelohde, S., and Humann, C. (1998). Comparative Evaluation of Four Daylighting Software Programs. ACEEE Summer Study on Energy Efficiency in Buildings Proceedings, American Council for an Energy-Efficient Economy.

University of Illinois, University of California, Lawrence Berkeley National Laboratory. (2016). EnergyPlus Engineering Reference The Reference to EnergyPlus Calculations. US Department of Energy, Washington, DC.

United States Environmental Protection Agency (EPA). (2009). National Action Plan for Energy Efficiency. *Energy Efficiency Program Administrators and Building Energy Codes*.

U.S. Department of Energy. Building Energy Codes Program. Retrieved from: https://www.energycodes.gov/development/commercial/prototype_models. (accessed November 2018).

U.S. Department of Energy. (2015). *EnergyPlus Engineering Reference: The Reference to EnergyPlus Calculations*. US Department of Energy, (c), 1–847.

Walsh, J. W. T. (1951). The early years of Illuminating engineering in Great Britain. *Transactions of the Illuminating Engineering Society*, *15*(3), 49–60.

Wang, N., Makhmalbaf, A., Srivastava, V., and Hathaway, J. E. (2017). Simulation-based coefficients for adjusting climate impact on energy consumption of commercial buildings. *Building Simulation*, *10*(3), 309–322. https://doi.org/10.1007/s12273-016-0332-1.

Ward, G. J. (1989). The RADIANCE Lighting Simulation and Rendering System. *21st Annual Conference on Computer Graphics and Interactive Techniques*, 459–472. https://doi.org/10.1145/192161.192286.

Ward, G. J., and Rubinstein, F. M. (1988). A new technique for computer simulation of illuminated spaces. Journal of the Illuminating Engineering Society, 1, 80–91.

Whitted, T. (1979). An improved illumination model for shaded display. *ACM SIGGRAPH Computer Graphics*, *13*(2), 14. https://doi.org/10.1145/965103.807419.

Wienold, J. (2009). Dynamic daylight glare evaluation. *Eleventh International IBPSA Conference: Building Simulation*, 944–951. https://doi.org/citeulike-article-id:11069372.

Wienold, J., and Christoffersen, J. (2006). Evaluation methods and development of a new glare prediction model for daylight environments with the use of CCD cameras. *Energy and Buildings*, *38*(Special Issue on Daylighting Buildings), 743–757.

Williams, A., Atkinson, B., Garbesi, K., and Rubinstein, F. (2011). *A Meta-Analysis of Energy Savings from Lighting Controls in Commercial Buildings*. LBNL-5095E.

Willmott, A. J., and Heckbert, P. S. (1997). *An Empirical Comparison of Radiosity Algorithms*. Technical Report CMU-CS-97-115; Carnegie Mellon University: Pittsburgh, PA, USA, 1997; pp. 7–10.

Wilcox, S., and Marion, W. (2008). *Users Manual for TMY3 Data Sets*. Technical Report NREL/TP-581-43156.

Wilson, W. T. (1941). An outline of the thermodynamics of snow melt. *Proceedings of the 9th Annual Western Interstate Snow Survey Conference. American Geophysical Union, Transactions*, Part I-B. Sacramento, California. 182–195.

Winkelmann, F. C. (1983). *Daylighting calculations in DOE-2*. LBL-11353.

Winkelmann, F. C., and Selkowitz, S. (1985). Daylighting simulation in the DOE-2 building energy analysis program. *Energy and Buildings*, *8*(4), 271–286.

Winkelmann, F.C., B.E. Birdsall, W.F. Buhl, K.L. Ellington, A.E. Erdem, J.J. Hirsch, and S. Gates. (1993). *DOE-2 supplement version 2.1E*. Report LBL-34947, Lawrence Berkeley Laboratory, Berkeley, CA.

Wortman, D. N., and Christensen, C. B. (1985). Variable-base degree-day correction factors for energy savings calculations. *ASHRAE Transactions*, *91*(pt 1B), 934–944. Retrieved from http://www.nrel.gov/docs/legosti/old/2435.pdf.

APPENDIX A

This appendix describes the process of developing the regression models and calculating the coefficient of determination of the models. The appendix consists of three section, describing the procedure for simple linear regression, multiple regression models, and the coefficient of determination of the models.

A.1. Developing Simple Linear Regression Model

The simple linear regression model can be formatted as shown in equation A.1.

$$y = \beta_0 + \beta_1 x_1 + \varepsilon \quad \text{A.1}$$

where *y* is the dependent variable, x_1 is the independent variable, β_0 is the y-intercept, β_1 is the slope, and ε is the random error term

β_0 and β_1 in equation A.1 are the population properties. The least-squares method estimates $\hat{\beta}_0$ and $\hat{\beta}_1$ minimizing the total squared prediction error. Lyman Ott and Longnecker (2001) has provided detailed information that yields equations A.2 and A.3.

$$\hat{\beta}_1 = \frac{\sum_i (x_i - \bar{x})(y_i - \bar{y})}{\sum_i (x_i - \bar{x})^2} \quad \text{A.2}$$

$$\hat{\beta}_0 = \bar{y} - \hat{\beta}_0 \bar{x} \quad \text{A.3}$$

where $\bar{x}$ and $\bar{y}$ in equations A.2 and A.3 are average of the independent and dependent variables, respectively.

A.2. Developing Multiple Regression Model

The multiple regression model, relating a dependent variable y to a set of independent variables can be written as shown in A.4.

$$y = \beta_0 + \beta_1 x_1 + \beta_2 x_2 + \cdots + \beta_k x_k + \varepsilon \quad \text{A.4}$$

where *y* is the dependent variable, $x_1, \ldots, x_k$ are the independent variables, β_0 is the y-intercept, $\beta_1, \beta_2, \ldots, \beta_k$ are the partial slopes, and ε is the random error term

As discussed in detail by Lyman Ott and Longnecker (2001), the following procedure using matrix notation can be used to calculate the least-squares estimates $\hat{\beta}_0, \hat{\beta}_1, \ldots, \hat{\beta}_k$ of the intercept and partial slopes:

Lets define the **Y**, **X**, and $\widehat{\boldsymbol{\beta}}$ matrices as:

$$\mathbf{Y} = \begin{bmatrix} y_1 \\ y_2 \\ \vdots \\ y_n \end{bmatrix}, \mathbf{X} = \begin{bmatrix} 1 & x_{11} & \ldots & x_{1k} \\ 1 & x_{21} & \ldots & x_{1k} \\ \vdots & \vdots & \ddots & \vdots \\ 1 & x_{n1} & \ldots & x_{nk} \end{bmatrix}, \widehat{\boldsymbol{\beta}} = \begin{bmatrix} \hat{\beta}_0 \\ \hat{\beta}_1 \\ \vdots \\ \hat{\beta}_k \end{bmatrix}$$

The desired vector of coefficients, $\widehat{\boldsymbol{\beta}}$, can be calculated using A.5[14]

$$\widehat{\boldsymbol{\beta}} = (\mathbf{X}^{\mathrm{T}}\mathbf{X})^{-1}\mathbf{X}^{\mathrm{T}}\mathbf{Y} \quad \text{A.5}$$

[14] Note that the matrix $\mathbf{X}^{\mathrm{T}}\mathbf{X}$ has an inverse as long as no x_i is perfectly collinear with other *xs*.

A.3. Calculating the Coefficient of Determination

As discussed in detail by Lyman Ott and Longnecker (2001), the coefficient of determination, $\boldsymbol{R^2_{y.x}}$ in simple linear regression models and $\boldsymbol{R^2_{y.x_1 \ldots x_k}}$ in multiple regression models can be calculated using A.6.

$$\boldsymbol{R^2 = 1 - \frac{\sum(y_i - \hat{y}_i)^2}{\sum(y_i - \bar{y})^2}} \qquad \text{A.6}$$

where $\boldsymbol{\hat{y}_i}$ is the *i*th predicted value and $\boldsymbol{\bar{y}}$ is the mean value of the dependent parameter.

APPENDIX B

This appendix includes the master list prepared for the simulations.

Table 15: Weather Files Master List for the Simulations

Number	Weather File Name	Climate Zone Number	Climate Subtype
1	USA_FL_Key.West.Intl.AP.722010_TMY3	1	A
2	USA_FL_Key.West.NAS.722015_TMY3	1	A
3	USA_FL_Marathon.AP.722016_TMY3	1	A
4	USA_FL_Miami.Intl.AP.722020_TMY3	1	A
5	USA_FL_Fort.Lauderdale.Intl.AP.722025_TMY3	1	A
6	USA_FL_Homestead.AFB.722026_TMY3	1	A
7	USA_FL_Fort.Myers-Page.Field.722106_TMY3	1	A
8	USA_AZ_Yuma.MCAS.699604_TMY3	1	B
9	USA_AZ_Phoenix-Sky.Harbor.Intl.AP.722780_TMY3	1	B
10	USA_AZ_Yuma.Intl.AP.722800_TMY3	1	B
11	USA_CA_Palm.Springs.Intl.AP.722868_TMY3	1	B
12	USA_CA_Blythe-Riverside.County.AP.747188_TMY3	1	B
13	USA_FL_Miami-Kendall-Tamiami.Executive.AP.722029_TMY3	2	A
14	USA_FL_West.Palm.Beach.Intl.AP.722030_TMY3	2	A
15	USA_FL_Naples.Muni.AP.722038_TMY3	2	A
16	USA_FL_Melbourne.Rgnl.AP.722040_TMY3	2	A
17	USA_FL_Vero.Beach.Muni.AP.722045_TMY3	2	A
18	USA_FL_Orlando.Intl.AP.722050_TMY3	2	A
19	USA_FL_Orlando.Executive.AP.722053_TMY3	2	A
20	USA_FL_Ocala.Muni.AWOS.722055_TMY3	2	A
21	USA_FL_Daytona.Beach.Intl.AP.722056_TMY3	2	A
22	USA_FL_Orlando-Sanford.AP.722057_TMY3	2	A
23	USA_FL_Jacksonville.Intl.AP.722060_TMY3	2	A
24	USA_FL_Jacksonville.NAS.722065_TMY3	2	A
25	USA_FL_Mayport.NS.722066_TMY3	2	A
26	USA_FL_Jacksonville-Craig.Field.722068_TMY3	2	A
27	USA_GA_Savannah.Intl.AP.722070_TMY3	2	A
28	USA_FL_Southwest.Florida.Intl.AP.722108_TMY3	2	A
29	USA_FL_Tampa.Intl.AP.722110_TMY3	2	A
30	USA_FL_Sarasota-Bradenton.Intl.AP.722115_TMY3	2	A
31	USA_FL_St.Petersburg-Clearwater.Intl.AP.722116_TMY3	2	A
32	USA_GA_Brunswick-Malcolm.McKinnon.AP.722137_TMY3	2	A
33	USA_FL_Tallahassee.Rgnl.AP.722140_TMY3	2	A
34	USA_FL_Gainesville.Rgnl.AP.722146_TMY3	2	A
35	USA_GA_Valdosta.Rgnl.AP.722166_TMY3	2	A
36	USA_FL_Pensacola.Rgnl.AP.722223_TMY3	2	A
37	USA_FL_Pensacola-Forest.Sherman.NAS.722225_TMY3	2	A
38	USA_AL_Mobile-Rgnl.AP.722230_TMY3	2	A
39	USA_FL_Panama.City-Bay.County.AP.722245_TMY3	2	A
40	USA_LA_New.Orleans.Intl.AP.722310_TMY3	2	A
41	USA_LA_New.Orleans-Lakefront.AP.722315_TMY3	2	A
42	USA_LA_New.Orleans-Alvin.Callender.Field.722316_TMY3	2	A
43	USA_LA_Baton.Rouge-Ryan.AP.722317_TMY3	2	A
44	USA_LA_Patterson.Mem.AP.722329_TMY3	2	A
45	USA_LA_Lake.Charles.Rgnl.AP.722400_TMY3	2	A
46	USA_LA_Lafayette.RgnlAP.722405_TMY3	2	A
47	USA_TX_Port.Arthur-Jefferson.Co.AP.722410_TMY3	2	A
48	USA_TX_Galveston.722420_TMY3	2	A
49	USA_TX_Houston-D.W.Hooks.AP.722429_TMY3	2	A
50	USA_TX_Houston-Bush.Intercontinental.AP.722430_TMY3	2	A

Table 15: (Continued)

Number	Weather File Name	Climate Zone Number	Climate Subtype
51	USA_TX_Houston-William.P.Hobby.AP.722435_TMY3	2	A
52	USA_TX_Houston-Ellington.AFB.722436_TMY3	2	A
53	USA_TX_College.Station-Easterwood.Field.722445_TMY3	2	A
54	USA_TX_Brownsville-South.Padre.Island.AP.722500_TMY3	2	A
55	USA_TX_Harlingen-Valley.Intl.AP.722505_TMY3	2	A
56	USA_TX_McAllen-Miller.Intl.AP.722506_TMY3	2	A
57	USA_TX_Corpus.Christi.Intl.AP.722510_TMY3	2	A
58	USA_TX_Corpus.Christi.NAS.722515_TMY3	2	A
59	USA_TX_Kingsville.722516_TMY3	2	A
60	USA_TX_Alice.Intl.AP.722517_TMY3	2	A
61	USA_TX_San.Antonio-Stinson.AP.722523_TMY3	2	A
62	USA_TX_Rockport-Aransas.Co.AP.722524_TMY3	2	A
63	USA_TX_San.Antonio.Intl.AP.722530_TMY3	2	A
64	USA_TX_San.Antonio-Kelly.AFB.722535_TMY3	2	A
65	USA_TX_Randolph.AFB.722536_TMY3	2	A
66	USA_TX_Austin-Mueller.Muni.AP.722540_TMY3	2	A
67	USA_TX_Austin-Camp.Mabry.722544_TMY3	2	A
68	USA_TX_Georgetown.AWOS.722547_TMY3	2	A
69	USA_TX_Victoria.Rgnl.AP.722550_TMY3	2	A
70	USA_TX_Palacios.Muni.AP.722555_TMY3	2	A
71	USA_TX_Waco.Rgnl.AP.722560_TMY3	2	A
72	USA_TX_McGregor.AWOS.722563_TMY3	2	A
73	USA_TX_Killeen.Muni.AWOS.722575_TMY3	2	A
74	USA_TX_Killeen-Fort.Hood.Rgnl.AP.722576_TMY3	2	A
75	USA_TX_Draughon-Miller.Central.Texas.AP.722577_TMY3	2	A
76	USA_TX_Dallas-Love.Field.722583_TMY3	2	A
77	USA_TX_Dallas-Fort.Worth.Intl.AP.722590_TMY3	2	A
78	USA_TX_Fort.Worth.NAS.722595_TMY3	2	A
79	USA_TX_Dallas-Redbird.AP.722599_TMY3	2	A
80	USA_LA_Alexandria-England.AFB.747540_TMY3	2	A
81	USA_MS_Biloxi-Keesler.AFB.747686_TMY3	2	A
82	USA_FL_Fort.Walton.Beach-Hurlburt.Field.747770_TMY3	2	A
83	USA_FL_MacDill.AFB.747880_TMY3	2	A
84	USA_FL_NASA.Shuttle.Landing.Facility.747946_TMY3	2	A
85	USA_GA_Albany-Dougherty.County.AP.722160_TMY3	3	A
86	USA_FL_Crestview-Bob.Sikes.AP.722215_TMY3	3	A
87	USA_FL_Whiting.Field.NAS.722226_TMY3	3	A
88	USA_LA_Fort.Polk.722390_TMY3	3	A
89	USA_TX_Lufkin-Angelina.Co.AP.722446_TMY3	3	A
90	USA_TX_Abilene-Dyess.AFB.690190_TMY3	2	B
91	USA_TX_Laredo.Intl.AP.722520_TMY3	2	B
92	USA_TX_Cotulla.AP.722526_TMY3	2	B
93	USA_TX_Hondo.Muni.AP.722533_TMY3	2	B
94	USA_TX_Del.Rio.722610_TMY3	2	B
95	USA_TX_Del.Rio-Laughlin.AFB.722615_TMY3	2	B
96	USA_TX_Wink-Winkler.County.AP.722656_TMY3	2	B
97	USA_AZ_Tucson.Intl.AP.722740_TMY3	2	B
98	USA_AZ_Davis-Monthan.AFB.722745_TMY3	2	B
99	USA_AZ_Safford.AWOS.722747_TMY3	2	B
100	USA_AZ_Casa.Grande.AWOS.722748_TMY3	2	B

Table 15: (Continued)

Number	Weather File Name	Climate Zone Number	Climate Subtype
101	USA_AZ_Luke.AFB.722785_TMY3	2	B
102	USA_CA_Barstow.Daggett.AP.723815_TMY3	2	B
103	USA_NV_Las.Vegas-McCarran.Intl.AP.723860_TMY3	2	B
104	USA_NV_Nellis.AFB.723865_TMY3	2	B
105	USA_CA_Imperial.County.AP.747185_TMY3	2	B
106	USA_CA_Palm.Springs-Thermal.AP.747187_TMY3	2	B
107	USA_SC_Charleston.Intl.AP.722080_TMY3	3	A
108	USA_SC_Beaufort.MCAS.722085_TMY3	3	A
109	USA_GA_Macon-Middle.Georgia.Rgnl.AP.722170_TMY3	3	A
110	USA_GA_Warner.Robins.AFB.722175_TMY3	3	A
111	USA_GA_Augusta-Bush-Field.722180_TMY3	3	A
112	USA_GA_Atlanta-Hartsfield-Jackson.Intl.AP.722190_TMY3	3	A
113	USA_GA_Fulton.County.AP.722195_TMY3	3	A
114	USA_GA_Dekalb.Peachtree.AP.722196_TMY3	3	A
115	USA_FL_Valparaiso-Elgin.AFB.722210_TMY3	3	A
116	USA_GA_Fort.Benning-Lawson.Field.722250_TMY3	3	A
117	USA_GA_Columbus.Metro.AP.722255_TMY3	3	A
118	USA_AL_Montgomery-Dannelly.Field.722260_TMY3	3	A
119	USA_AL_Maxwell.AFB.722265_TMY3	3	A
120	USA_AL_Dothan.Muni.AP.722268_TMY3	3	A
121	USA_AL_Fort.Rucker-Cairns.Field.722269_TMY3	3	A
122	USA_AL_Birmingham.Muni.AP.722280_TMY3	3	A
123	USA_AL_Auburn-Opelika.AP.722284_TMY3	3	A
124	USA_AL_Gadsen.Muni.AWOS.722285_TMY3	3	A
125	USA_AL_Tuscaloosa.Muni.AP.722286_TMY3	3	A
126	USA_AL_Anniston.Metro.AP.722287_TMY3	3	A
127	USA_MS_Meridian-Key.Field.722340_TMY3	3	A
128	USA_MS_Meridian.NAS.722345_TMY3	3	A
129	USA_MS_Hattiesburg-Laurel.AP.722348_TMY3	3	A
130	USA_MS_Jackson.Intl.AP.722350_TMY3	3	A
131	USA_MS_Natchez-Hardy.Anders.Field.722357_TMY3	3	A
132	USA_MS_McComb-Pike.Co.AP.722358_TMY3	3	A
133	USA_MS_Greenwood-Leflore.AP.722359_TMY3	3	A
134	USA_TX_Longview-Gregg.County.AP.722470_TMY3	3	A
135	USA_LA_Shreveport.Rgnl.AP.722480_TMY3	3	A
136	USA_LA_Shreveport.Downtown.722484_TMY3	3	A
137	USA_LA_Barksdale.AFB.722485_TMY3	3	A
138	USA_LA_Monroe.Rgnl.AP.722486_TMY3	3	A
139	USA_LA_Alexandria-Esler.Rgnl.AP.722487_TMY3	3	A
140	USA_TX_Nacogdoches.AWOS.722499_TMY3	3	A
141	USA_TX_Cox.Field.722587_TMY3	3	A
142	USA_TX_Fort.Worth-Alliance.AP.722594_TMY3	3	A
143	USA_TX_Fort.Worth-Meacham.AP.722596_TMY3	3	A
144	USA_TX_Lubbock.Intl.AP.722670_TMY3	3	A
145	USA_NC_Wilmington.Intl.AP.723013_TMY3	3	A
146	USA_NC_Fayetteville-Pope.AFB.723030_TMY3	3	A
147	USA_NC_Fayetteville.Muni.AP.723035_TMY3	3	A
148	USA_NC_Cape.Hatteras.723040_TMY3	3	A
149	USA_NC_Raleigh-Durham.Intl.AP.723060_TMY3	3	A
150	USA_NC_Pitt.Greenville.AP.723065_TMY3	3	A

Table 15: (Continued)

Number	Weather File Name	Climate Zone Number	Climate Subtype
151	USA_NC_Goldsboro-Seymour.Johnson.AFB.723066_TMY3	3	A
152	USA_VA_Norfolk.Intl.AP.723080_TMY3	3	A
153	USA_VA_Norfolk.NAS.723085_TMY3	3	A
154	USA_VA_Newport.News.723086_TMY3	3	A
155	USA_NC_Cherry.Point.MCAS.723090_TMY3	3	A
156	USA_NC_New.Bern-Craven.County.Rgnl.AP.723095_TMY3	3	A
157	USA_NC_New.River.MCAS.723096_TMY3	3	A
158	USA_SC_Columbia.Metro.AP.723100_TMY3	3	A
159	USA_SC_Florence.Rgnl.AP.723106_TMY3	3	A
160	USA_GA_Athens-Ben.Epps.AP.723110_TMY3	3	A
161	USA_SC_Greer.Greenville-Spartanburg.AP.723120_TMY3	3	A
162	USA_SC_Anderson.County.AP.723125_TMY3	3	A
163	USA_NC_Charlotte-Douglas.Intl.AP.723140_TMY3	3	A
164	USA_NC_Southern.Pines-Moore.County.AP.723143_TMY3	3	A
165	USA_NC_Hickory.Rgnl.AP.723145_TMY3	3	A
166	USA_NC_Winston.Salem-Smith.Reynolds.AP.723193_TMY3	3	A
167	USA_GA_Rome-Richard.B.Russell.AP.723200_TMY3	3	A
168	USA_AL_Huntsville.Intl.AP-Jones.Field.723230_TMY3	3	A
169	USA_AL_Muscle.Shoals.Rgnl.AP.723235_TMY3	3	A
170	USA_TN_Chattanooga-Lovell.Field.AP.723240_TMY3	3	A
171	USA_MS_Columbus.AFB.723306_TMY3	3	A
172	USA_MS_Golden.Triangle.Rgnl.AWOS.723307_TMY3	3	A
173	USA_MS_Tupelo.Muni-C.D.Lemons.AP.723320_TMY3	3	A
174	USA_TN_Memphis.Intl.AP.723340_TMY3	3	A
175	USA_TN_Jackson-McKellar.Sipes.Rgnl.AP.723346_TMY3	3	A
176	USA_AR_Little.Rock-Adams.Field.723403_TMY3	3	A
177	USA_AR_Little.Rock.AFB.723405_TMY3	3	A
178	USA_AR_Stuttgart.AWOS.723416_TMY3	3	A
179	USA_AR_Pine.Bluff.AP.723417_TMY3	3	A
180	USA_AR_Texarkana-Webb.Field.723418_TMY3	3	A
181	USA_AR_El.Dorado-Goodwin.Field.723419_TMY3	3	A
182	USA_AR_Fort.Smith.Rgnl.AP.723440_TMY3	3	A
183	USA_MO_Joplin.Muni.AP.723495_TMY3	3	A
184	USA_TX_Wichita.Falls.Muni.AP.723510_TMY3	3	A
185	USA_OK_Altus.AFB.723520_TMY3	3	A
186	USA_OK_Hobart.Muni.AP.723525_TMY3	3	A
187	USA_OK_Oklahoma.City-Will.Rogers.World.AP.723530_TMY3	3	A
188	USA_OK_Fort.Sill-Henry.Post.AAF.723550_TMY3	3	A
189	USA_OK_McAlester.Rgnl.AP.723566_TMY3	3	A
190	USA_OK_Lawton.Muni.AP.723575_TMY3	3	A
191	USA_VA_Petersburg.Muni.AP.724014_TMY3	3	A
192	USA_MD_Patuxent.River.NAS.724040_TMY3	3	A
193	USA_VA_Danville.Rgnl.AP.724106_TMY3	3	A
194	USA_NC_Fort.Bragg-Simmons.AAF.746930_TMY3	3	A
195	USA_FL_Tyndall.AFB.747750_TMY3	3	A
196	USA_GA_Savannah-Hunter.AAF.747804_TMY3	3	A
197	USA_GA_Valdosta-Moody.AFB.747810_TMY3	3	A
198	USA_SC_Shaw.AFB.747900_TMY3	3	A
199	USA_SC_Myrtle.Beach.AFB.747910_TMY3	3	A
200	USA_TX_San.Angelo-Mathis.AP.722630_TMY3	3	B

Table 15: (Continued)

Number	Weather File Name	Climate Zone Number	Climate Subtype
201	USA_TX_Marfa.AP.722640_TMY3	3	B
202	USA_TX_Midland.Intl.AP.722650_TMY3	3	B
203	USA_TX_Abilene.Rgnl.AP.722660_TMY3	3	B
204	USA_NM_Roswell.Industrial.Air.Park.722680_TMY3	3	B
205	USA_NM_Carlsbad.Cavern.City.Air.Terminal.722687_TMY3	3	B
206	USA_TX_El.Paso.Intl.AP.722700_TMY3	3	B
207	USA_NM_Truth.or.Consequences.Muni.AP.722710_TMY3	3	B
208	USA_AZ_Douglas-Bisbee.Douglas.Intl.AP.722735_TMY3	3	B
209	USA_CA_March.AFB.722860_TMY3	3	B
210	USA_CA_Riverside.Muni.AP.722869_TMY3	3	B
211	USA_CA_Burbank-Glendale-Passadena.Bob.Hope.AP.722880_TMY3	3	B
212	USA_CA_San.Diego-Lindbergh.Field.722900_TMY3	3	B
213	USA_CA_San.Diego-Montgomery.Field.722903_TMY3	3	B
214	USA_CA_Chula.Vista-Brown.Field.Muni.AP.722904_TMY3	3	B
215	USA_CA_San.Diego-North.Island.NAS.722906_TMY3	3	B
216	USA_CA_Camp.Pendleton.MCAS.722926_TMY3	3	B
217	USA_CA_Carlsbad.722927_TMY3	3	B
218	USA_CA_San.Diego-Miramar.NAS.722930_TMY3	3	B
219	USA_CA_Los.Angeles.Intl.AP.722950_TMY3	3	B
220	USA_CA_Hawthorne-Jack.Northrop.Field.722956_TMY3	3	B
221	USA_CA_Long.Beach-Daugherty.Field.722970_TMY3	3	B
222	USA_CA_Fullerton.Muni.AP.722976_TMY3	3	B
223	USA_TX_Childress.Muni.AP.723604_TMY3	3	B
224	USA_AZ_Kingman.AWOS.723700_TMY3	3	B
225	USA_AZ_Page.Muni.AWOS.723710_TMY3	3	B
226	USA_CA_Edwards.AFB.723810_TMY3	3	B
227	USA_CA_Lancaster-Gen.Wm.Fox.Field.723816_TMY3	3	B
228	USA_CA_Bakersfield-Meadows.Field.723840_TMY3	3	B
229	USA_NV_Mercury-Desert.Rock.AP.723870_TMY3	3	B
230	USA_CA_Fresno.Air.Terminal.723890_TMY3	3	B
231	USA_CA_Porterville.AWOS.723895_TMY3	3	B
232	USA_CA_Visalia.Muni.AWOS.723896_TMY3	3	B
233	USA_UT_Saint.George.AWOS.724754_TMY3	3	B
234	USA_CA_Sacramento.Exec.AP.724830_TMY3	3	B
235	USA_CA_Beale.AFB.724837_TMY3	3	B
236	USA_CA_Sacramento.Metro.AP.724839_TMY3	3	B
237	USA_CA_Stockton.Metro.AP.724920_TMY3	3	B
238	USA_CA_Modesto.Muni.AP.724926_TMY3	3	B
239	USA_CA_Red.Bluff.Muni.AP.725910_TMY3	3	B
240	USA_CA_Redding.Muni.AP.725920_TMY3	3	B
241	USA_CA_Fairfield-Travis.AFB.745160_TMY3	3	B
242	USA_CA_Lemoore.NAS.747020_TMY3	3	B
243	USA_NM_Holloman.AFB.747320_TMY3	3	B
244	USA_CA_Sandberg.723830_TMY3	4	B
245	USA_CA_Lompoc.AWOS.722895_TMY3	3	C
246	USA_CA_San.Luis.Obispo.AP.722897_TMY3	3	C
247	USA_CA_Point.Mugu.NAS.723910_TMY3	3	C
248	USA_CA_Santa.Barbara.Muni.AP.723925_TMY3	3	C
249	USA_CA_Camarillo.AWOS.723926_TMY3	3	C
250	USA_CA_Santa.Maria.Public.AP.723940_TMY3	3	C

Table 15: (Continued)

Number	Weather File Name	Climate Zone Number	Climate Subtype
251	USA_CA_Paso.Robles.Muni.AP.723965_TMY3	3	C
252	USA_CA_Monterey.NAF.724915_TMY3	3	C
253	USA_CA_Salinas.Muni.AP.724917_TMY3	3	C
254	USA_CA_Livermore.Muni.AP.724927_TMY3	3	C
255	USA_CA_Oakland.Intl.AP.724930_TMY3	3	C
256	USA_CA_Hayward.Air.Terminal.724935_TMY3	3	C
257	USA_CA_San.Francisco.Intl.AP.724940_TMY3	3	C
258	USA_CA_San.Jose.Intl.AP.724945_TMY3	3	C
259	USA_CA_Napa.County.AP.724955_TMY3	3	C
260	USA_CA_Santa.Rosa.AWOS.724957_TMY3	3	C
261	USA_CA_Ukiah.Muni.AP.725905_TMY3	3	C
262	USA_CA_Mountain.View-Moffett.Field.NAS.745090_TMY3	3	C
263	USA_NC_Jacksonville.AWOS.723069_TMY3	3	A
264	USA_TN_Nashville.Intl.AP.723270_TMY3	3	A
265	USA_TN_Dyersburg.Muni.AP.723347_TMY3	3	A
266	USA_AR_Fayetteville-Drake.Field.723445_TMY3	3	A
267	USA_AR_Flippin.AWOS.723447_TMY3	3	A
268	USA_GA_Marietta-Dobbins.AFB.722270_TMY3	4	A
269	USA_NC_Asheville.Rgnl.AP.723150_TMY3	4	A
270	USA_NC_Greensboro-Piedmont.Triad.Intl.AP.723170_TMY3	4	A
271	USA_TN_Bristol-TriCities.Rgnl.AP.723183_TMY3	4	A
272	USA_TN_Knoxville-McGhee.Tyson.AP.723260_TMY3	4	A
273	USA_TN_Crossville.Mem.AP.723265_TMY3	4	A
274	USA_MO_Poplar.Bluff.AWOS.723300_TMY3	4	A
275	USA_AR_Walnut.Ridge.AWOS.723406_TMY3	4	A
276	USA_AR_Jonesboro.Muni.AP.723407_TMY3	4	A
277	USA_AR_Siloam.Spring.AWOS.723443_TMY3	4	A
278	USA_AR_Bentonville.AWOS.723444_TMY3	4	A
279	USA_AR_Harrison.AP.723446_TMY3	4	A
280	USA_AR_Batesville.AWOS.723448_TMY3	4	A
281	USA_AR_Rogers.AWOS.723449_TMY3	4	A
282	USA_MO_Cape.Girardeau.Muni.AP.723489_TMY3	4	A
283	USA_OK_Clinton.Sherman.AP.723526_TMY3	4	A
284	USA_OK_Gage.AP.723527_TMY3	4	A
285	USA_OK_Vance.AFB.723535_TMY3	4	A
286	USA_OK_Oklahoma.City-Tinker.AFB.723540_TMY3	4	A
287	USA_OK_Oklahoma.City-Wiley.Post.Field.723544_TMY3	4	A
288	USA_OK_Stillwater.Rgnl.AP.723545_TMY3	4	A
289	USA_OK_Ponca.City.Muni.AP.723546_TMY3	4	A
290	USA_OK_Tulsa.Intl.AP.723560_TMY3	4	A
291	USA_VA_Richmond.Intl.AP.724010_TMY3	4	A
292	USA_VA_Farmville.Muni.AP.724017_TMY3	4	A
293	USA_VA_Melfa-Accomack.County.AP.724026_TMY3	4	A
294	USA_VA_Sterling-Washington.Dulles.Intl.AP.724030_TMY3	4	A
295	USA_VA_Fredericksburg-Shannon.AP.724033_TMY3	4	A
296	USA_VA_Quantico.MCAS.724035_TMY3	4	A
297	USA_VA_Manassas.Muni.AWOS.724036_TMY3	4	A
298	USA_VA_Davison.AAF.724037_TMY3	4	A
299	USA_MD_Salisbury-Wicomico.County.Rgnl.AP.724045_TMY3	4	A
300	USA_VA_Arlington-Ronald.Reagan.Washington.Natl.AP.724050_TMY3	4	A

Table 15: (Continued)

Number	Weather File Name	Climate Zone Number	Climate Subtype
301	USA_VA_Winchester.Rgnl.AP.724053_TMY3	4	A
302	USA_VA_Leesburg.Muni.AP-Godfrey.Field.724055_TMY3	4	A
303	USA_VA_Marion-Wytheville-Mountain.Empire.AP.724056_TMY3	4	A
304	USA_VA_Abingdon-Virgina.Highlands.AP.724058_TMY3	4	A
305	USA_MD_Baltimore-Washington.Intl.AP.724060_TMY3	4	A
306	USA_NJ_Atlantic.City.Intl.AP.724070_TMY3	4	A
307	USA_NJ_Millville.Muni.AP.724075_TMY3	4	A
308	USA_PA_Philadelphia.Intl.AP.724080_TMY3	4	A
309	USA_NJ_Belmar-Monmouth.County.AP.724084_TMY3	4	A
310	USA_PA_Philadelphia-NE.Philadelphia.AP.724085_TMY3	4	A
311	USA_PA_Willow.Grove.NAS.724086_TMY3	4	A
312	USA_DE_Dover.AFB.724088_TMY3	4	A
313	USA_DE_Wilmington-New.Castle.County.AP.724089_TMY3	4	A
314	USA_NJ_Trenton-Mercer.County.AP.724095_TMY3	4	A
315	USA_NJ_McGuire.AFB.724096_TMY3	4	A
316	USA_VA_Lynchburg.Rgnl.AP-Preston.Glen.Field.724100_TMY3	4	A
317	USA_VA_Staunton-Shenandoah.Valley.Rgnl.AP.724105_TMY3	4	A
318	USA_VA_Hillsville-Twin.County.AP.724107_TMY3	4	A
319	USA_VA_Roanoke.Rgnl.AP-Woodrum.Field.724110_TMY3	4	A
320	USA_VA_Blacksburg-Virginia.Tech.AP.724113_TMY3	4	A
321	USA_VA_Wise-Lonesome.Pine.AP.724117_TMY3	4	A
322	USA_WV_Beckley-Raleigh.County.Mem.AP.724120_TMY3	4	A
323	USA_WV_Bluefield-Mercer.County.AP.724125_TMY3	4	A
324	USA_WV_Charleston-Yeager.AP.724140_TMY3	4	A
325	USA_WV_Clarksburg-Harrison.Marion.Rgnl.AP.724175_TMY3	4	A
326	USA_WV_Morgantown.Muni-Hart.Field.724176_TMY3	4	A
327	USA_WV_Martinsburg-Eastern.WV.Rgnl.AP.724177_TMY3	4	A
328	USA_KY_Cincinnati-Northern.Kentucky.AP.724210_TMY3	4	A
329	USA_KY_Lexington-Bluegrass.AP.724220_TMY3	4	A
330	USA_KY_Louisville-Standiford.Field.724230_TMY3	4	A
331	USA_KY_Louisville-Bowman.Field.724235_TMY3	4	A
332	USA_KY_Jackson-Julian.Carroll.AP.724236_TMY3	4	A
333	USA_KY_Henderson.City.County.AP.724238_TMY3	4	A
334	USA_KY_Fort.Knox-Godman.AAF.724240_TMY3	4	A
335	USA_KY_London-Corbin-Magee.Field.724243_TMY3	4	A
336	USA_WV_Huntington-Tri.State.Walker.Long.Field.724250_TMY3	4	A
337	USA_WV_Parkersburg-Wood.County-Gill.Robb.Wilson.AP.724273_TMY3	4	A
338	USA_OH_Zanesville.Muni.AP.724286_TMY3	4	A
339	USA_OH_Ohio.State.University.AP.724288_TMY3	4	A
340	USA_OH_Cincinnati.Muni.AP-Lunken.Field.724297_TMY3	4	A
341	USA_IN_Evansville.Rgnl.AP.724320_TMY3	4	A
342	USA_IL_Mount.Vernon.AWOS.724335_TMY3	4	A
343	USA_IL_Carbondale-Southern.Illinois.AP.724336_TMY3	4	A
344	USA_IL_Belleville-Scott.AFB.724338_TMY3	4	A
345	USA_MO_St.Louis-Lambert.Intl.AP.724340_TMY3	4	A
346	USA_MO_St.Louis-Spirit.of.St.Louis.AP.724345_TMY3	4	A
347	USA_KY_Paducah-Barkley.Rgnl.AP.724350_TMY3	4	A
348	USA_KY_Somerset-Pulaski.County.AWOS.724354_TMY3	4	A
349	USA_IN_Huntingburg.Muni.AP.724365_TMY3	4	A
350	USA_IN_Terre.Haute-Hulman.Rgnl.AP.724373_TMY3	4	A

Table 15: (Continued)

Number	Weather File Name	Climate Zone Number	Climate Subtype
351	USA_IN_Monroe.County.AP.724375_TMY3	4	A
352	USA_IL_Springfield-Capital.AP.724390_TMY3	4	A
353	USA_IL_Quincy.Muni.AP.724396_TMY3	4	A
354	USA_MO_Springfield.Rgnl.AP.724400_TMY3	4	A
355	USA_MO_Columbia.Rgnl.AP.724450_TMY3	4	A
356	USA_MO_Rolla.National.AP.724456_TMY3	4	A
357	USA_MO_Jefferson.City.Mem.AP.724458_TMY3	4	A
358	USA_MO_Kaiser-Lee.Fine.Mem.AWOS.724459_TMY3	4	A
359	USA_MO_Kansas.City.Intl.AP.724460_TMY3	4	A
360	USA_MO_Kansas.City.Downtown.AP.724463_TMY3	4	A
361	USA_MO_Whiteman.AFB.724467_TMY3	4	A
362	USA_KS_Olathe-Johnson.County.Executive.AP.724468_TMY3	4	A
363	USA_KS_Wichita-Mid.Continent.AP.724500_TMY3	4	A
364	USA_KS_Wichita-Col.Jabara.Field.724504_TMY3	4	A
365	USA_KS_Wichita-McConnell.AFB.724505_TMY3	4	A
366	USA_KS_Chanute-Martin.Johnson.AP.724507_TMY3	4	A
367	USA_KS_Newton.AWOS.724509_TMY3	4	A
368	USA_KS_Dodge.City.Rgnl.AP.724510_TMY3	4	A
369	USA_KS_Garden.City.Muni.AP.724515_TMY3	4	A
370	USA_KS_Liberal.Muni.AP.724516_TMY3	4	A
371	USA_KS_Great.Bend.AWOS.724517_TMY3	4	A
372	USA_KS_Hays.Muni.AWOS.724518_TMY3	4	A
373	USA_KS_Fort.Riley-Marshall.AAF.724550_TMY3	4	A
374	USA_KS_Manhattan.Rgnl.AP.724555_TMY3	4	A
375	USA_KS_Topeka-Phillip.Billard.Muni.AP.724560_TMY3	4	A
376	USA_KS_Topeka-Forbes.AFB.724565_TMY3	4	A
377	USA_KS_Concordia-Blosser.Muni.AP.724580_TMY3	4	A
378	USA_KS_Russell.Muni.AP.724585_TMY3	4	A
379	USA_KS_Salina.Muni.AP.724586_TMY3	4	A
380	USA_NJ_Newark.Intl.AP.725020_TMY3	4	A
381	USA_NJ_Teterboro.AP.725025_TMY3	4	A
382	USA_NY_New.York-LaGuardia.AP.725030_TMY3	4	A
383	USA_NY_Islip-Long.Island.MacArthur.AP.725035_TMY3	4	A
384	USA_CT_Bridgeport-Sikorsky.Mem.AP.725040_TMY3	4	A
385	USA_RI_Block.Island.State.AP.725058_TMY3	4	A
386	USA_CT_Hartford-Brainard.Field.725087_TMY3	4	A
387	USA_PA_Reading.Mem.AP-Spaatz.Field.725103_TMY3	4	A
388	USA_PA_Harrisburg-Capital.City.AP.725118_TMY3	4	A
389	USA_PA_Pittsburgh-Allegheny.County.AP.725205_TMY3	4	A
390	USA_IL_Cahokia.AP.725314_TMY3	4	A
391	USA_IL_Decatur.AP.725316_TMY3	4	A
392	USA_IA_Keokuk.Muni.AP.725456_TMY3	4	A
393	USA_NY_New.York-J.F.Kennedy.Intl.AP.744860_TMY3	4	A
394	USA_NY_Republic.AP.744864_TMY3	4	A
395	USA_MD_Andrews.AFB.745940_TMY3	4	A
396	USA_NJ_Cape.May.County.AP.745966_TMY3	4	A
397	USA_VA_Langley.AFB.745980_TMY3	4	A
398	USA_VA_Martinsville-Blue.Ridge.AP.745985_TMY3	4	A
399	USA_KY_Fort.Campbell.AAF.746710_TMY3	4	A
400	USA_KY_Bowling.Green-Warren.County.AP.746716_TMY3	4	A

Table 15: (Continued)

Number	Weather File Name	Climate Zone Number	Climate Subtype
401	USA_TX_Dalhart.Muni.AP.722636_TMY3	4	B
402	USA_NM_Ruidoso-Sierra.Blanca.Rgnl.AP.722683_TMY3	4	B
403	USA_NM_Clovis-Cannon.AFB.722686_TMY3	4	B
404	USA_NM_Clovis.Muni.AWOS.722689_TMY3	4	B
405	USA_NM_Clayton.Muni.AP.723600_TMY3	4	B
406	USA_TX_Amarillo.Intl.AP.723630_TMY3	4	B
407	USA_NM_Albuquerque.Intl.AP.723650_TMY3	4	B
408	USA_NM_Farmington-Four.Corners.Rgnl.AP.723658_TMY3	4	B
409	USA_AZ_Prescott-Love.Field.723723_TMY3	4	B
410	USA_AZ_Winslow.Muni.AP.723740_TMY3	4	B
411	USA_CO_La.Junta.Muni.AP.724635_TMY3	4	B
412	USA_CO_Pueblo.Mem.AP.724640_TMY3	4	B
413	USA_CO_Trinidad-Las.Animas.County.AP.724645_TMY3	4	B
414	USA_CO_Grand.Junction-Walker.Field.724760_TMY3	4	B
415	USA_CA_Bishop.AP.724800_TMY3	4	B
416	USA_NV_Reno-Tahoe.Intl.AP.724880_TMY3	4	B
417	USA_NV_Fallon.NAS.724885_TMY3	4	B
418	USA_UT_Salt.Lake.City.Intl.AP.725720_TMY3	4	B
419	USA_NV_Lovelock-Derby.Field.725805_TMY3	4	B
420	USA_CA_Blue.Canyon.AP.725845_TMY3	4	B
421	USA_CA_Crescent.City-Jack.McNamara.Field.725946_TMY3	4	B
422	USA_CA_Montague-Siskiyou.County.AP.725955_TMY3	4	B
423	USA_ID_Boise.Air.Terminal.726810_TMY3	4	B
424	USA_OR_Pendleton-Eastern.Oregon.Rgnl.AP.726880_TMY3	4	B
425	USA_ID_Lewiston-Nez.Perce.County.AP.727830_TMY3	4	B
426	USA_WA_Pasco-Tri.Cities.AP.727845_TMY3	4	B
427	USA_WA_Walla.Walla.City-County.AP.727846_TMY3	4	B
428	USA_NV_Tonopah.AP.724855_TMY3	5	B
429	USA_WA_Whidbey.Island.NAS.690230_TMY3	4	C
430	USA_CA_Arcata.AP.725945_TMY3	4	C
431	USA_OR_Medford-Rogue.Valley.Intl.AP.725970_TMY3	4	C
432	USA_OR_North.Bend.Muni.AP.726917_TMY3	4	C
433	USA_OR_Eugene-Mahlon.Sweet.AP.726930_TMY3	4	C
434	USA_OR_Salem-McNary.Field.726940_TMY3	4	C
435	USA_OR_Corvallis.Muni.AP.726945_TMY3	4	C
436	USA_OR_Aurora.State.AP.726959_TMY3	4	C
437	USA_OR_Portland.Intl.AP.726980_TMY3	4	C
438	USA_OR_Portland-Hillsboro.AP.726986_TMY3	4	C
439	USA_OR_Astoria.Rgnl.AP.727910_TMY3	4	C
440	USA_WA_Olympia.AP.727920_TMY3	4	C
441	USA_WA_Hoquiam.AP.727923_TMY3	4	C
442	USA_WA_Kelso.AP.727924_TMY3	4	C
443	USA_WA_Bremerton.National.AP.727928_TMY3	4	C
444	USA_WA_Seattle-Tacoma.Intl.AP.727930_TMY3	4	C
445	USA_WA_Seattle-Boeing.Field.727935_TMY3	4	C
446	USA_WA_Snohomish.County.AP.727937_TMY3	4	C
447	USA_WA_Tacoma.Narrows.AP.727938_TMY3	4	C
448	USA_OH_Columbus-Port.Columbus.Intl.AP.724280_TMY3	4	A
449	USA_MA_Marthas.Vineyard.AP.725066_TMY3	4	A
450	USA_OH_Findlay.AP.725366_TMY3	4	A

Table 15: (Continued)

Number	Weather File Name	Climate Zone Number	Climate Subtype
451	USA_VA_Hot.Springs-Ingalls.Field.724115_TMY3	5	A
452	USA_WV_Elkins-Randolph.County.AP.724170_TMY3	5	A
453	USA_OH_Dayton.Intl.AP.724290_TMY3	5	A
454	USA_IN_Indianapolis.Intl.AP.724380_TMY3	5	A
455	USA_IN_Lafayette-Purdue.University.AP.724386_TMY3	5	A
456	USA_MO_Kirksville.Muni.AP.724455_TMY3	5	A
457	USA_KS_Goodland-Renner.Field.724650_TMY3	5	A
458	USA_KS_Hill.City.Muni.AP.724655_TMY3	5	A
459	USA_CT_Oxford.AWOS.725029_TMY3	5	A
460	USA_NY_Poughkeepsie-Dutchess.County.AP.725036_TMY3	5	A
461	USA_NY_White.Plains-Westchester.County.AP.725037_TMY3	5	A
462	USA_NY_Newburgh-Stewart.Intl.AP.725038_TMY3	5	A
463	USA_RI_Pawtucket.AWOS.725054_TMY3	5	A
464	USA_MA_Otis.ANGB.725060_TMY3	5	A
465	USA_MA_Plymouth.Muni.AP.725064_TMY3	5	A
466	USA_MA_New.Bedford.Rgnl.AP.725065_TMY3	5	A
467	USA_MA_Barnstable-Boardman.Poland.AP.725067_TMY3	5	A
468	USA_RI_Providence-T.F.Green.State.AP.725070_TMY3	5	A
469	USA_MA_Provincetown.AWOS.725073_TMY3	5	A
470	USA_CT_Hartford-Bradley.Intl.AP.725080_TMY3	5	A
471	USA_MA_Boston-Logan.Intl.AP.725090_TMY3	5	A
472	USA_MA_Worcester.Rgnl.AP.725095_TMY3	5	A
473	USA_MA_Norwood.Mem.AP.725098_TMY3	5	A
474	USA_PA_Harrisburg.Intl.AP.725115_TMY3	5	A
475	USA_PA_Washington.AWOS.725117_TMY3	5	A
476	USA_PA_Butler.County.AWOS.725124_TMY3	5	A
477	USA_PA_DuBois-Jefferson.County.AP.725125_TMY3	5	A
478	USA_PA_Altoona-Blair.County.AP.725126_TMY3	5	A
479	USA_PA_Johnstown-Cambria.County.AP.725127_TMY3	5	A
480	USA_PA_Wilkes-Barre-Scranton.Intl.AP.725130_TMY3	5	A
481	USA_PA_Williamsport.Rgnl.AP.725140_TMY3	5	A
482	USA_NY_Monticello.AWOS.725145_TMY3	5	A
483	USA_NY_Binghamton-Edwin.A.Link.Field.725150_TMY3	5	A
484	USA_NY_Elmira.Rgnl.AP.725156_TMY3	5	A
485	USA_PA_Allentown-Lehigh.Valley.Intl.AP.725170_TMY3	5	A
486	USA_NY_Albany.County.AP.725180_TMY3	5	A
487	USA_NY_Glens.Falls-Bennett.Mem.AP.725185_TMY3	5	A
488	USA_NY_Syracuse-Hancock.Intl.AP.725190_TMY3	5	A
489	USA_NY_Utica-Oneida.County.AP.725197_TMY3	5	A
490	USA_PA_Pittsburgh.Intl.AP.725200_TMY3	5	A
491	USA_OH_Akron.Canton.Rgnl.AP.725210_TMY3	5	A
492	USA_NY_Jamestown.AWOS.725235_TMY3	5	A
493	USA_OH_Cleveland-Hopkins.Intl.AP.725240_TMY3	5	A
494	USA_OH_Mansfield-Lahm.Muni.AP.725246_TMY3	5	A
495	USA_OH_Youngstown.Rgnl.AP.725250_TMY3	5	A
496	USA_PA_Erie.Intl.AP.725260_TMY3	5	A
497	USA_PA_Franklin-Chess.Lemberton.AP.725267_TMY3	5	A
498	USA_NY_Buffalo-Greater.Buffalo.Intl.AP.725280_TMY3	5	A
499	USA_NY_Niagara.Falls.Intl.AP.725287_TMY3	5	A
500	USA_NY_Rochester-Greater.Rochester.Intl.AP.725290_TMY3	5	A

Table 15: (Continued)

Number	Weather File Name	Climate Zone Number	Climate Subtype
501	USA_IL_Chicago-OHare.Intl.AP.725300_TMY3	5	A
502	USA_IL_Du.Page.AP.725305_TMY3	5	A
503	USA_IL_University.of.Illinois-Willard.AP.725315_TMY3	5	A
504	USA_IL_Peoria-Greater.Peoria.AP.725320_TMY3	5	A
505	USA_IL_Sterling-Rock.Falls-Whiteside.County.AP.725326_TMY3	5	A
506	USA_IN_Fort.Wayne.Intl.AP.725330_TMY3	5	A
507	USA_IN_Grissom.AFB.725335_TMY3	5	A
508	USA_IL_Chicago-Midway.AP.725340_TMY3	5	A
509	USA_IN_South.Bend-Michiana.Rgnl.AP.725350_TMY3	5	A
510	USA_OH_Toledo.Express.AP.725360_TMY3	5	A
511	USA_MI_Detroit.Metro.AP.725370_TMY3	5	A
512	USA_MI_Detroit-City.AP.725375_TMY3	5	A
513	USA_MI_Detroit-Willow.Run.AP.725376_TMY3	5	A
514	USA_MI_Mount.Clemens-Selfridge.ANGB.725377_TMY3	5	A
515	USA_MI_Howell-Livingston.County.AP.725378_TMY3	5	A
516	USA_MI_St.Clair.County.Intl.AP.725384_TMY3	5	A
517	USA_MI_Lansing-Capital.City.AP.725390_TMY3	5	A
518	USA_MI_Jackson-Reynolds.Field.725395_TMY3	5	A
519	USA_IL_Rockford-Greater.Rockford.AP.725430_TMY3	5	A
520	USA_IL_Moline-Quad.City.Intl.AP.725440_TMY3	5	A
521	USA_IA_Cedar.Rapids.Muni.AP.725450_TMY3	5	A
522	USA_IA_Atlantic.Muni.AP.725453_TMY3	5	A
523	USA_IA_Washington.Muni.AP.725454_TMY3	5	A
524	USA_IA_Burlington.Muni.AP.725455_TMY3	5	A
525	USA_IA_Des.Moines.Intl.AP.725460_TMY3	5	A
526	USA_IA_Charles.City.Muni.AP.725463_TMY3	5	A
527	USA_IA_Ottumwa.Industrial.AP.725465_TMY3	5	A
528	USA_IA_Carroll.Muni.AP.725468_TMY3	5	A
529	USA_IA_Chariton.Muni.AP.725469_TMY3	5	A
530	USA_IA_Clinton.Muni.AWOS.725473_TMY3	5	A
531	USA_IA_Creston.Muni.AP.725474_TMY3	5	A
532	USA_IA_Webster.City.Muni.AP.725478_TMY3	5	A
533	USA_IA_Waterloo.Muni.AP.725480_TMY3	5	A
534	USA_IA_Boone.Muni.AP.725486_TMY3	5	A
535	USA_IA_Fort.Dodge.AWOS.725490_TMY3	5	A
536	USA_IA_Storm.Lake.Muni.AP.725496_TMY3	5	A
537	USA_NE_Omaha-Eppley.Airfield.725500_TMY3	5	A
538	USA_NE_Lincoln.Muni.AP.725510_TMY3	5	A
539	USA_NE_Beatrice.Muni.AP.725515_TMY3	5	A
540	USA_NE_Grand.Island-Central.Nebraska.Rgnl.AP.725520_TMY3	5	A
541	USA_NE_Hastings.Muni.AP.725525_TMY3	5	A
542	USA_NE_Kearney.Muni.AWOS.725526_TMY3	5	A
543	USA_NE_Tekamah.AWOS.725527_TMY3	5	A
544	USA_NE_Omaha.WSFO.725530_TMY3	5	A
545	USA_NE_Bellevue-Offutt.AFB.725540_TMY3	5	A
546	USA_NE_Ainsworth.Muni.AP.725556_TMY3	5	A
547	USA_NE_Norfolk-Karl.Stefan.Mem.AP.725560_TMY3	5	A
548	USA_NE_Fremont.Muni.AP.725564_TMY3	5	A
549	USA_NE_Columbus.Muni.AP.725565_TMY3	5	A
550	USA_IA_Sioux.City-Sioux.Gateway.AP.725570_TMY3	5	A

Table 15: (Continued)

Number	Weather File Name	Climate Zone Number	Climate Subtype
551	USA_NE_Sidney.Muni.AP.725610_TMY3	5	A
552	USA_NE_North.Platte.Rgnl.AP.725620_TMY3	5	A
553	USA_NE_McCook.Muni.AP.725625_TMY3	5	A
554	USA_NE_Holdrege-Brewster.Field.725628_TMY3	5	A
555	USA_NE_Alliance.Muni.AP.725635_TMY3	5	A
556	USA_NE_Scottsbluff-W.B.Heilig.Field.725660_TMY3	5	A
557	USA_NE_Valentine-Miller.Field.725670_TMY3	5	A
558	USA_NH_Pease.Intl.Tradeport.726055_TMY3	5	A
559	USA_VT_Springfield-Hartnes.State.AP.726115_TMY3	5	A
560	USA_NH_Lebanon.Muni.AP.726116_TMY3	5	A
561	USA_NH_Laconia.Muni.AWOS.726155_TMY3	5	A
562	USA_NH_Keene-Dillant.Hopkins.AP.726165_TMY3	5	A
563	USA_MI_Grand.Rapids-Kent.County.Intl.AP.726350_TMY3	5	A
564	USA_MI_Benton.Harbor-Ross.Field-Twin.Cities.AP.726355_TMY3	5	A
565	USA_MI_Kalamazoo-Battle.Creek.Intl.AP.726357_TMY3	5	A
566	USA_MI_Muskegon.County.AP.726360_TMY3	5	A
567	USA_MI_Flint-Bishop.Intl.AP.726370_TMY3	5	A
568	USA_MI_Oakland.County.Intl.AP.726375_TMY3	5	A
569	USA_MI_Saginaw-Tri.City.Intl.AP.726379_TMY3	5	A
570	USA_MI_Manistee.AWOS.726385_TMY3	5	A
571	USA_MI_Oscoda-Wurtsmith.AFB.726395_TMY3	5	A
572	USA_WI_Milwaukee-Mitchell.Intl.AP.726400_TMY3	5	A
573	USA_WI_Manitowac.Muni.AWOS.726455_TMY3	5	A
574	USA_WI_Appleton-Outagamie.County.AP.726457_TMY3	5	A
575	USA_WI_Sturgeon.Bay-Door.County.AP.726458_TMY3	5	A
576	USA_WI_Watertown.Muni.AP.726464_TMY3	5	A
577	USA_IA_Fairfield.Muni.AP.726498_TMY3	5	A
578	USA_SD_Yankton-Chan.Gurney.Muni.AP.726525_TMY3	5	A
579	USA_SD_Rapid.City.Rgnl.AP.726620_TMY3	5	A
580	USA_SD_Pierre.Muni.AP.726686_TMY3	5	A
581	USA_ME_Wiscasset.AP.727135_TMY3	5	A
582	USA_NH_Manchester.Muni.AP.743945_TMY3	5	A
583	USA_IL_Aurora.Muni.AP.744655_TMY3	5	A
584	USA_MA_Lawrence.Muni.AP.744904_TMY3	5	A
585	USA_OH_Dayton-Wright.Patterson.AFB.745700_TMY3	5	A
586	USA_NM_Gallup-Sen.Clarke.Field.723627_TMY3	5	B
587	USA_NM_Taos.Muni.AP.723663_TMY3	5	B
588	USA_AZ_Grand.Canyon.National.Park.AP.723783_TMY3	5	B
589	USA_CO_Durango-La.Plata.County.AP.724625_TMY3	5	B
590	USA_CO_Lamar.Muni.AP.724636_TMY3	5	B
591	USA_CO_Colorado.Springs-Peterson.Field.724660_TMY3	5	B
592	USA_CO_Limon.Muni.AP.724665_TMY3	5	B
593	USA_CO_Golden-NREL.724666_TMY3	5	B
594	USA_CO_Aurora-Buckley.Field.ANGB.724695_TMY3	5	B
595	USA_CO_Akron-Washington.County.AP.724698_TMY3	5	B
596	USA_UT_Cedar.City.Muni.AP.724755_TMY3	5	B
597	USA_CO_Montrose.County.AP.724765_TMY3	5	B
598	USA_CO_Cortez-Montezuma.County.AP.724767_TMY3	5	B
599	USA_CO_Greeley-Weld.County.AWOS.724768_TMY3	5	B
600	USA_CO_Fort.Collins.AWOS.724769_TMY3	5	B

Table 15: (Continued)

Number	Weather File Name	Climate Zone Number	Climate Subtype
601	USA_NV_Ely-Yelland.Field.724860_TMY3	5	B
602	USA_WY_Cheyenne.Muni.AP.725640_TMY3	5	B
603	USA_CO_Denver.Intl.AP.725650_TMY3	5	B
604	USA_UT_Vernal.AP.725705_TMY3	5	B
605	USA_CO_Rifle-Garfield.County.Rgnl.AP.725717_TMY3	5	B
606	USA_UT_Provo.Muni.AWOS.725724_TMY3	5	B
607	USA_UT_Ogden-Hill.AFB.725755_TMY3	5	B
608	USA_ID_Pocatello.Muni.AP.725780_TMY3	5	B
609	USA_UT_Wendover.USAF.Auxiliary.Field.725810_TMY3	5	B
610	USA_NV_Elko.Muni.AP.725825_TMY3	5	B
611	USA_NV_Winnemucca.Muni.AP.725830_TMY3	5	B
612	USA_ID_Twin.Falls-Magic.Valley.Rgnl.AP-Joslin.Field.725866_TMY3	5	B
613	USA_ID_Burley.Muni.AP.725867_TMY3	5	B
614	USA_OR_Lakeview.AWOS.725976_TMY3	5	B
615	USA_WY_Gillette-Gillette.County.AP.726650_TMY3	5	B
616	USA_WY_Sheridan.County.AP.726660_TMY3	5	B
617	USA_WY_Cody.Muni.AWOS.726700_TMY3	5	B
618	USA_MT_Billings-Logan.Intl.AP.726770_TMY3	5	B
619	USA_ID_Caldwell.AWOS.726813_TMY3	5	B
620	USA_ID_Mountain.Home.AFB.726815_TMY3	5	B
621	USA_OR_Burns.Muni.AP.726830_TMY3	5	B
622	USA_OR_Redmond-Roberts.Field.726835_TMY3	5	B
623	USA_OR_La.Grande.Muni.AP.726884_TMY3	5	B
624	USA_OR_Baker.Muni.AP.726886_TMY3	5	B
625	USA_WA_Yakima.Air.Terminal-McAllister.Field.727810_TMY3	5	B
626	USA_WA_Wenatchee-Pangborn.Mem.AP.727825_TMY3	5	B
627	USA_ID_Coeur.dAlene.AWOS.727834_TMY3	5	B
628	USA_WA_Hanford.727840_TMY3	5	B
629	USA_WA_Spokane.Intl.AP.727850_TMY3	5	B
630	USA_WA_Fairchild.AFB.727855_TMY3	5	B
631	USA_WA_Spokane-Felts.Field.727856_TMY3	5	B
632	USA_WA_Pullman-Moscow.Rgnl.AP.727857_TMY3	5	B
633	USA_WY_Worland.Muni.AP.726665_TMY3	6	B
634	USA_MT_Missoula.Intl.AP.727730_TMY3	6	B
635	USA_OR_Sexton.Summit.725975_TMY3	5	C
636	USA_WA_Port.Angeles-William.R.Fairchild.Intl.AP.727885_TMY3	5	C
637	USA_WA_Quillayute.State.AP.727970_TMY3	5	C
638	USA_WA_Bellingham.Intl.AP.727976_TMY3	5	C
639	USA_WA_Tacoma-McChord.AFB.742060_TMY3	5	C
640	USA_NH_Concord.Muni.AP.726050_TMY3	5	A
641	USA_ME_Rockland-Knox.AWOS.726079_TMY3	5	A
642	USA_VT_Burlington.Intl.AP.726170_TMY3	5	A
643	USA_NY_Watertown.AP.726227_TMY3	5	A
644	USA_WI_Marshfield.Muni.AP.726574_TMY3	5	A
645	USA_MI_Pellston-Emmet.County.AP.727347_TMY3	5	A
646	USA_ME_Brunswick.NAS.743920_TMY3	5	A
647	USA_VT_Rutland.State.AP.725165_TMY3	6	A
648	USA_PA_Bradford.Rgnl.AP.725266_TMY3	6	A
649	USA_IA_Dubuque.Rgnl.AP.725470_TMY3	6	A
650	USA_IA_Mason.City.Muni.AP.725485_TMY3	6	A

Table 15: (Continued)

Number	Weather File Name	Climate Zone Number	Climate Subtype
651	USA_NE_ONeill-Baker.Field.725566_TMY3	6	A
652	USA_ME_Portland.Intl.Jetport.726060_TMY3	6	A
653	USA_ME_Sanford.Muni.AWOS.726064_TMY3	6	A
654	USA_ME_Waterville.AWOS.726073_TMY3	6	A
655	USA_ME_Bar.Harbor.AWOS.726077_TMY3	6	A
656	USA_ME_Bangor.Intl.AP.726088_TMY3	6	A
657	USA_VT_Montpelier.AP.726145_TMY3	6	A
658	USA_NH_Berlin.Muni.AP.726160_TMY3	6	A
659	USA_ME_Auburn-Lewiston.Muni.AP.726184_TMY3	6	A
660	USA_ME_Augusta.AP.726185_TMY3	6	A
661	USA_NY_Massena.AP.726223_TMY3	6	A
662	USA_MI_Houghton-Lake.Roscommon.County.AP.726380_TMY3	6	A
663	USA_MI_Cadillac-Wexford.County.AP.726384_TMY3	6	A
664	USA_MI_Traverse.City-Cherry.Capital.AP.726387_TMY3	6	A
665	USA_MI_Alpena.County.Rgnl.AP.726390_TMY3	6	A
666	USA_WI_Madison-Dane.County.Rgnl.AP.726410_TMY3	6	A
667	USA_WI_La.Crosse.Muni.AP.726430_TMY3	6	A
668	USA_WI_Eau.Claire.County.AP.726435_TMY3	6	A
669	USA_MN_Rochester.Intl.AP.726440_TMY3	6	A
670	USA_WI_Green.Bay-Austin.Straubel.Intl.AP.726450_TMY3	6	A
671	USA_WI_Wittman.Rgnl.AP.726456_TMY3	6	A
672	USA_WI_Wausau.Muni.AP.726463_TMY3	6	A
673	USA_WI_Mosinee-Central.Wisconsin.AP.726465_TMY3	6	A
674	USA_WI_Rice.Lake.Muni.AP.726467_TMY3	6	A
675	USA_WI_Phillips-Price.County.AP.726468_TMY3	6	A
676	USA_MI_Escanaba.AWOS.726480_TMY3	6	A
677	USA_MI_Menominee.AWOS.726487_TMY3	6	A
678	USA_IA_Estherville.Muni.AP.726499_TMY3	6	A
679	USA_IA_Spencer.Muni.AP.726500_TMY3	6	A
680	USA_SD_Sioux.Falls-Foss.Field.726510_TMY3	6	A
681	USA_SD_Brookings.AWOS.726515_TMY3	6	A
682	USA_SD_Huron.Rgnl.AP.726540_TMY3	6	A
683	USA_SD_Mitchell.AWOS.726545_TMY3	6	A
684	USA_SD_Watertown.Muni.AP.726546_TMY3	6	A
685	USA_MN_Glenwood.AWOS.726547_TMY3	6	A
686	USA_MN_St.Cloud.Muni.AP.726550_TMY3	6	A
687	USA_MN_Redwood.Falls.Muni.AP.726556_TMY3	6	A
688	USA_MN_Alexandria.Muni.AP.726557_TMY3	6	A
689	USA_MN_Marshall.Muni-Ryan.Field.AWOS.726559_TMY3	6	A
690	USA_MN_Fergus.Falls.AWOS.726560_TMY3	6	A
691	USA_MN_Faribault.Muni.AWOS.726563_TMY3	6	A
692	USA_MN_Red.Wing.Muni.AP.726564_TMY3	6	A
693	USA_MN_Morris.Muni.AWOS.726565_TMY3	6	A
694	USA_MN_Pipestone.AWOS.726566_TMY3	6	A
695	USA_MN_New.Ulm.Muni.AWOS.726567_TMY3	6	A
696	USA_MN_Owatonna.AWOS.726568_TMY3	6	A
697	USA_MN_Hutchinson.AWOS.726569_TMY3	6	A
698	USA_MN_Minneapolis-Crystal.AP.726575_TMY3	6	A
699	USA_MN_Willmar.Muni.AP.726576_TMY3	6	A
700	USA_MN_Edin.Prairie-Flying.Cloud.AP.726579_TMY3	6	A

Table 15: (Continued)

Number	Weather File Name	Climate Zone Number	Climate Subtype
701	USA_MN_Minneapolis-St.Paul.Intl.AP.726580_TMY3	6	A
702	USA_MN_Litchfield.Muni.AP.726583_TMY3	6	A
703	USA_MN_St.Paul-Downtown.AP.726584_TMY3	6	A
704	USA_MN_Mankato.AWOS.726585_TMY3	6	A
705	USA_MN_Fairmont.Muni.AWOS.726586_TMY3	6	A
706	USA_MN_Worthington.AWOS.726587_TMY3	6	A
707	USA_MN_Winona.Muni.AWOS.726588_TMY3	6	A
708	USA_SD_Aberdeen.Rgnl.AP.726590_TMY3	6	A
709	USA_MN_South.St.Paul.Muni.AP.726603_TMY3	6	A
710	USA_SD_Ellsworth.AFB.726625_TMY3	6	A
711	USA_WI_Ephraim.AWOS.726626_TMY3	6	A
712	USA_SD_Mobridge.Muni.AP.726685_TMY3	6	A
713	USA_MI_Sault.Ste.Marie-Sanderson.Field.727340_TMY3	6	A
714	USA_MI_Chippewa.County.Intl.AP.727344_TMY3	6	A
715	USA_MI_Rhinelander-Oneida.County.AP.727415_TMY3	6	A
716	USA_MI_Iron.Mountain-Ford.Field.727437_TMY3	6	A
717	USA_MI_Hancock-Houghton.County.AP.727440_TMY3	6	A
718	USA_MI_Ironwood.AWOS.727445_TMY3	6	A
719	USA_MN_Detroit.Lakes.AWOS.727457_TMY3	6	A
720	USA_MN_Mora.Muni.AWOS.727475_TMY3	6	A
721	USA_MN_Cambridge.Muni.AP.727503_TMY3	6	A
722	USA_MN_Benson.Muni.AP.727507_TMY3	6	A
723	USA_MN_Wheaton.AWOS.727533_TMY3	6	A
724	USA_MN_Austin.Muni.AP.727566_TMY3	6	A
725	USA_ND_Bismarck.Muni.AP.727640_TMY3	6	A
726	USA_ND_Dickinson.Muni.AP.727645_TMY3	6	A
727	USA_ND_Williston-Sloulin.Field.Intl.AP.727670_TMY3	6	A
728	USA_NY_Fort.Drum-Wheeler.Sack.AAF.743700_TMY3	6	A
729	USA_MN_Little.Falls.AWOS.726578_TMY3	6	A
730	USA_ND_Fargo-Hector.Intl.AP.727530_TMY3	6	A
731	USA_CO_Alamosa.Muni.AP.724620_TMY3	6	B
732	USA_CO_Eagle.County.Rgnl.AP.724675_TMY3	6	B
733	USA_WY_Laramie-General.Brees.Field.725645_TMY3	6	B
734	USA_WY_Casper-Natrona.County.Intl.AP.725690_TMY3	6	B
735	USA_CO_Craig.Moffat.AP.725700_TMY3	6	B
736	USA_WY_Green.River-Greater.Green.River.Intergalactic.Spaceport.725744_TMY3	6	B
737	USA_WY_Lander-Hunt.Field.725760_TMY3	6	B
738	USA_ID_Idaho.Falls-Fanning.Field.725785_TMY3	6	B
739	USA_CA_Truckee.Tahoe.AP.725846_TMY3	6	B
740	USA_MT_Glendive.AWOS.726676_TMY3	6	B
741	USA_MT_Lewistown.Muni.AP.726776_TMY3	6	B
742	USA_MT_Butte-Bert.Mooney.AP.726785_TMY3	6	B
743	USA_MT_Bozeman-Gallatin.Field.726797_TMY3	6	B
744	USA_ID_Salmon-Lemhi.AWOS.726865_TMY3	6	B
745	USA_MT_Glasgow.Intl.AP.727680_TMY3	6	B
746	USA_MT_Helena.Rgnl.AP.727720_TMY3	6	B
747	USA_MT_Great.Falls.Intl.AP.727750_TMY3	6	B
748	USA_MT_Havre.City-County.AP.727770_TMY3	6	B
749	USA_MT_Kalispell-Glacier.Park.Intl.AP.727790_TMY3	6	B
750	USA_MT_Cut.Bank.Muni.AP.727796_TMY3	6	B

Table 15: (Continued)

Number	Weather File Name	Climate Zone Number	Climate Subtype
751	USA_MT_Miles.City.Muni.AP.742300_TMY3	6	B
752	USA_MN_Orr.Rgnl.AP.726544_TMY3	7	—
753	USA_MN_Cloquet.AWOS.726558_TMY3	7	—
754	USA_MN_Ely.Muni.AP.727459_TMY3	7	—
755	USA_MN_Crane.Lake.AWOS.727473_TMY3	7	—
756	USA_MN_Eveleth.Muni.AWOS.727474_TMY3	7	—
757	USA_ND_Jamestown.Muni.AP.727535_TMY3	7	—
758	USA_CO_Gunnison.County.AWOS.724677_TMY3	7	—
759	USA_MT_Sidney-Richland.Muni.AP.727687_TMY3	7	—
760	USA_AK_Anchorage.Intl.AP.702730_TMY3	7	—
761	USA_AK_Anvik.702075_TMY3	7	—
762	USA_AK_Bethel.AP.702190_TMY3	7	—
763	USA_AK_Big.Delta-Allen.AAF.702670_TMY3	7	—
764	USA_AK_Cold.Bay.AP.703160_TMY3	7	—
765	USA_AK_Cordova.702960_TMY3	7	—
766	USA_AK_Dillingham.AWOS.703210_TMY3	7	—
767	USA_AK_Eielson.AFB.702650_TMY3	7	—
768	USA_AK_Homer.AP.703410_TMY3	7	—
769	USA_AK_Hooper.Bay.702186_TMY3	7	—
770	USA_AK_Iliamna.AP.703400_TMY3	7	—
771	USA_AK_Kenai.Muni.AP.702590_TMY3	7	—
772	USA_AK_King.Salmon.AP.703260_TMY3	7	—
773	USA_AK_Mekoryuk.702185_TMY3	7	—
774	USA_AK_Minchumina.702460_TMY3	7	—
775	USA_AK_Port.Heiden.703330_TMY3	7	—
776	USA_AK_Saint.Marys.AWOS.702005_TMY3	7	—
777	USA_AK_Shemya.AFB.704140_TMY3	7	—
778	USA_AK_Soldotna.702595_TMY3	7	—
779	USA_AK_St.Paul.Island.AP.703080_TMY3	7	—
780	USA_AK_Talkeetna.State.AP.702510_TMY3	7	—
781	USA_AK_Togiak.Village.AWOS.703606_TMY3	7	—
782	USA_AK_Unalakleet.Field.702070_TMY3	7	—
783	USA_AK_Valdez-Pioneer.Field.702756_TMY3	7	—
784	USA_AK_Valdez.702750_TMY3	7	—
785	USA_AK_Whittier.702757_TMY3	7	—
786	USA_NH_Mount.Washington.726130_TMY3	8	—
787	USA_AK_Ambler.701718_TMY3	8	—
788	USA_AK_Anaktuvuk.Pass.701625_TMY3	8	—
789	USA_AK_Barrow-W.Post-W.Rogers.AP.700260_TMY3	8	—
790	USA_AK_Bettles.Field.701740_TMY3	8	—
791	USA_AK_Deadhorse.700637_TMY3	8	—
792	USA_AK_Fairbanks.Intl.AP.702610_TMY3	8	—
793	USA_AK_Fort.Yukon.701940_TMY3	8	—
794	USA_AK_Gulkana.702710_TMY3	8	—
795	USA_AK_Kotzebue-Ralph.Wein.Mem.AP.701330_TMY3	8	—
796	USA_AK_McGrath.AP.702310_TMY3	8	—
797	USA_AK_Nenana.Muni.AP.702600_TMY3	8	—
798	USA_AK_Nome.Muni.AP.702000_TMY3	8	—
799	USA_AK_Northway.AP.702910_TMY3	8	—
800	USA_AK_Point.Hope.AWOS.701043_TMY3	8	—
801	USA_AK_Shishmaref.AWOS.701195_TMY3	8	—

APPENDIX C

C.1. Results of the Regulated Energy Consumption, Total Energy Savings, and Total Energy Savings Percentages in Each Climate Zone

This appendix includes the results of the building energy simulations of the ASHRAE Standard 90.1-2016 medium office prototype in each climate zone. The results include the regulated energy consumption of the models with and without daylight-responsive controls, the total energy savings, and the total energy savings percentages. The climate zone subtypes are discriminated using different shapes and colors to reveal the differences within each climate zone.

Figure 131 to Figure 138 show the regulated energy consumption of the ASHRAE Standard 90.1-2016 medium office prototype models in different climate zones. Figure 139 to Figure 146 show the regulated energy consumption of the ASHRAE Standard 90.1-2016 medium office prototype models without daylight responsive controls in different climate zones. The total energy savings are illustrated in Figure 147 to Figure 154 and the total energy savings percentage are shown in Figure 155 to Figure 162.

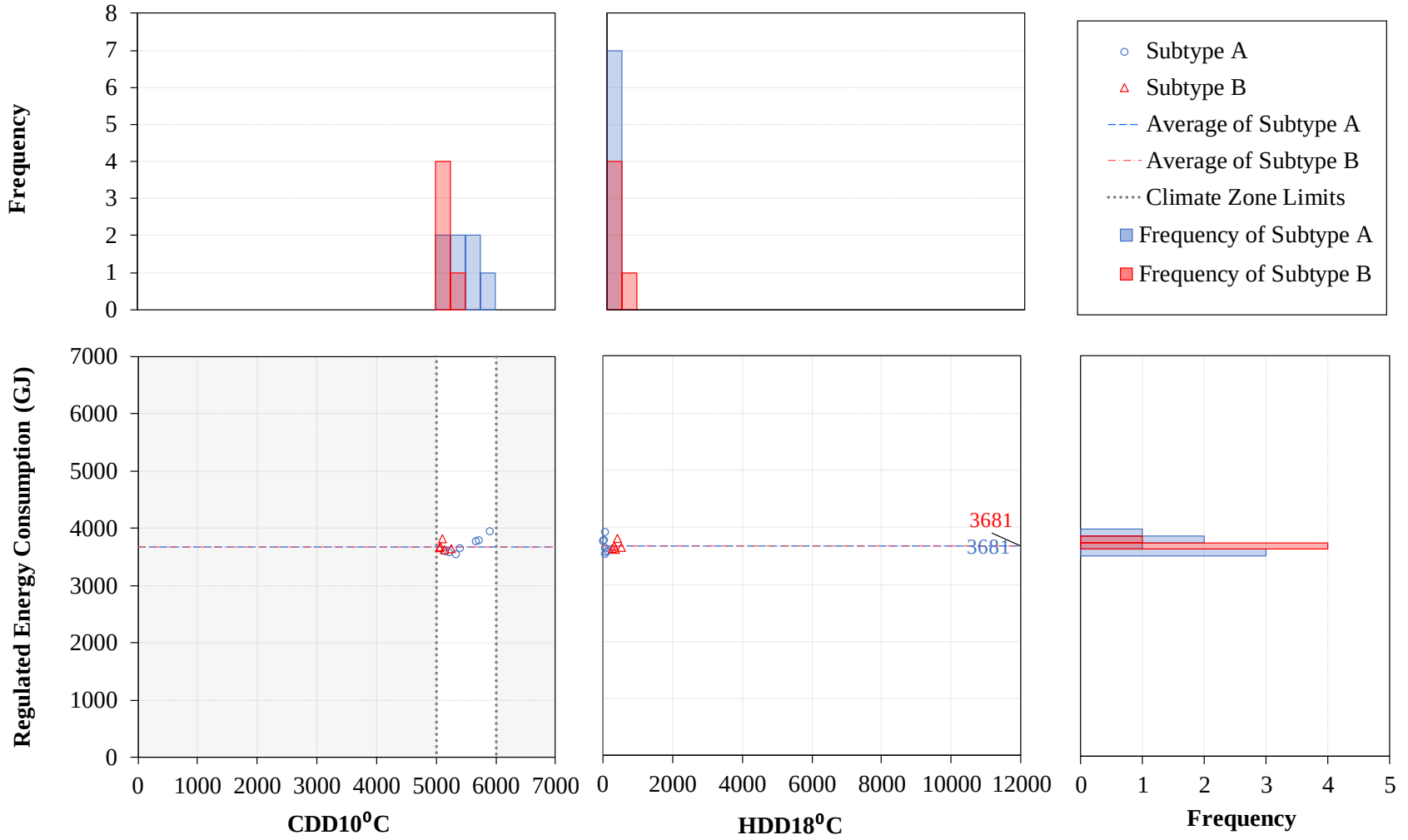

Figure 131: Regulated Energy Consumption of the ASHRAE Standard 90.1-2016 Medium Office Prototype Models in Climate Zone 1

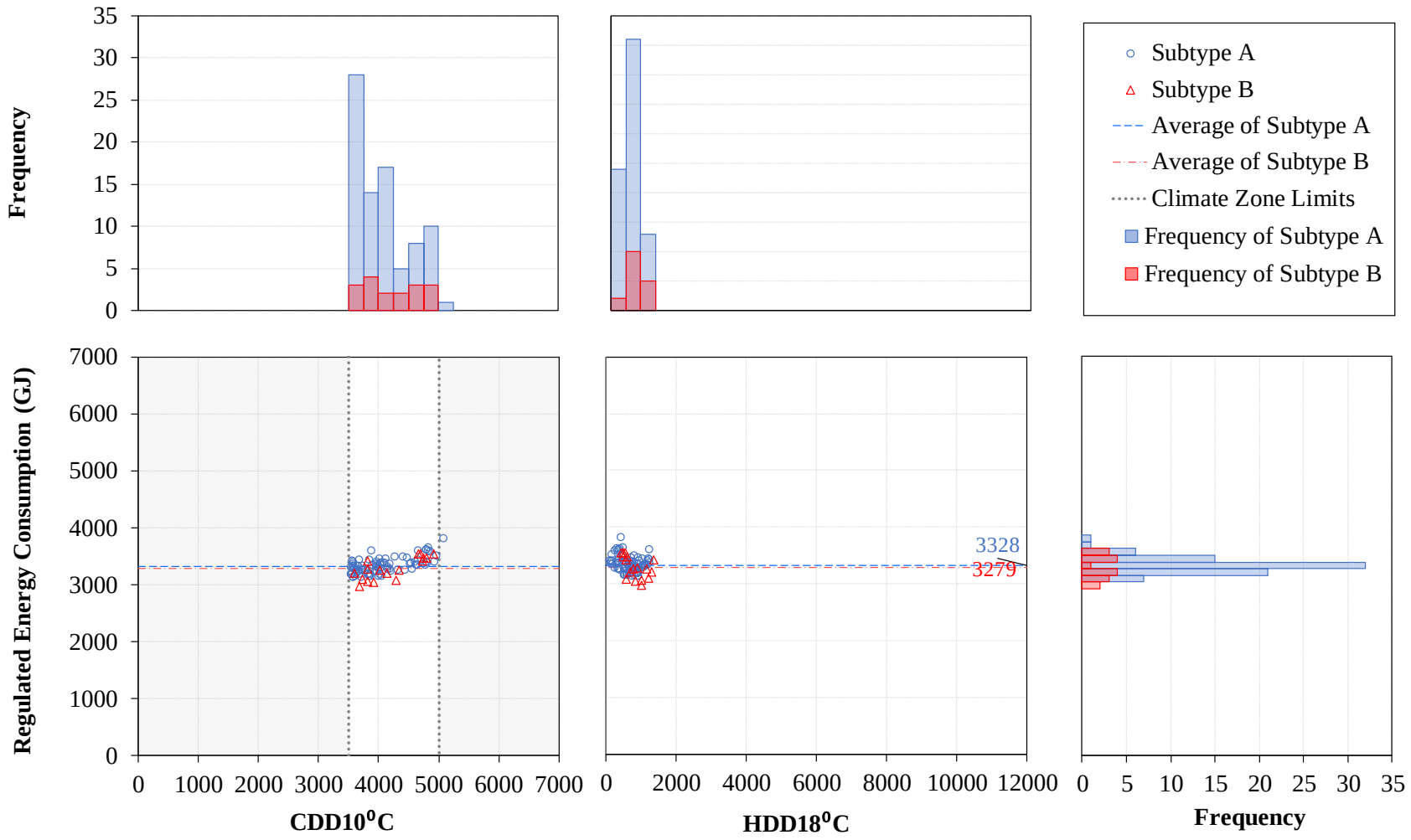

Figure 132: Regulated Energy Consumption of the ASHRAE Standard 90.1-2016 Medium Office Prototype Models in Climate Zone 2

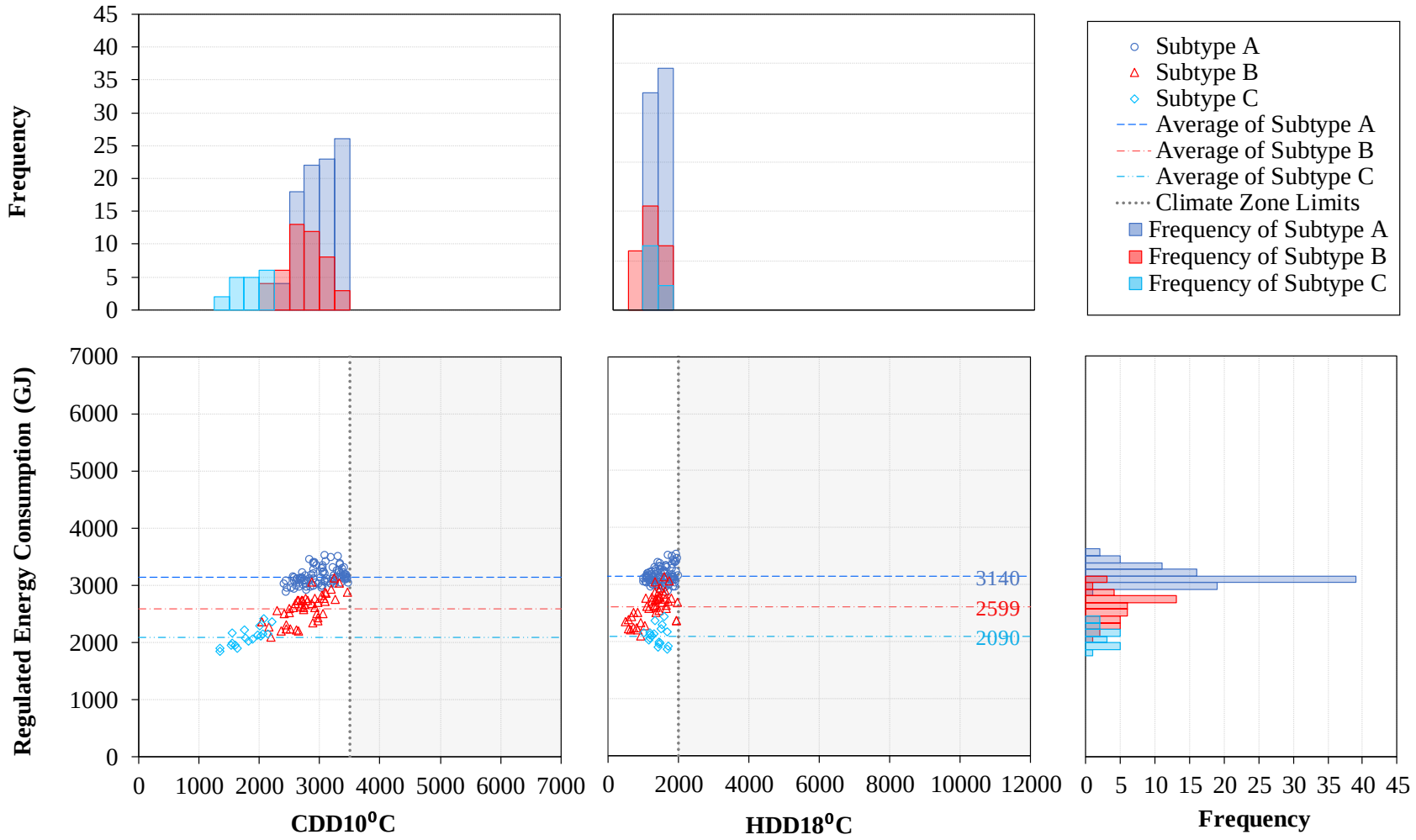

Figure 133: Regulated Energy Consumption of the ASHRAE Standard 90.1-2016 Medium Office Prototype Models in Climate Zone 3

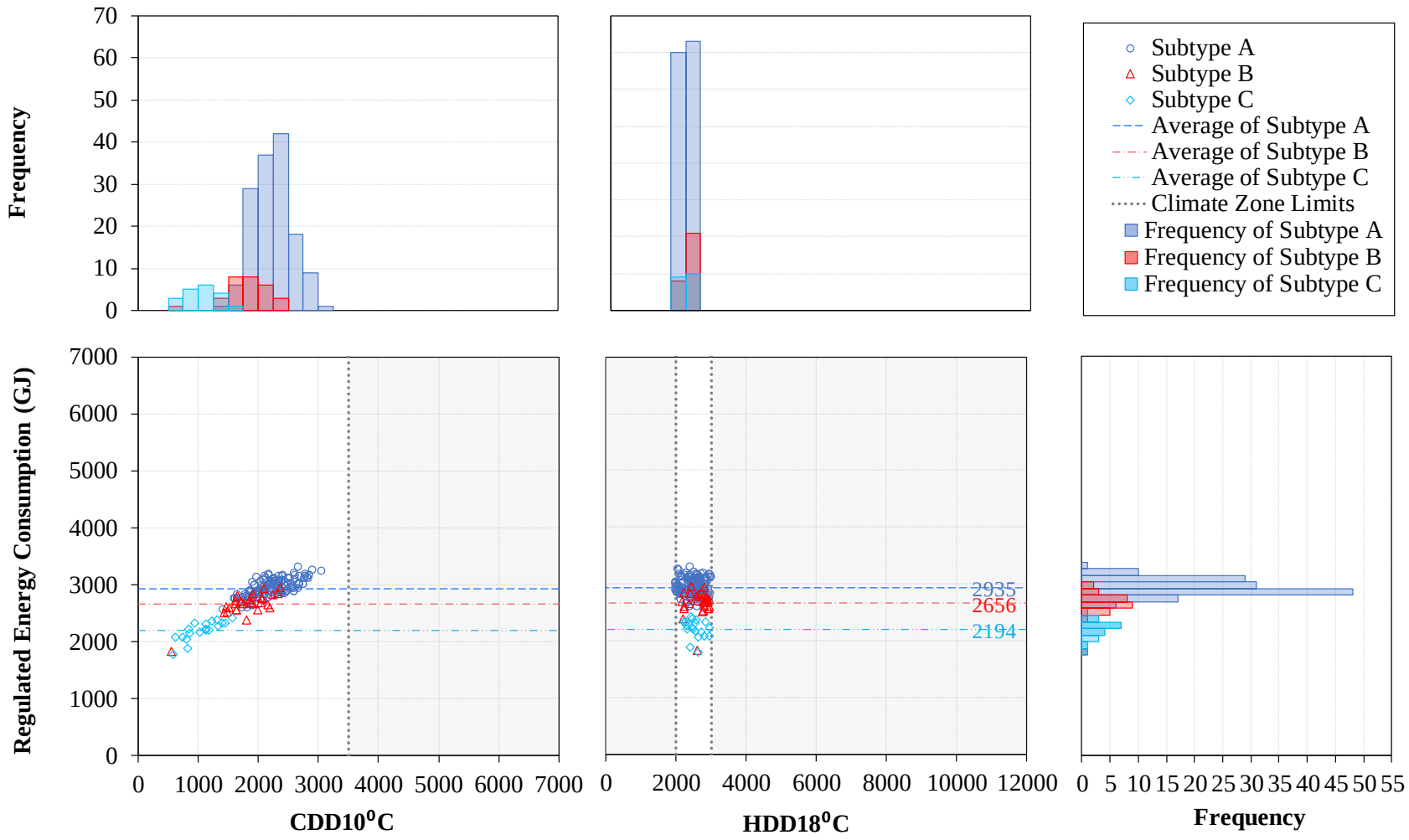

Figure 134: Regulated Energy Consumption of the ASHRAE Standard 90.1-2016 Medium Office Prototype Models in Climate Zone 4

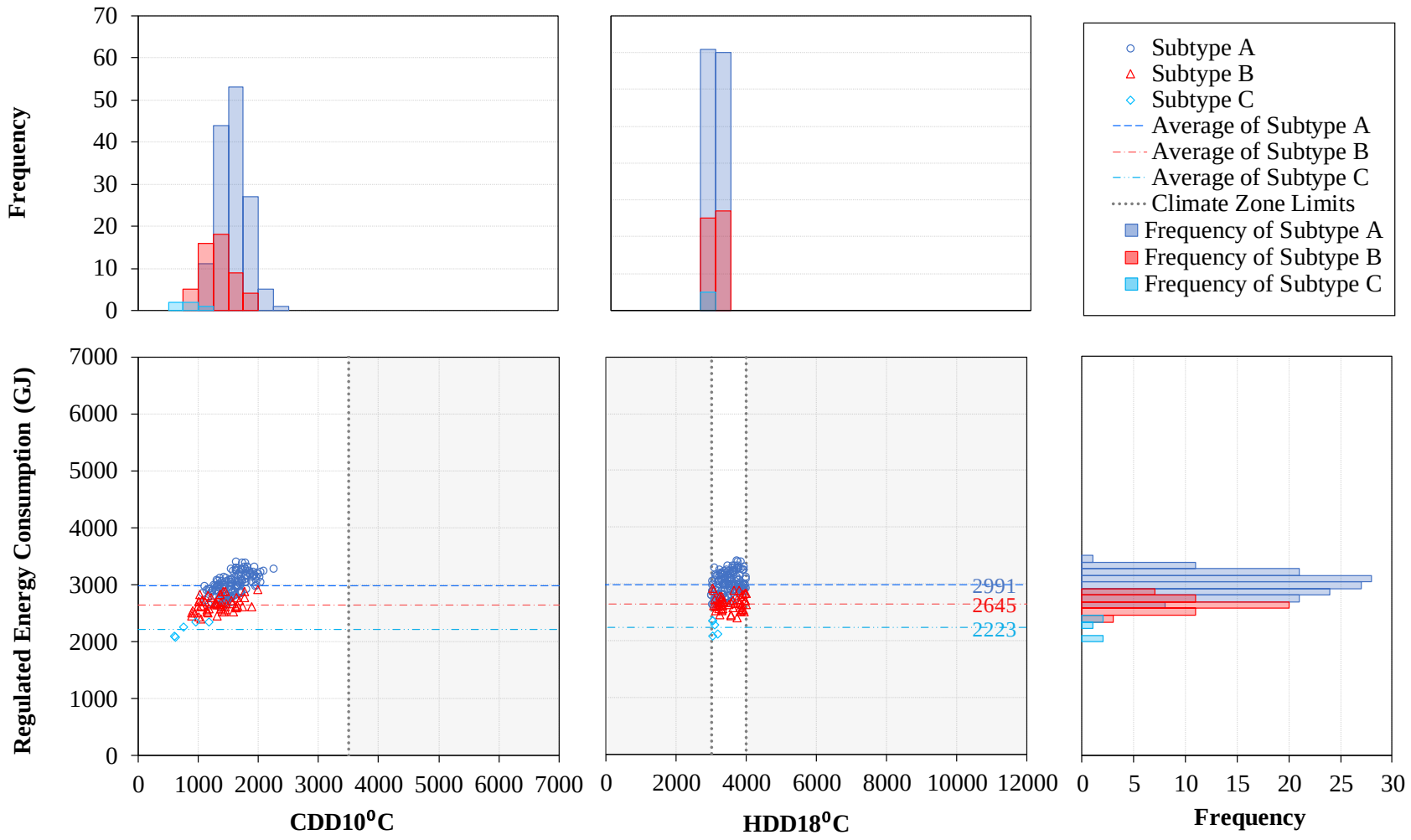

Figure 135: Regulated Energy Consumption of the ASHRAE Standard 90.1-2016 Medium Office Prototype Models in Climate Zone 5

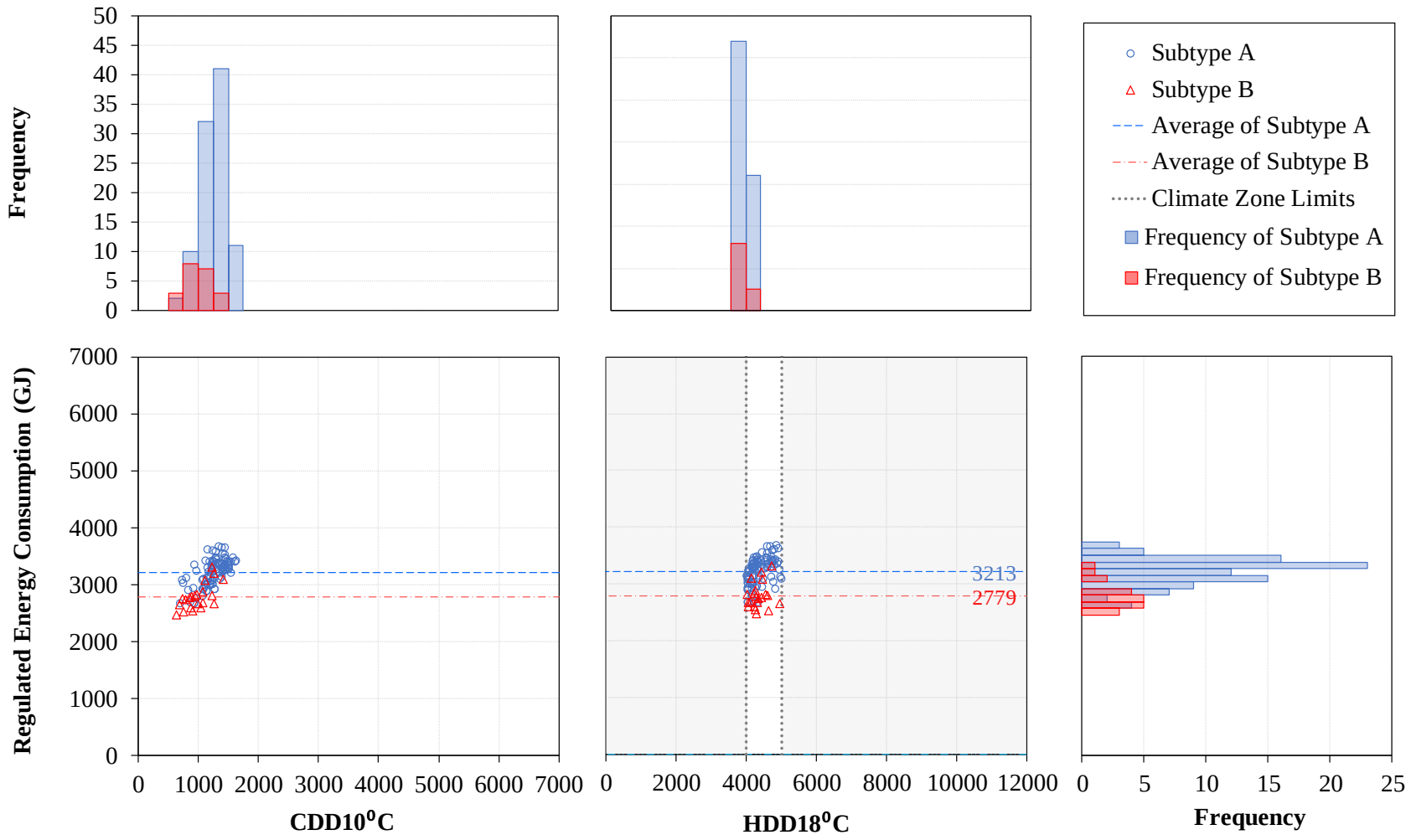

Figure 136: Regulated Energy Consumption of the ASHRAE Standard 90.1-2016 Medium Office Prototype Models in Climate Zone 6

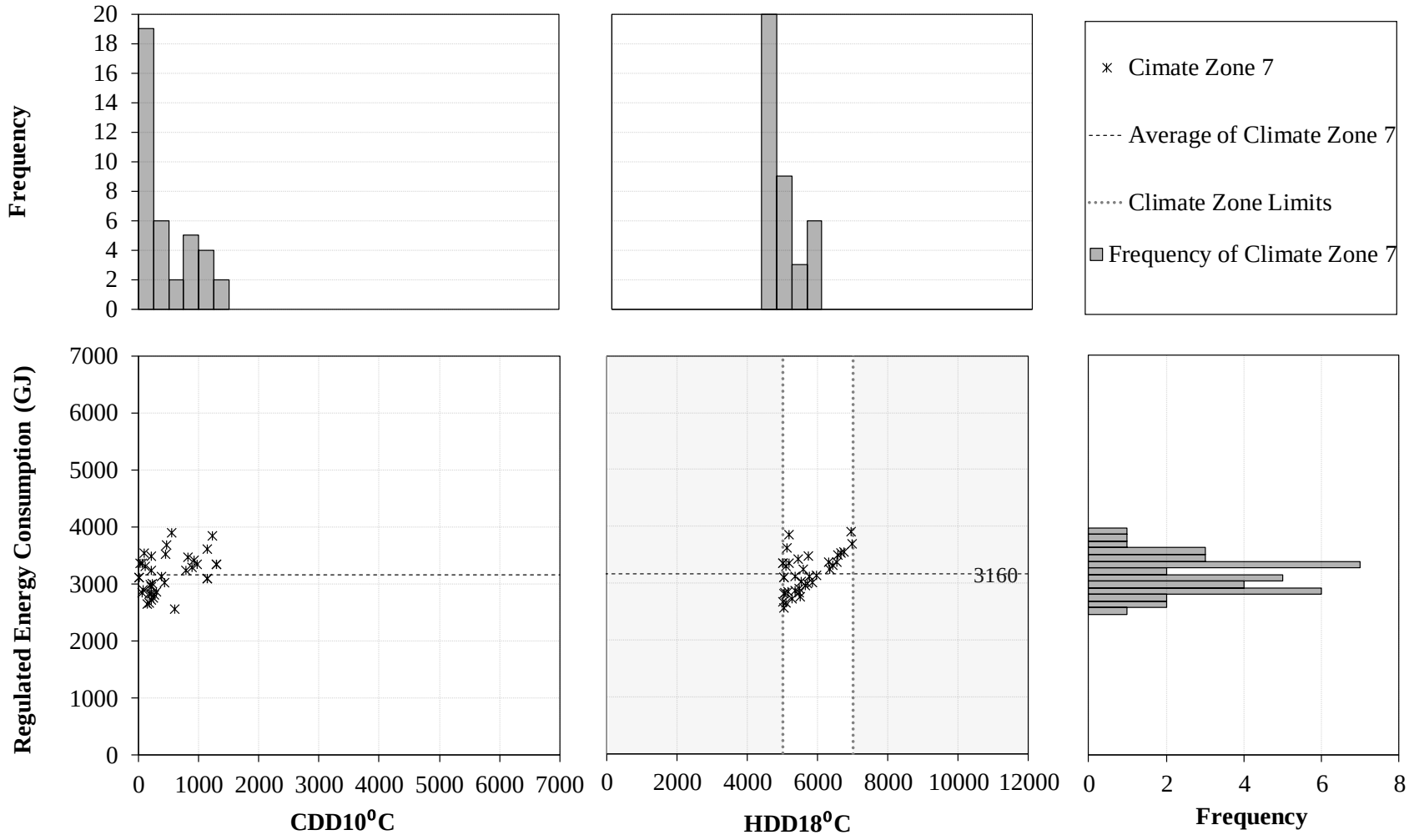

Figure 137: Regulated Energy Consumption of the ASHRAE Standard 90.1-2016 Medium Office Prototype Models in Climate Zone 7

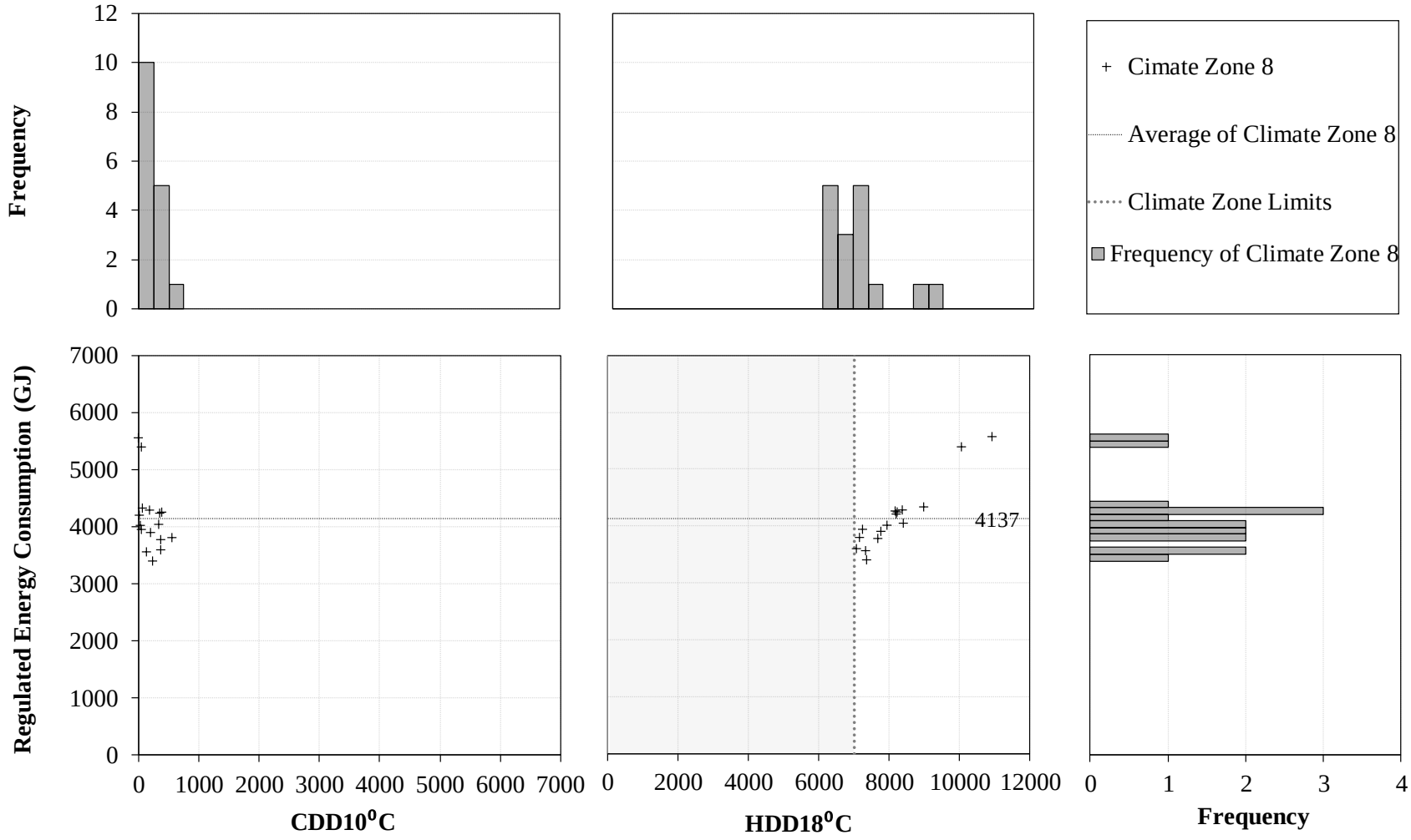

Figure 138: Regulated Energy Consumption of the ASHRAE Standard 90.1-2016 Medium Office Prototype Models in Climate Zone 8

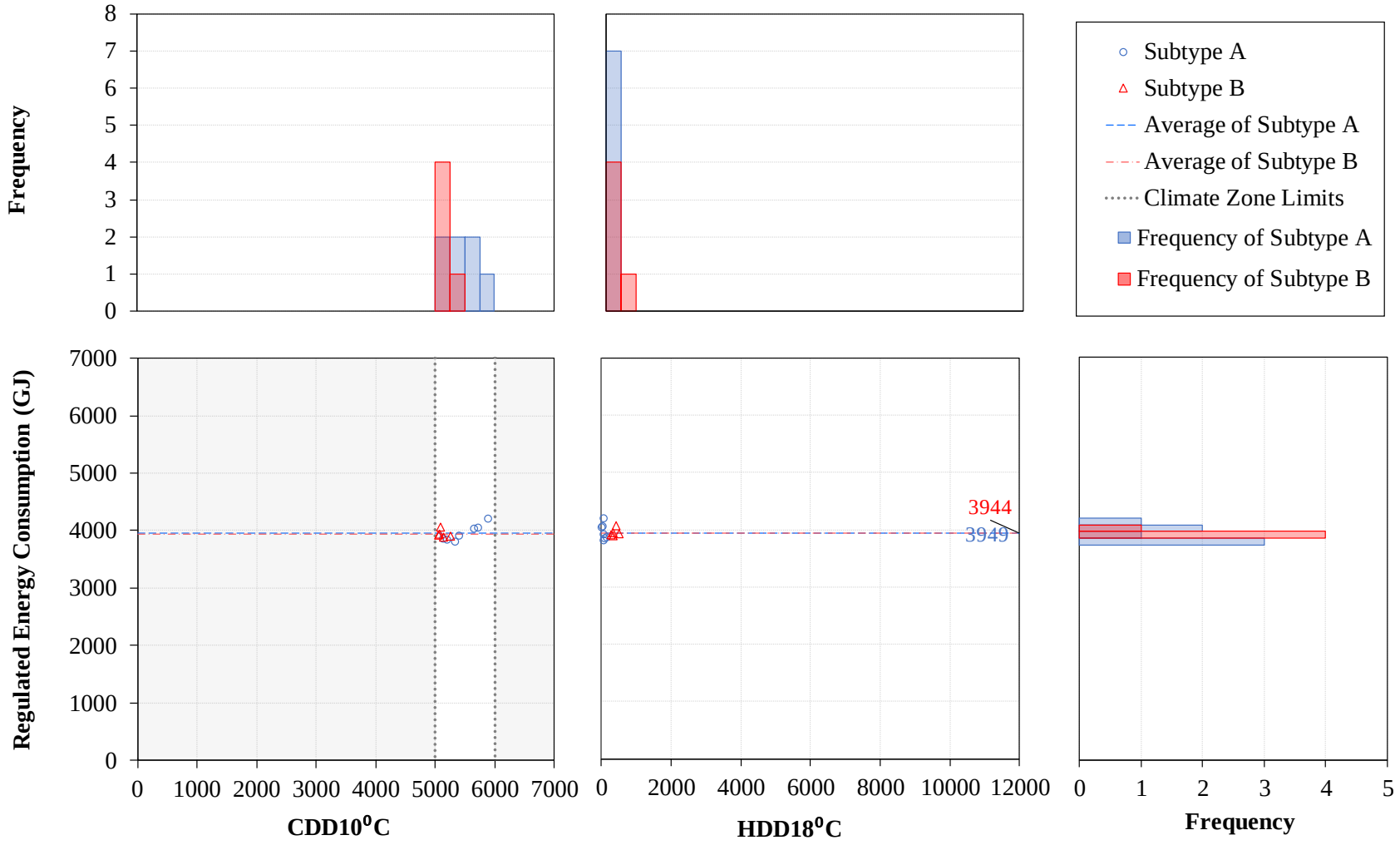

Figure 139: Regulated Energy Consumption of the ASHRAE Standard 90.1-2016 Medium Office Prototype Models without Daylight Responsive Controls in Climate Zone 1

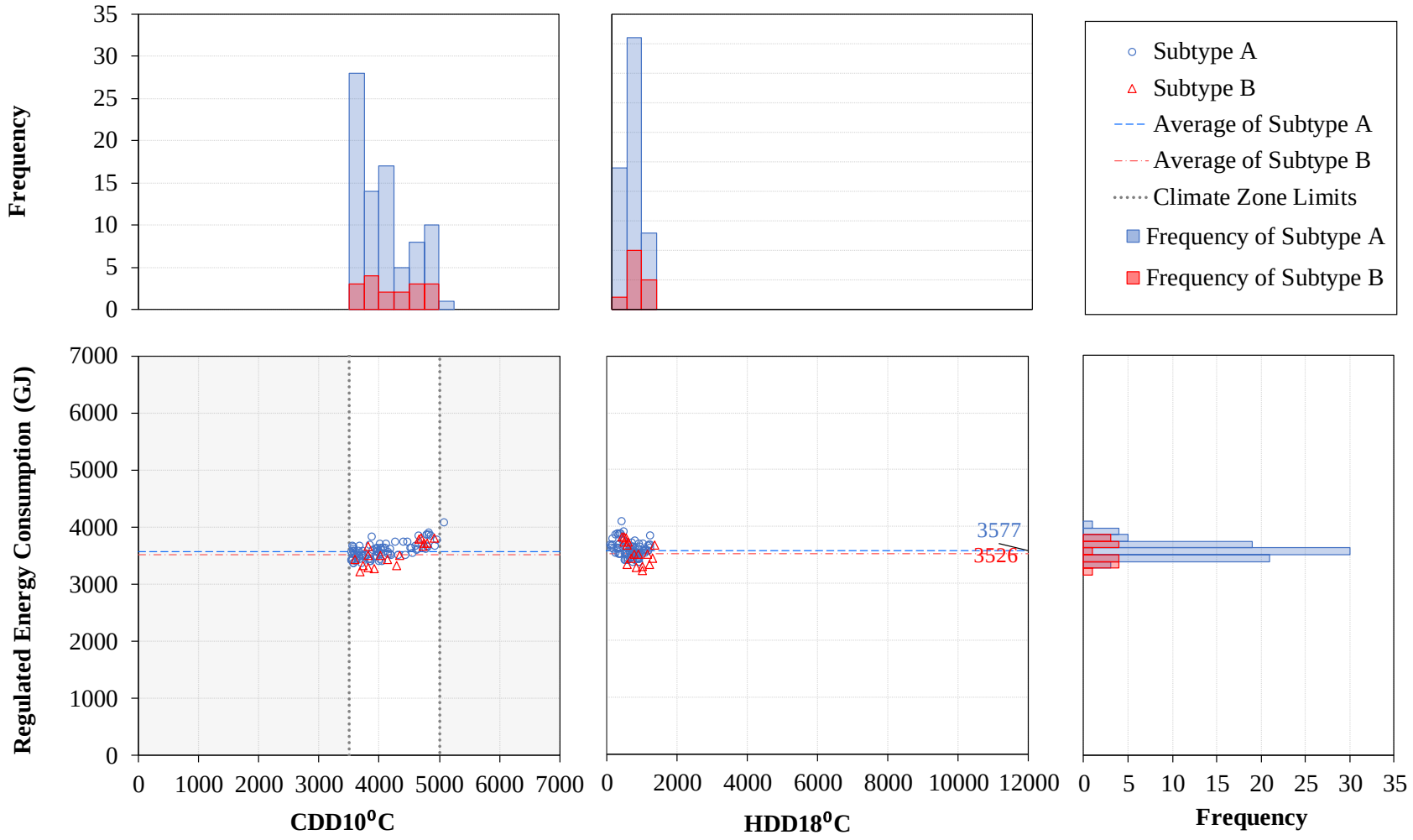

Figure 140: Regulated Energy Consumption of the ASHRAE Standard 90.1-2016 Medium Office Prototype Models without Daylight Responsive Controls in Climate Zone 2

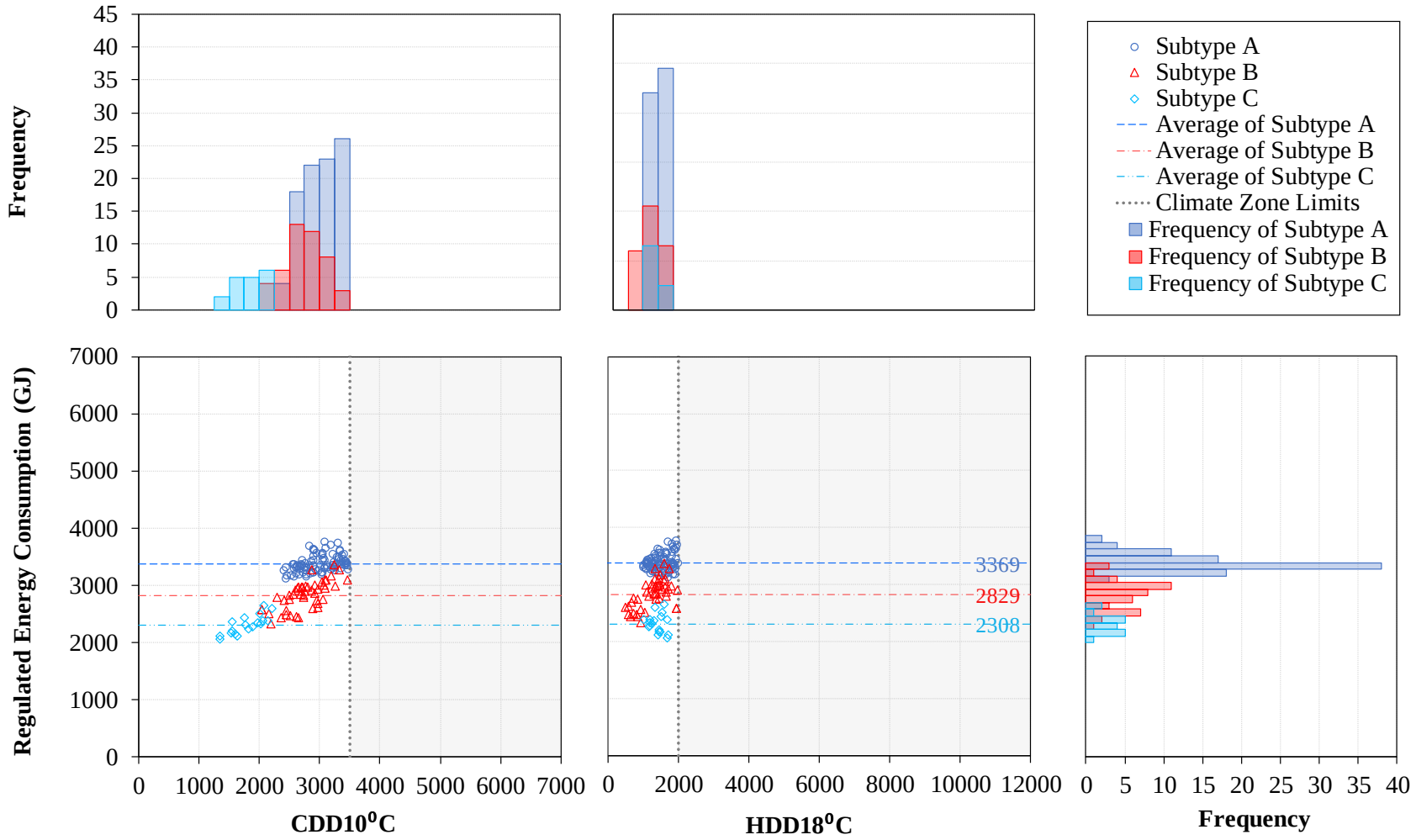

Figure 141: Regulated Energy Consumption of the ASHRAE Standard 90.1-2016 Medium Office Prototype Models without Daylight Responsive Controls in Climate Zone 3

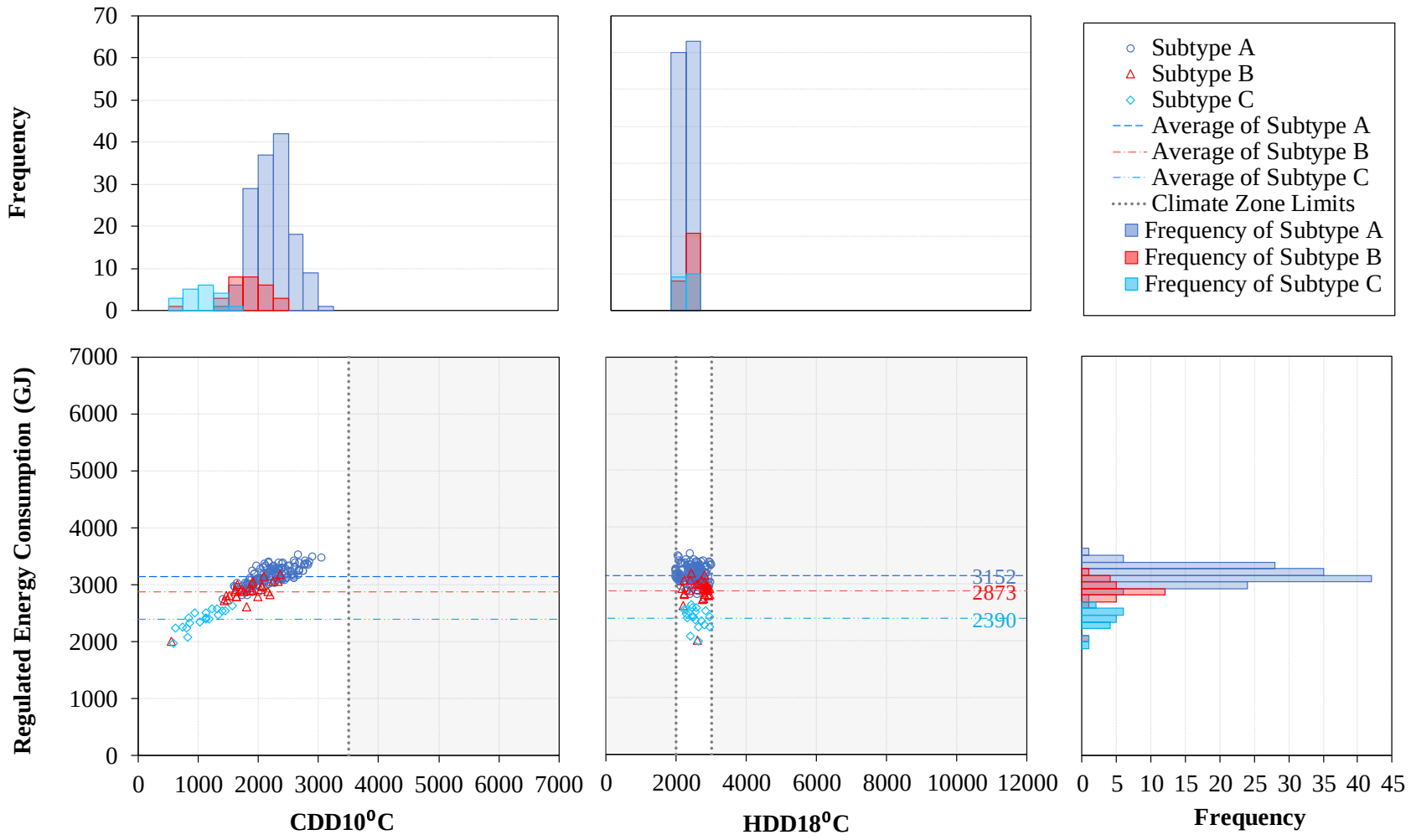

Figure 142: Regulated Energy Consumption of the ASHRAE Standard 90.1-2016 Medium Office Prototype Models without Daylight Responsive Controls in Climate Zone 4

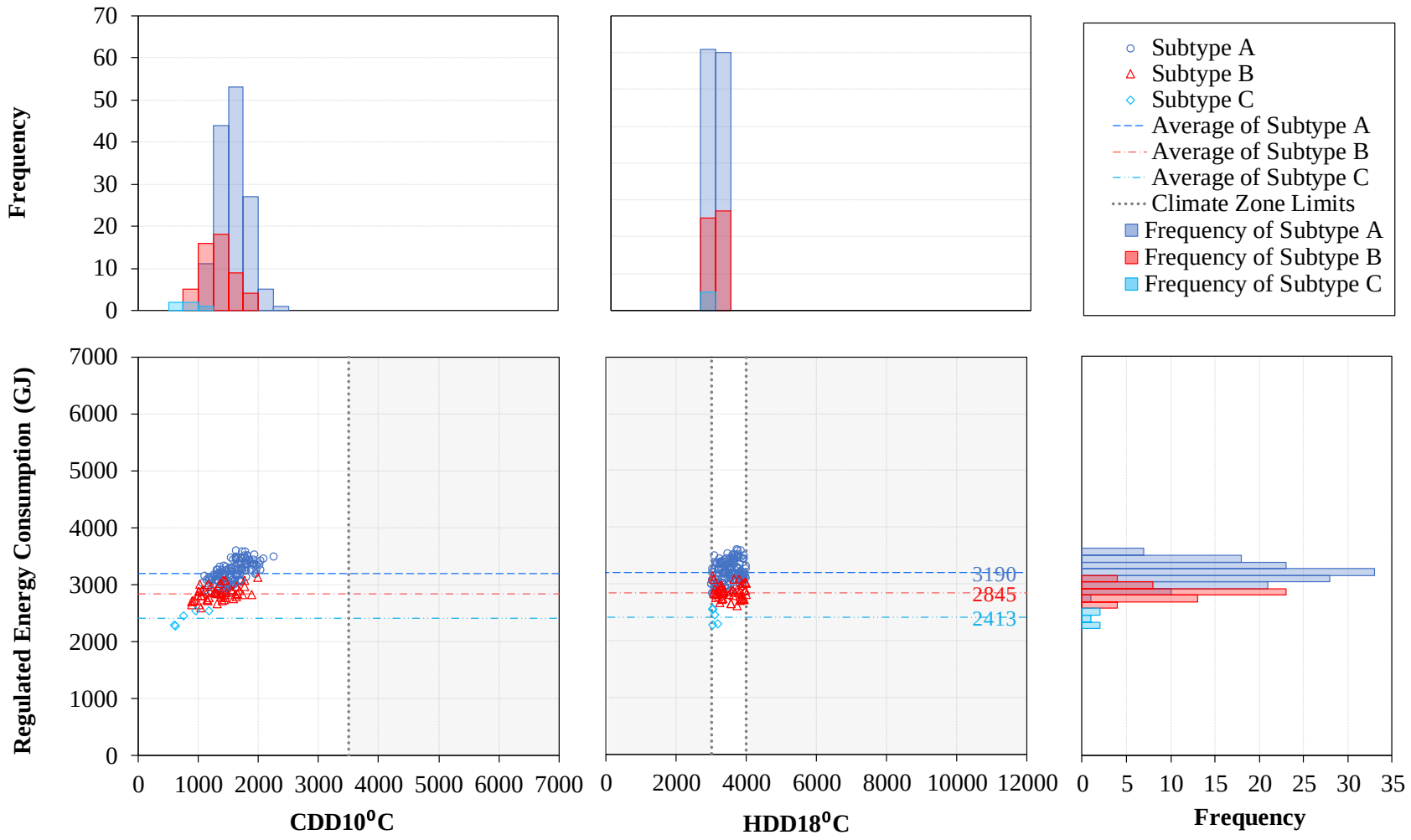

Figure 143: Regulated Energy Consumption of the ASHRAE Standard 90.1-2016 Medium Office Prototype Models without Daylight Responsive Controls in Climate Zone 5

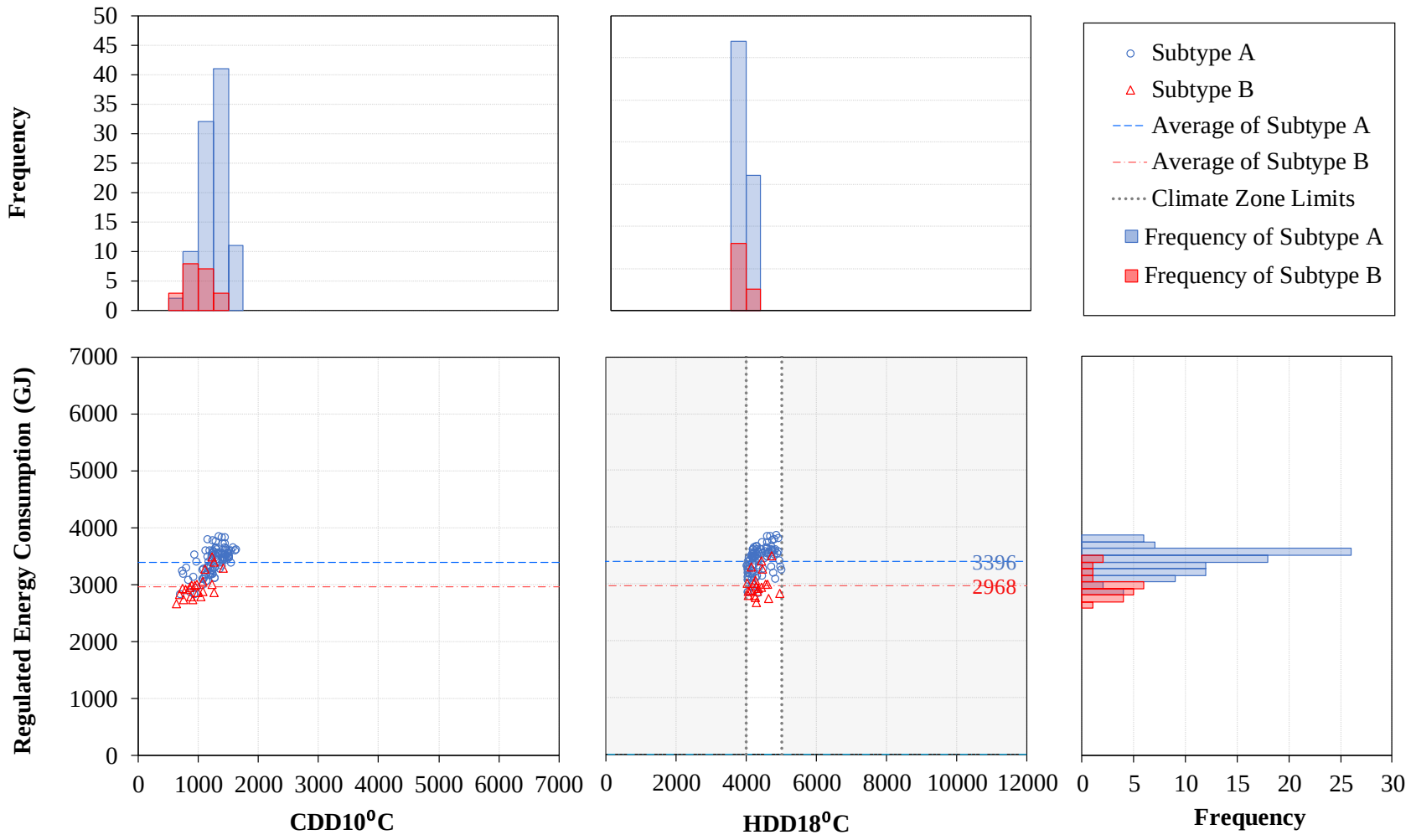

Figure 144: Regulated Energy Consumption of the ASHRAE Standard 90.1-2016 Medium Office Prototype Models without Daylight Responsive Controls in Climate Zone 6

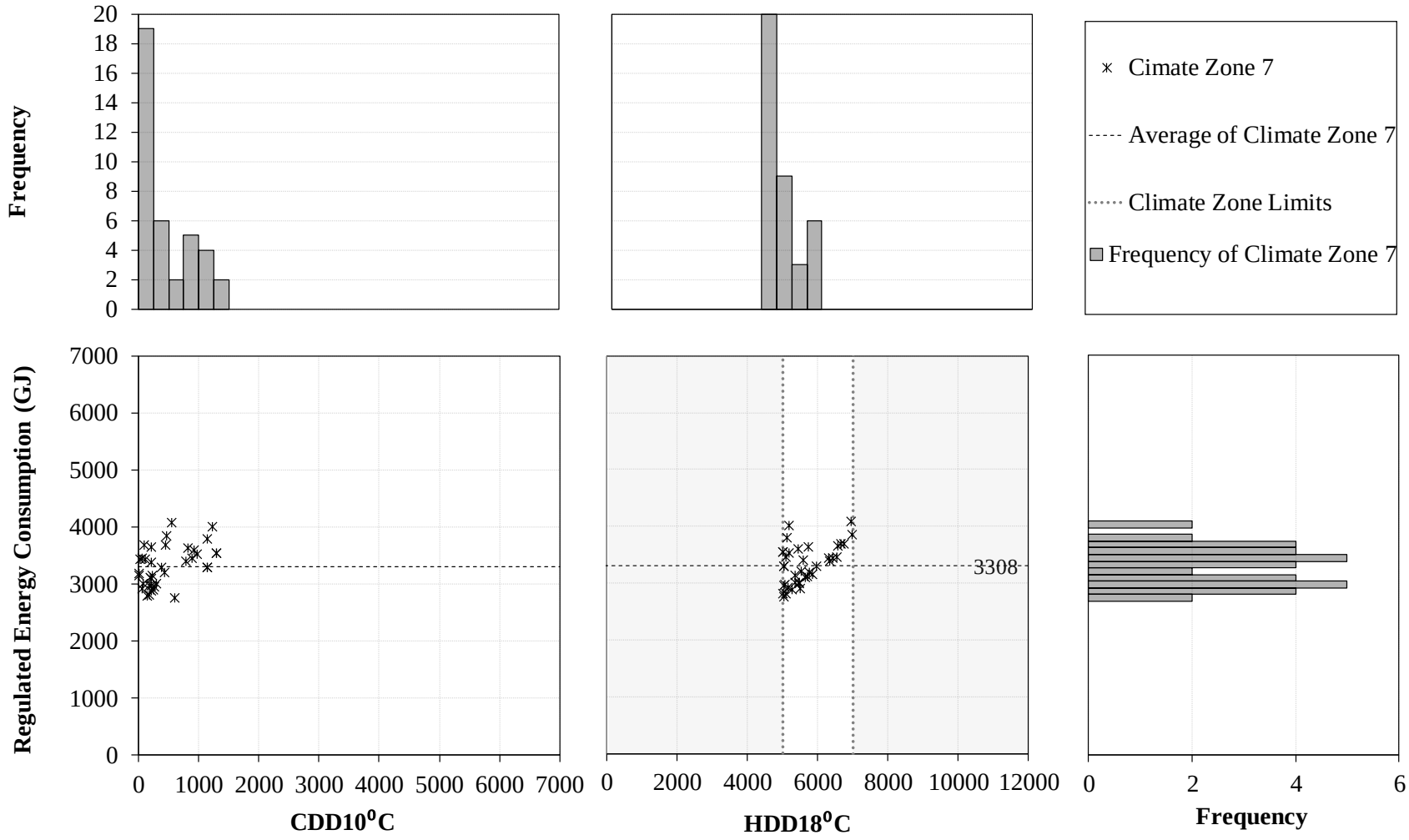

Figure 145: Regulated Energy Consumption of the ASHRAE Standard 90.1-2016 Medium Office Prototype Models without Daylight Responsive Controls in Climate Zone 7

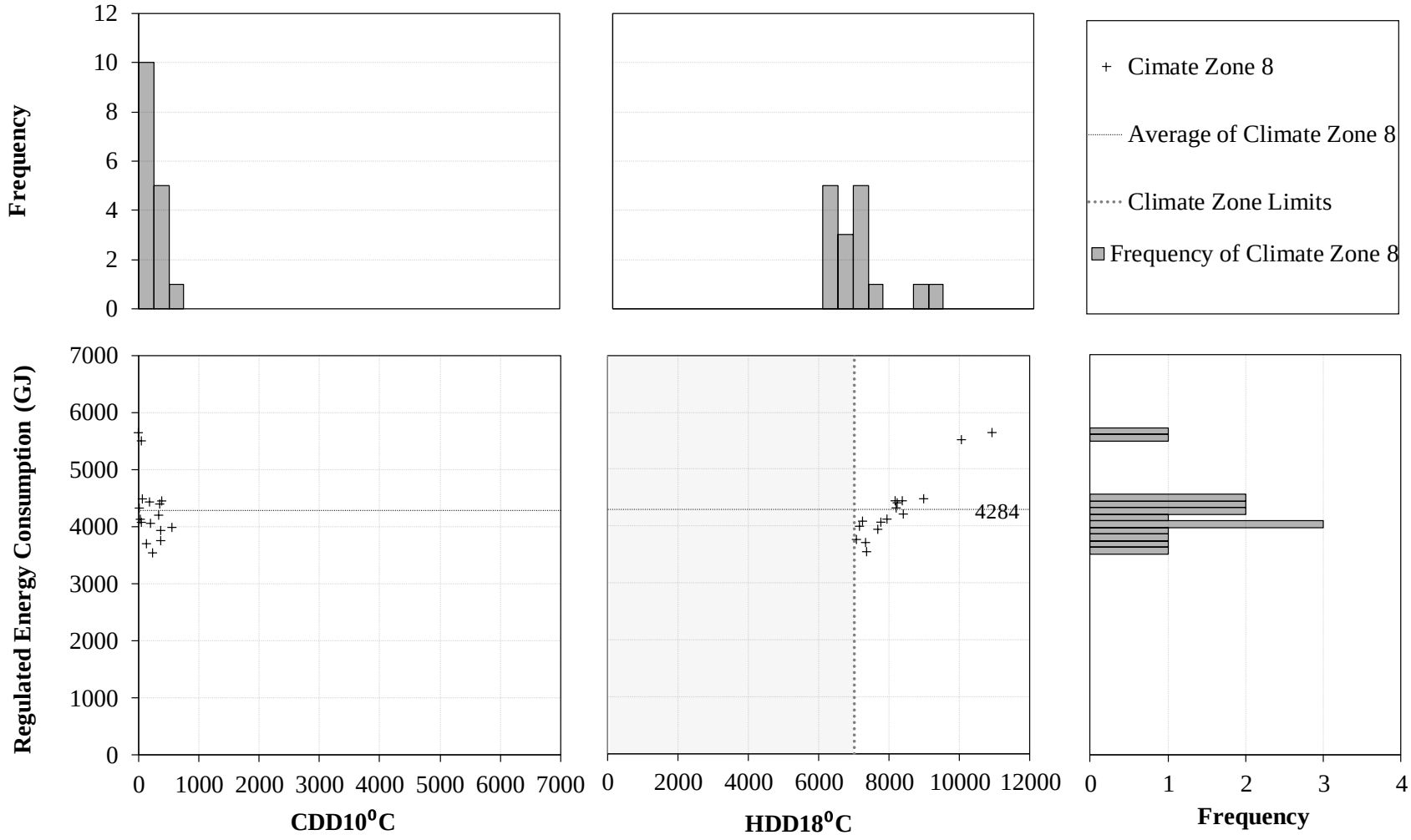

Figure 146: Regulated Energy Consumption of the ASHRAE Standard 90.1-2016 Medium Office Prototype Models without Daylight Responsive Controls in Climate Zone 8

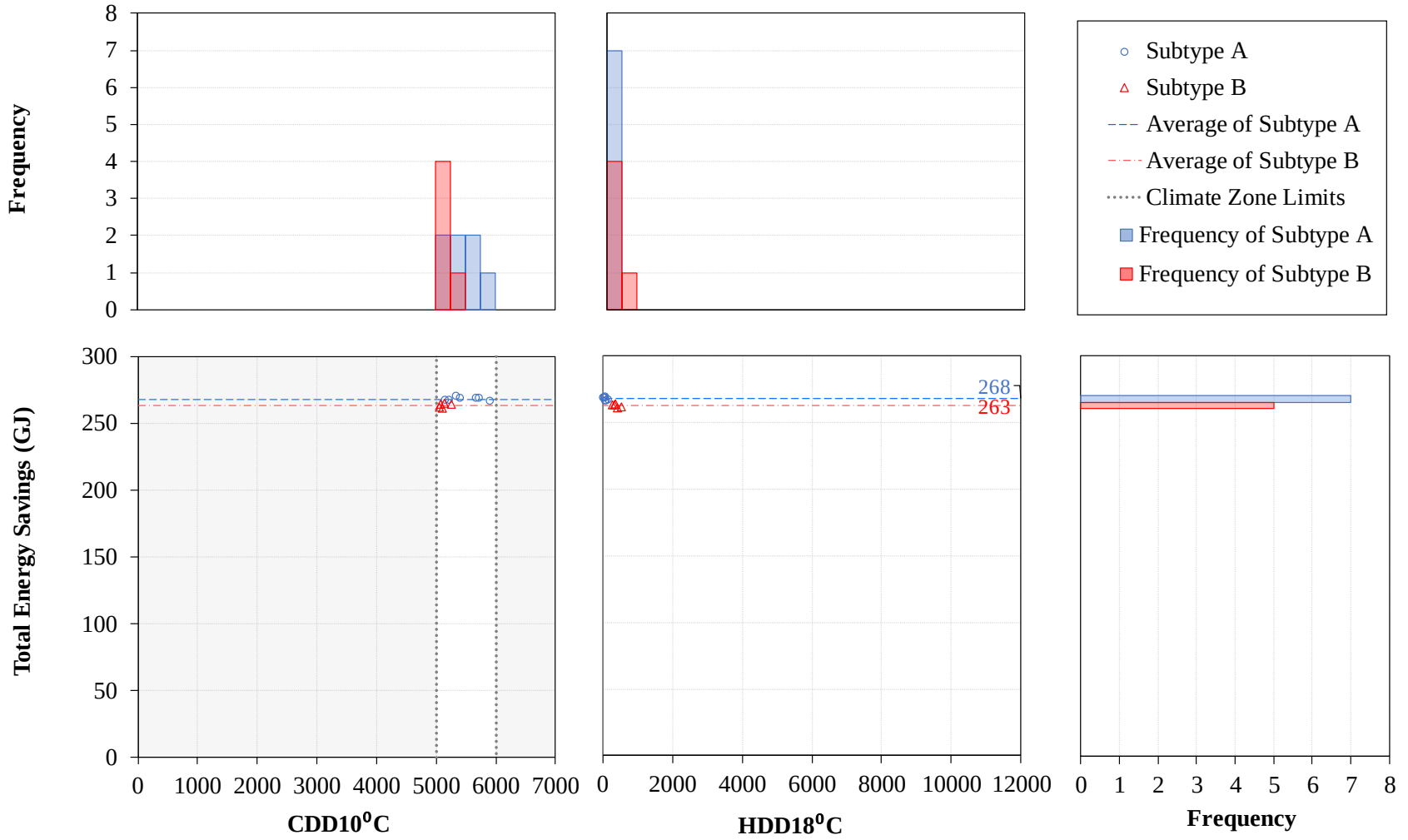

Figure 147: Total Energy Savings of the ASHRAE Standard 90.1-2016 Medium Office Prototype Models Associated with the Implementation of Daylight Responsive Controls in Climate Zone 1

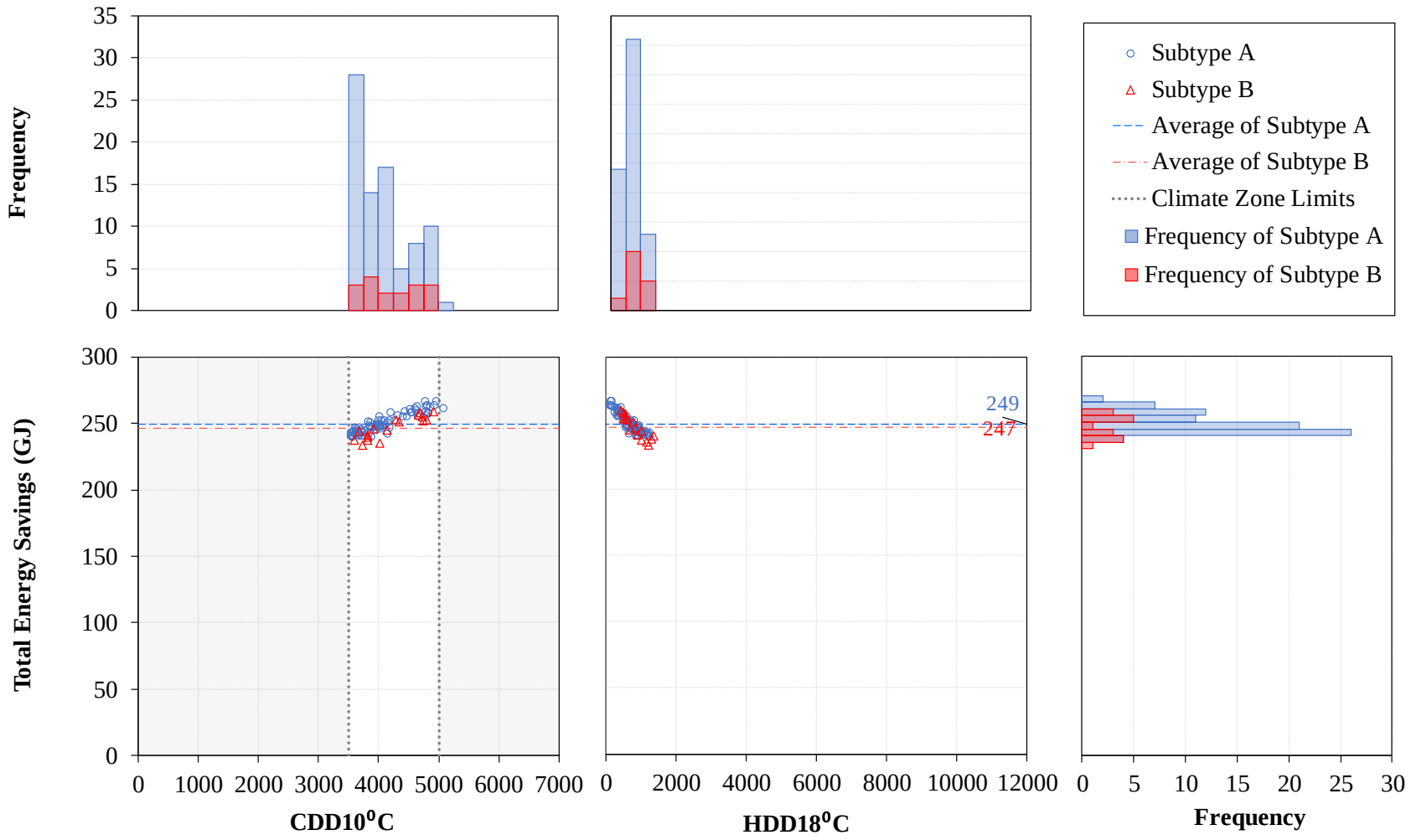

Figure 148: Total Energy Savings of the ASHRAE Standard 90.1-2016 Medium Office Prototype Models Associated with the Implementation of Daylight Responsive Controls in Climate Zone 2

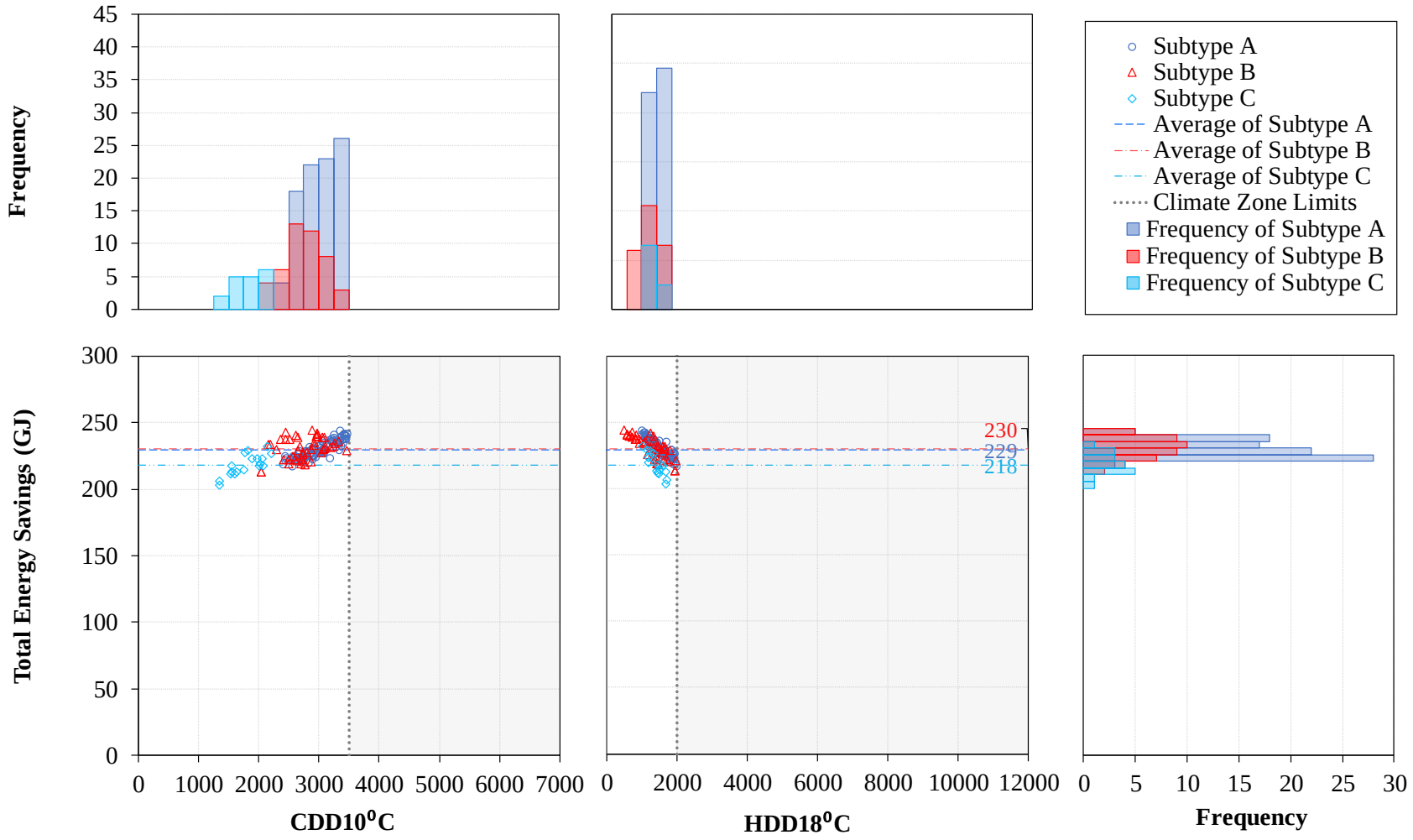

Figure 149: Total Energy Savings of the ASHRAE Standard 90.1-2016 Medium Office Prototype Models Associated with the Implementation of Daylight Responsive Controls in Climate Zone 3

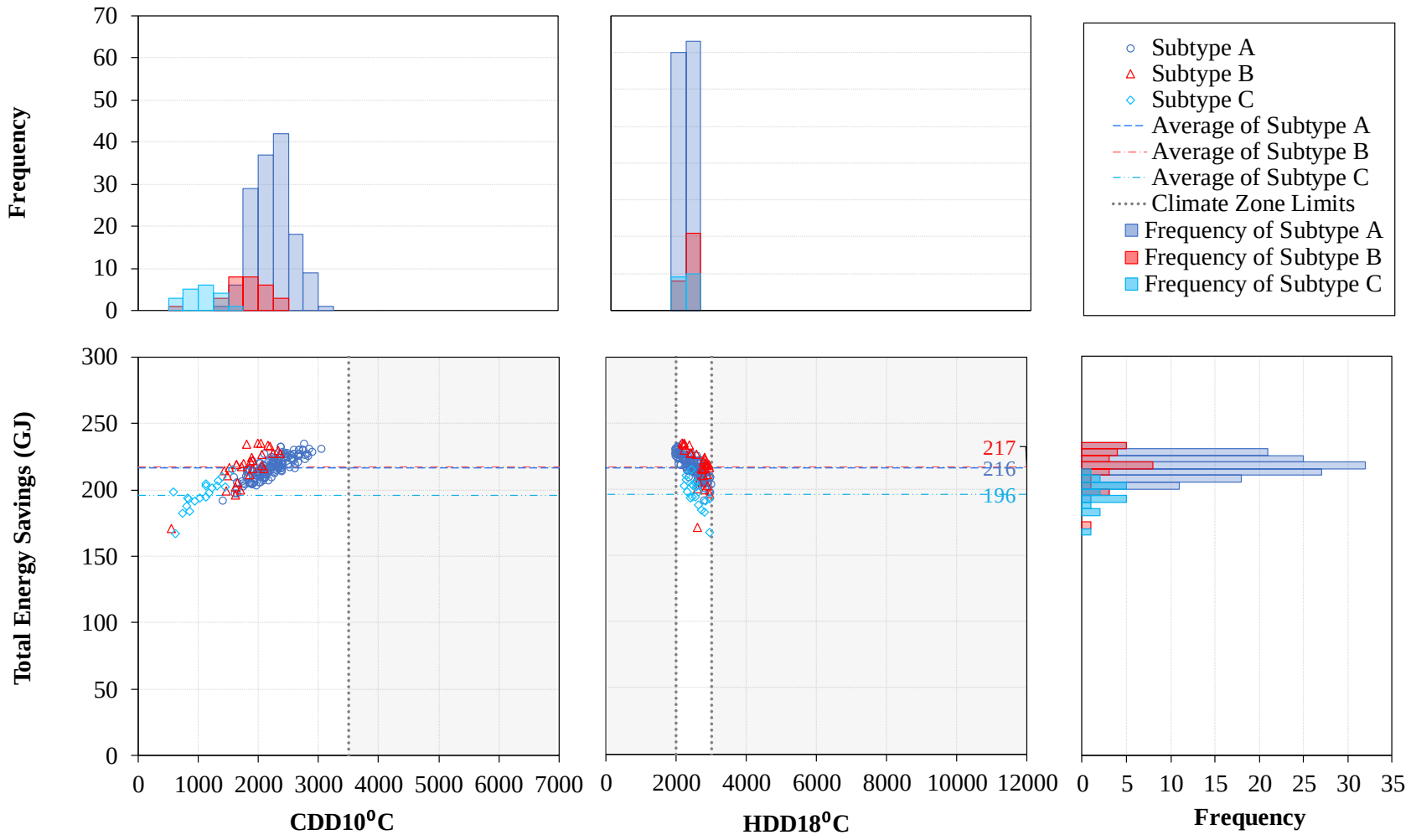

Figure 150: Total Energy Savings of the ASHRAE Standard 90.1-2016 Medium Office Prototype Models Associated with the Implementation of Daylight Responsive Controls in Climate Zone 4

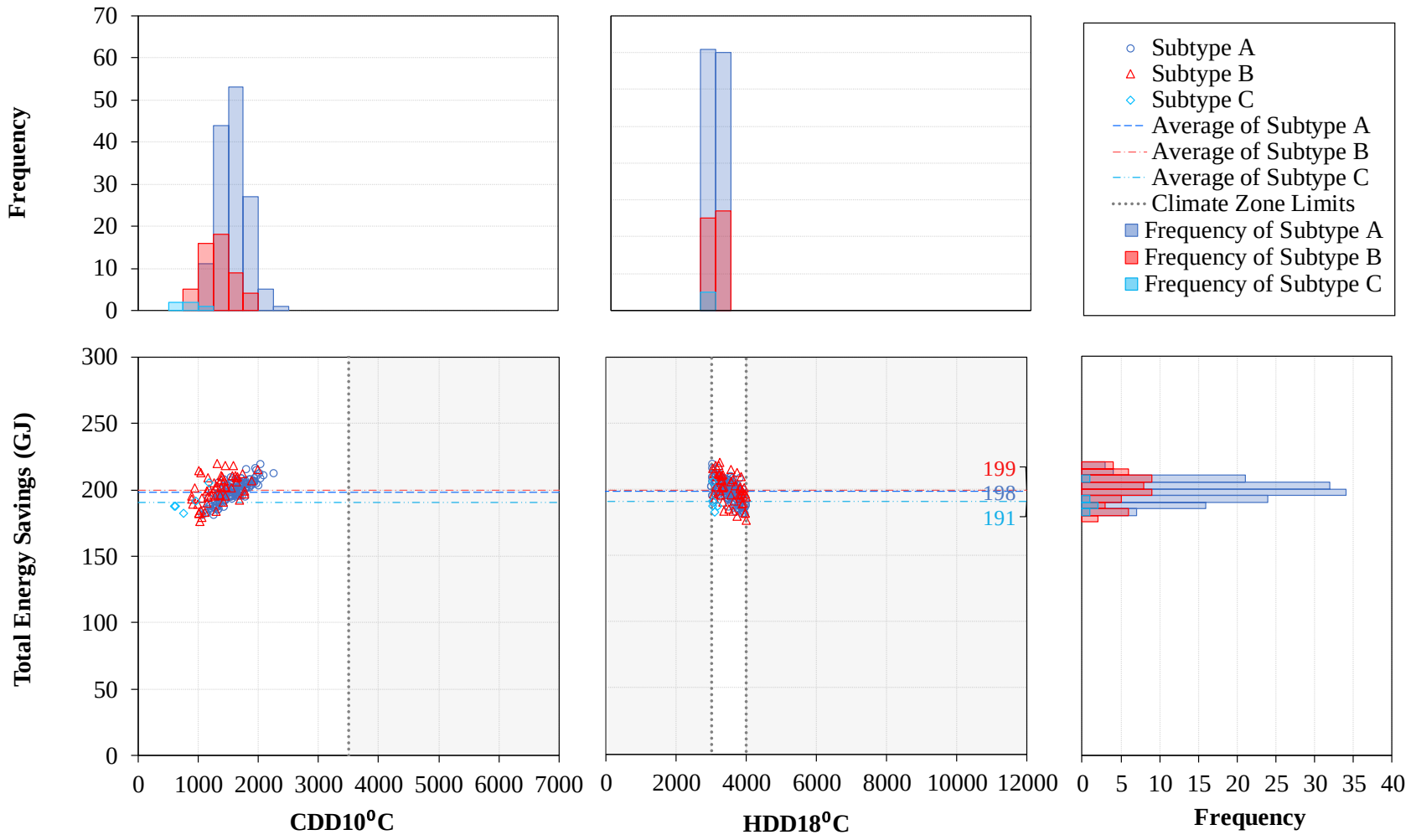

Figure 151: Total Energy Savings of the ASHRAE Standard 90.1-2016 Medium Office Prototype Models Associated with the Implementation of Daylight Responsive Controls in Climate Zone 5

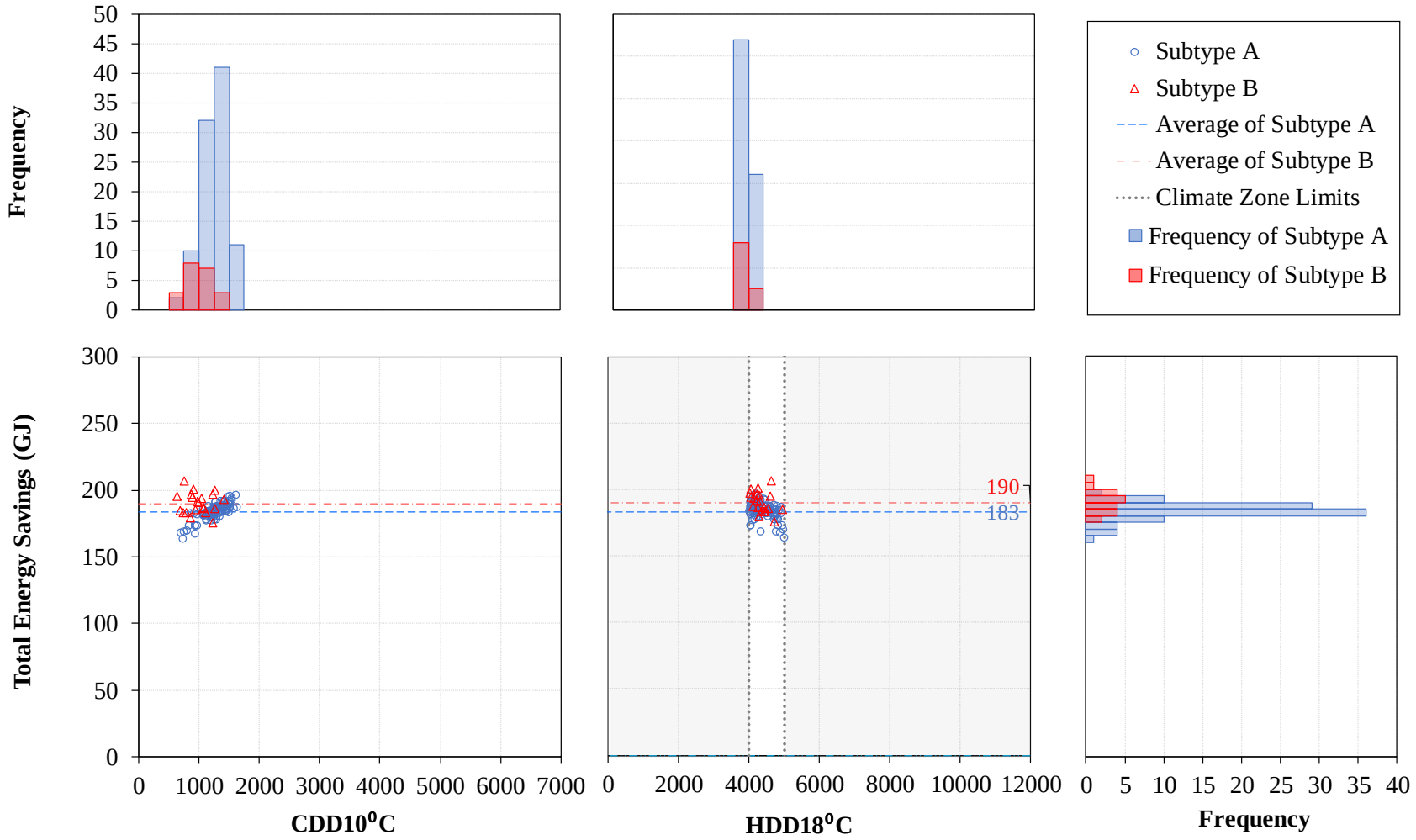

Figure 152: Total Energy Savings of the ASHRAE Standard 90.1-2016 Medium Office Prototype Models Associated with the Implementation of Daylight Responsive Controls in Climate Zone 6

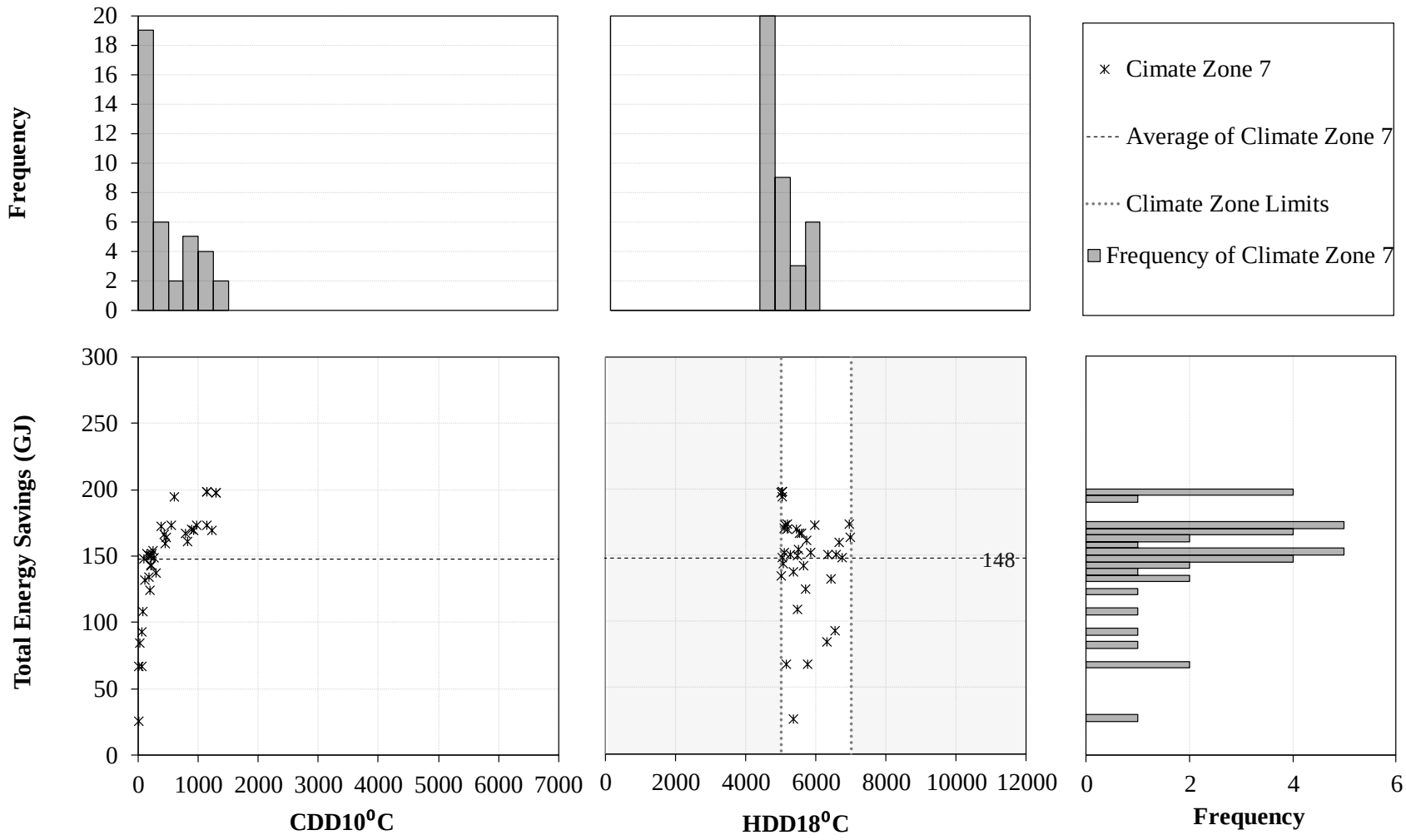

Figure 153: Total Energy Savings of the ASHRAE Standard 90.1-2016 Medium Office Prototype Models Associated with the Implementation of Daylight Responsive Controls in Climate Zone 7

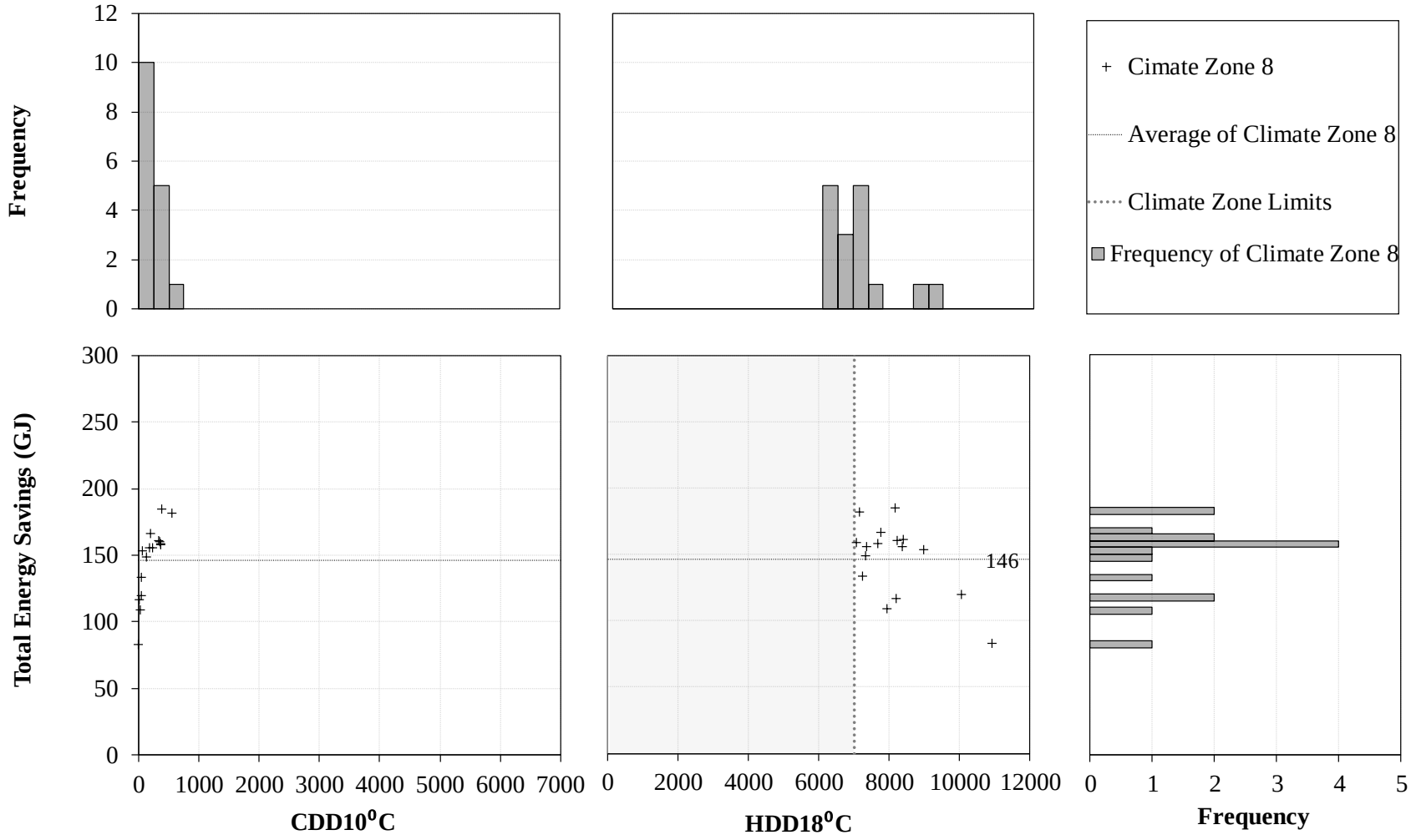

Figure 154: Total Energy Savings of the ASHRAE Standard 90.1-2016 Medium Office Prototype Models Associated with the Implementation of Daylight Responsive Controls in Climate Zone 8

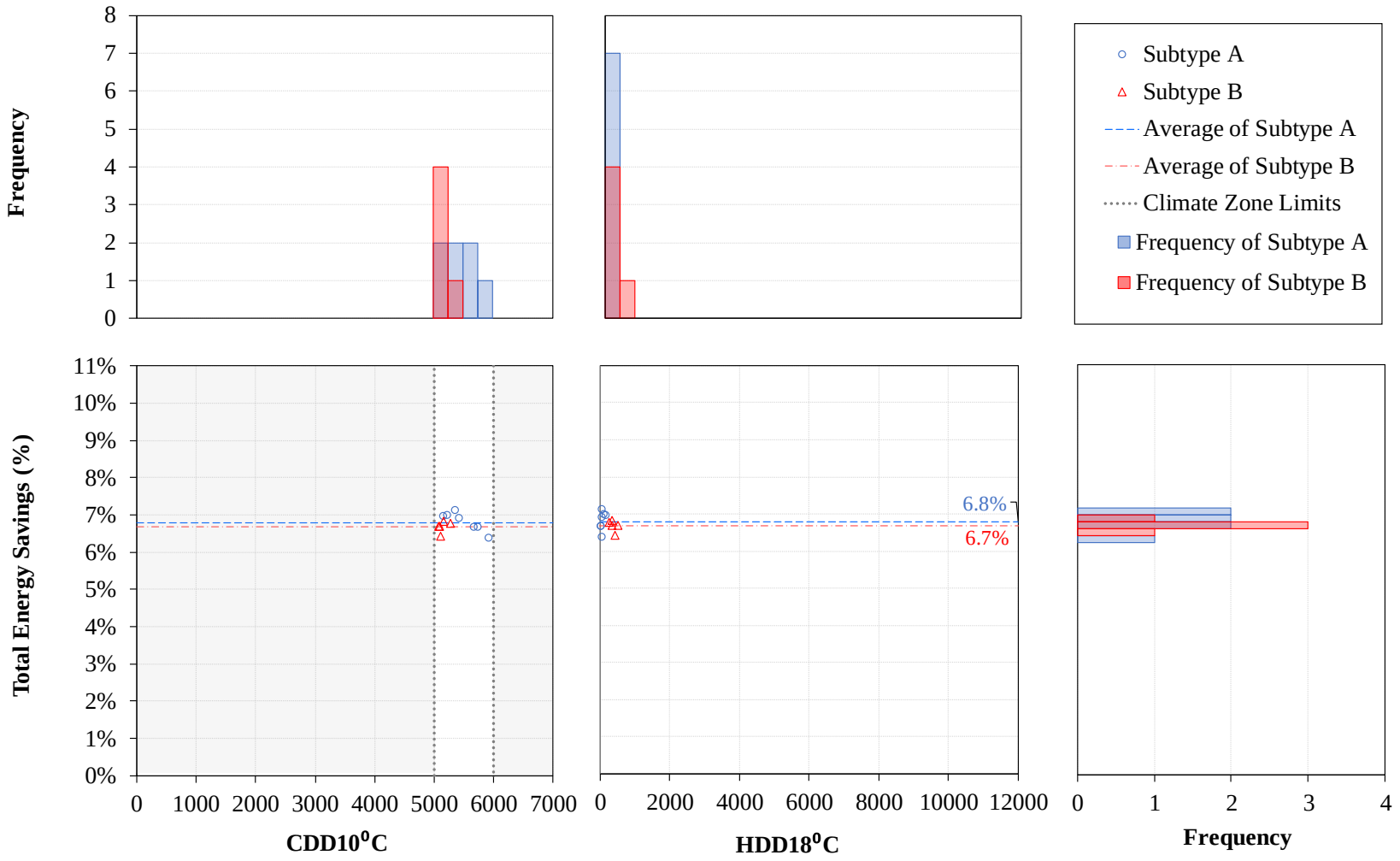

Figure 155: Total Energy Savings Percentage of the ASHRAE Standard 90.1-2016 Medium Office Prototype Models Associated with the Implementation of Daylight Responsive Controls in Climate Zone 1

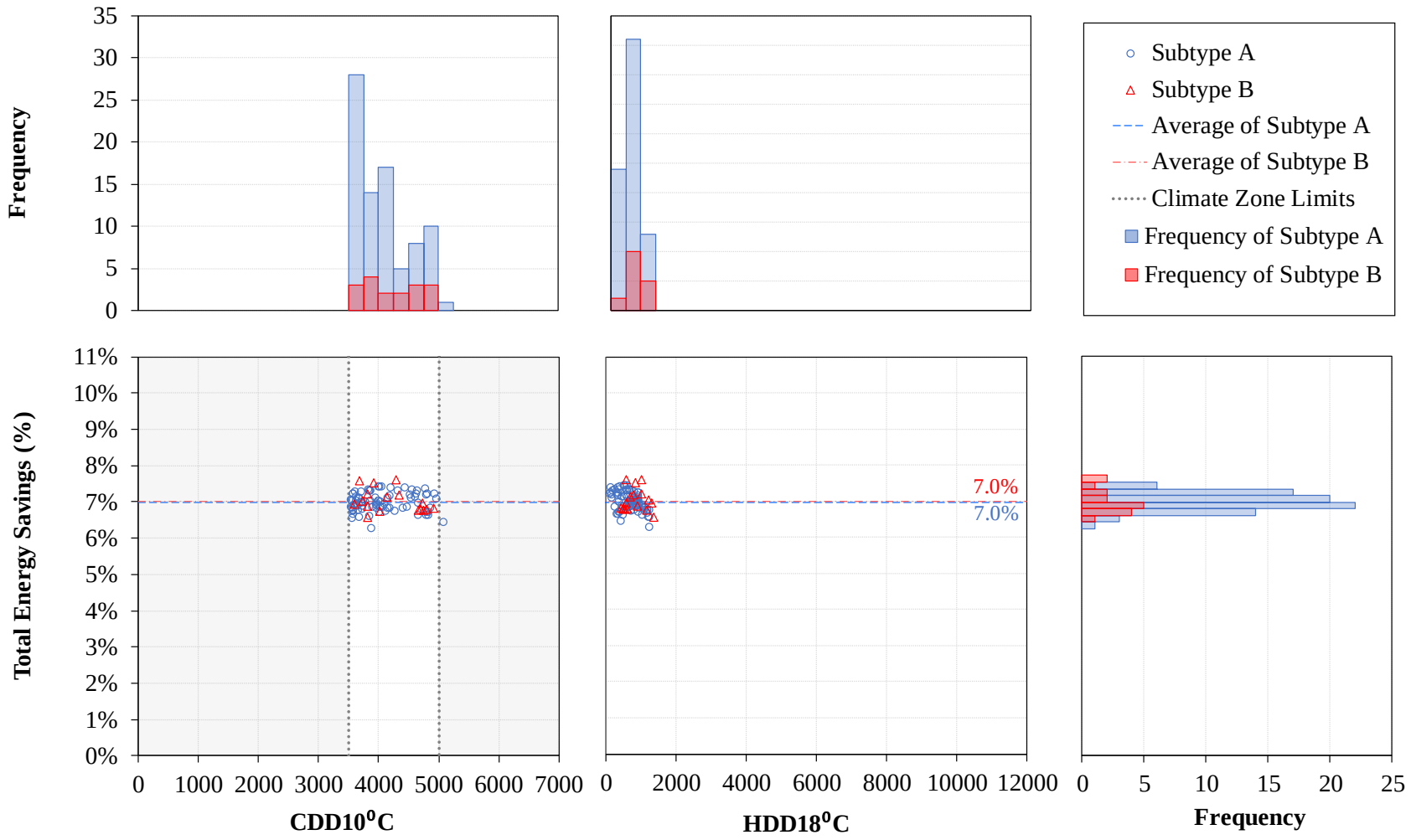

Figure 156: Total Energy Savings Percentage of the ASHRAE Standard 90.1-2016 Medium Office Prototype Models Associated with the Implementation of Daylight Responsive Controls in Climate Zone 2

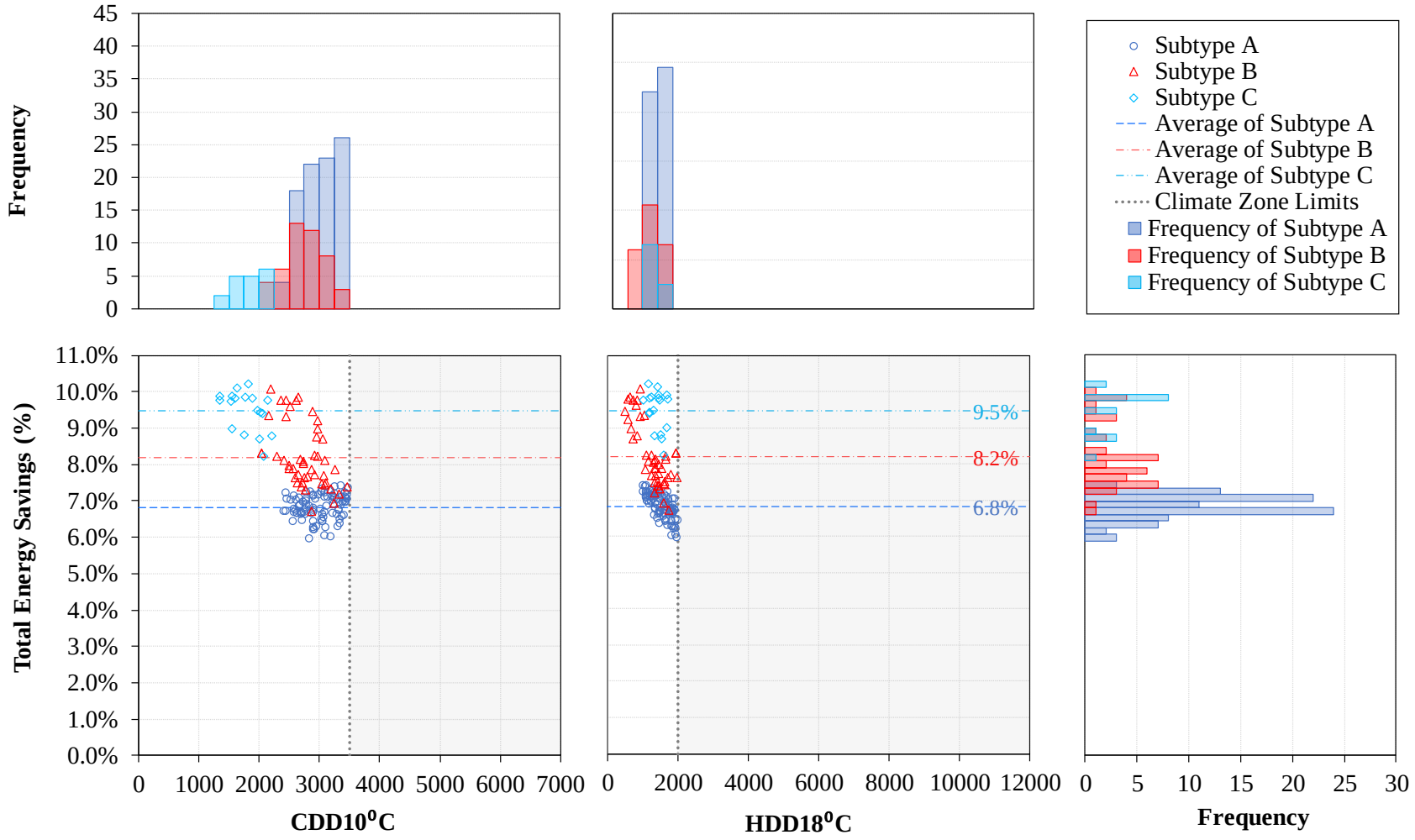

Figure 157: Total Energy Savings Percentage of the ASHRAE Standard 90.1-2016 Medium Office Prototype Models Associated with the Implementation of Daylight Responsive Controls in Climate Zone 3

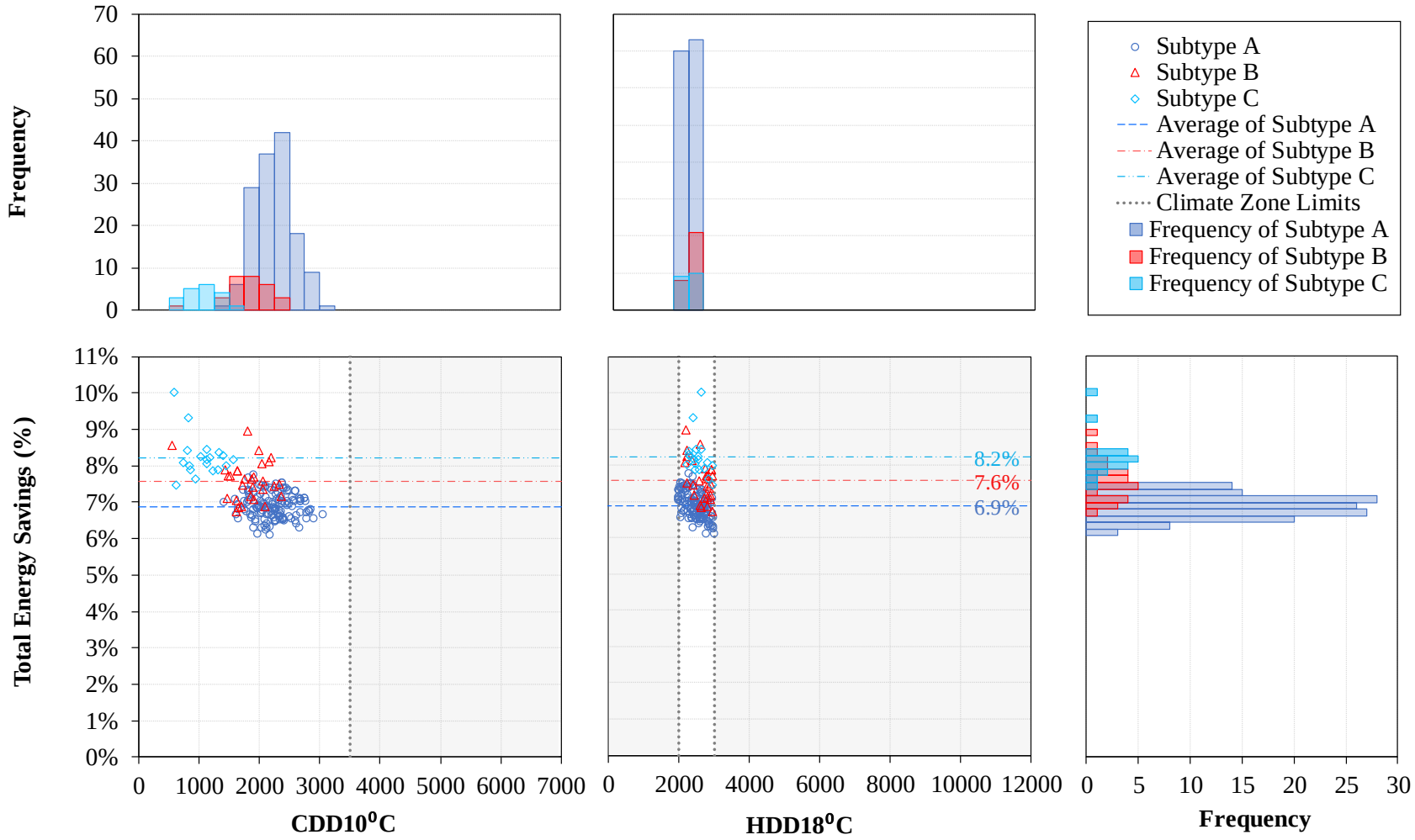

Figure 158: Total Energy Savings Percentage of the ASHRAE Standard 90.1-2016 Medium Office Prototype Models Associated with the Implementation of Daylight Responsive Controls in Climate Zone 4

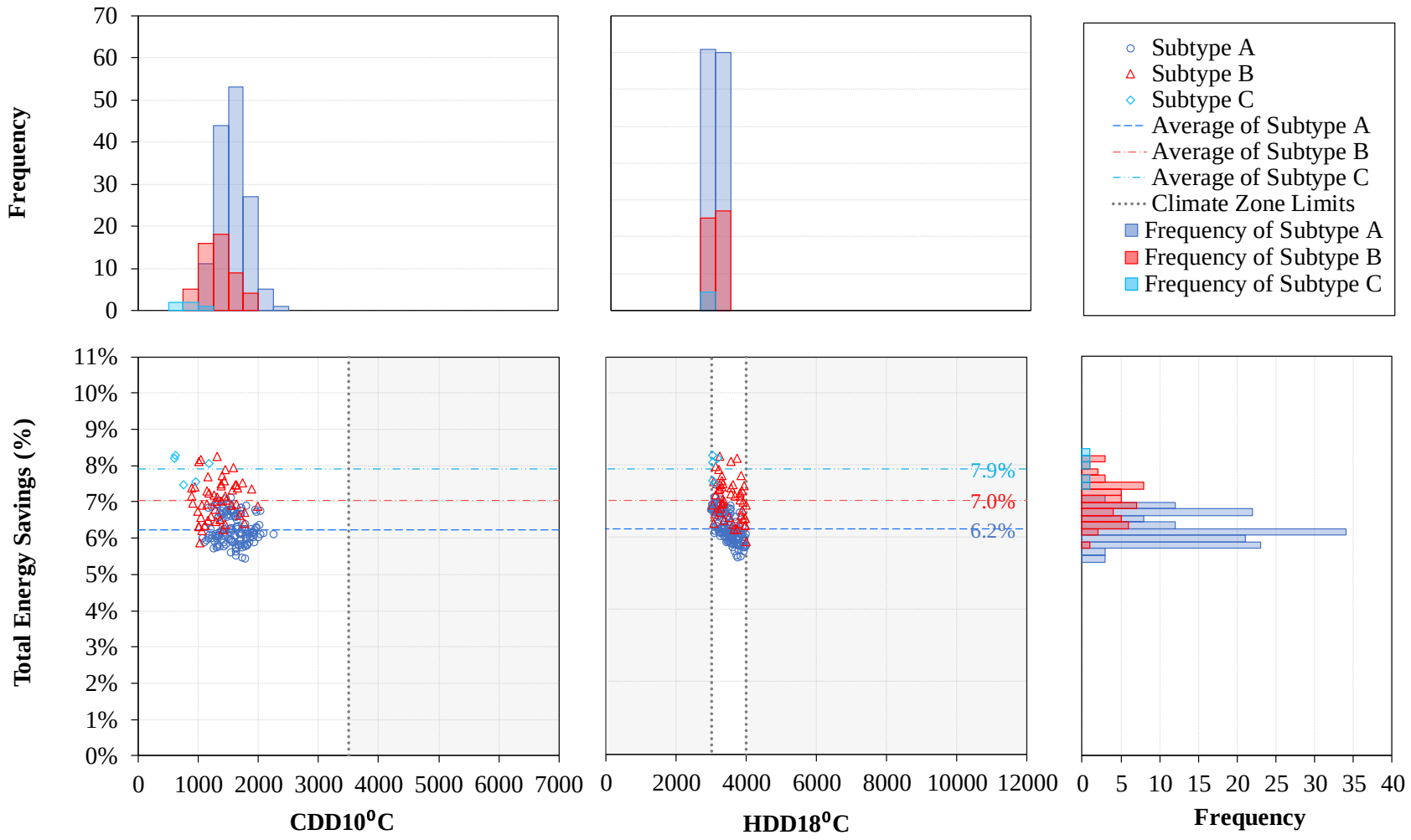

Figure 159: Total Energy Savings Percentage of the ASHRAE Standard 90.1-2016 Medium Office Prototype Models Associated with the Implementation of Daylight Responsive Controls in Climate Zone 5

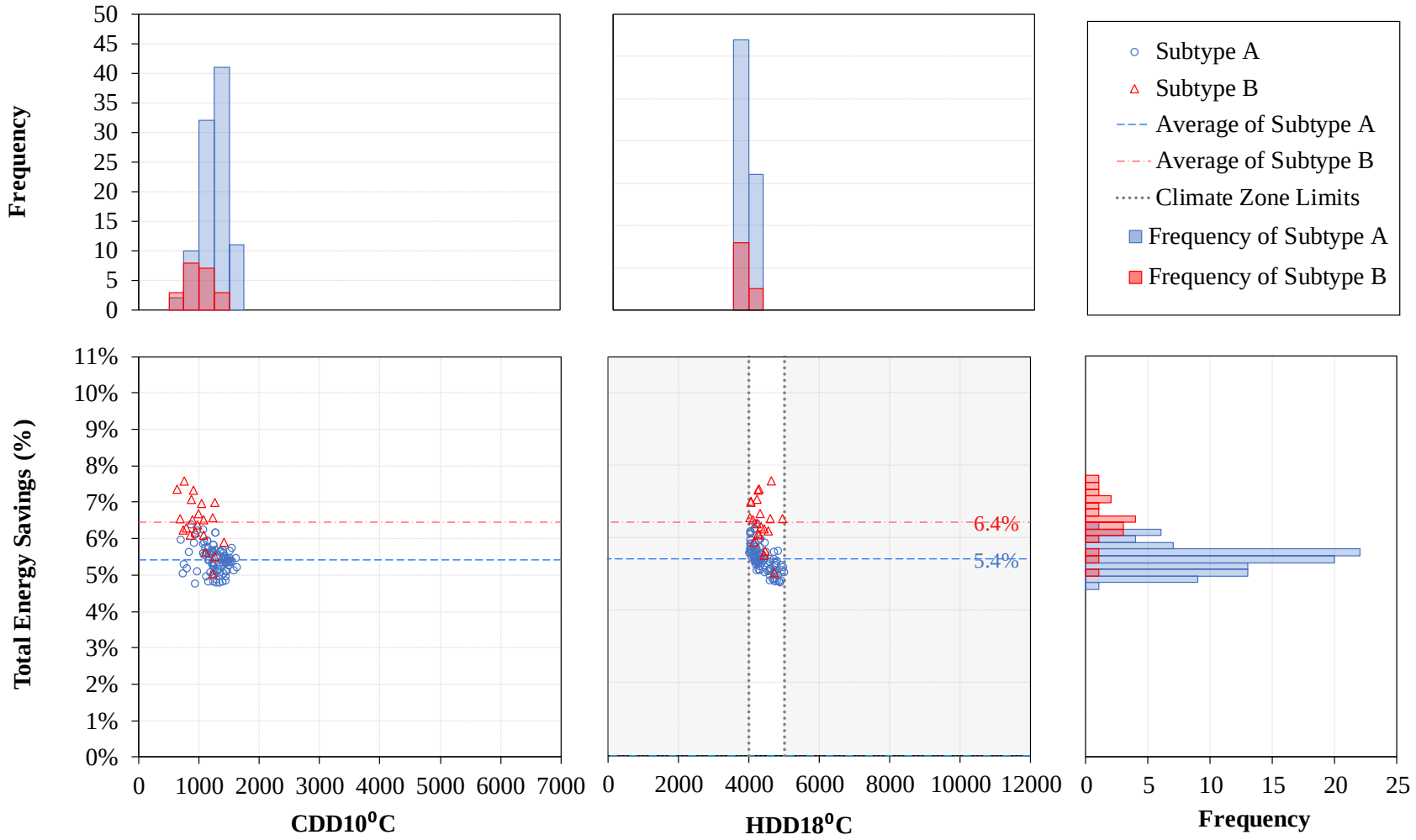

Figure 160: Total Energy Savings Percentage of the ASHRAE Standard 90.1-2016 Medium Office Prototype Models Associated with the Implementation of Daylight Responsive Controls in Climate Zone 6

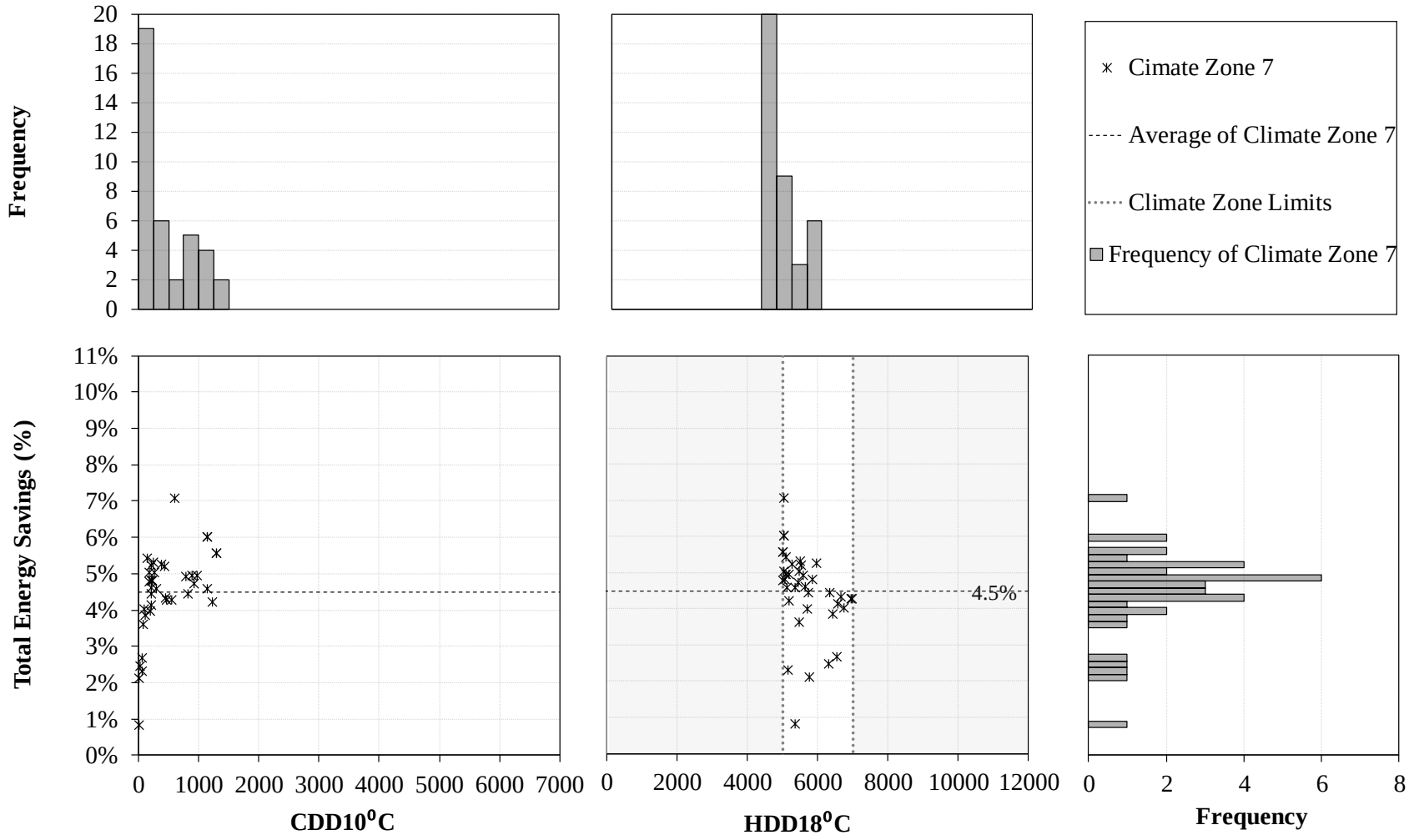

Figure 161: Total Energy Savings Percentage of the ASHRAE Standard 90.1-2016 Medium Office Prototype Models Associated with the Implementation of Daylight Responsive Controls in Climate Zone 7

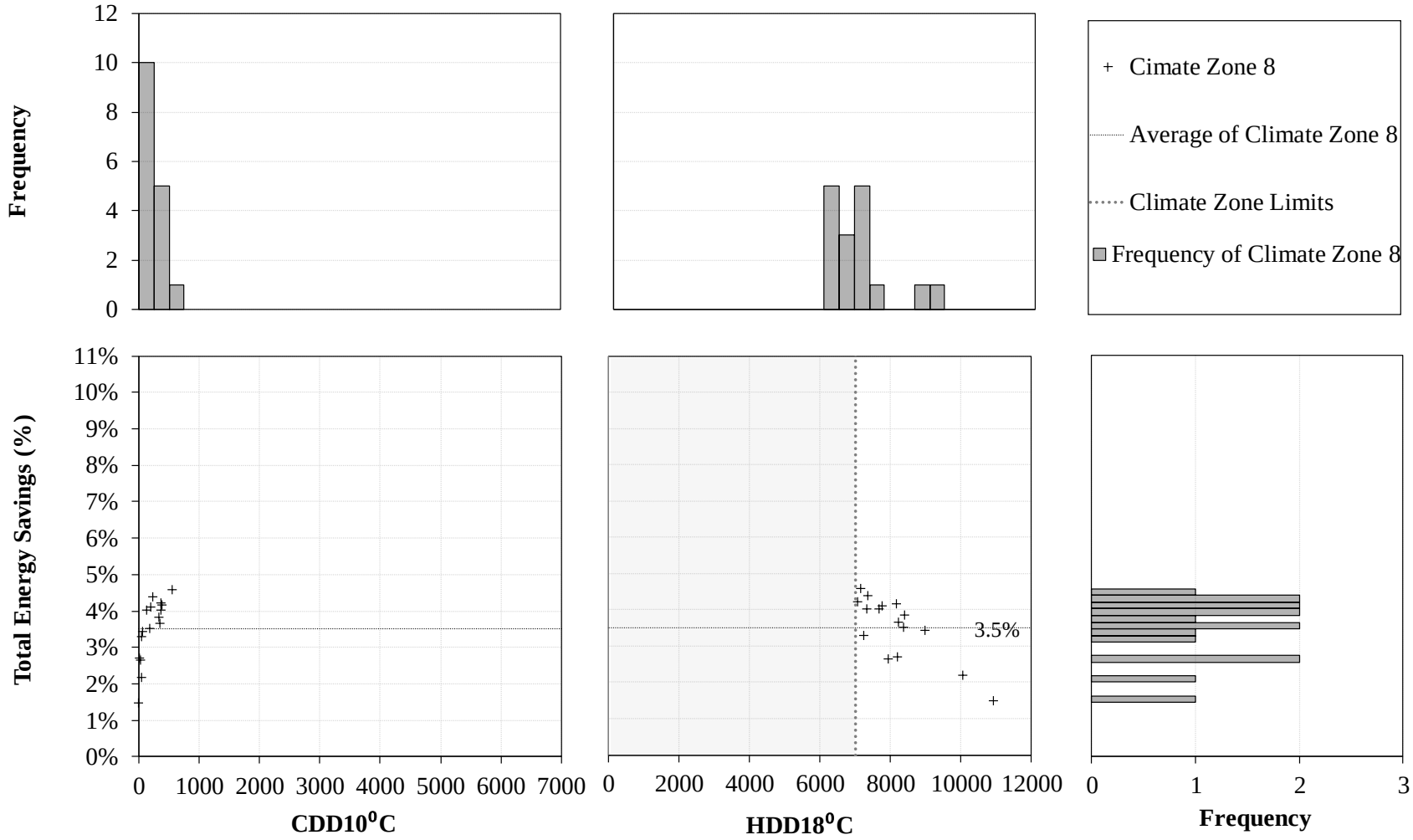

Figure 162: Total Energy Savings Percentage of the ASHRAE Standard 90.1-2016 Medium Office Prototype Models Associated with the Implementation of Daylight Responsive Controls in Climate Zone 8

C.2. Results for the Identical ASHRAE Standard 90.1-2016 Medium Office Prototype Model

This section includes the results of the simulations carried out on the identical ASHRAE Standard 90.1-2016 medium office prototype model, the model complied with the code for climate zone 4B, in different climates. Results include the regulated energy consumptions of the models with and without daylight responsive controls followed by the total energy savings and the total energy savings percentage for each case.

Figure 163 to Figure 165 show the regulated energy consumptions for the porotype model without daylight responsive control in different climates. Figure 166 to Figure 168 and Figure 169 to Figure 171 illustrate the total energy savings and the total energy savings percentages, respectively.

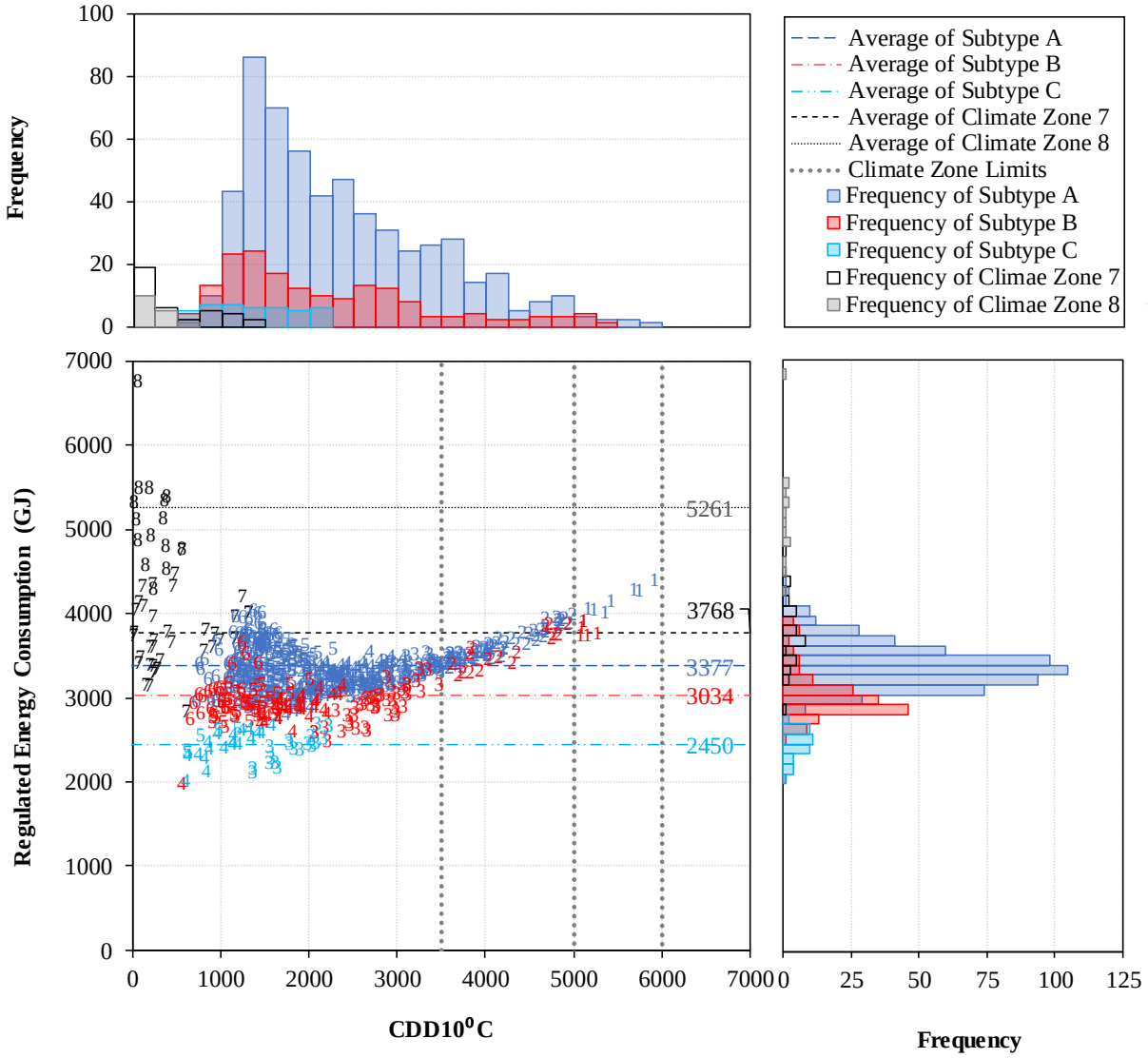

Figure 163: Regulated Energy Consumption of the ASHRAE Standard 90.1-2016 Medium Office Prototype Model for Climate Zone 4B without Daylight Responsive Controls with Respect to the HDD18°C of Different Weather Files

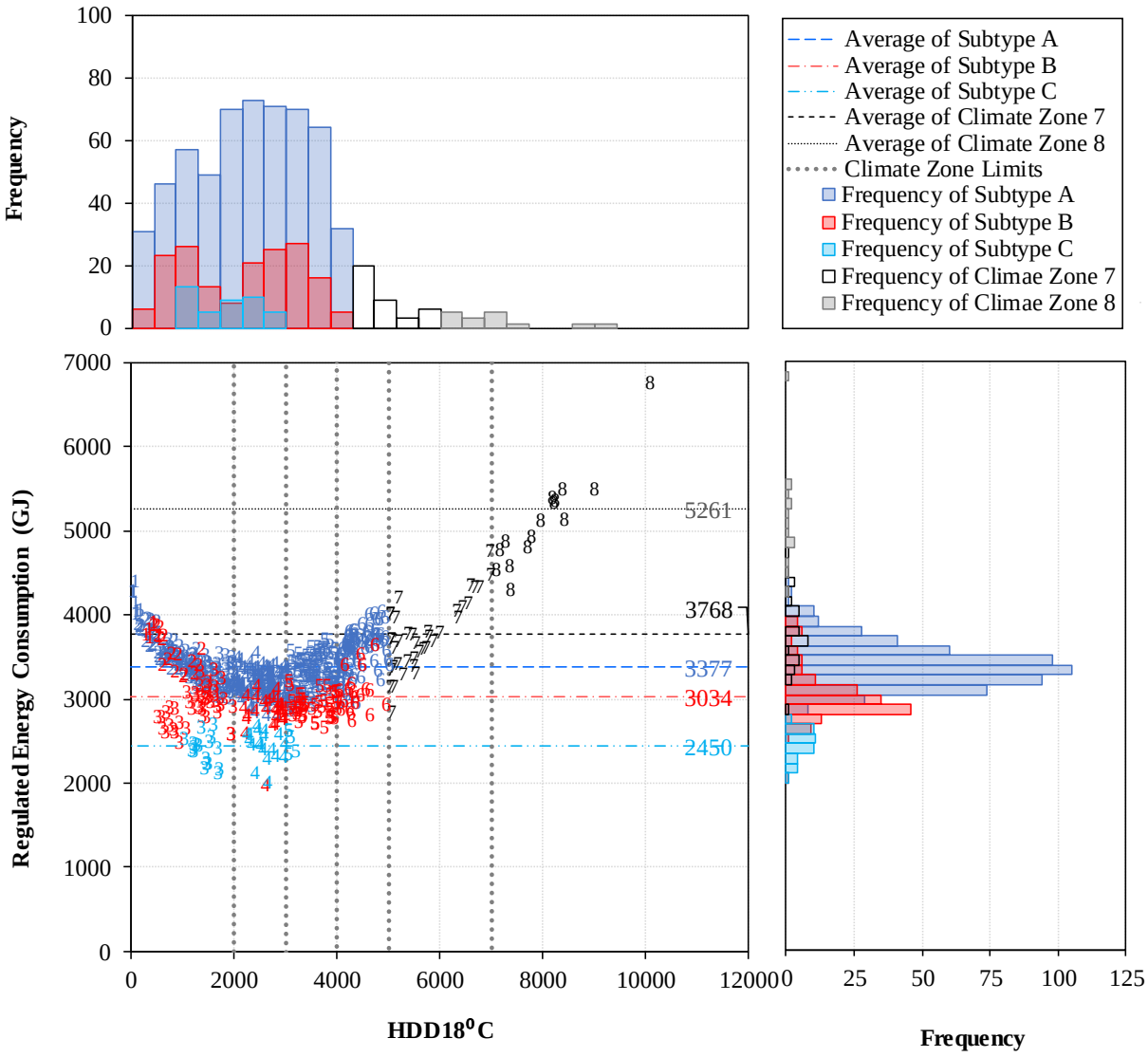

Figure 164: Regulated Energy Consumption of the ASHRAE Standard 90.1-2016 Medium Office Prototype Model for Climate Zone 4B without Daylight Responsive Controls with Respect to the HDD18°C of Different Weather Files

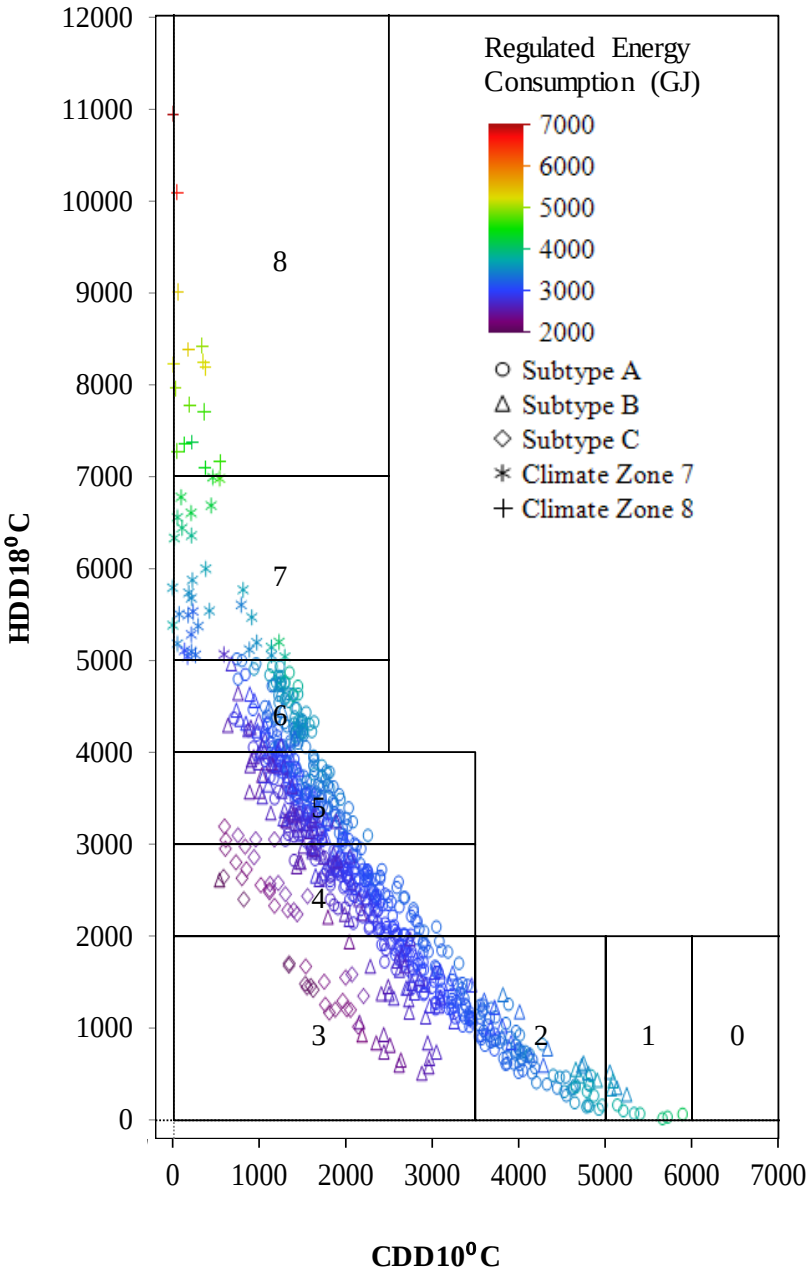

Figure 165: Regulated Energy Consumption of the ASHRAE Standard 90.1-2016 Medium Office Prototype Model for Climate Zone 4B without Daylight Responsive Controls in Different Climate Zones

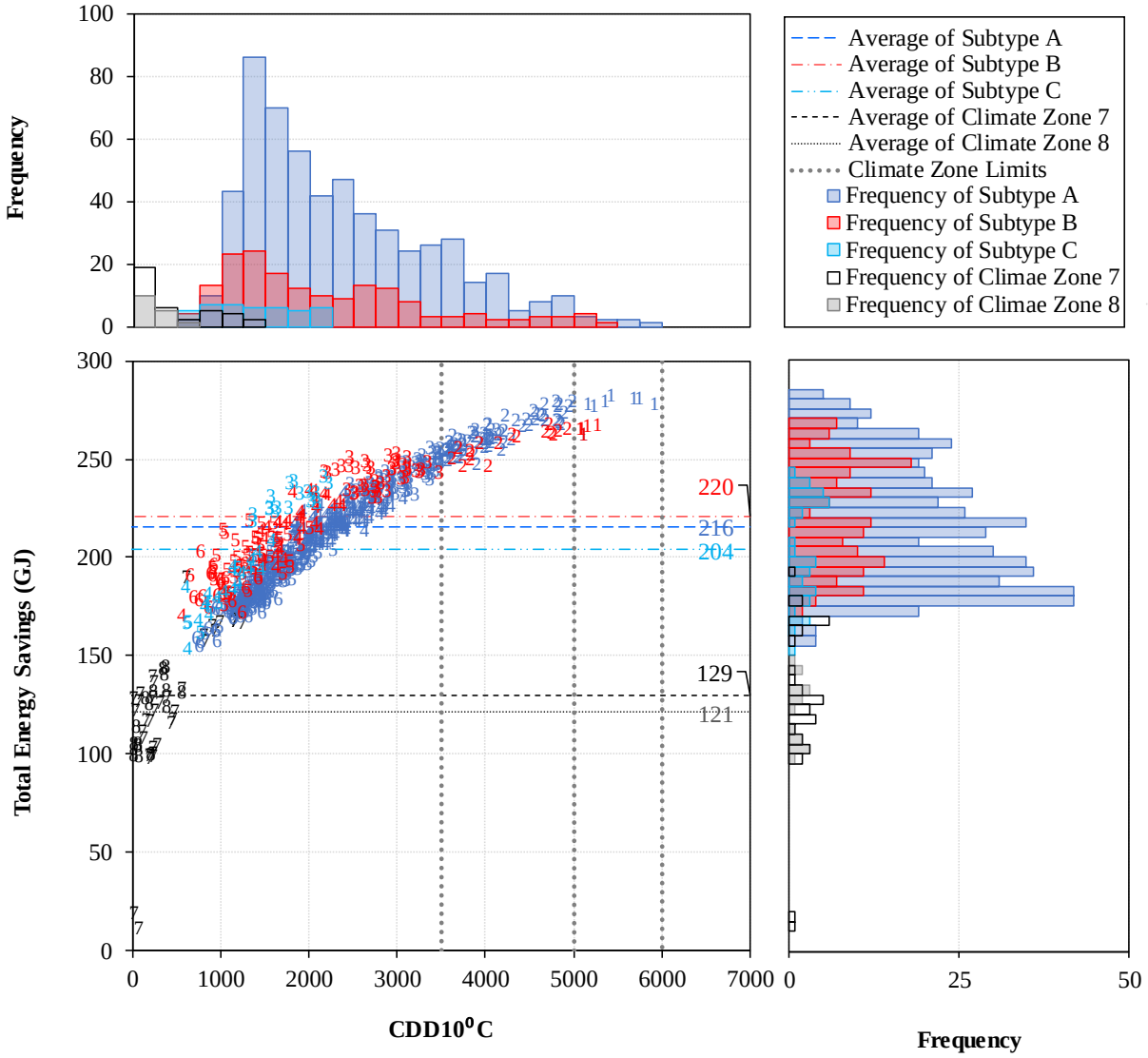

Figure 166: Total Energy Savings of the ASHRAE Standard 90.1-2016 Medium Office Prototype Model for Climate Zone 4B Associated with the Implementation of Daylight Responsive Controls with Respect to the CDD10°C of Different Weather Files

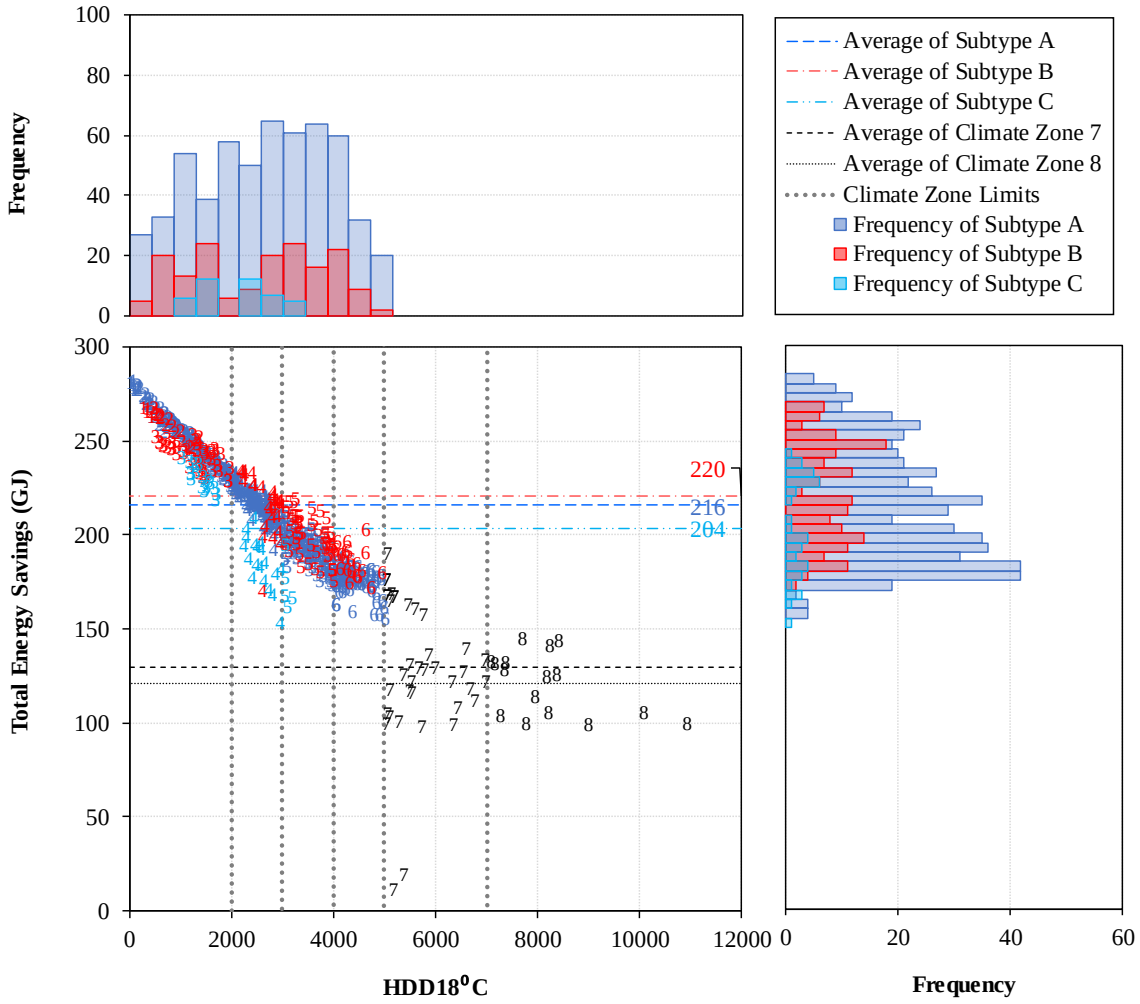

Figure 167: Total Energy Savings of the ASHRAE Standard 90.1-2016 Medium Office Prototype Model for Climate Zone 4B Associated with the Implementation of Daylight Responsive Controls with Respect to the HDD18°C of Different Weather Files

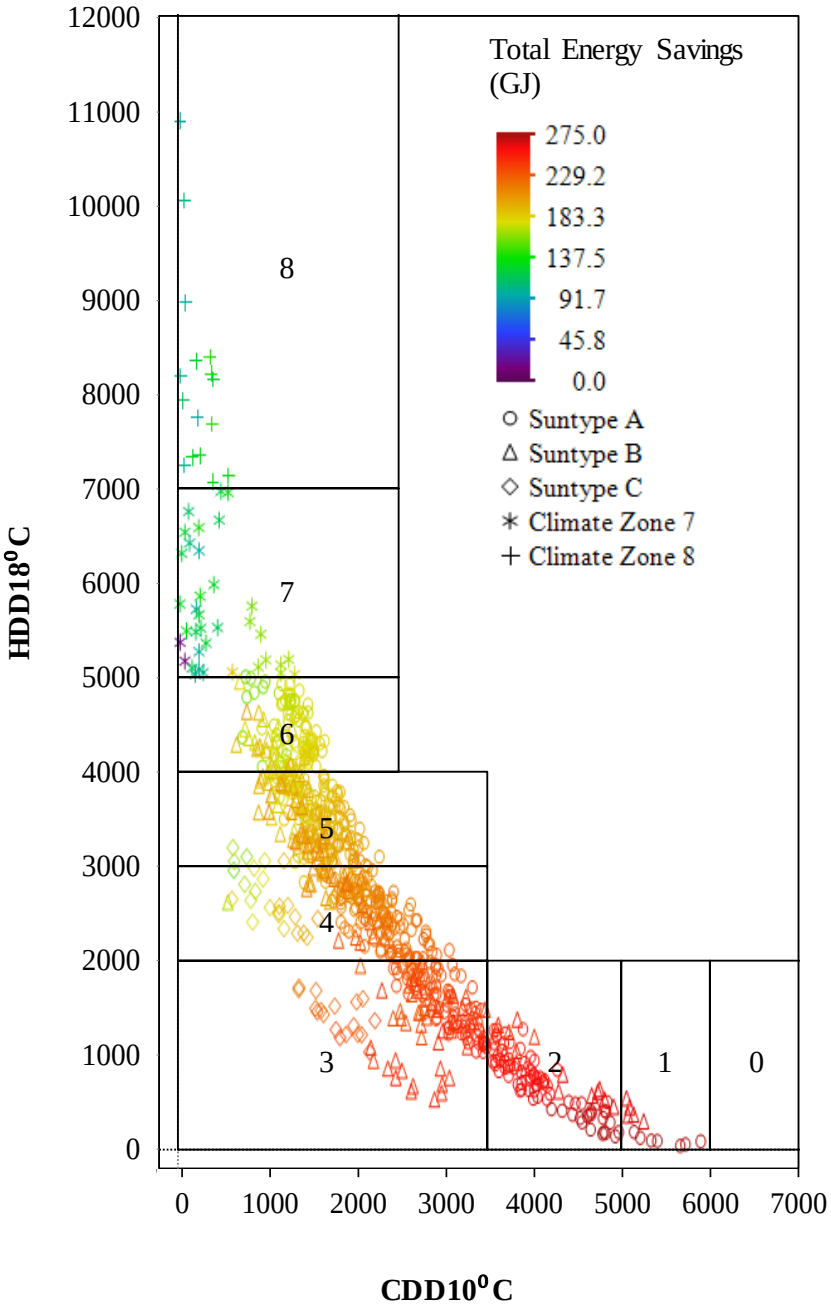

Figure 168: Total Energy Savings of the ASHRAE Standard 90.1-2016 Medium Office Prototype Model for Climate Zone 4B Associated with the Implementation of Daylight Responsive Controls in Different Climate Zones

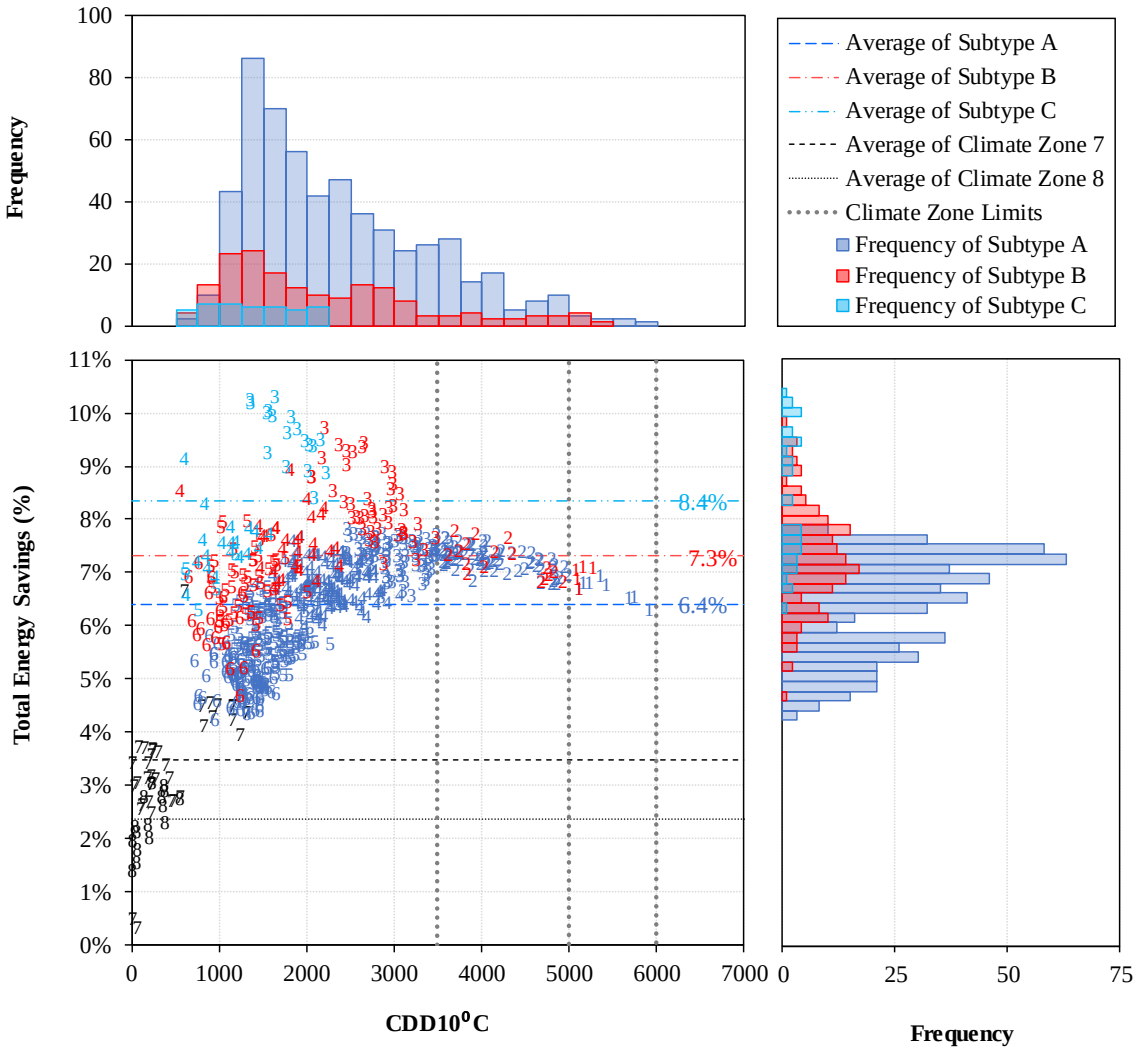

Figure 169: Total Energy Savings Percentage of the ASHRAE Standard 90.1-2016 Medium Office Prototype Model for Climate Zone 4B Associated with the Implementation of Daylight Responsive Controls with Respect to the CDD10°C of Different Weather Files

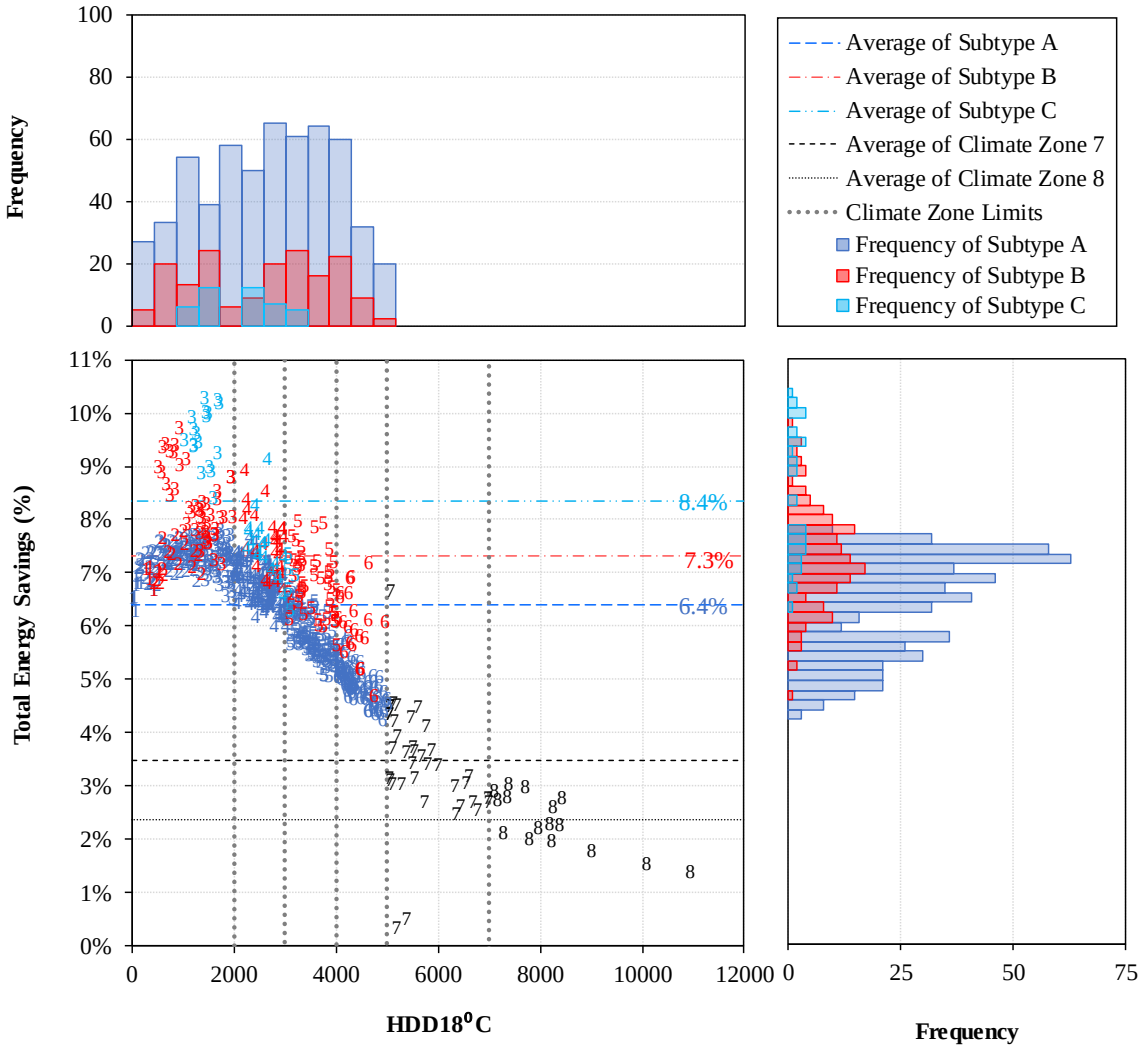

Figure 170: Total Energy Savings Percentage of the ASHRAE Standard 90.1-2016 Medium Office Prototype Model for Climate Zone 4B Associated with the Implementation of Daylight Responsive Controls with Respect to the HDD18°C of Different Weather Files

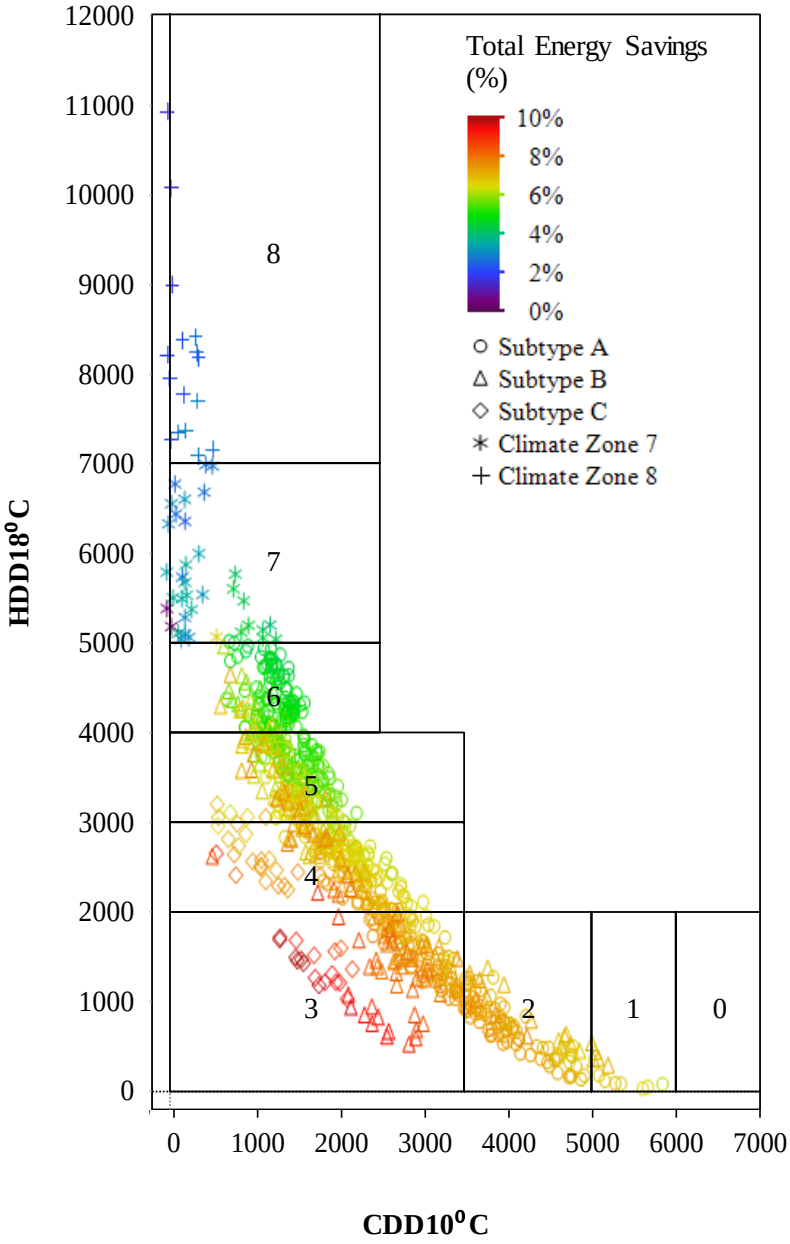

Figure 171: Total Energy Savings Percentage of the ASHRAE Standard 90.1-2016 Medium Office Prototype Model for Climate Zone 4B Associated with the Implementation of Daylight Responsive Controls in Different Climate Zones

C.3. Results for the Identical 24-Hour Operating Schedule Model

This section includes the results of the simulations carried out on the identical ASHRAE Standard 90.1-2016 medium office prototype model with 24-hour operation schedule. The model complied with the code for climate zone 4B and was modified as described in Section 3.4.3 for the 24-hour operation.

Figure 172 and Figure 173 show the regulated energy consumption of the model in different locations with respect to HDD18 °C and CDD10 °C, respectively. Results showed discrepancies between the energy consumption of the models with 24-hour operation schedule in different subtypes, similar to the discrepancies seen in the results of the models with office schedule. This shows the operating schedule of the models is not the main cause of the difference in energy consumption of the models in different subtypes.

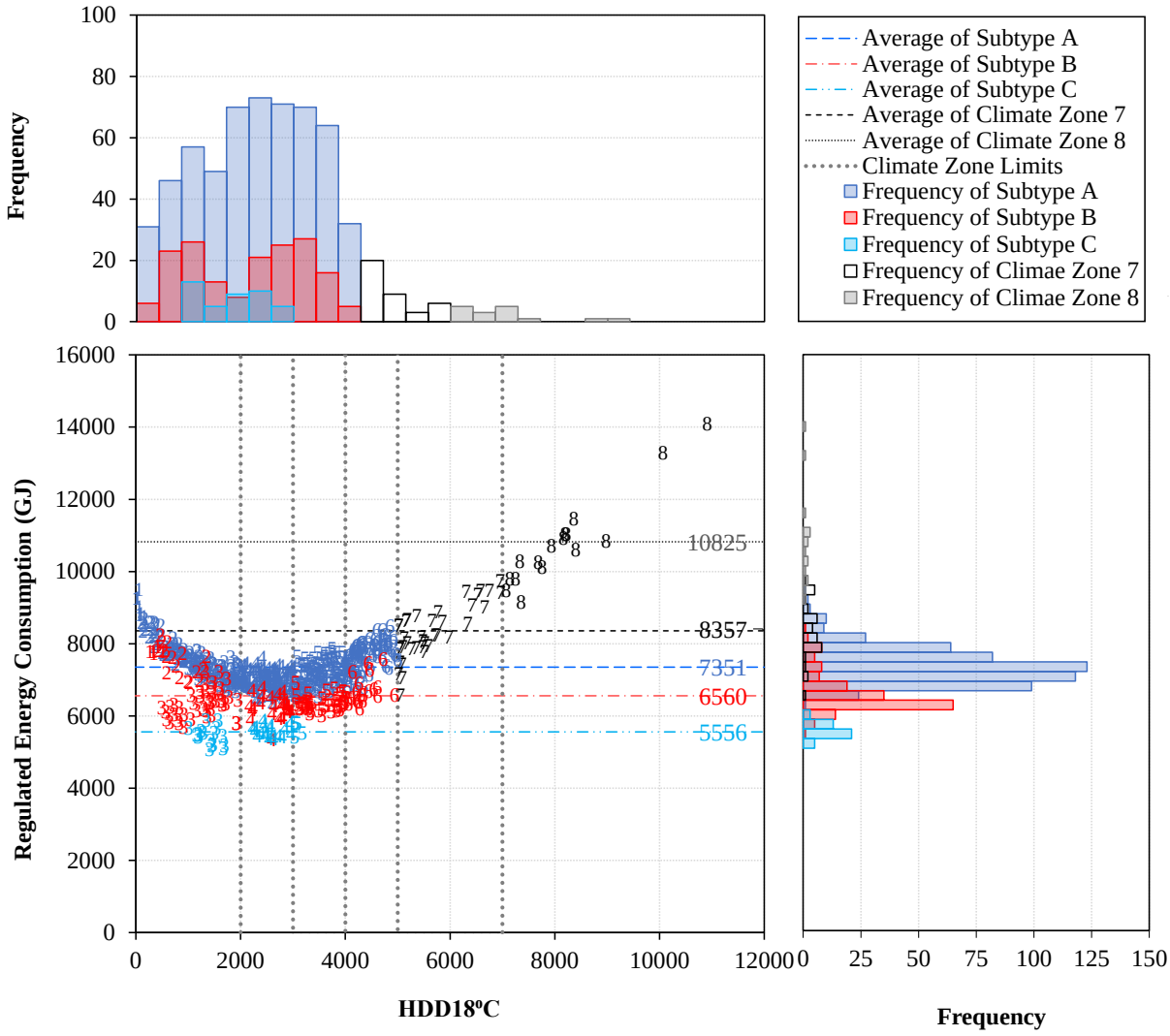

Figure 172: Regulated Energy Consumption of the 24-Hour Operating Schedule Model with Respect to the HDD18 °C of Different Weather Files

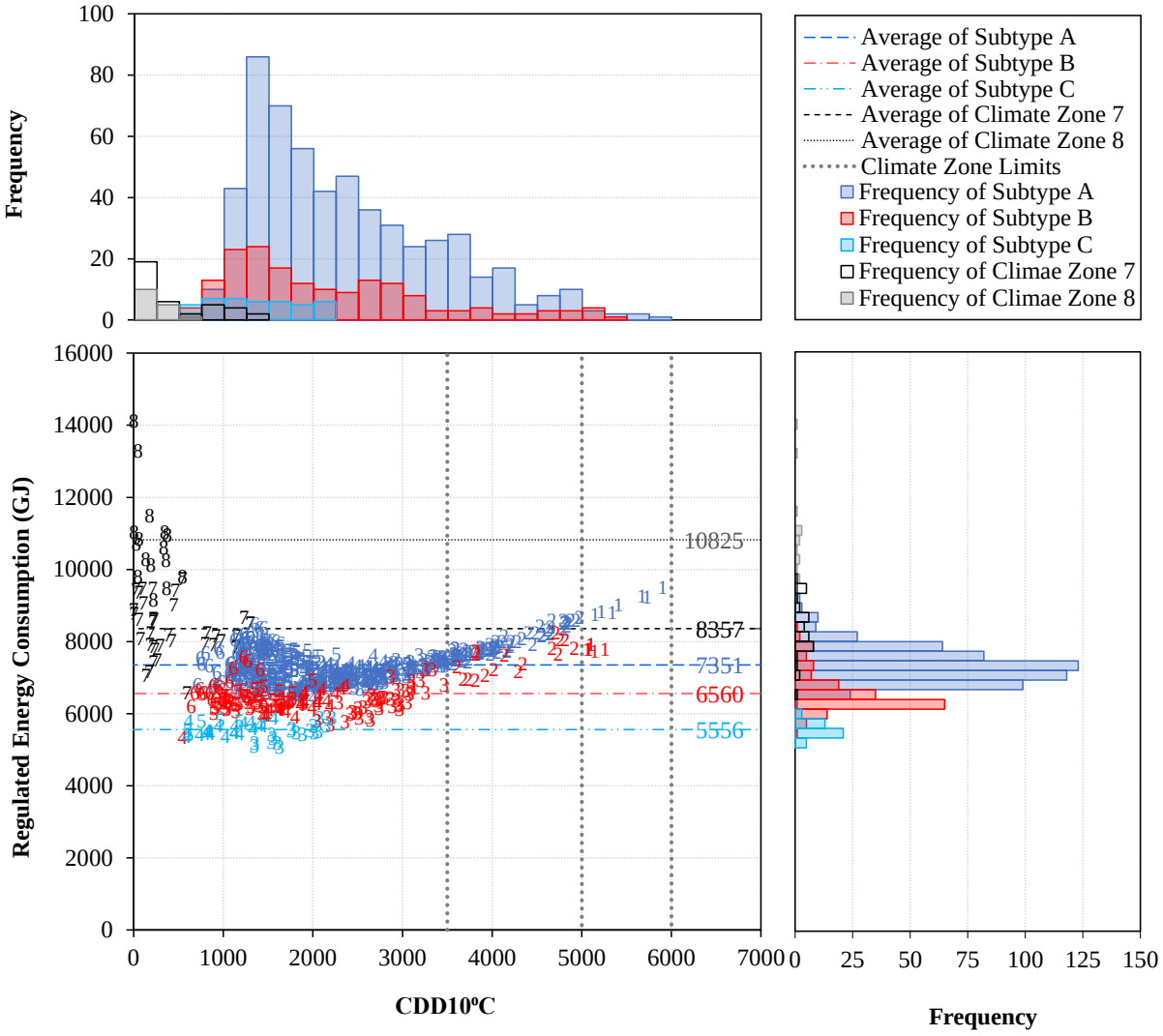

Figure 173: Regulated Energy Consumption of the 24-Hour Operating Schedule Model with Respect to the CDD10 °C of Different Weather Files